Ultra- and Extreme-Short Wave Reception

Principles, Operation, and Design

BY

M. J. O. STRUTT, D. TECHN. SC.

Electronics Consultant, N. V. Philips Co., Ltd.
Eindhoven, Holland.

1947

D. VAN NOSTRAND COMPANY, INC.

TORONTO NEW YORK LONDON

NEW YORK
D. Van Nostrand Company, Inc., 250 Fourth Avenue, New York 3
TORONTO
D. Van Nostrand Company (Canada), Ltd., 228 Bloor Street, Toronto
LONDON
Macmillan & Company, Ltd., St. Martin's Street, London, W.C. 2

PRINTED IN THE UNITED STATES OF AMERICA

PREFACE

The immense growth of the application of ultra- and extreme-short waves during World War II needs no further comment. The peace-time application of the experience thus gained calls for a coherent exposition of the principles and data at present available. It is the object of this book to offer these in such form as to admit of their direct application to individual reception problems. In his professional work of the past sixteen years the author had to acquaint himself with most phases of this field, being associated with the development of electronic tubes suited to these short waves ranging down to, say, 1 cm wavelength. Besides a number of experimental and theoretical data, partly unpublished or not yet widely circulated, published work from other sources has been assimilated so as to obtain an all-round exposition. Due attention has been drawn to restrictions still inherent to the treatment of some problems, with a view to stimulating further developments.

The frequency range treated is from about 6 to 30,000 mc/s thus covering the h.f. (3 – 30 mc/s), v.h.f. (30 – 300 mc/s), u.h.f. (300 – 3000 mc/s), and s.h.f. (3000 – 30,000 mc/s) ranges. Chapter I deals with the properties, propagation, reflection, and absorption of waves, including ionospheric data, as well as with signals, i.e., with the aspects of amplitude, phase, frequency, and impulse modulation. Chapter II contains information and data on spontaneous fluctuation noise of networks and tubes, due regard being given to the modern way of introducing noise figures. Section II.2.2, dealing with properties of noise figures, is thought to contain some items that may be new even to reception engineers. In Chapter III the relevant properties and data on reception antennas are given a unified treatment, including noise. Chapter IV deals with the links between antennas and receiving sets: transmission lines, wave guides, and resonant devices (circuits and cavities), illustrating their properties by data of actual examples. In order to give the reader an over-all picture of practical experimental data at present available, Chapter V contains a compilation of such data as well as a description of the experimental devices for obtaining them. Hereby it is hoped that experimental research by application of such devices might be stimulated in order to fill existing gaps in our present knowledge. Chapter VI deals with perhaps the most important stages of receivers: the entrance stages, including amplifier, mixer, regenerative

detector, and super-regeneration stages. Some possibilities of noise reduction mentioned in sections VI.1.2 and VI.2.4 are supposed to be not yet widely known. Finally, Chapter VII contains information on further reception stages such as second detector and output stages, frequency-modulation reception, impulse-modulation and single side-band reception, over-all design, including fading compensation, stabilized power supply, microphonic effects, and radar. A list of principal symbols has been added. Throughout the text practical units such as volts, amperes, ohms, etc., have been used.

Although the scope of the book may be evident from this summary, the separate treatment of reception as distinct from transmission perhaps needs some comment. The main reason, in the author's mind, lies in essential differences between the problems involved, such as the following: noise problems are often predominant with reception and mostly absent with transmission. Reception circuits and tubes nearly always involve low values of h.f. power, whereas high values are common in transmission. The number of receivers being by far larger than that of transmitters, different design problems are involved.

Decimal numbering of sections and subsections has been adopted, e.g., II.1.21 being a sub section of II.1.2, this being a division of II.1 and this in turn being a section of Chapter II. The equations in each section have been numbered *a*, *b*, *c*, etc., preceded by the section indication. Thus, reference to an equation automatically refers to its section, the section indication being repeated at the top of each page. Mathematical treatment has been cut down to a minimum, reasoning being in many cases substituted for elaborate formulas. The author has had in mind the production of a readable book of wide appeal, and the text has been prepared accordingly. Readers seeking more elaborate information on any detail are referred to the list of references given at the end of each section and corresponding to a bibliography of over 300 items dated between 1920 and 1946, preference being given to recent publications. With the aid of these references, the reader interested in any particular point will have little difficulty in pursuing his problem as far as seems necessary to his purposes.

It is a pleasure to extend my sincere thanks to colleagues and co-workers for assistance and discussion in the course of the work involved.

M. J. O. STRUTT

Eindhoven
April, 1947

CONTENTS

CHAPTER I

WAVES AND SIGNALS

The power captured by a receiver is carried by electromagnetic waves. These waves issue from a transmitter. On their path between transmitter and receiver they are subject to the processes of reflection and absorption, of propagation through different media, and to disturbances. A brief discussion of these processes, as far as they affect reception, will be given. The transmission of waves is for the purpose of conveying signals. Hence the different ways of implanting or modulating signals on waves will be discussed.

I.1 Waves

I.1.1. Spherical and plane wave trains. The waves in question are, for our purposes, either approximately spherical or plane. We shall start by a discussion of their main properties.

I.1.11. Field strengths and specific power. A transmitting antenna is supposed to be surrounded by a spherical surface of large radius compared to the antenna dimensions and to the wavelength of the waves issuing from the antenna. (The exact meaning of the term "wavelength" will be discussed later.) If the first condition is satisfied the entire antenna system may be supposed approximately to coincide with the center of the sphere. In any point of the spherical surface, the electric as well as the magnetic field strength is very nearly directed in the local tangential plane. Furthermore, the directions of both field strengths are very nearly mutually perpendicular. These simple rules are satisfied to a closer approximation if the sphere's radius is increased. The ensuing waves are indicated as "spherical waves." At a sufficiently great distance the waves issuing from any source may be regarded as being very nearly spherical.

Considering a small portion of the spherical surface, very little difference from a *plane* surface will be detected. Thus these spherical waves corresponding to such a small portion of the total surface very nearly coincide with plane waves. The electric- and magnetic-field

strengths at different points are approximately directed in parallel planes, corresponding field strengths being of parallel directions.

The electric-field strength **E** is expressed in volts/cm and the magnetic field strength **H** in amperes/cm. A definite relationship exists between both field strengths at the same point at any time:

$$\frac{\mathbf{E}}{\mathbf{H}} = 120\pi \approx 377 \text{ ohms.} \qquad \text{(I.1.11}a\text{)}$$

The specific power carried by a plane wave per cm^2 of its surface is denoted by **p** and expressed in watts/cm^2. It is related to **E** and **H** by the equation:

$$\mathbf{p} = \mathbf{EH}. \qquad \text{(I.1.11}b\text{)}$$

The bold-face type for these three quantities indicates their vector property, having a definite direction in space at any time. If their vector property does not matter, ordinary type is used for the same symbols. The direction of **p** is such that the positive directions of **E**, **H**, and **p** coincide respectively with thumb, first, and second finger of our right hand, pointing perpendicularly to each other. The direction of **p** indicates the direction in which the power is propagated. By Eqs. (*a*) and (*b*) we have for the amounts of **p**, **E**, and **H** the relationship:

$$p = \frac{E^2}{120\pi} = 120\pi H^2. \qquad \text{(I.1.11}c\text{)}$$

By these relations the field strengths resulting from a transmitter radiating uniformly in all directions may easily be evaluated. The above specific power at a point distant r from the transmitter radiating a power P watts is:

$$p = \frac{P}{4\pi r^2},$$

while E and H result from Eq. (*c*). For example, a transmitter of 200 kilowatts would cause an electric-field strength of about 120 μ volts/cm at 200 km distance and of about 5 μ volts/cm at 5000 km distance.

I.1.12. Polarization. The simplest waves are "singly periodic," meaning that both field strengths at any point of space are sine or cosine functions of time t, e.g., $\cos \omega t$. Here ω is indicated as "angular frequency" and $\omega = 2\pi f$, f being the frequency expressed in cycles/sec. In a singly periodic wave of linear polarization both field strengths are at

any point of space and at any instant parallel to a fixed direction, these directions for **E** and **H** being mutually perpendicular according to the preceding section. The direction of **E** coincides with what is called the direction of polarization. Both field strengths reach their maximum values at the same instant at any fixed point of space. No phase delay exists between them in free space or indeed in any medium free of absorption. As p is proportional to $1/r^2$, both E and H are proportional to $1/r$, and we may write:

$$E = \frac{A}{kr} \cos(\omega t - kr), \quad H = \frac{B}{kr} \cos(\omega t - kr), \qquad \text{(I.1.12}a\text{)}$$

these relations being valid at a large distance from the transmitter, such that $kr \gg 1$. Here $k = 2\pi/\lambda$ and λ is the wavelength of the waves in question. If r is increased by λ the expressions (a) retain approximately their original values as $kr \gg 1$. Instead of Eqs. (a) we shall use the often equivalent complex notation:

$$E = \frac{A}{kr} \exp(j\omega t - jkr), \quad H = \frac{B}{kr} \exp(j\omega t - jkr) \qquad \text{(I.1.12}b\text{)}$$

where $\exp(jx) = \cos x + j \sin x$ and $j = +\sqrt{-1}$. The real part of any resulting complete complex expressions resulting from our calculations will be used as a result. Thus Eqs. (a) are the real parts of Eqs. (b). These Eqs. (a) and (b) are the expressions of spherical singly periodic waves of linear polarization.

By the superposition of two linearly polarized waves of different directions of polarization and of equal single frequencies we obtain waves of a different kind. The simplest example is afforded by two waves of mutually perpendicular linear polarizations and a mutual phase difference of one quarter period, corresponding to a phase angle of $\pi/2$. It is well known that the resulting polarization of the composite wave rotates uniformly, one rotation coinciding with one period $2\pi/\omega$ of the waves. If the mutual phase angle has a value not coinciding with a multiple of $\pi/2$, the resulting composite waves have also a rotating polarization, one rotation again coinciding with one period of the waves, but this time not occurring at uniform speed. In the first case the composite wave is indicated as circularly polarized, in the second case

as elliptically polarized. At circular polarization the magnitude of the field strengths remains unaltered during rotation. Hence the corresponding vectors describe circles in space. At elliptical polarization their magnitude during rotation corresponds to the length of a rotating diameter in an ellipse.

A plane polarized wave is pictured in Figure 1. By the composition of several singly periodic waves of linear polarization and of different frequencies more intricate wave patterns may be obtained. Generally, however, their properties may be conveniently discussed by considering the simple component waves.

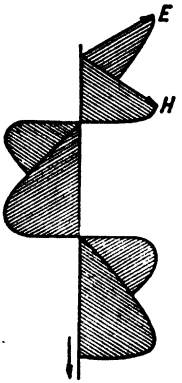

FIG. 1 Plane electromagnetic singly periodic wave of linear polarization, showing mutually perpendicular directions of electric-field strength E and of magnetic-field strength H, both being perpendicular to direction of propagation (downward).

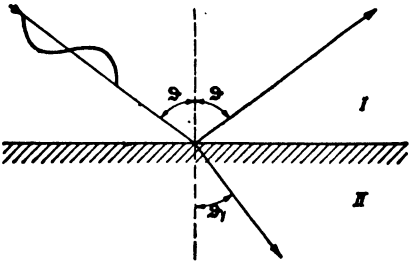

FIG. 2 Incidence of plane wave of linear polarization upon the plane boundary between two different media I and II, the angle of incidence being ϑ and that of refraction ϑ_1.

I.1.2. Reflection and absorption. In section I.1.1, waves in a space free of obstacles causing reflection and absorption were discussed. We shall now consider the effects of these processes on the waves in question.

I.1.21. Reflection of plane waves at a plane surface. A singly periodic plane wave train of linear polarization is supposed to be incident upon a plane boundary between two media of different properties (Fig. 2). The properties of a homogeneous medium relative to the propagation of electromagnetic waves depend on three quantities: frequency f, specific conductivity σ, and specific dielectric capacity ϵ, both at the frequency

in question. These quantities are active in the combination:

$$n^2 = j\frac{18 \times 10^{11}\sigma}{f} - \epsilon = \epsilon(j \tan \delta - 1). \qquad \text{(I.1.21}a\text{)}$$

The specific conductivity σ is expressed in mhos/cm. In a magnetic medium the value of n^2 is obtained by multiplication of the right-hand member of Eq. (a) by μ, this being the specific magnetic permeability. In most media occurring in this book we have $\mu = 1$. The quantity δ is indicated as "loss angle." Approximate values of ϵ, σ, and tan δ at different frequencies, expressed in megacycles/sec = mc/s and corresponding to different media, are shown in a table, assuming that the indicated values of σ and ϵ are independent of frequency.

MEDIUM	ϵ	σ	TAN δ AT 10 MC/S	AT 100 MC/S	AT 1000 MC/S	AT 10,000 MC/S
Sea water..	80	10^{-2}	22	2.2	0.22	0.022
Fresh water	80	10^{-5}	0.022	0.0022	0.00022	0.000022
Wet soil ...	10	5×10^{-5}	0.90	0.090	0.0090	0.00090
Dry soil....	5	10^{-6}	0.036	0.0036	0.00036	0.000036
Vacuum ...	1	0	0	0	0	0

The dependence of σ, ϵ, and tan δ on frequency was investigated for different types of soil between 500 cycles/s and about 600 mc/s. Some hitherto unpublished results are shown in Figures 3 and 4. The values of σ and ϵ corresponding to meadow soil of considerable moisture (presumably between 10 and 15% of its specific weight being due to water) were found to be approximately constant at frequencies between 500 and 2×10^7 cycles/s (reference *339*). It is possible that dry soil has a higher conductivity than wet soil at ultra-high frequencies but a lower conductivity at radio frequencies. For sea water σ was found to be constant between 500 and 10^6 c/s. Reflection takes place in such manner that the specific power of the reflected wave is propagated at an angle with the reflecting plane equal to that of the incident wave (see the angle ϑ in Figure 2). We assume that n^2 of Eq. (a) has the value n_1^2 in the medium I (Fig. 2) and the value n_2^2 in the medium II. The ratio n_2^2/n_1^2 is denoted by n_0^2. Two different cases will be dealt with: (a) the magnetic-field strength of the incident (and hence of the reflected) wave is parallel to the reflecting plane; (b) the electric-field strength of the incident and the reflected waves is parallel to the said

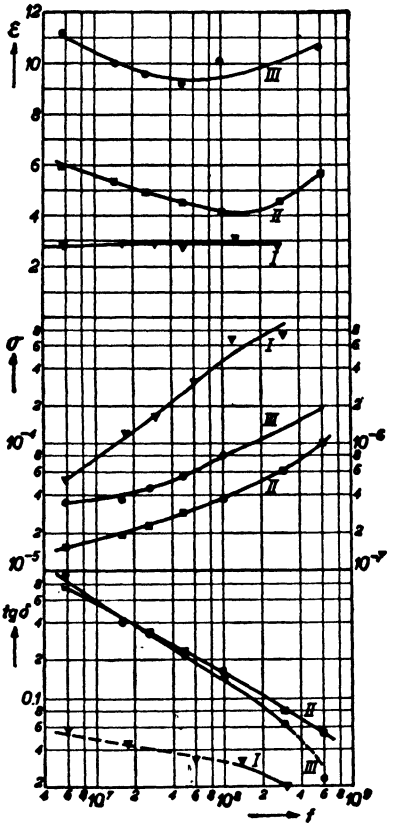

FIG. 3 Electric properties of garden soil between 50 and 600 mc/s. Upper part of figure: dielectric coefficient ϵ as dependent on frequency. Below this: specific conductivity σ (mhos/cm) as dependent on frequency. Lower part: tan δ (loss angle) as dependent on frequency. Curves marked I: dry soil; marked II: 5% moisture; marked III: 12% moisture.

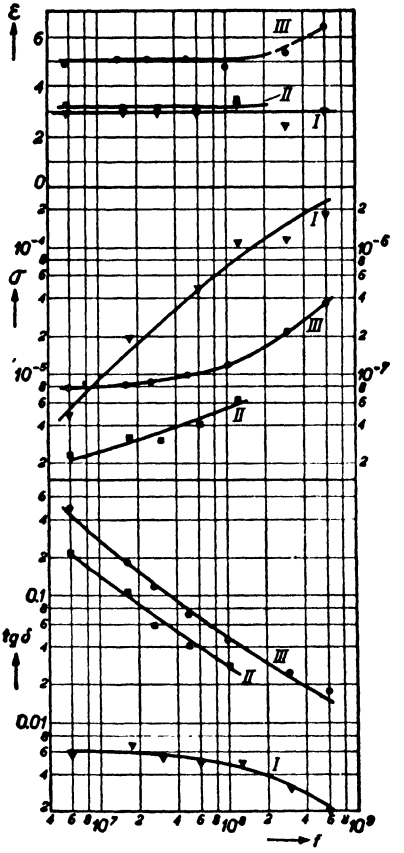

FIG. 4 As Fig. 3 but related to pure sand. Curves marked I: dry sand; marked II: 2.56% moisture; marked III: 5.6% moisture (water) added in weight to the sand.

Curves marked I of σ correspond to right-hand scale in both Fig. 4 and Fig. 3.

plane. In case (*a*) the ratio of the complex electric- and magnetic-field strengths in the reflected and incident waves is F_a. In case (*b*) the ratio of the similarly complex field strengths in the reflected and

incident waves is F_b. Then:

$$F_a = \frac{n_o^2 \cos\vartheta - \sqrt{n_o^2 - 1 + \cos^2\vartheta}}{n_o^2 \cos\vartheta + \sqrt{n_o^2 - 1 + \cos^2\vartheta}}, \qquad \text{(I.1.21}b\text{)}$$

$$F_b = \frac{\cos\vartheta - \sqrt{n_o^2 - 1 + \cos^2\vartheta}}{\cos\vartheta + \sqrt{n_o^2 - 1 + \cos^2\vartheta}}. \qquad \text{(I.1.21}c\text{)}$$

In case (a) the electric field strength component parallel to the reflecting plane is reversed in sign at reflection and in case (b) this applies to the magnetic field strength component parallel to the plane of reflection.

Obviously these ratios or "coefficients of reflection" are in general complex quantities having a modulus and a phase angle: $F_a = |F_a| \exp(j\psi_a)$ and $F_b = |F_b| \exp(j\psi_b)$, vertical dashes denoting the modulus or absolute value of the quantity placed between them. In terms of Eqs. (I.1.12b) the meaning of these coefficients is as follows:

Incident waves:

$|E| \exp(j\omega t - jkr)$, $|H| \exp(j\omega t - jkr)$,

Reflected waves:

$|EF_a| \exp(j\omega t + j\psi_a - jkr)$, $|HF_a| \exp(j\omega t + j\psi_a - jkr)$,

or

$|EF_b| \exp(j\omega t + j\psi_b - jkr)$, $|HF_b| \exp(j\omega t + j\psi_b - jkr)$. (I.1.21$d$)

Some actual values of F_a and F_b are shown in Figures 5, 6, and 7. If n_o^2 is complex, no zero occurs in the reflection coefficients, as is evident from Figure 7a.

A particularly simple case of reflection occurs at perpendicular incidence, the angle ϑ of Figure 2 being zero. Then:

$$F_a = \frac{n_o - 1}{n_o + 1} \quad \text{and} \quad F_b = -\frac{n_o - 1}{n_o + 1}. \qquad \text{(I.1.21}e\text{)}$$

In this case and in subsequent applications the value of n_o instead of n_o^2 occurs. We obtain from Eq. (I.1.21a):

$$n = n_r + jn_i = \pm\sqrt{|\epsilon|}\sqrt{-1 + j\tan\delta}. \qquad \text{(I.1.21}f\text{)}$$

The question as to which sign of the root ought to be chosen may be decided by the rule that n_r and n_i should be of *negative* sign. The reason for this will be apparent in section I.1.23. The calculation of n_r and n_i is simplified by Figure 8.

REFERENCES: *42, 80, 97, 114, 220, 237, 337, 338, 339.*

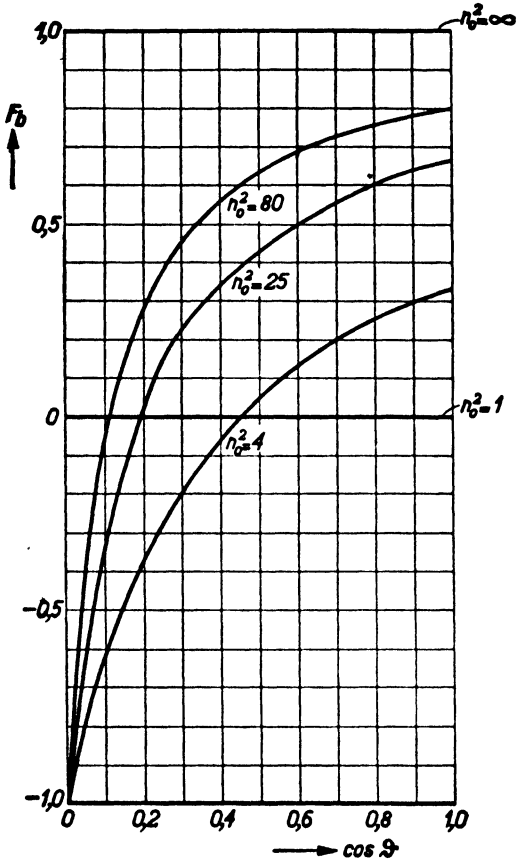

FIG. 5 Coefficient of reflection F_b as dependent on the angle of incidence ϑ corresponding to different values of the index of refraction n_0.

I.1.22. Directive patterns and wave-band distortions caused by plane reflection. Reflections at a plane boundary surface are of frequent occurrence in reception practice, the surface in question being the earth,

a lake, or the sea. We shall therefore examine some simple consequences of such reflections connected with reception antennas. A receptive antenna is situated at A (Fig. 9). Two separate parts of the incident plane wave reach A: one, indicated by W_1 in Figure 9, directly, and a second part, indicated by W_2, indirectly via reflection at B. Assuming the coefficient of reflection at B to be F (which might be either F_a or F_b, or a combination of both), its phase angle being ψ:

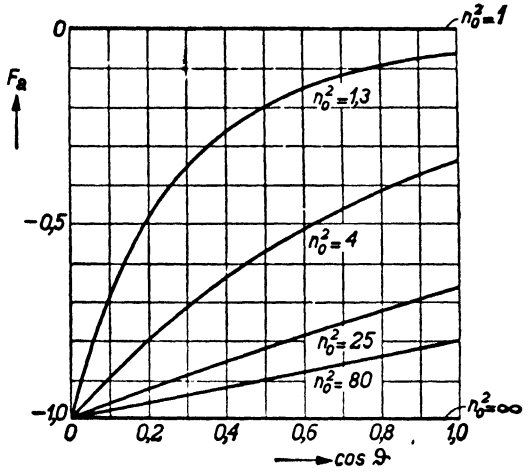

FIG. 6 As Fig. 5 but coefficient F_a instead of F_b.

$F = |F| \exp(j\psi)$, we may easily evaluate the resulting field strength at A. The wave W_2 has a path which is longer by the lengths $\overline{AB} + \overline{BC}$ in Figure 9 than the path of W_1. Indicating the height of the antenna above the earth by h (Fig. 9), we have obviously: $\overline{AB} + \overline{BC} = \overline{A'BC}$, A' being the image of A with respect to the surface T. As $\overline{A'BC} = 2h \cos \vartheta$, the wave W_2 is retarded by an angle $\varphi = (2\pi 2h \cos \vartheta)/\lambda$ with respect to W_1 because of the difference in path, λ being the wavelength in the upper medium. Hence the resulting field strength at A due to W_1 and W_2 is:

$$|\mathbf{E}|\{\exp(j\omega t) + |F| \exp(j\omega t - \varphi + \psi)\}, \qquad \text{(I.1.22}a\text{)}$$

$\mathbf{E}$ being the field strength of the unobstructed incident wave near A. Reverting Eq. (a) to real parts and omitting the factor $\cos \omega t$, we obtain a resulting field strength squared of:

$$|E|^2\{1 + 2|F| \cos(\varphi - \psi) + |F|^2\}. \qquad \text{(I.1.22}b\text{)}$$

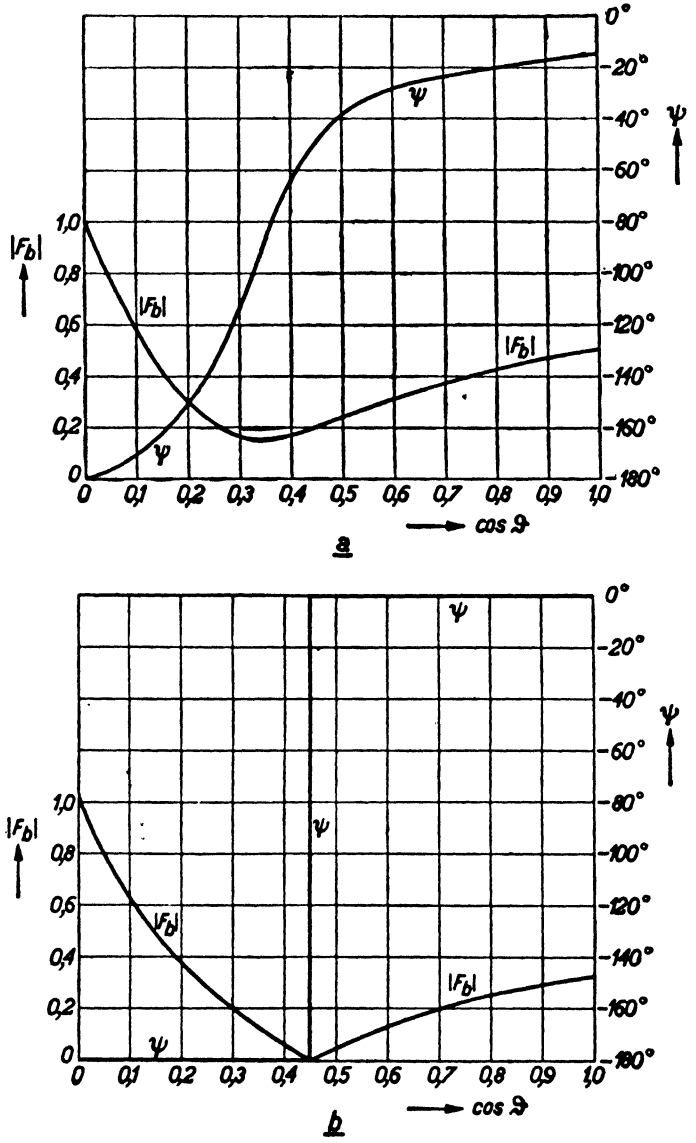

FIG. 7 Different representation of F_b as dependent on the angle of incidence ϑ. Modulus $|F_b|$ and phase angle ψ of reflection. Diagram *a* corresponds to $\epsilon = 6$ and $\lambda = \frac{1}{1200}\sigma$ being expressed in mhos/cm and the wavelength λ (measured in air) in *m*. Diagram *b* corresponds to $\epsilon = 4$ and $\sigma = 0$.

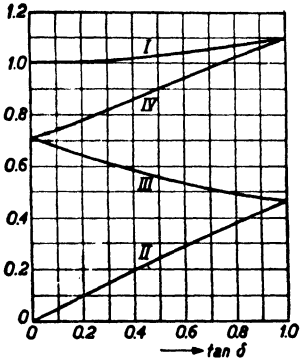

FIG. 8 Evaluation of n_o from complex values of $n_o^2 = \epsilon\,(-1 + j \tan \delta)$. Curves I and II represent the quantities $-\frac{n_i}{\sqrt{\epsilon}}$ and $-\frac{n_r}{\sqrt{\epsilon}}$ of eq. (I.1.21f) respectively, as dependent on tan δ (horizontal scale). If tan $\delta > 1$, the curves III and IV must be used, representing $-\frac{n_r}{\sqrt{\epsilon \tan \delta}}$ and $-\frac{n_i}{\sqrt{\epsilon \tan \delta}}$ of eq. (I.1.21f) respectively, while the horizontal scale in this case represents $\frac{1}{\tan \delta}$.

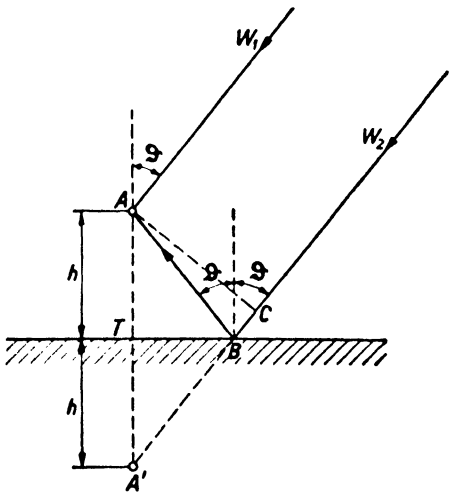

FIG. 9 Incidence of a plane wave on a reception antenna at A oriented horizontally with respect to the earth's surface T at a height h. The antenna receives the wave train W_1 directly and W_2 upon reflection at the earth's surface.

Several special cases of Eq. (*b*) are shown in Figure 10. Obviously directive patterns are created by reflection, their shape depending on the height h of the antenna, on its character (receiving electric- or magnetic-field strength of different orientation, or both), and on the

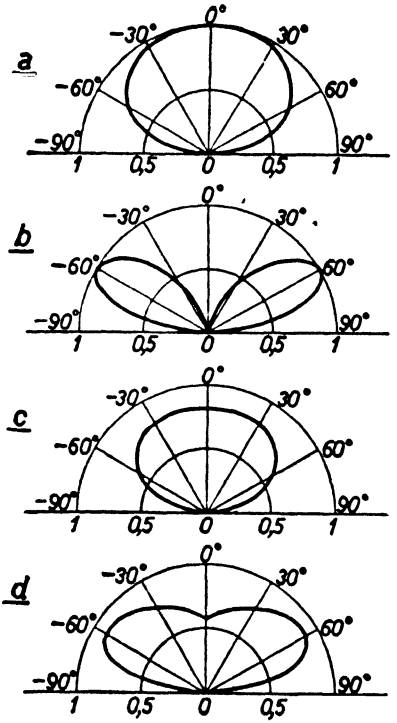

FIG. 10 Ratio of modulus of resulting field strength at antenna A of Fig. 9 to modulus of field strength of incident plane waves as dependent on angle ϑ of incidence of Fig. 9. Diagram *a*: Perfect reflection ($F_b = -1$), h being one-quarter wavelength λ. Diagram *b*: Perfect reflection, h being one-half wavelength. Diagram *c*: Index of refraction $n_o = 2$, h being $\lambda/4$. Diagram *d*: Index of refraction $n_o = 2$, h being $\lambda/2$.

nature of the reflecting medium below the boundary surface. In the above equations, E may be replaced by H, and F may be either F_a or F_b. Another example is shown in Figure 11 at perpendicular incidence ($\vartheta = 0$). A special case of practical interest is connected with a large value of tan δ compared to unity in Eq. (I.1.21*a*). In this case $F_a = +1$ and $F_b = -1$ at practically all angles of incidence. These reflection

coefficients result in simple effects on reception antennas of particular type.

First, consider an antenna consisting of a straight wire of vertical orientation with respect to the horizontal reflecting surface. Such an antenna captures only wave components, the electrical-field strength of which is of vertical direction or, as may be said with equal validity, the magnetic-field strength of which is parallel to the plane of reflection.

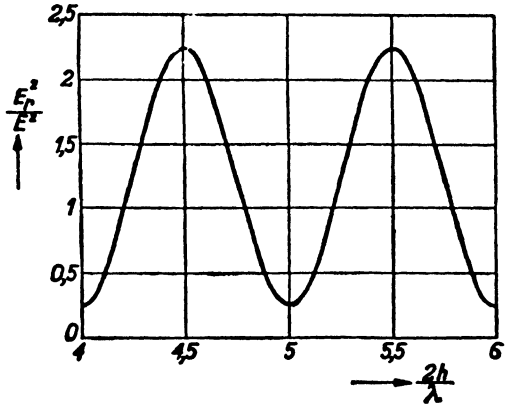

FIG. 11 Similar ratio as in Fig. 10 but at vertical incidence, the angle ϑ of Fig. 9 being zero. Horizontal scale: ratio of twice the height h of Fig. 9 to wavelength λ. Coefficient of reflection $F = -0.5$.

Hence this case is connected with $F_a = +1$. The result is that the reflecting surface has exactly the same influence on the antenna's action as the addition of a second image antenna below the reflecting surface of *equal* orientation as the original antenna (i.e., currents of equal amount flowing simultaneously in equal directions in both antennas). This is pictured in Figure 12*a* for a so-called half-wave antenna.

Secondly, we apply a similar argument to a wire antenna extending parallel to the surface of reflection. In this case only wave components of polarization parallel to that surface are received by the antenna. Hence this case is connected with $F_b = -1$. Again the action of the reflecting plane may be ascribed to an image antenna situated below it but now, owing to the negative sign of F_b, the image has an orientation opposite to that of the original antenna. In other words: the currents

in the image antenna are simultaneously of equal amount and of opposite direction with respect to those in the original antenna. This is illustrated in Figure 12*b* for a horizontal half-wave antenna.

The distortion of wave-band response in receiving antennas due to reflection may be illustrated by Figure 11. Assuming the band transmitted extending from λ_0 to $1.25\lambda_0$ and supposing $2h/\lambda_0 = 5$ while the transmitted field strengths are uniform over the band, the resulting field strengths at the receiving antenna are shown by the portion of

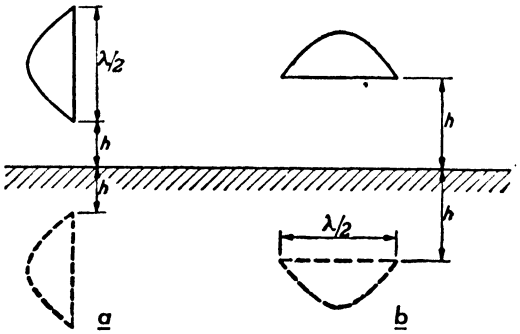

FIG. 12 Images equivalent to effect of perfectly reflecting plane. Diagram *a*: Wire antenna of vertical orientation and of approximately one-half wavelength. Diagram *b*: Similar wire antenna of horizontal orientation.

Figure 11 between $2h/\lambda = 4$ and 5. With television we might have λ_0 corresponding to 50 mc/s and the band extending to 40 mc/s. Reflections of this type might occur at skyscrapers or other buildings in city areas.

Another effect of reflections with television may be caused by the time lapse between the arrival of direct and reflected waves at the receiving antenna. If the total path difference is $2h$, the time lapse is $t_o = 2h/\lambda f$. Hence, at $2h/\lambda = 10$ and $f = 40$ mc/s we would obtain $t_o = 2.5 \times 10^{-7}$ secs. Owing to the high speed of the electronic pincer in the cathode-ray projector, time lapses of this order of magnitude result in visible distortion of the projected television image. Spurious images, called "ghosts," or blurring effects may arise.

The effect of reflection on the impedance of reception antennas will be discussed in section III.

REFERENCES: *73, 93, 338.*

I.1.23. Absorption and refraction. Thus far we have considered wave propagation only in nonabsorptive media. These have the common property that the corresponding value of n in Eq. (I.1.21a) is purely imaginary, as $\sigma = 0 = \tan \delta$. In such media the value of k in Eqs. (I.1.12a) and (b) is given by:

$$k = \frac{2\pi}{\lambda} = \frac{2\pi f}{3 \times 10^{10}} |n_i| = \frac{2\pi f}{3 \times 10^{10}} \sqrt{|\epsilon|}. \qquad \text{(I.1.23}a\text{)}$$

Hence k is purely real. But if σ is not zero, we obtain:

$$k = \frac{2\pi f}{3 \times 10^{10}} (|n_i| - j |n_r'|) = \frac{2\pi}{\lambda_0} - j \frac{2\pi f}{3 \times 10^{10}} |n_r| = k_o - j\alpha. \qquad \text{(I.1.23}b\text{)}$$

The propagation may in this case also be described by Eqs. (I.1.12b). Due to the complex value of k, an additional exponential decrease of field strength occurs:

$$E = \frac{A}{k_o r} \exp (j\omega t - jk_o r - \alpha r) \qquad \text{(I.1.23}c\text{)}$$

and a similar equation holds for H. This phenomenon is indicated as absorption. The result of this absorption may perhaps be judged best by considering the specific average propagated power, being the real part of EH^*, the asterisk indicating the conjugate complex value of H. We obtain from the above Eq. (c):

$$p = \frac{A^2}{k_o^2 r^2} \exp (-2\alpha r) \qquad \text{(I.1.23}d\text{)}$$

Disregarding the multiplier $A^2/k_o^2 r^2$, due to the spherical character of the wave in question, the power absorbed or dissipated in a stratum of unit length is the incident power multiplied by 1-exp (-2α). The values of 2α or of α are often indicated as coefficients of absorption. These coefficients have been expressed in a number of different ways in existing literature. The units for 2α have been: decibel/cm, db/km, db/mile, db/100 feet, and the units for α have been Neper/cm and Neper/km. If the specific power drops by 10 db which is by a factor 10 along one unit of length (cm, km, mile, etc.) the coefficient 2α is said to be 10 db/cm or 10 db/km, etc. If the square root of the specific power is multiplied by 1/2.718 after one unit of length, the coefficient α is said to be 1 Neper/cm or 1 Neper/km. The interrelation of these units may be seen from the following table.

		DB/CM	DB/KM	DB/MILE	DB/100 FT	NEPER/CM	NEPER/KM
(2α).....	db/cm	1	10^{-5}	0.621×10^{-5}	0.328×10^{-3}	8.69	8.69×10^{-5}
(2α).....	db/km	10^5	1	0.621	32.8	8.69×10^5	8.69
(2α).....	db/mile	1.61×10^5	1.61	1	52.8	14.0×10^5	14.0
(2α).....	db/100 feet	3048	0.03048	0.0189	1	2.66×10^4	0.266
(α).....	Neper/cm	0.115	0.115×10^{-5}	0.0714×10^{-5}	0.377×10^{-4}	1	10^{-5}
(α).....	Neper/km	0.115×10^5	0.115	0.0714	3.77	10^5	1

This table should be used *vertically*. Thus an absorption corresponding to 1 db/cm corresponds to 10^5 db/km or 1.61×10^5 db/mile or 3048 db/100 ft or 0.115 Neper/cm or 0.115×10^5 Neper/km, etc.

At the incidence of a wave on a boundary surface, part of its specific power is transmitted into the medium below that surface. If $n_o = n_2/n_1$ is real, the angle ϑ_1 of Figure 2 is given by the relation:

$$\frac{\sin \vartheta}{\sin \vartheta_1} = \frac{n_2}{n_1} = n_o. \qquad \text{(I.1.23}e\text{)}$$

Thus the angle of refraction is fixed by the angle of incidence in this case. The refracted waves are propagated following the direction of ϑ_1. But if n_o is complex, no real angle ϑ_1 results from Eq. (*e*) and hence no definite direction may be indicated for the refracted waves. If the specific power of the incident wave is unity, the specific power of the reflected wave is $|F_a|^2$ or $|F_b|^2$ in the two cases discussed in section I.1.21. The difference between the values for the incident and reflected waves is obviously the power imparted to the refracted waves. Hence this is $1 - |F_a|^2$ and $1 - |F_b|^2$ in these two cases. If $n_o^2 - 1 + \cos^2 \vartheta$ is real and negative in Eqs. (I.1.21*b*) and (*c*) $|F_a| = 1 = |F_b|$, and hence no refracted power here exists corresponding to what is called "total reflection." The border case occurs at $\cos^2 \vartheta = 1 - n_o^2$. Obviously n_o^2 is to be real and smaller than unity in such cases of total reflection (see section I.1.32).

Absorption occurs also in walls or strata bounded by parallel planes. Considering such a stratum of thickness D and an absorption corresponding to different values of the loss angle δ, the value of ϵ being 4, we obtain the curves of Figure 13a. Here λ denotes the wavelength corresponding to Eq. (I.1.23*b*) of the loss-free medium bordering on both sides of the stratum. Even if $\delta = 0$, a loss of transmitted power may occur due to pure reflection. This loss is increased by absorption in the stratum.

By the combined effects of reflection and absorption queer interference patterns may be created by plane incident waves, as shown in Figure 13b. The occurrence of such patterns should be borne in mind when considering indoor television reception antennas. They may seriously affect the wave-band response.

REFERENCES: *42, 80, 97, 117, 165, 253, 268, 297, 339.*

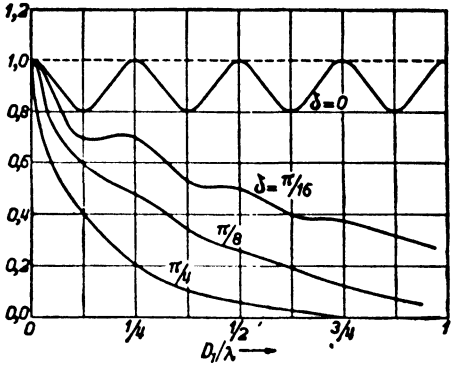

FIG. 13a Passage of plane wave train through a plane wall of thickness D perpendicular to the direction of propagation. Ratio of modulus of electric-field strength behind the wall at its surface to that of incident waves as dependent on ratio of D to wavelength λ (measured in air). Curves corresponding to different values of loss angle δ.

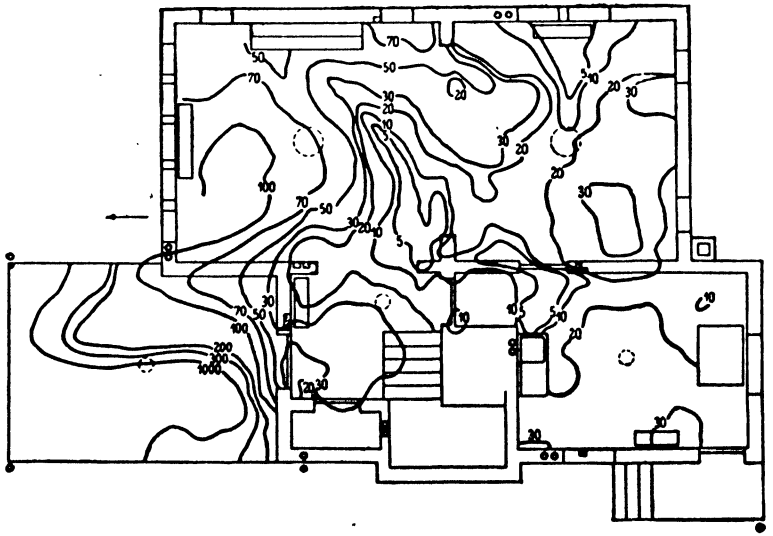

FIG. 13b Wave pattern inside a room as caused by reflection and refraction. Arrow indicates direction to transmitter. Wavelength in air 6 *m*. Figures indicate relative field strengths. Over-all largest width is about 40 ft.

I.1.24. Reflection by finite obstacles. The development of radar has given prominence to these cases of reflection. We shall assume that the transmitter is situated at such a distance from the reflecting obstacle that the waves impinging upon the latter are effectively spherical as described in section I.1 11. These impinging waves set up alternating electric charges and currents inside the obstacle if it is non- or badly conducting, and upon its surface if it is highly conducting (metallic). These currents make the obstacle itself act as a transmitter. Due to our assumptions, the waves thus emitted by the obstacle are effectively spherical when they arrive in the vicinity of the original transmitter. We may compare the effective power of the original transmitter radiating toward the obstacle with the effective power of the obstacle itself acting as a transmitter radiating toward the original transmitter.

A simple application of this reasoning will now be given. Consider a small wire transmitting antenna parallel to a plane metal wall at a distance r from it, large compared to the antenna dimensions and to the wavelength. The effect of the wall on the antenna (by Fig. 12*b*) may be completely described by an image antenna at a distance r behind the plane metal surface and oscillating counterphase to the original antenna. The power radiated by both antennas is obviously equal. This may be expressed a little differently by saying that the field strength created by the transmitter at a distance $2r$ (being the path to the obstacle and back again to the transmitter) is exactly the same in amount as that created by the image transmitter at the site of the original transmitter. This is obviously the situation with which we are faced in radar applications, as the positions of receiver and transmitter practically coincide. The ratio of effective transmitted to reflected power thus obtained might be termed the *radar coefficient* of the obstacle, its value for the above metal plane being unity. A radar coefficient unity causes the same field strength in amount at the transmitter site by reflection as is obtained at a distance twice that of the obstacle by unobstructed radiation in the direction under consideration.

If the linear dimensions of the obstacle are large compared to the effective wavelength in the adjacent medium, its reflective action at a distance r from the transmitter, large compared to the said dimensions, may conveniently be treated optically. Assuming the transmitter to be of a total power P radiating uniformly in all directions, the power intercepted by the obstacle is $P' = SP/4\pi r^2$, S being its intercepting

surface as seen from the transmitter. A part F^2 of this power P' may again be assumed to radiate uniformly in all directions, and hence the specific power at the transmitter site due to P' is:

$$p' = \frac{F^2 P'}{4\pi r^2} = \frac{P}{4\pi r^2}\frac{F^2 S}{4\pi r^2} = p\frac{F^2 S}{4\pi r^2}, \qquad \text{(I.1.24}a\text{)}$$

F^2 being the modulus squared of the surface's average coefficient of reflection and p the specific radiation power, due to the transmitter at the site of the obstacle. The radar coefficient O of the obstacle is, by Eq. (a):

$$O = \frac{F^2 S}{\pi r^2}. \qquad \text{(I.1.24}b\text{)}$$

Some examples may illustrate this. A circular disk of radius a has $S = \pi a^2$ and hence $O = F^2 a^2/r^2$. A spherical obstacle of radius a has the same radar coefficient. These values are all small compared to unity, even if $F^2 = 1$ as for most metallic surfaces.

It is interesting to compare Eq. (b) with some values obtained by exact calculation of diffraction at a metallic spherical surface of radius a. The values of $r^2 O/a^2$ which should be unity by Eq. (b) at values of ka large compared to unity are found to be (reference *287*):

ka	1	2	9	10	∞
$\frac{Or^2}{a^2}$	3.63	1	0.85	0.93	1

Hence the radar coefficient of small metallic spheres compared to the wavelength is much larger in proportion to their effective interceptive surface than the coefficient of larger spheres. Similar relationships may be expected with obstacles of different shapes.

REFERENCES: *69, 98, 169, 267, 287, 338, 340.*

I.1.3. Propagation. In this section some essential data on wave propagation between distant points of the earth's surface are presented. They are vital to an understanding of the different types of waves occurring at a reception antenna.

I.1.31. Layers of the ionosphere. The gas density of the earth's atmosphere decreases slowly from the surface upward. Part of the sun's radiation is absorbed by this gaseous atmosphere. Hence its

specific intensity is much larger at high altitudes than at the earth's surface. This radiation on the gas molecules causes ionization. Thus ultraviolet rays cause ionization of oxygen and of nitrogen molecules. At high altitudes the number of ions thus created per unit of volume is small because of the low gas density. At low altitudes it is small because of lack of ionizing rays due to absorption in the higher layers. Thus an altitude may be ascribed to each kind of rays in conjunction with specified constituents of the atmosphere for which an optimal number of ions of the kind under consideration is created. This altitude is of course liable to changes due to variations of radiation (e.g., between day and night) and of gaseous constitution. Of the great number of existing ionized layers of the ionosphere we shall quote here only a few together with their respective average daytime altitudes: D-layer at 50 km, E-layer at 120 km, F_1-layer at 200 km, F_2-layer at 300 km, etc. The properties of these different layers relative to wave propagation may be described by their effective value of n^2 (see Eq. I.1.21a):

$$n^2 = -1 + \frac{\omega_o^2}{\omega^2}, \quad \omega_o^2 = 36\pi 10^{11}\, N_e e e_o = 3.2\, N_e 10^9, \quad \text{(I.1.31}a\text{)}$$

N_e denoting the number of electrons per unit of volume (cm^3), e the electric charge of an electron (1.60×10^{-19} coulomb) and e_o the ratio of charge to mass of an electron multiplied by 10^7, its value being 17.6×10^{14} (cm^2/sec^2 volt). Though the layers, according to the above description of their origin, cannot possess abrupt boundaries and though n^2 will in general show appreciable variations within each layer, their behavior will be idealized by layers of uniform composition with sharp and locally plane boundaries. Assuming waves originating from the earth's surface or its nearer vicinity to be incident on such a boundary, the reflective properties will correspond to Eqs. (I.1.21b) to (d). The value of n_o^2 occurring in these reflection coefficients is the ratio of n^2 for the atmosphere below the layer and of n^2 according to the above Eq. (a). The former n^2 being substantially -1 for non-ionized parts of the atmosphere, we obtain:

$$n_o^2 = 1 - \frac{\omega_o^2}{\omega^2}. \quad \text{(I.1.31}b\text{)}$$

The simplest reflection occurs for waves of vertical incidence according to Eqs. (I.1.21e). Here obviously the moduli $|F_a|$ and $|F_b|$ become unity if either $n_o^2 = 0$ or n_o^2 negative. In all these cases what is

called *total* reflection occurs, the border case corresponding to $\omega = \omega_o$. This value ω_o is usually indicated as the *critical* angular frequency of the layer in question. It may be found experimentally by increasing

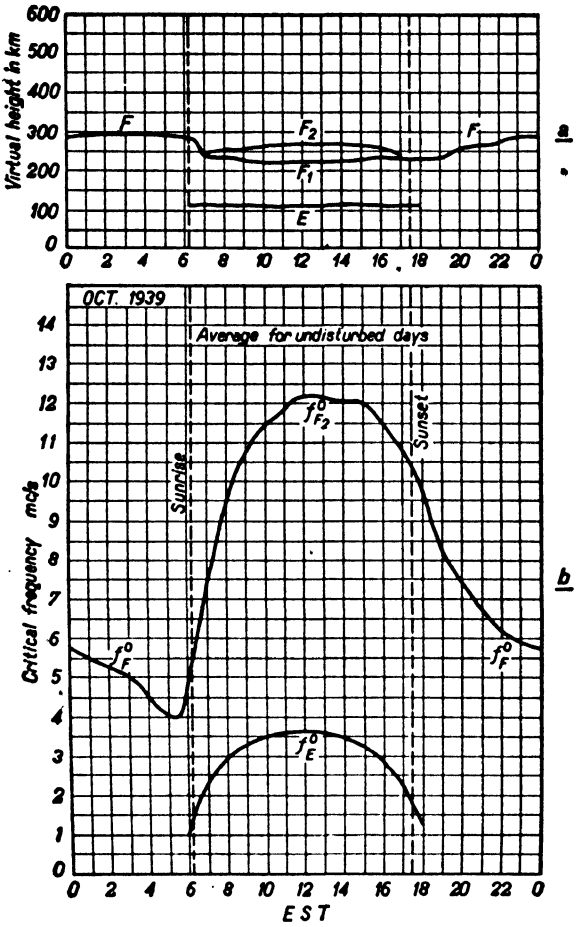

FIG. 14 Diagram *a*: Virtual altitude of F_2, F_1 and E layers at Washington, D.C., on undisturbed days (average) Oct. 1939. Diagram *b*: Average critical frequencies for the three layers of diagram *a*. Diagram *c*: Relation of average critical frequencies of F_2-layer to number of sunspots (reference *26*).

the angular frequency ω of the vertically incident waves until total reflection from the layer under consideration ceases, when the equation ($\omega = \omega_o$) obtains. The time lapse necessary for the waves to travel

upward and for the reflected waves to come down to the earth again may serve as a measure for the effective layer's altitude if simplifying assumptions are introduced as to the reflection and propagation processes. Examples of layer altitudes and critical frequencies $f_o = \omega_o/2\pi$ measured in this way are shown in Figure 14. Variations of these values in the course of a day are evident from this Figure 14. In

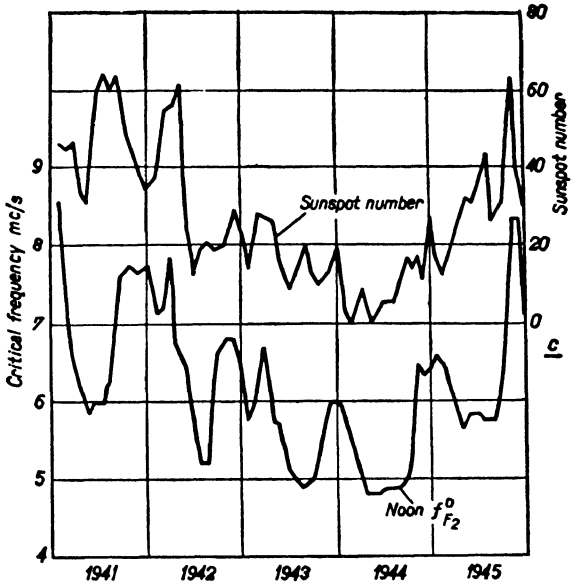

summer the altitudes are mostly higher and the critical frequencies are often somewhat lower than in winter for the F_2-layer. For the E-layer critical frequencies are usually higher in summer than in winter and altitudes are about equal under comparable conditions. Also 11-year variations corresponding to sunspot periods have been noticed.

REFERENCES: *21, 26, 87, 107, 124, 322, 384.*

I.1.32. Long-distance propagation. The ionospheric layers play a large part in long-distance propagation of short waves of frequencies mainly below 30 mc/s. Such waves are projected upward by the transmitting antennas, horizontal radiation being made relatively

negligible by the wave absorption of the earth's surface. These waves are then reflected by one or more of the ionospheric layers and the reflected waves are projected downward again. After a second reflection at the earth's surface they go upward again, and so on, until they arrive at the vicinity of the reception antenna. These reflections at the ionospheric layers may be dealt with approximately using the simplifying assumptions mentioned in the preceding section. The layers associated with effective reflections are mostly to have critical frequencies such that n_o^2 of Eq. (I.1.31b) is zero or negative. In these cases both reflection coefficients F_a and F_b of Eqs. (I.1.21b) and (c) are of modulus unity at all incident angles ϑ. Positive values of n_o^2 may also correspond to values of F_a and F_b of modulus unity if $n_o^2 - 1 + \cos^2\vartheta$ is negative, i.e., if $1 - n_o^2$ is larger than $\cos^2\vartheta$. In these cases if ϑ increases from zero upward, the moduli of the reflection coefficients increase steadily until they become unity from a definite angle ϑ_o onward till $\vartheta = \pi/2$. Waves projected upward at angles ϑ nearer zero than this critical angle ϑ_o are less effectively reflected. This affords an explanation of the well-known phenomenon called "skip distance," near-by short-wave stations sometimes being received much less effectively than more distant ones (Fig. 15). In general, propagation between two distant points of the earth's surface takes place along a path, the projection of which on the said surface is a great circle. Deviations from this rule are mostly negligible at distances beyond 1000 km. If the latitude and longitude of transmitter and receiver are given, this rule fixes a definite point of the compass at the receiver, from which the waves arrive. In order to calculate this compass direction, we first determine the latitudes l_t and l_r of transmitter and receiver both reckoned from the North Pole. Thus if the given latitude of a station is 50° north, l_t is 40°, and if the receiver is at 50° south l_r is 140°. Then take the difference γ_d of both longitudes, γ_d being less than 180°. Denoting the included angle between the compass direction at the receiver site pointing toward the transmitter and the northern direction by

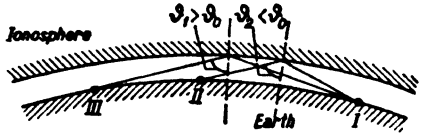

FIG. 15 Because the angle of incidence ϑ_2 of waves issuing from a transmitter at I and traveling to II is smaller than the critical angle ϑ_o, the signals received at II are far weaker than at III, corresponding to an angle of incidence ϑ_1 larger than the critical angle ϑ_o.

α_o, we obtain by spherical trigonometry:

$$\sin \alpha_o = \frac{\sin l_t \sin \gamma_d}{\sin a}, \quad \cos a = \cos l_r \cos l_t + \sin l_r \sin l_t \cos \gamma_d \tag{I.1.32a}$$

As an example, take a receiver near San Francisco and a transmitter near London. Then $l_r = 52°$, $l_t = 39°$, $\gamma_d = 122°$, and $\alpha_o = 33°$.

REFERENCES: *51, 107, 108, 125, 282.*

I.1.33. World maps of average propagation conditions. A second point in long-distance reception is related to the wavelengths which may be expected to be useful along a definite path. On the average

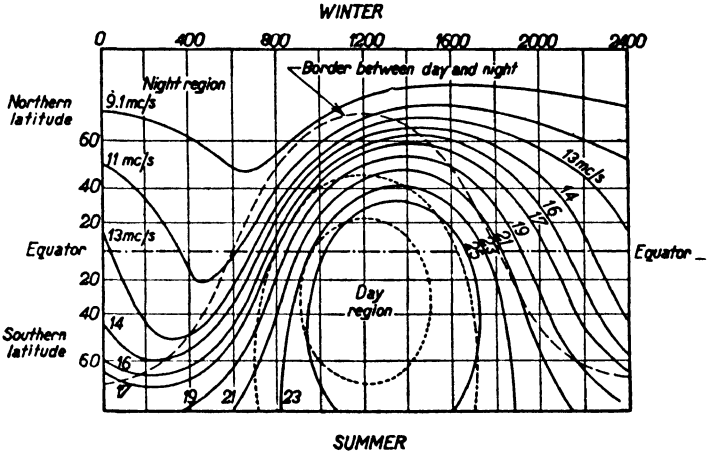

FIG. 16a Mercator world map picturing the state of the ionospheric F_2-layer approximately for the years 1946–47 in winter as well as in summer. The full curves correspond to definite values of critical frequency f_o indicated at each curve. The dotted curves correspond to values of definite E-layer ionic densities, causing attenuation of the propagated waves.

the state of the ionosphere is determined by the sun's relative position. In long-distance transmission the F-layers are most effective because of their considerable altitude. Two figures (Figs. 16a and 16b) show the average structure of this F-layer as mapped above the earth's surface using Mercator's projection, Figure 16a in winter and summer (December and June) and Figure 16b in autumn and spring (September and March). The figures attached to the full contours are critical

frequencies f_o and thus are immediately related to the local ionic density (Eq. I.1.31a). At a time t, fixed according to Greenwich mean time, the Greenwich meridian must coincide with the vertical line in the diagram corresponding to the time t on the upper scale. Obviously the entire earth's surface is then fixed relative to the ionic map. Now we have to draw a curve on this map corresponding to a great circle interlinking transmitter and receiver. This curve will intersect a

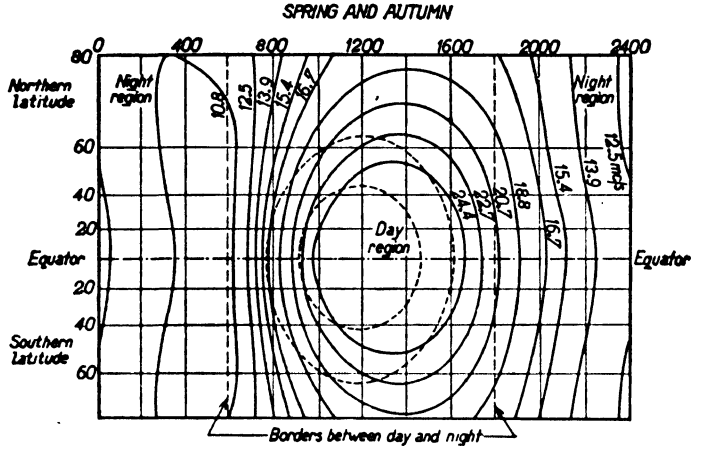

FIG. 16b Similar map as in Fig. 16a but corresponding to autumn and spring, the year being approximately 1946–47. The use of these maps is indicated in the text.

number of contours of the ionic map. The lowest frequency corresponding to one of these intersecting contours is the effective critical frequency for the transmission in question and the useful frequencies are below this effective critical frequency. As an example, consider a transmission from Rugby (England) to Cape Town at 1600 hours G.M.T. Using Figure 16a, the effective critical frequency is about 23 mc/sec. Hence 18.5 mc/s would seem to be a useful frequency for this transmission at this instant, and so it is. In general, if it is night along the path of transmission, the useful frequencies are lower than if it is day. Thus between New York and Amsterdam a useful daytime frequency is 16 mc/s, while at night 10 mc/s is often more suitable. Also during winter the useful frequencies are mostly higher than in summer. Some idea of the electric-field strengths generated at distant points by a transmitter radiating 1 kilowatt using a vertical half-wave

antenna may be obtained from Figure 17. The transmitter is situated at 50° north latitude and transmission takes place at 1200 hours local time at the transmitter in spring or autumn, the year being about 1941 (similar with respect to sunspots to 1952). The contours represent curves of equal field strength and the attached figures indicate db above (+) or below (−) 1μ V/m. In the shaded areas reception is impossible. The almost circular shaded area round the transmitter indicates the "skip" distance. The vertical dotted lines marked *R* and *S* coincide with sunrise and sunset.

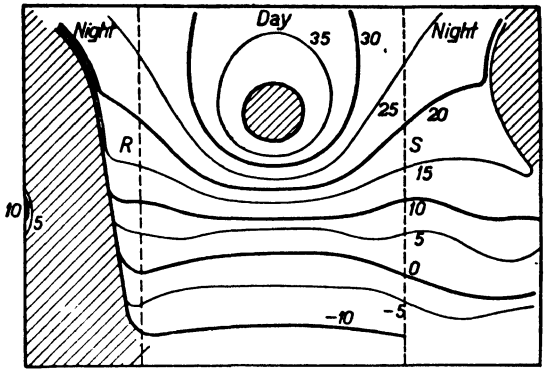

FIG. 17 Mercator world map, the transmitter being situated in the center of the shaded inner closed contour at 12 h. local time. Contours correspond to electric-field strengths as indicated in db above (+) or below (−) one microvolt/meter. The transmitter is supposed to radiate 1 kw using a vertical half-wave antenna. In the shaded areas reception is practically impossible.

The field strengths at reception are to be multiplied by the square root of the radiated power and of the gain (see subsection III.1.12) of the transmitting aerial over a half-wave antenna in the direction of propagation, if a power and an antenna differing from the above data of Figure 17 are used.

The Central Radio Propagation Laboratories of the National Bureau of Standards, Washington, D.C. issues monthly "Basic Radio Propagation Predictions," three months in advance, giving the optimum working frequencies for short wave communication. These "Predictions" are in essence similar to the maps of Figures 16a and 16b, together with a suitable transparent sheet on which the Mercator world map contours of the continents and islands are drawn. With the aid of such data an

advance determination of suitable transmission frequencies is possible for practically all paths.

In long-distance transmission single hop or multiple hop wave propagation may occur, corresponding to single or to several consecutive reflections at the ionosphere and at the earth's surface. Single hop transmission does not occur for distances beyond about 2200 miles (3500 km) via F-layer reflections and multiple hops occur often even at smaller distances. The maximum useful frequency (muf) of transmission is higher than the critical frequency f_o and is given by the equation:

$$\text{muf} = f_o \sec \vartheta \,. \qquad \text{(I.1.33}a\text{)}$$

if ϑ is the angle of incidence at the reflecting layer, assuming the radical in Eqs. (I.1.21*b* and *c*) to be zero and taking into account Eq. (I.1.31*b*). The angle ϑ varies with the distance of transmission and the height of the reflecting layer. The value of sec ϑ is unity at vertical incidence (zero distance), about 2.4 at 2000 km and about 3 at 3500 km distance for F-layer reflections. In long distance transmission a hop-distance of 2000 km is commonly adopted in estimating the useful frequency. The latter is often assumed to be between 50 and 85% of the muf, preferably nearer the upper limit in order to reduce absorption of the transmitted waves in the ionospheric layers.

REFERENCES: *25, 26, 51, 87, 124.*

I.1.34. Short-distance propagation. Though waves of frequencies above 30 mc/s have occasionally been propagated from Europe to the United States (references *21, 108, 275*), ionospheric conditions are usually such that reflection of these waves is poor. Hence only *direct* transmission between emitter and receiver is reliable at these frequencies. If h_{tr} denotes the altitude of the transmitting antenna above the earth's surface and h_{rec} that of the receiving antenna (both in meters), the maximum distance D at which both antennas are within sight of each other is:

$$D(\text{km}) = 3.57\left(\sqrt{h_{tr}(\text{m})} + \sqrt{h_{rec}(\text{m})}\right). \qquad \text{(I.1.34}a\text{)}$$

If the distance between transmitter and receiver is smaller than this, rays may arrive at the latter following mainly two different paths: directly along a straight line, and by single reflection at the earth's

surface. Interference patterns may result from the addition of such rays at the receiver. Moreover, diffraction at the earth level may still complicate this state of affairs (see Fig. 18). Whereas a gradual decrease of field strength below the horizon occurs at 7 m wavelength, abrupt decreases are obtained at centimeter-waves.

In these representations of Figure 18 no account is taken of the effect of the lower atmosphere. Though ionization is not appreciable, the dielectric coefficient ϵ is dependent on atmospheric density and humidity and thus gradually decreases at increasing altitude. The effects of this dependence are most noticeable if the path of transmission is inclined with respect to the earth's surface, as is the case between airplanes and ground stations. With light rays the effects of atmospheric inhomogeneity may sometimes be clearly seen at sunset, when the sun's disk assumes elliptical shapes. By these effects the field strength due to a transmitter below its horizon may be appreciably higher than would be deduced from Figure 18. Some examples of calculated electric-field strengths as dependent on altitude and distance, due to a vertical half-wave transmitting antenna carrying 1 amp at its center and situated at an altitude of 1 km, are shown in Figure 19 at 138 and 73 mc/s (reference *97*). These calculations have in part been confirmed experimentally under specified assumptions of atmospheric density and humidity.

If the angle of incidence at the earth's surface is near 90°, the reflection coefficients F_a and F_b according to Eqs. (I.1.21*b* and *c*) are both approximately equal to -1. Taking this into account a simple formula may be deduced for the approximate field strength at a height h_{rec} and a distance D from a transmitter of height h_{tr} and of any polarization, the transmitted power being P (watts) and the gain being g (see subsection III.1.12) in the direction of transmission over a dipole transmitting antenna.

$$E_{rec}\ (\text{volts/cm}) = 0.13\,\frac{\sqrt{Pg}}{D}\sin\left(\frac{2\pi h_{tr}h_{rec}}{\lambda D}\right) \qquad \text{(I.1.34}b\text{)}$$

The wavelength λ of the transmitter is expressed in meters as are D, h_{tr} and h_{rec}. This Equation is subject to the conditions that λ, h_{tr} and h_{rec} are less than one tenth of D.

REFERENCES: *21*, *49*, *51*, *69*, *97*, *107*, *108*, *114*, *170*, *253*, *267*, *275*, *276*, *337*, *380*, *393*, *395*.

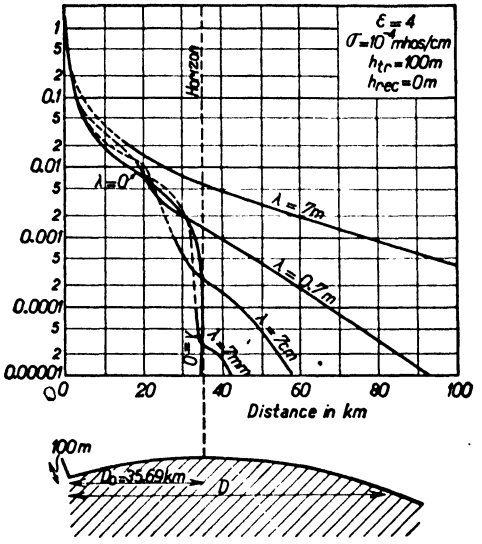

FIG. 18a Short-distance propagation up to the horizon and beyond, the properties of the soil (σ and ϵ) being as indicated, the altitude of the vertical transmitting dipole being 100 m and that of the receiver zero. Vertical scale indicates relative field strengths, the value near the transmitter being unity. Horizontal scale is distance from transmitter expressed in km.

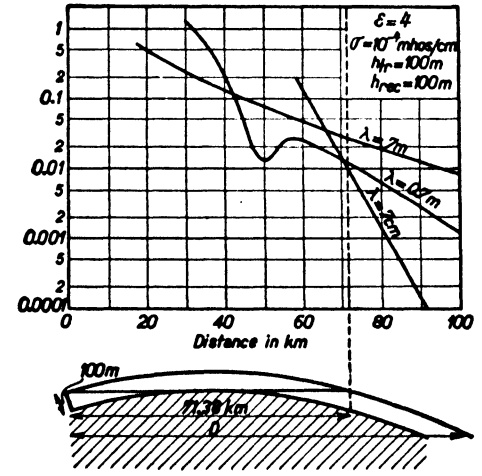

FIG. 18b Similar to Fig. 18a but the altitude of the receiver is also 100 m, as is that of the transmitter.

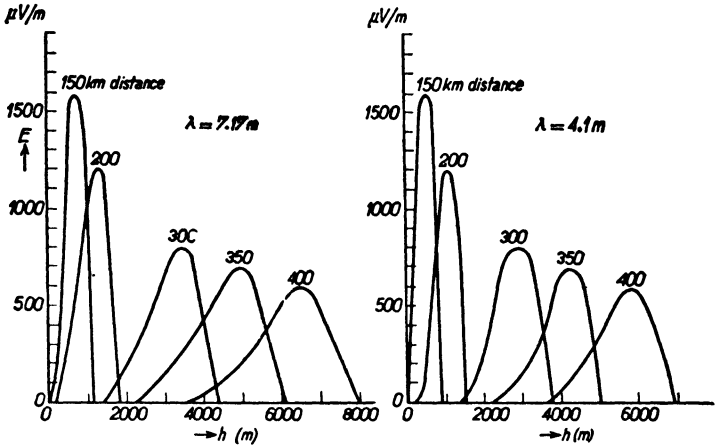

FIG. 19 Electrical-field strength due to a vertical half-wave antenna being fed with 1 amp r.m.s. current at its center and situated at an altitude of 1 km. Vertical scale: Field strength expressed in microvolts per meter. Horizontal scale: Altitude of receiver. Curves corresponding to different distances. Wavelength λ is indicated.

I.1.4. Disturbances of propagation. The effects dealt with in the preceding sections are subject to a number of disturbances caused by special conditions. Some of these will be treated briefly.

I.1.41. Regular ionospheric disturbances. The simple considerations of ionospheric reflections of sections I.1.31 and I.1.32 are only partly coincident with actual reflections due to the action of the earth's magnetic field. If a wave train is projected vertically upward at a place situated on the earth's magnetic equator, with the electric-field strength parallel to the earth's magnetic field, the ionospheric electrons move parallel to the latter field and hence their motion is not subject to its action. Reflection and refraction occur as described in the preceding sections, the corresponding rays being indicated as "ordinary" rays. But if the electric-field strength is perpendicular to the earth's magnetic field, the latter has a considerable influence on electronic motion. Reflection and refraction are altered and the corresponding rays are indicated as "extraordinary" rays. The critical frequency of extraordinary rays is higher than that of ordinary rays. If an angle exists between electric-field strength and the earth's magnetic field different from zero or a multiple of $\pi/2$, each incident wave train is split up into two reflected and two refracted wave trains, corresponding to these ordinary and extraordinary rays. At places on

the earth between the magnetic equator and magnetic poles the reflected and refracted waves are, in general, of elliptic polarization if the incident waves are of linear polarization. In the northern hemisphere the extraordinary rays are of polarization rotating clockwise and the ordinary rays of polarization turning counterclockwise. In the southern hemisphere these conditions are reversed. The waves are here viewed in the direction of propagation, assumed to be vertical. If this direction coincides with that of the earth's magnetic field, polarization is circular. By interference between ordinary and extraordinary rays at the receiving antenna, rapid changes of polarization and amplitude may and do frequently occur, necessitating suitable precautions against resulting strong signal-fading effects.

In the vicinity of critical frequencies the altitude of reflecting layers may show relatively large changes, e.g., between 190 and 450 km (F_1-layer) at frequencies of 4 to 4.5 mc/s. Considerable variations in angles of incidence may result even in such relatively small frequency intervals as 10 kc/s. In the above example the corresponding angle variation is 0.68 degree. Thus different propagation may occur at different frequencies of one frequency band, resulting in considerable distortion of the signals received (see section I.2).

The altitudes of reflecting layers and their local constitution may show rapid variations ascribed to what are believed to be ionospheric cloud motions. The points of reflection may thus change suddenly, and even the reflecting layers may alter, e.g., by a gap arising in the clouds of a lower layer. Obviously considerable variations of received field strengths may result from these effects. Some further resulting phenomena are: variations in vertical angles of arrival at the receiver of waves issuing from distant transmitters (Fig. 20) and variations in horizontal angles of arrival (Fig. 21).

Ionospheric properties are often dependent on the field strengths of incident waves, thus giving rise to non-linear effects in wave propagation. Among such effects are: generation of spurious frequencies and distortion of signals (reference *96*). The said dependence is particularly pronounced with waves of high specific power.

All these phenomena may be classified as "normal or regular disturbances," as they arise from effects occurring regularly without special outward causes (so far as is known).

REFERENCES: *87, 96, 124, 125, 282.*

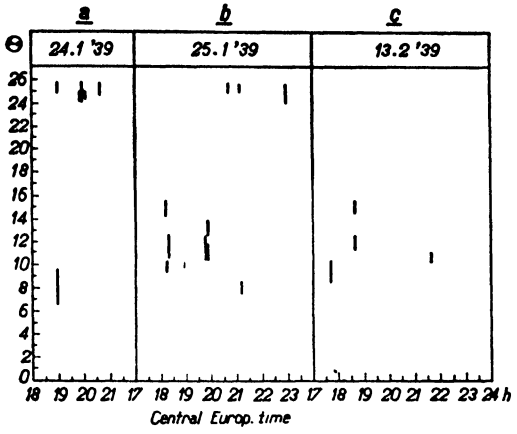

FIG. 20 Angles Θ of elevation at Berlin due to waves transmitted from Schenectady (vertical scale) as dependent on local time (horizontal scale). Usually several angles occur simultaneously.

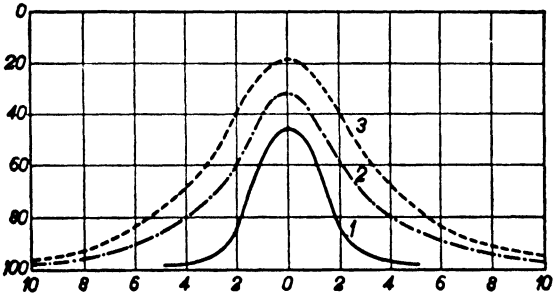

FIG. 21 Deviations from great-circle propagation, the deviation angles in degrees being indicated horizontally. Vertical scale: Percentage of observations at which a given deviation value is not surpassed. Curve 1: Reception near London from Berlin at a wavelength of 31.4 m. Curve 2: Reception near London from Prague, wavelength 44.6 m. Curve 3: Reception near London from U.S. transmitters at wavelengths between 31.4 and 36.

I.1.42. Irregular ionospheric disturbances. Variations in the sun's constitution are in many cases responsible for irregular disturbances. The known 11-year period of sunspots (maxima occurring in the years 1926/27, 1937/38, 1947/48, 1958, etc.) cause corresponding variations of ionization of the ionospheric layers and thence of critical frequencies, the latter being highest during sunspot maxima (reference *26* and Fig.

14). Another known source of ionospheric variations resides in variations of the earth's magnetic field. These are often caused by eruptive activity at the sun's surface.

Special disturbances of relatively short duration have been observed simultaneously on short as well as on medium waves. These disturbances probably stem from eruptions in the sun's chromosphere which produce considerable increases of ionization in the lower ionospheric layers. They are infrequent in periods of small sunspot activity (e.g., 1943/44), but increase in frequency in periods of maximal sunspots (e.g., 1947/48). The duration of these disturbances is up to about one hour, durations between 10 and 15 minutes being most frequent. They occur only along paths of propagation on the dayside and may result in complete disappearance of signals at reception sites. Simultaneously so-called "atmospherics" at medium-wave reception show marked increases. An example of such disturbances was observed in 1936, medium-wave atmospherics at Rabat and Tunis (both in North Africa) and Paris (frequencies between 27 and 31.6 kc/s) occurring simultaneously with disappearance of signals of 9.5 mc/s at Millis, Massachusetts. Another instance was a two-hour complete breakdown of transatlantic short-wave communication on Feb. 7, 1946.

Disturbances of short-wave propagation have been observed to occur simultaneously with northern lights (aurora borealis). The latter is known to be related to disturbances of the earth's magnetic field and probably also to activity on the sun's surface.

On the other hand, the "atmospherics" so common in long- and medium-wave reception are of less importance at short and ultra-short waves (see section I.1.44).

REFERENCES: *25, 26, 87, 124, 322, 384.*

I.1.43. Disturbances at ultra- and extreme-short waves. As these waves are normally used in short-distance propagation, ionospheric reflections being of minor importance, no pronounced effects due to ionospheric variations need be expected with such propagation. The disturbances occurring at these frequencies are due to interference of different rays of possibly different polarization propagated along different paths. Interference patterns are in general not stationary but liable to rapid variations. First we shall discuss interferences caused by reflections and diffractions at various types of obstacles. One example has been shown in Figure 13*b*. Another example, showing

the effects of hilly country in Switzerland, is shown in Figure 22. A third example shows the propagation of television waves over a densely built-up city area (New York), in Figure 23*a*.

Secondly, variations of field strength at a fixed reception site due to multiple-ray interference will be considered. In Figure 18 the field-strength curves have been flattened out a bit for the sake of simpler representation. In reality, the interference of multiple rays arriving at

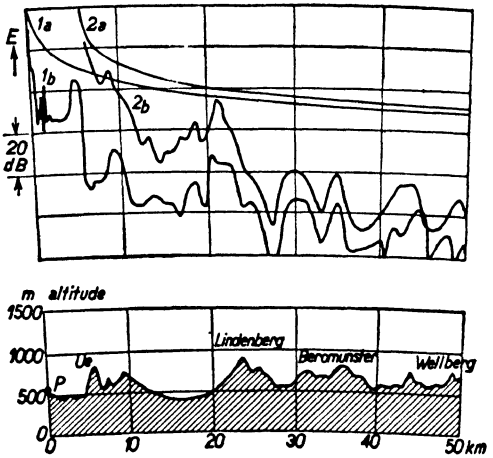

FIG. 22 Propagation of 40 mc/s waves across hilly country in Switzerland. Curves 1*a* and 1*b* are related to a transmitter at *P* (lower diagram), curves 2*a* and 2*b* to a transmitter at *Ue*, 1*a* and 2*a* being the reciprocal distance curves, while 1*b* and 2*b* are experimental curves. Due to Prof. F. Tank of Zurich.

the receiver causes oscillations of the field-strength curves amounting, in many cases, to between 3 and 20 db in power. By slight displacements of such interferences the field strength at a fixed receiver site may show similar variations. The conditions attending reception of these waves are illustrated by Figures 23*b*, *c*, and *d*. Large variations of field strength are in general more frequent in summer than in winter. Fog, rain, snow, and hailstorms usually cause comparatively few direct effects except at extremely short waves (see Fig. 23*e* and reference *297*).

Sometimes reflections of ultra-short waves (beyond 30 mc/s) at lower ionospheric layers have been found (references *108*, *275*), resulting in long-distance propagation of these waves over hundreds of miles (e.g., London–New York). It is obvious that such reflections, if they

occur, may also impair short-distance propagation by causing additional interfering rays. Reflections from passing objects, such as airplanes, may cause ray-interference and thence visible disturbances on a tele-

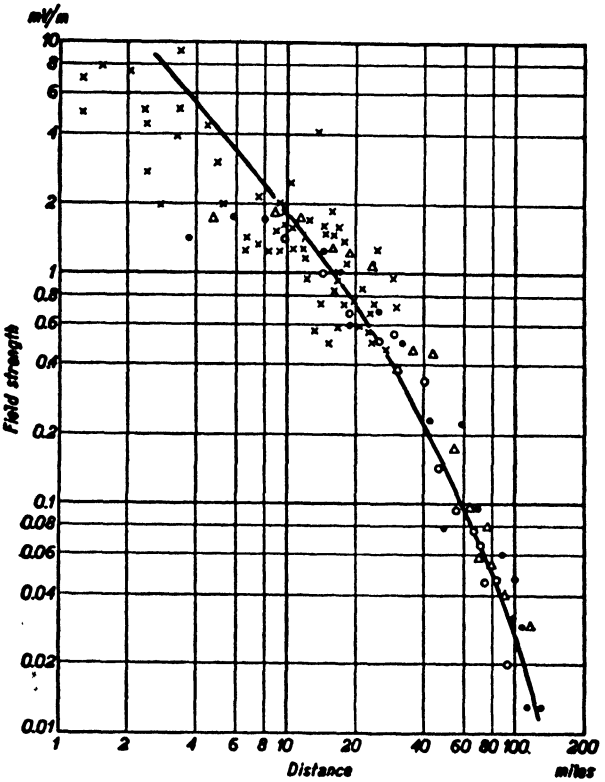

FIG. 23a Electric-field strength expressed in millivolts/meter (vertical scale) as dependent on distance in miles (horizontal scale) due to a 2-kw transmitter at 400 m altitude in New York, wavelength 6.8 m. The points indicated differently correspond to different directions from transmitter. (L.F. Jones, P.I.R.E. vol. 21 (1933) p. 349.)

vision screen. The effects of such reflections were described as early as 1931, based on 1929 observations, and were then applied for the detection of objects in rooms and on open grounds (e.g., trespassers). This may perhaps be indicated as an early application of radar (references *337, 340*).

REFERENCES: *108, 265, 275, 297, 337, 340.*

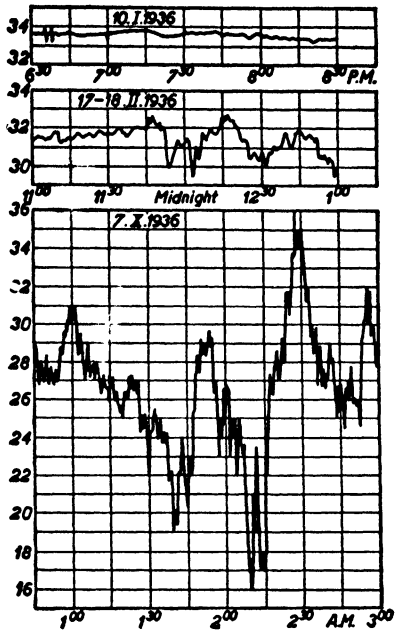

FIG. 23b Variations of electrical field in db above one microvolt/meter as dependent on time at 60 km distance and 2 m wavelength, the receiver being close behind the horizon. Transmitter power 4 watts. According to Ch. R. Burrows, A. Decino, and L. E. Hunt, P.I.R.E. vol. 26 (1938) p. 516.

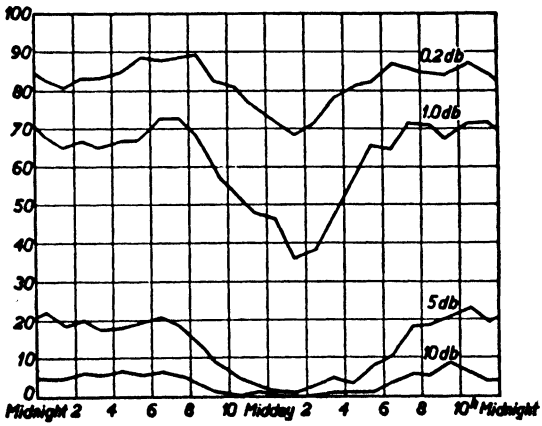

FIG. 23c Daily variations of amplitude of field-strength variations. Vertical scale: Percentage of time during which the hourly variation of field-strength amplitude is above the values indicated at the curves. Horizontal scale: Time. Conditions as in Fig. 23b. Same authors.

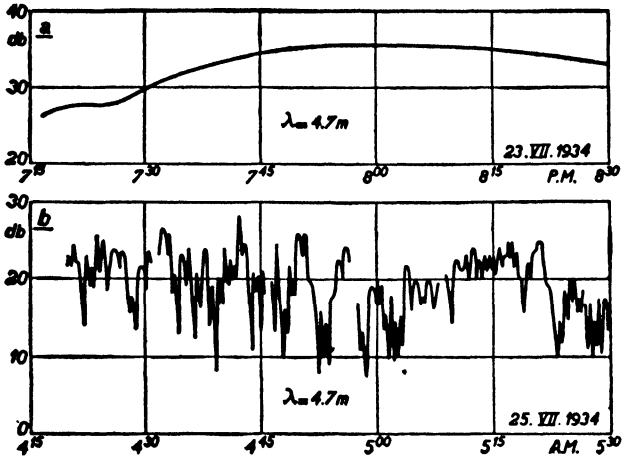

FIG. 23d Border cases of fading curves in transmission over sea. Vertical scale: Db reception power in relative arbitrary scale. Horizontal scale: Time. According to: C. R. Englund, A. B. Crawford, and W. W. Mumford, B. T. J. vol. 17 (1938) p. 489.

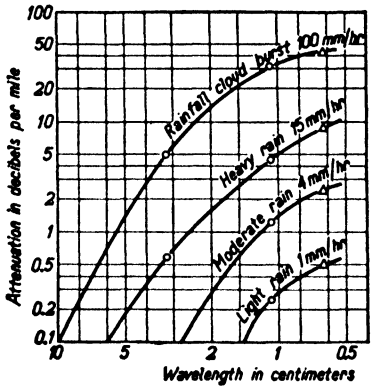

FIG. 23e Influence of rain on attenuation of centimeter waves. Due to S. D. Robertson, A. P. King, and G. E. Mueller, P.I.R.E. vol. 34 (1946) p. 178 and 181.

I.1.44. Man-made, atmospheric, and interstellar noise. Besides signal disturbances as described in the three preceding sections, other disturbing signals reach the reception antenna. These mostly cause "noise" in the sound stages of a receiver and are hence generally

indicated by this name. Probably the most important sources of such noise, especially in built-up areas, are man-operated. All sorts of apparatus operated by electricity may be sources of short- and ultra-short wave radiation, the resulting wavelength spectrum being more or less continuous, its specific power per unit of band width (assuming specific power to be proportional to band width) often decreasing toward the extreme-short waves. Dynamos and motors, high-power rectifiers, medical implements (e.g., diathermy), vacuum cleaners and household appliances, neon and similar lights, electric railways, high-tension lines, and motorcar and airplane ignition systems are among the most common sources of disturbances. Wide variations in specific disturbance power per kilocycle band width at different localities make it difficult to quote representative figures. A value of 10^{-15} watts per cm^2 and kc/s is often regarded as high and a value of 10^{-18} watts per cm^2 and kc/s as rather low in city areas up to 300 mc/s. Disturbance levels are particularly high in the vicinity of a source where the decrease with increasing distance is faster than corresponds to the $1/r^2$ law at longer distances. In such a vicinity the ratio of electric- to magnetic-field strength is in many cases larger than 377 ohms, which is the figure for the $1/r^2$ region (see Eq. I.1.11*a*).

Disturbance noises of a similar nature caused by thunderstorms and related atmospheric activities are commonly called "atmospherics." On the entire earth's surface an average of 2000 thunderstorms occur simultaneously, corresponding to about 100 strokes of lightning per second. The average dissipated power is about 10^{12} watts or 2 kw per square km. Only a small portion of this power is converted into atmospherics in our sense. The specific power of atmospherics is related to sunspot activity and shows 11-year periods. In summer it is generally much higher than in winter. A further daily period is superimposed, the minimum level mostly occurring at night. Different parts of the earth's surface show different densities of thunderstorms. South Africa is notorious for their frequency during its local summer. The noise level p_{kc} (specific power per kc/s) decreases with increasing frequency. At wavelengths beetwen 10 and 50 meters the minimum values of p_{kc} are about 2×10^{-21} watts/($cm^2 \times$ kc/s). Still lower values occur only during 5% of the time of observation. At decimeter and centimeter wavelengths this level is considerably lower, only atmospherics from sources at relatively short distances being received.

Experiments at frequencies between about 15 and 150 mc/s have shown (references *157*, *175*, *291*, *292*) that considerable noise is received from directions coinciding with the galactic region, the origin being beyond doubt extraterrestrial. The specific power p_{kca} per unit (radian) of spherical angle (the entire sphere being 4π units) and per kc/s in these directions was found to be about 10^{-20} watts/(cm^2 $\times$ kc/s $\times$ radian) at 30 mc/s. The resulting noise power captured by antennas may be larger than the values corresponding to the preceding two sources and hence this noise of stellar origin is of considerable practical importance. It has been found to be absent at frequencies between 10,000 and 30,000 mc/s. This cosmic noise is inversely proportional to a power of the frequency which lies between 2 and 3 in the range between 40 and 200 mc/s (reference *400*). The decrease of atmospheric noise at increasing frequency is faster above 10 mc/s. Thus a frequency region exists where both noises are of equal order of magnitude. This region is below about 10 mc/s at latitudes between 30 and 50 degrees. Below this frequency region cosmic noise becomes less important, particularly because of the ionosphere acting as a reflector.

Recent experiments (references *166*, *231*, *270*, *271*, *329*) have uncovered appreciable radiation by the sun at frequencies between 50 and 30,000 mc/s. The corresponding specific powers p_{kc} at 200 mc/s were often higher than 10^{-21} watts/(cm^2 $\times$ kc/s).

REFERENCES: *101*, *132*, *157*, *166*, *175*, *176*, *211*, *231*, *270*, *271*, *291*, *292*, *329*, *400*.

I.2. SIGNALS

A singly periodic wave of constant properties cannot convey any messages. In order to implant a message on such a wave it has to be *modulated*. Either one or several of its properties have to be varied according to a preconceived plan. We shall consider the variations of its different properties, which give rise to the different modes of modulation in present use.

I.2.1. Amplitude modulation (AM). Perhaps the oldest type of modulation arises by variation of the amplitudes of a singly periodic wave.

I.2.11. Singly periodic amplitude modulation. This type of modulation may perhaps best be explained graphically. The field strengths of a singly periodic unmodulated wave at a fixed position in space may be represented as dependent on time by a sine or cosine curve.

If this wave carries a singly periodic amplitude modulation the amplitudes of the sine or cosine curve vary in time as a sine or cosine curve. In the upper part of Figure 24 this is represented for a variation of amplitude between zero and a maximum value, its rate or frequency of variation being in this case exactly five times slower than the fre-

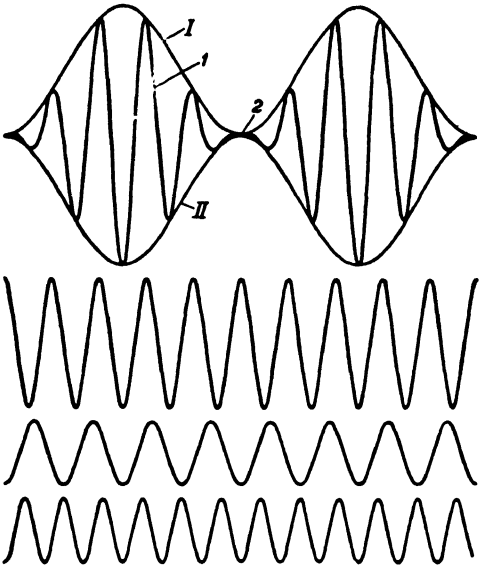

FIG. 24 Picture of an amplitude-modulated wave (upper diagram) with its carrier (next diagram) and both its side waves (remaining diagrams), the coefficient of modulation being unity.

quency of the unmodulated wave. The envelopes of the oscillating curve 1 are in this case two sine curves I and II, mutually tangent at the points of zero amplitude such as 2. Curve No. 1 may be decomposed into the three separate singly periodic curves shown in the lower part of Figure 24 in the sense that at every instant a point of curve 1 is obtained by adding the respective instantaneous deviations of these three curves from their central axes, associating opposite signs with deviations to either side of these axes. Hence the said three curves are together entirely equivalent to the curve No. 1. A different case of AM is shown in Figure 25; the enveloping curves of the amplitudes now intersect each other (upper part of Fig 25). Again the decomposition of the resulting curve No. 1 into three separate curves may

be carried out exactly as shown in Figure 24. A different and often applied representation of modulated waves makes use of their so-called spectrum. The amplitudes of the component waves are represented on a vertical scale and their respective frequencies on a horizontal scale. Thus the spectral representations corresponding to Figures 24 and 25

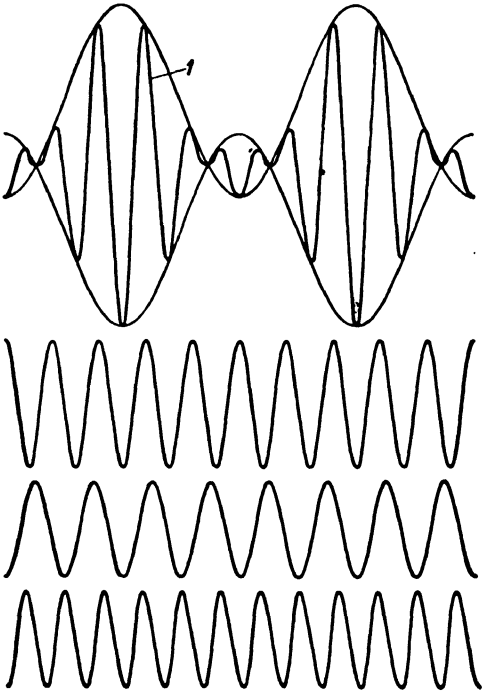

FIG. 25 As Fig. 24, but corresponding to a modulation coefficient of 1.5.

are as shown in Figure 26*a* and *b*. The frequencies of two of the component waves are situated symmetrically with respect to the central one, coinciding with the frequency of the unmodulated wave, indicated as the carrier. The former symmetric waves are called side waves. This spectral representation of Figure 26 does not, however, contain the complete information contained in Figures 24 and 25. The zeros of the three component waves in the lower parts of Figures 24 and 25 show a definite mutual situation, which does not enter into the spectral representations of Figure 26.

I.2.12. General representation of AM waves. In the usual treatment of alternating currents and voltages by vector diagrams, a singly periodic quantity of invariable properties is represented by a single straight line of length proportional to its amplitude. If the angular frequency is ω, this straight line rotates with uniform angular speed ω about one of its end points. The perpendicular projection of the rotating vector on any second straight stationary line represents the

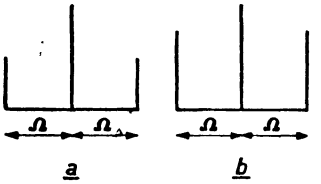

FIG. 26 Spectral representation of AM waves, the diagram *a* corresponding to Fig. 24 and the diagram *b* to Fig. 25. The moduli of carrier (center) and side waves are represented vertically and the corresponding angular frequencies horizontally, linear scales being used for both.

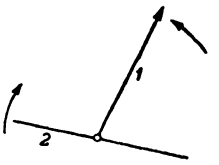

FIG. 27 Vectorial representation of carrier wave by the vector 1 rotating round its lower end at the angular frequency ω. Its perpendicular projection on the line 2 is its instantaneous value. If 1 rotates, 2 is stationary. Instead of this, 1 may be stationary while 2 rotates at the same uniform speed in the opposite direction.

oscillating quantity under consideration at every instant (see Fig. 27). Instead of a rotating vector and a stationary line of projection, we may also use a stationary vector and a uniformly rotating line of projection at the same angular speed but of opposite direction. We shall hereafter refer to this latter representation. The side waves of Figures 24 to 26 are of angular frequencies $\omega - \Omega$ and $\omega + \Omega$ respectively, Ω being the angular frequency of modulation. These side waves may be represented by two vectors in addition to the carrier-wave vector 1 of Figure 27 and rotating with respect to the latter stationary vector at angular speed Ω and in mutually opposite directions. In the AM as represented in Figures 24 to 26 the side-wave vectors are of equal lengths and of symmetrical positions with respect to the carrier vector. Thus Figures 24 and 26*a* correspond to Figure 28; the maximum instantaneous amplitude is twice that of the carrier vector and the minimum instantaneous amplitude is zero. In Figures 25 and 26*b*,

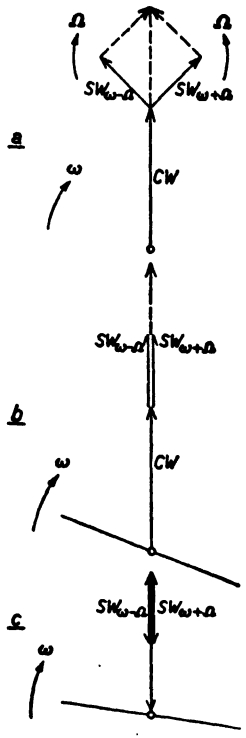

FIG. 28 Vectorial representation of an AM wave, the modulation coefficient being unity. Diagram *a*: Intermediate instantaneous position of side waves SW with respect to carrier wave CW. Diagram *b*: Instantaneous position of side waves such that maximum length of momentary vectorial sum is obtained, this being twice the total length of the CW vector. Diagram *c*: Momentary position of side waves such that a minimum length of instantaneous vectorial sum is obtained, this length being zero.

these values would be 2.5 times and −0.5 times (minus sign denoting reversal of direction) the carrier vector respectively. The ratio of the sum of the lengths of the two side-wave vectors to that of the carrier vector is indicated as depth of AM and denoted by m_a. Figures 24 to 26 and 28 show that the ratio of the amplitude of each side wave to that of the carrier wave is $m_a/2$.

Instead of one single angular frequency Ω of modulation, several such frequencies may be applied, resulting in a number of side waves twice the number of frequencies of modulation. The frequency band necessary to accommodate these frequencies of modulation is twice the highest value of Ω under consideration, as is evident from Figure 26.

The outstanding feature of *pure* AM, as indicated in Figures 24, 26*a*, and 28, is that the resulting instantaneous vector obtained by adding carrier-wave and side-wave vectors is of the same direction as the original carrier vector. Hence the instantaneous angular speed of rotation of the resulting instantaneous vector is invariable and equal to ω. In other words: the frequency of the resulting modulated wave is unchanged if compared with that of the unmodulated carrier. Only the latter's amplitude is altered, i.e., modulated. Hence the descriptive name, pure AM.

REFERENCES: *171, 286.*

I.2.2. Phase, frequency, and mixed modulation. We shall now discuss more modern types of modulation, which offer several advantages in comparison to pure AM.

I.2.21. Phase and frequency modulation (FM). In Figure 27, the angle included by the vector 1 and the line of projection 2 is indicated as "phase angle" at a fixed instant t, preferably $t = 0$. If the vector 1 is moved to and fro, its length remaining invariable while the line 2 is rotating uniformly, the phase angle is varied in a definite way. This alteration of the carrier wave is accordingly indicated as phase modulation. Denoting the phase angle by ϕ, we may impart a singly periodic modulation to it thus: $\phi = m \sin(\Omega t + \varphi)$, Ω being the angular frequency of modulation and φ an arbitrary phase angle. The instantaneous angular speed of the vector 1 with respect to the line 2 of projection is $\omega + d\phi/dt$. This expression also marks the instantaneous angular frequency of the phase-modulated wave. With the above singly periodic phase modulation, this resulting instantaneous angular frequency is:

$$\omega + \frac{d\phi}{dt} = \omega + m\Omega \cos(\Omega t + \varphi). \qquad \text{(I.2.21}a\text{)}$$

We shall now discuss a special case of phase modulation, in which the product $m\Omega$ is independent of the angular frequency Ω of modulation. Thus $m\Omega = \Delta\omega$, in which $\Delta\omega$ is a constant, indicated as angular frequency swing. This special case is called frequency modulation (FM), for obvious reasons. Using a representation similar to Figures 24 and 25, a singly periodic wave with singly periodic FM is shown in the bottom picture of Figure 29. This FM may be visualized by drawing a singly periodic wave on a rubber sheet and then applying extension of compression to some parts of the sheet so as to obtain the bottom curve of Figure 29.

For some purposes this graphical discussion of AM and FM waves may be usefully supplemented by formulas. If the carrier of a pure AM wave is represented by $A \cos \omega t$, the corresponding modulated wave may be represented:

$$\text{AM: } A\{1 + m_a \cos(\Omega t + \varphi)\} \cos \omega t. \qquad \text{(I.2.21}b\text{)}$$

By familiar trigonometric decomposition we obtain the equivalent equation:

$$\text{AM: } A \cos \omega t + \frac{m_a}{2} A \cos\{(\omega + \Omega)t + \varphi\} + \frac{m_a}{2} A \cos\{(\omega - \Omega)t - \varphi\}. \qquad \text{(I.2.21}c\text{)}$$

Thus we have the two side waves of angular frequencies $\omega + \Omega$ and $\omega - \Omega$ and of amplitudes $m_a A/2$, as represented in Figures 24 to 26 and 28, besides the carrier wave of angular frequency ω.

In the case of singly periodic FM of the carrier $A \cos \omega t$ we obtain, by Eq. (I.2.21a), the representation:

$$\text{FM: } A \cos \{\omega t + m \sin (\Omega t + \varphi)\}, \qquad \text{(I.2.21}d\text{)}$$

the expression $m \sin (\Omega t + \varphi)$ being the phase angle ϕ to which singly periodic modulation is applied. As with AM, the FM wave may also

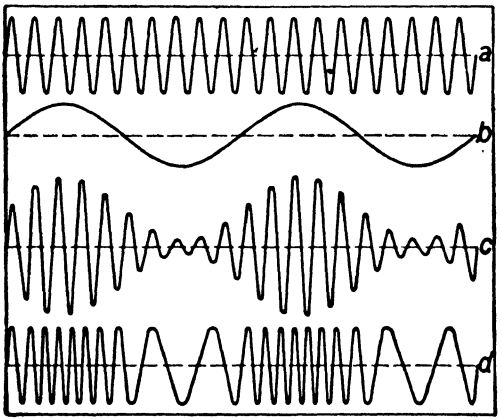

FIG. 29 Wave picture of AM and FM, diagram a representing the unmodulated carrier wave, diagram b representing the modulation, diagram c representing AM with a unity coefficient of modulation and diagram d representing FM.

be decomposed into components of a single frequency each. If m is small in comparison to unity, we obtain, as a first approximation:

$$\text{FM for } m \ll 1\text{: } A \cos \omega t + A \frac{m}{2} \cos \{(\omega + \Omega)t + \varphi\} + A \frac{m}{2} \cos \{(\omega - \Omega)t - \varphi - \pi\}. \qquad \text{(I.2.21}e\text{)}$$

Thus we have again one carrier and two side waves of angular frequencies $\omega + \Omega$ and $\omega - \Omega$. Comparing Eq. (e) with Eq. (c), it appears that the phase angle of the second side wave is $-\varphi - \pi$ in Eq. (e) as against $-\varphi$ in Eq. (c). Hence the vectorial representation of the side waves is different from figure 28 and is represented in Figure 30. The vectorial sum of the carriers wave (CW) and of the two side waves

(SW) of Figure 30 is a vector starting at 0 and ending on the straight line perpendicular to CW. Pure FM, however, corresponds to an invariable length of the carrier vector during the process of modulation. Hence the end of the resulting vector should be situated on a circle centered at 0. Thus it is seen that the decomposition of Eq. (*e*) can be approximately correct only if the SW vectors are small compared to CW, i.e., $m \ll 1$. If this condition is not satisfied, more than two side waves result from the decomposition of an FM wave. The spectral representations corresponding to several values of m are shown in Figure 31. Most of the appreciable side waves are contained within an interval of $\Delta\omega = m\Omega$ on each side of the carrier wave.

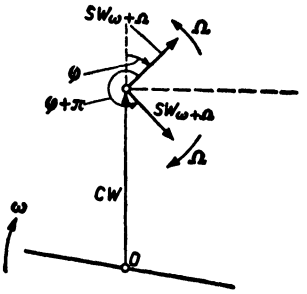

FIG. 30 Representation of a carrier wave vector CW with two side waves according to eq. (I.2.21*e*). The vectorial sum of the three vectors is always between 0 and some point on the broken line.

REFERENCES: *7, 58, 105, 171, 174, 286, 314.*

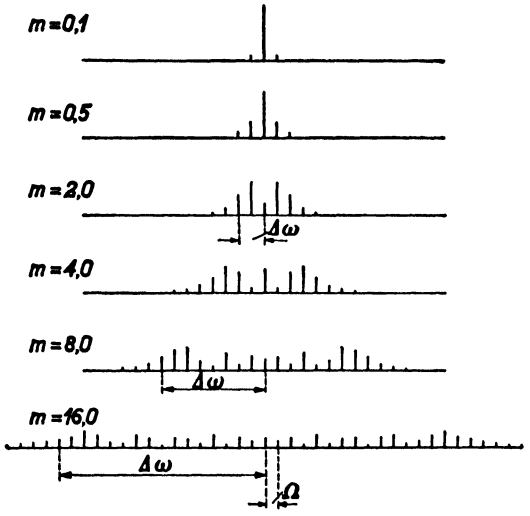

FIG. 31 Spectral representation of FM. Horizontal: Linear angular frequency scale. Vertical: Magnitude of the component waves on a linear scale. The modulation coefficients m are indicated, as well as the angular frequency swing $\Delta\omega = m\Omega$ and the angular modulation frequency Ω.

I.2.22. Mixed and distorted modulation. So far only pure AM and FM have been considered. For various purposes, however, other types of modulation are applied. One of the most common types in commercial communication is single side-wave modulation. If we remove one side wave in the AM pictures of Figures 24 to 26 and 28, only the carrier and a single side wave remain. In some cases the carrier is also suppressed and thus only a single side wave is transmitted. In other cases the carrier is only partly suppressed, thus leaving us with a relatively weakened carrier and a single side wave. One ad-

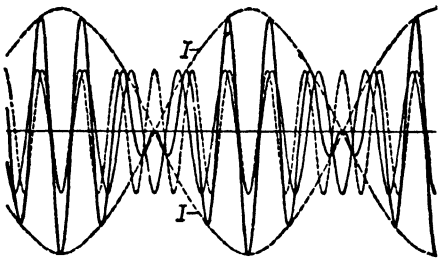

FIG. 32 Wave representation of single side-wave modulation. Full curve of varying amplitude represents resulting wave, I being its envelope. Full curve of constant amplitude is carrier and broken curve of constant amplitude is side wave. Angular modulation frequency Ω is one-quarter of angular carrier frequency ω.

vantage of all these procedures lies in the narrowing of the total band width required for transmitting modulation of frequencies within a given range. As compared to pure AM, at least half of the band width is eliminated. Besides creating space for accommodating more signal channels within a given frequency range, less distortion will in general be incurred by a single side-wave signal during transmission (see sections I.1.41 and 42). Furthermore, the power of the final transmitter stage is also cut down considerably, as no power is necessary to transmit the suppressed parts of the AM wave. The representation of these single side waves needs no further comment.

In the receiver, if linear detection is applied, the resulting signal after detection coincides with the envelope of the received modulated wave (see Figures 24, 25, and 29). The envelope of a single side wave with carrier has *not* the shape of a singly periodic curve (i.e., sine or cosine curve). An example is shown in Figure 32. This non-sinusoidal shape results in distortion at the output of the receiver. It may be minimized, however, by increasing the ratio of carrier amplitude to

side-wave amplitude. This may perhaps be discussed best by referring to Figure 28, omitting one side wave. If the CW is large in comparison to the remaining SW, the length of the modulated CW vector will approximately vary in proportion to cos $(\Omega t + \varphi)$, thus practically eliminating distortion of the linearly detected wave. This procedure is applied in single side-band reception, either relatively reinforcing the received carrier by local means or adding a new carrier of appropriate strength if no carrier is received. In general, the end point of the resulting vector will travel on a circle centered in the end point of the unmodulated CW vector and of radius equal to the SW vector (see Fig. 28). Its direction is therefore not invariable with respect to the unmodulated CW vector, and hence phase modulation as well as amplitude modulation results from single side-wave operation. It may be considered an example of mixed modulation.

The case of AM illustrated by Figures 25 and 26*b* also constitutes mixed or distorted modulation. In Figure 28 the lengths of the SW vectors are above one-half of that of the CW vector in the present case. Hence the resulting modulated CW vector reverses its sign in each period of modulation and thus its angular frequency is also altered abruptly. As soon as m_a is beyond $\frac{1}{2}$, AM results in distortion as mixed modulation is introduced. This is indicated in Figure 25, the envelope being no longer a sine or cosine curve. The present case of AM is often indicated by the term "over-modulation."

Another example of mixed or distorted modulation has already been mentioned in connection with Figures 30 and 31. If we eliminate (by the use of proper filters) from any of the FM waves represented in the latter figure all side waves except the two adjacent to the carrier, the picture of Figure 30 results; and we have already seen that besides FM, manifest in the wobbling of the CW vector, AM corresponding to the variation of its length is also present.

REFERENCES: *58, 73, 74, 76, 77, 105, 131, 171, 286.*

I.2.3. Impulse modulation and band-width considerations. In modern practice yet a third type of modulation, known as pulse or impulse modulation (IM), is being applied and will be discussed briefly. The interrelation of transmitted band width and message volume will be considered in the final section of the present chapter.

I.2.31. Impulse modulation (IM). Impulse modulation resembles AM in that the level of the transmitted wave is altered while its fre-

quency is kept invariable. Unlike AM, however, this variation of level is only between a fixed lower and upper wave level, barring any intermediate levels, the lower level being often negligible compared with the higher one. The necessary further variable in the modulation process may correspond to the length of time during which the wave is brought to its upper level before being restored to its original lower level. This "impulse duration" t_i has to be considered in relation to the period of the wave, this being $2\pi/\omega$. The quantity ωt_i constitutes a proper measure for the relative impulse duration. Its magnitude is determined by the quality factor of the tank circuits applied in transmission and reception (see section IV.2.11). If Q is the highest value of this factor, the building up of power in the corresponding circuit is governed by the exponential law: $1 - \exp(-\omega t/Q)$, ω being the resonant angular frequency and t the time. Substituting t_i for t and requiring the expression within brackets to be at least -1, we obtain the rule that ωt_i should be higher than Q—i.e., higher than the highest quality factor present. In this case the building up or decaying processes of power in the circuit under consideration are nearly completed within the duration of one impulse of shortest duration. Whereas this requirement fixes a lower bound for t_i, a higher bound is determined by the consideration that prolonged impulses would constitute an undesirable waste of transmitting power. Besides the impulse duration t_i the time lapse t_l between two adjacent impulses is important in IM. It should be longer than Q/ω for the same reasons as t_i, and is usually much longer than t_i for transmitter power considerations. The number of impulses per second is fixed by t_i and t_l and may be varied by altering t_l above its lower bound. The resulting angular impulse frequency $q = 1/(t_i + t_l)$ is usually well above audio frequency level. As with AM (Fig. 26) and FM (Fig. 31), a spectral representation of IM is useful for the discussion of its application. Assuming the pulses to be of exactly rectangular shape and $t_i = t_l$, whereas the low level is negligible compared to the high level, the spectrum is shown in Figure 33. The amplitudes of the two side waves adjacent to the first ones are $\frac{1}{3}$, those of the next ones $\frac{1}{5}$, of the next ones $\frac{1}{7}$, etc., of the highest amplitude. Neglecting the side waves less than $\frac{1}{10}$ in amplitude, a total band width of $18q$ or $9/t_i$ in frequency is obtained. If the pulses are not exactly rectangular but show a certain slope upward and downward with equal spacing, the more remote side waves drop faster in amplitude with increasing distance from the carrier. If $t_l \gg t_i$, the frequency q is

relatively much smaller but the decrease in amplitudes of the side waves with increasing order (starting from the carrier) is slower, thus often leaving the total required band width approximately unaltered at equal t_i.

The above type of IM is often indicated as "pulse-width" modulation for obvious reasons. Besides this type of IM a number of further types have found practical application. We shall mention here: "pulse-time" and "pulse-frequency" modulation. With the former, also called "pulse-position" modulation, the timing of a pulse of constant width

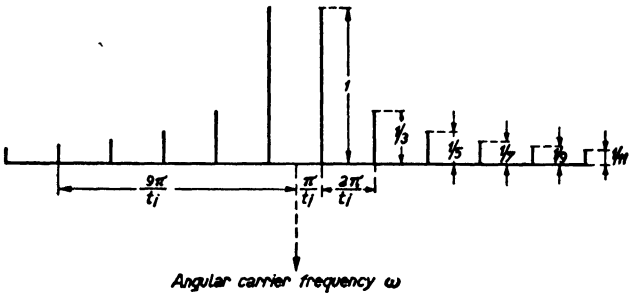

FIG. 33 Spectral representation of IM wave, the intervals between impulses t_l being equal to the impulse duration t_i. Horizontal and vertical scales are as in Fig. 31.

relative to a reference pulse of constant spacing and width is varied around a fixed mean value and conforms to the amplitude of the modulation to be transmitted (see Fig. 227). With the latter the repetition rate of a pulse of constant width is varied around a fixed mean value conforming to the amplitude of the desired modulation. Spectral decompositions of the two further types mentioned are somewhat similar to Fig. 33.

REFERENCES: *286, 296, 378, 407.*

I.2.32. Band-width considerations. As a first example of the relation between the messages transmitted and the required band width, we consider telephone communication. Usually a frequency band of width between 2 and 3 kc/s is assigned to such communication, 2.3 kc/s being a common figure. The interval between two adjacent channels of communication is usually 0.8 kc/s, thus bringing the total band width per channel to 3.1 kc/s. Normal speech carries between 50 and

150 words per minute (wpm), thus fixing the message volume expressed in wpm per cycle assigned band width.

As a second example, we consider telegraph communication using a system of 5 signals (dots and intervals) per letter or sign. Between two adjacent signs a further signal is required. With automatic apparatus 50 signals per second may be communicated, equivalent to 8 letter-signs per second. Using 50 signals per second, a band width of 80 c/s is required with an interval of 40 c/s between adjacent channels of communication. Hence a total assigned band width of 120 c/s per channel corresponds to about 80 wpm. The efficiency of this telegraph communication—i.e., the number of words per cycle/s assigned band width—is hence about 20 times that of the telephone communication. By using code and a more elaborate system (e.g., 7 or 10 signals per code-sign), much greater efficiency may be obtained. However, coding and deciphering of the messages increase the total time required for their communication.

As a third example, we consider television with an assigned band width of 6 mc/s. This may be compared to the communication of a great many wpm; think of the number of words required for an adequate description of all the detail contained in a television picture.

It is useful to include here some band assignments for different purposes at frequencies between 6 and 30,000 mc/s (50 meters and 1 cm wavelength in air). Sound broadcast services cover the ranges: 6.0–6.2, 7.2–7.3, 9.5–9.7, 11.7–11.9, 15.1–15.35, 17.75–17.85, 21.45–21.75, 25–26.6 mc/s. Television covers the channels: 44–50, 54–60, 60–66, 66–72, 76–82 and 82–88 mc/s, according to Federal Communications Commission assignments in the United States. Amateur services cover: 7.0–7.3, 14.0–14.4, 28–30, 56–60 mc/s, according to the 1938 international radio conference at Cairo. In the United States some further assignments by the F.C.C. are: 42–44, 72–76, 88–92 mc/s for non-government fixed and mobile services, 50–54 mc/s for amateur stations, 88–92 mc/s for non-commercial educational FM, 92–106 mc/s for FM stations, 106–108 mc/s for facsimile services. Because of the predominantly local character of wave transmission at frequencies beyond 30 mc/s, frequency assignments may well be different in separated regions of the earth.

REFERENCES: *207, 229, 286, 296.*

CHAPTER II

SPONTANEOUS FLUCTUATION NOISE

In some cases reception is essentially limited by noise of a random character caused by spontaneous fluctuations of electronic motion. In sound channels this is well known as a hissing noise, while in television the effect is similar to a snowstorm covering the picture. As a preliminary to an adequate treatment of reception, we shall consider some practical aspects of the generation and reduction of such noise.

II.1. Noise Due to Circuit Elements and Tubes

In this section the main sources of noise and their properties will be discussed.

II.1.1. General relations. Before embarking upon this discussion some relationships to which frequent reference will be made are presented in a convenient form.

II.1.11. Available power of a source. The sources of power active in the frequency range under consideration may be represented by a two-terminal generator of constant voltage amplitude, which in itself has zero internal impedance. The meaning of this is as follows: Let the generated voltage (r.m.s. value) be V_s and let an impedance Z be connected to the generator's terminals. Then the current I (r.m.s. value) is: $I = V_s/Z$. In order to represent completely the source under consideration, it is in many cases necessary to connect a definite impedance Z_s in series with one terminal of the generator. Thus, if we connect the remaining terminal of the generator to that of the impedance Z_s across a second impedance Z, the current through the latter impedance is: $I = V_s/(Z_s + Z)$. In general, the impedances, voltages, and currents are complex quantities in the sense stated in section I.1.11. If their complex character is to be stressed, boldface type will be used for the respective symbols. The voltage V arising across the impedance Z is obtained from the expression of I by multi-

plication by Z:

$$V = \frac{V_s}{Z_s + Z} Z = \frac{V_s}{Z_s} \frac{ZZ_s}{Z + Z_s} = I_s \frac{1}{\frac{1}{Z_s} + \frac{1}{Z}}. \qquad \text{(II.1.11}a\text{)}$$

This Eq. (a) suggests that the source of power may also be represented by a constant-current generator supplying the current I_s to the parallel connection of Z and Z_s. The current generator itself is to have infinite internal impedance, the impedance Z_s belonging to the source being paralleled to the current generator. Both representations of a power source—by a voltage generator or by a current generator—are depicted in Figure 34. The outer impedance Z is each time to be connected to the terminals nos. 1 and 2.

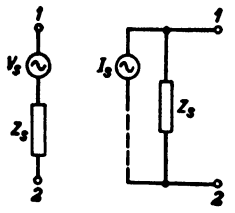

FIG. 34 Representation of a power source by a voltage generator of voltage V_s in series with an impedance Z_s or by a current generator of infinite internal impedance supplying the current I_s shunted to an impedance Z_s.

We shall now answer the question: What is the optimum average power which a source of this kind may deliver to an outer consumer's impedance **Z**? If **V** and **I** are the voltage across and the current through Z this power is:

$$P = \text{Real part of } (\mathbf{VI}^*) = \text{Real part of } \left(\frac{|V_s|^2 \mathbf{Z}}{|\mathbf{Z} + \mathbf{Z}_s|^2} \right),$$

the vertical bars denoting the absolute amount or modulus of the expression between them. If $\mathbf{Z} = R + jX$ and $\mathbf{Z}_s = R_s + jX_s$, R denoting a resistance and X a reactance, we obtain:

$$P = \frac{|V_s|^2 R}{(R + R_s)^2 + (X + X_s)^2}. \qquad \text{(II.1.11}b\text{)}$$

With V_s, R_s, and X_s given, the optimum value of P is attained if $X = -X_s$ and $R = R_s$. These conditions are indicated by the term: "matched" consumer's impedance. If they are satisfied, we obtain:

$$P_a = \frac{|V_s|^2}{4R} = \frac{|I_s Z_s|^2}{4R}, \qquad \text{(II.1.11}c\text{)}$$

and this expression is called the "available" power of the source under consideration. The second expression in (c) is obtained using

the constant-current generator mentioned above. Under the matched conditions as much power is consumed in the source's internal resistance R_s as in the outer resistance R. (It has been assumed that R_s and R are both of positive sign.)

II.1.12. Correlation and average values. The currents and voltages due to spontaneous electronic fluctuations represent quantities of random character. Take a current and let its instantaneous value be I. Measuring this instantaneous value many times over—e.g., at intervals spaced regularly—and taking the average of the measured values, the average current $\bar{I}$ is found, the horizontal bar denoting the averaging process. The difference $I - \bar{I}$ may be either positive or negative. The average value of its square, taken in the above sense, is the mean square current fluctuation or fluctuation current $\overline{i^2}$. In order to mark the difference between fluctuations and current values themselves, i is used as a symbol for the former and I for the latter. Now suppose that two fluctuation currents i_1 and i_2 flow through the same path on part of their course. Three cases may arise: (*a*) The fluctuations causing i_1 and i_2 are entirely correlated. In this case i_1 is a replica of i_2 on a magnified or reduced scale. Hence the resulting fluctuation current through the path is $i_1 + i_2$ and its mean square value is $\overline{(i_1 + i_2)^2}$. (*b*) The fluctuations are entirely uncorrelated or, in other words, independent of each other. In this case the resulting mean square fluctuation current is $\overline{i_1^2} + \overline{i_2^2}$. This rule is similar to the addition of a.c.'s of different frequencies. (*c*) The fluctuations are partly correlated. This case is obviously a combination of cases (*a*) and (*b*). Two partly correlated fluctuations may each be split up into one part completely correlated with a corresponding part of the other one and a second part noncorrelated to any part of the second one.

Fluctuating currents or voltages are often considered within a relatively narrow frequency interval Δf centered round a frequency f such that $\Delta f \ll f$. In this case the dependence of the fluctuating quantity upon time is in some ways similar to a singly periodic alternating quantity. The amplitude is not constant, however, but shows fluctuations of average period $1/\Delta f$, whereas the average frequency of oscillation coincides with f. By way of example, Figure 35 shows the actual registration of a fluctuation current in the case that Δf is approximately $f/14$.

REFERENCES: *118, 176, 247, 266, 294.*

FIG. 35 Representation of spontaneous fluctuations corresponding to a frequency interval Δf approximately equal to $\frac{1}{4}$ of its average frequency, round which it is centered.

II.1.2. Noise due to diodes and to resistances. One of the simplest known sources of noise is an electronic high-vacuum diode tube, which, under appropriate conditions of operation, produces a noise closely linked to that in an ohmic resistance.

II.1.21. Noise of high-vacuum electronic diodes. Consider part of an emitting cathode surface of unit area. The number of electrons emitted thermionically during a time interval t_o is n. If this number is measured over and over again each time during an equal interval t_o we obtain the average value $\bar{n}$ of n. The fluctuation $n - \bar{n}$ may be determined simultaneously and its mean square value $\overline{(n - \bar{n})^2}$ calculated. If the single events of electronic emission are completely independent, we obtain the relation:

$$\overline{(n - \bar{n})^2} = \bar{n} \qquad \text{(II.1.21}a\text{)}$$

from the theory of probability. This relationship is in agreement with experimental evidence. The electric charge emitted on the average during t_o is $\bar{n}e$ and the corresponding mean emission current $\bar{I}_e$ is $\bar{n}e/t_o$, the individual corresponding values being ne and $I_e = ne/t_o$. Using Eq. (a), we may deduce the mean square fluctuation of emission current:

$$\overline{i_e^2} = \overline{(I_e - \bar{I}_e)^2} = \frac{e^2}{t_o^2}\,\overline{(n - \bar{n})^2} = \bar{n}\,\frac{e^2}{t_o^2} = \frac{e}{t_o}\,\bar{I}_e. \qquad \text{(II.1.21}b\text{)}$$

In electronic applications we are, however, interested in the manifestation of these spontaneous fluctuations of electronic emission in circuits connected to the terminals of the tube under consideration. Taking a diode as the simplest type of tube, these manifestations may be widely different under different conditions of operation. The simplest case arises if the cathode and anode are both parallel planes of such area that relatively small contributions to the electronic current result from electrode regions near the edges. Furthermore, the anode voltage is supposed to be so high that all emitted electrons reach the anode and that the interelectrode field strength is uniform. Connecting anode and cathode by an outer lead of practically zero impedance, each electron

traveling from cathode to anode will cause a current pulse in the lead of the shape shown in Figure 36, the electronic transit time being τ. If the intervals t_o of Eq. (*b*) are large compared to τ, the current fluctuation in the outer short-circuit lead is exactly given by Eq. (*b*). If, however, t_o is comparable to or

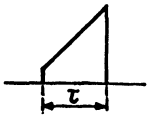

FIG. 36 Induced current pulse in a short-circuit connection of two parallel plane electrodes caused by an electron passing from the cathode to the anode under a uniformly accelerating field.

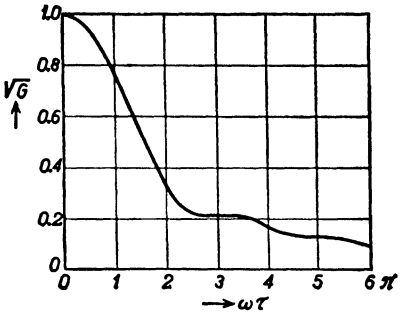

FIG. 37 Representation of the function G of eq. (II.1.21*d*) corresponding to the decline of induced fluctuation currents as dependent on $\omega\tau$ (horizontal scale).

even smaller than τ, the mean square current fluctuation in the outer lead may be much smaller than the value of Eq. (*b*).

The fluctuation currents under discussion contain components corresponding to all frequencies. It is useful to consider the mean square value $\overline{i^2}$ connected with an interval Δf, centered round a frequency f. The time interval $2t_o$ corresponds to $1/\Delta f$, and hence we obtain from Eq. (*b*):

$$\overline{i_e^2} = 2e\bar{I}_e\Delta f. \qquad \text{(II.1.21}c\text{)}$$

If f is such that $2\pi f\tau = \omega\tau$ is small compared to unity, Eq. (*c*) gives also the fluctuation current i in the outer lead; but if $\omega\tau$ is comparable to unity, we have:

$$\overline{i^2} = \overline{i_e^2}\, G(\omega\tau), \qquad \text{(II.1.21}d\text{)}$$

the function G being shown in Figure 37. The effect of these fluctuations in an outer lead having appreciable impedance may be found by assuming a constant-current generator of infinite internal impedance supplying the current i of Eq. (*d*). Parallel to this generator are the interelectrode impedance Z_d and the outer lead's impedance Z (Fig. 38).

If the conditions of operation of the diode are less simple, the fluctuations in the outer lead bear a more intricate relation to the emission fluctuations of Eq. (*c*). Generally:

$$\overline{i^2} = \overline{i_e^2} F_e, \qquad \text{(II.1.21}e\text{)}$$

the multiplier F_e varying according to the conditions described and the anode current I_a being substituted for I_e in Eq. (*c*).

As will be shown in the next section, the fluctuations of a diode in the exponential region of operation correspond exactly to those of its internal resistance R at half the cathode temperature T_c. In the space-charge limited region of operation this noise representation retains its validity if the multiplier 0.5 is replaced by 0.64 (references *288* and *311*). Thus F_e may be evaluated from:

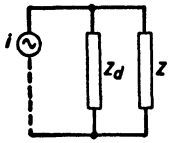

FIG. 38 Representation of a diode as a source of spontaneous fluctuations by a current generator of infinite internal impedance supplying the current i, shunted to the diode's interelectrode impedance Z_d and the outer impedance Z.

$$F_e = \alpha_e \frac{2KT_c}{eI_aR}, \qquad \text{(II.1.21}f\text{)}$$

the multiplier α_e being 0.5 or 0.64 as mentioned and K representing Boltzmann's constant (see Eq. II.1.22*a*). In the exponential region of operation F_e works out to be unity, while its value is between about 0.01 and 0.04 in most of the space-charge limited region. At saturation F_e is again unity. Thus the space charge in front of the cathode acts as an efficient threshold passing on only a small fraction of the initial fluctuations of the emission current.

REFERENCES: *141, 233, 247, 261, 288, 302, 311, 362, 376.*

II.1.22. Noise of ohmic resistances. If in the plane diode considered in the preceding section the effective anode voltage $-V_a$ is negative with respect to the cathode, the anode is reached only by those electrons whose motional energy of emission is equal to or larger than eV_a. Hence the anode current I_a is smaller than the emission current I_e, the relation being:

$$\frac{I_a}{I_e} = \exp\left(-\frac{eV_a}{KT}\right), \qquad \text{(II.1.22}a\text{)}$$

where K denotes Boltzmann's constant (1.38×10^{-23} joule per degree

Kelvin) and T the cathode's temperature expressed in degrees Kelvin (zero C. = 273 Kelvin). The value KT is the average effective motional energy of emitted electrons. From Eq. (*a*) we may easily calculate the current increment corresponding to a relatively small voltage increment:

$$\frac{dI_a}{dV_a} = -\frac{1}{R} = -\frac{e}{KT} I_a, \qquad \text{(II.1.22}b\text{)}$$

R being the interelectrode resistance due to electrons at small transit times compared to the inverse frequency in question: $\omega\tau \ll 1$ (see Eq. (II.1.21*d*) and Fig. 37).

We may suppose an ohmic resistance to consist of a conglomeration of minute diodes, both electrodes of each being at equal temperatures. Spontaneous voltages arise between the electrodes of each diode, causing a local flow of electrons one way or the other. Suppose that in one particular diode the voltage V_a is such that all electrons emitted by the electrode of lower voltage reach the other electrode whereas in the opposite direction emission is governed by Eq. (*a*). The resistance offered by this diode to the flow of current is given by Eq. (*b*), as the resistance associated with the current flow in the opposite direction is infinite and hence may be disregarded for our purpose. On the average, the current in either direction is of equal amount, the mean square fluctuation current being doubled if compared with the diode of the preceding section, having a thermionic cathode and a cold anode. Thus the total mean square fluctuation current for one diode is:

$$\overline{i^2} = 4eI_a\Delta f. \qquad \text{(II.1.22}c\text{)}$$

In order to obtain the corresponding mean square fluctuation voltage $\overline{v^2}$ we use the equations $\overline{v^2} = R^2\overline{i^2}$ and (*c*), and substitute the value of Eq. (*b*) for one multiplier R. The resulting values are:

$$\overline{v^2} = 4KTR\Delta f, \quad \overline{i^2} = \frac{4KT}{R}\Delta f. \qquad \text{(II.1.22}d\text{)}$$

The same reasoning may be applied to all miniature diodes of the actual resistance, thus obtaining the Eqs. (*d*) for the open-circuit mean square fluctuation voltage $\overline{v^2}$ and for the short-circuit mean square fluctuation current $\overline{i^2}$ of any ohmic resistance of R ohms. Such

a resistance may be replaced, as far as spontaneous fluctuations are considered, by a voltage generator of voltage v in series with a resistance R (the generator being of zero internal impedance) or by a current generator of current i and of infinite internal impedance acting in parallel to a resistance R. The available noise power of a resistance is, by Eq. (*d*):

$$P_a = KT\Delta f. \qquad \text{(II.1.22}e\text{)}$$

At 20° C. the value of KT is almost exactly 4.0×10^{-21} joule.

REFERENCES: *178, 247, 376, 390.*

II.1.3. Noise due to multi-element tubes and to networks. The noise in these more complex cases may be deduced from that in the two simple elements considered above: the diode and the ohmic resistance.

II.1.31. Noise due to triodes. The simplest of these tubes is the triode consisting of a cathode, a grid, and an anode placed in consecutive order. By the combined action of anode and grid voltages with respect to the cathode, part of the emitted electrons are drawn toward the former electrodes. We may replace the cathode-grid space by an equivalent diode, the anode of which is situated in the grid plane and has a voltage calculable from the combined action of grid and anode voltages. In reception triodes the grid is often given a negative and the anode a positive steady voltage for the purpose of preventing the grid from intercepting electrons (as far as possible). On these steady voltages relatively small alternating voltages are often superimposed. We are primarily concerned with the action of these latter voltages on the electronic stream in the tube. An alternating component arises in this electronic current from provoked local variations of electronic density as well as of electronic velocity. If these alternating voltages are sufficiently small, the resulting a.c.'s will be proportional to them. The alternating electronic current in the space between cathode and grid causes a corresponding alternating current in the outer circuit connecting the electrodes by induction of image charges on them. The screening action of the grid partly prevents the formation of image charges on the anode by these electrons, and we may assume approximately that no a.c. is caused by them in the outer circuit connecting grid and anode. Conversely, the electronic a.c. in the grid-anode space causes a corresponding a.c. in the outer circuit connecting these electrodes and only a relatively small a.c. in the grid-cathode circuit.

These simple notions may be directly applied to fluctuation currents. As was shown at the end of section II.1.12 and in Figure 35, these currents are similar to a.c.'s under appropriate conditions. The effect of electronic fluctuation currents on the outer circuits attached to the electrodes of a triode may be ascribed to two current generators of infinite internal impedance, one active between cathode and grid and the other between grid and anode. The interelectrode impedances between each pair of consecutive electrodes are in parallel to the outer

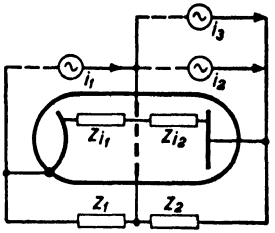

FIG. 39 Spontaneous fluctuations of a triode represented by two spontaneous current generators i_1 and i_2 of infinite internal impedances and active between cathode and grid and between grid and anode respectively, shunted to the interelectrode impedances Z_{i1} and Z_{i2} as well as to the outer impedances Z_1 and Z_2. The current generator i_3 corresponds to the transadmittance from grid to anode multiplied by the fluctuation voltage active between cathode and grid. In an ideal triode all three currents i_1, i_2, and i_3 are completely correlated.

impedances and to the current generators. Thus we obtain the picture of Figure 39. The two fluctuation currents i_1 and i_2 of the generators are completely correlated in an ideal triode in which all the electrons are passed by the grid of sufficiently negative steady voltage and in which no sources of fluctuations except the cathode exist.

The current generator supplying the current i_3 active between grid and anode in Figure 39 is due to the action of the fluctuation voltages of grid and anode with respect to the cathode. These voltages are again assumed correlated to i_1 and to i_2, and so is i_3. Definite phase relations exist between i_1, i_2, and i_3 regarded as a.c.'s in a relatively small frequency interval Δf centered around f.

The magnitude of $\overline{i_1^2}$ is given by Eqs. (II.1.21*e*) and (II.1.21*c*) in which I_e is to be replaced by the average anode current I_a in the case of a negatively biased grid capturing practically no electrons. The magnitude of $\overline{i_2^2}$ is approximately equal to $\overline{i_1^2}$ at frequencies below 600 mc/s in most triodes, but i_2 is retarded with respect to i_1 by a phase angle

approximately given by $\frac{1}{3}\omega\tau_1 + \frac{2}{3}\omega\tau_2$, if τ_1 and τ_2 represent the electronic transit times from cathode to grid and from grid to anode respectively. The frequency interval Δf under consideration is centered round the angular frequency ω. The value of i_3 is equal to $v_1\mathbf{Y}$ if v_1 is the effective fluctuation voltage acting between cathode and grid and if $\mathbf{Y}$ represents the complex transadmittance from grid to anode. By insertion of these values the fluctuations caused by a triode in any outer circuits connected to its electrodes may readily be evaluated.

REFERENCES: *11*, *12*, *219*, *262*.

II.1.32. Noise due to multi-element tubes. The simplest extension of the triode is a tetrode. The steady electrode voltages are often: control grid (adjacent to cathode) negative, screen grid (adjacent to anode) positive, and anode positive with respect to the cathode. A new source of fluctuations arises at the screen grid, as there being an element of chance in its intercepting an electron out of the stream or not. This element of chance corresponds to an electronic fluctuation current starting from the screen and passing on to the anode. This "partition" fluctuation current causes a correlated fluctuation current in the outer circuit connecting screen and anode, and may be ascribed to a current generator of infinite internal impedance active between those two electrodes. The partition fluctuations are uncorrelated to the cathode's emission fluctuations. Thus a tetrode may be represented by Figure 40. The interelectrode impedances Z_{i1}, Z_{i2}, and Z_{i3} are in parallel to the outer impedances Z_1, Z_2, and Z_3 attached to the electrodes and to the completely correlated current generators i_1, i_2, and i_3. The current generators i_4 and i_5 are also assumed correlated to i_1, i_2, and i_3, and are due to the combined action of correlated electrode voltages on the electronic stream. Finally, i_6 represents the uncorrelated partition fluctuation current.

Another extension is required by secondary emission. If an electronic stream hits an electrode at considerable speed, the latter starts emitting electrons on its own. This phenomenon is indicated by secondary emission. It entails fluctuations, uncorrelated to those of the impinging stream. Thus a tube incorporating a cathode, one grid, a secondary target, and an anode may be dealt with like the tube of Figure 40, the secondary target replacing the screen grid and i_6 representing the uncorrelated secondary fluctuation current. By combination the reader may now easily build up for himself the fluctuation picture

of a tube comprising a cathode, a control grid, a screen grid, a secondary target, and an anode such as those applied in some commercial tubes. Obviously Figures 39 and 40 may be considered as a repetition of Figure 38 applied several times over.

Besides preconceived secondary emission we often find this kind of emission with electrodes hit by fast electrons such as anodes and screen grids, and in these cases it must be considered detrimental.

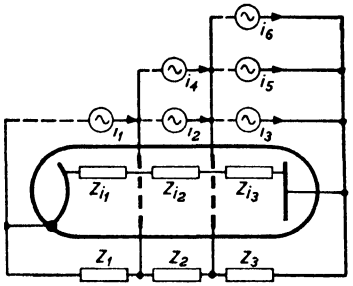

FIG. 40 Extension of the representation of Fig. 39 to a tetrode, i_1, i_2, and i_3 being completely intercorrelated fluctuation currents in the ideal case. The currents i_4 and i_5 are also asumed correlated to i_1, i_2, and i_3. The current i_4 corresponds to the transadmittance from the first control grid to the subsequent positive electrodes together, multiplied by the fluctuation voltage active between cathode and control grid. The current i_5 corresponds to the transadmittance from the control grid to the anode multiplied by the said fluctuation voltage, added to the transadmittance from screen grid to anode multiplied by the fluctuation voltage active between screen and cathode. The current i_6 is completely uncorrelated to the other currents and represents the partition fluctuations between screen and anode. The three inter-electrode impedances are represented by Z_{i1}, Z_{i2}, and Z_{i3}, while the outer circuit shunt impedances are Z_1, Z_2, and Z_3.

The secondary electrons are mostly emitted with speeds corresponding to a few volts (i.e., to the speed imparted to an electron on a parcourse of a few volts potential difference). Such electrons leave the target and then often encounter an electric field tending to reverse their original direction of motion. After completing a roundabout path in this field the secondary electrons are recaptured by the target. The spontaneous fluctuations of the secondary electronic emission give rise to the induction of corresponding fluctuation currents in an outer circuit connecting the target and adjacent electrodes; these fluctuations are uncorrelated to those of the primary impinging electronic stream. They may occur with diodes and multi-element tubes and may increase

the resulting mean square fluctuations in outer circuits considerably. With diodes their occurrence may often be prevented by keeping instantaneous anode voltages below, say, 5 volts, thus preventing secondary emission.

In the case of a tetrode with a negatively biased control grid i_1 and i_2 have the same values as i_1 and i_2 in the case of a triode in the preceding section, only replacing the average anode current I_a by the sum of the average anode current I_a and the screen grid current I_2 of the tetrode. The magnitude of i_3 is smaller than that of i_1 and i_2 in the proportion of I_a to $I_a + I_2$. The mutual phase angle of i_1 and i_2 is the same as for a triode. The phase retardation of i_3 with respect to i_2 is approximately $\frac{1}{3}\omega\tau_2 + \frac{1}{2}\omega\tau_3$ if τ_2 is the electronic transit time from control grid to screen grid and τ_3 the transit time from screen grid to anode. The positive bias voltages of the latter electrodes are assumed to differ relatively little. The above relations are approximately valid for most tetrodes below about 600 mc/s. The fluctuation current i_4 is equal to $v_1\mathbf{Y}$ if v_1 is the effective fluctuation voltage active between cathode and grid. The complex transadmittance $\mathbf{Y}$ is active between the control grid and a substitute electrode replacing the screen and capturing all electrons. This substitute electrode is to be given an appropriate positive bias voltage in order to simulate the combined action of the actual screen and anode on the electronic stream. The magnitude of i_5 bears to i_4 the ratio of I_a to $I_a + I_2$. It is retarded with respect to i_4 by an angle approximately equal to the retarding angle of i_3 with respect to i_2.

Finally the magnitude of i_6 is given by:

$$\overline{i_6^2} = 2e\frac{I_2 I_a}{I_2 + I_a}\Delta f\,. \qquad \text{(II.1.32}a\text{)}$$

Its phase angle is immaterial as it is uncorrelated to i_1, i_2, i_3, i_4 and i_5, which are assumed completely correlated among themselves.

REFERENCES: *55, 219, 247, 312, 319, 377.*

II.1.33. Noise due to networks and resonant circuits. In any network only the resistive elements are sources of spontaneous fluctuation power. This may be inferred from the fact that such power is dependent on temperature and only dissipative elements may absorb heat energy from the surrounding medium and convert part of it into fluctuation power. By this law it is a simple matter to evaluate the fluctuation

currents in any network containing resistances and reactances, the different resistance elements being allowed to have different temperatures. As a simple example we consider two resistances R_1 and R_2 at temperatures T_1 and T_2 with their terminals connected together. Making use of current generators, the total mean square fluctuation current flowing through the parallel arrangement of both resistances is (the individual fluctuations of the resistances being uncorrelated):

$$\overline{i^2} = \overline{i_1^2} + \overline{i_2^2} = \frac{4KT_1\Delta f}{R_1} + \frac{4KT_2\Delta f}{R_2},$$

and hence the fluctuation voltage generated at the terminals of the arrangement is:

$$\overline{v^2} = \overline{i^2}\left(\frac{R_1R_2}{R_1 + R_2}\right)^2 = 4K\Delta f\left(\frac{R_1R_2}{R_1 + R_2}\right)^2\left(\frac{T_1}{R_1} + \frac{T_2}{R_2}\right).$$

This expression assumes a simple value if $T_1 = T_2 = T$. Then we have:

$$\overline{v^2} = 4KTR\Delta f,$$

R denoting the composite resistance of the parallel connection. The available noise power is $KT\Delta f$ as in the case of a single resistance, as was predictable by this result being independent of the composition of the resistance under consideration.

In a more complex network it is convenient to make use of the notion of *gain* connected with a four-terminal network or "four-pole." In Figure 41 a resistance R with terminals $1'$ and $2'$ is connected to a general network containing resistances, reactances, and electronic tubes, current and voltage variations being so small that proportionality very nearly exists between them. This is usually expressed by saying that the network is very nearly "linear." The available power P between $1'$ and $2'$ is translated by the four-pole to an available power P_o between 3 and 4, the ratio of both being the "gain" g of the four-pole from its terminals 1, 2 to its output terminals 3, 4. Thus: $P_o = gP$. If no sources of power are included in the four-pole—i.e., no electronic tubes—g is either less than or equal to unity. Between 3 and 4 an impedance Z_o exists, looking into the four-pole, its real part being R_o. The open-circuit voltage between 3, 4 equivalent to the power P is then, by section II.1.11:

$$\overline{v^2} = 4R_oP_o = 4R_ogP = 4R_ogKT\Delta f. \qquad \text{(II.1.33}a\text{)}$$

This voltage is due to the fluctuations generated by the resistance R at a temperature T. A particularly simple result arises if the four-pole contains neither tubes nor resistances but only reactances. In this case we have $g = 1$, and hence the fluctuation voltage at the output is equal to the voltage corresponding to the real part R_o of the output impedance Z_o at a temperature T. If the network contains only reactances and several resistances at equal temperature, the above reasoning may be applied to each resistance in turn, the available

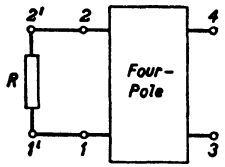

FIG. 41 Picture of a resistance R connected to the input terminals of a four-pole.

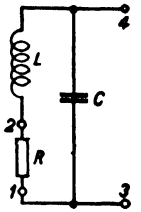

FIG. 42 Resonant circuit consisting of an inductance L in series with a resistance R shunted to a capacitance C. The output terminals are 3,4; the input terminals of the four-pole of Fig. 41 correspond to 1,2.

output power becoming $P_o = g_1P + g_2P + \cdots$, g_1, g_2, etc., being the gains from the resistances to the output terminals 3, 4 and P denoting the available power $KT\Delta f$ of each resistance. The sum $g_1 + g_2 + g_3 + \cdots$ being unity, we obtain the result that the available output fluctuation power is: $P_o = KT\Delta f$ and the open-circuit fluctuation voltage equivalent to that of the real part R_o of the output impedance Z_o. We may also argue that $P_o = KT\Delta f$ for any source at temperature T, and hence, necessarily, $g_1 + g_2 + g_3 + \cdots = 1$.

A particular application will be made to a resonant circuit shown in Figure 42. We want to obtain the open-circuit fluctuation voltage at the terminals 3, 4 due to R at a temperature T, L being an inductance and C a capacitance. By Eq. (a) we should evaluate R_o, which is:

$$R_o = \frac{R}{\omega^2C^2R^2 + (1 - \omega^2LC)^2},$$

and then: $\overline{v^2} = 4R_oKT\Delta f$. It is sometimes useful to have the value

of $\sqrt{v^2}$ corresponding to a resistance of R (kiloohms) at a temperature of 300° Kelvin and at different frequency intervals Δf (expressed in kc/s) at hand. This aim is served by Figure 43.

REFERENCES: *55, 118, 247, 390.*

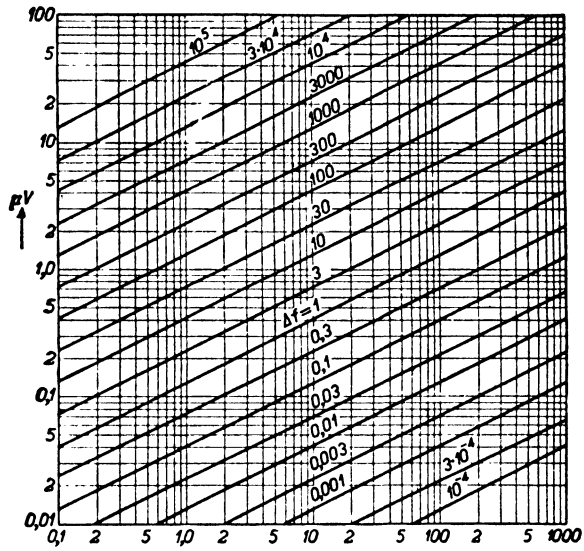

FIG. 43 R.m.s. spontaneous fluctuation voltage (vertical scale) in microvolts as dependent on the corresponding resistance R expressed in kiloohms (horizontal scale) causing the said fluctuations, the curves corresponding to different frequency intervals Δf expressed in kc/s.

II.2. NOISE RATIO AND NOISE FIGURE

The spontaneous fluctuation noise in receivers is hardly important in itself but quite important in relation to the signal under consideration. This comparison involves some useful notions.

II.2.1. Definitions. The discussion starts with the basic definitions and their interpretation.

II.2.11. Definition of noise ratio. In the subsequent definitions use is made of a linear four-pole as an agent (see Fig. 41). A source of signal power and a source of noise power are attached to the input terminals. Besides, the four-pole itself contains sources of noise but no sources of signal. We consider the available noise power P_{no} and the available signal power P_{so} at the output terminals 3 and 4. Their

ratio P_{no}/P_{so} is indicated as the available noise ratio at the output. This ratio may easily be measured by short-circuiting the terminals 3 and 4. The mean square noise current through this short connection being $\overline{i_o^2}$ and the square of the modulus of the r.m.s. signal current I_o^2, we have:

$$\frac{P_{no}}{P_{so}} = \frac{\overline{i_o^2}}{I_o^2}. \qquad \text{(II.2.11}a\text{)}$$

The proof of this relation may be based on section II.1.11. The real part of the impedance Z_o measured at the output looking into the terminals 3, 4 being R_o we have: $P_{no} = \overline{i_o^2} \times |Z_o|^2/4R_o$ and $P_{so} = I_o^2|Z_o|^2/4R_o$ by Eq. (II.1.11c). From this, Eq. (a) above follows directly. Similarly, if $\overline{v_{no}^2}$ is the open-circuit mean square noise voltage between the output terminals 3, 4 and V_o^2 the square of the modulus of the r.m.s. open-circuit signal voltage, the available noise ratio is:

$$\frac{\overline{v_{no}^2}}{V_o^2}.$$

The available noise power P_{no} at the output is obtained by adding two components. The first one is the available noise power P_{ni} of the input source multiplied by the gain g from input to output. The second one is due to the noise sources inside the four-pole. Both fluctuation noises are in general entirely uncorrelated. As the available signal power P_{so} at the output is obtained by multiplication of the available signal power P_{si} at the input by g, the available noise ratio at the output is in general larger than and under extremely favorable conditions (if the four-pole contributes no noise) equal to the available noise ratio at the input.

The above definitions apply only to a frequency interval Δf such that the gain g is constant throughout its range. If broader intervals are considered, some additional notions are necessary. In most reception four-poles, g is optimal at a definite frequency or within a definite frequency interval, its value then being g_o. Let its value at some other frequency be g. The effective band width B to be substituted instead of Δf into the relevant formulas is then found from:

$$B = \int_0^\infty \frac{g}{g_o}\, df, \qquad \text{(II.2.11}b\text{)}$$

while the effective gain g_e is:

$$g_e = \frac{1}{B}\int_0^\infty g\, df = g_o. \qquad \text{(II.2.11}c\text{)}$$

Using these expressions g_e and B instead of g and Δf, we may apply the above and the subsequent formulas to any four-pole of known gain-frequency curve.

REFERENCES: *127, 224, 250, 263, 264, 365.*

II.2.12. First definition of noise figure. Several definitions have been given of noise figures. We shall discuss two of them here, giving their interrelation; preference will be given in this book to the second one. The first definition, published almost simultaneously by independent sources in the United States and in Britain in 1944 (references *127, 224*), starts from the available noise ratios at the output and at the input of a four-pole. The ratio of these ratios—i.e., output over input—is called "noise figure F" of the four-pole. Thus:

$$F = \frac{P_{no}/P_{so}}{P_{ni}/P_{si}}. \qquad \text{(II.2.12}a\text{)}$$

In the simplest case the four-pole may consist only of short through-connections between its terminals 1 and 3 as well as between 2 and 4. In this case we have obviously $F = 1$. Another simple case arises if the four-pole contains exclusively passive reactances. As there are no noise sources inside the four-pole, we obtain also the value unity for F.

A case of special interest arises if two four-poles, of individual noise figures F_1 and F_2 and gains g_1 and g_2, are connected in cascade—i.e., with the output terminals of the first one attached to the input terminals of the second one. For the exact definitions of F_1, F_2, g_1, and g_2, reference is made to the relevant observations pertaining to the noise figures N_1, N_2 and associated gains below. The noise figure of the combination, regarded as one single four-pole, is called F. The gain g of the combination is: $g = g_1 g_2$. By the definition of Eq. (a), the available output noise power of a four-pole is:

$$P_{no} = FgP_{ni} = \frac{P_{no}}{P_{ni}} \times \frac{P_{si}}{P_{so}} \times g \times P_{ni},$$

the ratio P_{si}/P_{so} being $1/g$. The available noise output power due to

the input source being gP_{ni}, the component due to the four-pole is $(F-1)gP_{ni}$. Thus, in our cascade case we have:

$$P_{no} = F_1 g_1 g_2 P_{ni} + (F_2 - 1) g_2 P_{ni} = F g_1 g_2 P_{ni}.$$

Hence:

$$F = F_1 + \frac{F_2 - 1}{g_1}. \qquad \text{(II.2.12}b\text{)}$$

This process may obviously be extended to more than two four-poles connected in cascade.

REFERENCES: *55, 127, 224, 250, 263, 264.*

II.2.13. Second definition of noise figure. The second definition of noise figure, known since about 1939 (references *119, 197*), starts again from the available output noise ratio. We then determine the available input signal power necessary to make this available noise ratio equal to unity. This signal power is thereupon divided by KTB, T being the room temperature (e.g., 290° Kelvin) and B the effective band width in the sense mentioned in the preceding section. The resulting figure is called the noise figure N of the four-pole. At first sight this definition seems slightly more involved than the preceding one, but a little consideration will show that it is in fact equally simple. Expressed by a formula, we have:

$$\therefore\ N = \frac{P_{no}}{gKTB} = \frac{P_{no}}{KTB} \times \frac{P_{si}}{P_{so}} = \frac{P_{no}/P_{so}}{KTB/P_{si}}, \qquad \text{(II.2.13}a\text{)}$$

this noise figure being thus a direct measure for the available output noise power. Comparing Eqs. (II.2.13a) and (II.2.12a) indicates that the only difference is the substitution of KTB in the former equation for P_{ni} in the latter equation. Now, if the input noise source is at room temperature T, this substitution means no alteration at all, P_{ni} being then equal to KTB by Eq. (II.1.22e). But if the input noise source is at a different temperature T_i, we obtain from the two equations mentioned:

$$N = \frac{T_i}{T} F. \qquad \text{(II.2.13}b\text{)}$$

Thus N may in this case be larger or smaller than F. The practical value of N resides chiefly in its being a direct measure for the available

output noise power transferred to the input. As we shall see in later sections, it may be used as a measure of sensitivity of the four-pole in question, sensitivity being determined by the smallest available input signal value still receivable without being drowned in the noise level.

As in the case of F, we shall now consider two four-poles connected in cascade and of individual noise figures N_1 and N_2 respectively. These individual noise figures and the associated gains have to be defined carefully. Both four-poles are connected in cascade and the signal source is connected to the input of the first one. The individual gains are to be obtained under these particular conditions, as gains do in general depend on the impedance connected to the input terminals of the four-poles as well as on their own structures. The noise figure N_2 is to be obtained using a signal source at its input of impedance equal to the output impedance of the first four-pole in the sequence at a noise temperature equal to that of the source at the input of this first four-pole. The gain g_2 has to be obtained using a signal source of similar impedance at the input terminals of the second four-pole. The available noise powers at the outputs of the first and second four-poles while in cascade connection being P_{no1} and P_{no2}, we require an available signal power:

$$\frac{P_{no2}}{g_2} = \left(N_2 - \frac{T_i}{T}\right) KTB + P_{no1}$$

at the input of the second four-pole while in cascade connection in order to make the available noise ratio at its output equal to unity. This signal power is equivalent to:

$$\frac{P_{no2}}{g_1 g_2} = \frac{\left(N_2 - \frac{T_i}{T}\right) KTB}{g_1} + \frac{P_{no1}}{g_1}$$

at the input of the first four-pole. Upon division by KTB we obtain the noise figure N of the combination. Insertion of N_1 for $P_{no1}/g_1 KTB$ according to the definition yields:

$$N = N_1 + \frac{N_2 - \frac{T_i}{T}}{g_1}. \qquad \text{(II.2.13c)}$$

A value unity of N corresponds to a four-pole containing exclusively passive reactances combined with an input source of temperature T.

REFERENCES: *119, 127, 197, 224, 250, 263, 264.*

II.2.2. Properties of noise ratio and of noise figure. The importance of the notions of noise ratio and noise figure introduced in the preceding sections resides mainly in their properties, which are closely connected with numerous practical applications.

II.2.21. Properties corresponding to a single stage. We consider a four-pole of available output noise power P_{no} and gain g, its noise figure N being given by Eq. (II.2.13a). To this four-pole, feedback is applied, the uncorrelated additional noise sources (if any) introduced by the feedback circuit being disregarded. Feedback is to be such that a fraction α of the available output power is fed back to the input. This may be achieved by connecting a second four-pole of gain α between the output and input pairs of terminals of the original four-pole. The noise figure of this second four-pole connected to a source of room temperature T is then assumed to be unity or very nearly so. Let the available noise output power without feedback be P_{no}. Then a source of available noise power P_{no}/g may be connected to the input terminals of the four-pole, from which in itself all noise sources are now removed. The resulting available noise power at the output is the same as it was originally, i.e., P_{no}. Applying feedback to the noise-free four-pole alters its gain but has no effect upon the source of available noise power P_{no}/g connected to its input terminals. Similarly, the input signal source of available power P_{so}/g remains unaltered by feedback. At the output of the four-pole, including feedback, the noise ratio is P_{no}/P_{so} as it was without feedback, and the noise figure remains also unaltered. This result is expressed as:

Property A: If feedback is so applied to a four-pole that the effects of the additional noise sources of the feedback circuit are negligible, the noise figure of the circuit including feedback is equal to the original noise figure of the four-pole without feedback.

Adhering to the above example of an additional four-pole used as a means of feedback, the conditions of property A are satisfied if this four-pole contains exclusively passive reactances.

Coupling of the signal (and noise) source to the input of a four-pole may be so chosen that the resulting noise figure attains a minimum

value. When this is achieved and feedback according to property *A* is applied to the four-pole, the noise figure remains unaltered. By its definition, this noise figure is dependent on the impedance of the signal source presented to the input terminals. Hence this impedance remains unaltered by the feedback and so does the coupling coefficient. This may be expressed as:

Property B: If coupling between the signal source and the input of a four-pole is chosen so as to correspond to a minimum noise figure, the most favorable coupling coefficient remains unaltered by feedback according to property A.

It may be well to state that coupling corresponding to maximum gain is in general affected by feedback, but such coupling does not as a rule correspond to minimum noise figure.

REFERENCES: *369*, *401*.

II.2.22. Properties corresponding to a combination of stages. We now consider a $2q$-terminal device, having one pair of input terminals and $q - 1$ pairs of output terminals. This may be regarded as $q - 1$ separate four-poles with their input terminals connected in parallel. Each of these four-poles has its own noise figure, of which one is assumed to be the lowest. We apply feedback from the output of this particular four-pole to its input, according to property *A*. This feedback is assumed to be such that a very large gain figure of the four-pole in question results and is indicated as "nearly critical feedback," critical feedback corresponding to an infinitely large gain, to which our "linear" theory does not apply. By this nearly critical feedback the available noise power at the output as well as at the input of this particular four-pole is increased to such a high level as to drown completely the available noise power from any other sources at the input terminals. The same reasoning applies to the available signal power. Hence the noise ratios at the outputs of all the other four-poles become nearly equal to that of the selected one and so do the noise figures. Thus we are led to:

Property C: By applying nearly critical feedback from the output of lowest noise figure to the input of a $2q$-terminal stage, the noise figures corresponding to all the other outputs may be made to approach that of the output mentioned first.

In the discussion leading up to property C no correlation was assumed between the noise powers at the separate output pairs of terminals of the $2q$-terminal stage. In special cases of practical interest such correlation does exist. We shall assume, for simplicity, complete correlation between the noise at two pairs of output terminals. By proper feedback from one of these pairs to the input an additional noise may be created at the other output pair of terminals, being exactly counterphase to the original noise, and thus extinguishing the noise at these output terminals completely. Making the further assumption that by this feedback the signal power at the latter output terminals is not extinguished simultaneously, the noise figure corresponding to it may be made zero. Thus we obtain the

Property D: If the noise at two pairs of output terminals belonging to a $2q$-terminal device is completely correlated, feedback may be applied from one of these pairs to the input so that the noise at the other pair is extinguished. If by this feedback the signal at the latter pair is not extinguished simultaneously, its corresponding noise figure becomes zero.

Assuming two successive four-poles connected in cascade, having the individual noise figures N_1, N_2, and the gains g_1, g_2, we apply feedback from the output of the first stage to its input. By this feedback, if properly chosen, the gain g_1 is increased to g_1', and if critical feedback is approached g_1' is very much higher than g_1. In this case the noise figure of the combination of four-poles becomes, instead of the value given by Eq. (II.2.13c):

$$N' = N_1 + \frac{N_2 - \frac{T_i}{T}}{g_1'} \approx N_1.$$

Thus a decrease of over-all noise figure may be obtained; this is expressed by:

Property E: By applying nearly critical feedback from the output of the first of two successive four-poles to its input the over-all noise figure may be made to approach that of the first four-pole.

REFERENCES: *365, 396, 401.*

II.2.3. Applications. Though the main applications of the preceding definitions and properties to reception stages will be dealt with in

chapter VI, some simple applications of an introductory character are useful here by way of illustration.

II.2.31. Noise figures of four-poles consisting of single impedances. For the calculation of noise figures the composition of two sources of uncorrelated power, either in series or in parallel connection, is often required. Assuming two sources of available powers P_o and P_1, their impedances being Z_o and Z_1 with the real parts R_o and R_1, we shall first connect them in series. The resulting available power is:

$$P = \frac{P_o}{1 + \frac{R_1}{R_o}} + \frac{P_1}{1 + \frac{R_o}{R_1}}. \qquad \text{(II.2.31}a\text{)}$$

If they are connected in parallel we obtain a resulting available power:

$$P = \frac{P_o}{1 + \frac{R_1}{R_o}\left|\frac{Z_o}{Z_1}\right|^2} + \frac{P_1}{1 + \frac{R_o}{R_1}\left|\frac{Z_1}{Z_o}\right|^2}. \qquad \text{(II.2.31}b\text{)}$$

These equations are simple deductions from the rules mentioned in sections II.1.11 and 12. It is noteworthy that the sums of Eqs. (*a*) and (*b*) both yield $P = P_o$ if $P_o = P_1$, independently of the impedance values. Now consider a four-pole as shown in Figure 44, the impedance Z_1, or rather its real part, being at a temperature T_1. If we connect a source of available signal power P_s and impedance Z_o at a temperature T_o to the terminals 1, 2 the resulting available signal power at the terminals 3, 4 is:

$$P_s g_1 = \frac{P_s}{1 + \frac{R_1}{R_o}\left|\frac{Z_o}{Z_1}\right|^2}, \quad \text{whence } g_1 = \frac{1}{1 + \frac{R_1}{R_o}\left|\frac{Z_o}{Z_1}\right|^2}. \qquad \text{(II.2.31}c\text{)}$$

Eq. (*b*) gives us the available noise power at the terminals 3, 4 if the source is connected to 1, 2. Hence the noise figure N_1 becomes:

$$N_1 = \frac{T_o}{T} + \frac{T_1}{T}\,\frac{1 + \frac{R_1}{R_o}\left|\frac{Z_o}{Z_1}\right|^2}{1 + \frac{R_o}{R_1}\left|\frac{Z_1}{Z_o}\right|^2}. \qquad \text{(II.2.31}d\text{)}$$

This noise figure attains its lowest value if the ratio $R_1/R_o\left|Z_o/Z_1\right|^2$ in the numerator is decreased and made to approach zero. A high value

of $|Z_1|$ is obviously favorable to this aim. If Z_1 is a tank circuit, as shown in Figure 42, the value of $|Z_1|$ at the resonant frequency for which $\omega^2 LC = 1$ is: $Z_1 = L/CR$, and this is the highest value of $|Z_1|$ obtainable, the impedance being in this case purely real. If the frequency interval Δf under consideration is centered around this resonant frequency we obtain the lowest noise figure of the four-pole under discussion. Any detuning by which Δf is centered round a frequency off resonance entails an increase in noise figure N_1.

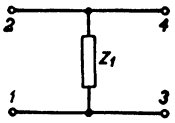

FIG. 44 Four-pole consisting of a single shunt impedance.

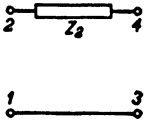

FIG. 45 Four-pole consisting of a single series impedance.

Another simple four-pole is shown in Figure 45, the impedance Z_2 being at a temperature T_2. Its gain may be obtained by reasoning like that applied above, a signal source of available power P_s and impedance Z_o at 1, 2 causing an available signal power at the output terminals 3, 4:

$$P_s g_2 = \frac{P_s}{1 + \dfrac{R_2}{R_o}}, \quad \text{whence } g_2 = \frac{1}{1 + \dfrac{R_2}{R_o}}.$$

By application of Eq. (*a*) we obtain the available noise power at the output and thence the noise figure:

$$N_2 = \frac{T_o}{T} + \frac{T_2}{T} \frac{1 + \dfrac{R_2}{R_o}}{1 + \dfrac{R_o}{R_2}}. \qquad \text{(II.2.31}e\text{)}$$

This noise figure attains its lowest value if R_2/R_o is made to approach zero. If the two four-poles of Figures 44 and 45 are connected in cascade, the output terminals 3, 4 of the network of Figure 44 being attached to the input terminals 1, 2 of the network of Figure 45, the resistance R_o in Eq. (*e*) has to be replaced by the real part R of Z, this

being the parallel connection of Z_o and Z_1. Thus:

$$\frac{R}{|Z|^2} = \frac{R_o}{|Z_o|^2} + \frac{R_1}{|Z_1|^2}, |Z| = \frac{|Z_o Z_1|}{|Z_o + Z_1|}, \quad \text{hence } R = \frac{R_o|Z_1|^2 + R_1|Z_o|^2}{|Z_o + Z_1|^2}$$

and:

$$N_2' = \frac{T_o}{T} + \frac{T_2}{T} \frac{1 + \dfrac{R_2|Z_o + Z_1|^2}{R_o|Z_1|^2 + R_1|Z_o|^2}}{1 + \dfrac{R_o|Z_1|^2 + R_1|Z_o|^2}{R_2|Z_o + Z_1|^2}}. \qquad \text{(II.2.31}f\text{)}$$

By application of Eq. (II.2.13c) the noise figure N of the cascade connection results directly from Eqs. (II.2.31f, d) and (c):

$$N = N_1 + \frac{N_2' - \dfrac{T_o}{T}}{g_1}$$

II.2.32. Noise figures of electronic tubes. The noise power attached to an impedance was in the preceding section given an arbitrary temperature. By this artifice the noise of diodes as shown in Figure 38 may be treated as the noise caused by the resistive part of the diode's impedance Z_d at a properly chosen temperature T_d. This will work out well as long as the resistive part is of positive sign —which is not always the case at extreme-high frequencies. As more complicated tubes such as triodes and multi-element tubes may be dealt with as a succession of diodes (see Figs. 39 and 40), this procedure may also be applied to them subject to a similar restriction. Due account should, however, be taken of correlation which causes a number of alterations to the pattern set up in the preceding section. Thus in an ideal triode all three fluctuation currents i_1, i_2, and i_3 of Figure 39 are completely correlated. Considering the input circuit of a triode amplifier stage, we obtain the picture of Figure 46, in which Z_o represents the impedance of the input signal source, Z_1 the impedance of the input tank circuit,

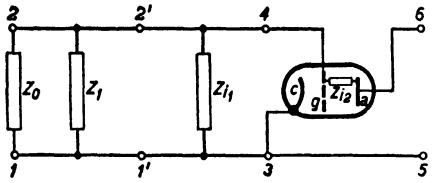

FIG. 46 Circuit corresponding to two shunt impedances Z_o and Z_1 shunted to the control grid and cathode terminals of a triode, the interelectrode impedance being Z_{i1}. The interelectrode impedance between grid and anode is Z_{i2}.

and Z_{i1} the impedance marked equally in Figure 39 between cathode and grid. The section of this picture between the terminals 1, 2 and 3, 4 may obviously be dealt with as a succession of two four-poles as shown in Figure 44. The further triode is contained in the four-pole between the terminals 3, 4 and 5, 6; this network is extremely simple, containing only one impedance Z_{i2} and thus being equivalent to the four-pole of Figure 45. The entire problem may therefore be treated in three simple steps. The only new feature resides in the complete correlation between the noise powers corresponding to Z_{i1} and to Z_{i2}.

Considering a series connection of two completely intercorrelated sources of power of impedances Z_{i1} and Z_{i2}, their real parts being R_{i1} and R_{i2} and of voltages V and $\alpha V \exp(j\varphi)$, α being a positive number and φ a phase angle of positive or negative sign, the resulting available power is:

$$P = \frac{|V^2|(1 + \alpha^2 + 2\alpha \cos \varphi)}{4(R_{i1} + R_{i2})} = P_1 \frac{1 + \alpha^2 + 2\alpha \cos \varphi}{1 + \dfrac{R_{i2}}{R_{i1}}}, \quad \text{(II.2.32}a\text{)}$$

if P_1 is the available power associated with the first source mentioned. This equation may be readily applied to the composition of the four-pole with terminals 1′, 2′, and 3, 4 and the four-pole with terminals 3, 4 and 5, 6 in Figure 46. After this, the composition with the further four-pole of terminals 1, 2 and 1′, 2′ may follow the lines indicated in the preceding section, as only uncorrelated noise powers are to be composed in this case (see sections VI.1.12, VI.1.22 and Figs. 150 and 153).

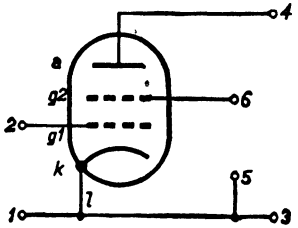

FIG. 47 Example of six-terminal network represented by a tetrode, the input terminals being 1,2 and the two pairs of output terminals 3, 4 and 5, 6 respectively.

As an example of a six-terminal device we consider a tetrode (Fig. 47). The complete amplifier tube acts between the input terminals 1, 2 and the output terminals 3, 4. An auxiliary pair of terminals 5, 6 is connected to cathode and screen grid. If we disregard all fluctuations except those due to current partition (corresponding to i_6 in Fig. 40), the resulting fluctuations at the pair of terminals 3, 4 are completely correlated to those at the pair 5, 6. We may apply feedback from 5, 6 to 1, 2 and discuss the effect at 3, 4. According to the argument

preceding property D of section II.2.22, the correlated fluctuations at 3, 4 may be completely extinguished by such feedback. The crucial question is whether the signal would be extinguished simultaneously by this procedure. From Figure 40 it is obvious that the partition fluctuation current i_6 flows counterphase (phase difference π) if viewed from the screen grid and from the anode respectively. On the other hand, the signal currents resulting from the input terminals 1, 2 generally have in-phase components to screen and anode (similar to the currents i_4 and i_5 of Fig. 40). Hence if the feedback is such that the partition fluctuation current to the screen is extinguished, the signal current to the anode is reinforced. Thus the noise figure completely correlated to partition fluctuations may be reduced to zero by application of such feedback. An entirely similar argument may be applied to fluctuations caused by secondary electronic emission.

REFERENCES: *197, 365, 367, 370, 372, 396, 401, 408.*

CHAPTER III

ANTENNAS

Antennas are the eyes for electromagnetic waves. They capture part of the specific power of those waves and make this captured power available at their terminals. The following discussion of their main properties has the aim of enabling the reader to construct an antenna suitable to his purpose.

III.1. Reception Antennas as Sources of Power

It is of fundamental importance to realize the concept of reception antennas as sources of power, signal power as well as noise power. The present sections are devoted to the elaboration of this concept.

III.1.1. Essential characteristics of reception antennas. This concept is closely related to the essential characteristics of reception antennas; these will be dealt with below.

III.1.11. Dipole antennas. If the complete system—incorporating the transmitting antenna with its two input terminals, the reception antenna with its pair of output terminals, and the intervening medium through which propagation takes place—is viewed, it may obviously be compared with a four-pole having such twin pairs of terminals. Under certain restrictions as to signal strength this four-pole is very nearly *linear*, i.e., a.c.'s at its output are proportional to alternating voltages at its input. A further restriction will be placed on the medium of propagation, excluding the effects of steady magnetic fields on ionic-layer properties (discussed in section I.1.41) which cause the splitting up into ordinary and extraordinary rays. The latter exclusion seems to be serious inasmuch as these effects are frequently present in long-distance transmission. However, as the theorem to be based on it is mainly applied to hypothetical antennas for the purposes of deduction, its effects are in reality far less serious than would appear at first sight. Under these restrictions the four-pole mentioned is *symmetric*, its gain being equal in either direction if identical antennas are used at

both ends. This is one way of expressing the reciprocity theorem of antennas (references *56*, *324*).

The crux of the present application of this reciprocity theorem is to assume one of the two antennas under consideration to be extremely simple. The simplest antenna known is the so-called dipole antenna, consisting of a straight wire with two suitable plates forming capacities at its ends, all dimensions being extremely small compared to one-quarter of a wavelength in the surrounding medium. If this antenna is interrupted at its center and an alternating voltage is applied to its resulting terminals, the alternating current along the wire is of approximately uniform strength. If this r.m.s. current is I_d, the electric-field strength E in the equatorial plane at a distance r, large compared to the wavelength, is:

$$E = \frac{60\pi}{r} I_d \frac{l}{\lambda} \qquad \text{(III.1.11}a\text{)}$$

l being the dipole's length and λ the wavelength in the surrounding medium, assumed to be air. In a direction including an angle Θ with the dipole's axis we have: $E_\Theta = E \sin \Theta$. The electric-field strength is of course polarized in a plane through the dipole's axis and is tangent to a sphere centered at the dipole's center. From these two equations we may easily obtain the total power radiated by the dipole:

$$P_r = 2\pi \int_0^\pi r^2 \sin \Theta \frac{E_\Theta^2}{120\pi} d\Theta = 80\pi^2 \frac{l^2}{\lambda^2} I_d^2 \quad \text{watts,} \qquad \text{(III.1.11}b\text{)}$$

using the expression (I.1.11c) for the specific power p of a plane wave. Equating this power P to $I_d^2 R_{rd}$, we obtain the radiation resistance R_{rd} of a dipole antenna in vacuum or air:

$$R_{rd} = 80\pi^2 \frac{l^2}{\lambda^2}. \qquad \text{(III.1.11}c\text{)}$$

In case that the surrounding medium is of dielectric coefficient ϵ, this expression must be multiplied by $1/\sqrt{\epsilon}$, λ then being the wavelength in this medium (section I.1.23). If a dipole is placed in a plane wave of polarization parallel to the dipole's axis and of electric-field strength E, the dipole being tuned to the angular frequency ω of the incident wave (i.e., $\omega^2 \times LC = 1$, L and C being the dipole's inductance and

capacitance), a current I will flow in the dipole, given by:

$$|I| = \frac{|E|l}{R_{rd}}. \qquad \text{(III.1.11}d\text{)}$$

Expressing E by P_r, using Eqs. (a) and (b) we obtain:

$$|I| = \frac{\sqrt{45P_r}}{r}\,\frac{l}{R_{rd}}. \qquad \text{(III.1.11}e\text{)}$$

REFERENCES: *56, 310, 324.*

III.1.12. Application of reciprocity theorem. Now the dipole transmitting antenna is replaced by a different antenna emitting radiation of equal polarization, the resulting electric-field strength depending on the elevation angle Θ and on the azimuthal angle φ by the function $\chi(\Theta,\varphi)$, this function being unity, if $\Theta = \pi/2$ and $\varphi = 0$. Assuming the squares of the resulting field strengths due to a dipole and to this transmitting antenna to have the ratio $1/g_r$ in the optimal direction, if total radiated powers are equal, we obtain:

$$g_r = \frac{\int_0^{\pi}\int_0^{2\pi} \sin^3\Theta\, d\Theta\, d\varphi}{\int_0^{\pi}\int_0^{2\pi} \{\chi(\Theta,\varphi)\}^2 \sin\Theta\, d\Theta\, d\varphi}, \qquad \text{(III.1.12}a\text{)}$$

this quantity being indicated as the radiation gain of the antenna over a dipole. This gain figure may be expressed in db.

The current induced in a tuned dipole reception antenna oriented in the plane of polarization and perpendicular to the radial distance r from the transmitting antenna ($r \gg \lambda$) is:

$$|I| = \frac{\sqrt{45g_rP}}{r}\,\frac{l}{R_{rd}}\,\chi(\Theta,\varphi), \qquad \text{(III.1.12}b\text{)}$$

P being the power radiated by the latter antenna. Expressing the power P by the voltage V at the input terminals of the transmitting antenna, of impedance $Z_r = R_r + jX_r$, we obtain:

$$P = \left|\frac{V}{Z_r}\right|^2 R_r,$$

and thus Eq. (*b*) may be transcribed:

$$|I| = \left|\frac{V}{Z_r}\right| \frac{\sqrt{45 g_r R_r}}{r} \frac{l}{R_{rd}} \chi(\Theta, \varphi). \qquad \text{(III.1.12}c\text{)}$$

We are now ready to apply the reciprocity theorem. Referring to Figure 48, the case considered in Eqs. (*b*) and (*c*) is pictured in the diagram marked *a*. In the diagram marked *b* the antennas are the same and of equal mutual position but the voltage V is applied to the tuned dipole antenna's input terminals now acting as a transmitter,

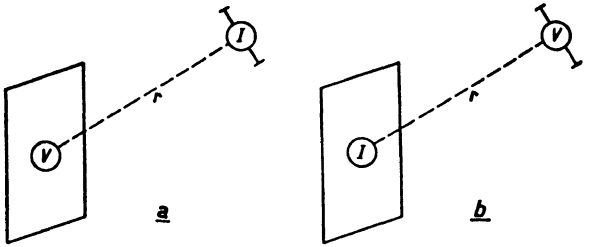

FIG. 48 Picture of a reception and a transmission antenna suitable for the application of the reciprocity theorem, the r.m.s. currents and voltages being I and V respectively.

and the current I is measured at the short-circuited terminals of the second antenna now used for reception. By this theorem, Eq. (*c*) applies equally as well to Figure 48*b* as to Figure 48*a*. Thus we have obtained the short-circuit output current I of an almost arbitrary reception antenna expressed in terms of the tuned transmitting dipole's input voltage V. We may still go one step further and express I in terms of the electric-field strength E created by the transmitting dipole at the reception antenna. Using Eq. (III.1.11*a*) and expressing I_d in terms of V as follows: $I_d = V/R_{rd}$, we obtain:

$$|E| = \frac{|V|}{r} \sqrt{\frac{45}{R_{rd}}} \qquad \text{(III.1.12}d\text{)}$$

and hence, by Eq. (III.1.12*c*) and using $l/\sqrt{R_{rd}} = \lambda/(\pi\sqrt{80})$:

$$|I| = \frac{|E|}{|Z_r|} \frac{\lambda}{\pi} \sqrt{\frac{g_r R_r}{80}} \chi(\Theta, \varphi). \qquad \text{(III.1.12}e\text{)}$$

The directional sensitivity is obviously described by the same angular

radiation function χ as the transmitted field strength created at a great distance by the same antenna used for transmitting purposes. In short, we may say: the radiation diagrams of an antenna used for reception or transmission are equal. Thus important deductions may be derived from the application of reciprocity.

REFERENCES: *45, 56, 60, 188, 310.*

III.1.13. Expressions of antenna characteristics. As mentioned above, a reception antenna may be considered as a source of power, and its characteristics as such will now be derived from the preceding expressions. In Eq. (III.1.12*e*) the current in a short-circuit connection of the antenna's output terminals was given. At the same time it is known that an impedance Z_r exists between these terminals if determined by means of an impedance-measuring device (see chapter V). This situation has already been discussed in section II.1.11. We may replace the reception antenna at its terminals by a constant-current generator of infinite internal impedance, generating the current I_o and acting in parallel to an impedance Z_r. Any outer impedance has to be paralleled to Z_r. The available power of this source is

$$P_a = \frac{|I_o|^2 \, |Z_r|^2}{4R_r}. \qquad \text{(III.1.13}a\text{)}$$

An equivalent representation of the reception antenna at its terminals is, according to section II.1.11, by a constant-voltage generator of zero internal impedance generating a voltage $|V_o| = |I_o Z_r|$ and acting in series with the impedance Z_r. Any outer impedance has to be connected in series with both voltage generator and Z_r. The available power, expressed by V_o, is:

$$P_a = \frac{|V_o|^2}{4R_r}. \qquad \text{(III.1.13}b\text{)}$$

The current I_o is given in Eq. (III.1.12*e*). By means of this latter equation and of the general expression $p = |E|^2/120\pi$ for the specific power of the incident plane waves (see section I.1.11) we obtain:

$$P_a = p \frac{3}{8\pi} \lambda^2 g_r \chi^2. \qquad \text{(III.1.13}c\text{)}$$

In the case of a dipole reception antenna: $g_r = 1$, and if the incident waves arrive from the direction of optimum sensitivity: $\chi = 1$. We

may ascribe the available power P_a at the antenna's terminals to a surface area S_e effective in capturing power from the incident wave system. This effective area is, by Eq. (*c*):

$$S_e = \frac{3}{8\pi} \lambda^2 g_r \chi^2. \qquad \text{(III.1.13}d\text{)}$$

In the case of a dipole, when $g_r = 1 = \chi$, this area is thus approximately equal to a square of face $\lambda/2.9$. At one single frequency the antenna's characteristics may thus be completely expressed by the ratio of its available power to the specific power p of the incident waves and by the complex impedance $Z_r = R_r + jX_r$ at its terminals. The ratio is the antenna's effective surface area S_e as given by Eq. (*d*). It is determined by the incident wavelength λ, the antenna's gain g_r (see Eq. III.1.12*a*), and its angular radiation function χ (or angular directivity).

We shall now consider a frequency range of given band width. At a given value of incident specific power p the above characteristics are dependent on frequency as far as are the impedance Z_r and the effective area S_e. The latter quantity is dependent on frequency by the three multipliers λ, g_r, and χ being so dependent. In most cases the reception antenna will be oriented in such a way as to have $\chi = 1$, and in such cases the frequency dependence of S_e is due to the two multipliers λ and g_r. This frequency dependence, a characteristic peculiar to the antenna under discussion, will be considered in section III.2 for some types of reception antennas. As soon as the frequency characteristics are known it is possible to evaluate the antenna's behavior throughout a frequency range of given width by an appropriate averaging process.

REFERENCES: *9, 116, 128, 310, 406.*

III.1.2. Noise of reception antennas. In order to bring our discussion of antennas in line with the noise considerations of chapter II, we shall now deal with the available noise power, from several causes, at the antenna's terminals.

III.1.21. Noise power captured. We shall first suppose the reception antenna to be situated inside an enclosure of dimensions large compared to the wavelengths under consideration. This enclosure is at a uniform temperature T_a and the radiation inside its walls is so-called "blackbody" radiation at equilibrium at that temperature. These physical

conditions are rarely met exactly in practical cases, but they make discussion easy and the effect of deviations from them will be discussed subsequently. The enclosure is pictured in Figure 49. If a small element of solid angle $\Delta\Gamma$ is drawn from this antenna, the element of specific power Δp incident on the antenna in a frequency interval Δf centered round a frequency f corresponding to a wavelength λ in the medium of the enclosure is, by radiation statistics:

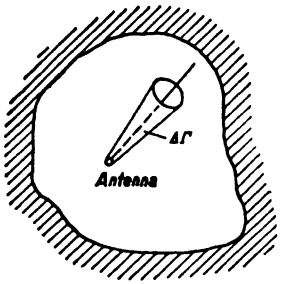

FIG. 49 Reception antenna in an enclosure the walls of which are at a uniform temperature and emit blackbody radiation. Cone of solid angle $\Delta\Gamma$.

$$\Delta p = \frac{2KT_a}{\lambda^2}\,\Delta f \Delta\Gamma. \quad \text{(III.1.21}a\text{)}$$

We recognize here upon division of Δp by $\Delta f \times \Delta\Gamma$ the specific power per unit of frequency and of solid angle already used in section I.1.44 as specific power p_{kca} per kc/s and per radian of solid angle. If this element Δp of specific power impinges upon an antenna of angular directivity χ and gain g_r, the resulting element ΔP_a of available power at the antenna's terminals is, by Eq. (III.1.13c):

$$\Delta P_a = \tfrac{1}{2}\Delta p \frac{3}{8\pi}\lambda^2 g_r \chi^2 = \frac{KT_a}{\lambda^2}\,\Delta f \Delta\Gamma \frac{3}{8\pi}\lambda^2 g_r \chi^2. \quad \text{(III.1.21}b\text{)}$$

The multiplier $\frac{1}{2}$ of Δp is due to the antenna's being assumed to be of linear polarization. The incident radiation has random polarization, and its component, polarized in the plane containing the antenna's direction of polarization, has only half of the total incident specific power. As the element $\Delta\Gamma$ of solid angle is equal to: $\Delta\Gamma = \sin\Theta\, d\Theta\, d\varphi$, we obtain an available power P_{na} upon integration over all elements $\Delta\Gamma$ of:

$$P_{na} = KT_a \frac{3}{8\pi} g_r \Delta f \int_0^{\pi}\int_0^{2\pi} \chi^2 \sin\Theta\, d\Theta\, d\varphi.$$

Using the value resulting from Eq. (III.1.12a) for the above integral, the value of P_{na} works out as:

$$P_{na} = KT_a \Delta f. \quad \text{(III.1.21}c\text{)}$$

Thus this available power corresponding to a frequency interval Δf

is exactly the same as that corresponding to a resistance at a temperature T_a according to Eq. (II.1.22*e*). The resistance at the antenna's terminals being the radiation resistance R_r, this result may be expressed by saying that under the present conditions the radiation resistance R_r at the antenna's terminals provides an available noise power P_{na} corresponding to the temperature T_a of equilibrium of the surrounding enclosure.

Under actual operating conditions the enclosure mentioned does not always exist. If the reception antenna is installed in the open, the earth's surface and parts of the reflecting ionospheric layers act as walls of an enclosure, but the temperature of these walls is not uniform nor do their characteristics coincide with conditions necessary for black-body radiation as was assumed in the above derivation. Hence, though Eq. (*c*) may still be used, the value of T_a to be inserted is somewhat doubtful and will often be an average of temperatures of surrounding objects on the earth's surface and of the ionosphere. At extreme-short waves highly directive antennas are often used, thus confining the received radiation to a relatively small solid angle centered round the direction of optimum reception. Under such conditions it is obvious that the effective temperature of distant objects within that solid angle determines the value of T_a in Eq. (*c*). In particular, if Δf is centered round a frequency above 30 mc/s, the ionospheric layers are hardly reflective and hence, if the antenna's optimum direction points toward the sky, a very low value of T_a, only slightly above zero, would be expected. This expectation has in many respects been borne out by experiments at frequencies of 300 to 30,000 mc/s. But at frequencies between 20 and 300 mc/s the experiments have revealed that extremely high values of T_a have to be associated with particular directions of the sky pointing toward the Milky Way. Values of 10,000 to 15,000 degrees were found at about 20 mc/s. Obviously radiation issuing from the region of the galactic agglomeration of stars is the cause of these phenomena (see section I.1.44 and references *175*, *291*, *292*). According to recent investigations the temperature mentioned is about 15,000° Kelvin at 40 mc/s, about 6000° Kelvin at 60 mc/s and about 2100° at 90 mc/s (reference *400*) above the temperature, associated with reception noise corresponding to other regions of the sky.

When highly directive reception antennas (parabolic reflector type) at frequencies between 3000 and 30,000 mc/s were pointed toward

the sun's disk, temperatures T_a of about 20,000° C. were found experimentally (reference *329*). This temperature coincides with the value usually associated with the sun's surface by astronomers at these frequencies (reference *231*). At lower frequencies, much higher effective temperatures of the sun's disk were derived theoretically (reference *231*) and confirmed experimentally (reference *271*), about a million degrees occurring at 200 mc/s.

REFERENCES: *44, 48, 157, 163, 166, 175, 231, 270, 271, 291, 292, 329, 400.*

III.1.22. Noise ratio and noise figures. As with other two- and four-terminal networks, a noise ratio as well as a noise figure may be assigned to a reception antenna. The antenna's noise ratio is the ratio of available noise power to available signal power at its terminals. The available noise power P_{na} being given by Eq. (III.1.21*c*) and the available signal power P_a by Eq. (III.1.13*c*), we obtain for the noise ratio the expression:

$$\frac{P_{na}}{P_a} = \frac{KT_a\Delta f}{p\,\frac{3}{8\pi}\lambda^2 g_r \chi^2}, \qquad \text{(III.1.22}a\text{)}$$

p being the specific power of the incident signal radiation. This noise ratio obviously depends on the band width Δf under consideration, as well as on the frequency round which Δf is centered and on the antenna's characteristics expressed by g_r and χ^2. From Eq. (*a*) we may conclude that a high value of radiation gain g_r is favorable to a low noise ratio, this being inversely proportional to g_r. Making use of Eq. (III.1.13*d*), we may say that the noise ratio is inversely proportional to the product of incident specific signal power and of the antenna's effective area S_e:

$$\frac{P_{na}}{P_a} = \frac{KT_a\Delta f}{pS_e}. \qquad \text{(III.1.22}b\text{)}$$

In the case of a dipole reception antenna, S_e is proportional to λ^2 and hence the noise ratio is directly proportional to the square of the frequency round which Δf is centered.

The noise figure of an antenna may be obtained by making the available signal power $P_a = pS_e$ of Eq. (*b*) equal to the available noise power and then dividing the resulting available signal power by KTB,

where T represents the room temperature. Thus we find:

$$N = \frac{T_a}{T} \qquad \text{(III.1.22}c\text{)}$$

for the antenna's noise figure. We shall adhere mainly to this definition in the course of the present book. Obviously this noise figure does not depend directly on the antenna's characteristics (gain and directivity), but only on the effective temperature T_a of the noise radiation captured. Inasmuch as this temperature depends on these characteristics, the noise figure N does so.

A different definition has been proposed for the noise figure of a reception antenna, starting from the concept of the complete system between the input terminals of the transmitting antenna and the output terminals of the reception antenna regarded as a four-pole. In this case the signal generator has to be connected to the input terminals of the transmitting antenna, the signal strength at these terminals being adjusted until a value of unity is obtained for the noise ratio of Eq. (*b*). If the ratio of available signal power at the reception antenna's terminals to the available signal power at the transmitting antenna's input terminals is $1/A$ (A being the power attenuation), we would obtain a value AT_a/T instead of Eq. (*c*) for the noise figure of a reception antenna. By the use of this definition the characteristics of transmitting as well as of reception antennas are directly involved in the noise figure.

REFERENCES: *44, 48, 127, 128, 267.*

III.2. CHARACTERISTICS OF SPECIAL RECEPTION ANTENNAS

In order to judge the suitability of a reception antenna for a definite purpose its characteristics, radiation gain g_r and angular directivity χ, must be known. These characteristics will now be discussed for certain types of frequent application.

III.2.1. Wire antennas. The antennas belonging to this type are based on the use of wires as main elements, a wire being in general an object of which one dimension largely exceeds the others.

III.2.11. Single-wire antennas. The most popular reception antenna consists of a single straight wire, interrupted at a suitable place so as to obtain a pair of output terminals. We shall assume that the total length of the antenna is $2l$ and that the interruption is

at the center of its length. The two ensuing terminals are supposed to be at a mutual distance, very small in comparison with one-quarter wavelength in the surrounding medium. The cross-section is assumed to be uniform, circular, and of radius a. With the antenna's characteristics the quantity $U = 2 \ln (2l/a)$, where ln is the Napierian logarithm, plays an important part. The ratio $2l/a$ is supposed to be

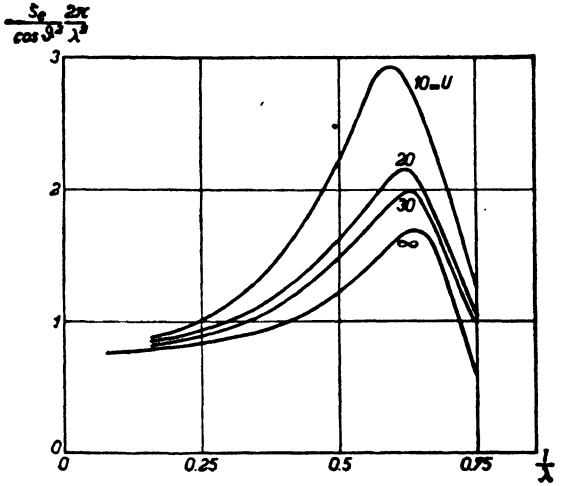

FIG. 50 Representation of the effective reception area S_e multiplied by 2π and divided by $(\cos\vartheta)^2$ times λ^2, ϑ being the angle included by the electric-field strength and a plane fixed by the direction of propagation and the antenna's axis and λ the wavelength in air. Horizontal scale: Ratio of l (half the antenna's length) to the wave length. Curves for different values of $U = 2 \ln \frac{2l}{a}$ (reference *194*).

such that U obtains a value above, say, 10. The direction of propagation of waves includes an angle $\pi/2 - \Theta$ with the wire's axis. The electric-field strength of the waves, being perpendicular to their direction of propagation, is assumed to include an angle ϑ with the plane fixed by the direction and the wire's axis.

The antenna is completely characterized by the available power P_a and by the impedance Z_r at its terminals. By Eqs. (III.1.13*c*) and (*d*) the available power is:

$$P_a = pS_e, \qquad \text{(III.2.11}a\text{)}$$

p being the specific power of the incident signal waves and S_e the antenna's effective area. Because of the circular symmetry round

the antenna's axis, S_e does not depend on the azimuthal angle φ in a plane perpendicular to the wire, but it does depend on the angles Θ and ϑ. The latter dependence is simple, S_e containing the multiplier $(\cos\vartheta)^2$ and no other function of ϑ. In the case $\Theta = 0$, i.e., for incident waves propagated perpendicularly to the antenna's axis, the

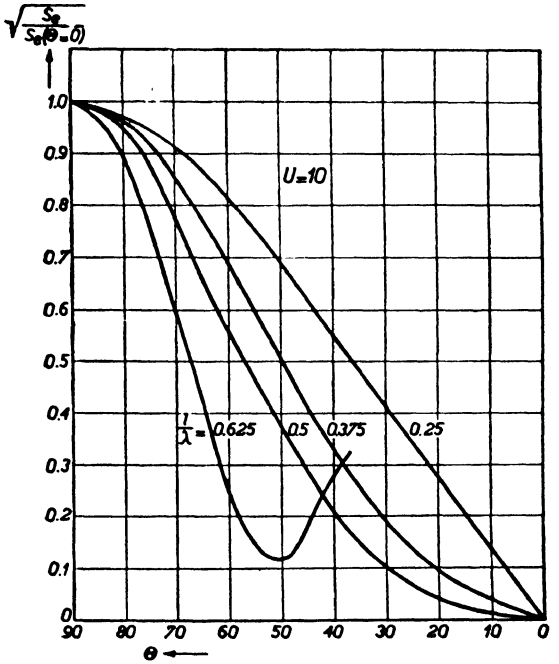

FIG. 51 Square root of ratio of effective reception area S_e at an angle of incidence Θ to S_e at $\Theta = 0$ as dependent on Θ (horizontal scale) if $U = 10$ (see Fig. 50). Curves for different values of ratio $\frac{l}{\lambda}$ (reference *194*).

value of $S_e/(\cos\vartheta)^2$ is shown in Figure 50 for four different values of U. From Figure 50 we may conclude that an antenna of total length $2l$, equal to about 1.25 wavelengths, has an optimum value of effective area under the conditions quoted. If the direction of arrival includes an angle with the antenna's axis, the effective area is altered considerably, as is shown by Figures 51 and 52, giving the square root of the ratio of S_e corresponding to an angle Θ to S_e if $\Theta = 0$, other conditions being equal. These two figures are equivalent to what may

be called directional-sensitivity diagrams, as their vertical scale is proportional to the generator voltage which may be substituted at the antenna's terminals for the action of the incident waves. As stated above, the antenna's impedance Z_r must be known, as well as its available power, in order to evaluate completely its effect in reception

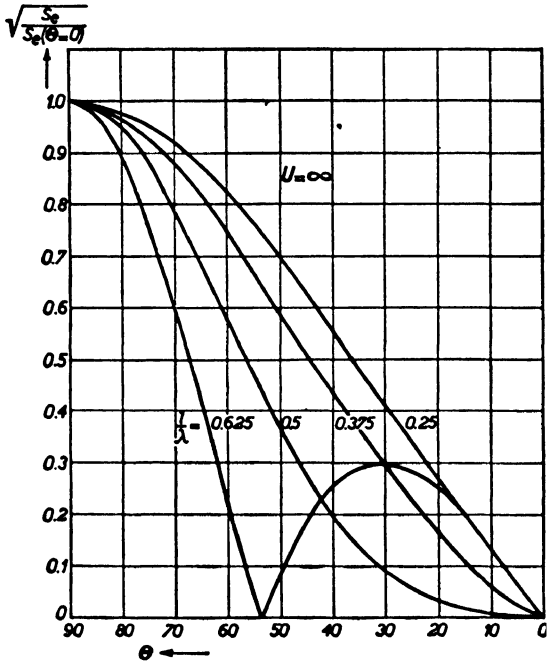

FIG. 52 Similar to Fig. 51 but for $U = \infty$ (reference *194*).

circuits. This impedance $Z_r = R_r + jX_r$ has a real part R_r which is approximately independent of U, whereas X_r is dependent on U. The value of R_r (sin $2\pi l/\lambda)^2$ is shown in Figure 53 as dependent on l/λ, while X_r is shown in Figure 54 for the particular case in which $U = 10$. Figures 50 to 54 give a fairly complete picture of the characteristics of straight, center-tapped wire antennas. In all the calculations from which these figures result, losses in the antenna wire itself (eddy currents) have been completely disregarded. In practice, this is justified only if good conductors, such as copper, are used. With

other conductors the available power at the terminals may be considerably less than would result from Figures 50 to 52.

REFERENCES: *28, 60, 103, 137, 147, 153, 191, 192, 194, 204, 206, 210, 236, 337.*

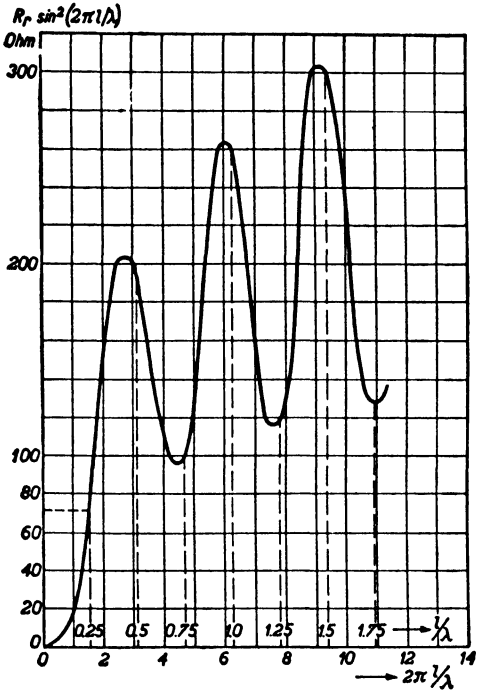

FIG. 53 Radiation resistance of a center-tapped straight antenna as dependent on the ratio l (half its length) to the wavelength λ. Vertical scale represents product of radiation resistance R_r and $\sin^2 2\pi \frac{l}{\lambda}$ (reference *210*).

III.2.12. Loop antennas. The wire antennas considered in the preceding section may be regarded as an extension of the dipole antennas discussed in section III.1.11. We shall now consider loop antennas of dimensions that are small compared with one-quarter wavelength in the surrounding medium. Such loop antennas may be regarded as simple elements much like dipole antennas. For the sake of simple derivations the loop is assumed to be a square of face a, its plane including an angle φ with the direction of the incident waves (Fig. 55),

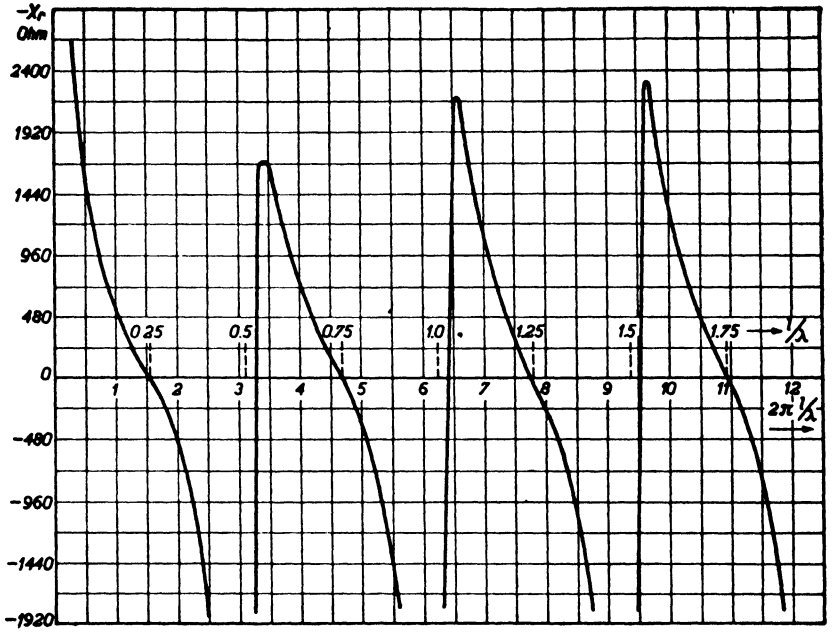

FIG. 54 Radiation reactance X_r of a center-tapped straight wire antenna as dependent on the ratio $\frac{l}{\lambda}$ if $U = 10$ (reference *210*).

The incident electric-field strength E being directed parallel to faces nos. 1 and 2 of the square loop, no voltage will result in faces nos. 3 and 4, as they are perpendicular to E. Let the field strength at 1 be E. Then the field strength at 2 is $E \exp(-jkb)$, where $k = 2\pi/\lambda$. The voltage received along 1 is (assuming the current to be uniform along this face) $V_1 = aE$, and the voltage along 2 works out as:

$$V_2 = aE \exp\left(-j\frac{2\pi b}{\lambda}\right) \approx aE\left(1 - j\frac{2\pi b}{\lambda}\right).$$

Hence the resulting voltage V_o of reception is, as $b = a \cos\varphi$:

$$|V_o| = |V_1 - V_2| = a\,|E|\,\frac{2\pi a|\cos\varphi|}{\lambda} = |E\cos\varphi|\,\frac{2\pi S_l}{\lambda}, \quad \text{(III.2.12}a\text{)}$$

$S_l = a^2$ indicating the loop's surface area. This result does not depend on the actual shape of the loop, as long as its dimensions are small as stated, its area being S_l.

By running a r.m.s. current I through the four dipoles constituting the square loop of Figure 55 its radiation at a distance, large compared with its dimensions and with the wavelength, may be calculated along the lines carried out in section III.1.11 for a single dipole. By integration of the specific power resulting herefrom over a sphere of large radius the total average radiation power is obtained. Equating this to I^2R_r, we find the radiation resistance R_r of a loop antenna:

$$R_r = \frac{320\pi^4}{\lambda^4} S_l^2 \quad \text{(Ohm)}. \quad \text{(III.2.12}b\text{)}$$

The available reception power is, as usual, $P_a = |V_o|^2/(4R_r)$ or:

$$P_a = \frac{|E|^2}{120\pi} \frac{3}{8\pi} \lambda^2 (\cos\varphi)^2$$

$$= p \frac{3}{8\pi} \lambda^2 (\cos\varphi)^2 = pS_e, \quad \text{(III.2.12}c\text{)}$$

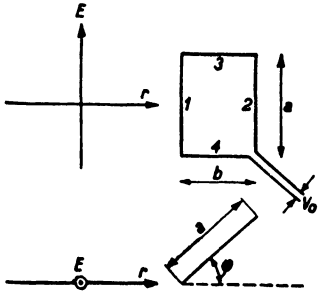

FIG. 55 Representation of square-loop antenna in an electric field of strength E.

the expression $|E^2|/(120\pi)$ being replaced by the specific power p of the incident waves according to section I.1.11 and S_e being the effective area of the reception loop antenna. This effective area is obviously quite comparable to that of a dipole reception antenna.

If proper balance is maintained to keep the two terminals of the loop at potentials of exactly equal amount and opposite phase with respect to receiver and to earth, the angular directivity expressed by $\cos\varphi$ may be useful as a means of locating the direction of a transmitter. This effect is sometimes used in so-called direction-finding apparatus. If unbalance exists, resulting in the potentials being of unequal amount and/or of non-opposite phase, the loop will in part act as a dipole reception antenna which has uniform response with respect to φ, and so the angular directivity will be impaired.

REFERENCES: *5, 46, 188, 279, 317, 337.*

III.2.13. Arrays of parallel wire antennas. We shall consider arrays of wire antennas with their axes mutually parallel. Perhaps the simplest of such arrays consists of two equal wire antennas, the length of each being one-half wavelength, situated in one plane as shown in Figure 56. Suppose that a plane signal wave of polarization parallel

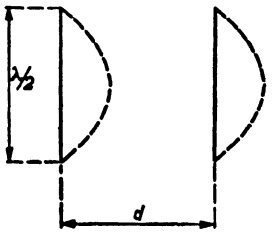

FIG. 56 Two parallel half-wave antennas.

to the antenna axes and of direction perpendicular to the plane fixed by the two antennas is incident on the array. What is the effective reception surface S_{e2} (see Eqs. III.1.13c and d) of both antennas, together upon in-phase addition of their generated voltages? The ratio of S_{e2} corresponding to two antennas to S_{e1} for two antennas, if the second one is removed to a great distance, is shown in Figure 57. Obviously a spacing d of about 0.7 wavelength affords optimal broadside reception conditions. By S_{e2} the available reception power under the conditions

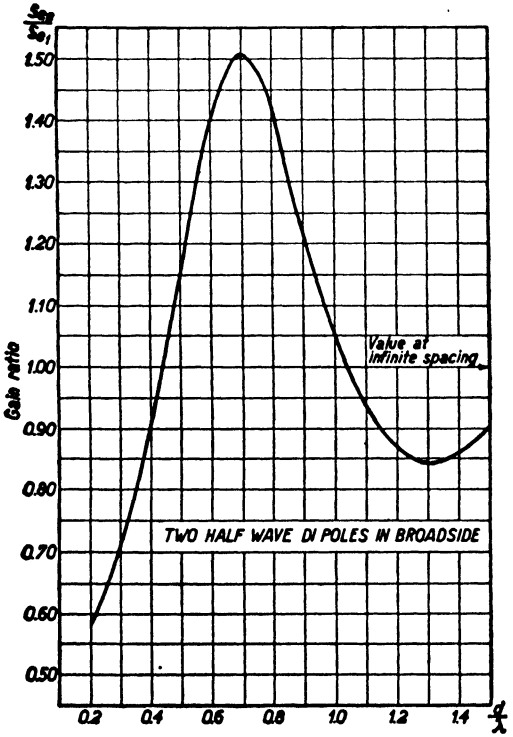

FIG. 57 Ratio of effective reception area S_{e2} for two parallel half-wave antennas at broadside reception upon in-phase addition of their output voltages to effective area S_{e1} of wide-spaced half-wave antennas. Horizontal scale: Ratio of distance d between antennas to wavelength λ (this and next Figure: reference *60*).

quoted is fixed according to Eqs. (III.1.13c) and (*d*). The impedance Z at the terminals of each antenna is made up of two components: $Z = Z_{11} - Z_{12}^2/Z_{11}$, where Z_{11} is the radiation self-impedance of a single half-wave antenna according to Figures 53 and 54

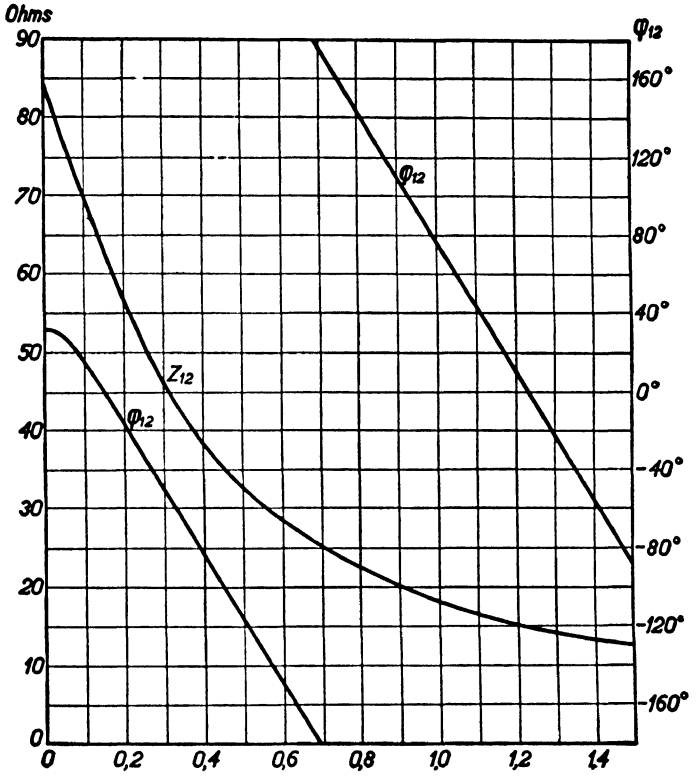

FIG. 58 Mutual impedance of two half-wave parallel antennas (Fig. 56) as dependent on the ratio $\frac{d}{\lambda}$ (horizontal scale). Modulus Z_{12} and phase-angle φ_{12}.

(i.e., $Z_{11} \approx 73 + j42.5$ ohms) and Z_{12} is the "mutual" impedance of both antennas as shown in Figure 58. If no radiation is incident on the antennas and a voltage generator of **V** volts and zero internal impedance is connected to the terminals of one antenna, a current $\mathbf{I} = \mathbf{V}Z_{12}/(Z_{12}^2 - Z_{11}^2)$ flows in a short-circuit connection of the central terminals of the second antenna. From Figure 58 we may conclude that the relative effect of the second antenna on reception by the first one

is already small at a spacing of one-half wavelength and becomes inappreciable at or beyond one wavelength.

Besides broadside reception by the two-antenna array of Figure 56, its response to waves arriving at an angle ϑ as indicated in Figure 59 is also interesting. The effective reception area S_e of each antenna depends on the angle ϑ of incidence as well as on the ratio of the spacing d to the wavelength λ in the surrounding medium. As an example, Figure 60 shows the ratio of the effective area S_{e2} of antenna no. 1 in Figure 59 in the presence of the second antenna no. 2, spaced at a

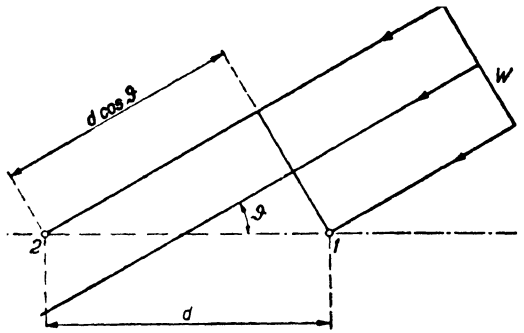

FIG. 59 Two parallel antennas 1 and 2 seen on top, together with incident waves W.

distance $d = \lambda/8$, to the effective area S_{e1} of antenna no. 1 if antenna no. 2 is removed to a large distance in dependence on the angle ϑ of incidence, for three cases: first, the self-impedance of antenna no. 2 is real and 73 ohms; second, this impedance is $73 - j50$ ohms; third, this impedance is $73 + j50$ ohms. The self-impedance of antenna no. 1 is in all three cases real and equal to 73 ohms. Obviously the second antenna acts as a wave director if its self-impedance has a negative reactance (capacitance in series with resistance) and as a wave reflector if its self-impedance has a positive reactance (inductance in series with resistance). The use of several such wave directors plus one wave reflector may entail considerable directivity. As an example, the arrangement of Figure 61 has an effective reception area as dependent on the angle of incidence shown in Figure 62. In the direction of maximum response the effective reception area in the case of Figures 61 and 62 was about 12.5 times the area corresponding to the single reception antenna upon removal of the directors and reflector.

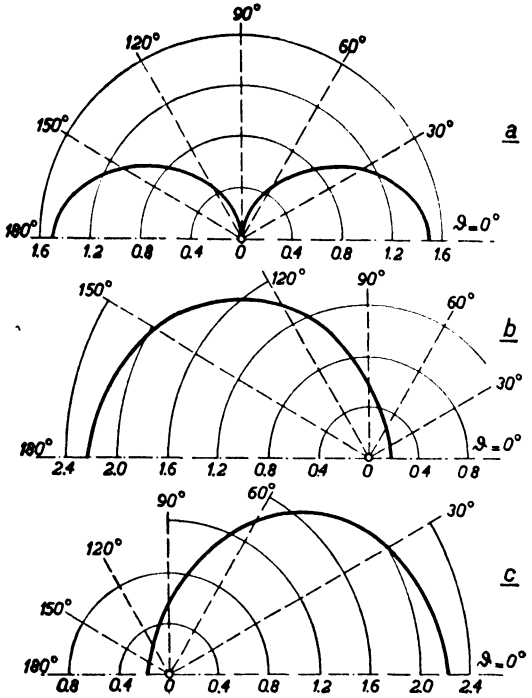

FIG. 60 Ratio of effective reception surface of antenna 1 of Fig. 59 in the presence of the disconnected antenna 2 to surface of antenna 1 without antenna 2 as dependent on angle ϑ of incidence according to Fig. 59. Diagram *a*: Reactance of antenna 2 is zero. Diagram *b*: Reactance of antenna 2 is -50 ohms. Diagram *c*: This reactance is 50 ohms. Resistance of antenna 2 for all three diagrams is 73 ohms and impedance of antenna 1 is a pure resistance of 73 ohms.

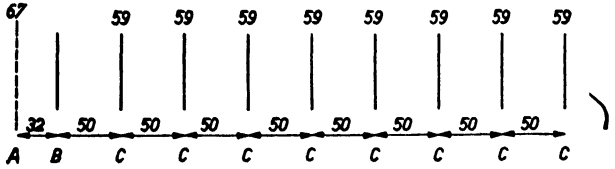

FIG. 61 Wave-director system consisting of one approximately half-wave transmitting antenna (second from left), one reflecting antenna (extreme left), and 8 directing antennas. Wavelength is 130 cm. (See reference *395*).

Another use of several parallel half-wave reception antennas in order to obtain an increase of effective reception area and of angular directivity is to arrange them in a suitable pattern in one plane. An

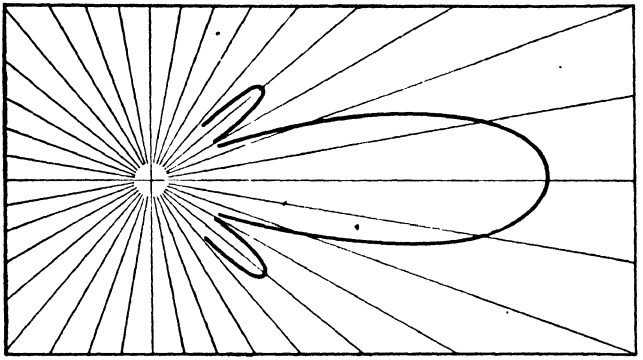

FIG. 62 Square root of effective reception area as dependent on angle of incidence corresponding to wave director of Fig. 61.

example is shown in Figure 63; the vertical spacing between the separate half-wave antennas as well as their individual length is about $\lambda/2$. Sometimes a second array of similar design is placed at a suitable distance

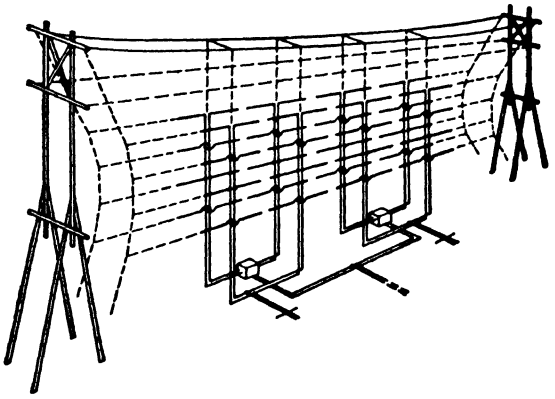

FIG. 63 Picture of an array of horizontal half-wave antennas suitable for reception as well as for transmission purposes, with a reflector array behind it.

behind the original array, as shown in Figure 63, in order to obtain reflector action. If a number q of half-wave antennas is used in one plane, an effective area S_e equal to q times the area corresponding to

one single antenna of this type is obtained in the direction of optimum response, if the mutual reaction is negligible and in-phase addition of the reception voltages is applied. With suitable arrays of considerable dimensions in comparison to the wavelength the gain may also be estimated roughly by assuming the effective reception area S_e of Eqs. (III.1.13c) and (*d*) to be approximately equal to the surface area of the array. The use of a suitable reflector array may raise this gain to almost $2q$. But actually, at a spacing of $\lambda/2$ between the individual antennas mutual reaction is not zero (see Fig. 58), and hence the gain is usually less. As an example, 36 half-wave antennas, each with a suitable reflector, are assumed to be arranged in a plane array, spacing between parallel antennas not with common axes being $\lambda/2$ and spacing between antennas of common axes being very small. The figures of the gains g_r obtained over one single half-wave antenna are tabulated:

NUMBER OF ANTENNAS ALONG HORIZONTAL AXIS	NUMBER OF ANTENNAS ALONG VERTICAL AXIS	GAIN g_r IN db
36	1	19.7
18	2	19.0
12	3	18.9
9	4	18.8
6	6	18.7
4	9	18.6
1	36	17.5

The gain disregarding mutual interaction would be $2q = 72$ or 18.6 db by the first rule above; and thus this rough estimate is not far wrong in the present case. By the second rule above we obtain $g = 73$ for 36 antennas along the horizontal axis. Complicated arrays like this are, of course, used only in commercial and military communication.

REFERENCES: *9, 60, 106, 116, 120, 151, 152, 154, 193, 204, 208, 209, 255, 300, 310, 395.*

III.2.14. Long-wire, rhombic, and V-shaped antennas. The antennas dealt with in the present section are generally of simple design and therefore useful to individual as well as to commercial reception. Straight wires stretched either horizontally or at an acute angle with the earth's surface have been commonly used as reception antennas. The reflecting action of the earth's surface, assuming, for simplicity, perfect reflection, is equivalent to a second wire, situated symmetrically

to the original one with respect to that surface. In symmetrically corresponding elements of the original and of the reflected wire the currents flow simultaneously in opposite directions, as indicated in Figure 64 (see also Fig. 12). Because of imperfect conductivity of the earth, losses occur, resulting in more complicated reflection effects and in loss of gain. When this fact was recognized, the long-wire antennas were duplicated by second wires causing effects similar to

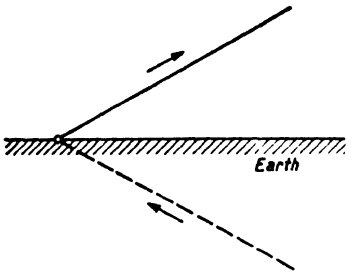

FIG. 64 Tilted reception antenna and its image with respect to the earth's surface.

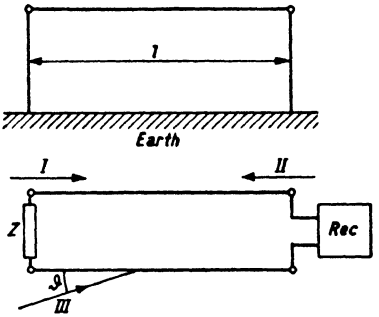

FIG. 65 Parallel-wire reception antenna, both wires being in a plane parallel to the earth's surface. I, II, and III indicate three different directions of incident waves. *Z* is a matching impedance, equal to the antenna's wave impedance and *Rec* a receiver.

those previously caused by the earth's reflection when using single wires. We shall now discuss such combinations of long-wire antennas, at first disregarding the effect of the earth. First, two wires are assumed to be parallel to the earth's surface at equal height and parallel to each other, as shown in Figure 65. If the incident waves arrive from the direction denoted by *I* in Figure 65 and are polarized parallel to the plane containing the two wires, a voltage is set up between them and a wave will travel along the pair of wires in that direction. A corresponding voltage will ensue at the reception terminals, and the impedance connected to these terminals is supposed to be such that no reflection of the traveling wave occurs at the reception end. This particular impedance is usually indicated as the wave or surge impedance of the pair of parallel wires (it will be dealt with fully in chapter IV).

If the incident waves arrive from the direction marked II in Figure 65, they will set up a voltage at the terminals of the impedance Z, which is again chosen to be equal to the said wave impedance. Thus no reflection occurs at Z and practically no voltage results from the waves

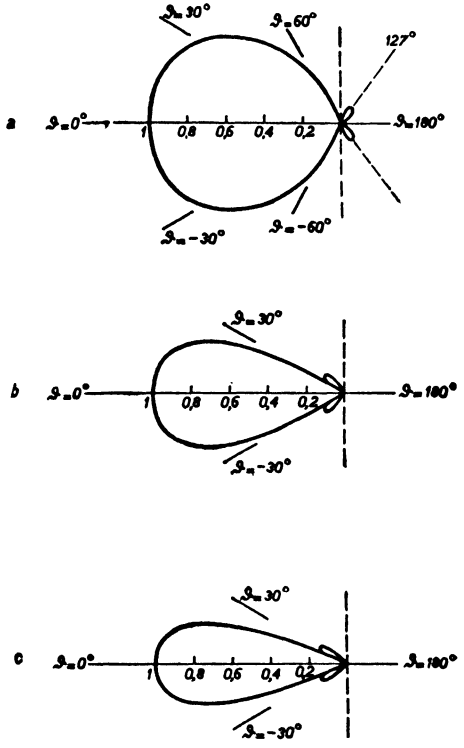

FIG. 66 Square root of effective reception area of antenna of Fig. 65 as dependent on angle of incidence ϑ of incoming waves. Diagrams a, b, and c correspond to $l = \lambda$, $l = 5\lambda$, and $l = 10\lambda$ respectively, Z of Fig. 65 being equal to the antenna's wave impedance.

II at the reception end. Hence the wave-antenna, as this device is often called, is unidirectional. The effective reception area S_e is dependent on the angle ϑ included between the direction of the incoming waves III (Fig. 65) and the wires, assuming the direction of incidence to be in the plane of the wires. Some relative values of $\sqrt{S_e}$ are shown in Figure 66 for different ratios of the wire length l to the wavelength λ.

An increase in gain may be obtained by the use of so-called rhombic antennas, as shown in Figure 67. The main difference with respect to the parallel-wire antennas is that the ends are now brought close together, the terminal impedances being again so chosen as to avoid reflection. With the antennas of Figures 65 and 67 the influence of the soil underneath the antenna on angular directivity and gain is very marked and may be discussed using the principles of section I.1.22. As an example, a rhombic antenna of 180 m over-all length and 50 m greatest width was stretched on four poles at 18 m height above the earth. At 17 m wavelength the gain g_r was about 15 db (or 32). At wavelengths of 20 m and of 36 m the gain was even larger.

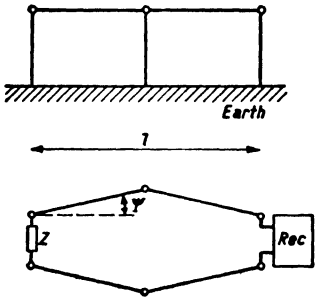

FIG. 67 Rhombic reception antenna of length l stretched parallel to the earth's surface. Z is equal to wave impedance of antenna and *Rec* indicates the receiver position.

In a number of cases arrays of rhombic antennas are used for commercial long-distance reception. Thus at Cooling, Kent, England, 16 rhombic antennas are spaced at regular intervals over a distance of two miles along the great circle toward a transmitting station of New Jersey, U.S.A., and used since 1942 for reception on five frequencies between 5 and 20 mc/s. By combining the signals from the individual antennas with suitable phase shifts the direction and major lobe of optimal response can be varied in the vertical plane. The system is equipped and calibrated to measure the angles of incidence of the incoming signals and their corresponding field strengths (reference *254*). Gain of parallel-wire antennas is usually smaller if they are of the same length as rhombic antennas. An important advantage of both types is the usefulness of one single antenna throughout a wide range of wavelengths (e.g., 15 to 65 m) without readjustments of antenna or terminal impedances.

If a rhombic antenna is halved, we obtain a V-shaped antenna. Because of the termination by a suitable impedance at the reception end only, reflection of traveling waves takes place at the open end and causes reception of incident waves from two opposite directions. In order to avoid reception from one of these directions a second V-antenna spaced suitably with respect to the first one and acting as a reflector may be used. If compared with a rhombic antenna, such a double

V-antenna offers several disadvantages (cost, frequency range, gain, directivity), and hence this type has been seldom used.

REFERENCES: *40, 41, 52, 67, 126, 136, 148, 173, 204, 254, 282, 300.*

III.2.2. Surface antennas. The antennas to be dealt with under the present heading are different from wire antennas in that the dimensions of their surfaces are all of comparable size. These antennas are suitable for extremely short waves, their dimensions being often comparable to or larger than the wavelength in the surrounding medium.

III.2.21. Parabolic reflectors. Two types of parabolic reflectors have been used extensively: cylindrical surfaces of parabolic shape and parabolic surfaces of revolution. In the cylindrical surfaces the antenna (half-wave or dipole type) is coaxial with the cylinder and situated at the focus of the parabola. The axial length is usually about two wavelengths, greater lengths being unfavorable to gain and to angular directivity on account of the secondary lobes then arising in the angular directive pattern in a plane containing the antenna. If the reflector measured at its open end is broad in comparison to the wavelength, the effective reception area S_e of the entire arrangement, incorporating a dipole or a half-wave antenna at the focus of the parabola, corresponding to the most favorable direction, is roughly equal to the surface area of the open end of the reflector. In applying this approximate rule it is assumed that no radiation reaches the reception dipole or half-wave antenna directly, as this might, by unfavorable phase relationships, cancel part of the reflected radiation reaching this antenna by way of the reflector surface. A simple means for achieving this aim is the use of a properly tuned reflector antenna 2 as shown in Figure 68. Another possibility is the use of a subsidiary small cylindrical reflecting surface instead of this reflector antenna. Some examples of actual and of calculated gains g_r by the above rule have been collected for parabolic reflectors of two wavelengths height, and of different widths b, using a suitable reflector antenna:

b/λ	ACTUAL GAIN	CALCULATED GAIN
2	12	11
4	23	22
6	33	33
8	44	44
10	50	55

In these calculations an effective height of $1.3 \times (\lambda/2)$ was assumed, the theoretical effective area S_e and gain being thus:

$$S_e = 1.3 \frac{b}{\lambda} \frac{\lambda^2}{2} \text{ and } g_r = \frac{S_e}{\frac{3\lambda^2}{8\pi}} = 1.3 \frac{b}{\lambda} \frac{4\pi}{3}. \qquad \text{(III.2.21}a\text{)}$$

Though this assumed height may seem somewhat arbitrary, it does not seem unreasonable. In some cases two parallel planes are added on both ends of the cylindrical surface and perpendicular to the latter, resulting in a more favorable radiation pattern.

Instead of a parabolic reflector of cylindrical shape made out of plate material, suitably galvanized to insure sufficient surface conductivity for a coefficient of reflection near unity, separate rods placed along a parabolic circumference are also used. If their mutual distance apart does not exceed one-half wavelength, the effect of such a rodtype reflector is similar to that of a full parabolic cylindrical surface.

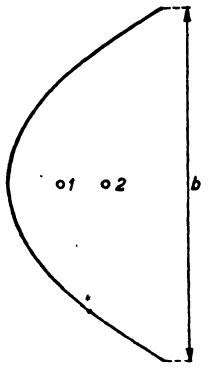

FIG. 68 Picture of a reflector shaped as a parabolic cylindrical surface with a reception antenna 1 at its focus and a reflector antenna 2.

Whereas the cylindrical parabola produces angular directivity mainly in a plane perpendicular to its axis, angular directivity in two mutually perpendicular planes may be achieved by the use of a reflector shaped as a parabolic surface of revolution. The optimal gain figures of such reflectors may again be approximately obtained from the surface area S_e corresponding to their open end by the application of the equation:

$$g_r = \frac{8\pi S_e}{3\lambda^2}. \qquad \text{(III.2.21}b\text{)}$$

Actual gain figures are mostly much less than this, sometimes by 50%, because of wave-interference effects. The application of a reflector antenna or of a relatively small reflecting surface of revolution similar to Figure 68 may increase the actual gain figure. In a plane perpendicular to the dipole or half-wave antenna the main lobe of the directive diagram has an opening angle, given approximately by $140\lambda/b$ degrees empirically, b being the diameter of the open end of the re-

flector. (See eqs. III.3.22*c* and *d* by which this angle would be $57 \times 2\lambda/b$.) In a plane perpendicular to this one the corresponding opening angle has approximately twice this value.

REFERENCES: *10, 85, 255, 267, 329, 393, 406.*

III.2.22. Antennas consisting of cones and horns. For several purposes such as wide-band reception and extremely short waves the reflector antennas of the preceding section are less suitable, and therefore different means of reception have been devised. As this section cannot give an exhaustive description of all the types of antennas suitable to achieve these aims, only a few examples will be given. All of these have evolved from a single prototype consisting of two metallic coaxial cones, the tops of which nearly coincide.

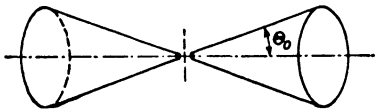

FIG. 69 Double-cone antenna with an angle of flare Θ_o.

One such construction is represented in Figure 69. This antenna is obviously similar to a half-wave antenna, except that the two parts are here cones instead of relatively thin cylinders. Its reception properties are also similar to those of a half-wave antenna, the gain being approximately 1.1, if the angle Θ_o determining the cones' shape (Fig. 69) is small compared with $\pi/2$. An important difference resides in its frequency response, which is wider than with a cylindrical half-wave antenna (see section III.3.12). Thus antennas of this type are particularly useful in television reception, and reception from several adjacent stations not too widely spaced, by means of a single antenna. Besides conical surfaces, other shapes have also been tried successfully. For example, two ellipsoids of revolution instead of the two cones of Figure 69, or two parts of hyperbolical surfaces of revolution, may be cited. Their reception properties are similar to those of the biconical antenna of Figure 69.

If the flare angle Θ_o is increased, a solid angle is included between the two conical surfaces, symmetrical with respect to the axis. Antennas of this shape have been proposed for television and wide-band transmission purposes, as power radiation is in a plane perpendicular to the axis and toward all sides, if this axis is vertical. For reception purposes this all-sidedness is of little use, and so two more plane surfaces through the center may be added so as to obtain a horn-shaped antenna

(Fig. 70*a*). The boundary surfaces consist of parts of two cones and of parts of two planes through the center. Similarly shaped antennas may be devised by deformation of the boundary surfaces. A very simple horn-shaped antenna is bounded by one single conical surface, the incident waves entering through its open end and proceeding toward the top. If the dimensions of the open end of the horn are large in comparison to the wavelength its gain may be obtained approximately by application of Eq. (III.2.21*b*), the optimal effective surface S_e being about 80% of the open-end surface of the horn. The actual gain will often be less than the figure thus obtained due to interference effects impairing the capture of the incident waves and their guidance to the apex of the horn where the reception device is situated. The detailed design of such horn antennas—which are, of course, suitable only for extremely short waves in the dm and cm ranges—will not be dealt with here. In order to obtain the gain mentioned, a considerable length in comparison to the wavelength is necessary. This length must also be large compared with the largest lateral dimension of the horn's open end—e.g., larger than 5 times the latter value—in order to obtain the optimal gain figure mentioned. If the horn is a cone its flaring angle Θ_o (see Fig. 69) should thus be smaller than, say, 6 degrees. Horns are sometimes used in combination with parabolic reflectors, the horn being fitted to the end of a suitably bent wave guide and flaring toward the reflector (e.g., in radar equipment).

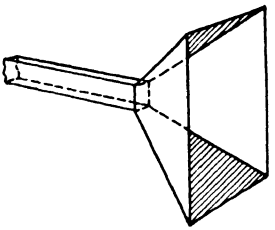

FIG. 70a Horn-type antenna connected to a rectangular wave guide.

Slotted pipes have also been used as antennas recently (e.g., reference *402*), the slots acting as outlets for the waves propagated through the pipes.

Lense action has been obtained by the application of transverse wave propagation between parallel conducting strips (see section IV.1.3). By a proper choice of the mutual distance of such strips the phase-velocity of the waves is increased. If this increase is applied along a longer path near the edges of the lense-substitute than near the center, a similar wave-concentrating effect results as in optical lenses. A simple means of obtaining this effect is shown in Fig. 70*b*, the metal sheets extending further along the direction of propagation near the edges than

near the center (reference *201*). These lenses may be applied in combination with suitable horns as shown in Fig. 70*b*.

REFERENCES: *15, 16, 17, 31, 54, 61, 185, 201, 214, 310, 327, 402, 406.*

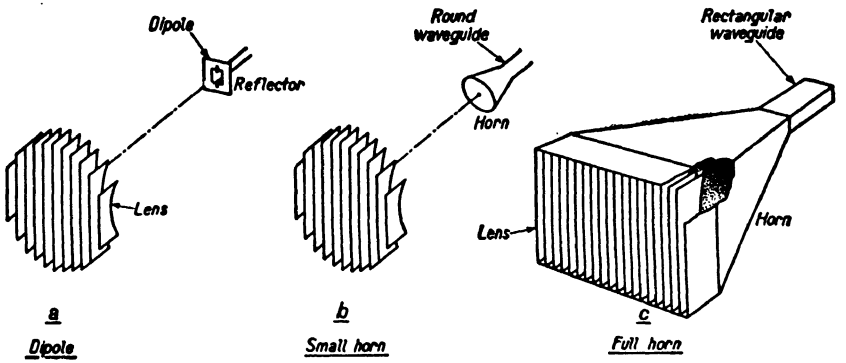

FIG. 70b Application of wave lenses consisting of parallel conducting strips of varying width, being smallest at the center and widening toward both ends. These lenses may be applied in combination with dipole and horn antennas as shown and result in an increase of gain.

III.3. NOISE, BAND-WIDTH, AND DESIGN CONSIDERATIONS

From the laws and facts discussed in chapters III.1 and III.2 a number of conclusions as to actual antenna noise, to band width, and to antenna design may be drawn. These are dealt with below.

III.3.1. Noise and band-width considerations. Minimum relative noise level and adequate band width to accommodate the signals to be received as well as to comply with further requirements are the primary aims of reception-antenna design.

III.3.11. Noise considerations. From Eq. (III.1.22*b*) we may conclude that the noise ratio at the terminals of a reception antenna with a given value of specific signal power is inversely proportional to the effective reception surface S_e and to the radiation gain g_r of the antenna for the direction in question. Hence reception antennas with the largest effective surface are most favorable as regards noise ratio. The same conclusion may be drawn from the second definition of noise figure in section III.1.22, the attenuation A being inversely proportional to S_e and to g_r. Hence the antenna's noise figure, according to this definition, is also inversely proportional to S_e. In the case of a single straight antenna with central terminals we see from Figure 50 that S_e

is optimal if the total length $2l$ is approximately equal to 1.25 wavelengths λ. Hence this particular antenna of the type considered corresponds to the lowest noise figure and noise ratio in the above sense. Considering arrays of wire antennas, the effective surface S_e, as well as the radiation gain, are increased by extending the array. Hence the noise ratio is decreased in inverse proportion. The array considered at the end of section III.2.13 has only 1/72 of the noise ratio and of the noise figure of a single half-wave antenna. Similarly V-shaped and rhombic antennas, with their considerable gain figures over dipole or half-wave antennas, have correspondingly low noise ratios and figures. Similar conclusions are valid for the surface antennas considered in sections III.2.21 and 22.

Besides noise arriving from all directions uniformly we have also to consider interstellar noise (sections III.1.21 and I.1.44), atmospheric noise arriving from particular directions, and man-made noise, also often highly directional. For all these, the antenna should be so designed as to afford optimal discrimination against such noise or, in other words, a minimum noise ratio. This may obviously be achieved particularly well if the directions of signal and of noise do not coincide. By increasing the antenna's directivity and gain for the signal direction the response to the noise is relatively decreased. On account of possible variations in the direction of incident signal waves the directivity may not, as a rule, be increased beyond a definite value, even if cost should be disregarded, which is often not tolerable (see section III.3.2). Even with relatively simple antennas such as half-wave wires or small loop antennas minimum or nearly zero response may often be achieved for the noise direction simultaneously with favorable response to the incident signals by application of proper angular directivity χ which is approximately proportional to $\sin \Theta$ in both cases, Θ being the angle included between the direction of arrival and the axes of either the loop or the wire. If, on the other hand, the directions of the noises and of the incident waves practically coincide, an increase of S_e and g_r for the direction will often not cause a decrease of noise ratio and noise figure.

REFERENCES: *44, 48, 127, 149, 163, 213, 249, 254, 263, 264, 282.*

III.3.12. Band-width considerations. Hitherto we have considered only the response of reception antennas to waves of a single frequency or of a relatively small frequency interval Δf centered round $f \gg \Delta f$.

We now extend the discussion to wider bands. Here we have to account for the frequency dependence of the available power P_a as well as of the antenna's impedance $Z_r = R_r + jX_r$. The simplest example is afforded by a dipole antenna, P_a being proportional to λ^2 by Eq. (III.1.13*c*) in which $g_r = 1 = \chi$ for the favored direction, and R_{rd} being proportional to $1/\lambda^2$ by Eq. (III.1.11*c*). Besides this radiation resistance we have still to consider the reactance X_r caused by the inductance L_r and capacitance C_r of the dipole antenna. At the tuning angular frequency ω_o we have $\omega_o^2 L_r C_r = 1$. The actual values of C_r and L_r depend on the construction of the dipole. At a frequency differing from the tuning position, the radiation impedance Z_r of the equivalent antiresonant circuit is:

$$Z_r = R_r + j\left(\omega L_r - \frac{1}{\omega C_r}\right) \qquad \text{(III.3.12}a\text{)}$$

and by inserting the value of Eq. (III.1.11*c*) for R_r and assuming constant values for L_r and C_r an approximate value of Z_r is obtained, valid in the vicinity of ω_o. This radiation impedance, together with the available reception power, completely determines the frequency dependence of the antenna's behavior in reception circuits. We may use a signal generator of voltage $|V_o| = \sqrt{4P_aR_r}$ and of zero internal impedance in series with R_r, C_r, and L_r as a complete substitute for the reception antenna at its terminals (see Fig. 71) 1, 2. With a dipole antenna, the product P_aR_{rd} is independent of frequency and so is V_o, if the incident waves are of fixed specific power. Assuming a resistance R_o to be connected to the terminals 1, 2, the power dissipated in R_o is

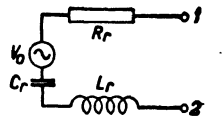

FIG. 71 Equivalent lumped circuit of a wire or horn-shaped antenna at its center taps 1,2.

$$P_o = \frac{|V_o|^2 R_o}{(R_r + R_o)^2 + \left(\omega L_r - \frac{1}{\omega C_r}\right)^2}. \qquad \text{(III.3.12}b\text{)}$$

If f_o is the resonant frequency $\omega_o/2\pi$ at which $\omega_o^2 L_r C_r = 1$, a deviation $f_o - f_1$ from this frequency is determined, at which P_o has exactly half its resonant value (P_o is hence 3 db down). Then $2|f_o - f_1| = f_o/Q$ and Q is called the quality figure of the circuit under discussion

(see also section I.2.31). The higher this quality figure, the more variation of P_o occurs at a given frequency deviation from the resonant frequency. We find from these definitions of Q and from Eq. (*b*):

$$Q = \frac{\omega_o L_r}{R_r + R_o} = \frac{1}{(R_r + R_o)\omega_o C_r}. \qquad \text{(III.3.12}c\text{)}$$

Thus Q may be decreased by increasing R_o if necessary.

We shall now consider the case of a half-wave antenna, first made out of a wire of constant diameter and then made out of two cones of small flaring angles Θ_o (see Fig. 69). In both cases, L_r and C_r may be approximately calculated from a quantity Z_o called the antenna's wave or surge impedance near its resonant length. This resonant length may be determined from Figure 54, taking X_r to be zero in a cylindrical antenna. Using the quantity $U = 2 \ln (2l/a)$ of section III.2.11, we have approximately:

$$Z_o = \begin{cases} 60U - 120 & \text{for cylindrical antennas,} \\ 60U & \text{for conical antennas.} \end{cases} \qquad \text{(III.3.12}d\text{)}$$

In the latter case, a is the radius of the cones' largest circles perpendicular to their axis and l the axial length of each cone from the apex to the said circle. It is assumed that $2l \gg a$ in each case. From Z_o we obtain:

$$\omega_o C_r = \frac{4}{\pi Z_o}, \quad \omega_o L_r = \frac{\pi Z_o}{4}. \qquad \text{(III.3.12}e\text{)}$$

These formulas indicate that Z_o may be increased by increasing U, and in conical antennas Z_o is larger than in cylindrical antennas if U is equal. The voltage V_o of Figure 71 in the vicinity of resonance corresponding to the half-wave antennas in question is nearly independent of frequency (see Figs. 50 and 53). From the first Eq. (*d*) and from Eqs. (*e*) and (*c*) it is obvious that a decrease of Q is obtained if the radius a of an antenna's cross-section is increased.

The Q figure of a double-cone antenna as pictured in Figure 69 in the case of angles Θ_o not very small compared with $\pi/2$ may still be calculated from Eqs. (*e*) and (*c*), but the second Eq. (*d*), expressing Z_o in terms of the cone's angle Θ_o, is no longer valid. Instead of this equation we have:

$$Z_o = 120 \ln \left| \operatorname{cotan} \frac{\Theta_o}{2} \right|. \qquad \text{(III.3.12}f\text{)}$$

If $\Theta_o \ll 1$ this expression obviously coincides with the second Eq. (*d*). But if Θ_o is near 40 degrees, Z_o will become of the order of magnitude of 120 or less, resulting in rather low Q figures suitable to wide-band reception.

The Q values of more complicated antennas and arrays are not readily adaptable to a simple treatment similar to that above. In general, if we use the equivalent circuit of Figure 71, the voltage V_o as well as the radiation impedance Z_r are dependent on frequency.

REFERENCES: *24, 61, 147, 163, 397.*

III.3.2. Design considerations. In designing a reception antenna its purpose should first be considered. We shall discuss two cases: (1) individual antennas for amateur and professional use, and (2) antennas for commercial communication.

III.3.21. Individual antennas. As cost is often a preponderant consideration, individual antennas usually need to be of simple design and yet best suited to their purpose. The half-wave antenna or simple loop constructions are effective.

First, the antenna's site has to be decided upon. The possibility of spurious reflections should be avoided. Such reflections may come from neighboring buildings, trees, overhead lines, masts, or hills as well as from the earth's surface. Besides stationary objects, passing aircraft, ships, and vehicles have been known to cause reflections and distortions (ghosts) of television pictures. It may sometimes be necessary to locate the reception antenna at some distance from the receiver itself and interconnect by means of a suitable transmission line (see chapter IV). If, however, this distance is so great as to cause undue attenuation by transmission losses it may be desirable to transfer part of the receiver, notably its u.h.f. stages (entrance stage and mixer stage—see section VI) to the antenna's site and to transmit intermediate-frequency signals to the receiver proper. It is not always easy to eliminate spurious reflections completely or even to predict all of them. Only the more obvious ones can be detected and taken care of beforehand. It will sometimes be necessary to alter the antenna after a trial period (reference *93*).

Similar measures will often be successful in the elimination or reduction of man-made noise. An antenna high in the air above a densely populated city area will pick up much less man-made noise than antennas at lower levels. If a particular source of noise is known, the antenna should be removed from its neighborhood.

A further point is polarization. In short-distance reception above or only a little below the horizon, polarization of the reception antenna should match that of the transmission antenna. In long-distance reception little correlation exists in most cases between polarizations of the waves near transmission and reception antennas. As was pointed out in sections I.1.41 and I.1.42, frequent changes of the polarization of incident waves are a common phenomenon. To reduce the disturbing effects of these changes and of fading phenomena, two separate reception antennas spaced several wavelengths apart and polarized differently have proved useful if proper addition of their output powers is applied. If the antennas are of simple design (e.g., half-wave wires), the slightly higher expenditure for such a double antenna may be entirely warranted by a considerable improvement of reception; this means seems readily applicable even to individual reception.

As to the band width of half-wave or of 1.25-wave reception antennas (the latter affording a much lower noise ratio), this may be made suitable for most purposes, including television reception. According to section I.2.32, the six television channels in the United States are allotted frequencies between 44 and 88 mc/s. If it is desired to receive all these channels on one single antenna system, special care is necessary. Assuming a drop of available power by 3 db at 44 and at 88 mc/s as compared with 66 mc/s, the Q figure required is: $Q = 66/44 = 1.5$. This extremely low quality may be obtained by the connection of a high ohmic resistance approximately independent of frequency to the antenna's terminals (see Eq. III.3.12c). The ensuing loss of power transferred to the receiver might, however, prohibit this measure. Thus the use of separate antennas for the reception of different television channels would be recommendable in such cases. Considering the channel of 44 to 50 mc/s, a Q of about 8 would correspond to a drop of 3 db in available power at 44 mc/s as compared with 47 mc/s. Assuming a cylindrical half-wave antenna tuned at 47 mc/s and of 1-inch radius, the surge impedance Z_o is approximately 460 ohms, corresponding to a Q of about 5.0 if short-circuited and of half this value if connected to a matched load resistance (73.1 ohms) (see also Fig. 133). With a 1.25-wavelength antenna the value of X_r is not nearly zero, as may be seen from Figure 54. By the use of a load impedance, connected to the terminals 1, 2 of Figure 71, of $R_o - jX_r$, the resulting reactance at the wavelength λ for which the antenna's length $2l = 1.25\lambda$ may be made zero or nearly so. The frequency dependence of S_e as

well as of R_r and X_r in the vicinity of this frequency have then to be taken into account, the latter dependences resulting from Figures 53 and 54 and the former (S_e) from Figure 50 or from Figures 51 and 52.

REFERENCES: *1, 39, 46, 61, 93, 136, 185, 402.*

III.3.22. Antennas for commercial reception. In these cases more elaborate designs are suitable, some of which may, of course, also be of use for individual reception. We shall first consider rhombic antennas and then arrays of half-wave antennas. With rhombic antennas the optimal angle ψ (see Fig. 67) is given by the equation:

$$\cos\psi = \frac{q-1}{q} + \frac{4}{\pi^2(2q-1)}, \qquad \text{(III.3.22}a\text{)}$$

the length of each of the four equal antenna wires being $q\lambda/2$, q being an integral number. As an example, if the length is $7\lambda/2$, we obtain an angle ψ of about 27 degrees. The height h above the earth's surface —this being assumed perfectly reflective ($F = -1$)—is determined by the angle ϑ included between the main direction of the incident waves and the earth and by the overall length l of the rhombic antenna (see Fig. 67) as follows:

$$\frac{l}{2\cos\psi} = \frac{0.37\lambda}{\sin^2\vartheta}, \quad h = \frac{\lambda}{4\sin\vartheta}. \qquad \text{(III.3.22}b\text{)}$$

Thus the optimum height and length are dependent on wavelength, though of course the width of the main directional lobe usually entails sufficient response over a rather wide range of frequencies. The width of the main lobe in both horizontal and vertical directions is decreased by increasing the lengths of the antenna wires. It is recommended to calculate the antenna's data for the shortest waves of the range to be received; if this is done, reception of longer waves is then often satisfactory. This was tested in a range of 7 to 23 mc/s (43 to 13 m wavelengths). The gain figures are often not readily predictable under practical conditions. An example was given at the end of section III.2.14. As with half-wave antennas in the preceding section, the use of two rhombic antennas at a mutual distance of several wavelengths, together with proper addition of the received powers, may cause a decrease of the effects of fading in long-distance reception (reference *126*).

The possible variations in direction of incidence with long-distance reception may be rated at about 3 degrees in a horizontal plane (azimuthal angle φ) and at about 5 to 30 degrees in a vertical plane (elevation angle Θ). The reception antenna should possess an angular directivity function $\chi(\Theta, \varphi)$ complying with these variations. Thus the lobe of main reception response should be of sufficient width horizontally as well as vertically. This requirement prohibits the use of too broad or too highly stacked arrays. On the other hand, the gain ought to be increased as much as possible in order to obtain high discrimination against noise. A favorable compromise between these two conflicting requirements must be aimed at. Gain figures of arrays have been dealt with in section III.2.13.

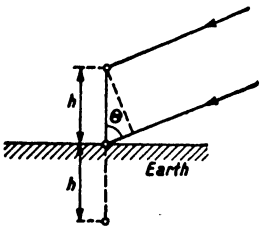

FIG. 72 Array of height h, hit by a plane wave at an angle Θ.

A simple estimate of the necessary height h and breadth $2l$ of an array in order to obtain a given azimuthal and elevational angular width of the main response beam will now be given. Assuming the azimuthal angle included between the plane of the array and the main direction of response to be φ, the difference in paths of two rays hitting the array at spots being l apart, resulting from a variation of φ by $\Delta\varphi$ is: $l \cos \varphi - l \cos (\varphi + \Delta\varphi)$, and this must be $\lambda/2$ if these rays—and hence any two rays hitting spots of the array, l apart horizontally—are to cancel each other. Hence, assuming $\Delta\varphi \ll 1$ we obtain:

$$l = \frac{\lambda}{2 \sin \varphi \times \Delta\varphi}, \qquad \text{(III.3.22}c\text{)}$$

the total width of the beam being $2\Delta\varphi$ radians in azimuthal angle. A similar reasoning applied to the height h, assuming a perfectly reflecting earth on which the array of vertical polarization is erected, yields:

$$h = \frac{\lambda}{2 \sin \Theta \times \Delta\Theta}, \qquad \text{(III.3.22}d\text{)}$$

Θ being the elevation angle included between the main direction of response and the plane of the array (see Fig. 72). As an example, if Θ is 70 degrees and $\Delta\Theta = 10$ degrees, we obtain: $h = 3\lambda$. At a wavelength of 20 m the array should therefore have a height of 60 m.

Problems of supports, poles, masts, cables, and buildings for housing the reception apparatus will be dealt with in chapter VII.

REFERENCES: *40, 41, 52, 126, 148, 168, 175, 282.*

III.3.23. Radiation resistance as affected by reflection. Besides gain and angular directivity, as determining the effective reception area S_e, the radiation resistance of antenna systems is an item of considerable importance to the design of further reception devices to be connected to the antenna's terminals. We shall start by dealing with the influence of the earth and of other reflecting surfaces on the radiation resistance of simple antennas and shall then proceed to arrays and other more complicated antennas. Considering a horizontal antenna, the effect of the earth's surface is simplest if reflection is perfect ($F = -1$). In this case, according to Figure 12*b*, an image antenna carrying exactly counterphase currents with respect to the original one accounts completely for this effect. If Z_{12} is the mutual impedance of original and image antenna, its real part being R_{12}, and if Z_{11} is the self-impedance of the original antenna without image or reflection, its real part being R_{11}, the resulting radiation resistance is:

$$R_r = R_{11} - R_{12}. \qquad \text{(III.3.23}a\text{)}$$

If we consider an antenna of vertical polarization and a perfectly reflecting earth's surface ($F = +1$), we have to apply Figure 12*a*, the image antenna carrying currents of equal amount and phase to the original one. In this case the resulting radiation resistance is:

$$R_r = R_{11} + R_{12}, \qquad \text{(III.3.23}b\text{)}$$

R_{11} and R_{12} having a similar value as in the case discussed above. The values of R_{11} and R_{12} being known in either case for half-wave antennas, the radiation resistances may be readily evaluated (for R_{12} of Eq. (*a*) see Fig. 58). In the case of dipole antennas of short length compared with a quarter wavelength the ratios R_r/R_{11} for the case of a horizontal and of a vertical dipole are:

$$\text{vertical dipole: } \frac{R_r}{R_{11}} = 1 + 3\frac{\sin\Lambda - \Lambda\cos\Lambda}{\Lambda^3},$$

$$\text{horizontal dipole: } \frac{R_r}{R_{11}} = 1 - 3\frac{(\Lambda^2 - 1)\sin\Lambda + \Lambda\cos\Lambda}{\Lambda^3}, \qquad \text{(III.3.23}c\text{)}$$

Λ being the ratio $4\pi h/\lambda$ and h the dipole's height above the earth. These expressions hold approximately also for half-wave dipoles if h is more than $\lambda/2$. With small loop antennas (section III.2.12), the effect of the earth is similar to that on dipole antennas, the above Eq. (a) being valid for a loop of horizontal plane and Eq. (b) for a loop of vertical

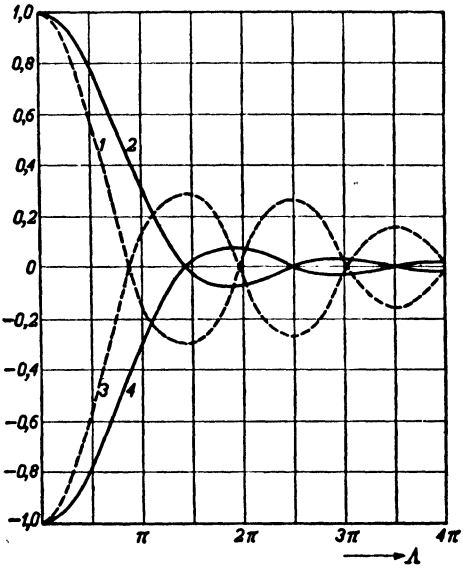

FIG. 73 Curves representing $-1 + R_r/R_{11}$ (vertical scale) as dependent on Λ (horizontal scale). Curve 1: Vertical loop antenna; curve 2: Vertical dipole; curve 3: Horizontal dipole; curve 4: Horizontal loop antenna. Here R_r is the radiation resistance taking perfect reflection into account, while R_{11} is the radiation resistance without reflection (e.g., at a great distance from the reflecting plane).

plane. The expressions of R_{12} are, however, different from the corresponding expressions in the cases of dipole antennas. Thus:

$$\text{vertical loop: } \frac{R_r}{R_{11}} = 1 + 3\,\frac{(\Lambda^2 - 1)\sin\Lambda + \Lambda\cos\Lambda}{\Lambda^3},$$

$$\text{horizontal loop: } \frac{R_r}{R_{11}} = 1 - 3\,\frac{\sin\Lambda - \Lambda\cos\Lambda}{\Lambda^3}. \qquad \text{(III.3.23}d\text{)}$$

A certain relationship between the expressions R_{12}/R_{11} for dipole and for loop antennas obviously exists. The Eqs. (c) and (d) are pictured

in Figure 73. If a horizontal antenna or a loop of horizontal plane comes close to a perfectly reflecting surface, the radiation resistance R_r approaches zero. If the reflecting surface has a coefficient of reflection of modulus less than unity, as with most actual surfaces, R_r will decrease to a finite value if the antenna's height is made to approach zero. This finite value will in most cases be small compared with the value of R_r at great heights. The effective reception area for the most favorable direction (see Fig. 10) approaches zero also in the first case of a perfectly reflecting earth and a decreasing height. So, of course, does the available reception power. Hence this situation should be avoided in reception antennas.

REFERENCES: *13, 60, 151, 154, 193, 310, 337, 395.*

III.3.24. Radiation resistance of arrays. Considering arrays of parallel half-wave antennas, disregarding the effect of the earth's surface, the simplest case is two equal antennas, their terminals connected in series. The resulting radiation resistance of each antenna being $R_{11} + R_{12}$ and R_{12} given by Figure 58, we see that a value of approximately $2R_{11} \approx 146$ ohms is obtained for each antenna, by bringing two equal half-wave antennas close together. The effective surface area corresponding to broadside reception remains unaltered if compared with a single antenna, and so does the available power. Hence we have a means of increasing the effective radiation resistance while retaining the available power per antenna. By bringing three equal parallel antennas close together, radiation resistance of each is tripled, etc. Upon proper connection of two antennas so as to obtain a "folded" unit (see Fig. 83) with broadside reception, the resulting voltage is twice that of a single antenna, while the corresponding radiation resistance at the resulting pair of terminals consists of 2 times $2R_{11}$ and is $4R_{11}$. Hence the total available reception power is not altered if compared with a single antenna as might have been anticipated. By proper spacing the available power may be increased, as appears from Figure 57, upon proper addition of the individual available powers.

Applying this reasoning to an array of q individual half-wave antennas, the resulting open-circuit voltage, disregarding mutual action, is upon proper addition at broadside reception, q times the open-circuit voltage of one antenna. The resulting radiation resistance, the individual resistances being in series, is q times that of one antenna. Hence the resulting available power is q^2/q or q times the amount for

one antenna. If the resulting radiation resistance is R_r, upon series addition of the individual resistances the gain in available power over one half-wave antenna is hence q^2R_{r1}/R_r, R_{r1} being the radiation resistance of one antenna remote from the other ones. This is also the ratio of effective reception area of the array to that of a single antenna. Thus in the case of two antennas (Fig. 57) the gain is:

$$g_r = 2\frac{S_{e2}}{S_{e1}} = \frac{4R_{11}}{2(R_{11} + R_{12})} = \frac{2R_{11}}{R_{11} + R_{12}}. \qquad \text{(III.3.24}a\text{)}$$

This gain is approximately equal to the gain g over one single dipole antenna (about 10% less than g actually).

Considering an array such as that discussed at the end of section III.2.13 with six antennas parallel horizontally at mutual distances of $\lambda/2$ and six antennas stacked vertically, the individual radiation resistances are given in the table below, R_r being obtained by adding them all, if a series connection of the individual antennas is applied.

75.4	93.1	86.0	86.0	93.1	75.4
59.9	67.8	69.4	69.4	67.8	59.9
64.0	79.0	74.4	74.4	79.0	64.0
64.0	79.0	74.4	74.4	79.0	64.0
59.9	67.8	69.4	69.4	67.8	59.9
75.4	93.1	86.0	86.0	93.1	75.4

Similar relationships may be derived if shunt connection of the individual antenna terminals of the array is applied.

REFERENCES: *60, 163, 193, 208.*

CHAPTER IV

WAVE CONDUCTORS AND RESONANT DEVICES

The available power obtained at the output terminals of an antenna system must be conducted to the input terminals of the receiver proper. This is achieved by the use of wave conductors and of resonator circuits and/or cavities. These means will now be discussed in some detail with a view to their most suitable design.

IV.1. Wave Conductors

The wave conductors in present use may be divided into two groups: transmission lines and wave guides. Their main difference resides in the dimensions in a direction perpendicular to power propagation relative to one-quarter wavelength in the dielectric medium. With the first group the dimensions are small and with the second group are comparable to or larger than (at least some of them) the quarter wavelength.

IV.1.1. Losses in u.h.f. fields. The peculiar behavior of u.h.f. fields causes losses and field patterns which are different from lower frequency fields.

IV.1.11. Eddy currents at conductive surfaces. At u.h.f. the electric-field strength outside and at a conducting surface is always directed very nearly perpendicular and the magnetic-field strength very nearly parallel to it. Both fields penetrate only very slightly into the interior of the conductor, the field strengths decreasing exponentially in amount reckoned in a direction perpendicular to the local surface. The depth d_o in this direction at which the moduli of both field strengths have decreased to the 1/2.718 part of their values at the surface is given (in cm) by:

$$d_o^2 = \frac{2\mu_o}{\omega\sigma\mu}, \qquad \text{(IV.1.11}a\text{)}$$

μ_o being equal to $10^9/4\pi$ in the present system of practical units, ω denoting the angular frequency of the field (c/s), σ the specific conductivity in question expressed in mhos/cm, and μ the magnetic permeability of the conducting material. In the case of copper, if f is the frequency in c/s, we obtain $d_o = 6.6/\sqrt{f}$. If the r.m.s. magnetic-field strength at the surface is H_o, the specific power p_o dissipated per cm^2 of the local conducting surface is:

$$p_o = \frac{H_o^2}{d_o \sigma}. \qquad \text{(IV.1.11}b\text{)}$$

Electric currents flow in the conductor at the vicinity of its surface (eddy currents), the r.m.s. current per cm of surface perpendicular to its local direction being equal in amount to H_o. Equating the specific power p_o to this current squared multiplied by a resistance ρ_o, which a square part of the conductor's surface 1 cm wide and 1 cm long (the latter dimension in the current's direction) offers to the eddy currents, we obtain:

$$\rho_o(\text{ohms}) = \frac{1}{d_o \sigma}. \qquad \text{(IV.1.11}c\text{)}$$

By the application of these equations the evaluation of eddy-current losses caused by particular u.h.f. fields offers few difficulties. What we have to learn from the field pattern outside the conducting surface is either the distribution of magnetic-field strength H_o at the surface or the eddy currents flowing in every part of the surface. A simple example is afforded by a straight cylindrical conductor of circular cross-section and of radius a. The u.h.f. current flowing through the conductor is by symmetry distributed uniformly along its circumference. Hence each part of it contributes equally to the total resistance, this being $1/(d_o \sigma 2\pi a)$ ohms per cm of axial length. The d.c. resistance of this length being $1/(\sigma \pi a^2)$, the ratio of u.h.f. to d.c. resistance works out as $a/2d_o$, which by Eq. (IV.1.11a) yields the well-known formula for this ratio of a circular u.h.f. conductor.

If the depth d_o of penetration is known for copper, its value for a different metal is obtained by multiplication by the square root of the ratio

σ_{copper} to σ of the metal in question. This multiplier is given in the table below for different metals:

Metal	$\sqrt{\frac{\sigma_{copper}}{\sigma_{metal}}}$
Aluminum	1.28
Brass	2
Cadmium	2.09
Chromium	1.23
Gold	1.19
Lead	3.57
Magnesium	1.63
Manganin	5.05
Palladium	2.52
Phosphor-bronze	2.47
Platinum	2.41
Rhodium	1.71
Silver	0.97
Tin	2.58
Zinc	1.89

This multiplier is also of direct application in obtaining the attenuation in wave conductors (see sections IV.1.2 and IV.1.3). The specific conductivity of pure copper is about 6×10^5 mhos/cm.

REFERENCES: *341*, *388*.

IV.1.12. U.h.f. impedance of resistors. In many circuits leakage resistance units are used, the d.c. resistance of which is between a few and some hundreds of k ohms. These units are usually shaped as cylinders, the length of which is several times the diameter, two small caps at the ends serving as contact connections for soldering them to other parts of the circuit (Fig. 74). The cylinders themselves often consist of ceramic material, covered by a relatively thin layer of a poor-conductivity mixture, e.g., of graphite with some additions. The a.c. impedance of these resistance units varies considerably in the ultra- and extreme high-frequency range. A value of 100 k ohms at low frequencies may well drop below 10 k ohms at 100 mc/s as regards the real part of the impedance. The reactance may be represented by a capac-

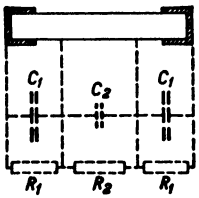

FIG. 74 Resistor unit with distributed capacitances C_1, C_2 and distributed resistance R_1, R_2.

ity, usually of the order of 1 pF, shunting the real part of Z, and this capacity often varies much less than the real part of Z up to a few hundred mc/s (see Fig. 136).

This behavior, which is in many cases essential to the application of such resistance units, may readily be explained by the stray capacities, shunting the different resistive parts of such a unit. Because of the connection caps at both ends, stray capacities are much higher near these ends than nearer to the center. We shall consider only three capacities, shunting the resistance, one capacity C_1 at each end, each shunting a resistance R_1 and a capacity C_2 near the center, shunting the resistance R_2 (see Fig. 74). It is assumed that the specific resistance of the layer is invariable throughout the frequency range considered, which is nearly always true, thus making $2R_1 + R_2$ equal to the d.c. resistance of the unit. The resulting impedance Z between the connectors, at an angular frequency ω is:

$$Z = \frac{2R_1}{1 + \omega^2 C_1^2 R_1^2} + \frac{R_2}{1 + \omega^2 C_2^2 R_2^2} - j\left(\frac{2R_1\omega C_1 R_1}{1 + \omega^2 C_1^2 R_1^2} + \frac{R_2\omega C_2 R_2}{1 + \omega^2 C_2^2 R_2^2}\right), \tag{IV.1.12a}$$

The over-all shunt capacity C is hence:

$$\frac{1}{\omega C} = \frac{|Z|^2}{\dfrac{2R_1^2\omega C_1}{1 + \omega^2 C_1^2 R_1^2} + \dfrac{R_2^2\omega C_2}{1 + \omega^2 C_2^2 R_2^2}}. \tag{IV.1.12b}$$

Assuming R_1 to be larger than R_2 and C_1 to be some few times C_2, the first terms of the real as well as of the imaginary part of Z predominantly determine the frequency dependence of Z as long as $\omega^2 C_2^2 R_2^2$ is still small compared with unity, whereas $\omega^2 C_1^2 R_1^2$ is comparable with or even much larger than unity. The real part of Z is, in this case, approximately:

$$\mathrm{Re}(Z) \approx \frac{2R_1}{\omega^2 C_1^2 R_1^2}, \tag{IV.1.12c}$$

and hence strongly variable with frequency. These simple Eq. (*a*) to (*c*) of course afford only a rather crude picture of the exact behavior, as many and even continuously distributed shunt capacities and series resistances should be taken into account instead of three. Even so, several essential features are duly expressed by these equations.

They afford some interesting means of decreasing the frequency dependence of Z and even of constructing leakage resistances of unusually high values of real impedance at extreme-high frequencies. In the first place, the effect of the shunting capacities C_1 at the ends of the unit may be decreased by decreasing R_1 in proportion to R_2—i.e., by applying a lower resistance per unit length near the end caps than near the center. This may be carried out by using an increased layer thickness near the ends, gradually decreasing to the center. Thereby $\omega^2 C_1^2 R_1^2$ may be much decreased and even made small, compared with unity, up to a few hundred megacycles. By choosing the resistance per unit length near the center, so that $\omega^2 C_2^2 R_2^2$ is small compared with unity too, units of approximately invariable real resistance value up to a few hundred megacycles may be obtained. The capacities near the ends, as well as near the center, may be decreased by decreasing the cylinder diameter. Miniature units—e.g., of one cm length and one mm diameter—constructed along these lines have been shown experimentally to satisfy practical requirements in the entire ultra-high frequency range. Their resistance values range from a few to some 50 k ohms.

REFERENCES: *29, 34, 78, 283.*

IV.1.2. Transmission lines. These wave conductors consist of two parallel lines, all dimensions in a plane perpendicular to the direction of power propagation being small compared with one-quarter wavelength. The lines may be of different shapes.

IV.1.21. General properties of transmission lines. Most transmission lines in practical use are of uniform shape throughout their length. We shall assume this condition to be satisfied. The voltage V between adjacent points on the two lines and the currents I in each line measured at these points (being of equal amounts and opposite directions in both lines) have a constant ratio if we consider a wave propagated freely along a transmission line. This ratio is called the surge or wave impedance Z_o of the line. In general Z_o is complex but with most actual lines Z_o is a purely real resistance or is very nearly real. Now consider a line terminated by an impedance Z connected to its end terminals. If a wave travels along the line it is in general partly reflected at this terminated end and part of its power is absorbed by Z. Denoting the current of the wave incident at Z by I and the voltage by V, the coefficient of reflection being F, the reflected current is $-FI$,

its direction being reversed to that of the incident current. The reflected voltage is FV and hence the total current at Z is $(1 - F)I$ and the total voltage $(1 + F)V$. The ratio of the latter voltage to the former current being Z, we have:

$$\frac{V}{I}\frac{1+F}{1-F} = Z.$$

Inserting the value $Z_o = V/I$ for the incident wave, we obtain:

$$\mathbf{F} = \frac{1 - \mathbf{Z}_o/\mathbf{Z}}{1 + \mathbf{Z}_o/\mathbf{Z}}, \quad \frac{\mathbf{Z}_o}{\mathbf{Z}} = \frac{1 - \mathbf{F}}{1 + \mathbf{F}}, \qquad \text{(IV.1.21}a\text{)}$$

which constitutes the expression for the complex coefficient $\mathbf{F}$ of reflection. Obviously, by Eq. (a), $\mathbf{F} = 0$ if $\mathbf{Z} = \mathbf{Z}_o$ which shows a fundamental property of the wave impedance: If a transmission line is terminated by its wave impedance, no reflection occurs and the line behaves similarly to one of infinite length. The above Eqs. (a) show that the relation between $\mathbf{F}$ and the ratio $\mathbf{Z}_o/\mathbf{Z}$ is a completely reciprocal one. The values of $\mathbf{Z}/\mathbf{Z}_o$ corresponding to a definite complex value of $\mathbf{F}$ may be obtained from Figure 75. By this reciprocity these curves may also be used in obtaining $\mathbf{F}$ from a given ratio $\mathbf{Z}/\mathbf{Z}_o$.

If a line of length l cm is terminated by its wave impedance Z_o, its voltage at the input terminals being V_i and at the output terminals V_o, the ratio V_o/V_i is a characteristic property of the line:

$$\frac{V_i}{V_o} = \exp(\gamma l) = \exp(\alpha l + j\beta l), \qquad \text{(IV.1.21}b\text{)}$$

γ being termed the propagation coefficient of real part α (attenuation coefficient) and imaginary part β (phase coefficient). The ratio of input current I_i to output current I_o is exactly equal to V_i/V_o, as the currents bear a constant ratio to the corresponding voltages. Thus the average input power P_i is related to the average output power P_o by:

$$\frac{P_i}{P_o} = \exp(2\alpha l) = \frac{1}{g} \qquad \text{(IV.1.21}c\text{)}$$

and this equation is similar to Eq. (I.1.23d) describing the absorptive propagation of waves in space. The attenuation coefficients 2α or α may be expressed in different units as shown in the table in section I.1.23. The gain g of a Z_o-terminated transmission line of length l is related in a simple way to the attenuation $2\alpha l$ as shown by Eq. (c).

We shall assume that one unit (cm) of length of both line conductors added together has a series resistance R_s. Hereby a loss of power of

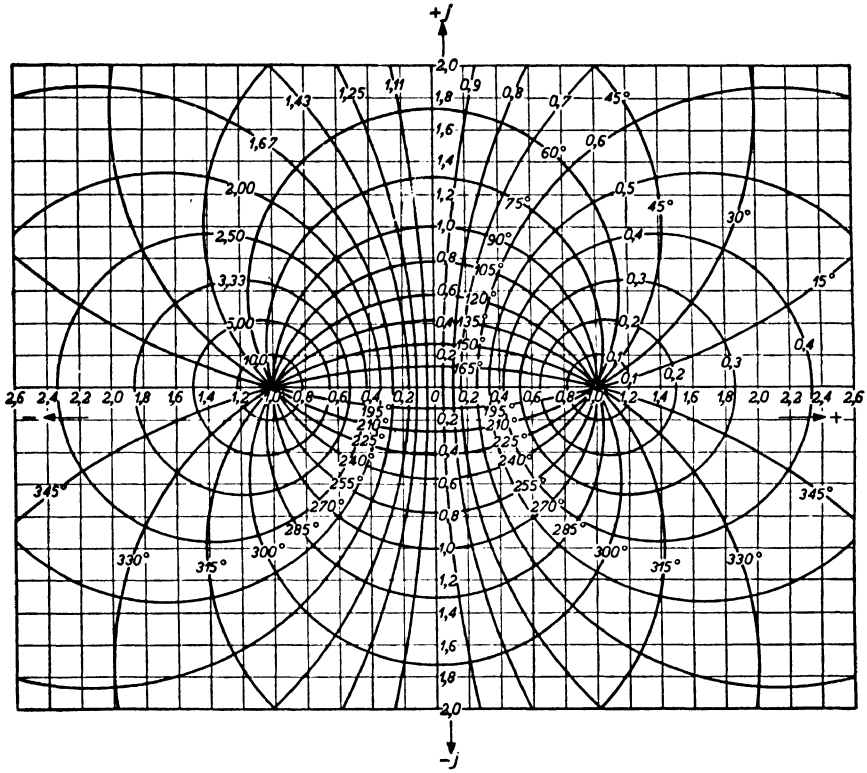

FIG. 75 Vertical scale: Ratio of imaginary part of terminal impedance to line wave impedance. Horizontal scale: Ratio of real part of terminal impedance to line wave impedance. Circles centered on the horizontal axis are loci for constant moduli of reflection coefficients (indicated at each circle). Circles centered on the vertical axis are loci for constant phase-angles of reflection coefficients (again indicated at each circle).

I^2R_s is caused, or, by $I = V/Z_o$, a ratio of power loss to transmitted power of

$$2\alpha_s = \frac{I^2R_s}{V^2/Z_o} = \frac{V^2R_s/Z_o^2}{V^2/Z_o} = \frac{R_s}{Z_o}, \qquad \text{(IV.1.21}d\text{)}$$

α_s being the attenuation coefficient due to series resistance. If we

assume no series resistance but a parallel resistance between one unit (cm) of length of the lines amounting to R_p the ensuing ratio of power loss to transmitted power is:

$$2\alpha_p = \frac{V^2/R_p}{V^2/Z_o} = \frac{Z_o}{R_p}, \qquad \text{(IV.1.21}e\text{)}$$

α_p being the attenuation coefficient due to parallel (leakage) resistance. The sum $\alpha_s + \alpha_p$ is the over-all attenuation coefficient α if no other causes of power loss are present.

If no power loss occurs, the ratio $V/I = Z_o$ on a Z_o-terminated transmission line is purely real. But if attenuation occurs, Z_o becomes complex. If attenuation is slight, we have:

$$\mathbf{Z}_o \approx |Z_o| \left(1 - j\frac{\alpha_s \lambda_o}{2\pi} + j\frac{\alpha_p \lambda_o}{2\pi}\right), \qquad \text{(IV.1.21}f\text{)}$$

assuming that each imaginary expression between parentheses is small compared with unity, λ_o being the wavelength on the transmission line, differing only slightly from the wavelength λ in free space. By Eq. (IV.1.21b) we have: $\beta = 2\pi/\lambda_o$.

REFERENCES: *50, 68, 232, 386.*

IV.1.22. Properties of sections of transmission lines. Considering a uniform transmission line of length l and terminated by an impedance Z_e, we want to evaluate its input impedance Z_i at the input terminals. If we connect these input terminals to a further line of equal structure, the reflection coefficient F_i of a wave incident on the said input is related to Z_i by Eq.(IV.1.21a):

$$F_i = \frac{1 - Z_o/Z_i}{1 + Z_o/Z_i}, \qquad \text{(IV.1.22}a\text{)}$$

while the coefficient of reflection F_e at the far end terminated by Z_e bears a similar relationship to the ratio Z_o/Z_e. A wave, incident on the input and traveling on to the far end, has to cover the length l twice before its reflected part arrives again at the input end. This entails the relation:

$$F_i = F_e \exp(-2\gamma l) = \frac{1 - Z_o/Z_e}{1 + Z_o/Z_e} \exp(-2\gamma l),$$

whence:

$$\frac{Z_o}{Z_i} = \frac{1 - F_e \exp(-2\gamma l)}{1 + F_e \exp(-2\gamma l)} = \frac{\operatorname{cotanh}(\gamma l) + Z_e/Z_o}{1 + \frac{Z_e}{Z_o}\operatorname{cotanh}(\gamma l)}. \quad \text{(IV.1.22}b\text{)}$$

The ratio Z_o/Z_i may in many cases be obtained graphically by applying Figure 75 twice, first to determine F_e from the given ratio Z_o/Z_e and second for the determination of Z_o/Z_i by the first relation of Eq. (*b*) after multiplication of F_e by $\exp(-2\gamma l)$, this relation being entirely similar to Eq. (IV.1.21*a*). The second relation of Eq. (*b*) is more suited to the discussion of particular cases. If the real part of γ is small in comparison with the modulus of its imaginary part, the hyperbolic function of Eq. (*b*) may very nearly be replaced by the corresponding trigonometric function cotan.

One of the most important types of line sections is the quarter-wave section: $l = \lambda_o/4$. Upon insertion of the values of Eqs. (IV.1.21*f*) and (IV.1.21*b*) for Z_o and for γ into Eq. (IV.1.22*b*), we obtain, if $Z_e = 0$:

$$\frac{R_i}{|Z_o|} = \frac{1}{\alpha l}\left(1 + \frac{\alpha^2\lambda_o^2}{4\pi^2}\right), \quad l = \frac{\lambda_o}{4}, \quad \text{(IV.1.22}c\text{)}$$

the resulting input impedance Z_i being real and equal to R_i. As αl is usually small, the ratio $R_i/|Z_o|$ is in most cases very large. Thus this quarter-wave low-loss line behaves as a very large real impedance. If its length is varied slightly the resulting impedance Z_i behaves similar to the off-tune impedance of a resonant circuit such as that pictured in Figure 42, the input terminals of this quarter-wave line being equivalent to the terminals 3, 4 of Figure 42. Defining the quality figure Q in a similar way to section III.3.12, the frequency difference from the tuning frequency f_o corresponding to a drop of $|Z_i|^2$ by 3 db being equated to $f_o/2Q$, we obtain:

$$Q = \frac{\pi}{4}\frac{1}{\alpha l}\left(1 + \frac{\alpha^2\lambda_o^2}{4\pi^2}\right), \quad l = \frac{\lambda_o}{4}. \quad \text{(IV.1.22}d\text{)}$$

This figure may be extremely high due to the smallness of αl with low-loss lines, values over 1000 being no exception.

Disregarding the losses and attenuation altogether, the behavior of some useful lengths of line sections is compiled below, Z_o being real and q being an integral number (reference *163*):

LINE LENGTH	FAR-END TERMINAL IMPEDANCE Z_e	NPUT MPEDANCE Z_i	EQUIVALENT LUMPED CIRCUIT
$l \ll \lambda_o$	$Z_e = 0$	$Z_i = j\frac{2\pi l}{\lambda_o} Z_o$	series inductance
$l \ll \lambda_o$	$Z_e = Z_o$	$Z_i = Z_o$	series resistance
$l \ll \lambda_o$	$Z_e = \infty$	$Z_i = \frac{Z_o \lambda_o}{j2\pi l}$	series capacitance
$l = (2q - 1)\,\lambda_o/8$	$Z_e = 0$	$Z_i = jZ_o$	series inductance
$l = (2q - 1)\,\lambda_o/8$	$Z_e = Z_o$	$Z_i = Z_o$	series resistance
$l = (2q - 1)\,\lambda_o/8$	$Z_e = \infty$	$Z_i = -jZ_o$	series capacitance
$l = (2q - 1)\,\lambda_o/4$	$Z_e = 0$	$Z_i = \infty$	tuned resonant circuit
$l = (2q - 1)\,\lambda_o/4$	$Z_e = Z_o$	$Z_i = Z_o$	series resistance
$l = (2q - 1)\,\lambda_o/4$	$Z_e = \infty$	$Z_i = 0$	tuned antiresonant circuit
$l = q\lambda_o/2$	$Z_e = 0$	$Z_i = Z_e = 0$	tuned antiresonant circuit
$l = q\lambda_o/2$	$Z_e = Z_o$	$Z = Z_e = Z_o$	series resistance
$l = q\lambda_o/2$	$Z_e = \infty$	$Z = Z_e = \infty$	tuned resonant circuit

REFERENCES: *33, 81, 94, 146, 163, 232, 258, 293, 321.*

IV.1.23. Wave impedance and attenuation. The wave impedance may be calculated from the power propagated through each cross-section if the electromagnetic field generated in the surrounding space is known. We shall consider two types of transmission lines which are of common occurrence in u.h.f. circuits (see Fig. 76). Of these the attenuation coefficients as well as the wave impedances will be given. The respective values of α and Z_o will be indicated by suffixes related to Figure 76, such as α_a, α_b, Z_{oa}, Z_{ob}. The values of 2α are given in db/100 feet and those of Z_o in ohms. In the case a of Figure 76 we have:

$$Z_{oa} = \frac{276}{\sqrt{\epsilon}} \lg_{10}\left(\frac{D + \sqrt{D^2 - d^2}}{d}\right) \approx \frac{276}{\sqrt{\epsilon}} \lg_{10}\left(\frac{2D}{d}\right), \quad \text{if } d \ll D, \tag{IV.1.23a}$$

ϵ being the dielectric coefficient of the surrounding medium, assumed to be of homogeneous isotropic structure (in vacuum $\epsilon = 1$). The ratio λ/λ_o of the wavelength in vacuum (air) to that on the line is very nearly equal to $\sqrt{\epsilon}$. In calculating the attenuation the frequency is

assumed to be so high that the depth d_o of penetration according to Eq. (IV.1.11a) is very small compared with the wire diameter d.

$$2\alpha_a = 2.2 \times 10^{-3} \frac{\sqrt{f(\mathrm{c/s})}}{Z_{oa} d(\mathrm{cm})} \frac{\sqrt{\frac{\sigma_{\mathrm{copper}}}{\sigma}}}{\sqrt{1 - \frac{d^2}{D^2}}} + 2.8 \times 10^{-6} f \tan \delta \sqrt{\epsilon} \qquad \text{(IV.1.23}b\text{)}$$

δ being the loss angle of the surrounding dielectric material (see Eq. I.1.21a) and σ the specific conductivity of the wires, being supposed of equal composition. In air and in vacuum the second component

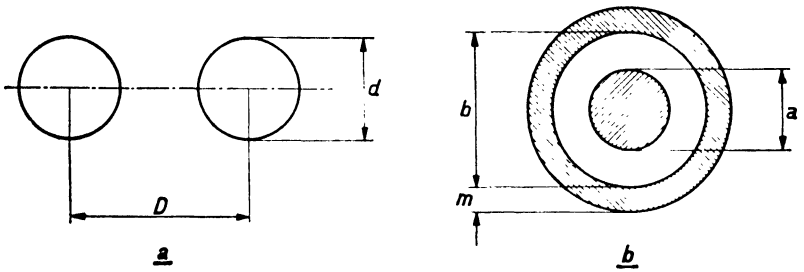

FIG. 76 Picture of parallel-wire-type transmission line (diagram a) and of coaxial line (diagram b).

of $2\alpha_a$ may often be neglected compared with the first one (except at high voltages near breakdown). There is still a third component of $2\alpha_a$ not included in the above Eq. (b) and pertaining to radiation of power into the surrounding space. The parallel-wire line obviously acts as a transmitting antenna, and its power radiation is equivalent to an additional attenuation. The exact amount of this radiation depends on the current distribution along the transmission line. As an approximate value pertaining to a quarter-wave line shorted at the far end, the equation:

$$2l\alpha_{ar}\ (db) = \frac{8.7 \times 240\pi^2 \left(\frac{D}{\lambda_o}\right)^2}{\sqrt{\epsilon} Z_{oa}} \qquad \text{(IV.1.23}c\text{)}$$

may be cited ($l = \lambda_o/4$). This value α_{ar} is additional to α_a of Eq. (b). The three subsequent components of α_a are hence respectively proportional to $\sqrt{f}$, f, and f^2, if f is the frequency of operation. At extreme-high frequencies, the latter part (α_{ar}) therefore becomes predominant.

As an example, the three components of α_a are shown in Figure 77 as dependent on the frequency f.

In order to avoid the radiation component of attenuation with

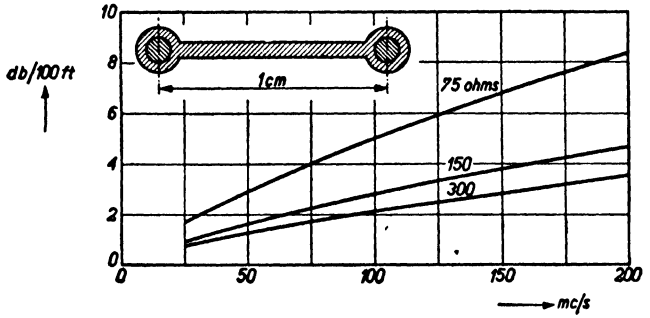

FIG. 77 Attenuation expressed in db per 100 ft (vertical scale) of parallel-wire lines constructed of two twisted leads, spaced by polyethylene insulation shaped as a strip containing the conductors (see upper figure). Horizontal scale: Frequency mc/s. Curves are related to lines of different wave impedances as indicated, of which upper figure pictures the one of 300 ohms. These curves show that the first part of eq. (IV.1.23b) dominates up to, say, 100 mc/s (proportionality to $\sqrt{f}$), while the second part and the radiation according to eq. (IV.1.23c) make themselves felt at higher frequencies. Loss angle of insulation is about 0.0004.

parallel-wire lines, enclosures of different shapes have been used, as shown in Figure 78. The corresponding wave impedance is less than without enclosure, an approximate value being (reference *200*):

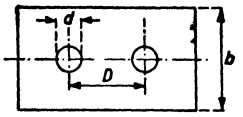

FIG. 78 Parallel-wire line enclosed in a rectangular shield.

$$Z_o = \frac{276}{\sqrt{\epsilon}} \lg_{10} \left[\frac{\tanh\left(\pi \frac{D}{2b}\right)}{\frac{\pi d}{4b}} \right]. \qquad \text{(IV.1.23}d\text{)}$$

The most useful lines at u.h.f. are, however, those of Figure 76b, i.e., concentric cylindrical lines. With these lines we have:

$$Z_{ob} = \frac{138}{\sqrt{\epsilon}} \lg_{10} \left(\frac{b}{a}\right), \qquad \text{(IV.1.23}e\text{)}$$

$$2\alpha_b = 0.55 \times 10^{-3} \frac{\sqrt{f}}{Z_{ob}} \left(\frac{1}{a} + \frac{1}{b}\right) \sqrt{\frac{\sigma_{\text{copper}}}{\sigma}} + 2.8 \times 10^{-6} f \tan\delta \sqrt{\epsilon}. \qquad \text{(IV.1.23}f\text{)}$$

It may be shown that α_b attains a minimum value if the ratio b/a is 3.6. The corresponding value of Z_{ob} is $77/\sqrt{\epsilon}$ ohms while the corresponding value of α_b becomes approximately:

$$2\alpha_b = 0.9 \times 10^{-5} \frac{\sqrt{f\epsilon}}{a} \sqrt{\frac{\sigma_{\text{copper}}}{\sigma}} + 2.8 \times 10^{-6} f \tan \delta \sqrt{\epsilon}.$$

Some measured values on coaxial cables of 75 ohms wave impedance and of different construction are shown in Figure 79. The theoretical value according to the above Eq. (*f*) for an air-spaced coaxial cable

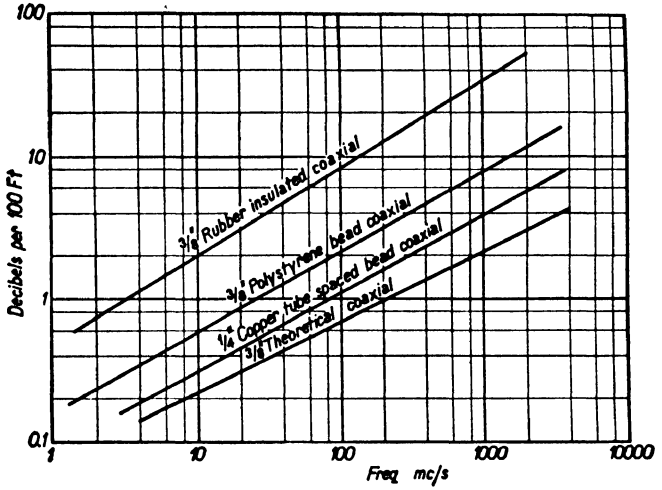

FIG. 79 Experimental data on attenuation of coaxial lines (reference *163*).

($\epsilon = 1$ and $\delta = 0$) is shown in the lowest curve, actual values being higher on account of various additional losses, e.g., in the dielectric insulating material. With good coaxial cables, however, the proportionality of α to $\sqrt{f}$ is satisfactory.

Finally we consider a quarter-wave coaxial line as discussed in connection with Eq. (IV.1.22c) and (*d*). It may be shown that R_i attains a maximum value if the ratio b/a is chosen to be 9.2. The maximum value of Q corresponds to minimum attenuation α and hence to a ratio b/a of 3.6. For an air-spaced quarter-wave section

of $b/a = 3.6$ and hence of 77 ohms wave impedance, the value of Q is:

$$Q_{max} = 5.2 \times 10^4 \frac{a}{\sqrt{\lambda}}, \quad a \text{ and } \lambda \text{ in cm.} \qquad \text{(IV.1.23}g\text{)}$$

In the dm wave range values of Q over 1000 may readily be obtained.

REFERENCES: *85, 95, 122, 200, 242, 281, 293, 332, 334.*

IV.1.24. Line transformers and line noise. The primary purpose of a transmission line is, in the case under discussion, to transmit power from the reception antenna to the receiver. In doing so it may be said to act partly as a transformer. We shall consider some special types of line transformers. Most transformers are based on the quarter-wave section. According to Eq. (IV.1.22*b*), disregarding losses, $\gamma l = j\pi/2$ and hence

$$Z_o^2 = Z_i Z_e \quad \text{or} \quad Z_e = Z_o^2/Z_i. \qquad \text{(IV.1.24}a\text{)}$$

By a proper choice of Z_o at a given value of Z_i, it is thus possible to obtain either a higher or a lower value of Z_e than Z_i. We may construct step-up or step-down transformers in this way. Owing to the losses, this transformation ratio cannot exceed a definite value for a particular quarter-wave section, this upper limit being $4Q/\pi$, which may be easily derived from Eqs. (IV.1.22*c*) and (*d*).

If a coaxial line is to be connected to a reception antenna, symmetrical with respect to its central terminals, as usual, some means must be inserted to prevent one antenna terminal from becoming grounded if connected to the outer tube of the line. An example is shown in Figure 80, called the quarter-wave skirt. The coaxial line is extended for one-quarter wavelength into the outer tube acting as a screen. By this skirt both conductors of the coaxial line, when connected to the balanced antenna terminals, attain a high impedance to ground. This skirt is effective over a considerable frequency range, its impedance Z at a frequency f somewhat different from the tuning frequency f_o being:

$$|Z| = Z_o \left| \tan\left(\frac{\pi}{2}\frac{f}{f_o}\right) \right|,$$

Z_o denoting the wave impedance of the outer skirt-tube with respect to the outer conductor of the coaxial line. This wave impedance may be made much higher than the Z_o-value of that line. Satisfactory effect of the skirt may thus be obtained from 240 to 360 mc/s. Another,

almost self-evident, example of a quarter-wave skirt is shown in Figure 81. The skirt may be combined with a quarter-wave line transformer as shown in Figure 82. Another transformer is the so-called folded half-wave antenna

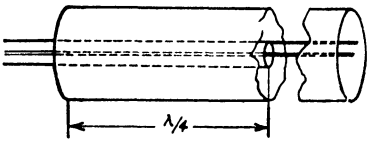

FIG. 80 Quarter-wave skirt used in transition from a coaxial line to a shielded double-wire balanced line.

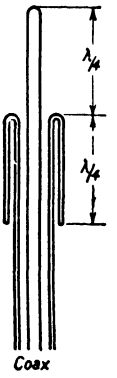

FIG. 81 Quarter-wave skirt used as part of a half-wave reception antenna connected to a coaxial line (reference *163*).

of Figure 83. By bringing two equal half-wave antennas close together the resulting radiation resistance, if measured at the terminals of one of them, the other one being short-circuited at its center, is approximately four times the radiation resistance of one of the antennas. Thus about $4 \times 73 = 292$ is obtained in this way. If one radiator has a smaller diameter, as in Figure 83, the step-up ratio may be below or above 4 (references *61*, *163*).

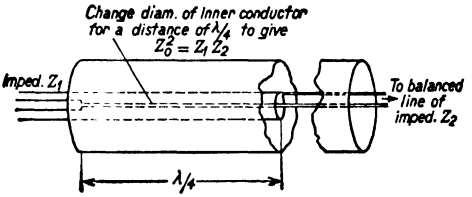

FIG. 82 Quarter-wave skirt combined with a quarter-wave transformer used in transition from a coaxial line to a double-wire shielded balanced line (reference *163*).

As regards the noise of a transmission line section, the rule of section II.1.33 may be applied; according to this, the available noise power at two terminals of a passive network (our line is such a network) at a uniform temperature T_l is $KT_l\Delta f$ and the corresponding impedance has the value measured at the terminals. If the line section has a

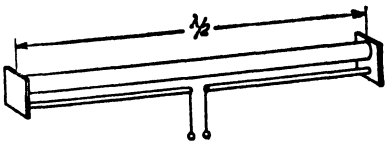

FIG. 83 Transformer circuit consisting of two parallel adjacent half-wave antennas, radiation coupled.

gain g and a temperature T_l, its noise figure is hence:

$$N_l = \frac{T_i}{T} + \frac{T_l}{gT}, \qquad \text{(IV.1.24}b\text{)}$$

T_i being the temperature at the output of the signal generator.

REFERENCES: *61, 163, 321, 332, 382, 383.*

IV.1.3. Wave guides. If the frequencies are increased beyond, say, 3000 mc/s, the transmission lines dealt with above become obsolete. Their place is then taken by the so-called wave guides.

IV.1.31. Fundamental properties of wave guides. These wave guides consist of hollow metal tubes, in the interior space of which the waves are transmitted from input to output end. Obviously wave motion in these guides is similar to that in free space, the difference being that a lateral concentration of the waves is obtained by the metal tube walls. In the propagation the general properties of electromagnetic fields near metal surfaces are satisfied, the electric-field strength being directed perpendicular to and the magnetic-field strength parallel to the surfaces in their vicinity. Under these conditions, only definite wave patterns are possible though an infinite sequence of such patterns exists. As in the case of transmission lines, we shall assume that all the field strengths are proportional to exp $(-\gamma z)$, z being a length directed parallel to the axis of the guide and γ a propagation coefficient as given in Eq. (IV.1.21b). The real part α of γ marks the attenuation coefficient and will again be expressed in db per 100 feet, other units being easily obtainable from the table of section I.1.23.

Some particular wave types have been found to afford simple approaches to more general types of wave transmission. In these types either the electric-field strength directed parallel to the guide's axis is assumed to be zero (indicated as transverse-electric or T-E wave), or the magnetic-field strength of this direction is assumed to be zero (indicated as transverse-magnetic type or T-M wave). Of the T-M as well as of the T-E waves, an infinite sequence of sub-cases exists, differing in field patterns though satisfying the general conditions of the type. For some simple cross-sections, such as circular or rectangular, the T-E and T-M waves have been studied in detail. Field patterns for circular cross-sections are shown in Figure 84. Attenuation co-

efficients α of the four wave types pictured in Figure 84 are shown for a particular guide in Figure 85.

Leaving out the case of the T-E_{01} wave which will be dealt with presently, attenuation is seen to rise very steeply below a definite frequency approximately corresponding to minimum attenuation in

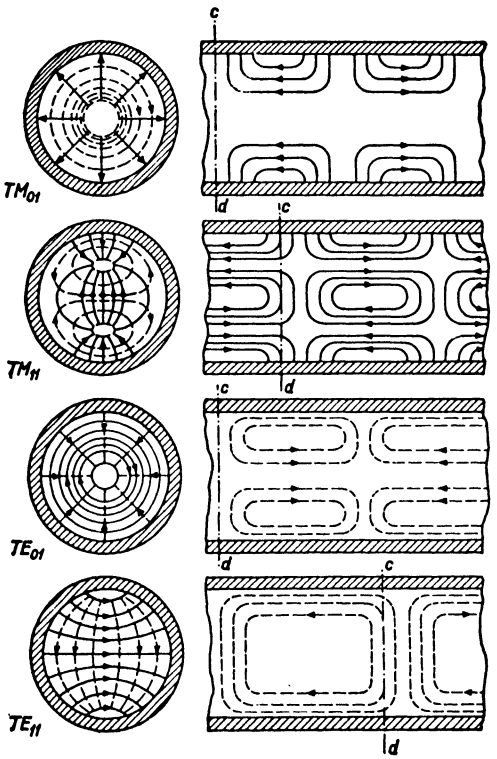

FIG. 84 Field patterns in a circular wave guide corresponding to the wave types indicated. Electric lines of force are full curves and magnetic lines of force are broken curves.

Figure 85. Below this frequency the guides become unfitted for practical use. Above this frequency attenuation is caused by eddy-current losses in the guide's walls and is proportional to the square root of the frequency, as is to be expected from this cause (see Fig. 79). In a guide of circular cross-section, the lowest frequencies suitable for

transmission, or rather, the corresponding longest wavelengths λ in the medium inside the guide, are directly related to the diameter D of the cross-section:

Wave type	T-M_{01}	T-M_{11}	T-E_{11}
λ/D	1.31	0.82	1.71

With the T-E_{01} waves, attenuation theoretically decreases if the frequency is increased (see Fig. 85). But unfortunately this exceptional

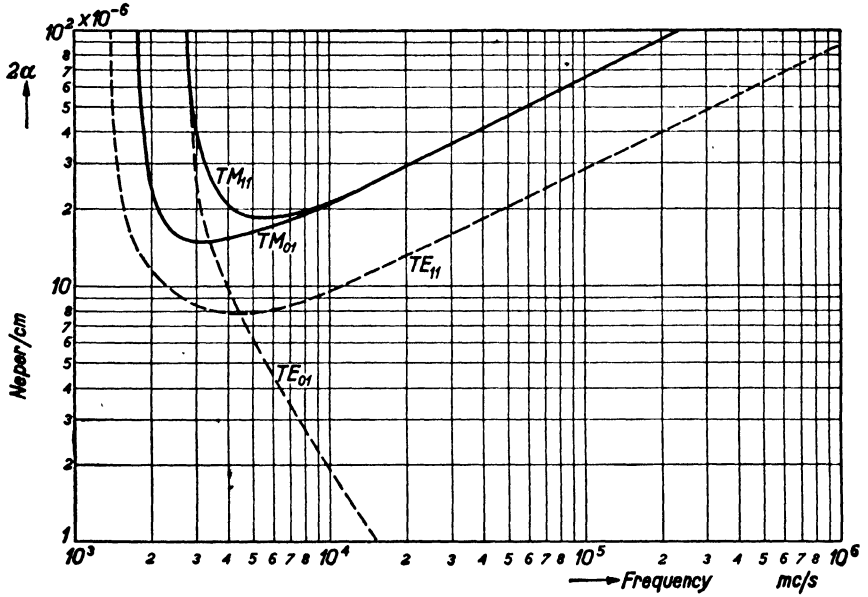

FIG. 85 Attenuation of some wave types in wave guides of circular cross-section, the inner copper tube diameter being 5 in. See table of section I.1.23 for other units of attenuation.

behavior is strictly dependent on an exactly symmetrical field pattern such as that shown in the T-E_{01} picture of Figure 84. Even a very slight departure from these conditions entails an attenuation curve similar to that of the other wave types in Figure 85. Thus no practical value should be attached to the T-E_{01} curve of Figure 85, as the attending conditions can hardly ever be realized in actual guides.

The two suffixes are closely related to the respective cross-sectional

field patterns. Thus, with T-M_{01} and T-E_{01} waves the patterns are of circular symmetry (suffix 0) and belong to the lowest frequency corresponding to this symmetry (suffix 1). With T-M_{11} and T-E_{11} waves there is one diameter of symmetry (first suffix 1), and the second suffix 1 indicates the lowest frequency corresponding to this symmetry. With T-M_{21} waves there would be two diameters of symmetry, etc. With T-M_{02} or T-M_{12} or T-M_{22}, etc., waves the second lowest frequency corresponding to the respective type of symmetry is indicated by the second suffix being 2, and so forth.

Similar relations exist with wave guides of different cross-sections. As a further example we shall discuss briefly some wave types and field patterns of guides of rectangular cross-section. Again we assume, first, that the electric-field strength directed axially is zero (T-E waves), and second, that the magnetic-field strength directed axially is zero (T-M waves). The simplest type of T-M waves has one focal point of magnetic lines of force in a cross-section as shown by Figure 86*a*, corresponding to the upper picture of Figure 84. This is usually indicated as the T-M_{11} wave. The need for a double suffix will appear presently. Other T-M-wave field patterns are shown in Figures 86*b* and 86*c*, being respectively indicated as T-M_{21} and T-M_{12} waves. The suffixes obviously indicate the number of focal points of the field patterns parallel to either side of the rectangular cross-section. A T-M_{31} wave has the pattern of Figure 86*d*. The electric lines of force are perpendicular to the magnetic ones shown in Figure 86. With the T-E waves the parts of electric and magnetic lines of force are reversed with respect to the equally suffixed T-M waves. As with the circular diameter, a lowest frequency exists for each wave type, below which attenuation becomes prohibitive. If a and b are the faces of the rectangular cross-section, the upper wavelength λ in the medium inside the guide corresponding to the

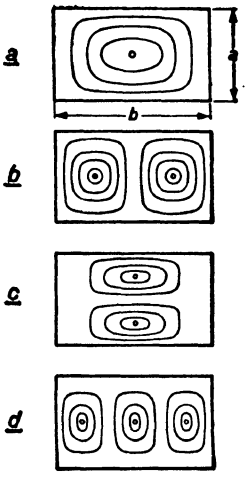

FIG. 86 Pictures of magnetic lines of force corresponding to various types of T-M waves in a rectangular guide. Diagrams a to d correspond to T-M_{11}, T-M_{21}, T-M_{12}, T-M_{31} waves respectively.

lowest frequency is given by:

$$\frac{4}{\lambda^2} = \left(\frac{q_a}{a}\right)^2 + \left(\frac{q_b}{b}\right)^2, \qquad \text{(IV.1.31}a\text{)}$$

q_a and q_b being equal to the respective suffixes of the wave indication. Thus in a square $a = b$ and the highest possible value of λ is obtained with $q_a = q_b = 1$, this value therefore being: $\lambda = a\sqrt{2} = 1.41 \times a$. This ratio of λ/a is somewhat smaller than the corresponding ratio in the case of a circular cross-section for T-E_{11} waves.

REFERENCES: *14, 35, 36, 57, 79, 212, 225, 308, 310, 325.*

IV.1.32. Comparison with lines and excitation. With rectangular and other guides of less symmetric structure than the circular ones, optimum ratios of the different principal dimensions of the guide's cross-section may be determined, corresponding to minimum attenuation in the range of operation (i.e., above the lowest border frequency). In the case of a rectangular guide transmitting T-M waves, the optimum ratio b/a depends on the suffix numbers q_a and q_b. If one is unity and the other is equal to 2, this ratio is 1.27; if both are equal to 2, this ratio is again unity, etc. The attenuation α expressed in db per 100 feet is shown, for some copper guides of optimal cross-sectional rectangular dimensions, in Figure 87 as dependent on frequency (reference *295*).

Comparing the present wave guides with the transmission lines of section IV.1.2, some practical points have to be taken into account. Considering, for example, the T-M_{01} wave of Figure 84, we might quite well assume a circular coaxial conductor at the center of the guide. The inter-conductor dimensions would still be such that ordinary transmission-line theory—e.g., the equations of section IV.1.23 giving the coefficients of attenuation—cannot be applied, as these require the dimensions to be small compared with a quarter wavelength. Therefore we would obtain what should be called a wave guide of coaxial shape. Considering the frequency corresponding to the T-M_{01} wave, this guide would be operated below its lowest frequency of operation and hence would show a very high attenuation compared with the minimum value corresponding to the T-M_{01} wave of Figure 85. If now, in order to comply with the requirements of a true coaxial transmission line, the cross-section should be decreased, the field strengths at the conductor surfaces corresponding to equal transmitted power, as with

the previous guide, would be much higher, entailing higher specific losses and higher attenuation. This latter figure would thus be much higher than that of the original T-M_{01} guide. A similar reasoning may be applied to different guides and wave types. At their given frequencies of operation the guides afford a much lower attenuation of transmitted power than any other known means of transmission.

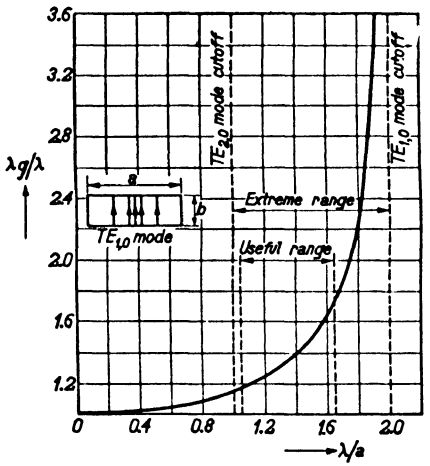

FIG. 87a Vertical scale: Ratio of wavelength λ_g along guide to wavelength λ in free space. Horizontal scale: Ratio of λ to width a of wave guide. Showing ranges and cut-off of T-E_{10} waves.

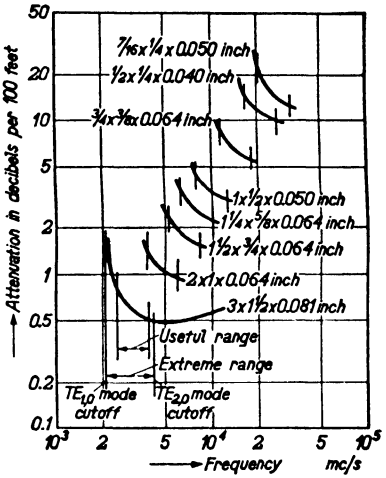

FIG. 87b Attenuation of T-E_{10} waves in wave guides of various dimensions as dependent on frequency.

We shall now consider the excitation of different wave types in guides. Taking first the T-M_{01} wave of Figure 84, a dipole or half-wave antenna placed along the axis of the guide will cause an electric-field strength pattern substantially as shown in the figure. With the T-M_{11} wave of Figure 84, two such antennas, excited counterphase, are needed, placed at the two focal points of the cross-section coaxially with respect to the guide. In the case of the T-E_{01} wave, a small loop antenna at its center would cause substantially the desired field pattern. Similar small transmitting antennas might be used for excitation of the respective wave types in a guide of rectangular cross-section (Fig. 86).

Here we consider a simple and very useful type of wave guide. It is of rectangular cross-section with one of its faces—say b—however,

small compared with one-quarter wavelength. The electric-field strength of T-E_{10} waves is directed parallel to this face in the guide's cross-section. It is zero at the surfaces of the *b*-faces, the magnetic-

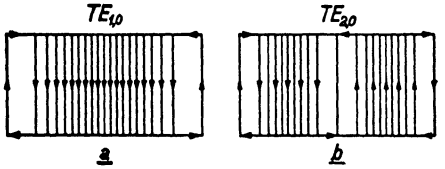

FIG. 88a Electric-field pattern of T-E_{10} and T-E_{20} waves in a rectangular guide.

field strength being almost everywhere parallel to the *a*-faces except in the vicinity of the *b*-faces (see Fig. 88 and references *246*, *316*). It offers particular advantages to measurements, as two adjacent points on

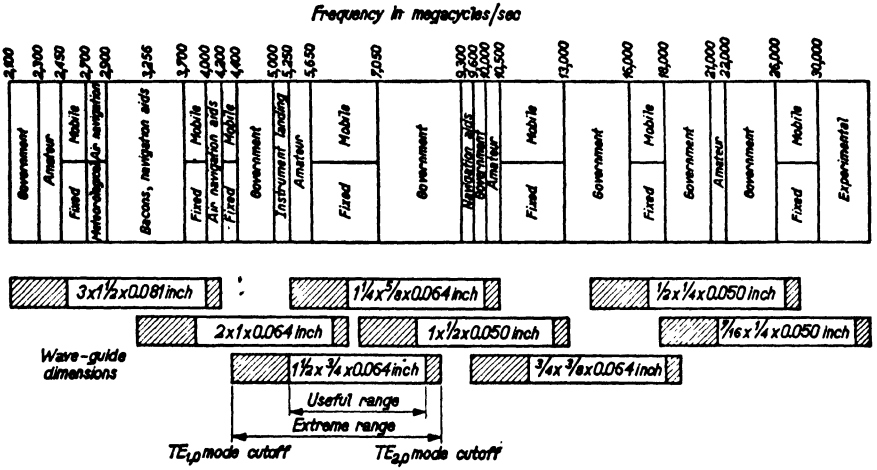

FIG. 88b Dimensions of various guides for T-E_{10} waves suitable for different frequencies in the u.h.f. and s.h.f. ranges as indicated.

opposite *a*-faces have a mutual distance small compared with one-quarter wavelength.

REFERENCES: *6, 19, 37, 43, 83, 241, 246, 295, 316, 326, 328.*

IV.2. RESONANT CIRCUITS AND CAVITIES

Besides antennas and wave conductors, means are used in reception as well as in transmission circuits to afford additional selectivity—i.e.,

discrimination between different wave ranges. These means are nearly always resonant circuits or resonant cavities.

IV.2.1. Lumped circuits. At frequencies below, say, 200 mc/s, circuits consisting of concentrated inductances and capacitances may be used. But even at these frequencies the additional capacitances and inductances caused by parts of wires or other conductors have often to be taken into account.

IV.2.11. Single resonant circuits at u.h.f. Such circuits are based on two elements: inductance coils and capacitances. Usually the capacitances are variable so as to allow adjustment of the resonance frequency, i.e., tuning, while the inductances are constant. Variations caused by temperature differences and by other secondary factors will be considered later. With inductances the quality figure Q, being the ratio of the modulus of coil reactance at resonance frequency to series resistance, is in many cases given high values by proper construction. Within a frequency range of 3 to 12 mc/s values for Q between 400 and 800 have been obtained with coils of about 3.7 μ henry using screening cans. Usually Q is lower, values of about 100 being common up to about 200 mc/s. With air condensers of proper design, tan δ need not be higher than 10^{-4} up to that frequency.

With circuits as shown in Figure 42 for which $Q \gg 1$, tan $\delta \ll 1$ and Q tan $\delta \ll 1$, the resonant impedance ($\omega_o^2 LC = 1$) at the terminals 3, 4 is approximately real and given by:

$$Z_{res} = \omega_o L Q = \frac{Q}{\omega_o C}. \qquad \text{(IV.2.11}a\text{)}$$

Assuming an angular frequency ω such that $|\omega - \omega_o| \ll \omega_o$, the modulus of the impedance Z at this frequency ω is approximately:

$$\frac{|Z|^2}{Z_{res}^2} = \frac{1}{1 + \dfrac{4(\omega - \omega_o)^2}{\omega_o^2} Q^2} = \frac{1}{1 + \zeta^2 Q^2}, \qquad \zeta^2 = \frac{4(\omega_o - \omega)^2}{\omega_o^2}. \qquad \text{(IV.2.11}b\text{)}$$

It is easy to see that the present definition of Q is perfectly equivalent with the one given previous to Eq. (III.3.12c). The total band width B of a resonant circuit is often defined as equal to twice the deviation in frequency from the resonant frequency, at which the ratio of Eq. (b)

has dropped to $\frac{1}{2}$. This band width B is simply related to Z_{res} and to Q:

$$Z_{res} = \frac{1}{2\pi BC} = \frac{Q}{\omega_o C}, \quad B = \frac{\omega_o}{2\pi Q}. \tag{IV.2.11c}$$

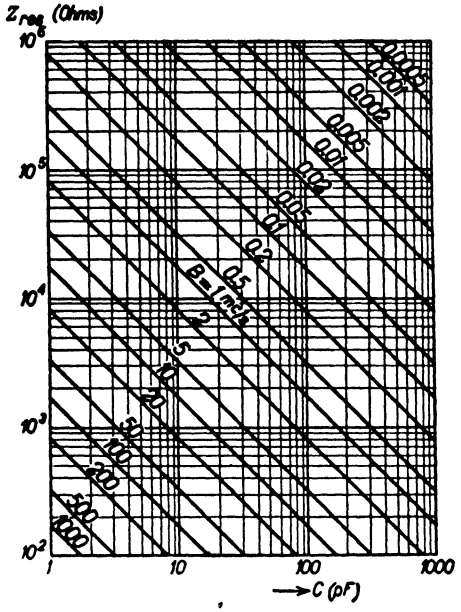

FIG. 89 Resonant impedance (vertical scale) as dependent on resonant circuit's shunt capacitance C (horizontal scale) at various band widths B.

This useful relation is pictured in Figure 89.

Whereas for the resonant circuit of Figure 42 the modulus of its impedance has a maximum value at resonance, circuits are sometimes needed which will show a minimum impedance at resonance. Two

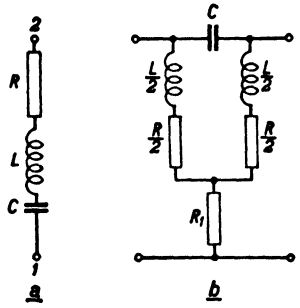

FIG. 90 Diagram a: Antiresonant circuit. Diagram b: Circuit of zero transfer impedance at an angular frequency ω_o given by $\omega_o^2 LC = 1$ if $R_1 = \omega_o^2 L^2/(4R)$.

such circuits are shown in Figure 90. With the circuit of Figure 90a, we have at $\omega_o^2 = 1/LC$:

$$Z_{res} = R \tag{IV.2.11d}$$

and at different frequencies:

$$Z^2 = R^2(1 + \zeta^2 Q^2), \tag{IV.2.11e}$$

Q and ζ having the same meaning as in Eq. (b) above. With the circuit of Figure 90b, the resonant transfer impedance Z_{res} is exactly zero

at $\omega_o^2 = 1/LC$. The value of R_1 is approximately equal to $\omega_o^2 L^2/(4R)$. The off-resonance transfer impedance Z (output open-circuit voltage over input current) is given by:

$$|Z^2| = \frac{(L/4CR)^2}{1 + \frac{1}{\zeta^2 Q^2}}, \qquad \text{(IV.2.11}f\text{)}$$

Q being $\omega_o L/R$ and ζ having the same meaning as in Eq. (*b*) above. The value of Z according to Eq. (*f*) is illustrated by Figure 91.

REFERENCES: *100, 138, 186, 226, 304, 359.*

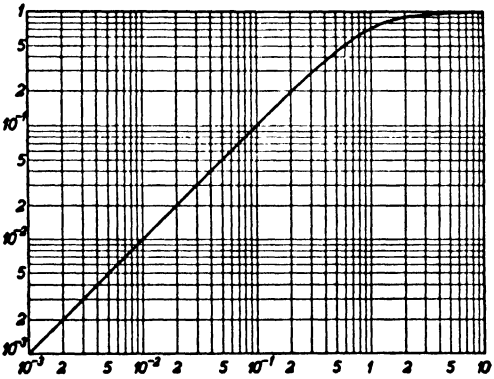

FIG. 91 Vertical scale: Ratio of impedance of circuit of Fig. 90*b* according to eq. (IV.2.11*f*), expressed in ohms to $L/(4CR)$. Horizontal scale: ζQ, being a measure for the frequency distance from the resonant position.

IV.2.12. Coupled resonant circuits. The theory of coupled resonant circuits has at present such a wide scope that we cannot here present anything like a comprehensive survey. Instead we shall discuss some simple examples of frequent practical occurrence with a view to the subsequent application of some notions considered to resonant cavities. In many cases a current generator of infinite internal impedance may be supposed to be connected to the input terminals of the four-pole constituted by the coupled circuits. In these cases an essential item of information often wanted is the ratio of the open-circuit voltage V across the output terminals at resonance to this voltage off-resonance or the inverse ratio. We shall quote this ratio in a number of simple

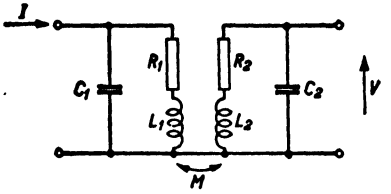

FIG. 92 Two resonant circuits coupled by a mutual inductance M.

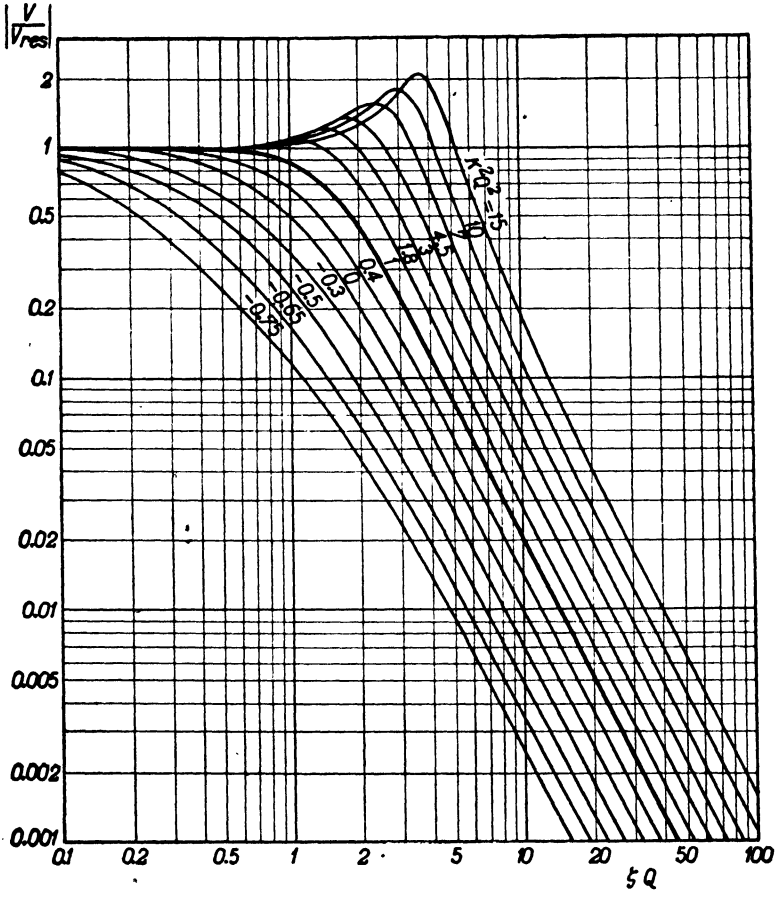

FIG. 93 Vertical scale: Ratio of output voltage V of network pictured in Fig. 92 to output voltage at resonance, assuming both resonant circuits to be equal. Horizontal scale: ζQ, being a measure for the frequency distance from resonance. Curves for different values of κQ, κ being the coupling coefficient M^2/L_1L_2 in the case of Fig. 92

cases. First, two resonant circuits coupled by a mutual inductance M will be considered (Fig. 92). This ratio works out approximately as:

$$\left|\frac{V}{V_{res}}\right|^2 = \frac{(1+\kappa^2Q^2)^2}{(1+\kappa^2Q^2)^2 + 2\zeta^2Q^2(1-\kappa^2Q^2) + \zeta^4Q^4}. \quad \text{(IV.2.12}a\text{)}$$

The underlying assumptions are: $\omega_o^2L_1C_1 = \omega_o^2L_2C_2$ (equal resonance frequencies), ζ^2 has the meaning of Eq. (IV.2.11b), $\omega_oL_1/R_1 = \omega_oL_2/R_2 = Q$, $\kappa^2 = M^2/L_1L_2$. It is supposed that $\zeta \ll 1$. This equation is illustrated by Figure 93. The extreme usefulness of Eq. (a) and of the curves of Figure 93 resides in their general applicability to coupled

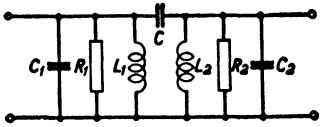

FIG. 94 Two resonant circuits coupled by means of a capacitance C as shown.

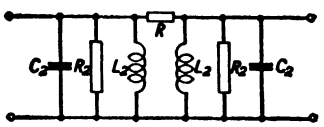

FIG. 95 Two resonant circuits coupled by means of a resistance R as shown.

circuits of different types of coupling. Thus, considering Figure 94 in which capacitive coupling is applied, we have simply to insert: $\kappa^2 = C^2/C_1'C_2'$ where $C_1' = C_1 + C$ and $C_2' = C_2 + C$, whereas the other symbols of Eq. (a) retain their significance. The negative values of κ^2Q^2 in Figure 93 pertain to a third type of coupling shown in Figure 95. In this case we have:

$$\kappa^2 = \frac{-1}{\omega_o^2R^2C_1C_2}, \quad Q_1 = \frac{\omega_oL_1}{R_1'}, \quad Q_2 = \frac{\omega_oL_2}{R_2'}, \quad \text{(IV.2.12}b\text{)}$$

$$\frac{1}{R_1} = \frac{1}{R_1} + \frac{1}{R}, \quad \frac{1}{R_2'} = \frac{1}{R_2} + \frac{1}{R}.$$

The curves of Figure 93 may also be applied to cases in which some of the above assumptions are invalid, if still $\zeta^2 \ll 1$, $Q_1 \gg 1$ and $Q_2 \gg 1$. We shall suppose that both coupled circuits have different resonance frequencies: $\omega_I^2L_1C_1 = 1$ and $\omega_{II}^2L_2C_2 = 1$, while $2\omega_o = \omega_I + \omega_{II}$, $\zeta_o^2\omega_o^2 = (\omega_{II} - \omega_I)^2$ the quality figures being Q_1 and Q_2, $1/Q = \frac{1}{2} \times (1/Q_1 + 1/Q_2)$, $\eta^2 = \frac{1}{4} \times (1/Q_1 - 1/Q_2)^2$. If the two coupled circuits are of equal quality but of different resonance frequencies, the coupling

coefficient κ^2 in Figure 93 and Eq. (*a*) must be replaced by $\kappa^2 + \zeta_o^2$. If the circuits are of equal resonance frequencies but of unequal quality figures, κ^2 in Figure 93 and Eq. (*a*) must be replaced by $\kappa^2 - \eta^2$.

REFERENCES: *226, 232, 381.*

IV.2.13. Optimal coupling and gain. Considering the ratio of V to I (see Fig. 92) in the case of Figure 94 we obtain:

$$\frac{\mathbf{V}}{\mathbf{I}} = \frac{j}{\omega_o\sqrt{C_1'C_2'}} \frac{\kappa}{\left(\frac{1}{Q_1} + j\zeta_1\right)\left(\frac{1}{Q_2} + j\zeta_2\right) + \kappa^2}, \qquad \text{(IV.2.13}a\text{)}$$

κ having the value indicated in connection with Figure 94, while $\zeta_1^2\omega_o^2 = 4(\omega - \omega_I)^2$ and $\zeta_2^2\omega_o^2 = 4(\omega - \omega_{II})^2$.

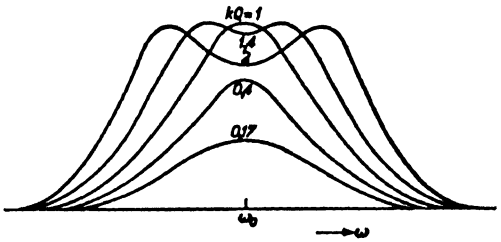

FIG. 96 Modulus of the ratio V/I of eq. (IV.2.13*a*) on a linear scale (vertical) as dependent on angular frequency (horizontal) in the case of two equal coupled circuits of resonant angular frequency ω_o. Curves for different values of κQ, κ being the coupling coefficient and Q the quality of the resonant circuits.

With equal resonance frequencies and quality figures, if $\zeta_1 = \zeta_2 = 0$, the ratio $|V/I|$ is proportional to $\kappa Q/(1 + \kappa^2 Q^2)$. If the coupling coefficient κ is in this case varied, this ratio attains a maximum modulus if $\kappa Q = 1$. This is usually indicated as critical coupling, and it entails that the voltages at the input and output pairs of terminals become equal. The modulus of the ratio of Eq. (*a*) in the case of equal resonance frequencies and quality figures is shown in Figure 96 as dependent on frequency and on coupling coefficient. The "humps" resulting from over-critical coupling are noteworthy. According to Eq. (*a*), small values of the circuit capacities are useful in obtaining a large modulus of the ratio V/I if the frequency dependence of the resonance curve, as determined by Eq. (IV.2.12*a*), is fixed. In the optimal case, the capaci-

tances C_1 and C_2 of Figure 94 may be made nearly equal to the capacitances of the devices connected to input and output terminals respectively.

Furthermore, a large modulus of the ratio V/I requires a maximum value of κQ, which is unity in the case of equal resonance frequencies and quality figures. But if the latter figures differ for both circuits while the resonance frequencies remain equal, κ^2 has to be replaced by $\kappa^2 - \eta^2$ in Eq. (IV.2.12a) determining the shape of the resonance curves. In order to maintain an unaltered shape of the resonance curve, κ^2 has therefore to be increased until $(\kappa^2 - \eta^2)Q^2$ attains the former value unity, Q being given by $1/Q = \frac{1}{2}(1/Q_1 + 1/Q_2)$. In the extreme case we might nearly make $1/Q_1$ zero and $2Q_2 = Q$, when κ^2 has to be replaced by $\kappa^2 - \eta^2 = \kappa^2 - 1/Q^2$. Hence, in order to retain the shape of the resonance curve according to Eq. (IV.2.12a) the value $\kappa^2 + 1/Q^2$ has to be substituted for κ^2, and as $\kappa^2 Q^2 = 1$ this entails a value of the modulus of Eq. (IV.2.13a) exactly $\sqrt{2}$ times the optimal value in the case of equal circuits. By this special choice of quality figures we have thus obtained a considerably larger ratio $|V/I|$ without impairing the shape of the resonance curve as determined by Eq. (IV.2.12a) and Figure 93 in any way.

The four-pole constituted by the two coupled circuits has a definite gain figure g if the impedance attending the current generator connected to the input terminals is fixed. Referring to Figure 94, we shall assume that the parallel resistance R_1 of the input circuit incorporates this impedance, assumed to be real. The available input power is thus $I^2 R_o/4$. By evaluating the real part of the impedance looking into the four-pole at its output terminals, the available output power may be obtained. Upon division by the available input power the gain, if $Q_1 = Q_2$, $\zeta_1 = \zeta_2 = \zeta$, $C_1 = C_2$, $R_1 = R_2 = R$ works out as:

$$g \approx \frac{R}{R_o} \kappa^2 Q^2 \frac{1}{|1 + \kappa^2 Q^2 - \zeta^2 Q^2 + 2j\zeta Q|}. \qquad \text{(IV.2.13}b\text{)}$$

Comparison of Eqs. (IV.2.12a) and (IV.2.13b) shows that the frequency dependence of g is entirely similar to that of the ratio $|V/V_{res}|$, the numerators of both expressions, containing this dependence, being equal. Thus Figure 93 also represents g if the vertical scale is changed accordingly. As our four-pole is a passive dissipative network, g is smaller than 1.

IV.2.14. Stray inductances and capacitances. In the present frequency range above 6 mc/s, the inductances and capacitances of short ends of wire and of metallic parts of a circuit may cause relatively considerable reactances or admittances. We shall start this discussion by giving the expressions of the inductances of short straight wires of circular diameter. In Figure 97, the self-inductance L corresponding

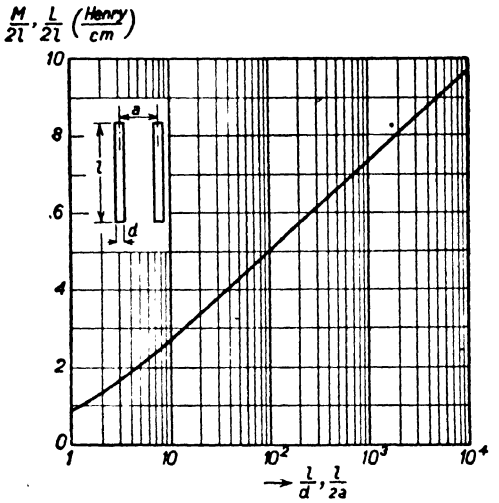

FIG. 97 Self-inductance L per cm length of a single straight section of circular wire of length l and of diameter $d \ll l$ as dependent on l/d. Same curve gives mutual inductance M per cm length between two such parallel wire sections at a distance $a \gg d$ as dependent on $l/2a$. One unit of vertical scale is 10^{-9} henry/cm.

to a single straight section of length l of a circular wire of diameter d being assumed small compared with l is shown in the curve. The same curve represents the mutual inductance M between two such parallel sections of wire at a distance $a \gg d$ but $a \ll l$. One unit on the vertical scale is 10^{-9} henry/cm.

The physical meaning of such inductances corresponding to straight sections of wire requires some further explanation. If we consider a loop of rectangular shape, its total inductance is equal to the sum of the inductances of the four face wires evaluated from Figure 97 minus the mutual inductances between each two different faces, the mutual inductances between parallel faces being evaluated from Figure 97.

As a numerical example, a wire of 10 cm length and 1 mm diameter has a self-inductance of 10.1×10^{-8} henry. If a second wire of equal dimensions is parallel to the first one at a distance of 0.5 cm, the mutual inductance is 55×10^{-9} henry. At 100 mc/s the corresponding reactances are 63 and 34 ohms respectively and these values may in many cases not be neglected. Figure 97 indicates that self-inductances may be decreased by increasing the wire diameters. This simple means has often been successfully applied with extreme-short wave tubes and circuits.

Besides ends of wires, metallic parts of chassis and other structures also have corresponding inductances though usually much smaller per unit of length than with wires. Still, in some cases, even these small inductances have to be taken into account.

Capacitances between separate sections of wires and between similar or other metallic parts of a circuit have often to be accounted for at u.h.f. In many cases these stray capacitances are of comparable amount to the variable tuning capacity. On the other hand, the leads and plates of such tuning capacitances have small but non-negligible inductances which may, in some cases, have an influence on the resonance curve obtained by varying the tuning capacity, as in reality the resonant circuit's inductance is simultaneously varied. Owing to these effects, lumped resonant circuits incorporating such variable tuning capacitances are to be used with care at frequencies beyond, say, 60 mc/s for measuring purposes.

The above curve of Figure 97 may be applied to obtain the self-inductance of resistance units, if capacitive effects (section IV.1.12) are negligible. From this self-inductance and the resistance, the Q value of this resistance unit may be evaluated; this Q value should be as *low* as possible for u.h.f. purposes, entailing short units of relatively considerable diameter.

REFERENCES: *140, 354, 356.*

IV.2.2. Cavity resonators. We have already considered one particular cavity resonator in section IV.1.23 when discussing a quarter-wave coaxial line. In the present section cavity resonators of various shapes will be considered.

IV.2.21. Resonant frequencies of cavity resonators. The simplest cavity resonators are based on wave guides as discussed in section IV.1.31. That section showed that a sequence of definite wavelengths

exists for every guide, corresponding to different types of wave propagation and having a limiting character inasmuch as longer waves of such types meet with excessive attenuation in the guide. Similar sequences of definite wavelengths occur in connection with electromagnetic resonance in cavities. Considering a cavity of rectangular shape and of faces a, b, and c, we again assume restrictions as to the field strengths. With T-M resonance the magnetic-field strength directed parallel to the face c is supposed to be zero, and with T-E resonance the similarly directed electric-field strength is zero. Discussing T-M resonance first, the magnetic-field strength directed parallel to the face a is of optimal amount at the planes containing the faces a and c. Assuming a plane wave propagated to and fro between these planes, the path b must be an integral multiple, say q_b, of half its wavelength. Similarly the path a must be an integral multiple, say q_a, of the half-wavelength in a direction of propagation parallel to a. Applying the same reasoning to a plane wave propagated parallel to c, we finally obtain the rule that:

$$\frac{4}{\lambda^2} = \left(\frac{q_a}{a}\right)^2 + \left(\frac{q_b}{b}\right)^2 + \left(\frac{q_c}{c}\right)^2. \qquad \text{(IV.2.21}a\text{)}$$

If we assume q_b and q_c to be zero, the above rule applies to a and a similar argument applies to b and to c. This equation is an obvious extension of Eq. (IV.1.31a) and determines the resonant wavelength in the medium inside the cavity corresponding to a T-M resonance fixed by three integral suffixes q_a, q_b, and q_c. Not all possible integral suffixes, however, correspond to actual electromagnetic fields. Thus the combination (0 0 0) leads to zero field strength throughout the cavity, and so do other combinations. The longest wavelength with T-M resonance results from $q_a = 1$, $q_b = 1$, $q_c = 0$ or (110) being:

$$\lambda_{110}^2 = 4a^2b^2/(a^2 + b^2). \qquad \text{(IV.2.21}b\text{)}$$

Similarly, with T-E resonance the longest wavelengths result from the combinations (011) or (101):

$$\lambda_{011}^2 = 4b^2c^2/(b^2 + c^2) \quad \text{or} \quad \lambda_{101}^2 = 4a^2c^2/(a^2 + c^2). \qquad \text{(IV.2.21}c\text{)}$$

We have given a special significance to the c direction in relation to T-M resonance or T-E resonance. Obviously no such special selection exists in general, and we may as well substitute a or b for c in the above

reasoning, thus obtaining different sequences of resonant wavelengths, of which, therefore, a somewhat dazzling diversity exists.

A rectangular cavity is only one out of many possibilities. Assuming a cylindrical cavity of circular cross-section and attaching the same meaning to the axial direction as above to a direction parallel to the face c, the axial length being l and the radius of the cross-section being r, we obtain for the longest wavelengths of T-M resonance and T-E resonance respectively:

$$\lambda = 2.61r \quad \text{and} \quad \lambda^2 = \frac{4}{\frac{1}{l^2} + \frac{0.344}{r^2}}. \qquad \text{(IV.2.21}d\text{)}$$

With a sphere of radius r, the longest wavelength of T-M resonance is: $\lambda = 2.28r$ and of T-E resonance: $\lambda = 1.40r$. These examples may, of course, be multiplied indefinitely.

REFERENCES: *18, 30, 43, 104, 181, 182, 203, 251, 310, 403.*

IV.2.22. Quality of cavity resonators. If by suitable means one of the possible resonant fields in a cavity is excited, the exciting power remaining constant while its frequency varies over a limited range in the vicinity of the resonance frequency, the field strengths in the cavity will show maximum amounts at resonance and a decline as soon as the exciting frequency deviates from this position. This behavior is similar to that of lumped resonance circuits. The relative amount of this decline at a given frequency deviation is connected with the cavity's quality figure corresponding to the particular resonant field in question. With an inductance coil the Q value is defined as $\omega_o L/R$, ω_o being the angular resonant frequency, L the coil's inductance, and R its series resistance. Multiplying denominator and numerator by the r.m.s. current I flowing through the coil, we note that LI^2 is the energy contained in the coil's magnetic field and RI^2 the power dissipated in the coil's wire. An entirely similar definition may be given of the Q value corresponding to a definite cavity resonance. It may be obtained as the ratio of the cavity's electromagnetic-field energy multiplied by the resonant angular frequency ω_o to the dissipated power in the cavity's walls. The denominator of this ratio being proportional to the ratio ω_o/μ_0 in which μ_0 denotes the same coefficient as in Eq. (IV.1.11a) and the numerator being proportional

to ρ_0, according to Eq. (IV.1.11c), we may write:

$$Q = \frac{\omega_o d_o \sigma}{\mu_0} Q_o. \qquad \text{(IV.2.22}a\text{)}$$

The reduced quality figure Q_o is exclusively dependent on the geometric shape of the cavity and not on the material of its walls or on the medium in its interior, its dimension being a length (cm). Considering a cube of face a, we have:

$$\lambda_{011} = a\sqrt{2} \quad \text{and} \quad Q_o = \frac{a}{6} = \frac{\lambda_{011}}{6\sqrt{2}}.$$

In the case of a sphere we obtain with T-M resonance:

$$\lambda = 2.28r \quad \text{and} \quad Q_o = \frac{r}{2.76} = \frac{\lambda}{6.30}$$

and for T-E resonance:

$$\lambda = 1.40r \quad \text{and} \quad Q_o = \frac{\lambda}{2.8}.$$

Thus the quality figure of a cube corresponding to T-M resonance for a face equal to a sphere's diameter is lower than that of the sphere, whereas the quality Q_o with T-E resonance of the sphere is the best of these three. As to the multiplier $\omega_o d_o \sigma / \mu_0$ of Eq. (a), this may be written as:

$$\frac{\omega_o d_o \sigma}{\mu_0} = \frac{2}{d_o} \approx \frac{5 \times 10^4}{\sqrt{\lambda}} \qquad \text{(IV.2.22}b\text{)}$$

in the case of copper walls and air as a dielectric medium inside the resonator, λ being the resonant wavelength in cm. At decreasing resonant wavelengths the quality figure Q, obtainable with a definite cavity and field pattern, will thus decrease. Comparing the above equations for the Q figure of cavities with the Q of Eq. (IV.1.23g) in the case of a resonant coaxial line, it is seen that the present values may be larger because of the ratio $a/\sqrt{\lambda}$ of that equation being smaller than $\sqrt{\lambda}/2.8$, if a is smaller than $\lambda/2.8$, which is necessary for the validity of Eq. (IV.1.23g). Generally the Q figures of a given cavity corresponding to the lowest suffixes of resonance are higher than those with higher suffixes.

REFERENCES: *18, 70, 310, 392, 403.*

IV.2.23. Cavities serving as coupling elements. Some simple examples of resonant lines serving as coupling elements have already been shown in section IV.1.24. A further example is shown in Figure 98*a*. A quarter-wave line is used here as a variable coupling element between the antenna line and the input electrodes of the first amplifier tube of the receiver. The equivalent lumped circuit of Figure 98*a* is shown in Figure 98*b*. The capacitance C of the figure is given by:

$$2C = C_t + \frac{2\pi l/\lambda}{\omega Z_o \sin^2\left(\frac{2\pi l}{\lambda}\right)}, \quad \tan\frac{2\pi l}{\lambda} = \frac{1}{\omega C_t Z_o},$$

l being the length of Figure 98*a*, Z_o the wave impedance of the line, and λ the wavelength. In addition to the example of Figure 98*a* in which a quarter-wave line is shortened by the application of a suitable capacity C at its open end, consider a resonant coaxial cavity in which this shortening process has

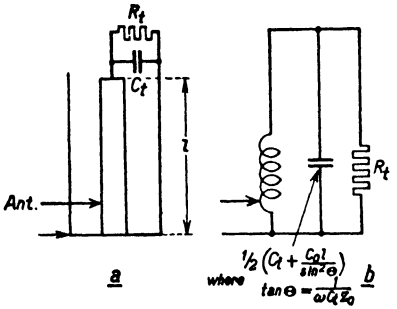

FIG. 98 Diagram *a*: Connection of an antenna transmission line to a coaxial resonant cavity of length l. Diagram *b*: Lumped circuit corresponding to the diagram *a*, C_o being the capacitance per unit of length of the coaxial cavity and Z_o its wave impedance.

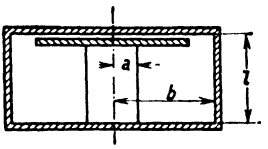

FIG. 99 Resonant cavity of dimensions a, b, and l which are small compared with one-quarter wavelength, with a capacitance between the top of the central stem and the top cover of the cylindrical cavity. This capacitance may be made adjustable.

been extended so as to obtain an axial length small compared with one-quarter wavelength (Fig. 99). This cavity may be regarded as being intermediate between a lumped resonant circuit and the cavities of the preceding sections. Its inductance is:

$$L = 4.60 l \lg_{10}\left(\frac{b}{a}\right) \times 10^{-9} \text{ henry}, \qquad \text{(IV.2.23}a\text{)}$$

while its series resistance works out as:

$$R = \rho_0 \left\{ \frac{l}{2\pi b} \left(1 + \frac{b}{a} \right) + \frac{2.30}{\pi} \lg_{10} \frac{b}{a} \right\} \text{ ohms}, \qquad \text{(IV.2.23}b\text{)}$$

ρ_0 being given by Eq. (IV.1.11c). From these equations the quality figure $Q = \omega_o L/R$ is obtainable directly, if required, as is the resonant impedance measured at the terminals of the lumped capacity C at the end: $Z_{res} = L/CR$. As with coaxial lines, an optimal value of Q is obtained if $b = 3.6a$, while the optimal value of the ratio b/a corresponding to a maximum resonant impedance Z_{res} is dependent on the ratio l/b thus:

l/b	0	0 25	0.5	1 0
(b/a) opt	9.2	10.1	11.0	12.8

The case of $l/b = 0$ corresponds to the optimal value $b/a = 9.2$ mentioned previously in the case of a quarter-wave resonant coaxial line (see end of section IV.1.23). The losses in the condenser plates have not been included in the above Eq. (b). If they are, the optimal value of the ratio b/a increases with decreasing ratio l/b between 3.6 if $l/b = \infty$ and 6.7 if $l/b = 0.05$ if Q is to be optimal. A constant term $\rho_0/8\pi$ has to be added to the expression (b) in this case. Resonant cavities of this type are suitable at frequencies between, say, 30 and 300 mc/s. Two types suitable for push-pull circuits are shown in Figure 100, in which means for tuning the condensers simultaneously may obviously be provided.

A further, slightly more involved, type is shown in Figure 101. In this the central conductor of the coaxial line connected with the antenna is tapped at a suitable height on the central stem of the cavity as in Figure 98a, a tuning condenser being provided at one end of this cavity similar to that of Figure 99. This resonant cavity's field is now coupled, through holes in a plate separating it from a further cavity, to the latter's field. The second resonating cavity is of similar type and also incorporates a tuning condenser at its end, supposed to be connected to the input electrodes of a receiver's entrance tube.

With frequencies from 300 to 10,000 mc/s the resonant cavities of the types discussed above have gradually to be replaced by cavities of dimensions comparable with the wavelength, as discussed in the

two preceding sections. Here again similar means of coupling through holes and taps with coaxial lines, as well as with wave guides, may be devised. At the highest frequencies a surface antenna (section III.2.22) may be coupled directly to a suitable wave guide which in

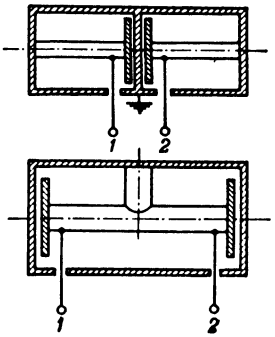

FIG. 100 Two push-pull constructions on the same principle as shown in Fig. 99, the outer terminals being 1 and 2.

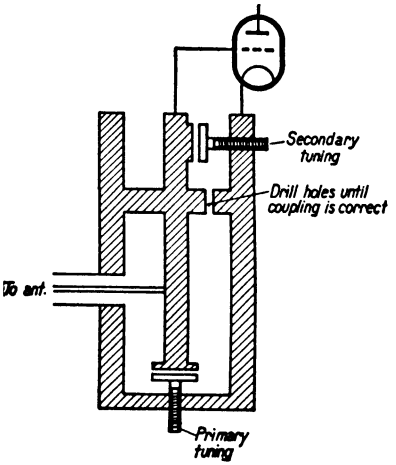

FIG. 101 Resonant device containing two cavities coupled through holes in the separating wall.

turn may be coupled directly to a suitable resonant cavity, perhaps traversed at the same time by an electronic stream necessary for amplification and/or detection purposes. These devices may be treated approximately by replacing them for calculation purposes by suitable coupled lumped circuits.

REFERENCES: *43*, *163*, *403*.

CHAPTER V

EXPERIMENTAL DEVICES AND DATA

Before we embark upon the design of the different receiver stages it is useful to give a brief exposition of some available experimental data on noise, antennas, lines, guides, resonant devices, and electronic tubes as well as of the means of obtaining them. This may give the reader a general picture as to the orders of magnitude of different effects and at the same time guide him in the performance of experiments and measurements by himself.

V.1. Standard Signal Sources at U.H.F.

In the frequency range under present consideration (6 to 30,000 mc/s), standard signal sources are equally useful for testing and experimental purposes as at radio frequencies. The requirements to be imposed on them, as well as the design considerations underlying their construction, differ considerably, however, from those at radio frequencies and it seems, therefore, useful to devote some space to their discussion.

V.1.1. General requirements. For many purposes standard signal generators at u.h.f. have to meet similar requirements, some of which will be described here.

V.1.11. Voltage, frequency, and modulation. The open-circuit u.h.f. output voltage should be adjustable between about 0.1 microvolt to 100 millivolts, with the additional possibility of obtaining one single fixed larger output voltage of, say, 1 volt. The former output voltages should be obtainable with a purely real output impedance, looking into the output terminals, of some 70 ohms, preferably invariable throughout the generator's frequency range but, if variable, being so in a definite way. At 100 mv the available output power is thus about 0.036 milliwatt. At the large output voltage the internal output impedance should not exceed, say, 500 ohms, thus obtaining an available output power of about 0.5 milliwatt. These output voltages should be measurable within about 5% of the nominal value.

The frequency should cover the entire range mentioned above in several and preferably not too many steps. At the highest frequencies, above, say, 1500 mc/s, a continuous adjustment of output frequency becomes increasingly difficult to obtain. In this upper range a number of fixed frequencies suitably chosen will, in many cases, cover present requirements. The output voltage should be as free as possible of harmonic frequency components, the total harmonic content not exceeding about 3%. If a certain frequency is adjusted on the scale its true value should differ less than by 5×10^{-3} times the nominal frequency from the latter value. Besides a primary adjustment of frequency, a secondary adjustment, varying the output frequency up to about 2%, should be possible.

Three kinds of modulation are generally required: AM, FM, and IM. With AM the frequency of modulation should be continuously variable from about 50 c/s to 100 kc/s with an also continuously variable degree of modulation up to about 80%. The required available modulation power to achieve the maximum modulation should not exceed about 0.25 watt (e.g., 24 volts across 600 ohms). If the modulation-frequency input voltage is constant, the degree of modulation should not vary by more than about 10% throughout the u.h.f. range of the standard generator. Special requirements must be imposed on distortion of modulation and upon undesirable modulation by hum and other disturbing sources. Finally the undesirable FM accompanying AM should be less than about 10^{-6}.

With FM applied to the standard generator, the modulation frequency should be up to about 20 kc/s and the frequency-swing up to about 100 kc/s at output frequencies above 100 mc/s. The required modulating voltage across 600 ohms should not exceed about 0.3 volt for each kc/s swing. Distortion of modulation should remain below 2% at 50 kc/s.

With IM the impulse duration should be allowed to vary between 0.5 and 10 microseconds at modulation frequencies between 50 c/s and 20 kc/s. The maximum width of the frequency band allotted to these IM signals should be about 2 mc/s. At the interruptions the remaining output voltage should not exceed 10% of the maximum output voltage.

It is obvious that the standard signal generator should contain suitable means of measuring and adjusting the respective items men-

tioned. A complete outline of further subsidiary requirements would exceed the scope of this section.

REFERENCES: *129, 135, 139, 269, 389.*

V.1.12. Stability of performance. Several undesirable and often uncontrollable effects may impair the stability of frequency as well as of output voltage. Some of these causes and the necessary limitations to be put on their effects will be discussed here. The main causes of variations are: variations of supply voltage and variations of temperature. If one of these items shows a variation of 10%, the other remaining unaltered, the ensuing variation of output voltage should not exceed 10%. The ensuing variation of output frequency should not exceed 10^{-5} of the nominal frequency at 10% supply-voltage variation and not exceed 10^{-3} at 10% variation of ambient temperature. Even if the latter is constant, the temperature of the standard generator, when in continuous operation, will gradually increase. The ensuing frequency variation after 1 hour of continuous operation at constant supply voltage should not exceed 10^{-5} of its nominal value per hour.

Even if the standard generator were of perfectly stable performance, the receiver or other device to be measured or tested will often not be so. In order to insure proper results, every test must therefore be performed within as short a time interval as possible. This essential point necessitates a number of subsidiary requirements connected with the standard source. The adjustments of frequency and output voltage of the latter must be such that they take very little time to perform. Thus the adjustment of frequency may suitably be carried out in two steps, the coarse tuning being done by means of a motor and the fine tuning by hand. Both means of tuning should be continuously and simultaneously adjustable. The indications on dials should be such that quick readings can be taken. The output voltage should require little or no readjustment, being automatically given the required value upon changing over from one frequency range to another.

In some cases the constant-frequency requirements will entail the use of thermostats for frequency-controlling elements such as crystals or resonant devices. Such thermostats should then be incorporated in the standard generator.

In order to afford mechanical stability during transport the entire construction of the standard source should be of proved rigidity, at the

same time not unduly hampering the dissipation of the heat generated in its tubes and resistive elements.

The required output up to about 3000 mc/s may suitably be shaped as a coaxial line of wave impedance of about 75 ohms. This output line should be of slight attenuation and rigid construction so as to prevent its twisting out of shape. At higher frequencies the output may take other shapes such as a small dipole antenna or loop of suitable design to be used in connection with proper wave guides. These output elements should also not be lacking in rigidity.

Finally, care should be excercised to avoid the undesirable effects of moisture.

REFERENCES: *53, 129, 135, 139, 156, 186, 256, 257, 269.*

V.1.2. Design considerations. The design of standard signal sources in the frequency range under discussion entails a number of considerations different from those governing such sources at radio frequencies. As some of these considerations are involved in most experimental work at u.h.f., discussion of them seems useful here.

V.1.21. Screening and shielding. At the present u.h.f. the depth d_o of penetration into metallic surfaces is so small that no h.f. power is transmitted through metal screening walls of reasonable thickness. Thus all spurious h.f. power must pass through slits and holes between or in such walls. Considering slits as pictured in Figure 102*a*, the voltage across the slit is obtained by multiplication of the a.c. I flowing on the inner wall-surfaces by the impedance Z across the slit. This impedance may often be represented by a resistance R in parallel to a capacitance C. The simple equivalent lumped circuit is shown in Figure 102*b*. The available spurious signal power at the slit is obviously:

$$P_a = \frac{|V^2|\ (1 + \omega^2 C^2 R^2)}{4R} = \frac{|I|^2 R}{4}.$$

In order to reduce this power as much as possible, I being given, R should be reduced. This may be achieved by introducing ground and polished faces at such slits and pressing the two parts together by a sufficient number of closely spaced bolts. Experience has proved that such measures, if carefully applied, may be successful. In some cases it may be advisable to use double screening as indicated in Figure 103*a*. In this case the equivalent lumped circuit is shown in Figure 103*b*, the

inductance L and capacitance C being shown in Figure 103*a*. If the moduli of Z_1 and Z_2 are small compared with the series impedance of the antiresonant combination LC, this double screening results in a

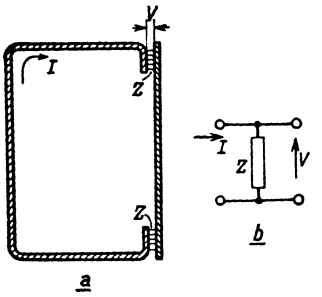

FIG. 102 Diagram *a*: Shielding by means of a metal box with cover separated by a narrow slit of over-all impedance Z. The equivalent lumped circuit is shown in the diagram *b*.

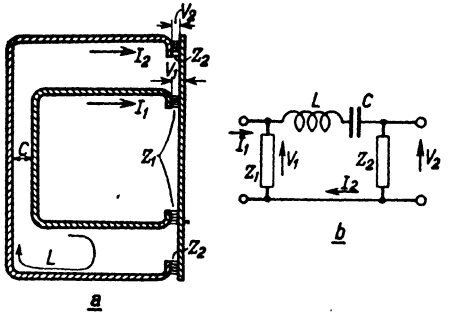

FIG. 103 Diagram *a*: Double shielding box with two consecutive slits, the effective inductance and capacitance of the interspace between the boxes being indicated by L and C respectively. The equivalent lumped circuit is shown in diagram *b*.

much lower available spurious power across the outer slit. In certain cases, however, if antiresonance of L and C occurs the effects may be detrimental. Besides slits of this kind, the bearings in metal walls

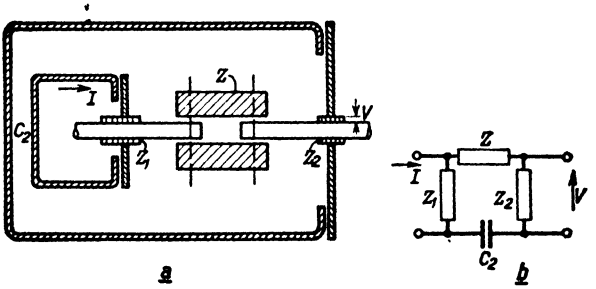

FIG. 104 Diagram *a*: Shielding of an axis penetrating a double shielding box by means of an interruption and an insulating link of impedance Z. Diagram *b* shows the equivalent lumped circuit (Figs. 102–110 see reference *269*).

used for the axes of switches and condensers are other examples of slits. In these cases double screening may be applied as pictured in Figure 104*a*, the equivalent lumped circuit being indicated in Figure 104*b*. The two metal sections of the axis in Figure 104*a* are interlinked by an

insulating part as shown, of impedance Z. This insulating part will in most cases be constructed of somewhat elastic material. The screened inner spaces must in any event be easily accessible. Hence bearings as shown should not be designed so as to penetrate removable metal covers or lids. A further point is the provision of sufficient outlets for the heat dissipated in the screened spaces.

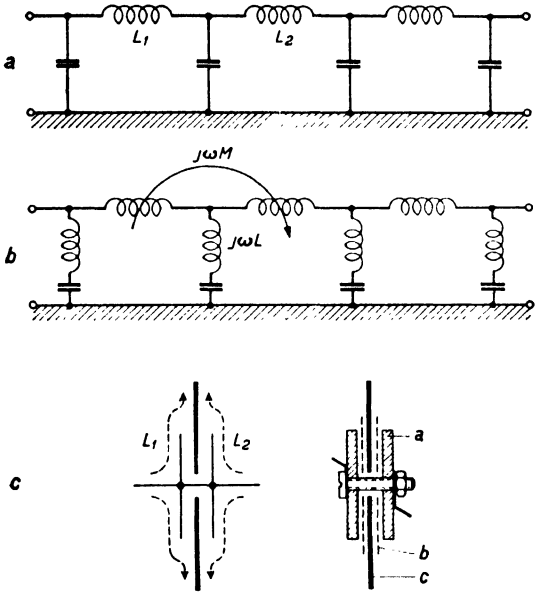

FIG. 105 Diagram *a*: Low-pass filter circuit. Diagram *b*: Mutual inductance M between the mazes or/and series inductance L of the capacitances make the filters ineffective at u.h.f. Diagram *c*: Construction of capacitances incorporating the inductances L_1 and L_2 but avoiding the inductances L and M of diagram *b*. Notation: *a*, conducting electrodes; *b*, insulating strips; *c*, part of compartment wall.

Besides screening of mechanical junctions as shown, the supply lines of mains and modulation power must also be properly screened. This is mostly achieved by means of low-pass filter circuits as shown in Figure 105*a*. Care should be exercised to avoid mutual inductance or series inductance at the capacitances as indicated in Figure 105*b*. In these cases the low-pass properties are ineffective at u.h.f. The capacitances of the low-pass filters may be constructed as shown in Figure 105*c*, incorporating the inductances L_1 and L_2 of Figure 105*a*. The parts *a* of Figure 105*c* act as metal condenser plates together with

the screening wall *c* between filter compartments, whereas *b* indicates insulating parts. The shape of a multi-section filter unit is shown in Figure 106, the inductances being placed inside separate screened compartments. A general picture of a doubly screened complete

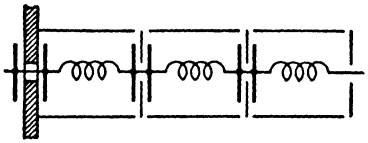

FIG. 106 Over-all picture of a three-maze filter network according to Fig. 105*a*.

standard signal generator is shown in Figure 107. Even the switches and instruments on the front panel are effectively screened.

The effect of spurious signal voltages ensuing from inefficient shielding on the desired output signal voltage is shown by Figure 108, curve *a* indicating the output voltage as dependent on attenuator adjustment

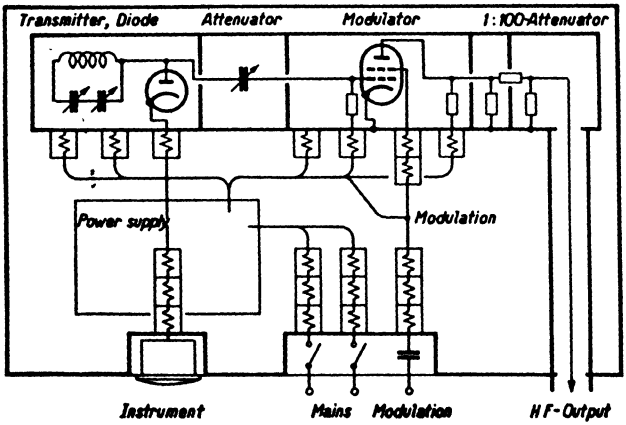

FIG. 107 Over-all diagram of standard signal generator showing its principal parts including low-pass filters.

without spurious signal, the latter voltage being shown by the dotted horizontal curve. If the spurious voltage is in phase with the desired voltage curve *b* results; if it is counterphase curve *c* shows the resulting output voltage.

REFERENCES: *269, 361, 402, 403.*

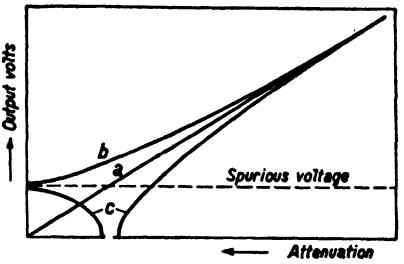

FIG. 108 Influence of spurious output voltage on over-all output volts of generator (vertical scale) as dependent on attenuation. Line *a*: Without spurious voltage. Curve *b*: With in-phase spurious voltage. Curve *c*: With counterphase spurious voltage.

V.1.22. Oscillator design. If we use direct oscillator stages (excluding superheterodyne circuits) the range of 6 to 300 mc/s may be covered in several steps by the use of proper circuits with lumped inductances and capacitances. A useful push-pull circuit is shown in Figure 109, V_a indicating the anode supply voltage, the cathode heater circuit being omitted. If the lumped *LC* circuit is replaced by part of a suitable transmission line or by a resonant cavity, a similar circuit may be effectively used up to about 2000 mc/s. The change-over between the different ranges obtainable with a single inductance by variation of the tuning capacitance necessitates interchangeable coils. A construction by which this is achieved is shown in Figure 110, the coils being arranged along the circumference of a circular wheel, motioned by a clicking mechanism as shown in the upper and lower part indicated by *c* and *h*, *c* being the axis of the driving disk. The coils not in use are automatically short-circuited in order to avoid spurious resonances. The coil-wheel itself has two bearings f_1 and f_2, the upper one of which is pressed onto the wheel by means of the metal spring *g*. Upon removal of this spring the entire wheel may be lifted out of its shield. The double tuning condenser *a* with its axis *b* may be connected to each coil in turn by means of two contacts as shown. The coil-wheel *e* is

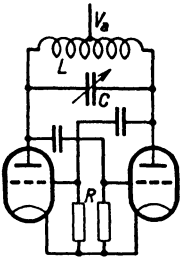

FIG. 109 Schematic diagram of push-pull oscillator stage. Tank circuit *L*,*C*. Bias resistors *R*. Capacitive feedback. Anode supply voltage V_a.

entirely shielded by a suitable cast-metal box *d*. The entire tube circuit is mounted on this box and thus forms a rigid unit together with the coil set. The gears and bearings connected with the condenser adjustment are kept in their proper positions by suitable spring action, thus avoiding any backlash. In this way the oscillator frequency may be adjusted within a few hundred c/s even at 300 mc/s. The condensers of Figure 110 are each of 12 to 50 pF, the Q of the coils at the said frequency being about 100 and higher for coils used at lower frequencies.

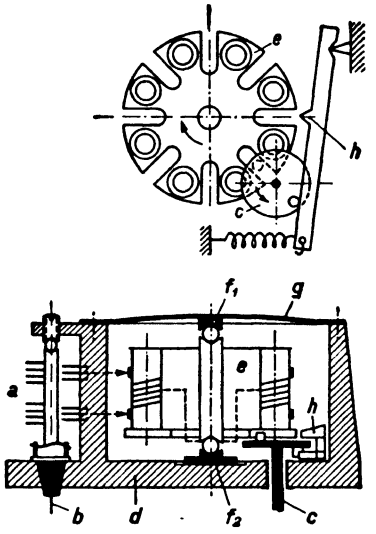

FIG. 110 Multiple-coil unit and tuning condenser of signal oscillator. Notation: *a*, tuning condenser; *b*, axis of t.c.; *c*, axis of motional disk of coil-wheel; *d*, container box of coil-wheel (cast-alloy); *e*, coil-wheel; f_1 and f_2, bearings of coil-wheel axis; *g*, metal spring; *h*, clicking mechanism of motional disk *c*.

It is essential that leads connecting tube, condenser, and coil terminals be as short as possible to avoid any additional unnecessary inductance. The resonant sections of transmission lines to be used at frequencies above 300 mc/s may be bent along a circular circumference so as to allow easy adjustment of their length by means of a centrally driven short-circuit slide. Owing to the requirements of stable operation, the power generated by the oscillator proper must be much in excess of the small power finally available at the output of the standard source. Such a relatively high level of generated power permits very loose coupling to subsequent stages, thus reducing the effects of feedback on the operative data of the oscillator stage. At the highest frequencies of the range in question (i.e., from 2000 to 10,000 mc/s) only relatively slight adjustment of the generated frequency is often contemplated, the oscillator stage being for the main part of fixed frequency. The use of suitable magnetrons or velocity-modulated tubes at these frequencies makes the necessary oscillator power readily available, several decawatts being obtainable even at 30,000 mc/s. As an example we may

cite an actual generator having a range of 2700–4200 mc/s using a velocity-modulated tube.

The generated voltage at the output of the oscillator stage must be measured at least on a relative scale in order to afford the possibility of its adjustment to a definite level. This aim is generally achieved by connecting a suitable diode or crystal detector across the output, using a suitable millivoltmeter on the front panel as an indicator. At the lower frequencies, up to about 600 mc/s, this instrument, together with the diode circuit, may easily be calibrated to an absolute scale; with appropriate care, this may be extended to about 1500 mc/s. At higher frequencies the absolute calibration calls for separate means, such as an electrostatic voltmeter of suitable design or air-expansion milliammeters with high-resistance heating wires.

REFERENCES: *3, 53, 91, 142, 156, 199, 238, 269, 301, 320, 352, 357, 361, 375.*

V.1.23. Modulator and attenuator stages. In order to avoid frequency drift of the oscillator stage and ensuing FM, the AM is in most cases carried out in a separate stage, sufficiently loose coupling being applied between this modulator and the oscillator stage. In Figure 107 this coupling is schematically indicated by a variable condenser called an *attenuator*. The modulator tube is in Figure 107 pictured as a tetrode, the modulating voltage being applied to the screen grid, the control grid, or the anode. Feedback of the modulator stage should be avoided by proper screening or/and by neutralization. By suitable design this modulator stage, which need not have any appreciable amplification, may be made to operate satisfactorily up to at least 1500 mc/s. At its output an attenuator affords a means of obtaining the lowest output level required. The electronic noise of the modulator tube may be suppressed relative to the inappreciable noise ensuing from the oscillator stage, even at the lowest output levels, by a suitable increase of the oscillator voltage at the modulator input and by applying additional attenuation at its output. The gain of the modulator stage as well as the adjustments of the attenuators determine the output signal level of the standard source. Thus this gain must be checked and properly adjusted from time to time. A special low-frequency voltage source is in some cases provided to achieve this checking by measuring the modulator performance as a l.f. amplifier, whereupon

adjustment by bias variation of the control grid affords a means of obtaining the desired gain (or rather loss).

With FM at the lower frequencies up to about 100 mc/s a common reactance tube circuit suitably coupled to the oscillator circuit may achieve the desired aim. An example of such a reactance circuit is shown schematically in Figure 111. Under proper conditions the impedance between the terminals of this circuit is equivalent to a resistance $1/Y$ in series with an inductance RC/Y, Y being the tube's transconductance. By variation of its grid bias this transconductance may be varied and thus an equivalent variation of the inductance is obtained. This variation causes a corresponding variation of frequency at the oscillator stage. It should be mentioned that the relative variation of frequency (i.e., the swing) is small compared with the frequency of oscillation above, say, 100 mc/s. Hence only a relatively slight variation of the oscillator circuit's reactance is necessary here. At the higher part of the oscillator frequency range a suitable frequency modulation may be produced by superposition of a proper modulation voltage on the oscillator's anode supply voltage. By careful design the AM accompanying the resulting FM may be limited.

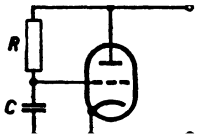

FIG. 111 Example of reactance circuit. Between the terminals shown an inductance is created, the magnitude of which may be controlled by biasing the grid.

With IM according to the requirements of section V.1.11 a revised AM system as described above may be used, the impulsive modulation voltage being applied to the modulator tube, thus varying its gain accordingly. In order to comply with the desired band width of 2 mc/s corresponding to the lowest impulse duration of 0.5 microsecond. special design of the modulator circuit is required.

Attenuator stages at the present u.h.f. are mostly of capacitive type. An example is shown in Figure 112. One fixed plate a_1 and a second plate a_2 of variable position are parts of a condenser. The distance between the plates may be varied by rotation of a_2 round the hollow axis b. The capacitance between a_1 and a_2 decreases logarithmically if their angular distance increases linearly. Thus a variation between 1 pF and 10^{-4} pF may be readily achieved. In order to obtain a constant input capacity of the entire attenuator if viewed from the oscillator, a second simultaneously and similarly varied condenser is

used, as shown in Figure 113, C_3 being a fixed capacitance, C_1 being an attenuator according to Figure 112, and C_2 a similar variable capacitance coupled mechanically to C_1. At frequencies above 500 mc/s the attenuator of Figure 112, instead of being designed for circular motion, is in many cases built for straight motion, the two adjacent plates being mounted inside a cylindrical tube. The lateral dimensions of the attenuator should be properly chosen at these frequencies subject to the

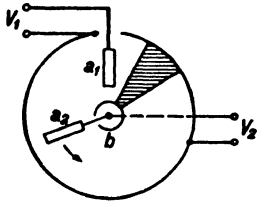

FIG. 112 Example of u.h.f. attenuator. The capacitance between the electrodes a_1 and a_2 decreases logarithmically in dependence on their mutual angular distance. The output voltage V_2 thus decreases logarithmically at a constant input-voltage level V_1.

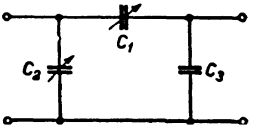

FIG. 113 Attenuator circuit creating an invariable input impedance if viewed from the left pair of terminals. C_3 is a fixed capacitance while C_1 and C_2 are equal and variable according to Fig. 112, their motion being coupled mechanically.

condition of being small compared with one-quarter wavelength. If this condition is not satisfied the radio-frequency calibration of the attenuator is no longer valid at the required u.h.f., and intricate if not unreliable subsidiary calibrations become necessary.

REFERENCES: *86, 119, 135, 197, 269, 318.*

V.1.3. Measurements of gain and of noise figure. Using u.h.f. standard signal generators as considered above, the gain and noise figures of reception stages may readily be measured. Such measurements and some data thus obtained will now be dealt with.

V.1.31. Measurements of gain. Measurements of gain are usually required in connection with either amplification or mixing stages. With amplifying stages the frequency connected with the output power

is equal to that of the input power. With mixer stages the frequency at the output is in general different and often much lower than the frequency at their input terminals. In both cases it should be observed that the gain figure does not depend on the input impedance of the subsequent stage to be connected to the output terminals of the stage in question. This may be concluded from the definition of the gain of a four-terminal device as being the ratio of its available output power to its available input power. Neither of these powers depends in any way on the input impedance of any subsequent stage. Hence we may adjust this input impedance to any value convenient for measuring purposes. For instance, it may be made equal to the purely real output impedance of the standard signal generator, often in the vicinity of 75 ohms.

Dealing with amplifier stages first, we shall assume that the input impedance of the subsequent stage, being either another amplifier stage or a mixer stage, is adjusted so as to be equal to the standard signal generator's output impedance. The receiver is then connected with its input terminals to the output of the standard signal generator, without making any adjustments at this connection. The output-voltage level of the generator is chosen so as to yield a clearly legible signal on an indicator at the receiver's output. With an AM receiver the standard signal generator is given AM well within the range of reception. With an FM receiver, proper FM is imparted to the standard signal generator. Care should be taken that the AM or the FM is such as to allow undistorted reception. When this is done, the output of the first stage is adjusted until at a fixed generator voltage and modulation level an optimum indication is obtained at the output. This is where the conditions of undistorted operation come in, insuring that an increased indication corresponds to a more favorable adjustment of output of the stage in question, imparting a larger proportion of its available output power to the subsequent stage. The means of adjustment, mainly consisting of a low-loss transformer—e.g., incorporating a quarter-wave line section (see sections IV.1.22 and 24) of proper wave impedance—should be such and of sufficient range that the most favorable adjustment may indeed be achieved, i.e., that the total available output power of the stage under discussion is transferred to the input of the subsequent stage. It may not always be easy to make sure that this condition is satisfied to a reasonable approximation but this is essential to the measurement.

When this condition is satisfied, the corresponding output indication of the receiver is noted. Thereupon the output of the stage in question is disconnected from the input of the subsequent stage and the standard signal generator's output is connected to the latter. No further adjustment is required in this connection, as both pairs of terminals are already of matched impedances, as mentioned at the start. The attenuator of the standard signal generator is then adjusted so as to obtain indication at the receiver's output exactly equal to that obtained previously with the first stage in position. The ratio of the second to the first attenuator reading represents the gain of the first stage in question, provided that these attenuator readings are in power terms. If they are in output-voltage terms the ratio of the readings has to be squared in order to obtain the gain figure. The proof of this procedure is almost trivial, as we have acted exactly in conformity with the definition of gain, the ratio of the attenuator readings (if in terms of power) being equal to the ratio of available output power to available input power of the stage in question. The gain figure thus obtained is, of course, not the optimum gain obtainable with the stage in question. This optimum gain involves matching of the stage's input to the output of the standard signal generator. In many u.h.f. receivers this matching is already approximately present, the stage's input being matched to the output of a coaxial transmission line of approximately 75 ohms wave impedance.

Several variants of the procedure as outlined are available. To mention one of them: Adjust the input of the stage in question to the output of the standard signal generator until a maximum indication at the receiver's output is obtained. Proceed in the same way with the output of the first stage in question and the input of the subsequent stage. Note the indication. Then disconnect the first stage, connect the standard generator's output to the input of the subsequent stage, and readjust the latter input until maximum indication at the receiver's output is reached. Adjust the generator's attenuator until the noted indication is reobtained. The gain is the ratio of the latter to the former attenuator readings (in terms of power). This procedure is, however, slightly more involved than the preceding one, and so are most other procedures.

If the stage in question is a mixer stage, the entire procedure as outlined remains exactly the same, with one single exception. When the standard signal generator is connected to the input of the subsequent

stage its frequency has to be adjusted to the carrier frequency of that stage, usually indicated as intermediate frequency. If this intermediate frequency is so low as to be outside the range of the standard signal generator, a second such generator has to be used, the modulation of which must be adjusted to exactly the same degree and properties as those of the first one. In addition, its output impedance should also be adjusted to exactly the same value as that of the first one, while the absolute (not only the relative) output levels of both generators should be exactly known so as to make comparison possible.

The relative calibrations of the attenuators of both generators may easily be checked with the aid of the receiver and its output indicator by connecting first the u.h.f. generator to the input of the first u.h.f. amplifier stage and then the second intermediate frequency generator to the input of the first i.f. stage. Upon variation of attenuator readings of both generators correspondingly and comparing the resulting output indications of the receiver, their equality may be checked. Automatic volume control (a.v.c.) has to be put out of operation when performing these measurements.

If reception antennas of horn type in conjunction with wave guides and resonant cavities are used, the measurement of over-all gain of the h.f. entrance stages of a receiver including its antenna may be carried out as follows. First, a standard signal generator or other suitable signal source is connected to a small dipole or half-wave antenna, situated in the direction of optimal response and having optimal polarization with respect to the receiver, the distance being larger than, say, 10 wavelengths. The specific radiation power p at the reception antenna may then be easily calculated. Second, a suitable standard signal generator of equal modulation is connected to the input terminals of an intermediate frequency stage of the receiver and adjusted until equal output is obtained as in the first case. From both figures (specific power p in the first and available power P_a in the second case) the gain of all stages preceding the input may readily be obtained, if a reasonable estimate is made of the effective surface S_e of the reception antenna.

REFERENCES: *32, 66, 129, 130, 227.*

V.1.32. Measurements of noise figure. The definitions of noise ratio as well as of noise figure involve linear reception stages. It is therefore essential that the non-linear stages of a receiver should be discarded. This applies especially to the second detector or rectifier

stage. The output of the last i.f. stage preceding the detector stage may then be selected for the connection of an indicator which should be responsive to r.m.s. values as exactly as possible. A thermoammeter will in many cases be suitable. In what follows such an indicator will be assumed at this position or at the output of any suitable preceding linear reception stage. First, the standard signal generator is connected with its output to the input terminals of the receiver's entrance stage with its oscillator out of operation, e.g., with the mains switched off. The receiver's a.v.c. is put out of action and the manual volume control is adjusted so that a well-defined reading is obtained at the output indicator. This reading obviously provides a relative measure for the receiver's available output noise power including all the stages preceding the output mentioned and at the selected position of the volume control. Evidence should be obtained that the output indication corresponds to random noise and not to hum.

Now the standard signal generator is switched on without modulation, its frequency being adjusted until an optimum output reading is obtained, while its level attenuator is brought to such a position that the previous output reading (i.e., with oscillator switched off) is exactly doubled (assuming the readings to be proportional to the squares of r.m.s. values). The generator's output voltage corresponding to this reading being V and its output resistance R, the available power at its terminals is $P_{si} = V^2/4R$ and this available signal power is obviously exactly equal to the available input noise power P_{ni} corresponding to the previous (i.e., the first) output reading. Upon division of P_{si} by KTB, the noise figure N of the receiver stages under consideration is obtained. The equivalent band width B of this succession of stages may be obtained by variation of the generator's frequency while keeping its output at a constant level, preferably such that the resulting output reading has at its peak many times the value of the first reading with the oscillator switched off. A curve may then be drawn giving the gain on a relative scale versus frequency. At the declining ends of this curve a correction corresponding to the inevitable noise indication must be applied to the output reading before obtaining the relative gain curve from it. Addition of signal and noise is here again such that the resulting reading is equal to the signal reading plus the noise reading, if the readings are proportional to the square of the r.m.s. output current (or voltage). From the relative gain-versus-frequency curve the value of B is obtained by graphic integration upon application of Eq. (II.2.11*b*).

By application of an automatic sweep to the oscillator frequency (i.e., of a suitable FM) coupled to the sweep electrodes of a cathode ray tube, the gain-versus-frequency curve may be viewed directly on the luminescent screen. The generator's output resistance being at room temperature T, the receiver's part of the noise figure N thus obtained is $N-1$.

We may also measure the noise figure of the reception antenna at various orientations and positions. To effect this the antenna has first to be attached to the receiver input terminals by using the means provided for this purpose. An output reading is then obtained at a definite adjustment of the manual volume control. This output reading obviously corresponds to the noise captured by the antenna and the receiver noise together. The antenna is then disconnected from the receiver's input terminals and the generator output connected to them, whereupon its level is adjusted so as to double the previous reading. The resulting noise figure N, obtained by division of the available generator output signal power by KTB, is equal to the noise figure of the receiver as measured by the above procedure plus the ratio T_a/T corresponding to the noise figure of the antenna according to the first definition in section III.1.22 (see Eq. c of that section). The value T_a represents the effective noise temperature of the real part of the antenna's impedance at the terminals which are to be connected to the receiver's input terminals (i.e., the output terminals of the transmission line connecting antenna and receiver). With a properly matched low-loss line this temperature is approximately equal to that at the antenna's output terminals. If we want to measure the antenna's noise figure corresponding to the second definition of section III.1.22, the standard signal generator has to be connected to the input terminals of a suitable transmitting antenna radiating toward the reception antenna in question.

By disconnecting successive stages of the receiver the noise figures of each of them may be obtained by application of the same procedure. In some cases it may be necessary to measure at least two successive noise figures in order to obtain the figure for a particular stage. This is especially true if the stage gain in question is not large compared with unity or if the subsequent stage has a noise figure large compared with that of the stage in question (see Eq. II.2.13c). As to the band width B obtained by the above procedure, this is obviously the over-all width of the succession of reception stages. If the bands of the last stages in the succession should be much wider than those of the first stages,

some confusion might arise as to the origin of the noise measured. To avoid this, the bands of the last stages should preferably be somewhat narrower than those of the first ones while centered round the same frequency.

At extreme-high frequencies beyond 3000 mc/s, the receiving antenna may be horn-shaped (see section III.2.22), a suitable wave guide being matched to its apex and this wave guide leading to a resonant cavity incorporating the entrance tube of the receiver (see Figs. 125 and 126). In such cases no "input terminals" of the receiver's entrance stage may be indicated unambiguously. A suitable procedure for measuring the receiver's noise figure in this case is to use a standard signal generator or other suitable power source connected to a tiny dipole antenna or half-wave antenna, having the direction and polarization of optimal response of the receiver at a distance of, say, 20 wavelengths. By measuring the receiver's noise by means of the above indicator with the signal source switched off and then doubling the indication by adjusting proper signal strength, the specific radiation power at the reception antenna may be calculated and thence, by multiplication by the antenna's effective surface area S_e, the available power at the output of the reception antenna may be obtained. The further procedure is then similar to that outlined above.

REFERENCES: *32, 66, 119, 121, 127, 135, 139, 197, 235, 250, 289, 302, 320, 391.*

V.2. IMPEDANCE AND POWER MEASURING DEVICES

Available power and impedance being the main data at the terminals of any device, we may argue that a standard signal generator is mainly connected with measurements of available power (and of corresponding gain figures). Thus we need separate devices in order to carry out the desired impedance measurements.

V.2.1. Devices using lumped circuits. Devices of this kind have been successfully applied up to about 300 mc/s. In their application some simple principles are involved which will be dealt with first.

V.2.11. Principles. The measurements are executed by comparison of the impedance in question with the impedance of a lumped resonant circuit, the impedance being connected in parallel to the circuit's terminals. Before this comparison the resonant impedance of the lumped circuit itself must be determined. This is carried out by using a simple oscillator and a suitable voltage indicator according to the diagram of

Figure 114*a*. If the oscillator is of invariable voltage and frequency, the diagram 114*a* may be replaced by Figure 114*b*, the oscillator being represented by a generator of constant current I and of infinite internal impedance in parallel to the coupling capacity C_o. Thus it is seen that this capacity is merely to be added to the circuit's capacity C. In general it is advisable to make C_o small (e.g., some tenths of a pF) in order to insure the invariability of the oscillator when detuning the circuit capacitance C. By Figure 114*b* it is seen that the voltage measured by the indicator V is equal to IZ, if Z is the circuit impedance

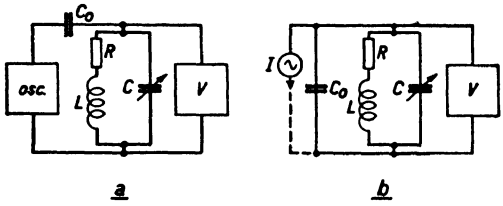

FIG. 114 Diagram *a*: Picture of signal oscillator *osc* acting on a resonant circuit LCR via a small condenser C_o, the voltage being measured by the voltmeter V. Diagram *b*: Equivalent circuit to diagram *a*, replacing the signal oscillator by a current generator I.

between its terminals 1 and 2. As I is constant, V is proportional to Z in our case. By detuning the circuit, varying C until the resulting impedance is in modulus exactly $1/\sqrt{2}$ times the resonant value, we obtain the relation:

$$Z_{res} = \frac{1}{\omega \Delta C} \qquad \text{(V.2.11}a\text{)}$$

ΔC being the deviation of C from its resonant position necessary to cause a drop of $|Z|$ to $Z_{res}/\sqrt{2}$ and of course an equivalent drop of the voltage V.

In these measurements two calibrations are necessary: one of the variable condenser C and the second one of the voltage indicator V. The calibration of C may be carried out at radio or audio frequencies, and if C is of suitable low-inductance design, this calibration may be valid up to about 300 mc/s. The voltmeters are either of the diode or of the crystal detector type, a corresponding circuit being pictured in Figure 115, D being either a suitable diode or a crystal rectifier.

The bias voltage is adjustable and the instrument A is usually a microammeter, of about one microamp full-scale deflection and 1000 ohms internal resistance. The condenser C_1 is usually such that the a.v. at the diode's terminals is equal to the voltage across the terminals of the impedance to be measured. The resonant frequency f_d of the diode (series inductance L_d of its leads with capacitance C_d between its electrodes giving $(2\pi f_d)^2 L_d C_d = 1$) must be much higher than that of the lumped circuit in question.

Diodes with f_d equal to about 3000 mc/s have sometimes been used (reference *368*). Crystal detectors of stable design have been used, their internal impedance being, however, sometimes as low as 30 ohms. In such cases they could be used only with either low-impedance circuits or with suitable series resistances attached to them in order to avoid excessive loading of the impedance under measurement. The calibration of the diode voltmeters may be carried out at audio or at radio frequencies by comparison with thermo-indicators and if they are of proper construction this calibration will remain valid in a relative sense up to at least 600 mc/s. In a relative sense this means that the voltage scale of the calibration curve will still represent volts at u.h.f. but these volts may be such that the scale value has to be multiplied with some multiplier dependent on frequency. Such a relatively known calibration obviously still satisfies the above requirements for the measurement of impedances. Direct u.h.f. calibrations of diode voltmeters of this kind have also been carried out by comparison with indications by thermoelectric couples and by thermo-expansion ammeters (see section V.2.3) and have confirmed previous observations. Besides, a check may be obtained at the frequency in question by determining the shape of the impedance-versus-tuning-capacity curve in the vicinity of resonance from the voltmeter readings and by comparing this experimental shape with the theoretical one.

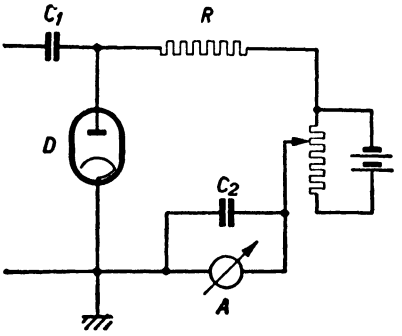

FIG. 115 Diode voltmeter circuit. Notation: D, diode or crystal rectifier; R, Resistor of some 0.2 megohms; A, microammeter; C_2 bypass, and C_1 coupling capacitance.

If a standard signal generator as considered in sections V.1.1 and V.1.2 is used in impedance measurements, we may dispense with the calibrated condenser described above. This generator may then be substituted for the oscillator of Figure 114, and by varying its frequency at a constant output level in the vicinity of the resonant frequency of the circuit under discussion, its resonance—i.e., impedance-versus-frequency curve—may be obtained. If Δf is the deviation from the resonant frequency causing a drop in modulus of impedance from 1 to $1/\sqrt{2}$, the resonant impedance is:

$$Z_{res} = \frac{1}{4\pi C \Delta f}, \qquad \text{(V.2.11}b\text{)}$$

C being the circuit's over-all parallel capacity. This is, of course, unknown. By adding a known small capacity to C we may, however, determine the corresponding variation of resonance frequency and thence the value of C. Thus in a way we still need a calibrated capacitance with this method.

When the resonant impedance of the circuit is known, any other impedance may be determined by connecting it in parallel to the circuit's terminals 1, 2. Representing the unknown impedance by a parallel connection of a resistance R_1 and a capacitance C_1, the latter is obtained from the variation of resonant frequency or of the calibrated tuning capacity of Figure 114. The value of R_1 is obtained from the variation of resonant impedance by connection of the unknown impedance to the circuit.

REFERENCES: *3, 20, 63, 91, 130, 142, 199, 228, 238, 243, 244, 320, 331, 352, 357, 361, 368.*

V.2.12. Examples. The devices to be considered are connected with measurements of tube impedances: input impedance (between cathode and control grid), output impedance (between anode and cathode), transadmittance (from control grid to anode), and feedback impedance (from anode to control grid). The apparatus built for these purposes covers a frequency range from about 6 mc/s to 300 mc/s. The separate parts of the devices were enclosed in adequately screened compartments (see section V.1.21), the different compartments being interlinked by u.h.f. coaxial lines where necessary.

By way of examples, the wiring diagrams of devices for the determination of output impedance and of feedback impedance are shown in

Figures 116 and 117. In these figures, the screened compartments, into which the measuring box is subdivided, are indicated by dotted lines. The alternating voltages, measured by the diode voltmeters,

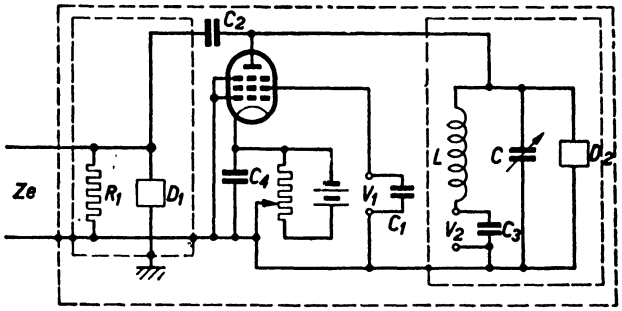

FIG. 116 Arrangement for the measurement of anode admittance in the meter-wave range. R_1, resistance of 1000 ohms; Ze, to transmitter; D_1 and D_2, diode voltmeters; C_1, C_3, and $C_4 = 2 \times 10^4\ pF$; $C_2 = 0.1\ pF$; V_1, screen grid and V_2, anode supply voltages; C, variable calibrated condenser of 15 pF maximum value.

range from some tenths of a volt to some volts, according to the circuit in use. In Figure 117 the transmitter voltage is connected to the

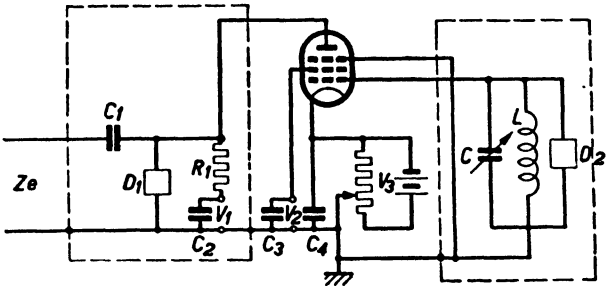

FIG. 117 Arrangement for measuring feedback admittances in the meter-wave range. Notation: Ze, to transmitter; D_1 and D_2, diode voltmeters; C_1, C_2, C_3, and C_4, condensers of $2 \times 10^4\ pF$; resistance R_1 of 500 ohms; V_1, voltage supply of 200 volts; V_2, supply of 100 volts; V_3, supply of 20 volts; C, variable calibrated condenser of 15 pF maximum value; L, inductivity of a tank circuit LC, tuned to the frequency in question.

tube's anode and measured at this electrode, while the tank circuit is connected to the tube's input and the voltage at this electrode is also measured. The tank circuit serves also as a means of observation

and elimination of spurious voltages in this case. Due to very small feedback admittances of modern tubes, if properly screened, in the wave ranges under discussion, the anode's alternating voltage had to be fixed at 3 to 30 volts in most cases, in order to obtain properly observable input voltages (some tenths of a volt). Only the modulus of feedback admittance is obtained in this way.

In the determination of transadmittance as regards modulus as well as phase angle, the circuit of Figure 118 was used. The transmitter voltage is connected to the input in this circuit, while the output voltage across a resistance R_o is measured by means of a diode voltmeter, preceded by a linear u.h.f. amplifier, including a mixer stage. The resistance R_1 and parallel capacity C_1 actually were constructed as a tank circuit of suitable resonant impedance used in a detuned position, connected in parallel to a reliably variable resistance of known u.h.f. calibration. This tank circuit's tuning condenser and parallel variable resistance were varied until the voltage across R_o was zero with the tube in normal operation. Then the tube's cathode heater voltage was switched off and the resonant impedance of the tank circuit with unaltered parallel resistance was measured. Let it be R_1. If ΔC is the variation in tuning capacity between both cases mentioned, the tube's transadmittance is $j\omega\Delta C - 1/R_1$. The measuring arrangement for this purpose, used between 7 and 30 m wavelength, is shown in Figure 119, while Figure 120 shows the over-all construction of the measuring devices described.

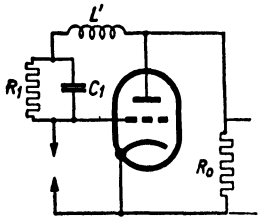

FIG. 118 Arrangement for measuring complex transadmittance from the control grid to the anode. Between control grid and cathode the applied a.v. is V_g. Between anode and cathode the a.v. is V_a. The inductance L' corresponds to the inevitable series inductivity of the leads to tube and to condenser C_1. The resistance R_1 consists of a tank circuit, bypassed by a variable calibrated resistance.

Special measuring devices were constructed for mixer tubes and stages. Here the relevant admittances are: h.f. input admittance, transadmittance between various electrodes—e.g., from oscillator input to signal input and vice versa, and from signal input to intermediate-frequency output. As the measurements have to be executed under operating conditions, one of the main problems to be solved is

the separation of alternating voltages of relatively little differing frequencies on signal-input or oscillator-input electrodes. This was achieved by the use of high Q circuits (e.g., resonant cavities). Rather elaborate set-ups have been constructed along the lines discussed above, as shown in Figure 120.

REFERENCES: *129, 143, 180, 256, 257, 290, 299, 352, 355, 356.*

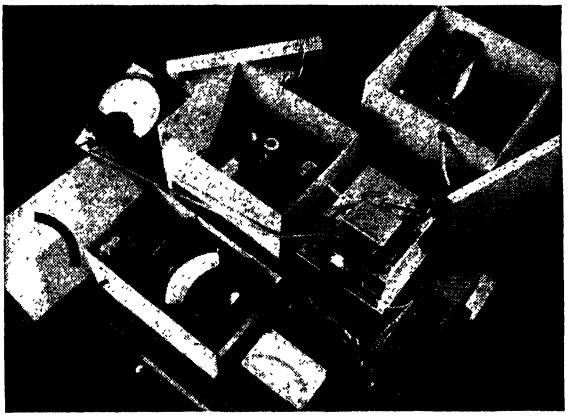

FIG. 119 Over-all picture of the arrangement for measuring complex transadmittances between 7 and 30 m wavelength. The boxes contain: Extreme right: signal transmitter. Center left: amplifier. Center right: variable condenser, variable resistance, tank circuit, diode voltmeter, and tube to be measured. Foreground left: microammeter of diode voltmeter. Right: supply voltage indicator.

V.2.2. Devices using transmission-line sections and cavities. At frequencies above 300 mc/s lumped circuits lose their efficiency owing to the inductances of sections of wire and to stray capacitances being almost of equal magnitude as the lumped circuit elements. Transmission-line sections are useful substitutes for lumped circuits until their dimensions perpendicular to the axes become considerable in comparison with one-quarter wavelength, at which point cavities become useful.

V.2.21. Devices based on quarter-wave resonance. Considering a quarter-wavelength section of a transmission line, its resonant impedance Z_{res} may be obtained by a procedure like that outlined in section V.2.11 in connection with Eq. (V.2.11a). By shortening the length of the section in question by an amount Δl starting from the resonant length

until a drop of the modulus of its open end impedance in the proportion of 1 to $1/\sqrt{2}$ is obtained we have:

$$R_{res} = Z_o \frac{\lambda}{2\pi \Delta l}, \qquad \text{(V.2.21}a\text{)}$$

Z_o being the section's wave impedance and λ the wavelength on the

FIG. 120 Over-all picture of arrangement for measuring mixer tubes and stages at about 2 m input wavelength and at intermediate frequencies of 0.5, 1, and 2 mc/sec. The box in the center consists of 8 compartments, containing the oscillator, the input signal source, the oscillator voltmeter, the input signal voltmeter, the input tank circuit, the tube, the output circuit plus amplifier, and finally, the output voltmeter. The lower boxes contain the supply sources.

line. This equation, like Eq. (V.2.11a), is valid only if Δl is small compared with $\lambda/4$. If a resistance is paralleled to the open end of the line section in resonance when coupled to a stable oscillator, the voltage across this open end will drop in proportion of the new combined resistance to Z_{res}. Thus a resistance may be measured. If a capacity C is paralleled to these open terminals the section has to be shortened by an amount l_c in order to reobtain resonance and in the case of a

low-loss line we have approximately:

$$\omega C = \frac{1}{Z_o} \tan\left(2\pi \frac{l_c}{\lambda}\right), \qquad \text{(V.2.21}b\text{)}$$

ω being the angular frequency in question and λ the wavelength. In order to carry out measurements of complex impedances conveniently, two line sections may be used according to Figure 121. Section I is always of length (slightly variable by means of a slide) nearly equal to one-quarter wavelength. Section II serves as a compensation for the parallel capacitance included in the impedance Z under measurement. A diode voltmeter is coupled to the terminals of the small loop near

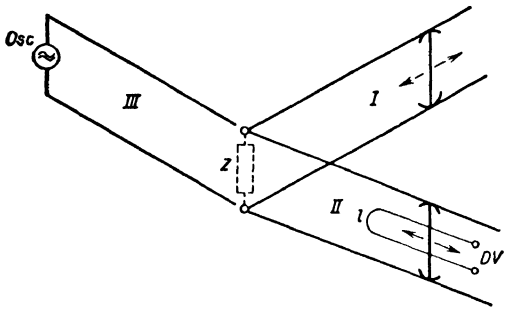

FIG. 121 Schematic picture of impedance measuring device consisting of the line sections I and II both provided with a sliding short-circuit at their far ends, the loop l of a diode voltmeter DV being connected to the slide of the section II. The impedance Z under measurement obtains its voltage from the generator *osc* via section III.

the short-circuit slide of section II. The generator is coupled to the impedance Z by means of a third suitable line section as shown. The limitations of this method may be derived from Eq. (*a*). As Δl in Eq. (*a*) is to be small compared with $\lambda/4$, the value of Z_{res} is obviously always large compared with Z_o, say, larger than $10Z_o$. If we connect a resistance to be measured in parallel to Z_{res} its value, in order to limit reading errors, should be comparable with Z_{res} and hence this resistance is also limited to values, say, larger than $10Z_o$. If we connect this resistance to the open terminals by interposition of a quarter-wave section of equal wave impedance Z_o, its value is transformed accordingly (see section IV.1.24) and we find that resistances smaller than, say, $Z_o/10$ may also be properly measured. A complete

picture of an impedance-measuring device according to the above description, of dimensions suitable at frequencies between 600 and 1000 mc/s, is shown in Figure 122. The three line sections of Figure 121 are clearly seen in the picture, each surrounded by a circular shield

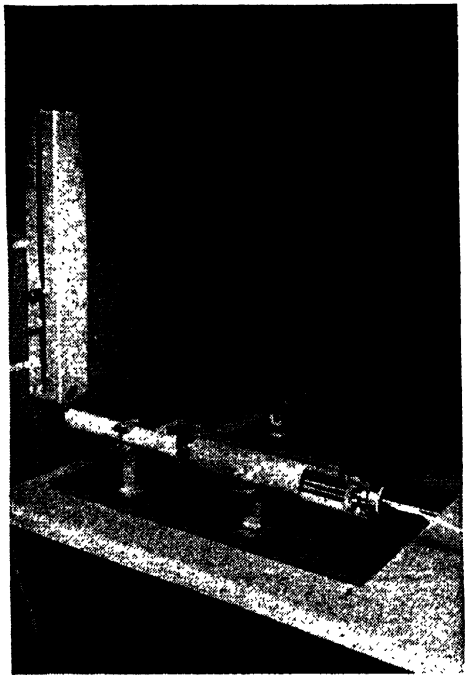

FIG. 122 Photograph of measuring device according to Fig. 121 suitable at about 600 to 1000 mc/s. At the left: Signal oscillator and coupling device. The three line sections are clearly shown, each consisting of two parallel conductors shielded by a tubular enclosure (reference *405*).

in order to avoid radiation losses and stray coupling (reference *405*). Adjustments of the short-circuit slides are carried out by means of micrometer nuts of suitable construction.

REFERENCES: *63, 65, 99, 102, 113, 129, 138, 143, 243, 256, 258, 361, 405.*

V.2.22. Devices based on non-resonant lines. In order to measure admittances, the conductive parts of which lie outside the range cited above, a parallel-line wave-conductor system has been used in a different

way. The method is based on the determination of the reflection coefficient F of Eq. (IV.1.21a) of an incoming wave at the admittance in question, connected across the parallel-wire line. On account of this reflection a voltage minimum arises at a definite distance in front of the admittance. By determining the location of this minimum relative to the connection of the admittance in question and from the shape of the voltage curve in its vicinity, the real and imaginary parts of the admittance may be obtained. From the diagram in Figure 75 it appears that admittances, the conductive parts of which are either

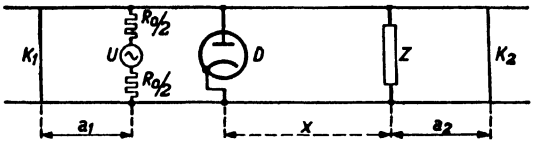

FIG. 123 Measuring device for impedance measurements. A parallel-wire line carries two short-circuit slides K_1 and K_2, a slide provided with two small resistances, the sum R_0 of which equals the line's wave impedance, and with a small loop U coupled to the signal generator and a slide carrying the diode D. The impedance Z is connected to the wires at a distance x from D and at a_2 from K_2.

too large or too small in relation to the wave admittance, may not be determined with any accuracy from the measured reflection coefficients. Hence the present method is best suited to the measurement of resistances of the same order as the wave impedance. The latter lies usually between 100 and about 300 ohms for most parallel lines, and hence the range of this method is limited to values of this order of magnitude.

It supplements the former method well, which deals preferably with resistances either several times smaller or larger than the wave impedance. A diagram of this conductor system is shown in Figure 123. The oscillator is coupled to the line at U in series with resistances, each equal to one-half of the wave impedance, a short-circuit slide K_1 being placed at a distance a_1, in such manner that this combination, as viewed from D, acts as a wave impedance at this end of the line. The impedance Z to be measured is connected at a distance a_2 from the short-circuit slide K_2 such that this combination, if viewed from D, acts as an impedance, exactly equal to the impedance to be measured, neutralizing lead and similar effects. The diode D is moved to a proper distance x from Z corresponding to minimum line voltage and the latter is de-

termined in the vicinity of this position. If the minimum voltage is V and if its modulus is $V\sqrt{2}$ at a distance x_1 from the minimum position, we obtain the equation:

$$\frac{(1 - |F|)^2}{|F|} = \left(\frac{4\pi x_1}{\lambda}\right)^2 \text{ if } \frac{4\pi x_1}{\lambda} \ll 1. \qquad \text{(V.2.22}a\text{)}$$

Hence the modulus $|F|$ is found from this shape of the voltage curve in the vicinity of the minimum position. From this modulus, the ratio of the corresponding resistance R to Z_o may be obtained using Figure 75. The phase angle ψ of F, which is also necessary to the determination of the ratio $\mathbf{Z}/Z_o$, is obtained from:

$$\frac{4\pi x}{\lambda} - \psi = \pi, \qquad \text{(V.2.22}b\text{)}$$

if x corresponds to the nearest minimum voltage position to $\mathbf{Z}$. Thus the complex value of F and hence by Figure 75 of $\mathbf{Z}/Z_o$ is known.

Many practical problems have turned up in the execution of measurements as described. Not all of these have as yet been solved in an entirely satisfactory manner. Two points may be mentioned by way of example. Diodes of very small physical dimensions have been constructed, but still, at the shortest waves (say 20 cm) the necessary distance between the line conductors is not sufficiently small (say 2 cm) with respect to one-quarter wavelength (say 5 cm). Neither is this true of the dimensions of the surrounding screening case. Hence crystal detectors have been constructed with outer dimensions of only a few mm and of stable performance, undisturbed by shocks, etc. These indicators have a number of advantages—e.g., no heating current is needed. But their impedance at the present frequencies is often extremely low, say some 10 to 50 ohms, and so no direct connection can be made, in most cases, to a line. Loosely coupled detectors, however, due to limited sensitivity, necessitate large voltages on the line and at the impedance connections. With reception tubes these large voltages do not agree with normal operating conditions in many cases. Another point is lack of symmetry. In most measurements it was found difficult to ascertain exact counterphase voltages at the points between which they are measured. This is often due to the third conductor—i.e., the surrounding screen—which is not exactly at a balanced voltage position with respect to the two line conductors.

REFERENCES: *65, 180, 183, 200, 256, 257, 299, 368, 383.*

V.2.23. Devices based on resonant cavities. These devices may be useful in obtaining data pertaining to the dielectric coefficient and the loss angle of dielectric media at extreme-high frequencies, as well as data pertaining to the interelectrode impedances of special types of tubes. As an example of the first type mentioned, we consider Figure 124, representing the cross-section of a cylindrical cavity resonator. At the center of the cylindrical circumference a small coupling loop *tr* is coupled to a transmitter or generator. Opposite this loop a second one indicated by *rec* is coupled to a suitable receiver. By operating the generator at the corresponding resonant frequency of the cavity a resonant field is created of which the electric-field strength between the plane parallel faces 1 and 2 is directed perpendicularly to them. The resultant field strength in the cavity is measured on a relative scale by the receiver attached to the loop marked *rec*. If the generator frequency is varied slightly in the vicinity of resonance until the field strength squared measured at *rec* has dropped by 3 db relative to its resonant value, the Q value of the cavity is obtained in terms of the frequency deviation Δf from the resonant frequency f using the familiar equation ($2Q = f/\Delta f$). Now a suitably shaped sample of the dielectric medium under measurement is brought between the centers of the faces 1 and 2 and the resulting Q value is determined, as well as the variation of the resonant frequency f. From these two data (variations of Q and f) and from the dimensions of the sample as well as of the adjacent faces 1 and 2, the values of the dielectric coefficient ϵ and of the loss angle δ may be obtained. Measurements of this kind have been successfully performed up to about 10,000 mc/s.

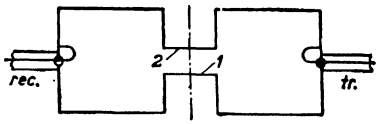

FIG. 124 Resonating cavity coupled to a signal oscillator: *tr* and to a voltmeter device: *rec.*

At extreme-high frequencies tubes of so called "lighthouse" type have been used, of which an example is shown in Figure 125. For applications of these tubes the equivalent impedances between each pair of adjacent electrodes are worth knowing. These may be obtained by a method similar to the one outlined above. The tube in question is mounted in a suitable resonant cavity 2 as shown in Figure 126. In this case the measurement pertains to the cathode-grid impedance. The cavity 1 enclosing the anode-grid portion is of much smaller dimensions than the cavity 2 and its lowest resonant frequency is much higher

than the excited fundamental resonant frequency of the cavity 2. Thus conditions approximating a short-circuit connection between anode and grid are obtained. In order to allow proper direct voltages to be applied to anode and grid, the cavities 1 and 2 are connected to the grid plane 3 by means of suitable ring-shaped capacitances C as shown. Sufficient capacitance of these connections is desirable in order not to impair the resonant Q value of cavity 2. The procedure is similar to the one outlined above, first measuring Q of cavity 2 with zero heater current and then under several selected operating conditions. From the variations of resonant frequency and of the corresponding Q value the equivalent impedance between cathode and grid caused by electronic emission and motion may be determined. A similar procedure may be applied to the anode-grid portion of the tube, interchanging the cavities 1 and 2.

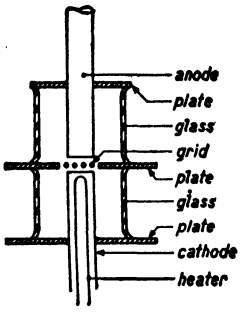

FIG. 125 Schematic picture of lighthouse triode.

REFERENCES: *65, 99, 104, 144, 203, 223, 290, 330, 392, 394.*

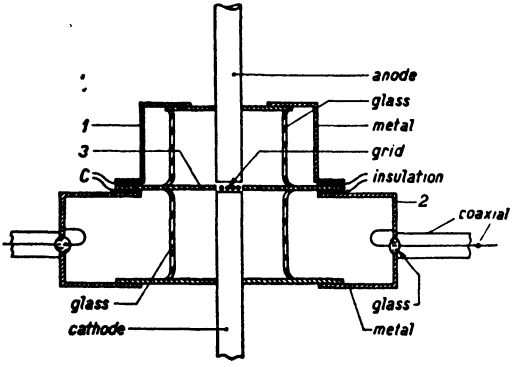

FIG. 126 Cavity 2 connected to the cathode and control grid of a lighthouse triode. Cavity 1, being much smaller than 2, is connected to anode and grid. Insulating sheets between the cavities and the grid electrode 3 create capacitances C serving as blocks.

V.2.3. Power-measuring devices. In a number of impedance measurements not only the impedance but also information concerning

the currents flowing through or the voltages created across those impedances is desired. The latter values are in the u.h.f. range almost exclusively obtained from the determination, by a suitable measuring device, of the power consumed.

V.2.31. Devices using current heating effects. The heating effects to be considered here are: incandescence, variation of resistance, expansion of a heated gas volume, and thermoelectricity. The current to be measured is in all three cases made to flow through a suitable wire of circular cross-section and of known impedance. In order to comply with the latter condition the wires must be of uniform structure. In many cases the length of the wires will be such as to cause non-uniform current amplitudes along their axes. Only if the length is very small compared with one-quarter wavelength in air will the current be distributed uniformly along the axis of a straight wire.

If the wire in question is heated to incandescence its temperature may be determined by pyrometric means or by activation of a photocell. If the current is of non-uniform distribution this fact will be revealed by pyrometric inspection. The relation between the local r.m.s. current in any spot of the wire and the corresponding temperature may be ascertained by a subsidiary check using d.c. For practically all purposes the difference in heating caused by skin-effect may be disregarded (reference *336*). From the temperature dependence of the wire's specific resistance, to be obtained from a subsidiary check using d.c., and from the current distribution obtained from the temperature distribution as specified above, the effective wire resistance under actual operating conditions may be determined. In series with this resistance a reactance $j\omega L$ exists, L being the wire's inductance to be obtained from Figure 97. Thus the current flowing through the wire, the power consumed in it, and its impedance are completely known.

In some cases the heating current flowing through a wire is too small to produce incandescence. In such cases the wire's resistance may be measured under operating conditions using d.c. No subsidiary check of the current distribution is readily obtainable in this case. Hence either this distribution must be derived from circuit considerations or the wire's length should be so small as to obtain uniform distribution. A considerable resistance of the wire being preferable in many cases, very thin wires (e.g., of 1 micron diameter or even less) of suitable material (e.g., tungsten) may be used to advantage. The check curve may be obtained at r.f. or using d.c. Devices of this kind have been

successfully used at 1500 mc/s with currents of a few milliamps. The skin-effect correction of wire resistance with very thin wires is small and may be obtained from:

$$\frac{R_{ac}}{R_{dc}} = 1 + 3 \times 10^3 \left(\frac{\mu\pi d^2\sigma}{4\lambda}\right)^2 \qquad \text{(V.2.31}a\text{)}$$

μ being the wire's effective magnetic permeability, λ the wavelength in air (cm), σ the wire's specific conductivity (mhos/cm), and d its diameter (cm). An example is shown in Figure 127.

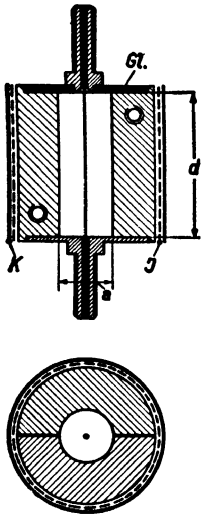

FIG. 127 Voltmeter (according to A. Ditl) acting on resistance-variation of a very thin central wire. Dimensions: a = 4 mm, d = 13 mm. Legend: J, polythene insulation; Gl, mica; K, copperfoil.

Another method applicable to small currents under similar additional conditions as described above makes use of a small bulb, filled with air, through which the wire is stretched. The bulb is connected to a suitable capillary tube containing a drop of colored liquid, the position of which may be determined by means of a scale. If a current flows through the wire the gas volume in the bulb expands and the drop moves. A check curve may again be obtained at r.f. or using d.c. In some cases two such devices have been used in a compensation circuit, d.c. being made to flow through one wire simultaneously with the a.c. through the other one. The d.c. is then adjusted until the liquid drop remains stationary when switching both currents on. An example is shown in Figure 128. Powers of about 10^{-5} watts have been successfully measured by these means with an error not exceeding 5% at about 1500 mc/s. The amount cited does not, however, constitute the lowest limit obtainable, as some scope for further development is present.

As thermoelectric couples are well-known means of current determination, only the special constructions of such devices to be used at u.h.f. are of particular interest here. The aim of these constructions is to minimize interaction between the two wires of different constitution at the junction of which a thermoelectric voltage is created, on the one hand, and the heater wire through which u.h.f. current flows, on

the other hand. A construction which was successfully operated at 1500 mc/s is shown in Figure 129 together with a more common type

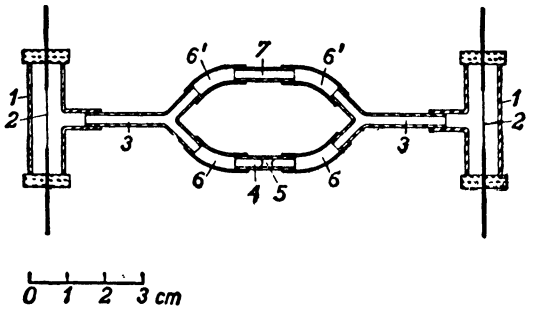

FIG. 128 Air expansion milliammeter. Legend: 1, polystyrene tube; 2, resistance wire (constantan of 20 microns diameter); 3, glass tubing; 4 and 7, glass capillary tubes, 7 being narrower than 4; 5, colored drop of liquid (alcohol). Through one of the wires 2, the a.c. to be measured is circulated, and through the second wire 2, a d.c. of equal magnitude, thus keeping the drop 5 at rest.

suitable at r.f. The powers that were measured successfully using these means are about equal to those described for the preceding case.

REFERENCES: *65, 142, 144, 199, 228, 256, 257, 320, 336, 357, 361, 388.*

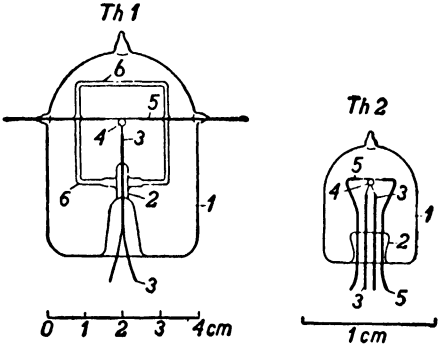

FIG. 129 Two high-vacuum thermocouples. Legend: 5, heating wire of 10 to 20 microns diameter; 4, pearl of insulating material; 3, two welded thermowires; 2, stem; 1, bulb; 6, glass support of heating wire 5.

V.2.32. Devices using effects of voltages. The best-known devices of this type are diode voltmeters (see Fig. 115) using either small diodes or crystal rectifiers. The former have the advantage of higher

impedance if of proper construction, whereas the latter may be of extremely small size (e.g., 6 mm over-all length) but are often of small impedance (less than 100 ohms). Diodes of small size with a directly heated tungsten wire cathode and a cylindrical anode, the resonant frequency of lead inductance together with interelectrode capacitance being about 3000 mc/s, are shown in Figure 130. Voltmeters using these diodes may be operated up to about this frequency if proper series

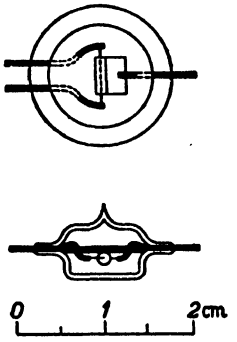

FIG. 130 Diode of small dimensions and low capacitance and lead inductance, suitable for voltage measurements up to about 2000 mc/s.

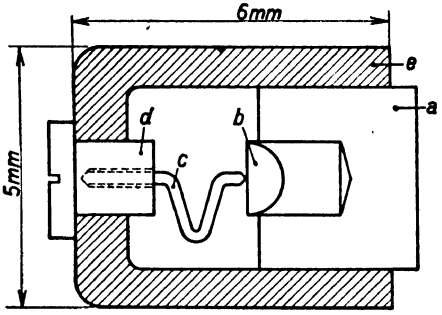

FIG. 131 Silicon crystal detector for u.h.f. and s.h.f. use. Notation: *a*, copper electrode holding silicon crystal *b*, on which tungsten wire *c* rests with its point, being held in position by the copper electrode *d* inside the insulating holder *c*.

resistance is applied to flatten out the resonance curve. The voltmeter reading will be less than with equal r.f. voltage at this frequency but a r.f. calibration curve may remain valid to a relative scale. A small crystal (silicon with some additions) detector construction of stable performance is shown in Figure 131. If used with a series resistance of about 1000 ohms the voltmeter sensitivity, using a crystal as described, is comparable to that of one using a suitable small-size diode.

A second effect used successfully at u.h.f. is the force created between the two electrodes of a tiny condenser, one electrode being made movable. Several constructions have been tried, small size being essential. Because of this, rather high voltages are required to activate the electrostatic voltmeter, values of the order of 100 volts being no

exceptions. Thus only rather large voltages may be measured in this way. Calibration is carried out using r.f. or direct voltages.

A third effect of u.h.f. voltages is the heating of dielectric media interposed between conducting electrodes. Only in few cases has this effect been successfully used for the quantitative determination of u.h.f. power. One such instance is worth mentioning on account of its relation to u.h.f. tube operation. Consider a diode with an indirectly heated cathode coated with the usual barium-strontium-oxide layer which has been activated to high emissivity by suitable previous processing. If an u.h.f. voltage is connected to the cathode and anode, it will have a heating effect on the cathode layer because of its conductivity and dielectric losses. This heating is additional to the one provided by the normal cathode heater. If a definite d.c. to the anode is caused by a proper r.f. interelectrode voltage before the application of an equal u.h.f. voltage, this current will be increased by the heating effect upon the application of the latter voltage. The heating power provided by the normal heating system may then be decreased until the d.c. is restored to its original value. Obviously this reduction of heating power is equal to the power dissipated in the cathode layer by the u.h.f. voltage. With layers of about 50 microns thickness values of one watt were obtained at a few u.h.f. interelectrode volts. By a reduction of the layer thickness to a few microns this effect practically disappeared. For this and for some additional reasons very thin cathode layers have been found essential to the u.h.f. operation of most types of tubes.

REFERENCES: *3, 65, 71, 72, 91, 92, 130, 200, 238, 239, 240, 244, 256, 257, 307, 331, 361, 368, 379, 404.*

V.3. GAIN, NOISE, AND IMPEDANCE DATA

The data presented under this heading are intended to afford instances of the application of devices described as well as to offer material useful in the discussion of subsequent chapters.

V.3.1. Gain and noise-figure data. Published data on gain and noise figures at u.h.f. and extreme-high frequencies are still somewhat scarce. Even so, by collecting the available evidence, satisfactory estimates of these figures may be made in the entire range from about 5 mc/s up to 30,000 mc/s.

V.3.11. Gain data of amplifier stages. We shall consider gain of h.f. amplifier stages of band width very small in comparison with the frequency of operation. With these stages tubes of three different types will be associated: first, tubes (pentodes) of conventional construction such as are used at r.f.; second, tubes of design such as are used in the range between 30 and 300 mc/s; third, tubes specially designed to give satisfactory performance at frequencies above 300 mc/s and in some cases even above 3000 mc/s. In each case the experimental gain figures pertain to optimal operating conditions, input and output of the stage in question being matched to the preceding and to the subsequent stage respectively.

Considering suitable amplifier stages using conventional r.f. tubes, optimal measured gain was between 3 and 4 at 150 mc/s. This gain was inversely proportional to the fourth power of the frequency between 15 and about 300 mc/s, increasing more slowly with decreasing frequency below the former limit. Thus gain figures between 30,000 and 40,000 would prevail at about 15 mc/s under optimal operating conditions, which is of course much higher than practical figures used in receiver design, the latter in most cases not exceeding 10,000. As higher figures are of little practical interest, we may perhaps in this sense state that the tubes under consideration are entirely satisfactory up to 20 mc/s and are of declining but still acceptable performance above this frequency up to about 70 mc/s. These figures all pertain to tubes with plastic sockets and of construction similar to the common octal-base metal or G-tubes. Tubes of all-glass construction without socket, the pins being directly pinched through the glass base, are mostly of more favorable performance, the optimal measured gain figure of a corresponding h.f. amplifier stage of suitable construction being between about 50 and 70 at 100 mc/s, this figure being again approximately inversely proportional to the fourth power of the frequency between, say, 300 mc/s and 20 mc/s. At equal frequencies these tubes thus afford about three times the optimal stage gain of the tubes of older construction.

Second, we now consider stages using tubes of special design for the range from 30 to 300 mc/s. In the first place, the prewar so-called acorn tubes come under this heading. At 150 mc/s optimal gains between about 25 and 30 were obtained; these figures compare favorably with those even of the all-glass tubes. Inverse proportionality of gain to the fourth power of the frequency again prevails between about

300 and 30 mc/s. With television tubes of suitable all-glass construction and high transconductance, similar to the type EF50, optimal gains were about equal to those of the acorn pentodes.

Third, tubes (triodes as well as pentodes) of special design under optimal operating conditions at frequencies above 300 mc/s will be considered. With some push-pull pentodes of dimensions comparable with those of the above EF50 type and of high transconductance (about 5 m mhos per electrode system) gains of about 50 have been obtained at 300 mc/s; these figures are considerably higher than those for tubes of the preceding types. Frequency dependence of g was again as stated above, up to about 600 mc/s. At the highest frequencies it has been found useful to derive gain figures from oscillator-circuit performance. If a tube is able to cause oscillations in a suitable feedback circuit at a given frequency, we may conclude that a gain figure exceeding unity may be obtained using the tube in a suitable efficient amplification stage at the frequency in question, avoiding feedback. For several tubes, especially triodes, the highest frequencies at which oscillator stages using them can possibly be made to operate are known. At these frequencies the gain of suitable amplification stages is at least unity. Assuming the gain to be dependent on frequency, as stated above, within a certain range, the resultant gain at any frequency within this range may obviously be deduced on the assumption of its being unity at the said limiting frequency. Thus with certain tubes of the lighthouse type (see Fig. 125) this limiting frequency is 5000 mc/s. Hence the optimal gain at 1000 mc/s may be about 600. Similar deductions may be made for other tubes of modern u.h.f. design. The basic equation for gain figures under the above conditions is:

$$g = \left(\frac{f_o}{f}\right)^4, \qquad \text{(V.3.11}a\text{)}$$

f_o being the frequency at which gain is unity and f the frequency of operation, the range of this equation usually extending from $f = f_o$ to at least $f_o = 10f$ and often beyond this.

If the width B of the frequency band in the amplification under discussion is considerable compared with the frequency round which it is centered, gain figures may be smaller than those quoted above. Gain may in such cases be inversely proportional to the square of B and practically independent of the central frequency of amplification.

Some experimental figures obtained with all-glass pentodes of the EF50 type as used in television are: about 4 at $B = 20$ mc/s and about 12 at $B = 10$ mc/s, the central frequency of the band B being about 40 mc/s. Thus the inverse proportionality to B^2 is not altogether verified because 10 mc/s is a border case between the two cases of B small and B large compared with the central frequency. In general, the course of the gain-frequency curve corresponding to wide-band amplification has the shape shown in Figure 132, the junction between the two fully traced parts being at a central frequency f_o depending on B and on stage and tube data. Under the present conditions the gain equation is:

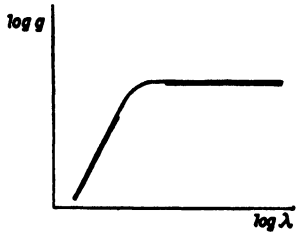

FIG. 132 General shape of gain-versus-frequency curve at v.h.f., u.h.f. and s.h.f.

$$g = \left(\frac{B_o}{B}\right)^2, \qquad \text{(V.3.11}b\text{)}$$

B_o being the band width at which gain is unity.

REFERENCES: *82, 88, 155, 163, 187, 195, 197, 202, 216, 218, 219, 223, 226, 298, 352, 353, 354, 356, 363, 364, 401.*

V.3.12. Gain data of mixer stages. Besides the tubes mentioned in the preceding section V.3.11, multi-grid mixer tubes are being used at frequencies below 60 mc/s and in some cases even beyond this frequency. We shall start by discussing a case pertaining to r.f. multi-grid mixer tubes of heptode type similar to type 6L7G, the input grid being adjacent to the cathode and the grid to which the local oscillator voltage is applied being separated from the input grid by an interposed screen grid. Input frequency is 50 mc/s, output (intermediate) frequency is 3 mc/s, and band width B about 1 mc/s. Optimal gain is about 4, this figure being inversely proportional to the square of the input frequency and to B at fixed i.f. within the range between 100 mc/s and 10 mc/s as regards input frequency.

At frequencies beyond 60 mc/s so-called single-grid mixing has been used frequently, both input and local oscillator voltages being applied to the input-control grid. The tubes used in single-grid mixer stages may be the same as those discussed above in relation to amplification

stages. Often the i.f. is small compared with the input frequency and the band width B is comparable with the i.f. round which it is centered at the output. In these cases, as in the one dealt with above, gain is found to be approximately inversely proportional to the input frequency squared and to B, the intermediate frequency remaining unaltered. With tubes of conventional r.f. design and all-glass construction, an optimal gain of about 6 is obtained under these conditions at 100 mc/s input frequency and B equal to 1 mc/s; this is comparable to the intermediate frequency (e.g. 10 mc/s). The range of input frequency for which the above proportionality rule holds is about 300 − 10 mc/s and the range of B relative to the output frequency about $\frac{1}{2}$ to $\frac{1}{10}$, the output frequency being lower than 10 mc/s. With the special tubes designed for the range up to about 300 mc/s—e.g., the acorn and the EF50 types—gain may be about 2 to 3 times the value of the latter tubes under equal conditions of operation as regards frequencies. The gain equation under the present conditions is:

$$g = \left(\frac{f_o}{f_{in}}\right)^2 \frac{B_o}{B}, \qquad \text{(V.3.12}a\text{)}$$

and the product $f_o^2 B_o$ may be obtained from any particular measured gain at known values of f_{in} and B.

At frequencies above 300 mc/s the intermediate frequency is often much higher than the band width B involved at the output. In these cases the gain figure becomes independent of B and inversely proportional to the square of the input frequency as well of the output frequency. Quoting a figure for a tube of lighthouse construction (as in section V.3.11), the input frequency being 3000 mc/s, the i.f. 150 mc/s, and the band width 2 mc/s, a mixer gain of about 100 to 150 may be obtained. In this case the gain equation is:

$$g = \frac{f_o^4}{f_{in}^2 f_{out}^2}, \qquad \text{(V.3.12}b\text{)}$$

the value of f_o being obtainable from any measured gain figure at known values of the input frequency f_{in} and of the output frequency f_{out}.

In a number of cases mixer stages using diode tubes have been used at input frequencies of the order of 300 mc/s and at higher frequencies. The optimal gain of a diode mixer stage obtainable is unity if no self-oscillation or regeneration occurs with the diode circuit in question. This is obvious from the consideration that such a circuit then consists

of passive impedances only (the diode also being of this type), and such a circuit can have only a gain that reaches unity at the utmost. With diodes of conventional design—i.e., with interelectrode distances of the order of 100 microns and non-negligible electrode lead reactances at the frequencies in question—gains of the order of 0.1 to 0.5 are often found in mixer stages at 300 mc/s input frequency, dropping to 0.01 at 1500 mc/s. These very low gains have resulted in excessive noise figures of receivers incorporating such stages. With diodes of proper construction and interelectrode distances of the order of 20 microns (e.g., lighthouse type), gains of the order of 0.3 to 0.5 at 3000 mc/s are obtainable. Using suitable silicon crystals instead of diodes, gain figures of about 0.3 have been obtained even at frequencies beyond 5000 mc/s.

REFERENCES: *32, 71, 72, 150, 159, 160, 161, 164, 196, 342, 344, 355, 359, 366, 404.*

V.3.13. Noise figures. In order to compare the noise figures obtained at u.h. and at extreme-high frequencies with those at r.f. some experimental figures related to amplifier and to mixer stages at the latter frequencies will be quoted first. In radio sets on the market, usually three wave bands are coped with (short waves: 6 to 23 mc/s; medium waves: 0.5 to 1.7 mc/s; and long waves: 150 to 380 kc/s), while two essentially different types still exist in which the entrance stage is an amplifier or a mixer stage. The highest noise figures are usually associated with the short-wave range and even these are usually not much above unity with the first type and not above 30 with the second type in sets of efficient design. In the other two wave ranges noise figures are usually between 1 and 5 with all types.

Using the conventional r.f. tubes (pentodes) in u.h.f. amplifier entrance stages above 30 mc/s at band widths small compared with the frequency of operation, the attendant noise figure increases with increasing frequency until figures in the neighborhood of 20 are reached at frequencies corresponding to unity gain (e.g., 200 mc/s). Similar relationships are valid in the case of special tubes designed for these frequencies, such as acorns or television tubes. When the noise figure exceeds about 5, it increases nearly proportionally to the square of increasing frequency up to the frequency corresponding to unity gain, at which noise figures in the vicinity of 20 are usually found. With tubes designed for operation above 300 mc/s such as push-pull pentodes

(section V.3.11), affording $g = 30$ at 300 mc/s, the limiting frequency f_o being about 700 mc/s according to Eq. (V.3.11a), noise figures between 10 and 30 are usually found at this frequency. This also holds good for the lighthouse type mentioned in section V.3.11, the noise figure being approximately proportional to the square of the frequency f of operation below the limiting frequency until N drops below about 5 at decreasing operational frequencies. These figures do not include a contribution of the subsequent stage.

Leaving out multi-grid mixer tubes, the noise figures of corresponding stages at frequencies up to about 30 mc/s being between 10 and 30, we shall refer only to pentode and triode tubes used as single-grid mixers. Under optimal conditions of operation and at band widths small compared with the input frequency, the noise figures of mixer stages incorporating these tubes are approximately equal to those of amplification stages using these tubes at a frequency equal to the input frequency of the mixer stages in question.

With wide-band amplification, the gain being approximately constant throughout the band width in question, the noise figure N is approximately proportional to the band width B as soon as N rises above about 5 (see section VI.1.23). At band widths corresponding to gain figures well above unity (say above 10) the noise figure N is usually small and below 10 or even 5, rising at increasing widths as stated. With wide-band mixing, too, in both cases corresponding to Eqs. (V.3.12a) and (b), the noise figure has about the values quoted with wide-band amplification as long as the gain figure is well above unity. The band width is nearly always small compared to the input frequency with such mixer stages. The actual noise figures found are under these conditions approximately equal to those given above for mixer stages at small band widths, and N is approximately independent of B.

Finally we shall quote some figures related to diode mixer stages at the entrance of receivers. Such stages operated at an input frequency of 300 mc/s, incorporating diodes of conventional interelectrode spacing (see end of section V.3.12), show noise figures of the entire receivers between about 10 and 30 under favorable conditions. With the same diodes noise figures of 500 to 1000 and even more were obtained for the corresponding receivers at a frequency of 1500 mc/s. These figures showed a marked improvement at the introduction of diodes of more suitable design, values between 10 and 20 being obtained at frequencies in the vicinity of 3000 mc/s, the corresponding stage gain

being between 0.1 and 0.5. These noise figures, according to Eq. (II.2.13*c*), show a considerable dependence on the noise figure of the intermediate frequency stage succeeding the diode; this value enters into the over-all figure multiplied by $1/g$ which may be 10. With specially careful construction of the second reception stage and of the diode mixer stage, noise figures of the order of 10 to 20 have been obtained above 3000 mc/s. With suitable crystals even lower figures may prevail.

REFERENCES: *32, 119, 135, 139, 162, 163, 196, 197, 235, 277, 329, 373, 404.*

V.3.2. Experimental data on impedances. Though the gain and noise figures of the preceding section V.3.1 give the reader an over-all picture of receiver performance at these frequencies, detailed understanding of this performance must be derived from impedance data such as will now be dealt with.

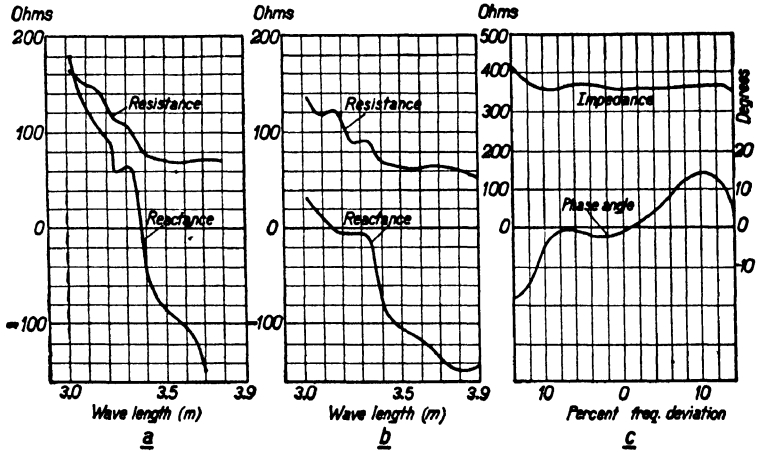

FIG. 133 Input impedance curves of half-wave antennas. Diagram *a*: No. 10 wire antenna. Diagram *b*: 1.5-inch copper pipe antenna. Diagram *c*: Double cone antenna of 13 degrees flare angle Θ_0 (see Fig. 69). In this latter diagram the modulus of the impedance is shown in the upper curve and its phase angle expressed in degrees in the lower curve. Vertical scales on the left are in ohms (reference *61*).

V.3.21. Antennas and impedance elements. In order to show the influence of shape on impedance at the terminals of a half-wave antenna, three sets of curves are presented in Figure 133. The curves of Figure

133*a* pertain to a half-wave antenna made of no. 10 wire connected to an open parallel-wire transmission line of equal wire size matched to the antenna at about zero reactance by means of a suitable low-loss transformer section (see section IV.1.24). The impedance is measured at the terminals of the line far from the antenna. The humps of the impedance curves are ascribed to reflections from near-by buildings. Even if these are flattened out, the useful band width is extremely low relative to the match-wavelength corresponding to zero reactance. The curves of Figure 133*b* pertain to a 1.5-inch copper pipe half-wave antenna occupying the same position as that of Figure 133*a* and fed through the same line (reference *61*). The useful relative band width of this antenna is considerably larger. For comparison, the impedance of a double-cone antenna of about 13 degrees flare angle Θ_o (see Fig. 69) is shown in Figure 133*c*, measured between the two tops. The length of the cone along its surface from apex to rim is about 0.365 wavelength at the center frequency. The magnitude of the impedance is nearly constant and its phase angle is less than 10 degrees within a band of approximately 20% of the center frequency. These figures tend to show the vast superiority of the double-cone antenna in wide-band reception. Adhering to the above relation of cone length to wavelength at the center frequency, the impedance at the latter frequency is given in relation to the flare angle Θ_o (see Fig. 69) in Figure 134.

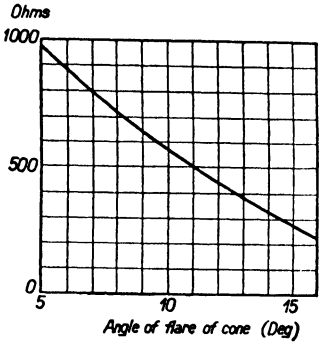

FIG. 134 Impedance at tuning position of a double cone antenna as dependent on the flare angle Θ_o (see Fig. 69). The length of one cone along its surface from apex to rim is 0.365 wavelengths (reference *61*).

The influence of reflection from the earth's surface on the impedance of a half-wave horizontal antenna, the frequency corresponding to zero average reactance of the antenna if at a great height above the surface, is shown in Figure 135. The soil in these measurements consisted of quartz sand, its dielectric coefficient ϵ being approximately 9.

Some data on the behavior of resistor units at u.h.f. are collected in Figure 136, giving the ratio of u.h.f. resistance R to d.c. resistance

R_o in dependence of the operating frequency. The curves pertain to the following units:

CURVE NO.	R_o =	LENGTH CM
1	100 k ohm	1.90
2	100 k ohm	3.50
3	25 k ohm	0.90
4	60 k ohm	2.20

the diameter being 0.40 cm in each case. The resistances of largest ratios of length to diameter show relatively the largest drop of resistance at the highest frequencies.

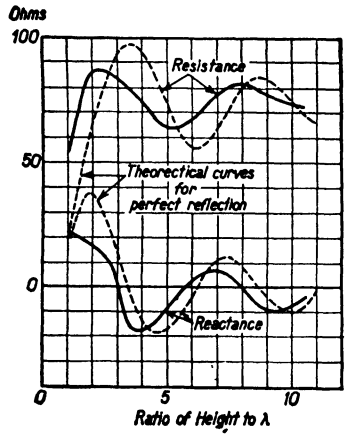

FIG. 135 Impedance of half-wave horizontal antenna at a frequency corresponding to zero reactance if at a considerable height compared with the wavelength, as dependent on the ratio height to wavelength (reference *61*).

At frequencies comparable with 300 mc/s, serious loss of gain may in some cases be caused by series resistance of contact joints, contact pins, and similar elements. Some experimental figures of present-day elements will be given here as illustrations. At 300 mc/s the series resistance of socket contact slips of good construction was found to be about 0.2 ohm; considerable variation existed, however, between individual specimens. In tubes of modern all-glass construction the series resistance of electrode leads has about the same value at 300 mc/s. With coaxial quarter-wave sections used as resonant elements the resulting Q and resonant impedance values may be considerably reduced if sliding contacts used for tuning purposes are not carefully constructed. Reductions of resonant impedance to $\frac{1}{5}$ its theoretical value have been observed at 300 mc/s due to this defect. Insulating plates between contacts—e.g., in tube sockets—should be constructed of low-loss material. With good plastic sockets conductances of 20μ mhos have been observed at 300 mc/s between adjacent pins, though values of 5μ mhos are obtainable using superior material.

REFERENCES: *13, 29, 34, 61, 78, 103, 283, 284, 315.*

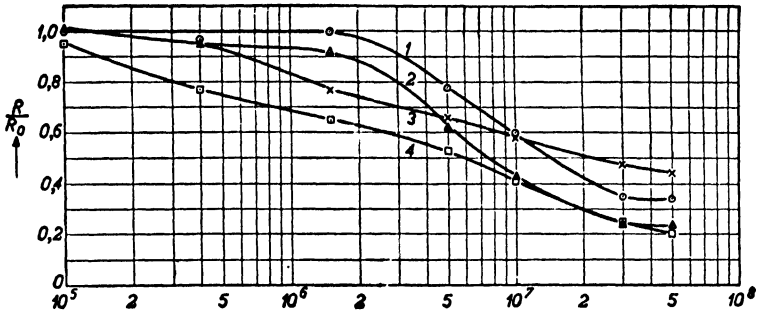

FIG. 136 Ratio of h.f. to r.f. resistance of several resistor units as dependent on the frequency c/s (horizontal scale). The curves are related to different shapes of resistors as mentioned in the text.

V.3.22. Impedances of amplifier tubes. An amplifier as well as a mixer tube may be regarded as a four-pole with two input and two output terminals, one of the former terminals being in most cases identical with one of the latter. In conventional stages this common terminal is the cathode, the other input terminal being the control-grid lead and the other output terminal the anode lead. In measuring the impedance between the input terminals, the output terminals are short-circuited as effectively as possible, and in measuring the output impedance the input terminals are short-circuited. Some resistance values obtained in this way, using conventional r.f. pentodes of octal-base design, are shown in Figures 137 and 138. Besides the values pertaining to normal operating conditions, resistances with unheated cathode and with a large negative bias voltage of the control grid are also shown, as well as the difference between two corresponding conductances. In this way the contributions resulting from electronic motion and from cathode heating may be separated. The input reactance may be ascribed to a capacitance, shunting these resistances, and this is similar at the output. The input capacitance with a large negative bias voltage is usually 1 to 1.5 pF smaller than the value corresponding to normal conditions of operation (6.5 pF), when the bias is between -2 and -3 volt. With tubes of suitable design for each frequency range, input shunt capacitance does not vary much at increasing frequency. Little variation of output capacitance is observed if the conditions of operation are altered. Some values of input and of output resistance pertaining to pentodes of all-glass construction

and of smaller size than those of Figures 137 and 138 are shown in Figures 139 and 140. The variation of input resistance upon variation of bias voltage is shown in Figure 141 for a tube of the same type as used in Figure 137, whereas Figure 142 contains similar information pertaining

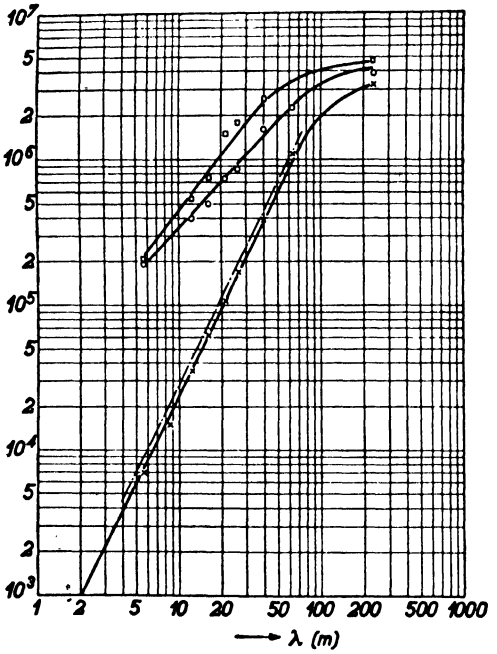

FIG. 137 Input resistance (cathode-control grid) of r.f. remote cut-off pentode expressed in ohms (vertical scale) as dependent on wavelength in m. Crosses: Tube under normal operating conditions of top transconductance. Circles: Unheated cathode. Squares: Largely negative bias. Broken curve: Resistance, which, if shunted to the biased resistance, gives the resistance under normal operation.

to output resistance. Finally input resistance of an acorn pentode under normal conditions of operation is shown in Figure 143.

From these figures the important inference may be made that input as well as output resistance is inversely proportional to the square of the operating frequency under normal conditions throughout the range considered. This rule has been confirmed up to about 700 mc/s with tubes of construction suitable to that frequency, and very probably holds up to 3000 mc/s with tubes of proper construction. Further-

more, anode resistance is shown to be inversely proportional to the transconductance from control grid to anode (Fig. 142), and so is input resistance.

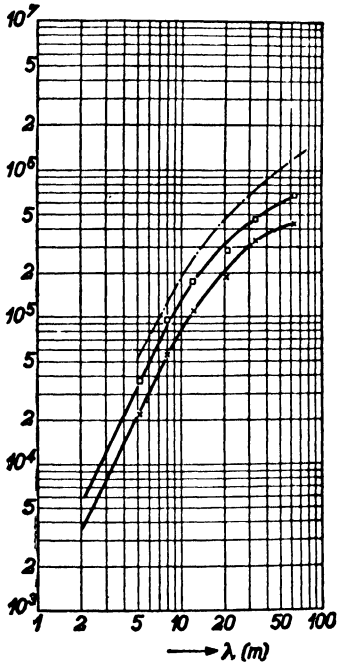

FIG. 138 Output resistance in ohms (cathode-anode) of same pentode as used in Fig. 137. Crosses: normal operation; squares: biased; broken curve: similar to broken curve of Fig. 137.

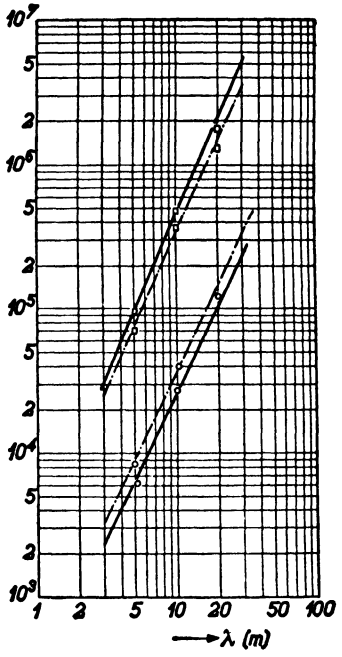

FIG. 139 Input resistance of r.f. and v.h.f. pentodes expressed in ohms (vertical scale). Circles: tube under normal operation. Squares: largely negative bias. Full curves: tube of socket type. Broken curves: tube of all-glass type. Input shunt capacitance under normal operation is about 6.3 *pF* and under biased operation about 5.3 *pF*, independent of frequency.

Besides input and output impedance, two more impedances are important in tube operation: transadmittance from grid to anode (the u.h.f. equivalent of r.f. transconductance) and the feedback impedance from anode to grid (u.h.f. equivalent of the r.f. feedback capacitance). This transadmittance was measured using low-impedance connections between input as well as between output terminals, thus offsetting

the effects of input and output impedance. Feedback impedance was measured similarly with unheated cathode. It was found that with suitable tubes the modulus of transadmittance was approximately equal to r.f. transconductance at any frequency up to 3000 mc/s. Besides this modulus, transadmittance acquires a phase lag at u.h.f.,

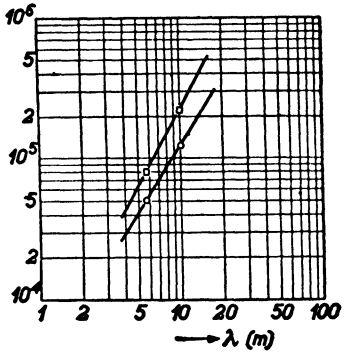

FIG. 140 Output resistance of v.h.f. all-glass pentode of Fig. 139 expressed in ohms (vertical scale). Circles: normal, and squares: biased operation.

$Y = |Y| \exp(-j\psi)$, the lag angle ψ being approximately proportional to frequency throughout this range with suitable tubes. Finally, the feedback capacitance was found to be considerably dependent on frequency at u.h.f. (see Fig. 144), the measured curve pertaining to a pentode of the type used in Figure 137. Obviously a frequency may be indicated at which feedback admittance becomes zero. It was found that this frequency may be shifted by proper stage construction to coincide with almost any desired frequency in the u.h.f. range (30–600 mc/s).

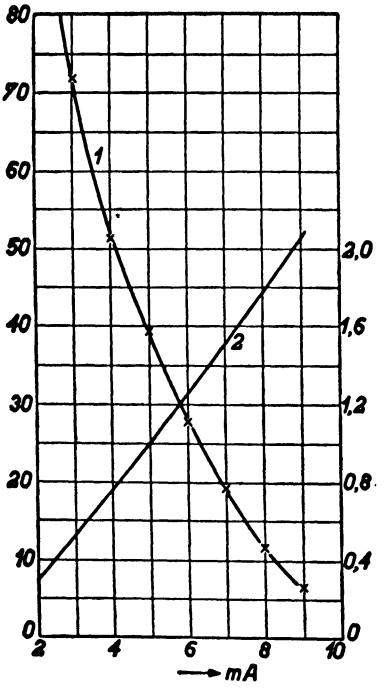

FIG. 141 Curve 1: Input resistance of r.f. socket-type pentode expressed in kiloohms (left vertical scale) as dependent on anode current (horizontal scale) at 60 mc/s. Curve 2: Transconductance (right vertical scale) expressed in m mhos.

REFERENCES: *123, 158, 163, 190, 195, 215, 216, 219, 285, 313, 345, 346, 348, 356, 362.*

V.3.23. Impedances of mixer and of diode tubes. Starting with mixer tubes of multi-grid type, we shall refer to a heptode tube as mentioned in section V.3.12. Input resistance at 50 mc/s input frequency under optimal operating conditions was found to be between 5 and 10 k ohms, input shunt capacity being about 8 *pF*. This resistance is inversely proportional to the input frequency squared between about 15 and 100 mc/s. The modulus of conversion transadmittance (corresponding to conversion transconductance at r.f.) was found to be about 0.5 m mhos,

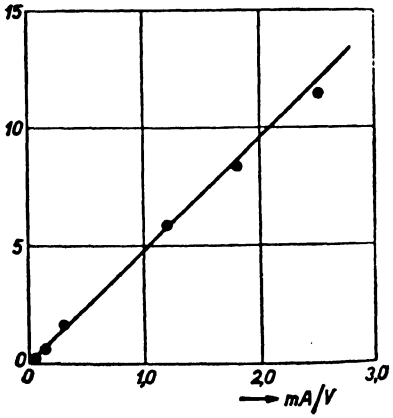

FIG. 142 Output conductance (vertical scale) expressed in μ mhos of r.f. socket type pentode as dependent on transconductance expressed in m mhos (horizontal scale) at 37.5 mc/s.

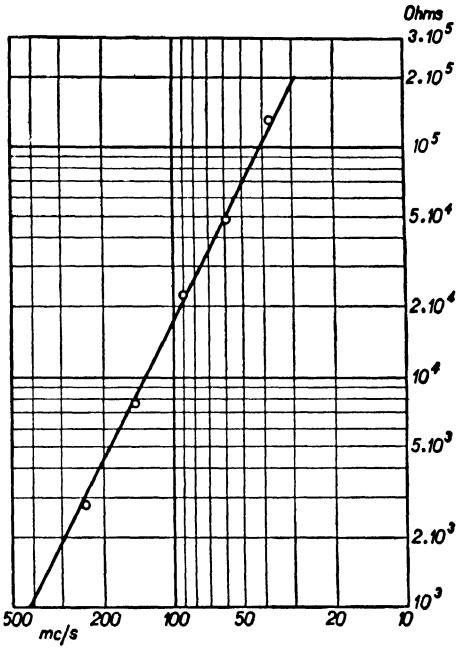

FIG. 143 Input resistance (cathode-control grid) of remote cut-off button pentode expressed in ohms (vertical scale) under normal operating conditions as dependent on frequency expressed in mc/s (horizontal scale).

which is practically the r.f. figure. The output or intermediate frequency being almost a r.f., the output impedance is approximately equal to the r.f. anode resistance and attending shunt capacity.

At higher frequencies we shall refer to similar tubes (pentodes and triodes) as those discussed in sections V.3.12 and V.3.13, using single-grid mixing. The input resistance was found to have about 2 to 4 times the value when used as an amplifier tube, conditions of operation being optimal both times. On the other hand, the modulus of con-

version transadmittance was about $\frac{1}{3}$ to $\frac{1}{4}$ of the modulus of transadmittance when used as an amplifier, conditions of operation being again both times optimal. Thus it may be stated that under these conditions the product of input resistance and modulus of transadmittance, that is, conversion transadmittance, is approximately equal in mixer and amplifier stages. This important experimental deduction is of great value in rating mixer and amplifier stages and in evaluating

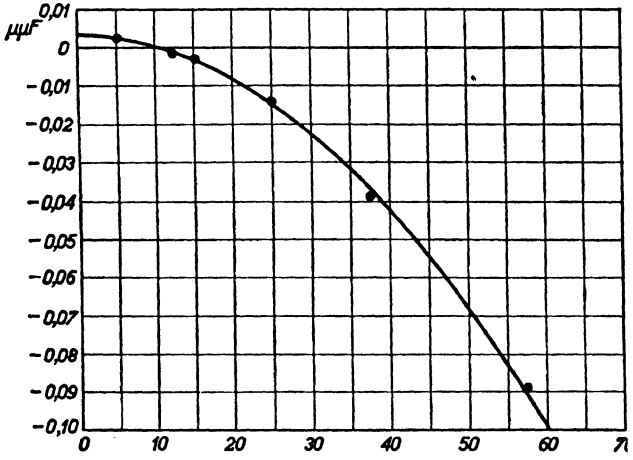

FIG. 144 Feedback capacitance (vertical scale) of r.f. socket-type pentode as dependent on frequency expressed in mc/s (horizontal scale). Operating conditions are of minor importance in this case.

their relative gain and noise figures. It may be applied to the entire range of operation up to input frequencies comparable with 3000 mc/s and probably higher, using tubes of suitable construction. With such tubes the input shunt capacitance is in most cases not dependent on frequency to any considerable extent within the range of useful operation.

We shall now consider diode tubes as used in mixer stages and in diode voltmeters. In order to show the losses due to cathode oxide-coating layers of about 30 and of 10 microns thickness, the interelectrode conductances of two diodes at 300 mc/s are given, no. 1 having a 30 and no. 2 a 10-micron layer, the other construction data being similar:

	$1/R_c$	$1/R_b$
diode no. 1	14μ mhos	45μ mhos
diode no. 2	11μ mhos	15μ mhos

The values R_c pertain to unheated cathodes and R_b to normally heated cathodes using large negative bias voltage at the anode. The interelectrode conductance is much affected by series resistance of the electrode and socket leads. All these points occur in amplifier tubes as well, but they are perhaps most easily studied with diodes. With the above diodes nos. 1 and 2 the interelectrode clearance was about 150 microns and the modulus of electronic admittance between the electrodes lower at 300 mc/s than at radio frequencies, thus causing a drop in optimal mixer-stage gain to, say, 0.3 at this frequency, and a similar drop in indication of diode voltmeters. At higher frequencies this drop becomes intolerable and different constructions with attending interelectrode clearances down to 40 and to 20 microns have to be introduced, as discussed in sections V.3.12 and V.3.13. Constructions similar to Figure 125 are suitable at the highest frequencies (e.g., 5000 mc/s).

REFERENCES: *233, 234, 239, 240, 272, 273, 277, 355, 383.*

V.3.24. Inferences from impedance figures. It seems useful to a proper understanding of u.h.f. amplifier and mixer stages to deduct the gain data of sections V.3.11 and V.3.12 from the impedance figures of the two sections preceding (V.3.22 and V.3.23). Disregarding the effect of feedback impedance (as this may in many cases be overcome by the application of suitable circuit design), and denoting the transadmittance of a tube by Y, its input resistance by R_{in}, and its output resistance by R_{out}, the optimal amplifier stage gain using that tube works out as:

$$g = \tfrac{1}{4}|Y|^2 R_{in} R_{out}. \qquad \text{(V.3.24}a\text{)}$$

This expression may be easily deduced. Assuming the input voltage to be V, the input power delivered to the stage is V^2/R_{in}, while its available output power is $\tfrac{1}{4}|Y|^2 V^2 R_{out}$ if the output shunt capacity is neutralized by the resonant circuit or cavity connected to the output. Thus the value of g is obtained upon division of the available output power by the input power. The expression (a) is valid if the over-all resonant impedance of the circuits or cavities connected to input and output are both upon transformation equal to R_{in} and R_{out} respectively. This condition may be complied with if the required band width of the stage does not exceed certain limits (into which we shall go later). From Eq. (a), as $|Y|$ is practically independent of frequency while

R_{in} and R_{out} are both found experimentally to be inversely proportional to the frequency squared within certain wide ranges, the value of g is seen to be inversely proportional to the fourth power of the frequency within the said range, in accordance with Eq. (V.3.11a). Inserting the experimental values of $|Y|$, R_{in}, and R_{out} for the particular tubes under discussion, the values of g cited in section V.3.11 are obtained.

If the band width B of the stage discussed is considerable, the resonance impedance of the input circuit or cavity being equal to $1/(2\pi BC_{in})$, and at the output being $1/(2\pi BC_{out})$, denoting the total input capacitance by C_{in} and the output capacitance by C_{out}, these values may be comparable with or even smaller than R_{in} and R_{out} respectively. Under the most favorable conditions C_{in} is approximately the input shunt capacitance and C_{out} the output shunt capacitance of the tube. As R_{out} is in general much higher than R_{in}, e.g., ten times higher, we shall obviously often be faced with the impedance $1/(2\pi BC_{out})$ becoming equal to R_{out} at increasing band width B before $1/(2\pi BC_{in})$ becomes comparable with R_{in}. The condition for the validity of Eq. (V.3.11b) is thus obviously that the product $2\pi BC_{in}R_{in}$ should be large compared with unity. The gain then becomes:

$$g = \tfrac{1}{4}\frac{|Y|^2}{(2\pi BC_{in})(2\pi BC_{out})}. \qquad \text{(V.3.24}b\text{)}$$

It should be mentioned that the coupling circuit artifice of section IV.2.13, allowing the gain to become four times the above figure, is not considered here. At band widths when Eq. (b) is valid, the significant tube properties determining stage gain are thus Y, C_{in}, and C_{out} instead of Y, R_{in}, and R_{out} if Eq. (V.3.24a) is valid. By inserting the values associated with different tubes the gain figures quoted in section V.3.11 for wide-band amplification are readily obtained, as is Figure 132 with the proper scales attached in the case under discussion.

For mixer stages, as the output frequency f_{out} is in most cases much lower than the input frequency f_{in} (this decrease of carrier frequency being the object of mixing), the output resistance will be much higher than the input resistance, even more so than with amplifier stages. At small band widths B the gain will be given by Eq. (V.3.24a), or, if the frequency dependences of R_{in} and R_{out} are taken into account, by Eq. (V.3.12b). The value of Y to be inserted into Eq. (V.3.24a) is the conversion transadmittance and, as we have seen in section V.3.23, the product $|Y|R_{in}$ is approximately equal, with single-grid mixer

tubes under conditions of optimal operation, to the value corresponding to the same tubes used as amplifiers. The resistance R_{out} being much larger in the mixer case, so will also be the gain according to Eq. (V.3.24a). At wide-band reception we obtain with mixer tubes the optimal gain equation:

$$g = \tfrac{1}{4}|Y|^2 R_{in} \frac{1}{2\pi B C_{out}}, \qquad \text{(V.3.24}c\text{)}$$

the condition being that $1/(2\pi B C_{out})$ is small compared with R_{out}. Thus we have reobtained Eq. (V.3.12a) as regards frequency dependence. By inserting the impedance values pertaining to particular tubes the figures quoted in section V.3.12 may readily be obtained.

REFERENCE: *401*.

CHAPTER VI

ENTRANCE STAGES OF RECEIVERS

The entrance stage of a receiver, if of sufficient gain, determines the receiver's noise figure almost exclusively. The chief aim in its design must be the reduction of this noise figure to as low a level as obtainable with the means in hand.

VI.1. Amplifier Stages

Using circuits of proper design, the aim announced may in many cases be most directly attained by the use of an amplifier stage, if tubes of satisfactory performance at the frequency under consideration are available.

VI.1.1. Entrance circuits. The entrance circuits under consideration are the links between the antenna or transmission-line output and the entrance terminals of the first tube.

VI.1.11. Versatile entrance circuits. At frequencies below 30 mc/s the antennas used in reception are often of similar construction to those used at r.f.; and often the same antennas are used at r.f. and at the high frequencies considered. The properties of individual antennas show marked differences, and the entrance stages of receivers should be designed to meet all occurring antenna constructions. This means that only a very loose coupling between antenna and entrance stage may be used, entailing that only a small portion of the antenna's available power is transferred to the entrance stage of the receiver. With the corresponding versatile entrance circuits several types of coupling may be applied, and we shall examine briefly the more common ones. First, we consider circuits in which satisfactory selectivity at the input terminals of the first tube is obtained by the use of a single resonant circuit (see section IV.2.11). Coupling between this resonant circuit and the antenna may be capacitive, inductive, and by transformer, the first two types each giving rise to two sub-types.

A picture containing the separate types of circuits and one combination of capacitive and transformer coupling is shown in Figure 145.

In Figure 145*a* the series connection of C_1 and of the antenna's impedance Z may be represented by an impedance $Z_1 = Z + 1/j\omega C_1$ while a current generator $VZ = I$ is substituted for the antenna's voltage generator V of Figure 145*a*. Thus we arrive at Figure 146,

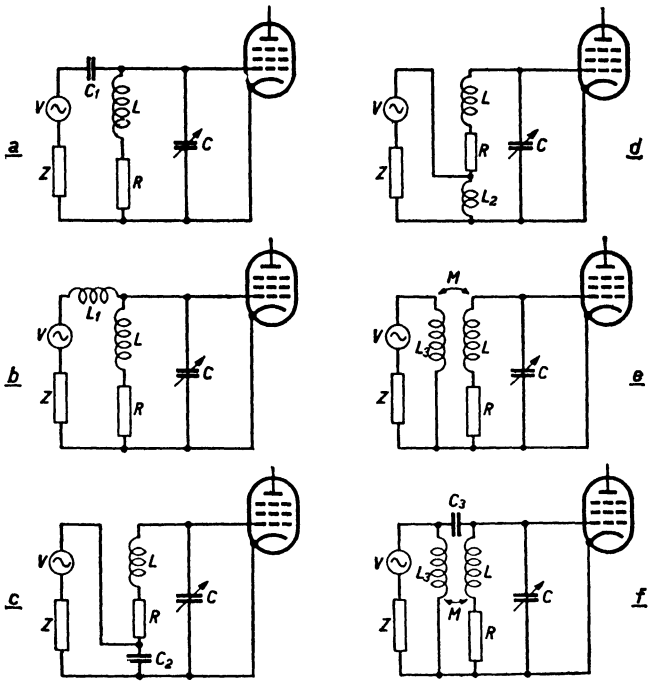

FIG. 145 Several methods of coupling the antenna to the input electrodes of the entrance tube of a receiver. Diagram *a*: Capacitive top-coupling. Diagram *b*: Inductive top-coupling. Diagram *c*: Capacitive bottom-coupling. Diagram *d*: Inductive bottom-coupling. Diagram *e*: Mutual inductance coupling. Diagram *f*: Combined coupling by mutual inductance and capacitance.

which circuit is obviously amenable to simple calculation. In order not to impair the selectivity of the resonant circuit too much, Z_1 should be large compared with the resonant impedance, and this again entails a rather small capacity C_1. If Z is also due to a capacitance C_a, the impedance Z_1 corresponds to a capacitance C_z given by $1/C_z = 1/C_1 + 1/C_a$, and C_1 should be small in order to keep C_z small compared with C. Similar simple considerations may be applied to the circuits 145*b*, *c*,

and d. The equivalent circuit of Figure 145e is shown in Figure 147, M being again the mutual inductance. This circuit of Figure 147 is suitable to simple treatment. Denoting Z by $1/j\omega C_a$ and $\omega_3^2 L_3 C_a = 1$, we obtain:

$$\frac{V_g}{V} = -j \frac{M}{L_3} \frac{\omega^2}{\omega^2 - \omega_3^2} Q, \qquad \text{(VI.1.11}a\text{)}$$

Q being the quality of the resonant circuit and V_g the voltage between cathode and control grid. If $\omega_3 \ll \omega$, Eq. (a) yields a ratio V_g/V independent of the angular frequency ω.

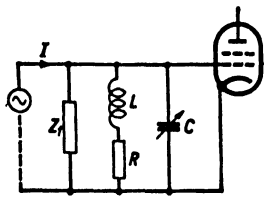

FIG. 146 Equivalent diagram to Fig. 145a, the voltage generator of the latter being replaced by a shunted current generator of infinite internal impedance (indicated by broken line) supplying the signal current I.

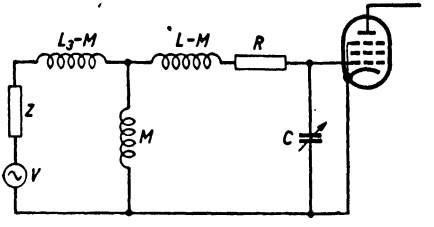

FIG. 147 Equivalent circuit diagram to Fig. 145e.

In some cases the selectivity attainable by the use of a single resonant circuit is not satisfactory and two coupled circuits as discussed in section IV.2.12 have to be applied. An example is shown in Figure 148, which may again be made suitable to simple treatment if the voltage generator is replaced by a current generator, then applying the results of sections IV.2.12 and 13. In the case of equal resonant circuits of quality Q, applying critical coupling, we obtain:

$$\frac{V_g}{V} = \frac{1}{2} \frac{C_z}{C_1 + C_z} Q,$$

C_z having the meaning indicated above. If compared with a single resonant circuit, this ratio V_g/V is only half of the value corresponding to Figure 145a, C_z, C, and Q being equal. In the case of non-critical coupling this ratio is even less.

From the above reasoning the frequency-response or selectivity curves near reasonance, as well as far off-resonance, may be obtained. In Figures 145*a* and 146 the ratio V_g/V approaches a value independent of frequency if $Z = 1/j\omega C_a$ and if the frequency is increased indefinitely. On the other hand, this ratio approaches zero if ω does so under the above assumption regarding Z. Thus we obtain roughly the upper curve *a* of Figure 149. Similarly we obtain the curve *b* of this figure in Figure 145*c*. In Figure 145*e* a curve similar to *c* of Figure 149 may result, if $\omega_3^2 = 1/L_3C_a$ is smaller than the angular resonance frequency squared. Thus selectivity near resonance is not impaired in the cases of Figures 149*a* and *b*, whereas it may be in the case of 149*c*. Far-off selectivity is of course much better with curve *c* than with curves *a* and *b*. If a set of two coupled resonant circuits, as in Figure 148, is used, near and far selectivity may in general be satisfactory.

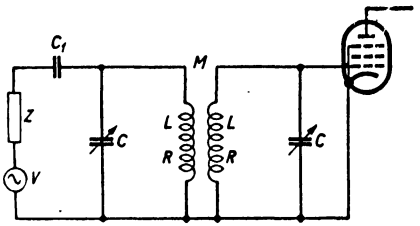

FIG. 148 Two resonant circuits coupled by means of an inductance M may be used between the antenna (represented by the voltage generator V and the impedance Z) and the input electrode of the receiver's entrance tube.

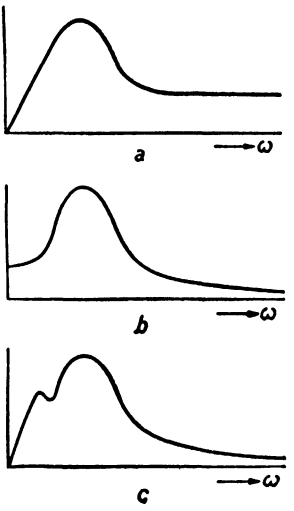

FIG. 149 Vertical scales: Ratio of tube input voltage to antenna voltage V (see Figs. 145, 147, and 148). Horizontal scales: Angular frequency. The upper curve *a* pertains to the circuit 145*a*, curve *b* pertains to Fig. 145*c* and curve *c* to Fig. 145*e*.

The lumped circuits discussed may be replaced by equivalent resonant line-sections or cavities.

VI.1.12. Fixed-antenna entrance circuits. With individual and commercial receivers specially designed for reception of the high frequencies under discussion, the reception antenna may be assumed to present a fixed and purely real impedance at the entrance terminals

of the receiver. This resistance R_a will, in many cases, be equal to the wave impedance of the transmission line interconnecting antenna and receiver. By application of a suitable transformer—e.g., a quarter-wave line section or a tap in conjunction with a resonant cavity (see section IV.2.23)—this resistance may be transformed to almost any suitable value. We shall denote the transformation ratio as viewed from the line output by w, thus obtaining a transformed resistance of w^2R_a. Besides this, we have two other impedances at the entrance terminals (grid-cathode) of the first tube: the resonant circuit's or cavity's impedance and the input-tube impedance, both being shunted to the above w^2R_a value. The input impedance of the tube may be assumed real (R_{in}), as its shunt capacity may be incorporated in the resonant circuit or cavity. We shall consider only frequencies f in the vicinity of the resonant frequency f_o, and at such frequencies the circuit's or cavity's impedance may be represented by a shunt connection of the resonant resistance R_{res} and of a capacity C such that the corresponding shunt susceptance at the frequency f is $4\pi(f - f_o)C$, the value of C being the total shunt capacity (tube input circuit) at the tube's entrance. Note the multiplier 4π instead of the usual 2π; this doubled value is due to the respresentation of our h.f. impedance by a shunt connection of R_{res} and C. We have now completely defined the impedance elements indicated between the terminals 1, 2 and 3, 4 in Figure 46:

$$Z_o = w^2R_a, \quad \frac{1}{Z_1} = \frac{1}{R_{res}} + j4\pi(f - f_o)C, \quad Z_{i1} = R_{in}.$$

If optimal gain between the terminals 1, 2 and 5, 6 of Figure 46 is to be attained, the total available power at 1, 2 should be transferred to the tube's input resistance $Z_{i1} = R_{in}$, implying that Z_1 should be real and R_{res} large compared with R_{in}, while $w^2R_a = R_{in}$. Picturing the tube of Figure 46 separately (see Figure 150), the real part R_{out} of its shunt output impedance is known experimentally (section V.3.22) to be much larger than R_{in}. Furthermore, we shall assume that proper precautions eliminating or minimizing feedback have been taken such that Z_{i2} may be disregarded in comparison with either R_{out} or R_{in}, being much larger in shunt connections. The problem is then much simplified and approximately optimum tube gain (section V.3.24):

$$g_{out} = \tfrac{1}{4}|Y|^2R_{in}R_{out}$$

may be secured between the terminal pairs 1, 2 and 5, 6.

The question now arises as to whether these optimal gain conditions do also correspond to minimum noise figure and if not, what other conditions do. In order to answer this question we shall evaluate the noise figure corresponding to the circuit of Figures 46 and 150. The noise-current generators supplying i_2 and i_3 of Figure 39, active between the grid g and the anode, may approximately be assumed active between the terminals 5 and 6 of Figure 150 as $R_{out} \gg R_{in}$ and as Z_{i2} may be disregarded. Both noise currents and also i_1 of Figure 39 are completely intercorrelated in an ideal triode, and this will be assumed here. The noise current flowing to the grid is $i_g = i_2 - i_1$, as indicated in Figures 39 and 150. After what was said in section II.2.32 and preceding sections, we may easily evaluate the resulting short-circuit noise and signal current between 5 and 6 of Figure 150. The resulting noise figure at these terminals is:

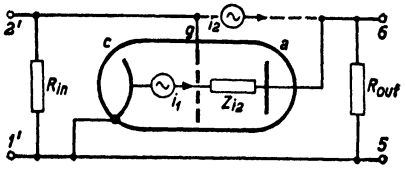

FIG. 150 Separate and more elaborate picture and equivalent circuit of the tube in Fig. 46. Notation: R_{in}, input resistance; i_1, noise-current generator active between cathode c and grid g; i_2, noise-current generator active between grid g and anode a; Z_{i2}, interelectrode impedance active between grid and anode; R_{out} output resistance.

$$N = \frac{T_a}{T} + \frac{T_{in}}{T} W,$$

$$W = \frac{w^2 R_a}{R_{in}} \left| 1 - \frac{\exp(j\phi)}{j} \right| \frac{i_2}{i_g Y R_{in}} \left| \left(\frac{R_{in}}{w^2 R_a} + 1 + j\omega C R_{in} \right) \right|^2 . \qquad \text{(VI.1.12a)}$$

Here T_{in} denotes the effective fluctuating temperature of R_{in}, according to $R_{in}\, \overline{i_g^2} = 4KT_{in}\Delta f$, i_2 the current of the noise generator active in shunt with R_{out} (see Fig. 39), $\omega = 4\pi(f - f_o)$, while ϕ is a phase angle dependent on the phase lags of the fluctuation currents i_1 and i_2 of Figure 39 and of the transadmittance Y:

$$\begin{aligned} Y &= |Y| \exp(-j\phi_a), \\ i_2 &= |i_2| \exp(-j\phi_2), \\ i_g &= j|i_g| \exp(-j\phi_g) = i_2 - i_1, \\ \phi &= \phi_a + \phi_g - \phi_2. \end{aligned} \qquad \text{(VI.1.12b)}$$

Obviously this noise figure N is dependent on the two variables:

$$\frac{R_{in}}{w^2 R_a} = x \quad \text{and} \quad \omega C R_{in} = y \tag{VI.1.12c}$$

and further dependent on the ratio:

$$\overline{\left|\frac{i_2}{i_g Y R_{in}}\right|^2} = a_o^2, \tag{VI.1.12d}$$

which is a quantity fixed by the data of the tube under discussion. In the case of optimal gain the conditions to be imposed on the quantities x and y of Eq. (c) are: $x = 1$ and $y = 0$, i.e., a matched purely resistive entrance circuit.

REFERENCES: *365, 367, 370, 371, 372.*

VI.1.2. Noise figure and gain. These will now be examined for fixed antenna entrance circuits.

VI.1.21. Conditions for a minimum noise figure. If we want a minimum noise figure, conditions differ from those corresponding to optimal gain. It is a simple matter to evaluate x and y of Eqs. (VI.1.12c) such that the noise figure of Eq. (VI.1.12a) or, which is equivalent, the quantity W of that equation, attain a minimum value. We shall only state the result here. The detuning of the input circuit should be such that:

$$a_o y = \cos \phi = a_o \omega C R_{in}, \tag{VI.1.21a}$$

by which the difference $f - f_o$ between the frequency f of operation and the resonant frequency f_o is completely fixed. If $\cos \phi$ is positive, the difference $f - f_o$ is also positive—i.e., the frequency of operation should be *higher* than the circuit's or cavity's resonant frequency f_o. If $\cos \phi$ is negative this is reversed. The second minimum condition fixes x:

$$a_o^2 x^2 = (a_o - \sin \phi)^2. \tag{VI.1.21b}$$

This condition thus requires a definite value of the entrance transformation ratio, and the resulting ratio x (Eq. VI.1.12c) is in general (if ϕ is not zero or a multiple of π) different from unity, which corresponds to optimal gain. The values of W in the noise Eq. (VI.1.12a) corresponding to these minimum noise conditions are shown in Figure

151 as dependent on a_o (see Eq. VI.1.12d) and on ϕ, positive as well as negative values of this phase angle being taken into account. If $\phi = \pi/2$ we would obtain zero for the minimum value of W.

Hitherto the correlation between i_1 and i_2 was assumed to be complete. If a non-ideal triode is used, or a tetrode instead of a triode, no complete correlation will exist between the fluctuations at the entrance

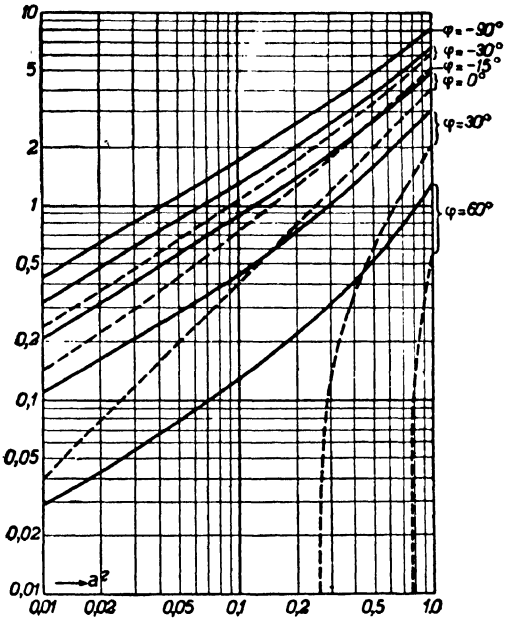

FIG. 151 Vertical scale: Value of W in the noise eq (VI.1.12a) corresponding to conditions of minimum noise ratio. Horizontal scale: a_o of eq. (VI.1.12d). Curves corresponding to different positive and negative values of phase angle ϕ according to eq. (VI.1.12b) (see references 371, 372).

(represented by i_1) and at the output (approximately represented by i_2). It is obvious that in such cases values of W larger than those of Figure 151 will result. The noise figure of a particular pentode tube was measured in an amplifier stage at $f = 300$ mc/s. The measured figures (the temperature T_a of the signal generator's output being T) are shown in Figure 152. It is apparent that a reduction of noise figure from 21 to 17 is obtained by detuning. At the detuned position the input transformation ratio (coupling) adjusted to a minimum noise

figure at the tuned position, should have been slightly altered to obtain a minimum noise figure again, but this was omitted. With the tube in question about 40% of the mean square output fluctuations were completely correlated to its input fluctuations. Thus we could hardly expect a larger reduction of noise figure by detuning than the 20% obtained, and Figure 152 may be said to offer satisfactory confirmation of our theoretical deductions. With triodes far greater reductions of noise figures are obtainable. We may conclude from Figure 152 that the phase angle of Figure 151 is positive in the present case, for otherwise the value of W could hardly be reduced at all by detuning, as the dotted curves for negative ϕ values in Figure 151 practically coincide with the full curves corresponding to a tuned circuit.

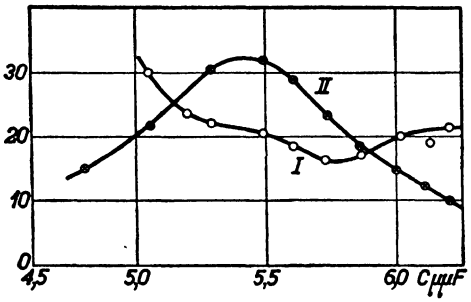

FIG. 152 Vertical scale: Noise figure of an entrance amplifier stage using a single resonant circuit and a pentode. Horizontal scale: Tuning capacitance. Curve I is related to the noise figure; curve II represents the ratio of output to input voltage squared of the stage on a linear relative scale and shows the tuning position (reference *197*).

As to the noise Eq. (VI.1.12*a*), all that is desired would be a reduction of W such that the second term in the sum expression of N—i.e., its part originating in the tube—is small compared with its first term, originating in the antenna. With tubes of suitable construction a_o^2 may be 0.5 at 300 mc/s. Thus in this case W cannot attain values below 0.2 by Figure 151 if ϕ is zero or negative, but W could easily be smaller if ϕ were 60 degrees positive. In most cases the ratio T_{in}/T is between 5 and 7 for oxide-coated cathodes, and we may judge from T_a/T and from W whether the above desirable condition is obtainable in any particular case as soon as a_o is known from experiments.

REFERENCES: *22, 197, 302, 370, 371; 372.*

VI.1.22. Grounded grid amplifier stages. At frequencies above 100 mc/s the output terminals of a tube amplifier are in some cases connected to control grid and anode instead of to cathode and anode, thus regarding the control grid as the common electrode to input and

output. Considering the optimum gain obtainable using a suitable tube in this way, disregarding feedback, we shall refer to r.f. values first. In a triode of rather high amplification factor μ_a—i.e., ratio of effective alternating voltages at the anode and at the grid causing equal electronic currents to be drawn from the cathode—this optimal gain figure is approximately $\mu_a/4$, if $\mu_a > 10$, whereas it is much higher with the cathode-base circuit as commonly used. At u.h.f., however, gain with the cathode-base circuit decreases very rapidly at increasing frequencies, whereas the decrease with the grid-base circuit is much slower, such that from a certain frequency onward its gain is larger than with the former circuit. The exact frequency where this happens depends on the tube in question. With the tubes suitable at frequencies between 30 and 600 mc/s this reversal often occurs between 500 and 2000 mc/s. Relatively similar relationships are found with tubes suitable at higher frequencies. From the preceding data the desirability of a high amplification factor μ_a with tubes to be used in a grid-base circuit may be inferred.

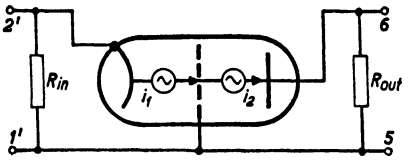

FIG. 153 Equivalent to Fig. 150 in the case of a grounded-grid amplifier stage.

In calculating the noise figure connected with a grid-base amplifier reference may again be made to Figures 46 and 150 only now interchanging cathode and control grid. Thus Figure 153 ensues, the values of R_{in} and R_{out} being, however, different from those in Figure 150 although the R_{out} values will in many cases not differ very much. With the noise currents in the tube the situation is a little different from Figure 150 as will be seen with reference to Figure 39. Instead of a noise current $i_g = i_2 - i_1$ active at the input of Figure 150 we have a noise current i_1 active in the case of Figure 153, while the noise current i_2 is active at the output of Figure 153 as it was approximately with Figure 150. The Eqs. (VI.1.12a) may easily be transcribed for the present case:

$$N = \frac{T_a}{T} + \frac{T_{in}}{T} W_o \qquad \text{(VI.1.22}a\text{)}$$

$$W_o = W \text{ (replacing } i_g \text{ by } i_1).$$

An equivalent reasoning to that of section VI.1.21 may be used in the

present case to obtain a minimum value of W_o and of the corresponding noise figure. We have only to replace ϕ by

$$\psi = \phi_a + \phi_1 - \phi_2 + \frac{\pi}{2}$$

$$i_1 = |i_1| \exp(-j\phi_1) \qquad \text{(VI.1.22}b\text{)}$$

and a_o by a quantity b_o:

$$b_o^2 = \left|\frac{i_2}{i_1 Y R_{in}}\right|^2, \qquad \text{(VI.1.22}c\text{)}$$

R_{in} having the value corresponding to the present case. Even Figure 151 may be used in the present case introducing the above changes. By Eq. (b) the angle ψ will in most cases be positive and near $\pi/2$ at not too high frequencies when the angles ϕ_a, ϕ_1, and ϕ_2, being approximately proportional to the operating frequency, are still small. Under similar conditions the angle ϕ of Eq. (VI.1.12b) would be very small. As was stated in connection with Figure 151, a phase angle ψ near $\pi/2$ would correspond to a complete elimination of W_o, this quantity then approaching to zero. Referring to Figure 154, the fluctuation currents i_1, i_2, and i_g are represented by vectors, being approximately singly periodic a.c.'s within a narrow frequency interval Δf compared with the operating frequency f. The phase angle φ_{12} of Figure 154 is proportional to f. Thus i_1 and i_2 are of nearly equal direction and magnitude and i_g is small compared with either of them at not too high frequencies f. This entails that the optimal W_o is much smaller in the case of a grid-base amplifier than with a cathode-base amplifier, according to Figure 151. Thus we would expect an almost zero contribution of tube noise to the over-all noise figure in this case. This has been confirmed experimentally with a triode of conventional design and at a frequency of about 100 mc/s. The grid-base circuit, using suitable tubes at the frequencies under consideration, is thus seen to be useful from a noise point of view as it is with respect to gain.

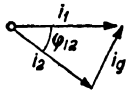

FIG. 154 Phase angle φ_{12} between the fluctuation currents i_1 and i_2 of Figs. 150 and 153. The difference of i_1 and i_2 is i_g and flows to the grid.

REFERENCES: *22, 90, 197, 198, 302, 372, 401.*

VI.1.23. Wide-band amplification. Referring to the discussion of section V.3.24, wide-band amplification is assumed to imply that stage gain is independent of frequency within the range considered. The reception antenna is in most cases linked to the receiver by a transmission line. If a tuned half-wave antenna and a coaxial line are used, both may be nearly matched at the antenna end as the antenna's radiation resistance is approximately equal to the line's wave inpedance, assuming the line to be of optimal design (see section IV.1.23). In the vicinity of the tuning position the antenna's impedance will be:

$$Z = R_r(1 + j\zeta Q), \qquad \text{(VI.1.23}a\text{)}$$

R_r being the radiation resistance, Q the antenna's quality figure, and ζ having the sense of Eq. (IV.2.11b). Inserting this impedance value into Eq. (IV.1.22b) and assuming R_r to be equal to the line's real wave impedance Z_o, we obtain an output impedance

$$Z_{out} = Z_o\left(1 + j\zeta Q\,\frac{\operatorname{cotan}\beta l - 1}{\operatorname{cotan}\beta l + 1}\right), \qquad \text{(VI.1.23}b\text{)}$$

if the product ζQ is small compared with unity. The line losses have been neglected. Eq. (b) shows that the phase angle of the output impedance Z_{out} of the transmission line may be either larger or smaller than the angle at the antenna. A small phase angle results, if βl is an odd integer multiplied by $\pi/4$, as the numerator of the fraction within parentheses then vanishes. In many cases the phase angle at the line's output will be larger than at the antenna, calling for a particularly low value of Q corresponding to the latter in order to insure proper wide-band response. Antenna designs complying with this requirement have been considered in section III.3.12.

We shall assume that a total band width B, corresponding to a 3 db drop of gain on either side of resonance, is required at the input of the first amplifier tube. If the over-all shunt capacitance at these terminals is C, this band width results in a resonant impedance at the input of $1/(2\pi BC)$. The input circuit may be represented by Figure 46, Z_o being the transformed output impedance of the transmission line, Z_1 the resonant impedance of the input resonant device (circuit or cavity) and Z_{i1} the tube's input resistance. By the wide-band definition mentioned at the start of this section VI.1.23, the value of $Z_{i1} = R_{in}$ is large compared with the present over-all resonant impedance $1/(2\pi BC)$,

which is thus approximately constituted by the shunt connection of $Z_o = w^2 R_a$ and $Z_1 = R_1$:

$$2\pi BC = \frac{1}{w^2 R_a} + \frac{1}{R_1}. \qquad \text{(VI.1.23}c\text{)}$$

Optimal gain from the antenna up to the entrance terminals of the first tube is obtained if no extra loss of power is incurred in the resistance R_1, thus requiring this to be large compared with the over-all resonant impedance. Thus coupling for optimum gain yields a transformation ratio w given by:

$$w^2 = \frac{1}{R_a 2\pi BC}. \qquad \text{(VI.1.23}d\text{)}$$

If the frequency band of which amplification is desired is made equal to B, its ends will incur a drop of gain of 3 db. To avoid this, the band B might be made larger than the said frequency band.

In evaluating the input noise figure, use may again be made of Eq. (VI.1.12a), introducing appropriate conditions. As R_{in} is large compared with $w^2 R_a$ according to our present assumptions, the expression for W is simplified to:

$$W \approx \left|\frac{i_2}{i_g Y R_{in}}\right|^2 \frac{R_{in}}{w^2 R_a}. \qquad \text{(VI.1.23}e\text{)}$$

By the introduction of:

$$\overline{i_g^2} = \frac{4KT_{in}\Delta f}{R_{in}}, \qquad \overline{i_2^2} = 4KT|Y|^2 R_f \Delta f, \qquad \text{(VI.1.23}f\text{)}$$

R_f being often indicated as "noise resistance" of the tube in question, we obtain from Eqs. (e) and (VI.1.12a):

$$N = \frac{T_a}{T} + \frac{R_f}{w^2 R_a} = \frac{T_a}{T} + R_f 2\pi BC. \qquad \text{(VI.1.23}g\text{)}$$

The first term represents the antenna's noise contribution and the second term the tube's noise contribution. The latter's relative significance may easily be estimated from Eq. (g). With modern wide-band tubes, R_f is often about 1000 ohms while C may be about 15 pF. At a band width B of 4 mc/s we obtain for the second term of the noise figure the value 0.4. This is always nearly negligible in comparison

with the first term, which often exceeds unity at carrier frequencies of some 40 mc/s. Band widths of about 50 mc/s at a carrier frequency of, say, 100 mc/s would be required to make the second term's contribution to the over-all noise figure appreciable.

In order to connect the noise figure in the present case still further with tube properties, the fluctuation resistance R_f may be written in the form:

$$R_f = \frac{T_f}{T\,|Y|}, \qquad \text{(VI.1.23}h\text{)}$$

$|Y|$ being the modulus of tube transadmittance as before and T_f a temperature which is in many cases between 4 and 10 times the room temperature T. Thus the tube's contribution to the input noise figure becomes:

$$\frac{T_f}{T}\,\frac{2\pi BC}{|Y|},$$

favoring tubes with a low ratio $C/|Y|$ of input shunt capacitance to modulus of transadmittance.

REFERENCES: *197, 302, 365.*

VI.1.3. Means of obtaining improved tube performance. As we have seen from experimental figures in section V.3.2, tube performance as regards gain is in many cases below what would be desirable. Means of improving tube performance will be discussed in section VI.1.3.

VI.1.31. Gain-improving circuits. From the data of section V.3.2 the main cause of the reduction of gain with relatively narrow-band amplifier and mixer stages is seen to be the decrease of input resistance and output resistance if the operating frequency is increased. Thus the circuits to be discussed in the present section aim at an increase of these resistances. One of the simplest of them makes use of an unbypassed resistance in the cathode lead of a tube with indirectly heated cathode (see Fig. 155). The capacitance C_f between the cathode sleeve and the heater circuit is shunted across the unbypassed resistance R_3 of this figure, thus still leaving us with a slight bypass capacitance. By R_3 the effective transadmittance Y of the tube is reduced in modulus to Y_1, approximately according to:

$$|Y_1| = \frac{|Y|}{|1 + YR_3|}. \qquad \text{(VI.1.31}a\text{)}$$

At the same time the input resistance of the tube is considerably increased, as shown by the experimental data of Figure 156. At 60 mc/s the input resistance is increased from 10 to about 30 k ohms, while the reduction of transadmittance according to Eq. (*a*) amounts to about 20% of its original value. The output resistance is also increased by the unbypassed cathode lead resistance but relatively much less. Thus, at 60 mc/s corresponding to curve 1 of Figure 156 the

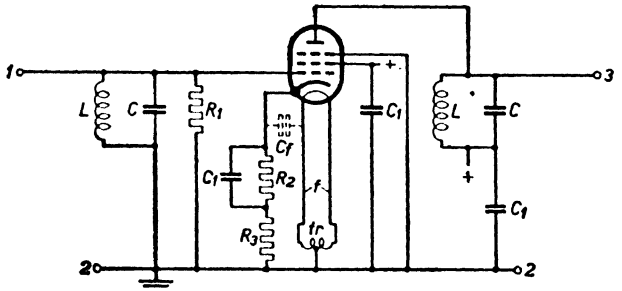

FIG. 155 Circuit serving to increase the input resistance of a pentode amplifier stage at v.h.f. Notation: 1,2 entrance and 2,3 output terminals of the stage; L,C, input resonant circuit; R_1, leakage resistance of some hundreds of kiloohms; C_1, blocking condensers (some 10,000 pF); R_2, bias resistance bypassed by C_1; f, heater wires; tr, heater transformer; C_f, capacitance between heater and cathodes leeve; R_3, unbypassed resistance causing an increase of stage input resistance (between 10 and 100 ohms for most pentodes).

optimal stage gain is multiplied by about 2 by the insertion of R_3 in Figure 155, and similar figures may be obtained at different frequencies. This circuit is useful up to about 150 mc/s.

Another simple means of obtaining an increased gain is based upon the knowledge that the input resistance of tubes at u.h.f. is to a considerable extent due to the inductance of the cathode lead. This inductance serves as a passage for the output a.c. and the voltage set up by this current causes a degenerative feedback from output to input, resulting in a decreased input resistance. If a low-loss capacitance is connected in series with the cathode lead, the ensuing antiresonant circuit being tuned at the frequency of operation, the effect of this inductance is neutralized and thus the input resistance is increased. This circuit is active only in the vicinity of the antiresonant frequency, whereas the preceding one is effective over a wider range, as shown by

Figure 156. Still, with amplifiers used at fixed operating frequencies a useful increase of gain—e.g., by 3 to 5 db—may be achieved. The inductance being, in many cases, of the order of magnitude of 10^{-8} henry, the required capacitance at 40 mc/s is about 1550 *pF*. If the

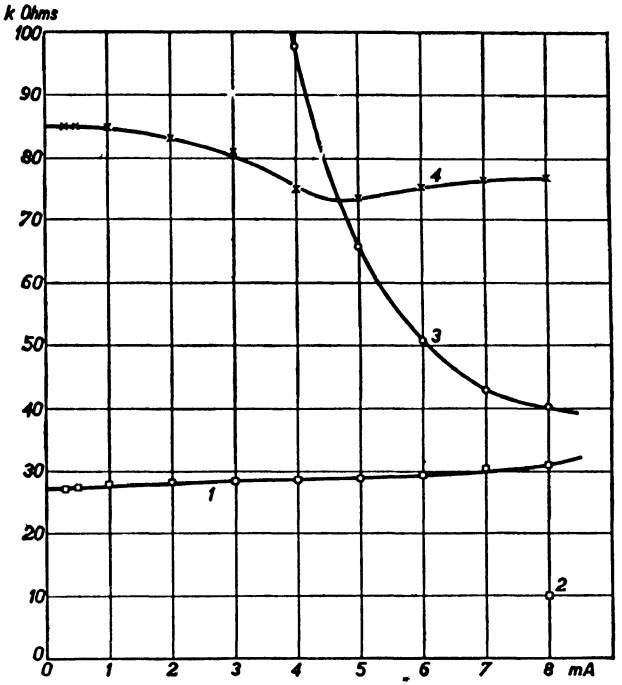

FIG. 156 Input resistance expressed in kiloohms (vertical scale) of a v.h.f. remote cut-off pentode applying an unbypassed resistance R_3 according to Fig. 155 of 125 ohms at 60 mc/s (curve 1) as dependent on anode d.c. (horizontal scale) controlled by grid bias. Curves 3 and 4 pertain to 30 mc/s, curve 3 corresponding to $R_3 = 0$, and curve 4 to $R_3 = 125$ ohms. Point 2: at 60 mc/s and $R_3 = 0$.

capacitance is smaller than the antiresonant value, a further reduction of input resistance by the ensuing regenerative feedback results.

Very effective increases of gain at frequencies up to about 300 mc/s may be obtained by the use of a double cathode lead, one connected to the input and one to the output circuit (see Fig. 157). Obviously the degenerative feedback by the cathode-lead inductance causing a reduction of input resistance is effectively reduced if a proper tube construction is applied. Furthermore, by the use of a capacitance

indicated by C_1 in Figure 157 a regenerative feedback may be introduced, resulting in an increase of input resistance. A similar capacitance, indicated by C_2 in Figure 157, may cause a regenerative feedback resulting in an increased output resistance. Thus we may obtain an

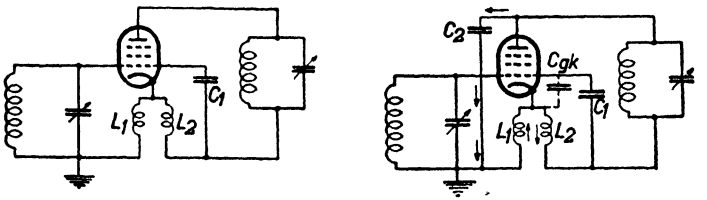

FIG. 157 Diagram to the left: Double cathode lead of a v.h.f. pentode, the inductances being L_1 and L_2 and a capacitance C_1 being added from the lower end of L_2 to the control grid. Diagram to the right: Addition of a further capacitance C_2 between the anode and the lower end of L_1.

appreciable increase of gain (e.g., 5 to 8 db) by the application of a double cathode lead (reference *364*).

As the causes of a reduction in input as well as output resistance of amplifier stages up to about 600 mc/s are to a considerable extent connected with inductances of the electrode leads, an increase of these

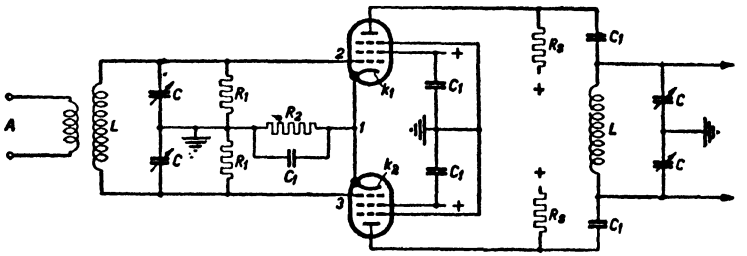

FIG. 158 Push-pull amplifier stage utilizing two pentodes. Notation: L,C,C, input and output resonant circuits; C_1, blocking condensers; R_1, leakage resistors; R_2, bias resistance; K_1 and K_2, cathodes; R_s, series resistors of anode voltage supply; A, antenna coupling.

resistances may be expected from the application of proper push-pull circuits in which no a.c. flows through the leads in question. Considering Figure 158, the a.c. in the lead connecting the input resonant circuit (LC) with the point 1 is zero in the ideal case of exactly equal halves of the entire push-pull stage, as the two a.c.'s corresponding to each

part cancel each other in this lead. The two leads connecting the point 1 with the cathodes of the tubes retain their degenerative effects resulting in reduced input resistance. It is thus recommendable to shorten these leads as much as possible. This may be achieved by the construction of two electrode systems within one tube bulb, connecting their individual cathodes by a relatively broad strip. Considerable success has been attained by the application of such constructions and optimal gain figures up to 100 have been obtained in push-pull stages

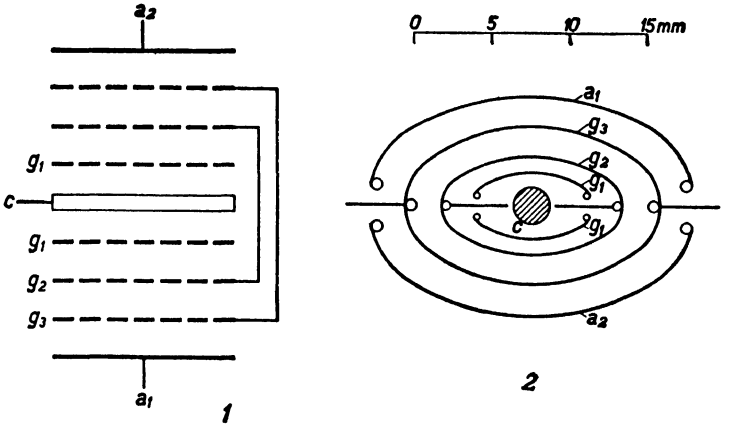

FIG. 159 Internal construction of push-pull pentode. Picture 1: connections. Picture 2: cross-section perpendicular to cathode axis. Notation: c, cathode; g_1, control grids; g_2, screens; g_3, suppressor grids; a_1 and a_2, anodes.

using such double-system tubes of suitable electrode dimensions and spacings (down to 70 microns) at about 300 mc/s. If a single cathode is used, both electrode systems acting upon different faces of it, the reduction of degenerative lengths of cathode lead has been carried to its limit (see Fig. 159). Unfortunately, tube manufacturers have in some cases hesitated to apply this construction for fear of unequal electrode clearances ensuing on either side of the cathode as a result of the manufacturing process.

REFERENCES: *158, 346, 352, 353, 354, 363, 364.*

VI.1.32. Noise-reducing circuits. Besides the circuits discussed in section VI.1.2, aiming at a reduction of noise figure by proper entrance coupling and (if required) circuit detuning, further means of reducing

the noise figure may often be successfully applied. A useful circuit of this type aims at reduction of the noise resulting from current partition in tetrodes and pentodes. This circuit constitutes an application of the principles discussed in property *D* of section II.2.22 and at the end of section II.2.32 (Fig. 47) and is shown in Figure 160. A resistance *R* is connected to grid and cathode, representing the resonant impedance of a resonant circuit incorporating the total shunt capacitance between the electrodes, including *C* of Figure 160. This capacitance *C*, together with the inductance *L*, constitutes the feedback circuit connecting the subsidiary pair of output terminals (nos. 5 and 6 of Fig. 47) with the input terminals 1, 2. We may consider this *LC* combination as a four-pole containing only passive reactances and thus having a gain equal to unity and a noise figure also equal to unity (see sections II.2.21 and 22). An approximate evaluation of the effect of this circuit, valid if $\omega^2 LC \ll 1$, ω being the angular frequency of operation, will now be given, disregarding all noise currents not completely correlated with the partition fluctuations in question. The partition fluctuation current generator active between screen grid and anode causes a partition current i_p through *L* and a completely correlated fluctuation voltage v_p results between cathode and control grid. By the transadmittance Y_2 (assumed to be real) active between control grid and screen grid, the total partition fluctuation current through *L* is $i_p + Y_2 v_p$ and hence a corresponding voltage $(i_p + Y_2 v_p) j\omega L$ ensues across *L*, resulting in a voltage $(i_p + Y_2 v_p)\omega^2 LCR$ across *R*, this voltage being by our assumption equal to v_p. Thus:

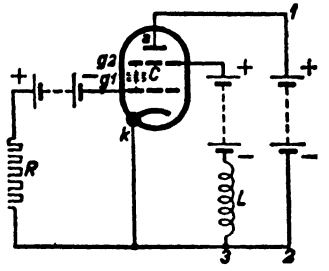

FIG. 160 Circuit for the suppression of partition fluctuations at the output of a tetrode. Notation in text.

$$v_p = \frac{i_p}{Y_2}\frac{R_i}{R_2}, \quad \frac{1}{R_2} = Y_2\omega^2 LC, \quad \frac{1}{R_i} = \frac{1}{R} - \frac{1}{R_2}.$$

The value R_i represents the resulting input resistance of the stage with noise-reducing circuit. Hence the effect of the latter circuit is regenerative, corresponding to a negative shunt resistance component $-R_2$ at the input. If *Y* represents the transadmittance from control grid to anode the resulting partition fluctuation current circulating between

screen grid and anode is:

$$i = i_p\left(1 - \frac{Y}{Y_2}\frac{R_i}{R_2}\right). \qquad \text{(VI.1.32}a\text{)}$$

Thus it may be annihilated by a proper choice of R_2, i.e., of L and C. This evaluation takes no account of phase angles of Y_2 and Y but by the theorem D of section II.2.22 we may conclude that the essential result is not affected by such angles.

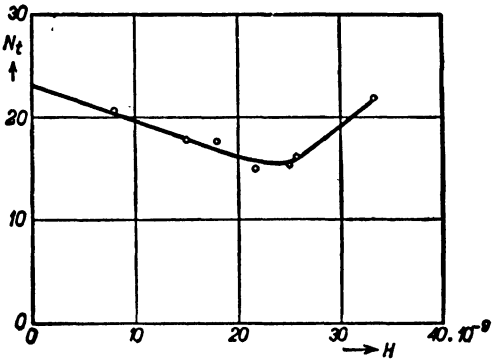

FIG. 161 Noise figure (vertical scale) of an amplifier stage using a pentode and adding extra series inductance to the screen-grid lead (horizontal scale). By the application of the circuit according to Fig. 160 a substantial reduction of noise figure is obtained (reference *197*).

An experimental confirmation of this annihilation of partition fluctuations was obtained at 300 mc/s. In an entrance amplifier stage of a receiver a pentode was applied. The mean square partition current fluctuations amounted to about $\frac{1}{3}$ of the total mean square output fluctuations. Hence by a proper application of the circuit of Figure 160 no decrease of over-all mean square output fluctuations to less than about $\frac{2}{3}$ of its original value may be expected. The noise figure of this amplifier stage was measured as dependent on the extra inductance L inserted into the screen grid lead (Fig. 161). A decrease of noise figure from 23 to 15 was obtained, increasing L from zero to 25×10^{-9} henry. This ratio 15/23 is close to the expected decrease to $\frac{2}{3}$ of the original value. With this tube:

$$|Y| = 7 \text{ m mhos}, \quad |Y_2| = 0.9 \text{ m mhos}, \quad R = 500 \text{ ohms}, \quad C = 2\,pF.$$

Hence $1/R_2 = 2.2 \times 10^{-4}$ mhos at $\omega = 2\pi 3 \times 10^8$ cycles/sec. Assum-

ing the total screen lead inductance to be 35×10^{-9} henry (25×10^{-9} henry extra inductance and 10×10^{-9} henry original lead inductance) the expression between parentheses in Eq. (VI.1.32*a*) works out as 0.04, which again affords satisfactory confirmation of the above theory.

The regenerative effect of the screen lead inductance may be combined with its noise-reduction properties. But in most cases optimal noise reduction calls for an inductance, the regenerative effect of which, as in the above example, is relatively unimportant. By using a tap T on the inductance L (Fig. 162) at an intermediate position between its terminals A and B we may achieve annihilation of partition fluctuations at the output (in Fig. 162 pictured as a short-circuit connection between the anode a and the tap T) while at the same time using the entire inductance between A and B for regeneration. It is perhaps needless to say that the above noise reduction and regeneration may also be applied to push-pull circuits.

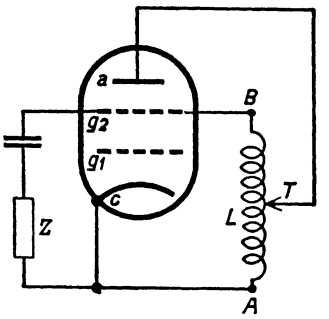

FIG. 162 Noise-reduction circuit similar to Fig. 160 but with a tap T on the inductance L between its terminals A and B. The inductance between B and T may be adjusted so as to obtain a minimum value of partition fluctuations in the output lead connecting the anode a and the tap T. The total inductance between A and B may be chosen so as to yield a proper value of regeneration to the input in order to obtain an increased stage gain.

REFERENCES: *197, 363, 396, 401, 408.*

VI.1.4. Feedback, gain control, and distortion. The performance of amplifier stages is in many cases appreciably affected by feedback, by the requirements of gain control, automatic or manual, and by distortion of the amplified signals.

VI.1.41. Feedback. Because of the feedback occurring to a certain extent in most stages and tubes under consideration, the input impedance is dependent on the impedance at the output. Ascribing the feedback to a capacitance C_f (see section V.3.22), the resulting input admittance becomes:

$$\frac{1}{Z_{in}} = \frac{1}{Z_1} + \frac{j\omega C_f Y}{\frac{1}{Z}}, \qquad \text{(VI.1.41}a\text{)}$$

Z_1 denoting the input impedance if the output is short-circuited, and Z being the total impedance between the output terminals. The output admittance $1/Z$ will be represented by a shunt connection of a conductance $1/R$ and of a susceptance $j\omega C$. As soon as the real part of the input admittance $1/Z_{in}$ becomes negative and of sufficient amount by manipulation of $1/Z$, instability results and oscillations may be started, often prohibiting the application of the stage for amplification purposes. We shall derive a necessary limitation of the admissible feedback capacitance C_f from the requirement of the said total input conductance to be positive. By Eq. (*a*) we obtain:

$$\frac{1}{R_{in}} = \frac{1}{R_1} + \omega C_f |Y| R \left(\frac{\sin \psi + \omega CR \cos \psi}{1 + \omega^2 C^2 R^2} \right), \quad \text{(VI.1.41}b\text{)}$$

the transadmittance Y being complex: $Y = |Y| \exp(-j\psi)$ at the present u.h.f. (see section V.3.22) and identifying the output resistance with R. By the output impedance of the preceding stage being shunted to Z_{in} the total input conductance without feedback will always be higher than $1/R_1$ (assumed to be positive). If the second term of Eq. (*b*) contributes a negative conductance which is smaller in amount than $1/R_1$, stability will prevail under all possible input coupling conditions, assuming the preceding stage to have a positive output conductance. By section V.3.22, C_f may be of positive or of negative sign at u.h.f. Assuming C_f to be negative, the expression of Eq. (*b*) between parentheses should be positive and as large as possible under the conditions most favorable to instability. Hence $\omega CR = (1 - \sin \psi)/\cos \psi$ if $\psi < \pi/2$ and the limiting condition to C_f is:

$$|Y \omega C_f R R_1| < \frac{2}{1 + \sin \psi}. \quad \text{(VI.1.41}c\text{)}$$

If C_f is positive, the expression between parentheses should be negative and of as large modulus as possible. Hence: $\omega CR = -(1 + \sin \psi)/\cos \psi$ and the ensuing condition becomes:

$$|Y \omega C_f R R_1| < \frac{2}{1 - \sin \psi}, \quad \text{if } \psi < \pi/2. \quad \text{(VI.1.41}d\text{)}$$

Whereas the limit (*c*) decreases if ψ increases from zero to $\pi/2$, the limit *d* increases and hence becomes more favorable. If input and output coupling of the stage in question are adjusted corresponding to optimal gain, R_1 must be replaced by $R_1/2$ and R by $R_2/2$, the value R_2 being

the tube's output resistance. Hence a larger modulus of feedback capacitance $|C_f|$ may be tolerated in this case.

Besides the possible instability ensuing from too large moduli of feedback capacitance, a reduction of gain is caused by feedback. If the optimal gain of a stage disregarding feedback is:

$$g_o = \tfrac{1}{4}\,|Y|^2 R_1 R_2, \qquad \text{(VI.1.41}e\text{)}$$

the optimal gain taking feedback into account becomes approximately:

$$g = \frac{g_o}{|1 + \tfrac{1}{2}j\omega C_f Y R_1 R_2|}, \qquad \text{(VI.1.41}f\text{)}$$

assuming total input and output tube impedances to be real and equal to R_1 and R_2 respectively.

Using triodes in amplifier stages, the effective feedback often requires special measures aiming at its reduction in cathode-base circuits. These special so-called "neutralization" circuits have been applied in many

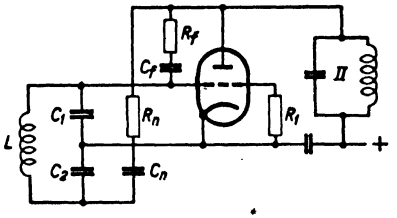

FIG. 163 Neutralization of feedback at v.h.f. and u.h.f. by means of a resistance R_n in series with a capacitance C_n.

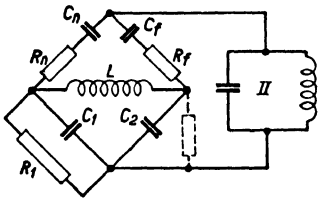

FIG. 164 Equivalent bridge-circuit to Fig. 163. The dotted shunt resistance to C_2 may be caused by additional losses.

varieties and no exhaustive discussion will be attempted here. Assuming the feedback in a cathode-base triode to be represented by a series connection of a resistance R_f and of a capacitance C_f at u.h.f., a suitable neutralization circuit, using an additional capacitance C_n and resistance R_n, is shown schematically in Figure 163. This diagram may be represented by a bridge circuit as shown in Figure 164, which is perhaps self-evident. Instead of a capacitive tap on the input tank circuit, an inductive tap may be used, as well as taps of both kinds on the output resonant circuit, instead of on the input circuit. Another simple means of neutralization is connected with the application of a suitable push-pull circuit as shown in the schematic Figure 165, which is also perhaps

self-evident. Instead of triodes, tetrodes or pentodes may be used in similar circuits, neutralization being applied to the screen grids in the latter cases (Fig. 166). By the screen lead inductances and the capacitances between screen grids and control grids this neutralization has an effect similar to that of Figure 165.

If grid-base circuits using triodes are applied, the effective feedback capacitance, being now between cathode and anode instead of between grid and anode, is much reduced if compared with cathode-base circuits. Hence no neutralization need be applied in many such cases though a certain reduction in optimal gain according to Eq. (V.1.31*f*) must be taken into account.

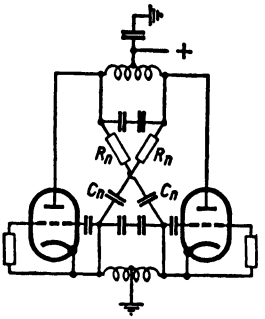

FIG. 165 Neutralization of feedback at v.h.f. and u.h.f. in a push-pull triode circuit (see caption of Fig. 166).

With push-pull circuits lack of balance sometimes occurs, by which the voltages of corresponding electrodes (e.g., control grids or anodes) are not exactly counterphase and of equal magnitude. If satisfactorily small feedback is achieved for balanced voltages, the unbalanced parts may still suffer from considerable feedback, corresponding electrodes being in shunt connection for these unbalanced voltages. It is in some cases necessary to provide special means of ascertaining balanced conditions (e.g., by using suitable taps for the ground connections at the anode and grid coils of Figure 165 or by using unequal neutralizing values R_n and C_n in the two connections). In other cases special neutralization of unbalanced feedback has to be applied, for which a circuit similar to Figures 163 and 164 may be suitable.

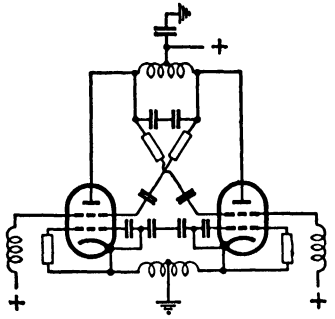

FIG. 166 Neutralization of feedback at v.h.f. and u.h.f. in a push-pull tetrode circuit. The short-circuit connections between cathodes and control grids in Figures 165 and 166 are in error and should be replaced by inductances, while the cathodes should be grounded directly.

By the circuit indicated in Figures 160 and 162, aiming at a suppression of partition fluctuations at the output, an increase of feedback is involved, as voltages are set up between screen and cathode, which, by the screen-control grid capacitance, directly result in output voltage components landing on the input. If the feedback capacitance is C_f previous to the insertion of the inductance L, the value upon insertion is:

$$C_{f1} = C_f - \omega^2 C L C_{a2} = C_f - \frac{C_{a2}}{YR_2}, \qquad \text{(VI.1.41}g\text{)}$$

C_{a2} denoting the capacitance between anode and screen grid. Assuming $C_{a2} = 1\ pF$, $YR_2 = 150$, $C_f = 3 \times 10^{-3}\ pF$, we obtain $|C_{f1}| = 4 \times 10^{-3}\ pF$. Thus the increase in feedback capacitance is almost negligible in this example. With pentodes, the capacitance C_{a2} is often smaller than $1\ pF$ because of the screening effect of the suppressor grid. In such cases the increase of feedback is hardly appreciable if full suppression of partition fluctuations is aimed at. If, however, the screen inductance L is increased beyond the value appropriate to full suppression, in order to obtain regeneration and an increased gain, the effect on feedback capacitance must be taken into account by means of Eq. (g). When it is known, a decision upon its effect on stage operation may be reached by means of the preceding Eqs. (c), (d), and (f).

REFERENCES: *280, 302, 346, 348, 353, 354, 356, 364.*

VI.1.42. Volume control and distortion. The available input power at the entrance of the first amplifier stage of a receiver may vary widely by variations of the specific signal power at the reception antenna, due to fading and to other causes (see section I.1). If an invariable adjustment of receiver gain should be maintained, inevitable overloading and distortion would result at the higher signal levels, if proper reception of the lower levels were obtained. Conversely, if overloading at the higher levels were avoided, poor reception of the lower levels would ensue, the level difference of specific signal power being often 40 db or more. As these variations in signal level often occur in rapid succession, only automatic volume (or gain) control can provide proper means of avoiding the said undesirable effects. While the exact design of a.v.c. will be dealt with in chapter VII, we shall consider only the means of a.v.c. and its effects on amplification in the entrance stages here. The most popular a.v.c. is by variation of control-grid bias voltage. In some cases bias control has been applied simultaneously

with variation of screen-grid voltage in pentodes (more negative bias corresponding to a higher screen voltage) by insertion of a properly bypassed high resistor (e.g., 50 k ohms) in series with the screen-grid voltage supply. In other cases negative bias voltage has been applied to the suppressor grid of a pentode. It may be well to discuss briefly the effects of these biasing procedures on amplification and especially on distortion. If a singly periodic signal voltage of amplitude V_o is applied to the input of an amplifying tube, assuming its output to be short-circuited, the output a.c. will in general not be singly periodic. We may, however, select the output current component of equal frequency as the input voltage. It may be shown that this output current amplitude I_o is not exactly proportional to the input voltage amplitude, but is given by:

$$I_o = |Y_1|V_o + |Y_3|V_o^3 + |Y_5|V_o^5 + \cdots \qquad \text{(VI.1.42}a\text{)}$$

etc. By applying singly periodic AM to the input voltage, writing $V_o(1 + m_a \cos \Omega t)$ instead of V_o and inserting this into Eq. (a), the output current is not only modulated by the angular frequency Ω but also by multiples of Ω and the output current has a modulation coefficient m_a' which is larger than m_a. We obtain approximately:

$$\left|\frac{m_a' - m_a}{m_a}\right| = \left|\frac{Y_3}{Y_1}\right| V_o^2 (2 - \tfrac{3}{4}m_a^2). \qquad \text{(VI.1.42}b\text{)}$$

If m_a is near to 1, serious distortion might arise from this effect upon rectification, but at small values of m_a little harm is done, in most cases. The modulation coefficient m_2 of the output current with twice the angular frequency Ω is approximately:

$$\left|\frac{m_2}{m_a}\right| = \left|\frac{Y_3}{Y_1}\right| \tfrac{3}{2}m_a V_o^2. \qquad \text{(VI.1.42}c\text{)}$$

If two different modulation frequencies corresponding to Ω_1 and Ω_2 are present in the input signal, the output current shows a coefficient $m_\pm$ of modulation, corresponding to the angular frequencies $\Omega_1 \pm \Omega_2$, which is approximately:

$$\left|\frac{m_\pm}{m_{a1}m_{a2}}\right| = 3\left|\frac{Y_3}{Y_1}\right| V_o^2. \qquad \text{(VI.1.42}d\text{)}$$

Finally, if two signals, one of amplitude V_o and a second of amplitude V_c, are present at the input, their carrier frequencies showing relatively

little difference, while V_o is unmodulated and V_c is modulated at an angular frequency Ω with a modulation coefficient m_a, the output current corresponding to the carrier frequency of V_o shows a modulation m_c with the angular frequency Ω, which is approximately:

$$\left|\frac{m_c}{m_a}\right| = 4\left|\frac{Y_3}{Y_1}\right| V_c^2. \qquad \text{(VI.1.42}e\text{)}$$

This effect is called cross-modulation. Obviously all these distortion effects depend on the ratio Y_3/Y_1 and this is dependent on the local

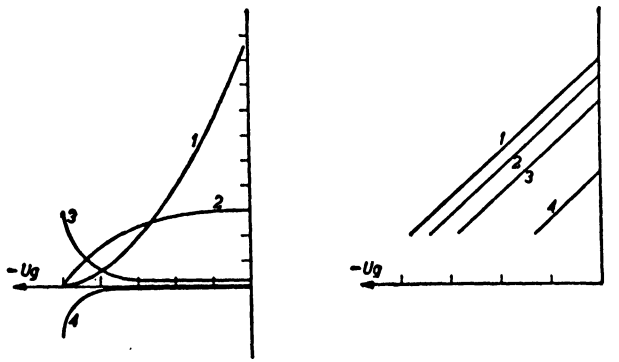

FIG. 167 Left diagram: Curve no. 1 represents the short-circuit anode current (vertical linear scale) as dependent on the control-grid bias voltage (horizontal linear scale) in the case of an ideal tube construction. Curves 2 to 4 represent the first, second, and third differential coefficients of curve 1. Thus the ratio of curves nos. 4 and 2 becomes very large near the cut-off point of curve no. 1. Right diagram: The curves 1 to 4 represent the same quantities as in diagram *a* on a vertical logarithmic scale, the horizontal scale being linear (bias voltage) in the case of a "remote cut-off" characteristic curve. Here the ratio of curves nos. 4 and 2 is constant throughout the course of curve no. 1.

curvature of the tube characteristic according to which the short-circuit anode current is dependent on the control grid voltage. The ratio described is proportional to the ratio of the third to the first differential coefficients of the anode current curve in question. This ratio is shown in Figure 167 for two types of curves. Obviously the type of diagram *b* is to be preferred if large bias voltages and corresponding volume control are to be applied. But unfortunately such a full logarithmic or "exponential" anode-current curve cannot well be applied,

as it would entail too large anode d.c.'s at small bias voltages. Such large anode d.c.'s result in correspondingly large noise currents and would cause intolerable noise figures of the stage in question. For this reason a compromise is often applied in which the anode-current curve is of type 167*a* at small bias voltages and of type 167*b* at medium bias voltages, falling back on type *a* at very large bias values. Thus tolerable anode d.c. and noise are combined with tolerable distortion effects. Though this general pattern of amplifier tube is now of almost universal application, rather wide differences in individual choice of compromise exist between tubes of different manufacturers.

Besides the distortion effects mentioned above, some further effects caused by volume control must be considered. As is evident from the impedance data of section V.3.22, both the input resistance R_1 and the output resistance R_2 are considerably increased by the application of control-grid bias voltage. Hereby a mismatch at the input as well as at the output results, if a particular coupling has been adjusted at a definite bias. The increase of these resistances also entails variations of band width. The seriousness of these effects depends on the particular case under discussion and will be dealt with in chapter VII. But some means of avoiding at least part of these variations will be considered here. From Figure 156 in comparison with Figure 141 it is obvious that a suitable unbypassed cathode-lead resistor as shown in Figure 155 may cause a nearly constant input resistance over a considerable range of bias voltage. This measure also causes a second effect to be much decreased: the variation of input shunt capacitance by bias variation. A nearly constant input capacitance may be obtained over a considerable bias range. As for the variation of output shunt capacitance by alteration of bias voltage, this effect is very small and practically negligible. But suitable remedies for the attending variation of output resistance R_2 are still somewhat lacking.

With wide-band amplification the variations of input and output resistances are in general not of great importance, but the variation of input capacitance, if unremedied, may have an undesirable effect. The center of the band under consideration may be shifted by this variation of capacitance and this shift may result in distortion, e.g., in television. Hence the application of a suitable unbypassed cathode-lead resistor is specially recommendable in these cases.

If gain-improving or noise-reducing measures of sections VI.1.2 and VI.1.3 are applied, gain control by variable bias is not admissible as

a rule, because the inherent variations of tube data upset the action of the circuit in question.

REFERENCES: *22, 96, 123, 187, 190, 260, 285, 302, 313, 346, 362.*

VI.2. MIXER STAGES

In many cases a mixer stage is preferable to an amplifier stage at the entrance of a receiver. The main properties of different mixer stages will be discussed here.

VI.2.1. Single- and multi-grid tube mixer stages. A full understanding of the relevant properties of u.h.f. mixer stages necessitates a discussion of their general operation as well as of the performance of particular types.

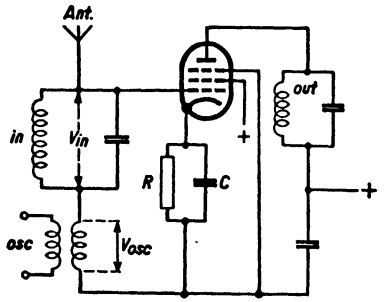

FIG. 168 Single-grid mixer circuit, the oscillator as well as the input voltages acting between cathode and first control grid.

VI.2.11. Operation of single-grid mixers. With single-grid mixers the input and the oscillator voltage are both applied to the tube input. The simplest way of achieving this consists of a series connection of both voltages as shown in Figure 168, the oscillator voltage V_{osc} being injected by means of a small coil, assuming a separate oscillator stage supplying this voltage. The anode lead contains a circuit resonant at the intermediate or output frequency, this being usually the difference between oscillator and input frequency:

$$\omega_{out} = |\omega_{osc} - \omega_{in}|. \qquad \text{(VI.2.11a)}$$

If the output angular frequency ω_{out} is small compared with the input angular frequency ω_{in}, the oscillator's angular frequency ω_{osc} is obviously close to the latter and undesirable interaction may thereby be created between the oscillator and the input circuit of Figure 168. In some cases the oscillator coil was inserted into the cathode lead in series with the bypassed bias resistance R, but at u.h.f. interaction remains appreciable via the tube's input impedance and besides this an extra input loading is caused by the cathode-lead inductance (see section

VI.1.31). A circuit which avoids interaction is shown in Figure 169, at the same time deriving the oscillator voltage from the mixer tube itself. With this circuit, however, some loss of gain is involved between the antenna and the tube entrance due to the bridge connections. We shall discuss some push-pull mixer stages in section VI.2.4 which, if applied correctly, are free of such interaction.

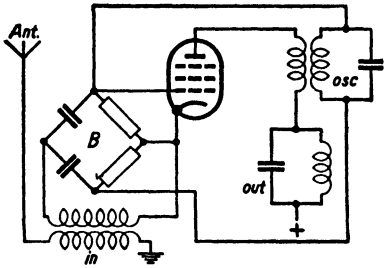

FIG. 169 Single-grid mixer circuit avoiding interaction between input and oscillator by the use of bridge connections.

The operation of a single-grid mixer stage may be discussed best by considering the transadmittance versus grid bias voltage curve (Fig. 170). By application of a proper steady bias voltage (R and C of Fig. 168) the oscillator voltage in this case varies between -10 and -2 volt, causing a transadmittance versus time curve as shown in the lower part of Figure 170 and more fully in Figure 171, together with the resulting anode current I_a versus time. An interval 2π on the horizontal scale of Figure 171 corresponds to one full period of the oscillator voltage. The transadmittance versus time curve of Figure 171 may be decomposed into singly periodic components:

$$Y = Y_o + Y_1 \cos \omega_{osc}t + Y_2 \cos 2\omega_{osc}t + \cdots . \quad \text{(VI.2.11}b\text{)}$$

The separate values Y_o, Y_1, Y_2 are dependent on ω_{osc} and on the input angular frequency ω_{in} under application. They are in general complex at u.h.f. and real at r.f. Evaluating the anode current if an input voltage $V_i \exp(j\omega_{in}t)$ is applied, we obtain components of several frequencies from which we now select only those of angular frequency $\omega_{out} = |\omega_{in} - \omega_{osc}|$. This is, by Eq. ($b$): $\frac{1}{2}Y_1V_{in}$, the multiplier $\frac{1}{2}$ resulting from the decomposition of $\cos \omega_{osc}t$ into its exponential elements. The value $Y_1/2$ is usually indicated as conversion transadmittance Y_{conv}. A rough estimate of its value at r.f. in relation to the top value of Y in the course of one oscillator period may be obtained from Figures 170 and 171. The value of Y oscillates between zero and this top value during one oscillator period. Hence Y_1 will approximately be half and Y_{conv} about $\frac{1}{4}$ of the top value of Y. It is, in most cases, of efficient mixer operation between $\frac{1}{3}$ and $\frac{1}{5}$ of the latter value.

At u.h.f. this relation is approximately valid in connection with the moduli of these admittance values.

Besides the conversion transadmittance, the values of effective input and output impedances under operating conditions are important data

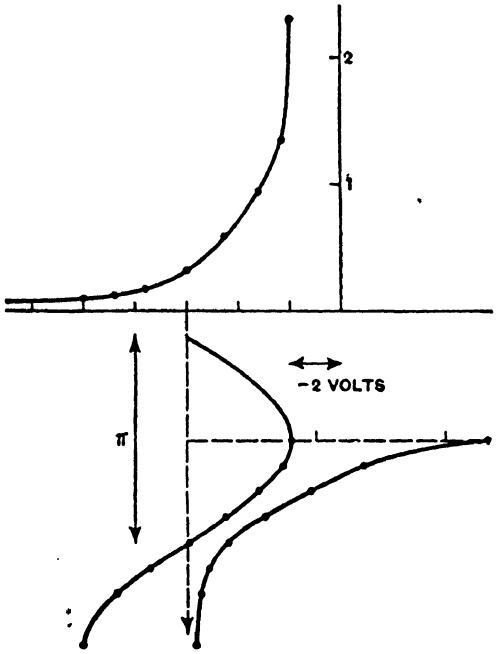

FIG. 170 Upper curve: Transconductance (m mhos, vertical scale) versus grid bias voltage (volts, horizontal scale) of a remote cut-off pentode. Lower left curve: Grid oscillator volts versus time (vertical scale). Lower right curve: Ensuing transconductance (horizontal scale) versus time.

of performance. In Figure 141 experimental data of the input resistance of an amplifier tube as dependent on bias voltage are shown. Assuming the input and oscillator frequencies to be incommensurable and the corresponding voltages to be of random mutual phase, the effective input resistance active at the angular frequency ω_{in} is obtained by averaging (taking the arithmetical mean value) over one period of oscillator voltage. As soon as the oscillator as well as the steady bias voltages are known, the resistance versus time curve may be obtained from a curve as shown in Figure 141 by a graphic procedure similar

to that of Figure 170. Under conditions of operation similar to those of Figure 170 an effective input resistance results, several times that at top transadmittance in an amplifier stage. A similar procedure may be applied to the input capacitance as well as to the output impedance. With the latter value the above assumptions of incommensurability and mutually random phase between input and oscillator frequencies and voltages are sufficient to justify the application of the above averaging process in obtaining the output impedance effective

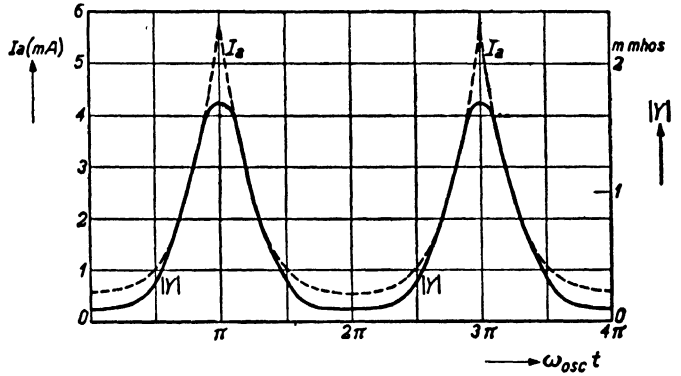

FIG. 171 Anode current I_a and transconductance Y (vertical scales) versus time ensuing from operational conditions similar to Fig. 170.

at the intermediate angular frequency ω_{out}. With the output resistance, a value several times that at top transadmittance in an amplifier stage results from the averaging process as indicated (see Fig. 140). These data—conversion transadmittance Y_{conv}, effective input resistance R_{in}, and output resistance R_{out}—determine the optimal gain:

$$g = \tfrac{1}{4}|Y_{conv}|^2 R_{in} R_{out}, \qquad \text{(VI.2.11c)}$$

if the band width B is such that $2\pi BC \ll 1/R_{in}$ and $\ll 1/R_{out}$ (i.e., with very narrow band mixer stages, C being the input or output capacitance respectively). In many cases, as $\omega_{out} \ll \omega_{in}$ and $R_{out} \gg R_{in}$, we have $2\pi BC_{in} \ll 1/R_{in}$ but $2\pi BC_{out} \gg 1/R_{out}$ and the effective gain becomes:

$$g = \tfrac{1}{4}|Y_{conv}|^2 \frac{R_{in}}{2\pi BC_{out}}. \qquad \text{(VI.2.11d)}$$

These data combined with those of section V.3.22 may be used to

obtain a check and confirmation of the experimental gain data of single-grid mixer stages mentioned in section V.3.12. With most mixer stages, even triodes, the effects of feedback capacitance on gain and on possible instability may be disregarded because of the small impedance which the input circuit offers to voltages of output frequency. If it is not negligible, feedback may be evaluated on the basis of the equations of section VI.1.41. In these cases, feedback active at the input, the oscillator and the output frequencies should be examined, inserting the impedance values at these respective frequencies.

REFERENCES: *32, 150, 160, 161, 163, 187, 190, 196, 302, 342, 344, 359, 362, 401.*

VI.2.12. Operation of multi-grid mixer stages. The multi-grid mixer stages now in us for frequencies above, say, 6 mc/s input frequency, are in many cases of the heptode type, this name being derived from the Greek word for the number (7) of electrodes involved (cathode, 5 grids and anode). We shall abstain from a description of other multi-grid mixers. The grids, counted from the cathode, have the following functions: control grid, screen, second control grid, screen and suppressor (of secondary electrons), the control grids being of negative bias, the screens of positive steady voltages and the suppressor usually connected to the cathode. One of the two control grids is connected to the oscillator voltage and the other one to the input voltage, the latter usually corresponding to the first control grid, though the reverse connection is sometimes used. We shall, however, refer to the former situation. The object of providing mutually screened grids for input and oscillator voltages is to prevent mutual interaction between the respective circuits. Though this aim is attained in a satisfactory manner at r.f., interaction remains present above, say, 6 mc/s, and usually increases if the input frequency is increased.

In order to discuss the operation of a mixer tube as described, we consider the transadmittance from the input control grid to the anode as dependent on the bias of the oscillator control grid (Fig. 172). Obviously a transadmittance versus time curve results from the action of oscillator voltage, which is very similar to that of Figure 171 in the case of a single-grid mixer. The subsequent discussion is entirely along the same lines as set forth in the preceding section and we need not repeat it here. As a result a conversion transadmittance is obtained

which is between about $\frac{1}{3}$ and $\frac{1}{5}$ in modulus of the transadmittance at zero bias of the oscillator grid (referring to moduli at u.h.f.).

As with single-grid mixers, we have to deal with effective input and output impedances besides transadmittance. With output impedance the situation is much the same as in the case of single-grid mixer tubes and no further comment is needed. With input impedance a slight

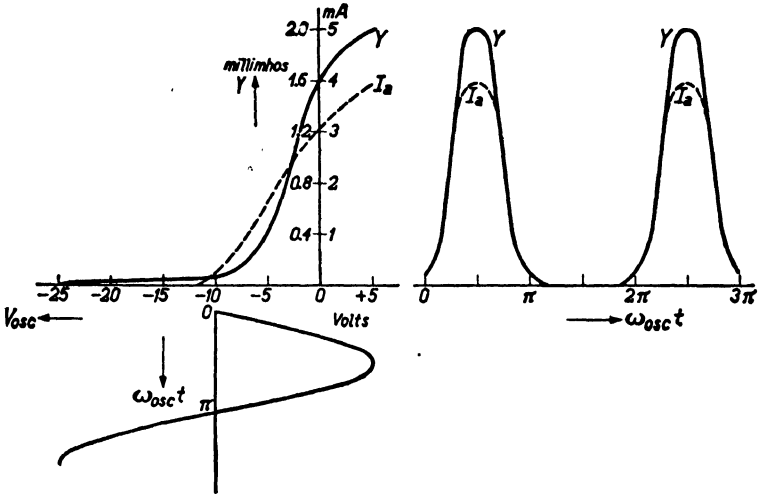

FIG. 172 Transadmittance of multi-grid mixer tube (full curves) from input signal grid to anode as influenced by oscillator swing (lower figure) as well as anode current (broken curves) under same conditions.

difference results from the electronic motion in the heptode. If the bias voltage of the second control grid is made increasingly negative, the resistance between the first control grid and the cathode decreases due to additional space charge resulting from electrons the direction of which is reversed by the decelerating field in the space preceding the second control grid. This effect is shown for a particular tube in Figure 173 at a frequency of 21 mc/s, the input conductance as well as the input shunt capacitance being recorded in dependence of bias on the second control grid. Obviously the present situation differs from that connected with a single-grid tube, where the input conductance and the shunt capacitance both decrease with increasingly negative bias. The upshot is that by application of the averaging procedure mentioned in the preceding section the effective input resistance becomes

lower than the value at zero bias of the second control grid, instead of higher, as in the case of a single-grid mixer. By this effect the gain figures of a heptode mixer stage are considerably lower than those of comparable single-grid mixers at frequencies above, say, 15 mc/s. The usefulness of heptode mixer tubes beyond about 60 mc/s is, therefore, doubtful, unless of special construction.

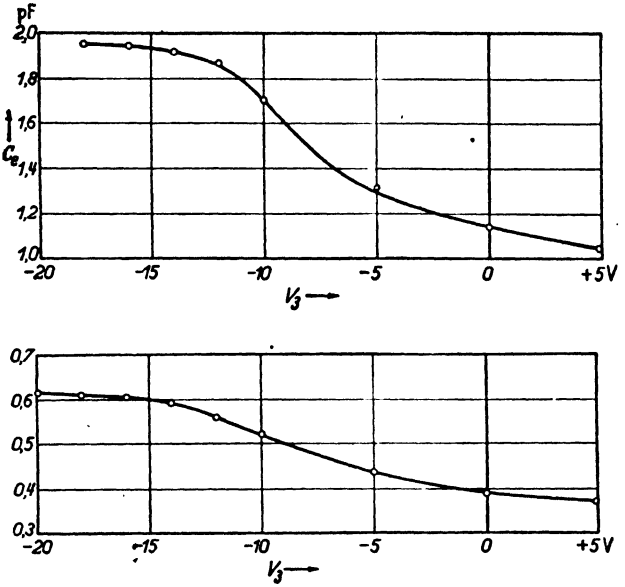

FIG. 173 Input capacitance variation C_e (expressed in pF on vertical scale in upper picture) and input conductance expressed in units equal to 0.1 milli mhos (vertical scale in lower picture) of a heptode tube measured between the grid nearest to the cathode and the cathode as dependent on the voltage of grid 3 (horizontal scale) under normal operating conditions of the other electrodes

As to the interaction between both control grids and their attached circuits, this is due, first, to electrostatic capacitance (often limited to some 0.02 pF by the interposed screen grid) and, second, to electronic motion between these grids. The electronic stream being modulated by both voltages at their respective frequencies, induction of alternating charges at corresponding frequencies upon the respective grids will result. By the reversing electronic motion in the space preceding the second control grid induction of alternating charges of

oscillator frequency on the input control grid ensues. These alternating charges result in spurious and undesirable voltages of the wrong frequencies being set up across the circuits connected to the said grids. Thus we obtain interaction, which increases at higher frequencies. Several remedies, such as suitable neutralizing impedances, have been applied, and within a limited range of frequencies satisfactory performance may be obtained in this way.

Some curves showing conversion transadmittance in dependence of oscillator voltage are shown in the case of a modern heptode and for a single-grid mixer pentode in Figure 174, the oscillator voltage swing being equal to the steady bias voltage in each case. These typical curves indicate that oscillator voltage should exceed a definite amount corresponding to top conversion transadmittance, when minor variations of oscillator voltage will have relatively little effect on gain.

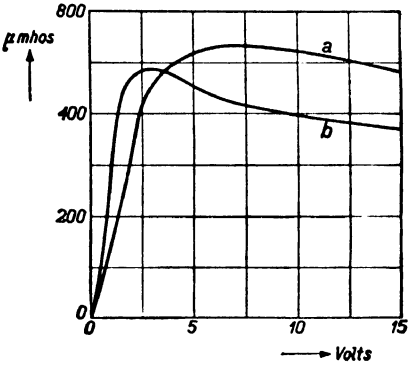

FIG. 174 Conversion transadmittance (vertical scale, expressed in micro mhos) of single-grid mixer according to Fig. 170 (curve *b*) and of multi-grid mixer (curve *a*) as dependent on oscillator voltage in volts (r.m.s. value).

REFERENCES: *150, 159, 160, 161, 163, 302, 342, 344, 349, 350, 351, 355, 358, 360, 362, 401.*

VI.2.13. Interference effects. As with amplification stages, volume or gain control of mixer stages is in general desirable, and in many cases a.v.c. will be applied to the entrance mixer stage. This volume control is, in most cases, based on bias regulation of the input grid voltage. Again as with amplifier tubes, the anode-current amplitude I_o of output frequency (assuming the output terminals to be short-circuited or nearly so) is dependent on the amplitude of input voltage V_o (of input angular frequency ω_{in}) by an equation which is formally identical with Eq. (VI.1.42*a*) so that we need not repeat it here, $|Y_1|$ now representing the modulus of conversion transadmittance and $Y_3|$, $|Y_5|$, etc., the respective quantities corresponding to transadmittance at higher input voltage levels. From this equation the various distortion effects connected with mixer operation may be derived and the results correspond entirely to those obtained in the case of amplification

(see section VI.1.42). In fact, the Eqs. (*b*, *c*, *d*, and *e*) of that section may be applied directly to the present case, thus obtaining the increase of AM coefficient, the AM coefficient of twice the fundamental frequency of modulation, the AM coefficients of differences of modulation

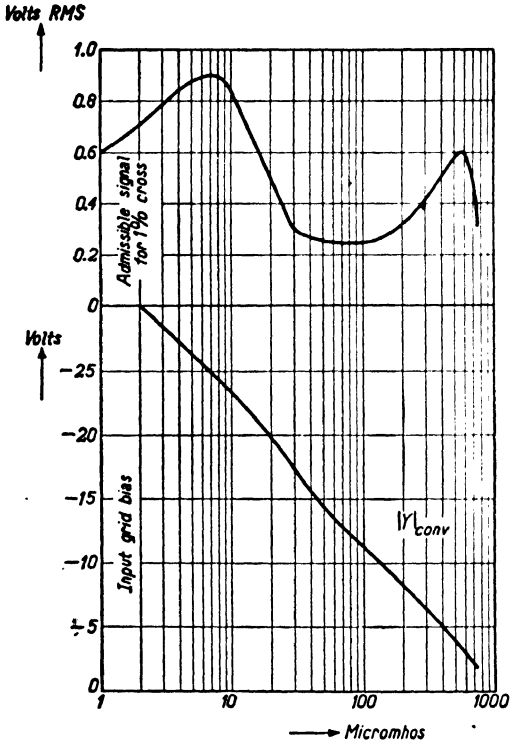

FIG. 175 Conversion transconductance (horizontal scale of lower curve) as dependent on input grid bias (vertical scale of lower curve) of typical triode-heptode mixer valve. Admissible input signal r.m.s. voltage causing 1% cross-modulation (vertical scale of upper curve) as dependent on conversion transconductance (horizontal scale).

frequencies, and the coefficient of cross-modulation at the output. As with amplification, a conversion transadmittance versus bias curve sloping down gradually at increasingly negative bias voltages is required in order to keep the distortion effects within tolerable bounds. Some curves related to the same heptode mixer tube as Figure 174*a* are shown in Figure 175, the lower curve corresponding to the conversion trans-

conductance (at r.f.) versus input bias voltage and the upper curve giving the input cross signal voltage for which the cross-modulation ratio according to Eq. (VI.1.42*e*) is exactly 1%. From the former curve the almost exactly exponential dependence of conversion transconductance on bias voltage will be noted, causing the more or less constant level of the latter curve according to the said equation. By this remote cut-off character of the former curve a rather large anode current at low bias voltages is caused, and this tends to increase the noise figure (as will be further elaborated in section VI.2.14).

A second type of interference is inherent in the mixing process and has no parallel in amplification. Besides the required relation between the three frequencies under consideration:

$$\omega_{out} = |\omega_{in} - \omega_{osc}|, \qquad \text{(VI.2.13}a\text{)}$$

additional equations of the type:

$$\omega_{out} = |q_{in}\omega_{in} - q_{osc}\omega_{osc}| \qquad \text{(VI.2.13}b\text{)}$$

may be satisfied simultaneously, q_{in} and q_{osc} being integers. Suppose that one of the Eqs. (*b*) is approximately satisfied, the right-hand side being relatively little different from the left-hand side. Then we will have at the output one a.c. of angular frequency ω_{out} corresponding to Eq. (*a*) and a second a.c. of an angular frequency relatively little different from ω_{out}, corresponding to Eq. (*b*). Both a.c.'s give rise to output voltages that are further amplified and subsequently arrive at the rectification stage (or second detector stage, the mixer stage being sometimes indicated as first detector). By the process of rectification a beat note of frequency corresponding to the difference between the frequencies of the said two a.c.'s is created and this beat note at the output of the rectification stage may be harmful to reception. With superheterodyne sound receivers such beat notes give rise to the well-known whistles, and this type of interference is therefore sometimes called "whistling notes". We have thus far assumed that only one singly periodic input voltage, besides the oscillator voltage, is active upon the mixer tube. By lack of selectivity, however, several input voltages of different carrier frequencies may be simultaneously present at the mixer tube's input terminals. Suppose that one (desired) voltage of angular fequency ω_{in} and a second spurious voltage of angular frequency ω'_{in} are present. Then, besides Eq. (VI.2.13*a*) the equation:

$$\omega_{out} = |q_{in}\omega_{in} \pm q'_{in}\omega'_{in} \pm q_{osc}\omega_{osc}| \qquad \text{(VI.2.13}c\text{)}$$

may be approximately valid (in the above sense) simultaneously. Again, beat notes or whistles may be created, giving rise to undesirable interference. This process may obviously be extended to an arbitrary number of spurious input voltages. Thus the possibilities of obtaining beat notes are many. Fortunately, not all of these potential whistles are of equal strength, i.e., output current at the mixer stage. If the integral multiplier of an input frequency in Eqs. (*c*) or (*b*) is q (i.e., either q_{in} or q'_{in}) the r.m.s. output a.c. corresponding to the equation in question is proportional to $|V_{in}|^q$, i.e., to the q^{th} power of the input voltage of the frequency multiplied by q in one of the equations. As these spurious input voltages are mostly relatively small, the beat notes diminish rapidly in strength if q increases. Hence only the lowest integers q_{in} or q'_{in} in Eqs. (*b*) and (*c*) need be considered, i.e., only unity or two at most. Furthermore, the beat notes diminish in strength if q_{osc} in Eqs. (*b*) and (*c*) is increased, though in general more slowly than in the preceding case.

Some particular cases of multiple input response of mixer stages will now be considered by way of examples. First, the so-called image response which plays a considerable part in most u.h.f. mixer stages. With it the spurious angular frequency is $\omega'_{in} = \omega_{osc} + \omega_{out}$, if the desired relation is $\omega_{in} = \omega_{osc} - \omega_{out}$; or, conversely, if the former equation represents the desired relation, the spurious angular frequency satisfies the second one. The reason for the name "image" will be evident from this explanation as the difference between ω_{osc} and both input angular frequencies is of equal modulus. This image response may be effectively eliminated only by the application of a sufficiently selective circuit preceding the mixer tube. At u.h.f. such selectivity is, however, often difficult to obtain because of the smallness of ω_{out} relative to ω_{osc} (and to ω_{in} or ω'_{in}) and thus image response often persists to a considerable degree and its resulting effects, especially in relation to noise (see section VI.2.14), must be faced. Another spurious response which has been found to cause trouble at somewhat lower frequencies corresponds to $q_{osc} = 2$ and $q'_{in} = 2$ in Eq. (*c*), q_{in} being zero. For instance, if $\omega_{in} = 2\pi \times 10$ mc/s, $\omega_{out} = 2\pi \times 0.5$ mc/s, $\omega_{osc} = 2\pi \times 10.5$ mc/s, $\omega'_{in} = 2\pi \times 10.251$ mc/s, we obtain $2 \times 10.5 - 2 \times 10.251 = 0.498$ mc/s, and a beat note of 2 kc/s results with the desired output frequency of 500 kc/s. These examples might be extended almost without end.

Besides the above interference effects which are due to non-linearity

of the mixer action, its output voltages and currents being only approximately proportional to input voltages and currents (though of different frequencies), further interferences have been found to arise from the interaction between oscillator and input circuits. Only one instance will be given pertaining to a heptode mixer tube. By such interaction a certain amount of input voltage arises at the oscillator grid and by a mixing process in the oscillator stage this is converted to a voltage of output frequency at the oscillator grid, being then amplified directly to the mixer output. If of unfavorable phase, the resulting output a.c. may cause a reduction of the total a.c. of output frequency and hence of mixer-stage gain. Several similar examples of undesirable effects caused by interaction could be given, all of them pointing to the necessity of avoiding their primary cause (interaction).

REFERENCES: *343, 344, 349, 351, 355, 358, 359, 360, 362.*

VI.2.14. Noise figures. In a triode amplifier tube of ideal construction the noise-current generators supplying the fluctuation current i_1 between cathode and grid and i_2 between grid and anode are completely intercorrelated (see Fig. 39). If the same triode is applied in a mixer stage, the relevant noise currents generated between cathode and grid on the one hand and between grid and anode on the other are not completely correlated. This is mainly due to their respective frequency intervals Δf being centered round different frequencies, corresponding to the input and output circuit. Thus the output noise current corresponding to an interval Δf centered round f_{out} is partly due to noise-current components, originally centered round f_{out} and to components, originally centered round other frequencies (among these is f_{in}) and finally centered round f_{out} by the action of the oscillator voltage, causing a variation of transadmittance of fundamental angular frequency ω_{osc}. With multi-grid mixer tubes, applying single or double grid mixing, this correlation between relevant noise currents and voltages at the input and at the output is still weaker, due to the effects of current partition fluctuations. As an approximation satisfactory in most cases, we shall assume a complete incorrelation between the noise current i_1 at the input and the tube-noise current i active at the output in a frequency interval Δf centered round f_{out}. This output noise current i is given by the equation:

$$\overline{i^2} = 4KT_f|Y_o|\Delta f, \qquad \text{(VI.2.14}a\text{)}$$

$|Y_o|$ being the modulus of average transadmittance during each oscillator period (see Eq. VI.2.11*b*) and T_f being approximately equal to 0.6 to 5 times the tube's cathode temperature expressed in degrees Kelvin under normal conditions of operation. Using the same procedure that was applied in obtaining Eq. (VI.1.12*a*), the noise figure of a mixer entrance stage, conforming to Figure 46 as regards the circuit between antenna or transmission line output and tube input, works out as:

$$N = \frac{T_a}{T} + \frac{T_{in}}{T}\frac{w^2 R_a}{R_{in}} + w^2 R_a R_f \left(\frac{1}{R_{in}} + \frac{1}{w^2 R_a}\right)^2, \quad \text{(VI.2.14}b\text{)}$$

the symbols having the same sense as in Eq. (VI.1.12*a*) and R_f being the "noise resistance" according to Eq. (VI.1.23*f*), replacing Y by Y_o. We may now determine the transformation ratio w so as to obtain a minimum noise figure. This optimum ratio is given by:

$$w^4 R_a^2 \left(\frac{1}{R_{in}^2} + \frac{1}{R_f R_{in}}\frac{T_{in}}{T}\right) = 1$$

and yields a minimum noise figure:

$$N_{min} = \frac{T_a}{T} + 2\frac{R_f}{R_{in}} + 2\sqrt{\left(\frac{R_f}{R_{in}}\right)^2 + \frac{R_f}{R_{in}}\frac{T_{in}}{T}}. \quad \text{(VI.2.14}c\text{)}$$

Thus the noise figure is dependent only on the ratio R_f/R_{in}, considering T_a/T and T_{in}/T as given and unalterable constants. It is useful to observe that this same Eq. (*c*) applies in the case of an amplifier stage if the correlation between i_1 and i_2 is disregarded, and if the over-all input circuit is resonant at the frequency of operation. The noise resistance R_f is, by its definition in Eq. (VI.1.23*f*), practically independent of frequency. Thus the only frequency dependence in Eq. (*c*) is due to R_{in} being inversely proportional to the frequency squared. Disregarding the second term under the square root sign of Eq. (*c*) this frequency dependence of R_{in} involves a direct proportionality of the variation of N to the square of the frequency of operation. This is in accordance with experimental data on mixer-stage noise stated in section V.3.13. As to the actual values of noise figures obtained by application of the above Eq. (*c*), we have primarily to consider the relevant values of R_f and R_{in}. With triode mixer tubes at cathode-base operation, the value of R_f is about equal to $4/|Y_o|$, which, under

optimal conditions of operation, amounts to about $12/|Y_{max}|$, the trans-admittance $|Y_{max}|$ corresponding to optimum operation as an amplifier. Thus R_f is about three times larger with a triode mixer than with a triode amplifier; and we have seen in section VI.2.11 that R_{in} with single-grid mixers has also about three times the value corresponding to the same tube as an amplifier. From this we conclude that the ratio R_f/R_{in} with single-grid mixers has about the same value as with amplifier tubes. With multi-grid mixers of heptode type, however, R_{in} is about 2 to 4 times smaller than with the same tube in an amplifier stage and, R_f being about 3 times larger, the ratio R_f/R_{in} acquires between 6 and 12 times the value correspond ng to the same tube used in an amplifier stage. With suitable triodes at 300 mc/s, the ratio R_f/R_{in} in cathode-base amplifier stages may be about 1.5, increasing proportionally to the square of the frequency of operation, and with suitable pentodes the ratio may be about 2. The same values apply to single-grid mixer stages, thus, assuming T_{in}/T to be 6 and T_a/T to be unity, obtaining a noise figure N of about 10 to 20 at 300 mc/s according to Eq. (*c*). With heptode tubes at 30 mc/s, we have a ratio R_f/R_{in} of about 5, and from this Eq. (*c*) yields a noise figure of about 25. At lower frequencies these noise figures decrease rapidly until they become finally equal to T_a/T.

With wide-band mixer stages such that $2\pi BC_{in}R_{in} \gg 1$, B being the band width corresponding to a drop of gain of 3 db on either side of resonance, C_{in} denoting the input capacitance and R_{in} the input resistance of the mixer tube, the noise figure is given by:

$$N = \frac{T_a}{T} + R_f 2\pi BC_{in} \qquad \text{(VI.2.14}d\text{)}$$

instead of by the above Eq. (*c*), the input transformation ratio w (coupling) being obtained from:

$$w^2 R_a 2\pi BC_{in} = 1 \qquad \text{(VI.2.14}e\text{)}$$

instead of from the equation preceding (*c*). If R_f is comparable with R_{in} we may assume that $R_f 2\pi BC_{in} \gg 1$, but in many cases R_f will be much smaller than R_{in} under the conditions of operation being discussed. As an example, we assume $R_f = 4000$ ohms, $B = 4$ mc/s, and $C_{in} = 15\ pF$. Then $2\pi \times BC_{in}R_f$ is about 1.5. The tube's contribution to

the over-all noise figure according to Eq. (*d*) becomes inappreciable in this example. Attention is drawn to the equality between Eq. (VI.2.14*d*) and Eq. (VI.1.23*g*).

REFERENCES: *342, 351, 359, 362, 367, 373, 401.*

VI.2.2. Diode and crystal mixer stages. These stages have become increasingly popular at extremely high frequencies on account of their excellent properties under suitable conditions of operation. We shall examine these conditions and state clearly these optimal properties.

VI.2.21. Operation. The operation of a diode mixer stage may be discussed referring to Figure 176. The oscillator voltage V_{osc} is applied to the diode circuit by means of a relatively small coupling coil of negligible impedance. Besides the diode D itself, which may be replaced by a suitable crystal detector unit, the circuit contains an impedance R_{out} resonant at ω_{out}, an impedance R_{in} resonant at ω_{in}, and a resistance R bypassed by a capacitance C of such value that $\omega RC \gg 1$, in which ω may be either ω_{in}, ω_{osc}, or ω_{out}. The impedances R_{in} and R_{out} are supposed to be very small at any frequency not coinciding with their resonant frequencies. Thus at the oscillator's angular frequency ω_{osc} the total diode series circuit offers negligible impedance except as regards the diode itself. By the oscillator voltage acting on the diode, its admittance Y is varied in synchronism with this voltage:

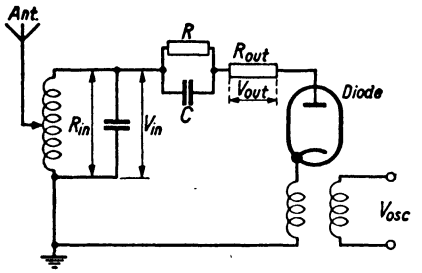

FIG. 176 Diode mixer circuit (schematic).

$$Y = Y_o + Y_1 \cos \omega_{osc} t + Y_2 \cos 2\omega_{osc} t + \cdots . \quad \text{(VI.2.21}a\text{)}$$

Assuming the interelectrode distance of the diode to be sufficiently small or the oscillator frequency to be sufficiently low, or both, the values Y, Y_o, Y_1, etc., are nearly real if the input frequency also is sufficiently low, i.e., of the same order of magnitude as the oscillator frequency (thus $\omega_{out} = |\omega_{osc} - \omega_{in}|$ being small compared with either of the angular frequencies). The values of Y_o, Y_1, etc., are dependent on the properties of the diode as well as on the applied resistance R. At positive bias voltages on the diode's anode with respect to its cathode,

the dependence of anode d.c. on the bias voltage is often nearly linear, or may, within a definite range of current and voltage, in many cases be approximated by a straight line. The slope of this line—i.e., the voltage increment over the current increment—is then indicated as the diode's internal resistance. It will be assumed that R is large compared with this internal resistance over the entire range of operation. If this condition is satisfied, the dependence of diode admittance on time is represented by a curve similar to that of Figure 171 but with the peaks much narrower relative to their height. In the extreme case of very narrow peaks we have the relations: $2Y_o \approx Y_1 \approx Y_2$, etc. In other cases, Y_1, Y_2, etc., are smaller than $2Y_o$. By the action of the input voltage $V_{in} \exp (j\omega_{in}t)$ on the diode circuit with its vibrating diode admittance, several current components arise, one of which:

$$-\tfrac{1}{2}Y_1V_{in} \exp \{j(\omega_{in} - \omega_{osc})t\}$$

has the angular frequency $\omega_{out} = \omega_{in} - \omega_{osc}$, which will be assumed to be the desired relationship between the three frequencies in question; thus ω_{in} is higher than ω_{osc}. This a.c. causes a voltage across the output resonant impedance R_{out} and the ensuing output voltage causes an a.c. of angular frequency ω_{out} which, by Eq. (a) is:

$$V_{out} \exp (j\omega_{out}t)Y_o$$

and the direction of which is opposite to the previous current of the same frequency. Hence the total a.c. of angular frequency ω_{out} is:

$$-\tfrac{1}{2}Y_1V_{in} + V_{out}Y_o = -\frac{V_{out}}{R_{out}}.$$

We may express V_{out} by V_{in}, using this equation, and thus find:

$$\frac{V_{out}}{V_{in}} = \frac{\tfrac{1}{2}Y_1}{\dfrac{1}{R_{out}} + Y_o}.$$

The available input power may be assumed as: $V_{in}^2/4R_{in}$. The admittance of the diode circuit to the output voltage V_{out} across the resistance R_{out} may be found by evaluating the total current of angular frequency ω_{out} resulting from V_{out}, taking into account the ensuing voltage arising across R_{in} by conversion due to the vibrating diode admittance and the resulting current of angular frequency ω_{out}. The

output admittance of the diode circuit is:

$$Y_{out} = Y_o - \frac{\frac{1}{4}Y_1^2}{\frac{1}{R_{in}} + Y_o} \qquad \text{(VI.2.21}b\text{)}$$

and the ensuing available output power is hence $V_{out}^2 Y_{out}/4$. Thus the gain, being the ratio of available output power to available input power, works out as:

$$g = \frac{\frac{1}{4}Y_1^2}{(Y_o R_{in} + 1)\left(Y_o^2 - \frac{1}{4}Y_1^2 + \frac{Y_o}{R_{in}}\right)}. \qquad \text{(VI.2.21}c\text{)}$$

Under the conditions of operation corresponding to sharp and narrow peaks of diode admittance as dependent on time, mentioned above, we have $2Y_o = Y_1$. If we assume furthermore that $Y_o R_{in}$ is large compared with unity, the gain of our diode mixing circuit becomes unity according to Eq. (*c*). The entire circuit being in effect a series connection of passive impedances, a gain amounting to unity is the highest value ever attainable. If it occurs, no loss is incurred in the diode circuit itself.

The diode mixer circuit, if viewed from the terminals of the output impedance R_{out} or from the terminals of the input impedance R_{in}, shows a similar aspect. In fact, its properties are entirely symmetrical between the two pairs of terminals. This is revealed in its input admittance:

$$Y_{in} = Y_o - \frac{\frac{1}{4}Y_1^2}{\frac{1}{R_{out}} + Y_o}, \qquad \text{(VI.2.21}d\text{)}$$

this expression being symmetrical with respect to Eq. (*b*) of the output admittance. If considered as a device situated between the said two pairs of terminals, the diode circuit may be pictured as a four-pole. Its exact equivalent network structure is shown in Figure 177, the three impedances being:

$$\frac{1}{Z_1} = \frac{1}{Z_3} = -\tfrac{1}{2}Y_1 + Y_o, \quad \frac{1}{Z_2} = \tfrac{1}{2}Y_1,$$

if the voltages and currents are assumed to be of orientation as shown in the figure.

Thus far we have assumed that the input impedance R_{in} has an

appreciable value only at the input angular frequency ω_{in}, supposed to be equal to $\omega_{osc} + \omega_{out}$. At u.h.f., however, the input circuit's impedance at the image angular frequency $\omega'_{in} = \omega_{osc} - \omega_{out}$ is in many cases comparable with the value at ω_{in} as $\omega_{out} \ll \omega_{osc}$. In these cases the diode or crystal mixer circuit may be regarded as a six-terminal network, the two pairs of input terminals corresponding respectively to ω_{in} and to ω'_{in} while the output pair of terminals corresponds to ω_{out}. The gain is affected likewise by this image response. Whereas an optimal value of unity may be obtained under favorable conditions if image-frequency impedance is zero, this optimal figure drops to $\frac{1}{2}$ if image-frequency impedance is equal to input-frequency impedance. This loss of 3 db results from additional power loss incurred in the image-frequency impedance being real and equal to the resonant impedance at ω_{in}.

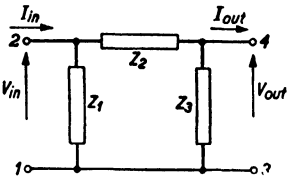

FIG. 177 Equivalent four-pole representation of diode mixer circuit.

REFERENCES: *32, 71, 92, 130, 163, 164, 277, 302, 347, 366, 373, 401, 404.*

VI.2.22. Noise figures. We shall first consider the noise figure corresponding to the mixer stage itself, though by its low gain the noise figure of the subsequent intermediate frequency stage enters into the over-all entrance noise figure appreciably. In evaluating this noise figure use may be made of the diagram of Figure 177, assuming that the three impedances (all of them real) shown are uncorrelated sources of noise. This assumption yields results confirming those obtained by different reasonings as well as by experiments and is thus shown to be correct. Evaluating the resulting available noise power at the output terminals 3, 4 of Figure 177, the equations of section II.2.31 may almost be applied directly as soon as the temperature T_f corresponding to the fluctuation sources is known. With diodes incorporating a heated cathode, T_f is often between 0.5 and 0.7 times the cathode temperature. With crystals, T_f is in most cases between 1 and 2 times the room temperature. The resulting noise figure, disregarding image response, is:

$$N = \frac{T_a}{T} + \frac{T_f}{T} Y_o R_{in} \left[\frac{\left(Y_o + \frac{1}{R_{in}}\right)^2}{\frac{1}{4}Y_1^2} - 2 \frac{Y_o + \frac{1}{R_{in}}}{Y_o} + 1 \right]. \quad \text{(VI.2.22a)}$$

This equation is worthy of discussion and offers several interesting viewpoints. In the first place, the condition $Y_o R_{in} \gg 1$, which is conducive to a high gain figure, is obviously also favorable to a low noise figure. Second, the expression within square brackets contains parts of different sign owing to the negative signs in Figure 177. If these parts are of equal amount they may thus cancel. The conditions for such canceling are: $Y_o R_{in} \gg 1$ and $2Y_o = Y_1$, and are thus identical with those causing the gain figure to approach unity. Under these conditions the remarkable situation may thus be obtained that the mixer tube's or crystal's contribution to over-all entrance noise is completely eliminated.

If image response is taken into account, conditions are less favorable and no complete elimination will in general be obtained. However, even so, the noise contribution of the diode tube or crystal to the entrance noise figure may often be made of relatively negligible amount.

If the gain of the mixer stage is g, its noise figure being N_1 and that of the subsequent intermediate frequency stage N_2, the over-all entrance noise figure becomes:

$$N = N_1 + \frac{N_2 - \frac{T_a}{T}}{g}. \qquad \text{(VI.2.22}b\text{)}$$

Thus a relatively considerable contribution of the noise of the subsequent amplifier stage may always be expected, even if gain approaches unity, which will often be impossible, e.g., owing to image response. As was stated in section V.3.12, gain figures of diodes of conventional interelectrode spacing (e.g., 100 microns) show a considerable drop in mixer stages already at, say, 300 mc/s, a pertinent figure being 0.3. At 2000 mc/s the corresponding gain often drops to figures comparable with 0.01. In such cases the noise figure N_2 of the subsequent stage is considerably magnified and over-all figures between 100 and 1000 may result. This situation may be very much improved either by the use of diodes of unconventionally small spacings (e.g., 20 microns) or of suitable crystals. Taking image response into account, gain figures approaching 0.5 may be obtained at frequencies of 3000 mc/s and even beyond this, resulting in correspondingly low noise figures, as already mentioned in sections V.3.12 and 13.

REFERENCES: *32, 72, 163, 250, 373, 401, 404.*

VI.2.3. Oscillator stages. The oscillator stages used in mixer stages involve a number of separate considerations and thus merit a special treatment.

VI.2.31. Operation. A triode oscillator circuit is shown schematically in Figure 178. Disregarding the effect of feedback capacitance and incorporating the tube's input and output impedances in the outer circuit, a part wV_a of the anode's a.v. is fed back to the grid, and by the tube's transadmittance Y this grid a.v. is amplified to the anode circuit, thus obtaining the condition of sustained oscillation:

$$wYZ = 1, \qquad \text{(VI.2.31}a\text{)}$$

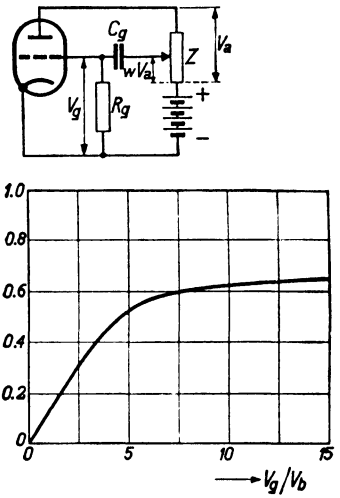

FIG. 178 Upper picture: Schematic diagram of triode oscillator circuit. Lower picture: Efficiency (vertical scale) as dependent on the ratio of grid voltage V_g to cut-off bias V_b.

Z representing the resonant impedance of a suitable tank circuit or cavity. By the grid leakage resistance R_g the tops of the oscillator voltage swing will only be relatively slightly positive on the grid with respect to the cathode. Thus, if this swing increases, the anode-current versus time curve will assume a shape similar to that shown in Figure 171. The r.m.s. value of the fundamental frequency component of this anode-current curve divided by the r.m.s. grid a.v. yields the effective value of Y to be inserted into Eq. (a). Thus this effective transadmittance decreases in modulus at increasing grid a.v. If w and Z in Eq. (a) are regarded as fixed, this equation yields directly the required value of Y, and this value in time determines the corresponding grid a.v. (and hence the anode a.v.) according to the above reasoning.

The ratio of the available h.f. power at the terminals of Z to the direct power supplied to the anode is the oscillator's efficiency. This is small at small oscillator voltages and gradually rises until a value is reached at a definite a.v. beyond which little is gained by a further increase of a.v. In Figure 178 this efficiency is shown in dependence on the ratio of grid a.v. V_g to the cut-off bias voltage V_b at the grid (corresponding to nearly zero anode current). High efficiency values

like those of Figure 178 are obtainable with conventional r.f. triodes or triode parts of combination tubes up to, say, 50 mc/s. Beyond this frequency top efficiency gradually decreases owing to several causes such as: increasing losses in the tube (e.g., electrode leads) and in parts of the oscillator circuit. Special constructions have been devised, with which this decrease of efficiency occurs at higher frequencies, and with lighthouse tubes such as are shown in Figure 125 oscillations still occur at 5000 mc/s though efficiency is low at this frequency.

An oscillator circuit suitable at frequencies up to about 2000 mc/s is shown in Figure 179*a*, the longer wave equivalent being shown in Figure 179*b*. In Figure 179*a* the resonant circuit *LC* of Figure 179*b* is constituted by the transmission-line section shown, the cathode being tapped to the resonant circuit by means of the capacitances C_1 and C_2 in Figure 179*b* and by C_{cg} and C_{ca} in Figure 179*a*. The resonant line of Figure 179*a* may be replaced by a suitable resonant cavity. A lighthouse triode coupled to a suitable resonant cavity oscillator circuit is shown in Figure 179*c*. The shape of the efficiency versus frequency curve of most oscillator tubes is similar to Figure 180, the frequency f_o being in many cases about $\frac{1}{4}$ to $\frac{1}{3}$ of the frequency at which oscillation becomes impossible. The latter frequency, as well as f_0, is to a considerable extent dependent on the resonance frequencies of the tube in question. These angular resonance frequencies ω_{res}, like those of a diode (see section V.2.32 and Fig. 130), are determined by the product of lead inductance L and interelectrode capacitance C according to $\omega_{res}^2 LC = 1$. A tube will in many cases fail to oscillate at a frequency somewhat below the lowest resonance frequency thus obtained. With suitable constructions similar to Figure 125 these resonance frequencies are above 5000 mc/s and thus oscillations may be obtained almost up to such frequencies.

However, as will be discussed more fully in section VI.2.33, oscillation is in itself not sufficient. The oscillation frequency is required to be stable within rather narrow limits, and, moreover, the oscillation power to be delivered to the mixer circuit must be such that optimal mixer operation may be ascertained (see Fig. 174). Both requirements point to tolerable lower limits of generated power and of efficiency. Beyond 3000 mc/s sufficient power is sometimes difficult to obtain by the use of triode circuits and magnetrons have been used instead. Devices of this kind affording ample power at 10,000 mc/s and at operating direct voltages as low as 200 volts have been constructed, the

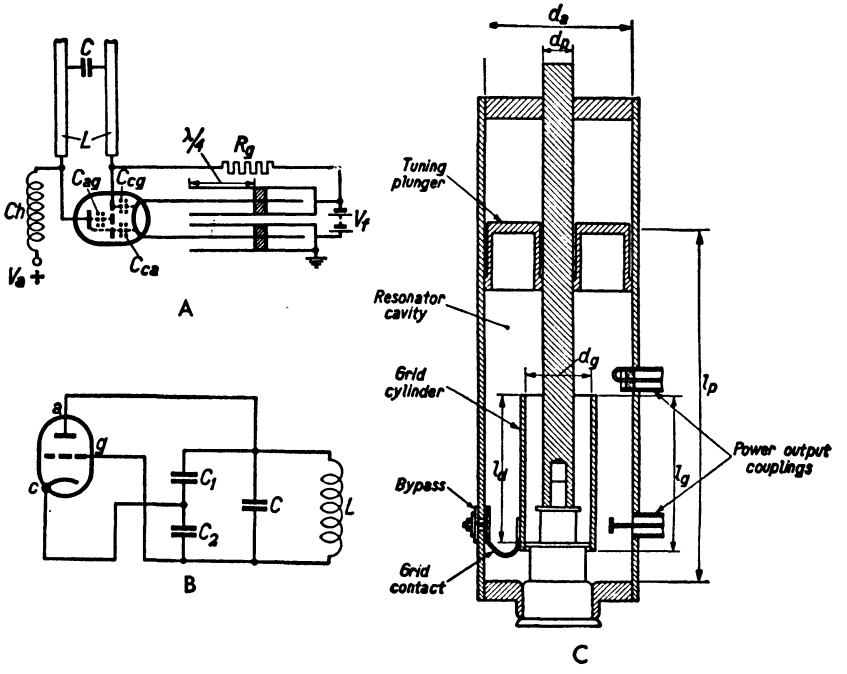

FIG. 179 Picture *a*: Resonant transmission-line circuit connected to a triode. The anode supply voltage V_a is fed through a choke *Ch*. Quarter-wave resonators are inserted into the heater wires and a leakage resistor R_g is connected between grid and cathode. Picture *b*: R.f. equivalent circuit of diagram *a*. Picture *c*: Lighthouse triode of type 2 C 40 connected to a resonating coaxial line circuit. Dimensions: d_a: 1 to 1/2 in., d_p: 9/16 in., d_g: 13/16 in., while l_g, l_p, and l_d are dependent on the oscillator frequency as follows:

Frequency mc/s	l_g	l_p	l_d *(inches)*
3 300	1.37	2.0	1 17
3 000	1.75	2.4	1.55
1 500	3.8	6.2	2.35
1 000	5.6	9.4	1.78

cavity resonators being incorporated in the magnetron. As an example, see Figure 181, in which such cavities have been drilled out of a solid metal block. The central cathode emits the electrons and by the axial magnetic field a "cloud" of them revolves on an orbit round the cathode. By the motion of this cloud past the narrow slits connecting the individual cavities with the central orbital space, currents are induced in the cavities and the resulting alternating voltages across the slits react on the electrons. Output powers of 100 watts at 30,000 mc/s are obtainable continuously by the use of such devices (reference *112*). In most mixer stages at frequencies beyond 2000 mc/s input frequency a reflex klystron is used in the oscillator stage (see Figure 181c). In this tube the electrons emitted by the cathode are accelerated by a steady electric field and shot past a slit connected to a resonant cavity. Alternating voltages ensue across this slit, reacting on the electron beam. The electrons are then decelerated by an inverse steady electric field and reversed so as to pass the slit again at such a phase delay that the alternating power oscillating in the cavity is reinforced. Part of this power is fed to the mixer stage via the small coupling loop shown in Figure 181c. Reflex klystrons are in operation up to and beyond 30,000 mc/s (see reference *134*).

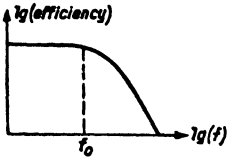

FIG. 180 Logarithm of efficiency (vertical scale) of oscillator circuits as dependent on logarithm of frequency (horizontal scale).

Besides generating oscillator power the oscillator stage also acts as a source of noise power. This is at once obvious by the consideration of Figure 39, as the noise currents i_1 and i_2 connected with electronic motion act directly as noise sources creating a definite output-noise power. The exact evaluation of this noise power has scarcely been effected yet at u.h.f. We may, however, say that the ratio of generated oscillator power to noise power will in general increase at increasing efficiency levels as the average number of electrons moving in the tube at a definite oscillator power decreases. Hence a high efficiency, preferably corresponding to the curve of Figure 180 below the frequency f_o, is recommendable from this point of view as from several others. The

FIG. 181 Pictures of magnetrons and reflex klystron suitable as oscillator at frequencies up to 10,000 mc/s. Picture 181*a*: Two cuts of a power magnetron. Picture *b*: Internal structure of a cavity magnetron showing resonant cavities and tuning straps. Picture *c*: Reflex klystron including attached resonant cavity.

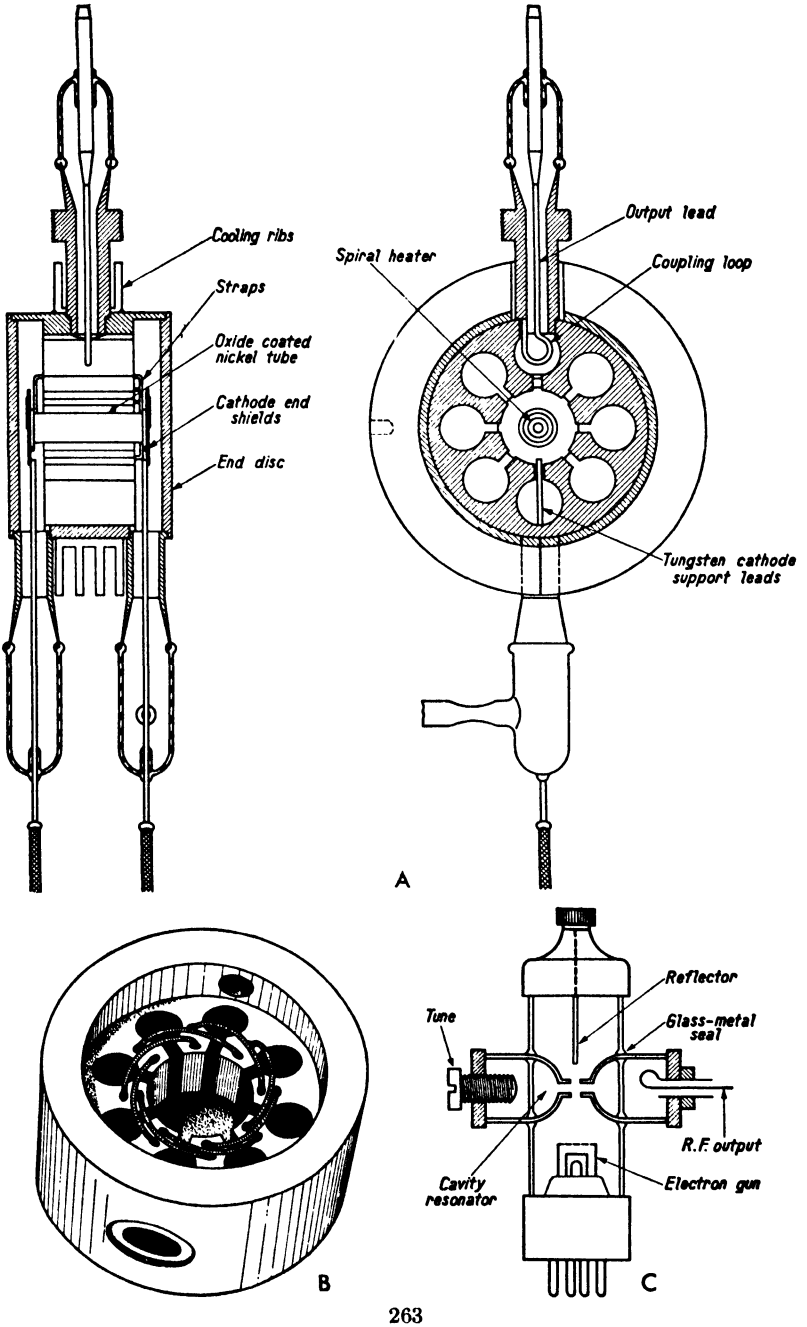
Cooling ribs
Straps
Oxide coated nickel tube
Cathode end shields
End disc
Output lead
Spiral heater
Coupling loop
Tungsten cathode support leads
A
B
Tune
Reflector
Glass-metal seal
R.F. output
Cavity resonator
Electron gun
C

noise power in the case of a high Q resonant circuit used in the oscillator stage corresponds substantially to a frequency interval Δf centered round the oscillator frequency. This is important in estimating its effects in mixer circuits. With magnetrons and reflex klystrons, as with triodes, a noise power is generated at the stage's output simultaneously with the oscillator power. Here again, no definite estimates are yet available, but it seems reasonable to assume that high efficiency will tend to decrease the noise power in relation to the oscillator power (references *318* and *373*).

REFERENCES: *4, 38, 82, 88, 111, 112, 134, 145, 155, 186, 202, 217, 222, 223, 248, 305, 306, 309, 318, 373, 375.*

VI.2.32. Over-oscillation and padding. A cause of disturbances sometimes arising in oscillator stages and its simple remedies are worth mentioning. Assuming the values of leakage resistance R_g and bypass capacitance C_g of Figure 178 to be very large, the starting process of oscillations in the circuit will be considered. Initially the grid is at zero bias voltage with respect to the cathode and transadmittance Y is hence of maximum modulus. Small spontaneous fluctuation voltages between grid and cathode are amplified to the anode circuit and cause a rapidly increasing oscillation voltage at the terminals of that circuit. The rate of increase is approximately proportional to $1 - \exp(-\omega_o t/2Q)$, ω_o being the angular oscillator frequency, t the time, and Q the quality factor of the resonant circuit. Hence the final oscillator voltage is approached after a lapse of time comparable with Q/ω_o. The grid must acquire a proper bias voltage with respect to the cathode, approximately equal to the amplitude of the grid's a.v. The time required to set up this bias voltage is comparable with the product $R_g C_g$ (see Fig. 178). Assuming this product to be much larger than the value Q/ω_o, the oscillator voltage will, at a given moment, shortly after switching the power supply on to the oscillator stage, be much larger than the corresponding bias voltage. If now the bias voltage increases, a situation may arise in which the modulus of Y required to keep the high oscillator voltage in being is higher than the actual value of $|Y|$. In such cases the oscillator voltage decreases, and as the bias lags behind, it decreases too much. Subsequently it increases again and the value thus attained is again too high, etc. This phenomenon is known as over-oscillation, and stages in which it occurs may be unsuited to mixer operation. As Q/ω_o is often smaller at h.f. and u.h.f. than at r.f., the

ratio of $R_g C_g$ to Q/ω_o may be higher at u.h.f. than at r.f. if R_g and C_g are given similar values in both cases. Remedies against over-oscillation are thus: First, decrease of the product $R_g C_g$ until it is comparable to or smaller than Q/ω_o. Second, increase of grid d.c. drawn from the cathode at a given bias by proper grid construction. Third, increase of Q.

Problems of padding arise if the local oscillator of a mixer stage is required to operate within a given frequency range which is considerable in comparison with the average frequency of the range. We shall depict the entrance resonant circuit of the mixer stage (assuming that no two coupled circuits are applied) as well as the resonant circuit of the oscillator stage by lumped circuits as shown in Figure 182. The main tuning condensers (indicated by C in Fig. 182) are assumed to be equal, this being the most convenient situation. We have, then, three quantities, indicated by a, C_s, and C_f in Figure 182, with which to insure a proper output frequency of the mixer stage to be created throughout the required range of input frequencies. In many cases it is customary to choose an oscillator frequency which is higher than the input frequency. If the output frequency is not inappreciable compared with these frequencies, a higher oscillator frequency leads to a smaller ratio of lowest to highest oscillator frequency of the range than the converse choise of a lower oscillator frequency. If the range is relatively large, such a lower ratio may cause a simplified design of the oscillator stage. If the output frequency is inappreciable compared with these frequencies the choice at issue is immaterial from this point of view. An exact compliance with the equation $\omega_{osc} - \omega_{in} = \omega_{out}$ throughout the range is of course impossible using the means given in Figure 182. As we have three parameters a, C_s, and C_f, the equation may be satisfied at three predetermined frequencies.

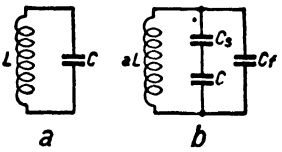

FIG. 182 Padding circuit (diagram b) supposed to be equivalent to simple resonant circuit (diagram a).

The deviation of the actual output frequency of the mixer stage from the exact one at any position of the input frequency is, of course, required to be as small as possible. In general, the deviation y is under the present conditions given by a curve as shown in Figure 183, if the oscillator frequency is proportional to x and the range of oscillator frequencies represented on the x-scale is from $x = -1$ to $x = +1$.

The choice of the three points at which $y = 0$ is governed by the requirement that the modulus of y should be as small as possible throughout the range considered. This is a well-known mathematical problem, solved by Tchebycheff. The maximum values of $|y|$ should occur at the ends of the range and at the intermediate points corresponding to maximum deviations. The shape of the resulting curve is represented by the equation $y = \frac{3}{4}x - x^3$, and this corresponds exactly to the curve drawn in Figure 183. The three points where $y = 0$ are: $x_1 = 0$, $x_2 = \sqrt{\frac{3}{4}}$ and $x_3 = -\sqrt{\frac{3}{4}}$. If the latter two points are brought closer together, the two maxima of $|y|$ between them decrease but the other

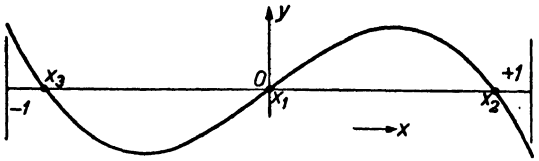

FIG. 183 Tchebycheff curve applicable to padding problems.

two maximum deviations increase. The reverse situation occurs if x_2 and x_3 are further removed from each other. If the range of oscillator frequencies is from f_a to f_b, the three frequencies corresponding to x_1, x_2, and x_3 are respectively $f_1 = (f_a + f_b)/2$, while $f_2 = f_1 + (f_b - f_a) \times \sqrt{\frac{3}{16}}$ and $f_3 = f_1 - (f_b - f_a) \times \sqrt{\frac{3}{16}}$. The actual calculation of a, C_f, and C_s corresponding to this choice of frequencies is rather intricate and several graphical methods have been devised for its execution. Their representation is, however, outside the scope of this book. In some cases special importance is attached to a selected interval of the entire frequency range under consideration and the value of $|y|$ is then required to be as small as possible within the said interval, without, however, undue increase of $|y|$ in the remaining range. In such cases deviations from the above Tchebycheff procedure may be appropriate.

REFERENCES: *156, 375.*

VI.2.33. Frequency drift and control. Frequency drift is a term applied to all variations of oscillator frequency due to other than predetermined causes. As a first cause of frequency drift, variations of supply voltage (e.g., mains voltage) may be mentioned. As such voltage variations affect the tube's properties (impedances and transadmittance), their effects may be decreased by a loose coupling of the

tube to the resonant circuit. Such loose coupling calls for a large optimal efficiency of the oscillator tube at the frequency in question, leaving ample scope for a decrease of efficiency caused by the loose coupling. Moreover, special measures may be taken to stabilize the direct supply voltages independently of these variations, e.g., by the use of proper feedback in the rectifier and supply unit feeding the receiver in question (see section VII.4 and Figure 239).

A second cause of frequency drift, common in many receiving sets on the market, is caused by the application of gain control to the mixer stage. By such control the impedances of the mixer tube are altered and thus variations of the connected oscillator stage may occur, causing frequency drift. The remedy obviously lies in a loose coupling of oscillator to mixer. Ample output-power generation of the oscillator stage is desirable in order to facilitate the application of such loose coupling, still obtaining sufficient available local oscillator power at the corresponding mixer terminals. Both causes of frequency drift mentioned are active through resulting variations of capacitance at the oscillator's resonance circuit. Thus, if the total capacitance of this circuit is increased, relatively less variation of capacitance and hence of frequency will ensue. By such an increase of circuit capacitance its resulting resonant impedance is, however, decreased (if Q remains unaltered) and conditions of oscillation may become less favorable. Essentially this remedy acts somewhat similarly to a looser coupling.

A very serious cause of frequency drift is to be found in temperature variations of the oscillator circuit. These are often due to heating by the power losses in the tube as well as in the attached circuit. Besides, a general heating of the receiver by power losses in further stages may add to the rise in temperature of the resonant circuit and of its attached elements. Unlike the frequency drift resulting from the preceding two causes, the present drift is in many cases very gradual and thus more suitable to be decreased by means such as automatic frequency control. This rise in temperature is in many cases active in causing frequency drift by way of ensuing variations of capacitance. Now, essentially a pure capacitance free of losses cannot be altered by temperature variations. The latter can be active only through losses occurring in the capacitances in question. Hence low loss angles of all applied insulating materials will be favorable to low capacitance variations per degree of ambient temperature rise. Another partial remedy may be found in efficient heat transport and ventilation, thus keeping

the ensuing temperature variations within narrow limits. In some cases special capacitances having an adjustable specific variation dependent on ambient temperature have been applied to neutralize the variations of circuit capacitances within a limited range of temperature. Careful design is needed for the successful application of this remedy.

As a final cause of frequency drift, variations of ambient air pressure may be mentioned, such as may occur in airplanes flying at varying altitudes. Here the ambient temperature may also show large variations—e.g., from −40 to +40° C. These severe conditions must sometimes be met by special design, the description of which is mainly outside the scope of the present book.

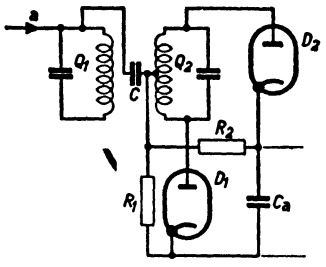

FIG. 184 Automatic frequency control circuit. Input a.c. at a, output voltage V_d across C_a.

The manual control of frequency by means of suitable tuning knobs will not be dealt with here (see section VII.4). We are, however, concerned with the automatic control of oscillator frequency designed to offset frequency drift or for other purposes. This automatic control is often active through two separate resonant circuits, the resonance frequencies of which are situated on either side of and at some suitable distance from the desired frequency. The latter may be the i.f. carrier frequency obtained by the mixing process of local oscillator and of input frequency. A diode rectifier circuit is connected to each of the separate resonant circuits. If, by frequency drift of the local oscillator, the i.f. approaches the resonant frequency of one of these circuits, a d.v. is created by rectification, the d.v.'s resulting from either diode circuit being of opposite signs. A pertinent diagram is shown in Figure 184. The direct voltage V_d created at the output of this stage as dependent on the variation Δf in frequency at its input is shown in Figure 185. Thus the control voltages rise sharply in modulus if fre-

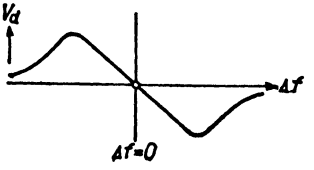

FIG. 185 Output voltage V_d across C_a of Fig. 184 as dependent on the frequency deviation Δf from the center frequency between the two tuning positions of the resonant circuits of Fig. 184.

quency deviations on either side of the adjusted zero position occur. These control voltages are applied to the oscillator stage by way of a suitable voltage-controlled reactance. A tube circuit serving as such has been shown in Figure 111. If direct control voltages of opposite directions are applied to this reactance circuit, its reactance is altered accordingly and frequency variations of opposite directions are caused in the connected oscillator circuit. The adjustment may be made such that these controlled variations offset the original drift activating the control circuit. In the design of automatic frequency control (a.f.c.) circuits of this kind a number of problems arise, such as the positions of the resonance frequencies to be chosen for the two resonant circuits of Figure 184, the delay in the application of control voltage to the oscillator, delay in time as well as delay in voltage level being involved.

REFERENCES: *53, 146, 156, 177, 315, 351, 375.*

VI.2.4. Improvement of performance and selection of tubes. As with amplifier stages, several means may be indicated with mixer stages, resulting in an improved performance as regards gain or noise or both. Subsequent to this discussion some rules governing the selection of amplifier, mixer, and oscillator tubes will be considered.

VI.2.41. Gain of single- and multi-grid stages. In considering mixer stages the four-pole concept has already been introduced in section VI.2.21, due regard being given to the difference in frequencies at the input and at the output terminals. This aspect of mixer stages was somewhat extended in the final paragraph of that section, when image response was taken into account, the resulting network being a six-terminal one. We shall drop image response here but proceed to extend the equivalent network to a single pair of input terminals connected to many pairs of output terminals. At each pair of output terminals only one corresponding frequency will be considered. The sequence of frequencies involved results directly from the representation of transadmittance under the action of local oscillator voltage as given by Eq. (VI.2.11*b*). Multiplying this transadmittance by the input voltage $V_{in} \exp(j\omega_{in}t)$, we obtain the output angular frequencies:

$$\omega_{in}, \quad |\omega_{osc} - \omega_{in}|, \quad |\omega_{osc} + \omega_{in}|, \quad |2\omega_{osc} - \omega_{in}|, \quad |2\omega_{osc} + \omega_{in}|, \cdots,$$

etc., and each of these frequencies may be associated with one separate pair of output terminals, e.g., resulting from a corresponding interrup-

tion of the output lead connecting the tube's output electrodes. In order to dispel undue anxiety in the reader's mind, it may be well to mention that only two of these output pairs of terminals will be needed in the course of this section. From each of these output pairs of terminals feedback to the input terminals may be applied. We have, in fact, before us a multi-terminal network of the kind considered in properties *C* and *D* of section II.2.22.

By application of regenerative feedback active at the input frequency, some impedances at the input of the mixer stage in question may be improved, thus obtaining an improved stage gain. For examples of such improvements reference may be made to section VI.1.31. The circuit of Figure 155 may be applied directly in the present case as the cathode lead of a mixer tube carries currents corresponding to each of the frequencies mentioned above and in particular an a.c. of input angular frequency ω_{in} which is active in a circuit as shown in Figure 155. The unbypassed resistance R_3 should be active only at the angular frequency ω_{in}, and in order to achieve this aim it may be replaced by a suitable resonant circuit tuned to this frequency and of negligible impedance at other frequencies. Thus improvements of input impedance as depicted in Figure 156 may be obtained, while no attending reduction of modulus of conversion transadmittance, similar to that of Eq. (VI.1.31*a*), need be present. The transadmittance affected in the present case corresponds to Y_o of Eq. (VI.2.11*b*), whereas Y_1 remains unaltered, thus resulting in an unaltered conversion transadmittance. Another example of feedback active at ω_{in} is to be found in the circuit of Figure 157. By the proper application of a double-cathode lead and appropriate regeneration considerable improvements of input impedance and of gain may be obtained.

If improvements of effective output impedance of the mixer stage are desired, regenerative feedback active at ω_{out} may be applied. Examples may again be found in the circuits of section VI.1.31. It is obvious that such feedback circuits may be applied to triode as well as to multi-grid mixer tubes.

Another means of improving gain may be found in the application of suitable push-pull circuits. With mixer stages, push-pull possibilities are many, and we can discuss only some of them here. In general we have the three different circuits: input, oscillator, and output. Each of these may be in push-pull or in shunt—i.e., the respective corresponding pairs of tube terminals obtaining either counterphase or

in-phase voltages of the three frequencies. Thus we have eight different cases:

CASE NO.	INPUT	OSCILLATOR	OUTPUT
1	push-pull	push-pull	push-pull
2	push-pull	push-pull	shunt
3	push-pull	shunt	push-pull
4	push-pull	shunt	shunt
5	shunt	push-pull	shunt
6	shunt	push-pull	push-pull
7	shunt	shunt	push-pull
8	shunt	shunt	shunt

Now the most obvious connections in the case of two triodes, tetrodes, or pentodes correspond to the use of cathode and grid as input as well as oscillator terminals while the output terminals are anode and cathode. Even if we adhere to these connections there is still some further scope for variation, as each pair of terminals may be connected to the corresponding pair of the other tube in equal or in reversed orientation. If of equal orientation, case no. 2 of the above table gives rise to a useful circuit if tubes of proper construction are applied, the advantages as to u.h.f. input impedance being similar to those discussed in connection with Figure 158 in the case of push-pull amplifier stages. If permutations of the electrodes are allowed in devising push-pull mixer circuits, at least 48 possibilities arise in the case of two triodes, but not all of them, of course, are useful. It may be well, however, to call attention to some of them by way of examples (see Fig. 186).

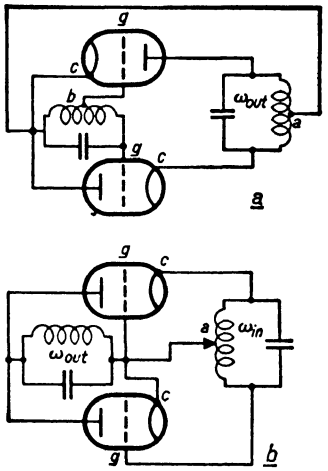

FIG. 186 Two unconventional circuits each using two triodes in double-unit mixer stages. The two resonant circuits shown in each diagram are tuned to the input angular frequency ω_{in} and to the output angular frequency ω_{out} respectively. The oscillator connections may be inserted into the leads starting from the adjustable tap points marked *a*.

In this figure only the input and output resonant circuits have been indicated by ω_{in} and ω_{out} respectively. The oscillator terminals may be inserted in the lead connecting *a* and the input of diagram *a* and in the lead connecting the points *a* and the output of diagram *b*. In diagram *b*, one tube is used in a cathode-base connection and the other in a grid-base connection. The interested reader might find fascination in unraveling various specimens of the at least 48 and probably more possibilities in the case of two triodes.

REFERENCES: *373*, *401*.

VI.2.42. Noise of single- and multi-grid stages. First some attention will be given to the subject of oscillator noise and its influence on output noise in mixer stages. As we have seen in the concluding paragraph of section VI.2.31, the noise generated by an oscillator stage of proper design corresponds mainly to frequencies in an interval centered round the oscillator frequency. The electronic current in the mixer tube contains fluctuation components of all frequencies and these may, by mixing with the oscillator stage's noise, entail noise-current components centered round any frequency and in particular round the input frequency and round the output frequency. If we assume that the noise voltage issuing from the oscillator stage is sufficiently small, the r.m.s. noise currents created in the mixer's output lead by this mixing process will be proportional to the oscillator's r.m.s. noise voltage, in accordance with Figure 174. (Compare the linear parts of curves *a* and *b* in Fig. 174 at small oscillator voltages.) The magnitude of the output noise-current components thus created will in general be smaller than that of the noise-current components uncorrelated to oscillator noise, the latter being obtained by an amplification process more efficient than the mixing mentioned. The grid of a mixer tube connected to the oscillator stage acts similarly to the grid of a single-grid mixer, if we regard the oscillator voltage and its accompanying noise voltage. Thus it is seen that at the mixer's output noise-currents, completely correlated with oscillator noise and having frequencies centered round the oscillator frequency and its multiples, will be present. In general, little harm will be caused by these noise-current components. Feedback active at one of these frequencies should be avoided in order to prevent an undue increase in their magnitude, when harm might be caused by mixing with other noise components issuing from the mixer tube itself.

We shall now leave the subject of oscillator noise and consider possible improvements in noise figures of mixer stages by the application of suitable feedback. Starting from the concept of a mixer stage as a multi-terminal network with a single pair of input terminals and several pairs of output terminals, we may first answer the question as to what noise figures must be assigned to these latter pairs individually. Considering in particular output pairs of terminals associated with the angular frequencies ω_{out} and ω_{in}, we have shown in section VI.2.14 and V.3.13 that under proper and favorable conditions of operation the noise figures of triode mixer stages may be approximately equal in these cases. If, however, the mixer is operated under less favorable conditions—e.g., at too small oscillator voltage level—the noise figure associated with the ω_{in}-terminals may be lower and in some cases even much lower than the figure corresponding to the ω_{out}-terminals. In such cases the application of feedback active at ω_{in} may improve the noise figure corresponding to ω_{out}, and at nearly critical feedback the latter noise figure will approach that corresponding ω_{in}. This is a simple application of property C of section II.2.22. The feedback active at ω_{in} may be obtained by insertion of a proper impedance Z into the cathode lead of a cathode-base mixer stage as shown schematically in Figure 187. This impedance must correspond to a capacitance at ω_{in} and be of negligible amount at any other frequency. We may obtain such an impedance by using a resonant circuit tuned to an angular frequency slightly lower than ω_{in}.

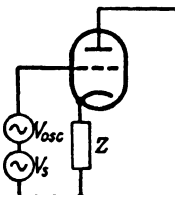

FIG. 187 Feedback by an impedance Z, equivalent to a capacitance at the input frequency, inserted into the cathode lead of a single-grid mixer stage.

Another example of noise-figure reduction by the application of feedback in multi-grid stages will now be given in which the reduction may be considerable even at optimal conditions of mixer operation. Considering a heptode mixer tube (Fig. 188), the partition fluctuations caused by the screen grids nos. 2 and 4 do not circulate in the lead between the points B and c. This is a simple deduction from the general picture of partition fluctuation currents discussed in section II.1.32 in connection with Figure 40. The partition fluctuations do

circulate in the leads issuing from the point C and other than that leading to B. In particular their full strength is present in the output lead connecting the anode a with the point D, which lead usually contains the output terminals connected to the circuit resonant at ω_{out}. We now apply feedback active at ω_{in} by the use of a similar impedance Z inserted into the cathode lead as mentioned in connection with Figure 187. This feedback may be considered as corresponding to a pair of output terminals at ω_{in} with the particular property that the related noise figure is that of a triode (no partition fluctuations) used as an amplifier. It is hence several times (10 or more even at optimal mixer operation) lower than the noise figure corresponding to the mixer's output terminals at ω_{out}. By the application of nearly critical feedback in this way the noise figure of the mixer's output at ω_{out} may be made to approach that of the said output at ω_{in}, which output might be imagined to have terminals inserted into the lead connecting the points B and c of Figure 188. Thus a very considerable reduction of noise figure may be obtained by this type of feedback, being again an application of property C of section II.2.22.

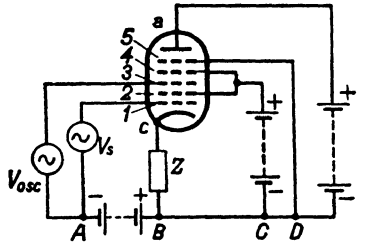

FIG. 188 Feedback similar to that of Fig. 187 but applied to a multielectrode mixer stage.

By nearly critical feedback of the type considered, as it is regenerative, instability might be caused. To avoid this a second and this time degenerative feedback may be applied. Considering again the case pictured in Figure 188, the noise figure corresponding to the currents of angular frequency ω_{out} or ω_{in} in the lead connecting the anode a and the point D may be made to approach the said triode-amplifier value by the feedback connected with the impedance Z. Once this low output noise figure is attained, it cannot be altered by the application of feedback from the output to the input, according to property A of section II.2.21. This latter feedback may be chosen such that it is degenerative at ω_{in}, thus undoing the instability that might be caused by the previous regenerative feedback. We might insert an impedance Z_1 into the lead connecting the anode a and the point D, equivalent to a capacitance at ω_{in} and of negligible amount at other frequencies. The terminal on the anode side of this impedance may then be connected

to the control grid no. 1 of the mixer tube across a proper series connection of a resistance and a capacitance. Without regard to phase angles of transadmittances a capacitance would be sufficient but at frequencies comparable with or larger than 30 mc/s a resistance in series with the capacitance may have a favorable effect. Several other applications of feedback may be devised aiming at a reduction of noise figure. All of them are based on the properties of noise figures set forth in section II.2.2.

REFERENCES: *274, 373, 401.*

VI.2.43. Diode mixer stages. With diode mixer stages we shall consider a number of circuits aiming at an improved performance as regards gain, noise, and further properties. First we shall discuss some applications of the push-pull principle. As was mentioned in section VI.2.41, eight fundamental cases of push-pull circuits exist. The two diodes or crystals may be used with their corresponding electrodes in equal or in reversed orientation. Thus each of the eight fundamental circuits has two possible applications, entailing 16 different possibilities in all. As examples the circuits corresponding to the cases numbered 4 and 7 of the table in section VI.2.41 will be discussed (Fig. 189). In cases 4*b* and 7*b* the diodes (pictured as contact detectors) are of parallel and in cases 4*a* and 7*a* of mutually reversed orientation. It is simple to show that no output voltage is created in cases 4*b* and 7*b* of angular frequency $\omega_{out} = |\omega_{in} - \omega_{osc}|$, these circuits thus being of no practical use in most cases. By reversing one diode the circuits 4*a* and 7*a* are, on the contrary, suited to the creation of such an output voltage approximately proportional to the input voltage of angular frequency ω_{in}. With the circuit 4*a* a voltage of oscillator frequency may arise across the push-pull input resonant circuit if its impedance is not negligible at ω_{osc}. With the circuit 4*b* this is impossible, assuming perfect balance, i.e., exactly equal diodes and further elements in each half of the circuit. But the whole circuit is unfortunately unsuited to mixer operation of the usual kind. A useful circuit in which no oscillator voltages will under proper conditions arise at the input is no. 3 of the table in section VI.2.41. This situation may in some cases be desirable in order to avoid interaction as well as radiation of oscillator signal power by the input reception antenna. Such radiation might disturb reception of near-by sets.

The conditions conducive to optimum gain have already been mentioned in section VI.2.21. We shall now look into them a little more closely and particularly from the viewpoint of diode or crystal proper-

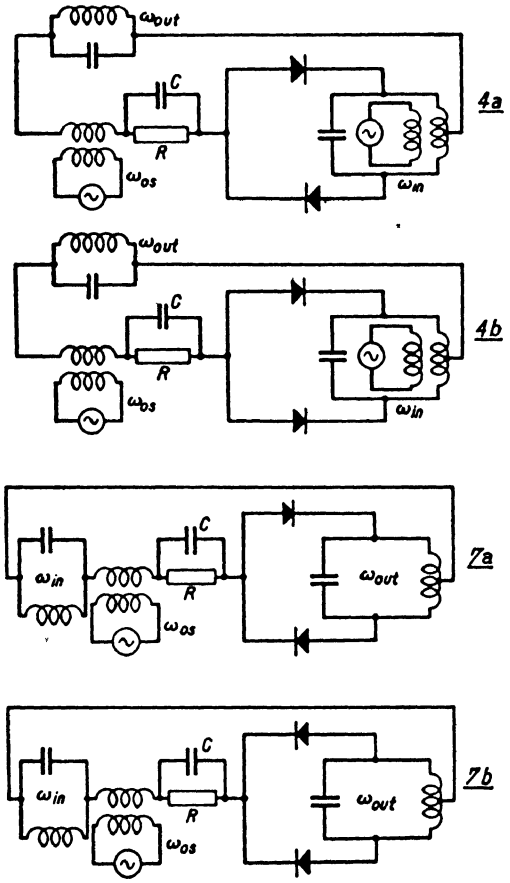

FIG. 189 Double-unit diode mixer stages, the diodes being represented by detector symbols. The tuned circuits are indicated by their angular tuning frequencies. The indications 4*a*, 4*b*, 7*a*, 7*b* refer to the table of possible cases in the text.

ties. An important condition for optimum gain was shown to be $Y_o Z_{in} \gg 1$. This condition may be approached by raising the diode's admittance Y_o or by increasing the resonant impedance Z_{in} of the resonant input circuit. The first means, implying the use of special

diodes, may only in part be attained by an increased surface area of the diode's electrodes, for such an increased area entails a directly proportional increase of interelectrode capacitance C_d. With a given band width B, the value $2\pi BC_dZ_{in}$ must, however, be small compared with unity, and if C_d is increased this would entail a decreased value of Z_{in}, adverse to the condition $Y_oZ_{in} \gg 1$ for optimal gain. Hence the said increase of Y_o should be obtained by a decrease of interelectrode clearance (e.g. to 20 microns or less at u.h.f.). If the diodes contain sources of losses—such as cathode oxide coating, lead series-resistance, getter-layers absorbing power, etc.—these losses may be represented by a corresponding shunt resistance across the diode's terminals. It is obvious that this shunt resistance may constitute a serious limitation to an increase of Z_{in} and hence the losses should be cut down as much as possible by the application of a proper diode construction. If a crystal rectifier is used instead of a diode, the conduction in one direction is not zero as with an ideal electronic diode but remains at a finite value. The crystal's current versus applied voltage curve may be idealized by Figure 190 in a number of cases. This curve shows that a diode admittance corresponding to the left portion of the curve remains active at all voltages. The crystal's performance may hence be represented by a corresponding constant admittance on which an oscillating admittance is superimposed. This constant admittance limits the attainable value of Z_{in} which, taking into account the already not very high value of Y_o, makes adherence to the condition $Y_oZ_{in} \gg 1$ difficult. It is therefore necessary to use crystals, the reversed conductance of which is extremely small with respect to the value corresponding to the favorable direction. Ratios between 1/200 and 1/1000 have been obtained and these may afford satisfactory conditions for u.h.f. and s.h.f. mixer operation.

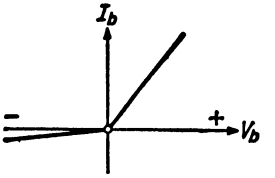

FIG. 190 Crystal detector operating characteristic showing d.c. as dependent on applied voltage V_b.

With noise, too, the condition $Y_oZ_{in} \gg 1$ is of fundamental importance in obtaining low figures. Hence similar observations as were made above are pertinent to this case.

By the use of proper feedback we may try to increase the value of Z_{in}. As an example a subsidiary feedback triode circuit may be used

for this purpose, thus increasing the resonant impedance of the input circuit by regeneration. Obviously an increase of gain as well as a decrease of noise figure of the mixer stage may be obtained in this way under suitable conditions. As with all feedback circuits of this kind, the output noise figure of the mixer stage can never be lower than that corresponding to the triode oscillator stage used in the feedback circuit. Thus a reduction of mixer noise figure may only be obtained if and when the triode stage's figure is lower than the original mixer figure.

The diode mixer circuits under consideration are at present practically unrivaled as regards low noise figures at s.h.f. The use of velocity modulation tubes in first-stage amplifiers leads to far higher noise figures (references 252 and 372) but recently similar tubes called "traveling wave tubes" have been shown to yield noise figures as low as 10 at s.h.f. (reference 205).

REFERENCES: *205, 252, 273, 302, 372, 401.*

VI.2.44. Selection of tubes. Considering tubes for amplifier stages first, the two cases of relatively narrow-band and of wide-band amplification have to be discussed separately. With both types of amplification the relevant tube properties are: transadmittance (modulus), input impedance, and output impedance. Experiments have shown that the modulus of transadmittance does not vary considerably at increasing frequency with tubes of suitable construction and a similar conclusion applies to the input shunt capacitance C_{in} as well as to the output shunt capacitance C_{out} up to frequencies at which stage gain becomes too low for practical purposes. The input shunt resistance R_{in} as well as the output shunt resistance R_{out} are approximately inversely proportional to the modulus of transadmittance, other conditions remaining equal. This results from experimental (see Figures 141 and 142) as well as from theoretical data. Furthermore, both resistances are inversely proportional to the square of the frequency of operation within a large range of practical importance. Thus they may be expressed by:

$$\frac{1}{R_{in}} = |Y|(t_{in}f)^2 \quad \text{and} \quad \frac{1}{R_{out}} = |Y|(t_{out}f)^2, \qquad \text{(VI.2.44}a\text{)}$$

t_{in} and t_{out} denoting time values dependent on tube construction. Their order of magnitude is usually about 10^{-9} secs.

The predominant data of an amplifier stage are: band width B and frequency f round which this band width is centered. Starting from these data, it is evident from the gain curve of Figure 132 that the highest gain obtainable with any particular tube corresponds to the case that gain is practically independent of frequency, i.e., to the conditions of what was termed wide-band amplification:

$$2\pi BC_{in}R_{in} \gg 1 \quad \text{and} \quad 2\pi BC_{out}R_{out} \gg 1, \qquad \text{(VI.2.44}b\text{)}$$

the second condition being in most cases satisfied if the first is. Hence we should try to select a tube satisfying the conditions (b) at the given frequency f of operation. If no such tube is available, the type of tube with which these expressions have the largest values will be the most suitable, i.e., will yield the highest stage gain. If the conditions (b) are satisfied, optimal stage gain is:

$$g = \frac{1}{4}\frac{|Y|^2}{(2\pi BC_{in})(2\pi BC_{out})}, \qquad \text{(VI.2.44}c\text{)}$$

and the multiplier $\frac{1}{4}$ may under favorable conditions become unity according to sections V.3.24 (see paragraph below Eq. (b) of that section) and IV.2.13. Of all the tubes satisfying the conditions (b), those having the highest value of:

$$\frac{|Y^2|}{C_{in}C_{out}} \qquad \text{(VI.2.44}d\text{)}$$

are the most suitable in obtaining high stage gain. This value of Eq. (d) thus constitutes a figure of merit for all the types of tubes satisfying Eqs. (b) at the given frequency f of operation. Now suppose that the latter frequency is so high or the band width B so narrow that no suitable tubes can be found satisfying the conditions (b). Suppose further that, instead of being large, the expressions of Eq. (b) are small compared with unity. Then the gain is, by Eqs. (V.3.24a) and (VI.2.44a):

$$g = \frac{1}{4}\frac{1}{(f^2t_{in}t_{out})^2}. \qquad \text{(VI.2.44}e\text{)}$$

Hence in this case the tubes having the lowest values of $t_{in} \times t_{out}$ corresponding to Eqs. (VI.2.44a) are the most suitable in obtaining a high

stage gain. The expression $1/(t_{in}t_{out})$ constitutes a pertinent figure of merit in this case, of which the highest values are the most favorable.

Turning our attention now to mixer stages, we have three predominant data determining stage performance: band width B and the frequencies f_{in} at the input and f_{out} at the output round which B is centered. Again we assume first that the conditions of Eqs. (*b*) are satisfied at the given values of f_{in} and f_{out}. Then stage gain is given by the equivalent of Eq. (*c*), replacing Y by the conversion transadmittance Y_{conv}, which bears a fixed relation to optimal transadmittance Y under proper conditions of mixer operation. Hence in this case the tubes having the highest values of the expression in Eq. (*d*) are the most suitable in obtaining a high stage gain. With some mixer stages the second condition (*b*) may be satisfied but the first condition (*b*) not, the expression $2\pi BC_{in}R_{in}$ being rather small compared with unity. Stage gain is then given by Eq. (V.3.24*c*) and the relevant figure of merit of the tubes in question is:

$$\frac{|Y|}{C_{out}t_{in}^2}. \qquad \text{(VI.2.44}f\text{)}$$

Finally, if both expressions of Eq. (*b*) are small compared with unity, we fall back upon Eq. (*e*) above and the pertinent figure of merit of the tubes at issue is $1/(t_{in}t_{out})$.

Of all the possibilities mentioned, the type of tube yielding the largest stage gain may not always be the most suitable owing to subsequent properties, of which noise is predominant, some other ones being distortion and applicability of a.v.c. As for noise, we shall assume that the gain of the entrance stage is sufficiently high to prevent the noise of the subsequent stage from being appreciable in the over-all noise figure of the set, which in this case coincides with the figure corresponding to the entrance stage. With this figure, only the part contributed by the entrance tube needs discussion here. Assuming the first condition of Eq. (*b*) above to be satisfied, that part, with amplifiers as well as mixers, is given by: $2\pi BC_{in}R_f$, according to Eqs. (VI.2.14*d*) and (VI.1.23*g*), R_f being the tube's noise resistance (see its definition in Eqs. (VI.1.23*f*) and (*h*)). The pertinent figure of merit of the tubes in question is hence R_fC_{in}, and this product should be as low as possible. If, however, the tube's contribution to total stage noise is already inappreciable, no attention needs be given to its further decrease.

If, instead of the first condition of Eq. (*b*) being satisfied, this ex-

pression is small compared with unity, we have to consider two cases: amplifiers and mixers. With triode amplifiers the results of sections VI.1.2 are pertinent. According to them, the lowest noise figure, at proper operating conditions, is obtained with tubes having the lowest value of a_o (see Eq. (VI.1.12*d*) and Fig. 151) if a cathode-base circuit is used and having the lowest value of b_o (see Eq. VI.1.22*c*) if a grid-base circuit is considered. We may translate these quantities into those familiar from the above discussion:

$$a_o^2 = \frac{T}{T_{in}} \frac{R_f}{R_{in}}, \quad b_o^2 \approx /+ f^2 t_{in}^2 + \cdots. \qquad \text{(VI.2.44}g\text{)}$$

The ratio T/T_{in} decreases at increasing cathode temperature. Assuming the latter temperature to be fixed, the remaining variable of a_o^2 is the ratio R_f/R_{in} which should be as low as possible. With grounded grid amplifiers the value of t_{in} (see Eqs. (*a*) of the present section) should be as low as possible, which condition is also conducive to a high stage gain. If tetrode or pentode amplifier tubes are used, the r.m.s. partition fluctuation current should be as low as possible compared with the r.m.s. cathode emission fluctuation current, subject, however, to conditions of satisfactory screening action (i.e., sufficiently low feedback capacitance) by the screen grid.

With mixer stages under the present conditions we may derive from Eq. (VI.2.14*c*) the condition that R_f/R_{in} constitutes a figure of merit as regards the noise contribution of the mixer tube. This ratio should be as low as possible.

With diode mixer tubes and crystals the discussion of section VI.2.43 already affords sufficient material pertinent to the selection of proper types and hence no further space need be devoted to that subject here.

Finally, a few words will be devoted to the selection of suitable triodes for oscillator purposes. If oscillation at an upper frequency f_o is required, the resonant frequencies of input and output electrodes (lead inductances together with interelectrode capacitances) are required to be higher than f_o using the oscillator circuit under consideration. Subject to these requirements the tubes showing the highest optimal stage gain at f_o under "narrow-band" conditions are in general the most suitable and may show the highest efficiency in an oscillator stage. This is also favorable as regards oscillator noise relative to the oscillator power output.

REFERENCES: *22, 354, 365, 367, 372, 398, 401.*

VI.3. Amplifier stages in which feedback is essential. The stages discussed in the preceding two sections VI.1 and VI.2 may be regarded as standard types of wide application. In some cases different stages have been applied, mostly with a view of obtaining simplified receiver sets, using fewer tubes and parts.

VI.3.1. Detector and reflex circuits. With the detector stages in question regenerative feedback is applied with a view of obtaining an increased stage gain. With the reflex circuits feedback is not, as a rule, regenerative but is such as to use one stage twice over for amplification of the same modulation at different carrier frequencies.

VI.3.11. Regenerative detector circuits. Regenerative feedback as a means of obtaining an increased gain is already familiar from preceding sections. In the present case such regenerative feedback is applied to an entrance stage incorporating a detector (rectifier) circuit for the demodulation of AM signals. A simple circuit of this kind is shown in Figure 191, the antenna being replaced by an input-current generator of infinite internal impedance supplying the current I. The input resonant circuit has a Q value equal to $\omega L/R$ and the tube is of transadmittance Y, assumed to be real. The input voltage V between grid and cathode of the tube in question (being supposed to be a tetrode) is given by the equation:

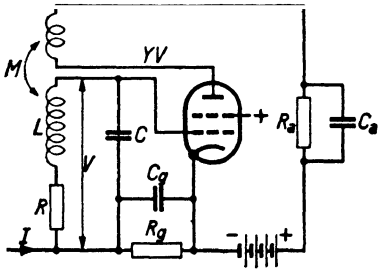

FIG. 191 Schematic diagram of regenerative detector circuit.

$$\mathbf{I}(j\omega L + R) = \mathbf{V}\{(1 - \omega^2 LC) + j\omega(CR - YM)\}, \quad \text{(VI.3.11}a\text{)}$$

M being the mutual inductance shown in Figure 191. If $\omega^2 LC = 1$ and simultaneously $CR = YM$, the feedback is indicated as being critical. By Eq. (a) the value of $\mathbf{V}$ would then become infinite at finite values of $\mathbf{I}$. But at the ensuing high input voltage levels the transadmittance Y is no longer independent of this input voltage. We have seen in section VI.1.42 that the transadmittance is in this case given by

$$Y = Y_1 - Y_3 |V|^2 + \cdots, \quad \text{(VI.3.11}b\text{)}$$

the sign of the second term being in most cases negative (this was

immaterial in Eq. (VI.1.42*a*)) at high values of Y. Inserting the transadmittance of Eq. (*b*) into Eq. (*a*) and applying critical feedback corresponding to the conditions: $\omega^2 LC = 1$ and $CR = Y_1 M$ we obtain approximately, if $Q = \omega L/R \gg 1$:

$$\mathbf{I}\omega L = \omega Y_3 M \, |V|^2 \mathbf{V} \quad \text{or} \quad \frac{|V|^3}{|I|} = \frac{L}{Y_3 M}. \qquad \text{(VI.3.11}c\text{)}$$

Without feedback ($M = 0$) the resulting grid input voltage works out as:

$$\left|\frac{V'}{I}\right| = \frac{L}{CR} = \frac{Q}{\omega C}. \qquad \text{(VI.3.11}d\text{)}$$

Hence we obtain the fundamental equation:

$$\frac{|V|^3}{|V'|} = \frac{CR}{Y_3 M} = \frac{Y_1}{Y_3}, \qquad \text{(VI.3.11}e\text{)}$$

expressing that the third power of input voltage including critical feedback is directly proportional to the input voltage without feedback. The ratio of input voltage, including feedback, to input voltage without feedback is thus dependent on the input voltage level in question. As a practical example we may assume Y_1/Y_3 to be, e.g., 10 (volts)^2. Then if $|V| = 100$ m volts the said ratio is 1000, and if $|V|$ is 100 microv. the ratio becomes 10^9. Thus a very considerable extra gain may be obtained by the present application of feedback.

The input signal, if of AM type, is demodulated by the grid circuit of Figure 191 (see section VII.1) and the modulation is amplified by the tube, resulting in a corresponding l.f. output voltage at the terminals of the resistance R_a in the tube's anode lead. The tube thus serves a double purpose: First, it provides a suitable means of obtaining feedback active at the h.f. input and, second, it serves as a low-frequency amplifier. As we shall see more elaborately in the succeeding section, such double usage of a single tube constitutes the main characteristic of a reflex circuit.

In the preceding discussion we have assumed the transadmittance Y, as well as its components Y_1 and Y_3, to be real for the sake of simplicity. At the present high frequencies this condition is, of course, not satisfied in many cases. But, if Y_1 as well as Y_3 are complex, a similar reasoning to the above one may be applied, involving no essentially new arguments. If $Y_1 = Y_{r1} + jY_{i1}$, the conditions of

critical feedback are: $1 + \omega Y_{i1} M - \omega^2 LC = 0$ and $CR = Y_{r1} M$. A slight alteration of the equation for the ratio of input voltage including feedback to input voltage without feedback also results in the present case.

We shall devote a little more space to the circuit of Figure 191. From Eq. (*d*) it is apparent that a high input voltage without feedback is obtained using a high Q input circuit. Of course this is also conducive to a high input voltage applying feedback, according to Eq. (*e*).

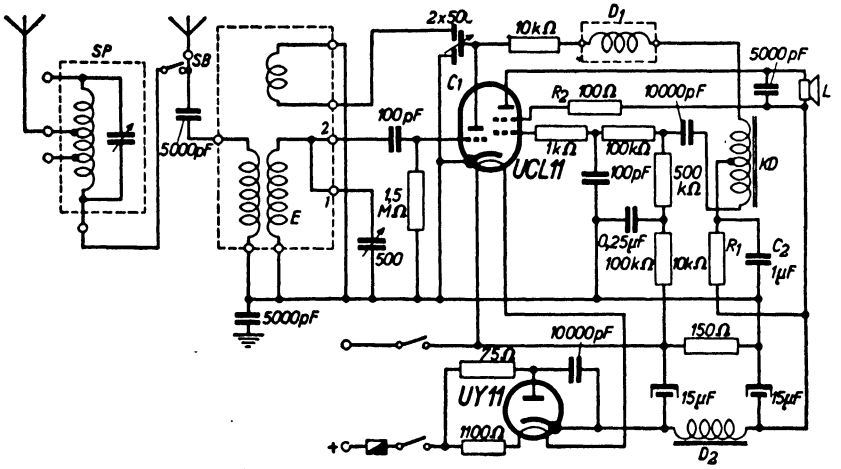

FIG. 192 Regenerative detector receiving set. Legend: *SP*, selector circuit; *SB*, switch; *E*, transformer; D_1, choke; *KD*, adjustable auto-transformer; D_2, l.f. choke.

The notion of noise figure being only applicable to *linear* devices according to section II.2, no direct evaluation of such a figure is obtainable in the present essentially non-linear case. We may state, however, that regenerative feedback by the use of a tube as in Figure 191 will in general tend to increase the available noise-to-signal ratio existing at the input terminals of the tube previous to feedback, as the tube represents an additional source of uncorrelated noise. Hence, though obtaining an increased gain, we cannot hope to obtain as low available noise ratios at the tube input terminals as with properly designed amplifier or mixer stages.

As an example of a complete all-mains (a.c./d.c.) receiver set using only two tubes in all and incorporating a feedback circuit as considered in Figure 191, we discuss Figure 192; this set. with suitable inductances.

is operative at about 6 to 20 mc/s. The antenna is connected to a selector circuit *SP*, which is switched off or on by means of the switch *SB*. The antenna coupling to the input resonant circuit is effected by means of a transformer *E*, while the feedback may be controlled by means of the variable condenser C_1. The tube of European type *UCL*11 shown is a triode-tetrode. The l.f. signal from the triode's anode is conducted across the choke D_1 for purification from h.f. components and is then connected to the iron-core autotransformer *KD* of controllable transformation ratio. The output l.f. voltage of this transformer is supplied to the control grid of the tetrode. Upon l.f. amplification the l.f. signal from the anode of the tetrode is fed to the loudspeaker *L* shown in the figure. The magnitudes of the various element parts are indicated (except the h.f. coils), D_2 being a choke used in the power supply unit (see section VII.4). The set's sensitivity may be of the order of 100 microvolts, full output being obtained at this input.

VI.3.12. Reflex circuits. As already mentioned, reflex means the multiple use of the same tube for amplification at different carrier frequencies. A simple example has been dealt with in Figures 191 and 192, the first carrier frequency being the h.f. input frequency and the second carrier frequency (subsequent to demodulation) being zero with sound modulation. The multiple use of a tube produces a number of extra circuit problems, resulting from the necessity of obtaining a proper separation of the different carrier frequencies in question. By the non-linearity of tube performance several possibilities of interaction between the different signals following the same tube path may be created. Assuming the two signals in question to be a h.f. AM signal and a l.f. signal, we shall consider two interactions: First, disturbance of the h.f. by the l.f. signal, and second, disturbance of the l.f. by the h.f. signal. In this discussion account must be taken of the l.f. signal's being, in most cases, of much higher voltage at the tube's input terminals than the h.f. signal. This condition is not satisfied with Figures 191 and 192, where both signals are of equal magnitude. Assuming the said condition to be valid, the disturbance of the h.f. by the l.f. signal will often be much more serious than the inverse disturbance. That disturbance essentially takes the form of a disturbing modulation which is additional to the already existing modulation of the h.f. signal. The disturbing modulation entails modulating frequencies equal to those of the l.f. signal as well as multiples of these

frequencies. By the former frequencies an increase or a decrease of the original AM of the h.f. signal may be caused, depending on the relative phase angles of the disturbing modulation with respect to the original modulation. By the latter frequencies distortion of the resulting demodulated l.f. signal arises. Hence this disturbing modulation should be avoided as far as possible. Means to this effect are: First, the use of a tube of the remote cut-off type and of gradually sloping

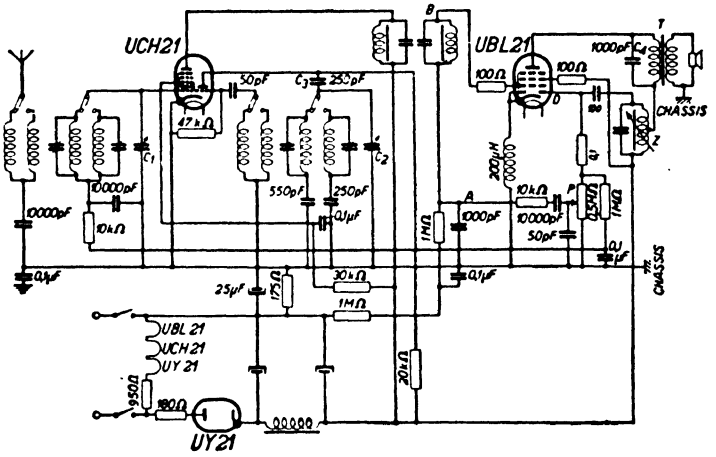

FIG. 193 Diagram of a reflex receiving set using a triode-heptode tube UCH21 and a twin-diode-pentode output tube UBL21 (European types). For description of operation see text.

anode current versus grid bias curve. Second, a decrease of the l.f. signal at the tube's input terminals. The latter means is, of course, in contrast to the chief aim of reflex circuits, consisting in the creation of large gain using only few tubes.

As an example of a reflex receiving set, the diagram of Figure 193 will be discussed briefly. This diagram contains two amplifier tubes (*UCH*21 and *UBL*21) and a power supply rectifier (*UY*21), the set being of all-mains (a.c./d.c.) type and suitable at two wave ranges, e.g., 6–20 mc/s and 2–6 mc/s. The antenna coupling to the input resonant circuit is effected by means of a transformer (see Fig. 145*e*). The heptode part of the tube marked *UCH*21 is used as a mixer tube, the oscillator stage incorporating the triode part of the said tube. The i.f. signal from the anode of the mixer tube is connected to the entrance of a set of two coupled i.f. resonant circuits. From the output terminals of this

coupling set the i.f. signal is conducted to the control grid of the tube *UBL*21, a double-diode-pentode, thus serving as an i.f. amplifier in the first place. The l.f. output transformer T is bypassed by the condenser C_4, thus allowing the amplified i.f. signal to be fed to the diode D via the i.f. circuit Z and a condenser of 100 pF. In the diode circuit demodulation of the AM i.f. signal is obtained, and the resulting l.f. signal of the diode stage is conducted via the potentiometer P and via A and B to the control grid of the pentode part of the tube *UBL*21. This tube thus serves in the second place as a l.f. amplifier (reflex). The l.f. signal from its output is fed to the loudspeaker via the l.f. transformer T. As a special measure counteracting possible non-linear interaction of l.f. and i.f. signals in the tube *UBL*21, a choke of 200 μ henry has been inserted into its cathode lead. This choke effects a degenerative feedback promoting linearity in the i.f. amplification by the said tube. The entrance part of this set being a normal multigrid mixer stage, its noise figure may be of the order of magnitude of 20 if constructed properly.

VI.3.2. Super-regeneration. Whereas the regenerative feedback discussed in section VI.3.11 was such that no actual oscillations ensued, the present application of feedback makes use of such oscillations as a means of obtaining an increased gain.

VI.3.21. Operation. The circuit of a super-regeneration stage bears some resemblance to that of Figure 191. The feedback is, however, in the present case over-critical, meaning $\omega^2 LC = 1$ and $YM > CR$ in Eq. (VI.3.11a). By this over-critical coupling oscillations are started in the resonant circuit; this process has been described in some detail in sections VI.2.31 and 32. The essential difference of the present super-regeneration from ordinary oscillation resides in a variable bias voltage being applied to the control grid of the tube in question. We shall suppose for simplicity that this bias voltage is made to vary between two fixed levels, the variations themselves being almost abrupt or at least taking place within time intervals, small with respect to the intervals during which the bias voltage remains at each of the two fixed levels. These levels are so chosen that oscillations are started at one of them but not at the other one, the transadmittance obtaining a too small value in the latter case (see Eq. VI.2.31a). The means of obtaining the said variations of bias voltage automatically will be dealt with later. As soon as the bias level conducive to oscillations is reached, oscillations will be started in the resonant circuit.

Two cases may arise: either a received signal acts on the said circuit or no such signal is present. Assuming the first case, the signal's carrier frequency is supposed to coincide approximately with the circuit's resonant frequency. The oscillator voltage across the tuning condenser of the resonant circuit will in this event rise approximately exponentially starting from a level corresponding to the value of the input signal voltage, the exponent in question being $\omega_o t/2Q$, Q representing the resonant circuit's quality and ω_o its resonant angular frequency. Now the bias variations mentioned above are timed such that the low bias level comes into effect shortly before the oscillation voltage has grown to its ultimate value, discussed in sections VI.2.31 and 32. From the moment when this decrease of bias level occurs, the oscillator voltage decreases again, this decrease involving again approximately an exponential function of exponent $\omega_o t/2Q_1$, Q_1 being the circuit's quality under the present bias conditions. The bias level remains unaltered until the voltage level corresponding to the input signal voltage under the present conditions is obtained. Then the bias is again varied to its high level, exciting oscillations, and the entire process starts over again. Referring to the circuit of Figure 191, the oscillator voltage amplitude between grid and cathode roughly rises and falls according to the upper full enveloping curve of Figure 194, the lower full curve representing the abrupt variations of bias voltage. The second upper curve corresponds to an initial input signal voltage of smaller amplitude than the upper former curve.

By the action of the grid leakage resistance R_g and of its bypass capacitance C_g the individual oscillations of voltage between grid and cathode are flattened out and only slow variations of oscillator amplitude are registered by the d.c. flowing through R_g. Thus a voltage is created at the grid, approximately given by the surface area enclosed by the enveloping upper curve of Figure 194. At a lower level of initial input voltage the surface area is smaller, as indicated by the second upper curve. The final value of oscillator amplitude is reached later in this case by a time interval Δt, approximately expressed by:

$$\frac{\omega_o \Delta t}{2Q} = \ln\left(\frac{V_{in}}{V'_{in}}\right), \qquad \text{(VI.3.21}a\text{)}$$

the input amplitude V_{in} being larger than V'_{in}. This time interval Δt represents a measure for the difference in grid voltages V_g obtained

in the rectification process corresponding to the input voltages V_{in} and V'_{in}:

$$\Delta V_g = \frac{\Delta t V_{max}}{2t_o}, \qquad \text{(VI.3.21}b\text{)}$$

V_{max} being the maximum oscillator voltage according to Figure 194 and t_o being the time during which the bias voltage is at its high level (see Fig. 194), this time being of sufficient duration for the oscillator voltage to reach V_{max} starting from V'_{in}. Assuming an AM input signal we have:

$$V_{in} = V_o(1 + m_a \cos \Omega t), \quad V'_{in} = V_o.$$

By inserting this into Eq. (*a*) and by series development of the logarithmic function we obtain:

$$\Delta t = \frac{2Q}{\omega_o}\left(m_a \cos \Omega t - \tfrac{1}{2}m_a^2 \cos^2 \Omega t + \cdots\right). \qquad \text{(VI.3.21}c\text{)}$$

Thus at small values of the AM coefficient m_a compared with unity, the voltage variations ΔV_g active between grid and cathode are approximately proportional to $m_a \cos \Omega t$ according to Eqs. (*b*) and (*c*), only the first term of the series in the latter equation then being involved. The other terms of this series give rise to distortions of the rectified signal if compared with the initial modulation. They may often be disregarded if $m_a < 0.5$.

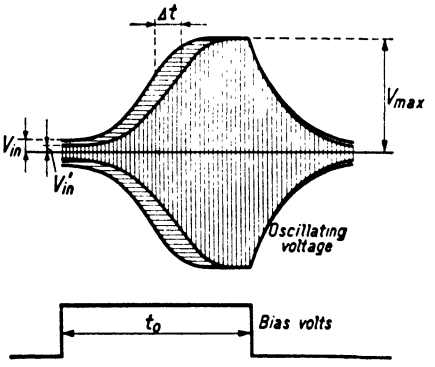

FIG. 194 Upper picture: Oscillating voltages ensuing from two starting levels, V_{in} and V_{in}' respectively, and finally building up to the same voltage V_{max}. Lower picture: Bias voltage as dependent on time, caused by quenching oscillator.

The rectified l.f. grid voltage is amplified by the same tube and gives rise to a corresponding voltage in the anode circuit, e.g., across R_a of Figure 191. Thus a reflex circuit is also involved in the super-regeneration under discussion, though this is not essential to the over-all operation.

We shall now devote some further discussion to the variations of bias level, essential in the operation of super-regeneration. These

variations are often carried out at a supersonic rate if the input signal has AM at sound frequencies. They may be achieved by means of a special oscillator operating at supersonic frequency. An approximately sine-shaped oscillator output voltage may be transformed into the abrupt voltage variations shown in the lower part of Figure 194 by means of a suitable transducer or the latter may be generated by a suitable RC-oscillator circuit. This transformation is, however, not essential, as the super-regenerative circuit will also operate at sine-shaped variations of bias voltage. These variations may also be created by the tube circuit itself. In this case we can make a useful application of the over-oscillation procedure described in section VI.2.32. If the half-period of these over-oscillations is made to coincide with t_o of Figure 194, the required periodic variations of bias voltage will occur automatically.

REFERENCES: *8, 184.*

VI.3.22. Gain and noise. From Eq. (VI.3.21*b*) we conclude that V_{max} and Δt should be as large as possible while t_o should be as small as possible in order to obtain an optimal value of ΔV_g. Hence t_o will preferably be chosen such that the voltage V_{max} is just attained starting from, say, V_o:

$$t_o = \frac{\omega}{\omega_o} \ln \left(\frac{V_{max}}{V_o} \right). \qquad \text{(VI.3.22}a\text{)}$$

The gain g of the stage in question will be defined as being the square of the ratio of ΔV_g at $\Omega t = \pi$ to $m_a V_o$. Thus:

$$g = \left\{ \frac{V_{max}/V_o}{2 \ln (V_{max}/V_o)} \right\}^2. \qquad \text{(VI.3.22}b\text{)}$$

As V_{max} is in most cases of the order of magnitude of some volts and V_o may be some microvolts, gains of 10^{10} are obtainable in a single stage by super-regeneration. The frequency f_b of the bias level variations is $1/(2t_o)$ and is often of the order of magnitude of the resonant frequency f_o divided by Q. Thus, if $Q = 100$ and $f_o = 300$ mc/s, we obtain $f_b = 3$ mc/s.

In order to satisfy the conditions underlying this operation of a super-regeneration stage, the value of the product $R_g C_g$ of Figure 191 must be such that $\Omega R_g C_g \ll 1$. This condition is imposed by the requirements of a proper detection process of the AM signal (see section VII.1). But $f_b R_g C_g$ must be large compared with unity in order to allow the enveloping voltage curve of Figure 194 to develop properly.

Thus f_b must be much larger than the highest frequency of modulation. This condition is not hard to comply with in the case of a u.h.f. carrier frequency.

The noise level with super-regeneration results largely from the initial noise voltage present at the terminals of the resonant circuit at the start of the high bias level period. If no input signal is present, fluctuation voltages of frequencies centered round the resonant frequency of the input circuit will start oscillations, the ultimate amplitudes of which will be of random magnitude, as are the initial voltages. If the signal voltage to be received by the stage in question is comparable with the r.m.s. fluctuation voltages at the start of the high level bias period, the ultimate voltages attained at the end of this period will also be of comparable magnitude. The noise figure of the stage may hence be calculated by evaluating the available noise power at the terminals of the resonant circuit at the starting instant mentioned above. This available power being $KT\Delta f$, the noise figure works out as unity. But in this reasoning the noise contributions by the tube have been disregarded. Taking them into account will probably result in noise figures of, say, 5 under appropriate conditions of operation. Figures like this may be considered as favorable in view of the particularly high gain involved.

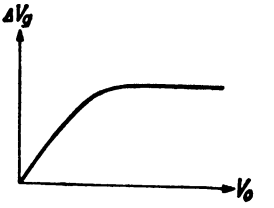

FIG. 195 L.f. voltage ΔV_g at output of super-regenerative stage as dependent on signal carrier voltage V_o at the input. Limiting effect of super-regeneration.

Finally we shall discuss a limiter effect, inherent to a super-regeneration stage under proper conditions of operation, assuming a fixed value of t_o. If an AM signal is present at the stage's input, the l.f. voltage ΔV_g at the tube's input terminals will increase at very small signal carrier input voltages until a value of the latter voltage occurs at which the ultimate voltage V_{max} is just reached during the fixed value of t_o. If the input carrier voltage is increased further, practically no corresponding increase of ΔV_g ensues, thus obtaining the curve shown in Figure 195. A super-regeneration stage has hence properties corresponding to an automatic volume control. This has been confirmed by experiments. The said property is similar to the action of a limiter stage (see section VII.2) in FM reception.

REFERENCES: *8*, *184*.

CHAPTER VII

FURTHER STAGES AND OVER-ALL DESIGN

Though the entrance stage of a receiver is doubtless the most important in many respects, including noise figure, its further stages also contribute materially to its over-all performance. Their detailed and comprehensive discussion is outside the scope of this book and many of them are familiar from the common radio set. But some stages merit discussion from the special viewpoint of ultra short wave reception and these will be considered here.

VII.1. Rectification (Detection) and Output Stages

When the signal has passed through mixer and amplifier stages, its modulation content must be separated from the carrier frequency. This is essentially the purpose of a detection stage. Upon detection the signal is made to pass through one or more output or "power" stages intended to supply the required signal power at the set's output.

VII.1.1. Rectification stages. Several types of rectification (detection) circuits have been proposed of which some will be treated here with a view of examining their properties for the present purposes.

VII.1.11. Diode rectification. The signals arriving at the entrance of a rectification stage are of AM type, other types of modulation of the received signals at the entrance of the receiver having been converted to AM prior to their arrival at the detector entrance. Two types of AM will be considered, single side-band signals and double side-band undistorted AM.

Dealing with the single side-band case first, we shall assume that only one single side-wave component is present and that its amplitude is small compared with the carrier amplitude. The received signal wave at the entrance of the set is usually not of this type. The presence of multiple side-frequency components need not be taken into account, as each component may be dealt with similarly to the single one considered here. If the carrier amplitude is not originally large compared with the side-frequency amplitude it will often be given relatively more

amplification (see section VII.3.2) in order to obtain the relationships mentioned above at the entrance of the detector stage. We shall further assume that the difference Ω between the angular frequencies of the carrier and the side-wave is small compared with the angular frequency ω_c of the carrier. This condition is in most cases satisfied at u.h. carrier frequencies. A diagram of a detector stage suited to these conditions is shown in Figure 196. The input resonant circuit is of resonant impedance R_{in} at the carrier's angular frequency ω_c as well as at the angular side-frequency $\omega_c + \Omega$. The bias resistance R and its bypass capacitance C are such that $\omega_c RC \gg 1$ and $\Omega RC \gg 1$. The output resistance R_1 and its bypass capacitance C_1 satisfy the conditions: $\omega_c R_1 C_1 \gg 1$ and $\Omega R_1 C_1 \ll 1$, this combination thus representing a nearly pure resistance R_1 at Ω. The l.f. transformer *tr* at the output is assumed to be of ratio 1 : 1, and reasonably free of losses, its aim being to prevent d.c. from passing through R_1. The transformer's inductance in conjunction with C_1 resonates neither at ω_c nor at Ω.

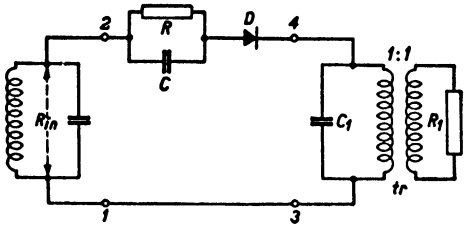

FIG. 196 Diode rectification (second detection) stage. Legend: R_{in}, resonant impedance of input circuit; R, resistor; C, bypass condenser; D, diode; *tr*, transformer; C_1, bypass condenser; R_1, output resistance.

Comparing the circuit of Figure 196 with the diode mixer circuit of Figure 176, all elements of the latter are seen to have corresponding counterparts in the former circuit (R_{out} in Fig. 176 corresponding to R_1 in Fig. 196), with the exception of the coupling coil for the oscillator voltage. In the present case we have originally to deal with two frequencies: carrier and side-wave, as with the said mixer, and the relationship of their amplitudes corresponds entirely to that between oscillator and input frequency in the mixer case. The two cases may indeed be treated in a similar way if we deal with the carrier voltage of Figure 196 as with the oscillator voltage of Figure 176. By the action of the carrier wave in combination with R and C, the diode's or crystal detector's admittance oscillates between almost zero and a maximum value, its dependence on time being similar to the Y curve of Figure 171 and its representation being given by Eq. (VI.2.21*a*), if ω_{osc} is replaced by ω_c. The theory of a diode mixer stage of section VI.2.21 may be

applied to the present case with only slight changes. In particular the gain g, meaning the ratio of the available l.f. power of angular frequency Ω at the terminals 3, 4 to the available power of frequency $\omega_c + \Omega$ at the terminals 1, 2 of Figure 196, is given by Eq. (VI.2.21c). It approaches unity under the conditions: $Y_o R_{in} \gg 1$ and $Y_1 \approx 2Y_o$. The latter condition requires the resistance R of Figure 196 to be large compared with the internal diode resistance (see section VI.2.21 subsequent to Eq. (a)). The signal as well as the noise issuing from the receiver's entrance stage(s) having gone through considerable amplification previous to the rectification stage in question, the additional noise caused by the latter stage may in most cases be disregarded. The noise arriving at the input terminals 1, 2 of Figure 196 together with the signal is detected similarly, and the gain relative to the available noise power is equal to that corresponding to the signal. Hence the available noise ratio at the entrance is equal to that at the output terminals 3, 4. The definition of this ratio in the present case is: ratio of available noise power in a relatively small frequency interval Δf centered round $\Omega + \omega_c$ to available signal power at $\Omega + \omega_c$ in the entrance case and both powers being centered round Ω at the output.

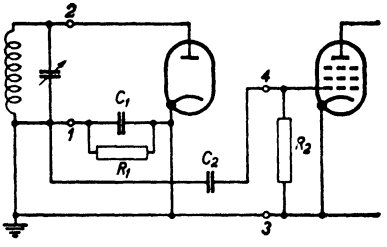

FIG. 197 Diode detector stage connected to a subsequent l.f. amplifier stage.

We now come to the detection of AM signals of symmetric and undistorted double side-band modulation. If the carrier amplitude were large compared with the side-wave amplitudes, the operation of a suitable diode detector stage could be discussed on the basis of a mixer stage under image-response conditions. But in most cases this condition is *not* satisfied and we shall hence not introduce it. A common diode detector circuit is shown in Figure 197, the input terminals being 1, 2 and the output terminals 3, 4, connected to the input terminals of the subsequent l.f. stage. Assuming an AM signal voltage at the input terminals 1, 2 given by the equation:

$$V_o\{1 + m_a \cos(\Omega t + \varphi)\} \cos \omega t$$

(see Eq. 1.2.21b), the values R_1 and C_1 of Figure 197 are required to satisfy the condition: $\omega R_1 C_1 \gg 1$, R_2 and C_2 satisfying the condition

$\Omega C_2 R_2 \gg 1$. In many cases we have also: $\Omega C_1 R_1 \ll 1$. Under these conditions we may discuss two cases: First, V_o large compared with $KT_c/e = V_T$, T_c being the cathode's temperature and e the electronic charge. Second, V_o small compared with V_T. In the first case the amplitude of the voltage of angular frequency Ω arising at the terminals 3, 4 is proportional to $V_o m_a$. In the second case it is proportional to $V_o^2\{1 + m_a \cos(\Omega t + \varphi)\}^2$. Hence the first case is indicated as "linear" and the second one as "square law" detection. In the second case we obviously meet with considerable distortion if m_a is not extremely small. Therefore the first case is preferable and conditions of operation should be chosen accordingly, meaning sufficient over-all gain of the stages preceding the detector.

VII.1.12. Equivalent networks and wide-band detection. Considering "linear" detection, we shall first discuss the equivalent impedance of the detector stage if viewed from the terminals 1, 2 and then its equivalent network at the output terminals 3, 4. The input impedance at the terminals 1, 2 is to be evaluated at the angular carrier frequency ω as well as at the two angular side-wave frequencies $\omega \pm \Omega$. At the carrier-wave frequency we may assume the shunt capacitance of the entire network to the right of the input resonant circuit of Figure 197 to be incorporated in the tuning capacitance of this circuit, tuned to the said frequency. Thus the detector circuit's input impedance at the terminals 1, 2 is a pure resistance at ω, and this resistance approaches $R_1/2$ if V_o becomes larger than 10 times V_T and if $R_2 \gg R_1$. At smaller ratios V_o/V_T it is smaller. At the two side-wave frequencies the input impedance consists of a shunt connection of a resistance with a susceptance, positive at the higher frequency and negative at the lower frequency. The resistance R_{in} in question is given by (see Fig. 197):

$$\frac{1}{R_{in}} = \frac{2}{R_1} + \frac{2}{R_2}. \qquad \text{(VII.1.12}a\text{)}$$

The shunt susceptance active at the angular frequency $\omega \pm \Omega$ is:

$$\frac{1}{X_{in}} = \pm \frac{\tan \psi}{R_{in}}, \qquad \text{(VII.1.12}b\text{)}$$

ψ being the phase delay of the input modulation current with respect to the corresponding voltage, the upper and lower sign corresponding to $\omega \pm \Omega$ respectively. Thus we obtain the equivalent input networks

pictured in Figure 198, the diagram *a* pertaining to the carrier ω (if $R_2 \gg R_1$ in Figure 197) and *b* to the side waves $\omega \pm \Omega$.

If wide-band detection is considered, the diode's characteristic curve (i.e., d.c. versus bias voltage) may often be approximated by a straight line of slope $1/R_i$ (compare the similar reasoning of the preceding section VII.1.11). Applying this approximation, the above Eqs. (*a*) and (*b*) are valid if R_1 and R_2 are large compared with R_i, e.g., $R_1 > 100\,R_i$. At the output terminals 3, 4 of Figure 197 the detector circuit may be represented by a constant l.f. voltage generator of voltage V_{out} and of zero internal impedance, acting in series with a resistance R_s on a shunt connection of R_1, R_2, and C_1 (see Fig. 199). The capacitance C_2 of Figure 197 is assumed to satisfy the conditions: $\Omega C_2 R_2 \gg 1$, $\Omega C_2 R_1 \gg 1$, necessary to the validity of the shunt connection of R_1, R_2, and C_1 in Figure 199. The expression for V_{out} is:

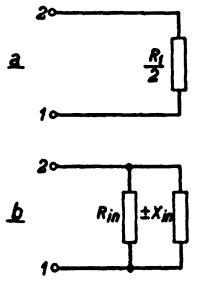

FIG. 198 Substitute diagrams at input terminals 1,2 of diode detector stage (see Fig. 197). Diagram *a* is valid for carrier frequency and diagram *b* at the side frequencies.

$$V_{out} = m_a' V_o. \qquad \text{(VII.1.12c)}$$

The ratio of m_a' to m_a is shown in Figure 200 for the linear detector under discussion as dependent on the ratio R_1/R_i if $R_2 \gg R_1$. The ratio m_a'/m_a is hardly different from unity if R_1/R_i is larger than, say, 50. Furthermore, the value of R_s of Figure 199 may also be obtained from Figure 200 if $R_2 \gg R_1$. It is seen to become small compared with R_1, if R_1/R_i is increased beyond, say; 50. We have now all the elements necessary to a complete discussion of the circuit of Figure 197. The h.f. amplifier stage preceding the detector circuit shown in Figure 197 may be represented at its output by a voltage generator: $V_{in}\,(1 + m_{in} \cos \Omega t) \times \cos \omega t$ in series with a resistance R_a representing the output resistance of

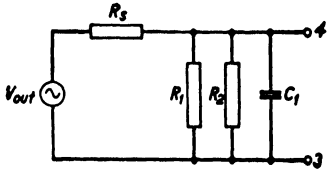

FIG. 199 Substitute diagram at the output terminals 3,4 of diode detector stage (see Fig. 197).

the preceding tube circuit. Assuming the resonant impedance of the tank circuit shown in Figure 197 to be R_{res} and its tuning capacitance to be C_t, we obtain a change of AM coefficient from the original value m_{in} to m_a at the terminals 1, 2. This change is caused by the difference in

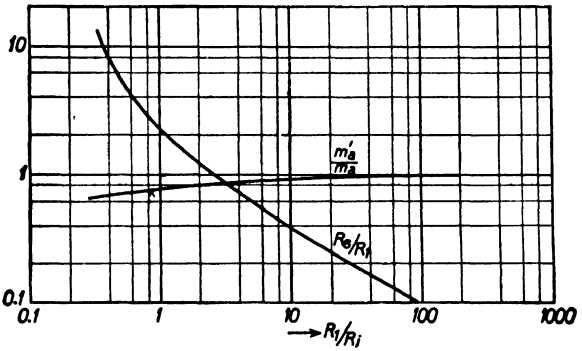

FIG. 200 Curves representing ratio of m'_a to m_a (see eq. VII.1.12c) and of R_s to R_1 (see Figs. 199 and 197) as dependent on ratio of R_1 to R_i, the latter being the diode's internal resistance.

input impedance at the carrier and at the side-wave frequencies (see Fig. 198). Thus (reference *301*):

$$m_a = m_{in} \cos\varphi \frac{R_{in}}{R_1} \frac{R_1 + 2R_{res}}{R_{in} + R_{res}},$$

$$\tan\varphi = 2\Omega \left(C_t + \frac{1}{\Omega X_{in}}\right) \frac{R_{res}R_{in}}{R_{res} + R_{in}}, \qquad \text{(VII.1.12d)}$$

$$V_o = V_{in} \frac{R_p}{R_a + R_p}, \quad R_p = \frac{R_{res}R_1}{2R_{res} + R_1}.$$

Inserting these values into Eq. (VII.1.12c) and Figure 199, the evaluation of the resultant l.f. voltage at the output terminals 3, 4 is a simple matter.

We shall now discuss some limitations imposed on the AM coefficient in order to avoid distortion. Considering Figure 201, the d.c. through the diode is shown vertically in dependence on the bias voltage active at the diode's electrodes (horizontal scale) at several values of the h.f. r.m.s. voltage $V_o/\sqrt{2}$ as indicated. If $R_2 \gg R_1$ and $\Omega C_1 R_1 \ll 1$, the ratio of l.f. instantaneous voltage at the diode's electrodes to the l.f. instantaneous current through the diode is R_1, and thus the straight

line marked R_1 in Figure 201 is in this case the locus of all corresponding points. But if the condition $\Omega C_1 R_1 \ll 1$ is dropped, the loci become approximately ellipses as shown. If the AM coefficient is such that the ellipse marked III is obtained, serious distortion would ensue, cor-

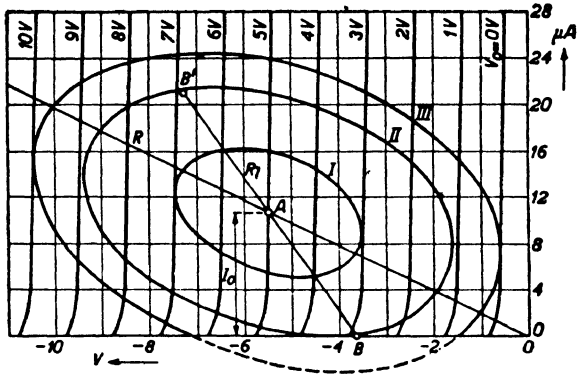

FIG. 201 Curves representing diode current (vertical scale expressed in microamps) as dependent on bias voltage (horizontal scale) at different amplitudes V_e of applied alternating voltage. The line OA corresponds to a load resistance R_l of 0.5 megohm. The three ellipses are loci of momentary corresponding l.f. voltage and current values, the coefficients of AM being 0.4 for curve I, 0.78 for curve II, and 1.0 for curve III. The line BAB' corresponds to a load resistance R_l which is smaller than R_l.

responding to the broken part of this curve, which is obviously not properly detected. The ensuing limitation is approximately:

$$m_a^2 (1 + \Omega^2 R_1^2 C_1^2) < 1. \qquad \text{(VII.1.12}e\text{)}$$

The three ellipses of Figure 201 represent the following AM coefficients: I: 0.4; II: 0.78; III: 1.0. Another limitation arises if the condition $R_2 \gg R_1$ is dropped, though $\Omega C_1 R_1 \ll 1$. In this case the straight line marked R_l in Figure 201 represents the locus of corresponding l.f. current and voltage values, R_l being the resistance resulting from the shunt connection of R_1 and R_2. If the AM coefficient is larger than that corresponding to a swing between the points B' and B of the said line, the ensuing l.f. voltage shows distortion. Referring to the internal diode resistance R_i, the maximum tolerable AM coefficient $m_{a\,max}$ is shown in Figure 202 for different values of R_l/R_1 as dependent on the ratio R_1/R_i.

With wide-band detection the application of diodes having small values of internal resistance R_i is essential in order to obtain an optimum

value of l.f. output voltage of the detector stage. This may be seen from Figures 199 and 200, R_s assuming considerable values in relation to R_1 if R_1/R_i is not large compared with unity and m_a' dropping far

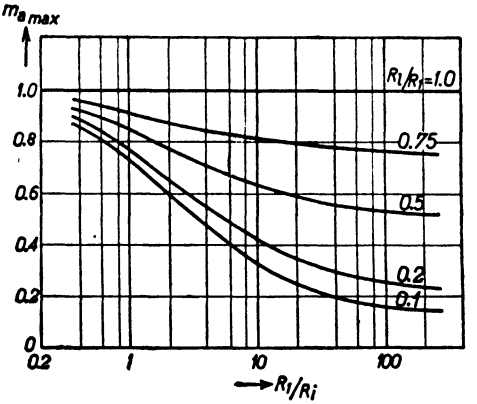

FIG. 202 Maximum admissible coefficient $m_{a\,max}$ of input AM of a detector stage as dependent on ratio of R_1 to R_i (see Fig. 200) for different values of the ratio R_l/R_1 (see Fig. 201 and text).

below m_a in this case. Now R_1 becomes rather low with wide-band detection, owing to the condition $\Omega R_1 C_1 \ll 1$, and thus R_i should be lower still in order to avoid loss of gain. As a simple example of this

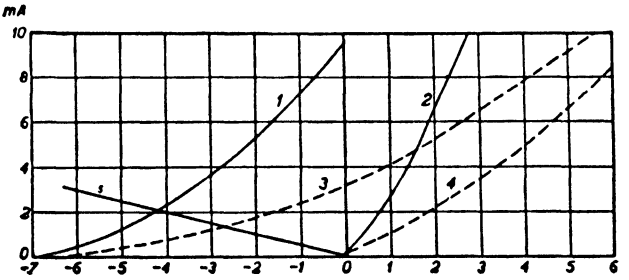

FIG. 203 Diode currents (vertical, expressed in milliamps) as dependent on bias voltage (horizontal scale). Curves 1 and 3 correspond to an applied a.v. of 5 volts r.m.s., the curves 2 and 4 to zero a.v. The straight line corresponds to a load resistance of 2000 ohms.

effect we consider Figure 203. The straight line shown corresponds to $R_1 = 2000$ ohms, while $R_2 \gg R_1$. The full and broken curves correspond to two different diodes, the former being a special wide-band

type and the latter a conventional r.f. tube type. With the curves 1 and 3 the r.m.s. voltage (unmodulated) active at the detector's entrance is 5 volts, with the curves 2 and 4 it is zero. The detected l.f. voltages result from the intersections of the straight line with the curves 1 and 3. Obviously the wide-band diode affords much better detection. Still, if R_1 were large compared with R_i, the optimum detected voltage would be approximately $5\sqrt{2} = 7.1$ volts, whereas it is only 58% of this value with the best diode shown and 37% with the conventional r.f. diode. The importance of low R_i values is thus stressed, keeping, however, the diode's shunt capacitance C as low as possible. Hence we have to resort to small interelectrode clearance in order to achieve the aim under discussion, i.e., optimal efficiency of detection, diodes of smallest product R_iC being most suitable.

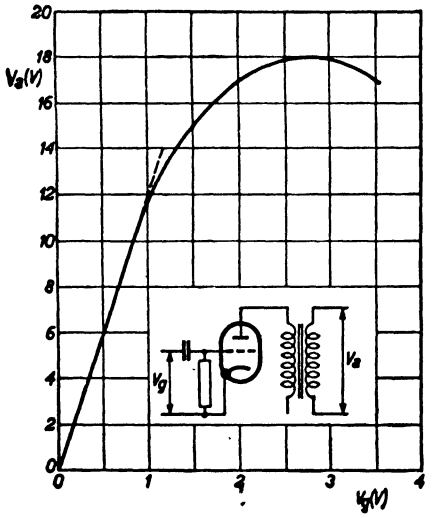

FIG. 204 Grid rectifier stage and corresponding rectification curve showing l.f. output voltage V_a as dependent on r.f. input voltage V_g.

REFERENCES: *301*, *359*.

VII.1.13. Grid and anode rectification. In some cases the control grid of a triode or multi-grid tube (tetrode or pentode) has been used instead of the diode in the preceding two sections. As an example, a corresponding diagram is shown in Figure 204, together with the detection curve of an AM input signal. The output voltage of the detector stage is nearly proportional to the input carrier voltage V_g within a limited range of input signal. Beyond this no proportionality exists and serious distortion may arise. The cause of this fact resides in the curvature of the anode current versus grid bias curve near cut-off bias voltages. This region of operation should therefore be avoided. With wide-band detection the internal resistance R_i corresponding to the grid-cathode space of the tube is in many cases too high to afford efficient undistorted detection (see end of preceding section VII.1.12).

Another mode of detection sometimes used tentatively is so-called anode-bend detection. Detection is in these cases mainly caused by the curvature of the anode current versus control grid bias curve. Owing to the nature of this curve the l.f. anode current I caused by a modulated input voltage between control grid and cathode is approximately proportional to the square of this voltage. Thus:

$$I \sim V_o^2\{1 + m_a \cos(\Omega t + \varphi)\}^2 = \tag{VII.1.13a}$$

$$V_o^2\{1 + 2m_a \cos(\Omega t + \varphi) + \tfrac{1}{2}m_a^2 + \tfrac{1}{2}m_a^2 \cos(2\Omega t + 2\varphi)\}.$$

This equation shows that the l.f. output voltage created by the l.f. current across a resistance in the anode lead is only approximately proportional to the modulation content of the input h.f. voltage, if the AM coefficient m_a is small compared with unity. The ratio of the output l.f. voltage of twice the AM frequency to that of simple AM frequency is $\frac{1}{2}m_a$. Thus distortion is considerable, if m_a exceeds, say, 0.2. For this reason anode-bend detection is hardly used if distortion matters, which is in most cases of sound and television detection. Only with some cases of IM detection—e.g., connected with radar—its application might lead to a slight simplification of the set, as the detection diode is eliminated.

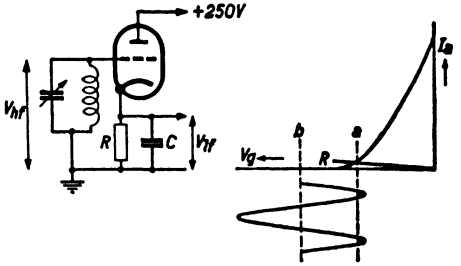

FIG. 205 Rectification (detection stage), the h.f. input voltage being V_{hf} and the l.f. output voltage V_{lf}. The diagram at the right pictures the stage's functioning.

By application of a special circuit, anode detection may be given similar properties as diode detection (Fig. 205). The cathode bias resistance R is chosen such that no grid current is caused even by large signal input voltages, while the bypass capacitance C satisfies the equation: $\Omega CR \ll 1$. If the input signal voltage is small compared with the cut-off voltage of the anode current versus grid bias curve (see Fig. 205), detection occurs at the point a of this curve and is caused substantially by curvature effects (see Eq. (a)) when distortion may be considerable. At large input signal voltages, however, detection

is linear and similar to that with a diode circuit. A corresponding signal voltage is shown in Figure 205 together with the locus of l.f. current and voltage values corresponding to a resistance R, this locus being a straight line in our curve diagram. Some experimental results obtained by application of the circuit of Figure 205 are shown in Figure 206. Two values of AM coefficient m_a are applied corresponding to the full ($m_a = 0.9$) and to the broken ($m_a = 0.3$) curves in the figure. The distortion squared d^2 is defined as the ratio of the sum of the squares of l.f. voltages of twice, three times, four times, etc., the fundamental AM frequency to the sum of the squares of all l.f. component voltages at the output. No appreciable advantage of this circuit in comparison with a suitable diode circuit is apparent whereas it may be at a disadvantage at wide-band detection, as R_i may be higher than with suitable diodes. Summing up, the methods of detection mentioned in the present section are hardly recommendable in general if compared with suitable diode detector circuits as discussed in the two preceding sections VII.1.11 and 12.

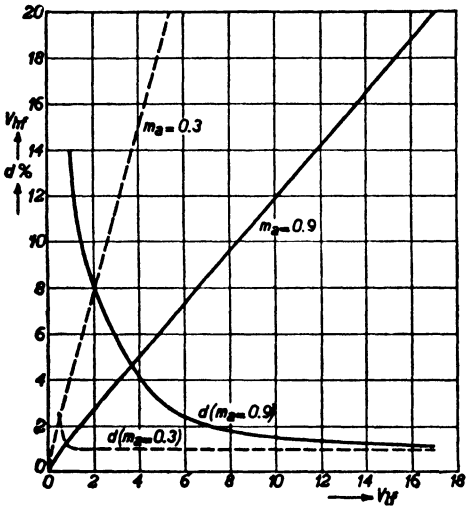

FIG. 206 Resulting detection and distortion of stage according to Fig. 205. Vertical scale represents h.f. input voltage as well as percentage d of distortion. Horizontal scale represents l.f. output voltage. Curves starting from zero are detection curves, other curves being distortion. Coefficient m_a of AM is indicated at each curve.

VII.1.2 OUTPUT AND VIDEO STAGES

This title is intended to cover all the stages of a receiver subsequent to the rectification or second detection stage as dealt with in section VII.1.1.

VII. 1.21. Operation. The stages in a receiver, subsequent to rectification, may be indicated as l.f. stages, implying that the lower

frequency limit of the band under amplification is adjacent to zero, being, e.g., 50 or 100 c/s. The upper frequency limit may be some 10 or 15 kc/s with sound stages and some 2 to 5 mc/s with video stages in television receivers, while values of about 1 mc/s are common with impulse receivers (e.g., radar). The stages in question may be classified as low-power stages directly succeeding the detector and a subsequent (or more) high-power stage (s).

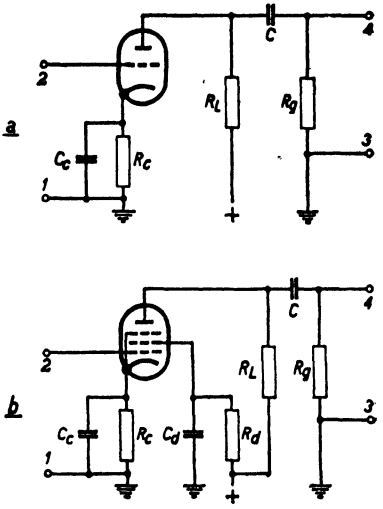

FIG. 207 Two conventional l.f. amplification circuits using a triode and a pentode respectively.

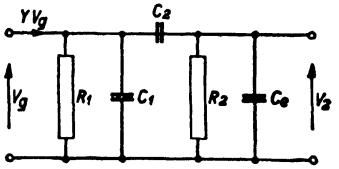

FIG. 208 Simplified amplification circuit, representing the tube by a current generator supplying a current equal to the product YV_g of tansconductance and input l.f. voltage.

In receivers RC coupling is in most cases applied between subsequent stages. Two conventional circuits suitable for sound amplification are shown in Figure 207. The values of the capacitances and resistances are subject to a number of conditions of which we quote the following, assuming ω_l to be the lowest angular frequency of the band under amplification:

$$\omega_l C_c R_c \gg 1, \quad \omega_l C_d R_d \gg 1.$$

Assuming the parallel connection of tube plate resistance and R_L to be equivalent to a resistance R_1 and the total shunt capacitance across R_1 to be C_1, the circuits under discussion may be simplified as shown in Figure 208, in which $\Omega C_c R_2 \ll 1$ at all frequencies within the band. The effect of the tube has been represented by a current generator YV_g, Y being the transconductance from control grid to anode and V_g the control-grid l.f. voltage. The voltage ratio V_2/V_g is shown in

modulus and phase angle in Figure 209, introducing the abbreviations:

$$\omega_u = \frac{1}{R_1 C_1}, \quad \omega_l = \frac{1}{R_2 C_2}, \quad y = \frac{\omega}{\sqrt{\omega_u \omega_l}}, \qquad \text{(VII.1.21}a\text{)}$$

ω_u being the upper and ω_l the lower angular frequency limit of the band under amplification. For television purposes the phase angle

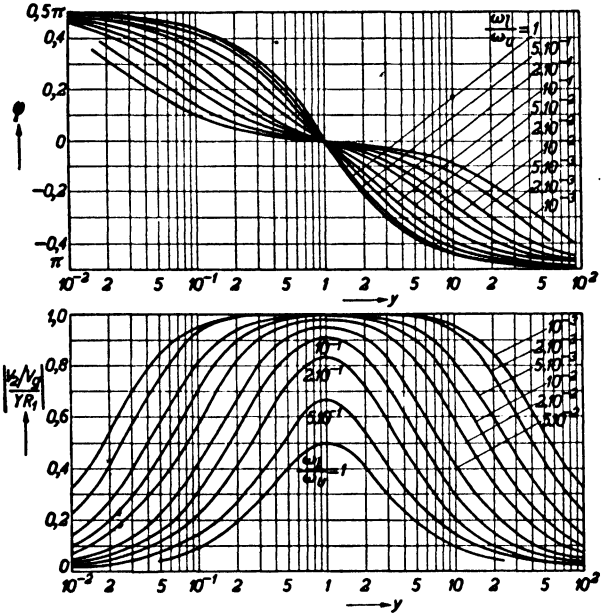

FIG. 209 Ratio of l.f. output voltage V_2 to input voltage V_g of an amplification stage according to Fig. 208 as dependent on y, this being the ratio of the operational angular frequency ω to $\sqrt{\omega_l \omega_u}$.

should be proportional to the frequency in the band at issue, which is approximately true in Figure 209. By Figures 207–209 it is simple to design suitable stages complying with given values of ω_u and ω_l. The distortion in impulse amplification using one and two subsequent amplifier stages of the type considered, is pictured in Figure 210. Assuming the impulse duration to be t_i, the product $\omega_u t_i$ should be large compared with unity, e.g., > 100, in order to obtain an undistorted impulse shape at the amplifier output.

With wide-band amplification, means for extending the amplified band width are required in some cases. Some corresponding interstage coupling networks are shown in Figure 211*a*, the network I being a simplified version of Figure 208, the lower angular frequency ω_l being

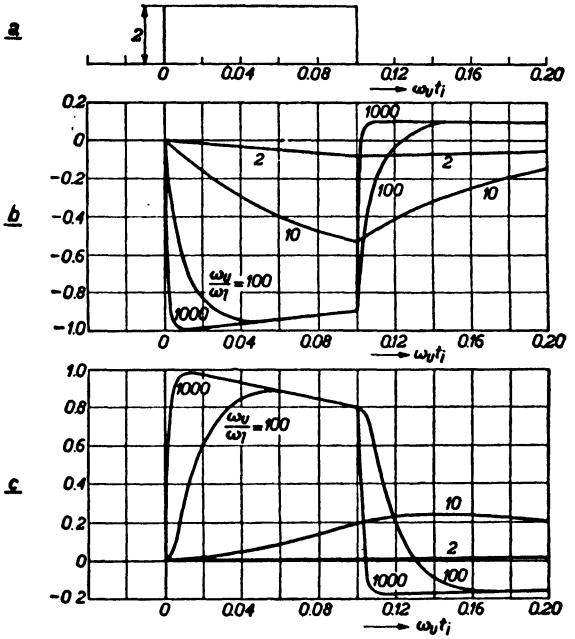

FIG. 210 Distortion of an input voltage impulse of exactly rectangular shape and duration t_i (diagram *a*) by an amplification stage according to Fig. 207 is shown in diagram *b* for four ratios of upper to lower border frequencies. Diagram *c* pertains to two equal subsequent amplification stages. Horizontal markings should be $\omega_l t_i$.

negligible with respect to ω_u. In Figure 211*b* the frequency responses of the networks of Figure 211*a* are shown. Thus the network V has a considerably extended response. Subjecting the networks of Figure 211*a* to a sudden rise of input current (corresponding to the start of an impulse), the resulting output voltage rise is shown in Figure 212. It is doubtful, from this Figure 212, if the network V is really better than I, considering impulse amplification. Thus improvements in frequency response need not necessarily lead to improved impulse response.

We now come to high-power output stages and their accessories. The power tubes of these output stages may be used in three ways,

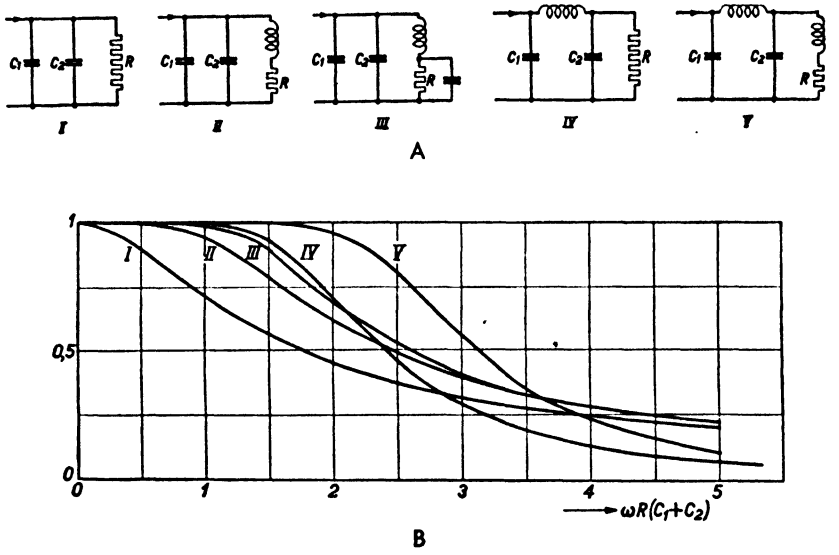

FIG. 211 The five diagrams of Fig. 211*a* represent common circuits for l.f. broad-band amplification, the entering current supplied by a current generator (arrows) being I. The corresponding ratios of output voltage V to IR (vertical scale, R see Fig. 211*a*) as dependent on frequency are plotted in Fig. 211*b*. Both figures taken from Philips techn. Rev. July 1941 pp. 196–197, paper by J. Haantjes.

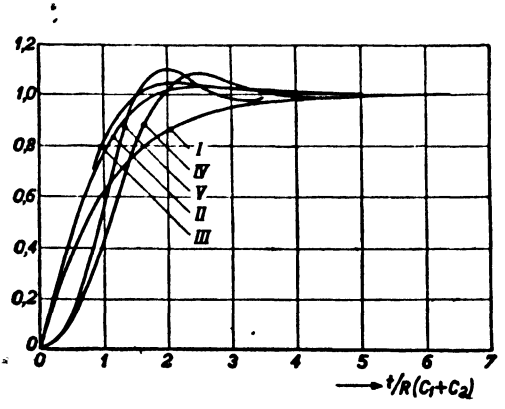

FIG. 212 If the input current rises abruptly from zero to I the ratio of output voltage V to IR (vertical scale) is dependent on time t (horizontal scale) as shown for the five networks of Fig. 211*a* (from same source as Fig. 211).

indicated as class A, class B and class A/B amplification and pictured in Figure 213. If two class B or A/B tubes are applied in a push-pull stage, the components of any even multiple of the input frequency cancel each other at the output (Fig. 214). This feature is greatly

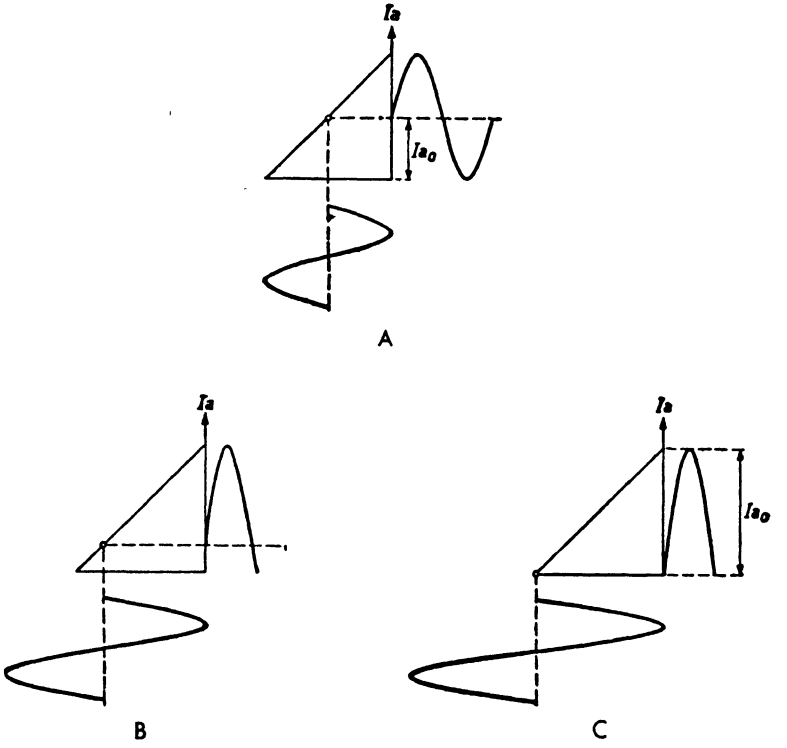

FIG. 213 Diagram *a*: Linear anode current (vertical scale) versus grid bias (horizontal scale) curve and alternating grid voltage corresponding to class A amplification. Diagram *b*: Similar to *a*, but corresponding to class *A*/B. Diagram *c*: Class *B*.

responsible for the application of such stages in order to minimize output distortion. Instead of a phase difference of 180 degrees as with push-pull stages, we may apply voltages to the input terminals of two tubes, having a phase difference of 120 degrees. In this case the output current components of 3, 6, 9, $\cdots$ times the fundamental frequency cancel at the output. This is shown in Figure 215 in the

case of the output current component of 3 times the fundamental frequency.

If triodes are used in the power stage, avoiding grid current, the relevant data are: top anode voltage V_{ao} and anode resistance R_a. If grid current is tolerated, the data are V_{ao} and $R_o = 2V_{ao}/I_a$, the value I_a indicating the top anode current at the highest (positive) grid voltage.

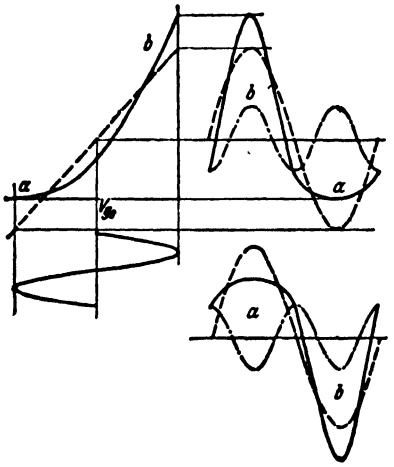

FIG. 214 Push-pull class A/B amplification. The resulting anode currents are pictured in the diagrams at the right. The broken curves correspond to a linear anode current versus grid bias curve and the full curves to a quadratic curve. The second harmonic anode current component causes an increase at *b* and a decrease at *a* in the latter case. The resulting second harmonics are counterphase and thus cancel each other at the output.

With pentodes, the relevant data are also V_{ao} and R_o. Three possible applications of two output tubes are shown in Figure 216: one single triode (or pentode), two tubes in parallel, and two tubes in push-pull connection. The consumer's resistance is indicated by R_l and its equivalent at the primary side of the output transformer by R. Optimal output power is obtained if R is matched to the effective output resistance of the tube combination under optimal conditions of operation. Efficiency is the ratio of optimal l.f. output power consumed in R_l to the supply power of the anode circuit. The said optimal conditions have been compiled in the table below:

CIRCUIT	R	OUTPUT POWER	EFFICIENCY
One triode class A, no grid current	$2R_a$	$V_{ao}^2/16R_a$	25%
One pentode class A, no grid current	R_o	$V_{ao}^2/2R_o$	50%
Two triodes parallel class A, no grid current	R_a	$V_{ao}^2/8R_a$	25%
Two pentodes class A, parallel	$R_o/2$	V_{ao}^2/R_o	50%
Two triodes class A, push-pull	$4R_a$	$V_{ao}^2/8R_a$	25%
Two pentodes class A, push-pull	$2R_o$	V_{ao}^2/R_o	50%
Two triodes class B, push-pull, no grid current	$2R_a$	$V_{ao}^2/8R_a$	39%
Two pentodes class B, push-pull	R_o	V_{ao}^2/R_o	78%
Two triodes class B, push-pull with grid current	R_o	V_{ao}^2/R_o	78%
One triode class A with grid current	R_o	$V_{ao}^2/2R_o$	50%
Two triodes class A, push-pull with grid current	$2R_o$	V_{ao}^2/R_o	50%
Two triodes parallel class A with grid current	$R_o/2$	V_{ao}^2/R_o	50%

If push-pull stages are applied, the preceding driver stage must provide proper push-pull input voltages for the output stage. In other words, it must act as a phase-inverter for one pair of the push-pull tube input terminals. Two circuits of this type are shown in Figure 217. In the diagram 217*a* the triode I acts as driver for one of the push-pull tubes while the triode II acts as a phase inverter. In the diagram 217*b* the triode *T* drives the push-pull tube *A* while the input voltage of the push-pull tube *B* is obtained from the output of *A*. In some cases a space-charge grid tube or a tube incorporating a secondary emission electrode have been used as drivers of a push-pull stage. The description of such stages is, however, outside the scope of this book.

REFERENCES: *27*, *86*, *226*, *302*, *303*, *335*, *374*, *381*.

VII.1.22. Microphonic and similar effects. As their name indicates, microphonic effects are caused by the action of mechanical motion—e.g., sound waves—on parts of a receiver, such as condensers, particularly tuning condensers, coils, tube bases, tube electrodes, transformers, resistances, switch gear, parts of the chassis, etc. By the motion of such parts small l.f. voltages may be set up at some electrodes of the set. Upon amplification these voltages may result in audible or visible (television) effects at the set's output. Mechanical action of this kind may be expected especially in sets installed in airplanes, cars, tanks,

vessels, etc. Its prevention calls for special constructional measures aiming at immunity of the parts mentioned against mechanical action. Such immunity may be promoted by rigid construction of the parts themselves and by screening from such action by the provision of proper

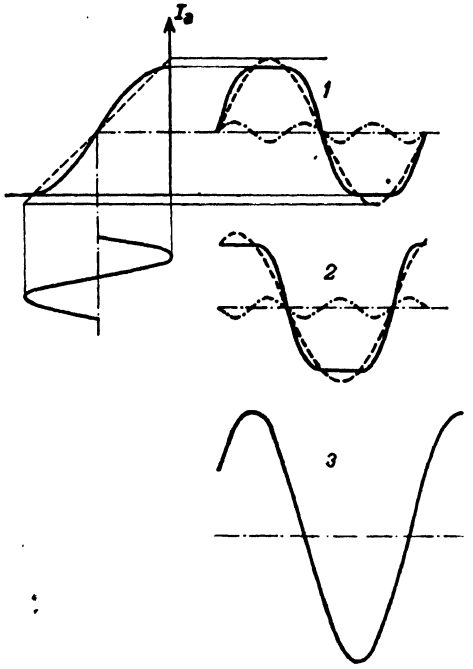

FIG. 215 Similarly to Fig. 213*a*, an anode current versus grid bias curve (left) causing third harmonic anode-current components resulting from a singly periodic input voltage is shown. If two tubes are used and the input voltages have a phase difference of 120 degrees, as shown in diagrams marked 1 and 2, the resulting output current (see diagram 3) is singly periodic, as the third harmonics cancel each other.

obstacles in its path. As an example we may mention: screening enclosures and acoustic insulation—e.g., by interposition of rigid walls separated by rubber cushions between the source of mechanical disturbances and the sensitive parts.

The effects mentioned may result in electro-acoustic feedback causing howling sounds in the loudspeaker of a sound receiver. Such sounds will probably be familiar to most users of short-wave sets. Even before howling—i.e. electro-acoustic oscillation—is started, regenerative electro-

acoustic feedback may result in effects somewhat resembling reverberation of the sound issuing from the loudspeaker. By resulting high l.f. voltage levels non-linear distortion may also be caused at some frequencies within the band transmitted. It is obvious that these

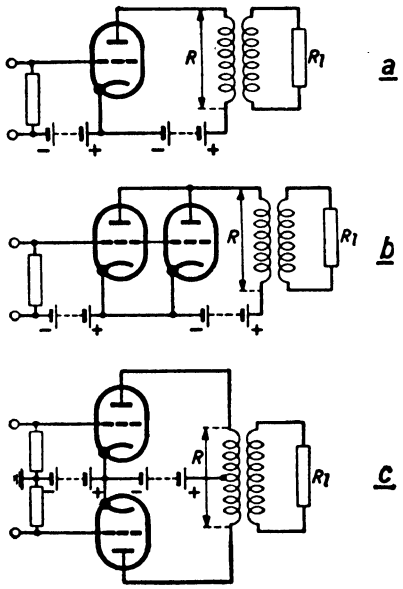

FIG. 216 Three diagrams of output stages. *a*: single tube; *b*: two tubes in parallel; *c*: two tubes connected in push-pull.

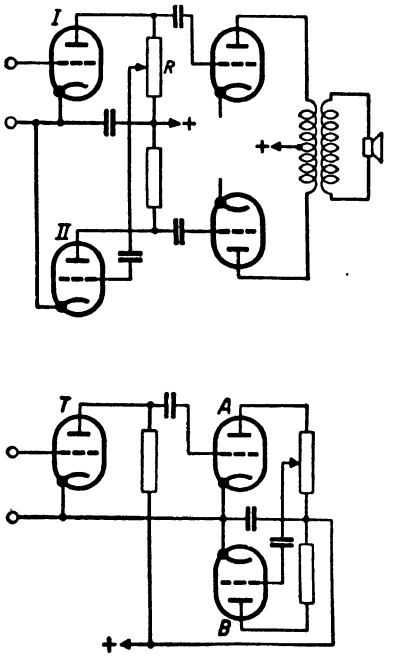

FIG. 217 Upper diagram: Pre-amplifier of a push-pull stage, the triode II acting as a phase reverser with respect to I. Lower diagram: Pre-amplifier of a push-pull stage, phase reversing of the input to the power tube *B* being obtained by deriving a suitable output voltage from tube *A*.

effects are in most cases undesirable and call for the provision of appropriate means for their prevention. In order to be able to judge the effects of such means quantitatively, a simple experimental procedure for their determination is needed. The loudspeaker Lou_1 belonging to the set in question (see Fig. 218) is disconnected from the output terminals 1, 2 of the set's output stage and is instead connected to a

suitable l.f. signal generator *SG*. The terminals 1, 2 are connected to an exactly similar loudspeaker Lou_2 placed outside the set and surrounded by a soundproof box *B* in such manner that no sound issuing from it can reach any part of the set. Then the signal generator *SG* is operated throughout the frequency range under consideration, the resulting input voltage V_1 of the set's loudspeaker Lou_1 being measured as dependent on frequency. By microphonic effects of parts in the set, a voltage V_2 will result at each frequency at the terminals of the auxiliary loudspeaker Lou_2. As long as V_2 is smaller in amount than V_1 no electro-acoustic oscillation or howling can occur. If, however, V_2 is larger in amount than V_1, such howling may occur, provided that a proper phase relation exists at the corresponding frequency between these voltages. As examples some experimental curves of this kind are shown in Figure 219. In the upper diagram the voltage V_2 is at all frequencies much smaller than V_1, and this set is quite safe as regards microphonic howling. But in the lower diagram the voltage V_2 is at some frequencies larger in amount than V_1. Actually, howling occurred with this set in the vicinity of 1600 c/s, as may be expected from the curves. Proper measures—i.e., acoustic screening of the set's parts from the sound issuing from the set's speaker—may be introduced and their effects may then be inspected by repetition of the experiment described.

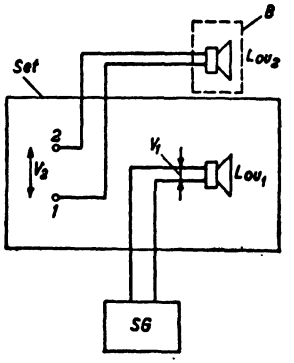

FIG. 218 Arrangement for measuring the microphonic level of a receiver set. Legend: *Lou*, loudspeaker; *SG*, signal generator; *B*, soundproof box containing Lou_2.

The parts that are in many cases responsible for the trouble under discussion are tubes, especially battery types in which the filaments may be susceptible to mechanical oscillation, tuning condensers, and iron-core transformers (osillations of plates). Modern tubes have been improved by their manufacturers and are in many cases safe, except if too large gain is applied subsequent to detection. The present trend to decrease the over-all size of tubes and hence also the electrode sizes, seems to be favorable as regards microphonic effects, the resonance frequencies being increased to higher values at which higher specific attenuation will tend to make resonances less harmful microphonically.

Besides electro-acoustic regenerative feedback, purely electric feedback may also occur at l.f. If part of the output l.f. voltage of a set or a stage is fed back to the input of a preceding stage, two cases may arise. If the preceding stage is of different frequency of operation —e.g., i.f. or h.f.—the feedback voltage arising at its input may cause additional modulation of its output signal. If the preceding stage is

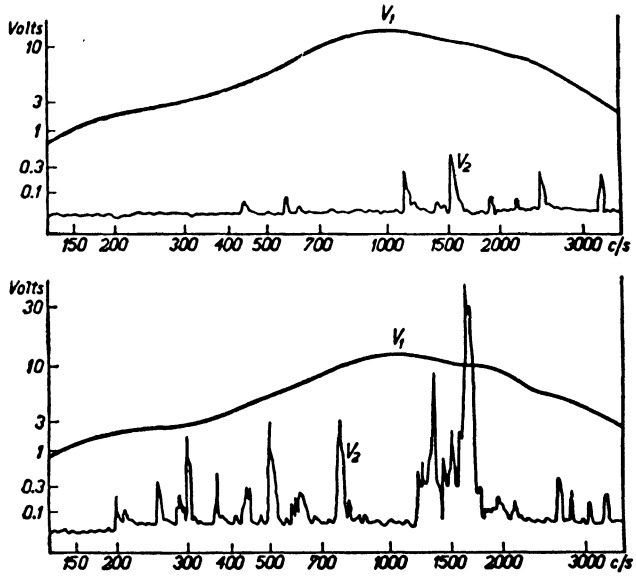

FIG. 219 Output volts V_1 at the terminals of Lou_1 of Fig. 218 and V_2 at the terminals of Lou_2, as dependent on frequency of modulation of input signal. Upper picture: Non-microphonic set, as V_2 is always smaller than V_1. Lower picture: probable microphonic action as V_2 is sometimes above V_1 (reference *302*).

of equal frequency, the feedback in question may cause oscillation as soon as the feedback voltage is of equal or larger amount than the original input voltage and at the same time of a phase favorable to regeneration. Effects of this type have been experienced in many cases, both stages in question being often of equal frequency. In some cases feedback occurs at extremely low frequencies, causing what is known as "motorboating." By cutting out such low frequencies from the band under amplification this effect may be stopped. As a general rule the avoidance or decrease of electric coupling between output

and input is a remedy against regeneration as considered. Such coupling may be due to stray capacitance between the output and input terminals in question, to stray mutual inductances, stray coupling by the use of common feeder lines and supply units, etc. By proper screening, applying screening cans and/or panels and by insertion of proper filter networks into the supply lines, such stray coupling may be effectively decreased. As an example we assume a l.f. amplifier having 1 k ohm resistance at its input and output terminals as well as a capacitance of 1 pF between both pairs. At 16 kc/s the feedback is about 10^{-4} in voltage ratio. This is equivalent to a gain of about 80 db. Hence the over-all amplifier gain, in order to avoid regeneration, may not be larger than this value. If the feedback is required to amount to less than 10% of over-all voltage amplification, the latter may not exceed 1000, corresponding to a gain of 60 db.

REFERENCES: *138, 280, 302, 304.*

VII.1.23. L.f. Noise output of a receiver. We shall assume that an AM signal of modulation coefficient m_a together with random noise of uniform distribution throughout the band width $2B$ are present at the entrance of the rectification (second detector) stage. Both signal and noise power are assumed to be such that noise contributions due to the detector or subsequent l.f. stages are relatively negligible. In the case of an FM receiver we shall assume that FM has been properly converted into AM in a converter stage preceding the detector stage. If m_a is fixed, we shall first examine the dependence of the output l.f. noise ratio on the input carrier voltage, assuming the input noise power to be small compared with the input signal power.

At small values of detector input signal voltage compared with $V_T = KT_c/e$ (see section VII.1.11), rectification takes place according to a square law, the current through the detector being proportional to the square of input voltage. The latter may be written as (see Eq. I.2.21c):

$$V_o \cos \omega t + \tfrac{1}{2} m_a V_o \cos \{(\omega + \Omega)t + \vartheta\} + \tfrac{1}{2} m_a V_o \cos \{(\omega - \Omega)t - \vartheta\} + v_{n1}\sqrt{\Delta f} \cos (\omega + \omega_1)t + v_{n2}\sqrt{\Delta f} \cos (\omega - \omega_2)t. \quad \text{(VII.1.23}a\text{)}$$

In this expression the fourth and fifth components of the sum denote noise voltages corresponding to a relatively very small frequency

interval Δf centered round the angular frequencies $\omega + \omega_1$ and $\omega - \omega_2$, which are within the band $2B$ under consideration. Squaring this expression, we need only take into account the resulting components of frequencies between zero and B. These are:

$$2m_a V_o^2 \cos(\Omega t + \vartheta) + 2V_o v_{n1}\sqrt{\Delta f}\cos\omega_1 t + 2V_o v_{n2}\sqrt{\Delta f}\cos\omega_2 t.$$

Only products of the carrier wave and of the other components of Eq. (*a*) have been taken into account. This implies that m_a is not too high—e.g., $m_a < 0.5$—thus justifying the neglection of products of side waves and noise and of noise-noise components. The first of these three components corresponds to the signal and the latter two to the noise. We may conclude that the output noise power of the detector is proportional to the input carrier voltage V_o squared, while the output noise ratio is expressed by:

$$\frac{2V_o^2\overline{v_n^2}2B}{2m_a^2V_o^4} = \frac{\overline{v_n^2}2B}{m_a^2V_o^2} = \frac{P_{in}}{m_a^2P_{is}}, \qquad \text{(VII.1.23}b\text{)}$$

$\overline{v_n^2}$ denoting the m.s. noise voltage amplitude, P_{in} the input noise power, and P_{is} the input signal power contained in the carrier wave. Thus the output noise ratio is $1/m_a^2$ times the input noise ratio if the latter is taken relative to the carrier wave.

We shall now examine the rectification of signal and noise if the former voltage is large compared with $V_T = KT_c/e$, thus considering linear detection. It is simple to show that the output noise power is in this case ultimately independent of the input signal voltage if the latter is large in relation to the r.m.s. input noise voltage. We may here refer to the discussion of linear single side-wave detection in section VII.1.11. Each noise component corresponding to a relatively small frequency interval Δf at the detector input may be regarded as a side wave to the carrier. Its corresponding output voltage is thus proportional to the input voltage and independent of the carrier voltage, which acts similarly to a local oscillator voltage. The same argument applies to the over-all output noise voltage. The dependence of l.f. output noise power on h.f. input carrier power of a detector stage is thus as follows: proportionality to the input carrier power at small values of the latter approaching independence of input carrier power if its value is increased steadily.

In evaluating the ratio of output noise power to output signal power with linear detection, the simplest assumption implies an ideal detector

circuit (see Fig. 198) in which $|X_{in}| \gg R_{in}$, $R_{in} = R_1/2$ and thus $R_2 \gg R_1$. The h.f. power delivered by the two side waves of an AM signal to the detector circuit is then approximately equal to the l.f. power consumed at its output, both being $m_a^2 V_o^2/2R_1$. Under these conditions it is reasonable to assume that the l.f. output noise power is approximately equal to the h.f. input noise power. Thus the ratio of l.f. output noise to signal power is approximately equal to the h.f. input ratio of noise to carrier wave power divided by m_a^2. This simple relationship will be approached with an ideal detector circuit at increasing values of input carrier voltage. An entirely adequate theory of l.f. noise ratio under less simple conditions is still somewhat lacking. Experimental evidence is in support of the said relationship, revealing deviations at lower input voltage levels, for which no completely adequate formulas have as yet been given.

REFERENCES: *23*, *121*, *289*, *302*, *391*.

VII.2. FM RECEPTION

The frequencies allotted to FM transmission are at present in the United States between 88 and 106 mc/s (see end of section I.2.32). Hence FM reception certainly comes into the scope of this book.

VII.2.1. Principles. The operation of FM receivers involves some stages that do not occur with sound or vision reception, and it is to these stages that special attention will be given in relation to the principles under discussion.

VII.2.11. Conversion and detection. Assuming an input FM signal expressed by (see Eq. I.2.21*d*):

$$A \cos\left\{\omega t + \frac{\Delta\omega}{\Omega} \sin(\Omega t + \vartheta)\right\}, \qquad \text{(VII.2.11}a\text{)}$$

$\Delta\omega$ being the angular frequency swing and Ω the angular frequency of modulation, Figure 31 shows that the most important side waves of the infinite number corresponding to the spectral representation of this FM signal are contained within a frequency band of width $\Delta\omega/\pi$ centered round the carrier frequency $\omega/2\pi$. If the modulation frequencies correspond to sound, $\Omega/2\pi$ may be up to, say, 15 kc/s. As will be shown later, a relatively large value of $\Delta\omega$ is favorable to the final quality of reception. A useful value is $\Delta\omega = 2\pi \times 75$ kc/s. The total required band width would then be somewhat larger than 150

kc/s and all the stages, including the antenna and transmission line, up to the first l.f. stage have to be designed in compliance with this band width. As pure FM is assumed, the magnitude of the instantaneous h.f. amplitude vector is independent of time (see Fig. 29). Such a signal cannot be directly detected by a linear or a quadratic detector (see section VII.1.1), as these devices act on differences in amplitude. Hence the FM must be converted into AM before such detection can be achieved. The corresponding converter stage has not been considered in this sense before, but we shall show that the circuit of Figure 184 may be applied for the present purpose if the resonant circuits are tuned to frequencies, distant slightly more than $\Delta\omega/2\pi$ on each side from the intermediate carrier frequency $\omega_i/2\pi$. In this case the resulting detected l.f. voltage V_d is shown in Figure 185. Obviously the FM is converted into AM and properly detected thereafter by this circuit. Different circuits have also been proposed for the present purpose, but the one of Figure 184 is adequate. The sequence of stages thus far discussed is hence: h.f. amplifier stage (may be left out), mixer stage, i.f. amplifier stage (s), converter-detector stage of Figure 184, l.f. stages, loudspeaker.

Considering the converter-detector stage of Figure 184 in greater detail, it is seen that an approximately linear dependence of the detected output voltage on the frequency difference Δf from the carrier frequency $\omega_i/2\pi$ (Fig. 185) requires the resonant frequencies of the two tank circuits of Figure 184 to be sufficiently removed from the latter frequency. If $\Delta\omega/2\pi$ is the frequency swing, these resonant frequencies may be situated at a distance $\Delta\omega/\pi$ on either side of the carrier frequency. The values Q_1 and Q_2 belonging to the two resonant circuits may be chosen to be both equal to $\omega_i/2\Delta\omega$ corresponding to the said distance of the resonant frequencies from the carrier frequency. The capacitances C and C_a may also be chosen to be equal, both being subject to the conditions: $\omega_i(R_1 + R_2)C \gg 1$ and $\Omega(R_1 + R_2) \times C \ll 1$. In a practical case (see section VII.2.2), when $\omega_i = 2\pi \times 2.1$ mc/s, the values of C and C_a may both be 50 pF while R_1 and R_2 may both be 100 k ohms.

REFERENCES: *7, 105, 314.*

VII.2.12. Noise figure of a FM receiver. It is important to be aware of the fact that the converter-detector circuit described in the preceding section VII.2.11 is insensitive to a pure AM input signal. The carrier

frequency of such an AM signal remains unaltered while its amplitude varies in accordance with the AM in question. Hence Δf in Figure 185 remains zero and so does the detected voltage V_d. For simplicity we assume the entire noise of the receiver to be issuing from a noise source at its entrance. Instead of a continuous noise spectrum we shall first discuss the disturbance caused by a single-frequency disturbing signal adjacent to the unmodulated carrier wave, the latter being $A \cos \omega_i t$ and the former $A_d \cos \{(\omega_i + \omega_d)t + \vartheta\}$ at the entrance terminals of the converter-detector circuit of Figures 184–185. Using the vectorial representation of Figures 27–28, the sum of these two signals is shown in Figure 220. From this picture we may conclude that the resulting wave is of the type indicated in section I.2.22 by the term "mixed modulation." If A_d is small compared with A, the phase angle ϕ of the carrier wave vector (Fig. 220) varies approximately according to $\phi \approx A_1 \sin(\omega_d t + \vartheta)$, A_1 being the ratio A_d/A. Hence the FM imparted to the carrier wave by the disturbance in question is $d\phi/dt \approx \omega_d A_1 \cos(\omega_d t + \vartheta)$. The AM of the carrier wave caused by the disturbance may be disregarded, as it does not result in a corresponding output voltage of the converter-detector. From Figure 185 we may conclude that the detected voltage is proportional to $\omega_d A_1$. The final band width of the receiver is $\Omega/2\pi$, if Ω denotes the highest angular modulation frequency under discussion. Thus we are interested in angular frequencies ω_d ranging from zero up to Ω. Assuming the relevant proportionality factor mentioned to be q, the power of the disturbing signal to be detected is: $q^2\omega_d^2 A_1^2$. Now the phase angle ϑ included in the above representation of the disturbing signal has a random character if the disturbance is due to fluctuation noise, the angular frequencies then being uniformly distributed over the range from zero to Ω. Thus the noise power to be detected is:

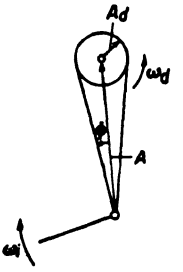

FIG. 220 A carrier wave of amplitude A and angular frequency ω_i modulated by a single side wave of amplitude A_d. If A_d is small compared to A, the result is almost pure FM.

$$\frac{1}{2\pi} A_1^2 q^2 \int_0^{\Omega} \omega_d^2 d\omega_d = \frac{1}{3} q^2 \left(\frac{A_1^2 \Omega}{2\pi}\right) \Omega^2.$$

If a pure FM signal of swing $\Delta\omega$ is present at the receiver's entrance, its power to be detected, on the same basis as the above noise, is expressed by: $q^2(\Delta\omega)^2$. Hence the relevant noise to signal ratio at the converter's input becomes:

$$\frac{1}{3}\left(\frac{A_1^2\Omega}{2\pi}\right)\left(\frac{\Omega}{\Delta\omega}\right)^2$$

The expression $(A_1^2\Omega)/2\pi$ represents the comparable ratio at the entrance of an AM receiver of effective band width $\Omega/2\pi$. Thus the ratio of the noise figure of a FM receiver of angular swing $\Delta\omega$ and top angular modulation frequency Ω to the noise figure of an AM receiver corresponding to the same modulation is:

$$\frac{N_{FM}}{N_{AM}} = \frac{1}{3}\left(\frac{\Omega}{\Delta\omega}\right)^2. \qquad \text{(VII.2.12}a\text{)}$$

This ratio of the two comparable noise figures may obviously be reduced by reducing the ratio $\Omega/\Delta\omega$. Unfortunately, the effective band width necessary for the FM receiver is about $\Delta\omega/\pi$ and thus a reduction of the ratio automatically implies an increase of this band width, as Ω is fixed by the nature of the transmitted information (e.g., sound). A useful proportion is $\Omega/\Delta\omega = \frac{1}{10}$ to $\frac{1}{5}$, thus causing a reduction in noise figure between 0.01 and 0.04 of the comparable value with an AM receiver.

In the above reasoning the disturbing signal and later the noise were superimposed on an unmodulated signal. If they are, however, added to a pure FM signal, an additional noise term crops up at detection using the device of the preceding section VII.2.11. This additional term results from the AM of the desired signal caused by the disturbance in conjunction with the corresponding FM. At the start of the present section we have mentioned that pure AM does not affect the converter-detector circuit under consideration, but the presence of such AM completely correlated to a corresponding FM does cause an output voltage of the circuit. This effective combination of AM and FM occurs only if the desired signal carries FM, and in that case the corresponding noise power to be detected on the same basis as the expression above is $q^2(\Delta\omega)^2/2$. Thus the ratio of noise figures as expressed by Eq. (a) must in this case be altered into:

$$\frac{N_{FM}}{N_{AM}} = \frac{1}{3}\left(\frac{\Omega}{\Delta\omega}\right)^2 + \frac{1}{2}. \qquad \text{(VII.2.12}b\text{)}$$

The reduction in noise figure to be effected by a suitable choice of the ratio $\Omega/\Delta\omega$ seems hence to be rather limited, as the resulting noise figure of a FM receiver would, in the most favorable case, be half of that of a comparable AM receiver.

REFERENCES: *77, 105, 314, 399.*

VII.2.13. Noise reduction. A reduction of the ratio of Eq. (VII.2.12*b*) may be effected in two different ways. In the first place, we may eliminate the AM (see Fig. 220) responsible for the second and largest noise figure contribution in that equation. This elimination of AM may be achieved by a stage known as a "limiter." In this stage the output voltage is of approximately unvariable level as soon as the

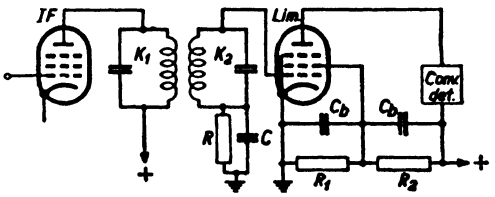

FIG. 221 Intermediate frequency stage *IF* and subsequent limiter stage *Lim* of a FM receiver, the next stage being a converter-detector. The resonant circuits K_1 and K_2 are coupled.

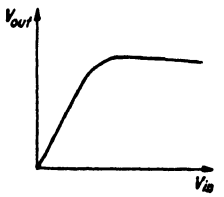

FIG. 222 Output voltage of a limiter according to Fig. 221 as dependent on its input voltage.

input voltage exceeds a definite amount. A suitable circuit effecting such limiter action is shown in Figure 221. By the leakage resistance R and bypass capacitance C, satisfying the condition: $\omega_i RC \gg 1$, a negative bias voltage is applied to the control grid of the pentode marked *Lim*, increasing at increasing input voltage amplitudes. Thus the corresponding transconductance and stage gain are effectively decreased at increasing input voltage levels and the output voltage remains at an approximately constant level if the input voltage amplitude exceeds a minimum value. A corresponding curve is shown in Figure 222. If this limiter stage is inserted before the converter-detector of Figure 184 the noise figure of the FM receiver corresponds substantially to Eq. (VII.2.12*a*), thus eliminating the term $\frac{1}{2}$ of Eq. (VII.2.12*b*).

The second means of achieving the same objective consists in the application of a suitable feedback. This feedback differs from the usual feedback affecting amplitude levels in a similar way as FM differs

from AM. It is effective through a variation of frequency of the local oscillator stage which is proportional to the frequency swing of the signal at the input of the converter-detector stage. With a FM input signal of angular carrier frequency ω modulated by a frequency swing $\Delta\omega$, the local oscillator is assumed to be of angular frequency ω_{osc} with a frequency swing $\Delta\omega_{osc}$. Thus the i.f. signal is of angular frequency $\omega_i = \omega - \omega_{osc}$ and of frequency swing $\Delta\omega - \Delta\omega_{osc}$. The detected signal is then of amplitude proportional to $\Delta\omega - \Delta\omega_{osc}$, and this is assumed to be equal to the oscillator's swing $\Delta\omega_{osc}$ divided by a multiplier α. Hence:

$$\Delta\omega_{osc} = \frac{\alpha}{1 + \alpha}\Delta\omega$$

and the detected signal amplitude becomes proportional to:

$$\Delta\omega\left(1 - \frac{\alpha}{1 + \alpha}\right) = \frac{\Delta\omega}{1 + \alpha}. \qquad \text{(VII.2.13}a\text{)}$$

If α is given a large value compared with unity, the oscillator swing $\Delta\omega_{osc}$ tends to become independent of α, while the detector's output voltage is divided by $1 + \alpha \approx \alpha$ according to Eq. (a). Referring to the argument preceding Eq. (VII.2.12b), we obtain a noise power corresponding to combined and correlated AM and FM of $q^2(\Delta\omega)^2/2(1 + \alpha)^2$ instead of $q^2(\Delta\omega)^2/2$. Hence Eq. (VII.2.12b) must in the present case be replaced by:

$$\frac{N_{FM}}{N_{AM}} = \frac{1}{3}\left(\frac{\Omega}{\Delta\omega}\right)^2 + \frac{1}{2(1 + \alpha)^2}. \qquad \text{(VII.2.13}b\text{)}$$

By a proper choice of frequency feedback the second term may thus be reduced until it becomes inappreciable and we fall back substantially upon Eq. (VII.2.12a). By the feedback in question the detected voltage becomes approximately independent of the input signal amplitude and hence the influence of fading on FM reception is also effectively reduced. A similar effect is obtained by the limiter stage, provided that its input signal exceeds a minimum level.

REFERENCES: *7, 59, 62, 105, 399.*

VII.2.2. Operation. In the present section the operation of FM receivers based on the principles discussed in section VII.2.1 will be considered in some detail.

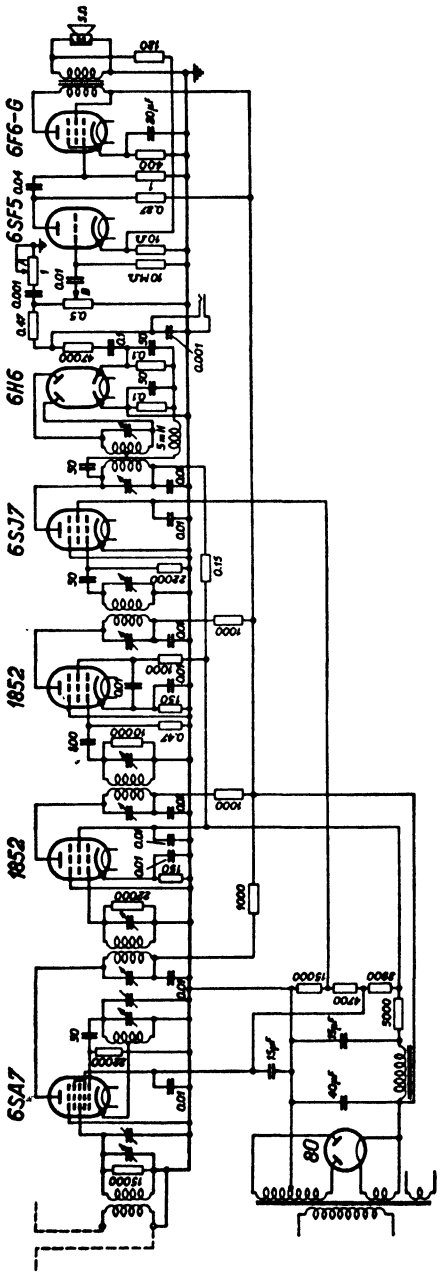

FIG. 223 FM receiver diagram. Tube types are indicated. Numbers of small values at resistors, e.g., 0.47 or 0.15 are megohms; larger values indicate ohms. Numbers of small values at capacitors are microfarads; larger values indicate micromicrofarads.

VII.2.21. Example and tests of a FM receiver. A complete FM receiver diagram including a limiter stage is shown in Figure 223. The entrance tube is a multi-grid mixer of the self-oscillating type (tube type 6SA7). The oscillator circuit is connected to the cathode and to the adjacent control grid, the subsequent screen grid being grounded. The input voltage is active between the screen and the subsequent second control grid, while a second screen connected to the first one, a grounded suppressor grid, and an anode complete the sequence of 7 tube electrodes. With the present receiver the input carrier frequency is about 40 mc/s while the i.f. is 2.1 mc/s. The mixer stage is succeeded by two i.f. amplifier stages (tubes 1852), interconnected by three sets of two coupled resonant circuits each. The band width corresponding to these i.f. stages is variable in order to accommodate different frequency swings between 15 and 75 kc/s. The next stage is a limiter (tube 6SJ7) corresponding to the diagram of Figure 221. Then comes the converter-detector stage corresponding to Figure 184, with the addition of a choke coil of 5 m henry, intended to reduce the damping of the coupled resonant circuits by the detector diodes (tube 6H6), having separate cathodes. Subsequent to this converter-detector stage are a l.f. amplifier (tube 6SF5) and output stage (tube 6F6G).

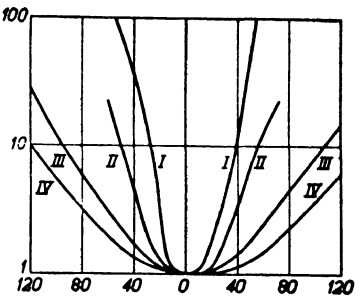

FIG. 224 Selectivity curves of the set of Fig. 223. Vertical scale: Required unmodulated input signal voltage for obtaining a definite fixed output level of the last i.f. stage (a.v.c. out of action) as dependent on frequency deviation from center position (expressed in kc/s). Curves I, II, III, and IV correspond to settings of 15,30,60, and 75 kc/s frequency swing.

Some tests were carried out using this receiver. In the first place some selectivity curves (unmodulated input signal voltage causing a fixed output voltage of the final i.f. stage, on a relative logar scale, versus input signal frequency) are shown in Figure 224. The curves marked I, II, III, and IV correspond to frequency swings of 15, 30, 60 and 75 kc/s. Using undistorted FM signals at the receiver's input, the l.f. output power contained less than 3% distortion at all bandwidth settings cited. The l.f. ouput power versus frequency curve is

flat within 6 db between 50 and 10^4 c/s. Frequency drift of the local oscillator was about 20 kc/s during an observation of 40 minutes after switching the receiver on. At an i.f. band width corresponding to a swing of 15 kc/s the set could be operated as an AM receiver by putting the converter-detector stage out of action and using the 6SJ7 tube as a grid detector (see section VII.1.13). Thus a comparison between AM and FM receiver performance could readily be obtained.

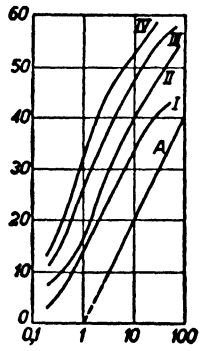

FIG. 225 Vertical scale: Ratio of signal sound output to noise output powers expressed in db. Horizontal scale: Ratio of input signal voltage to equivalent input noise voltage. Curves I, II, III, IV correspond to frequency swings of 15, 30, 60, and 75 kc/s. Curve *A* corresponds to an AM signal supplied to the same receiver, making suitable adjustments.

In order to check the noise reduction obtained by the application of FM, a noise source was used consisting of a three-stage amplifier of carrier frequency equal to the i.f. of the FM receiver (2.1 mc/s). By gain control of this amplifier its output noise could be varied. The output terminals of this noise source were connected to the input terminals of the first i.f. stage of the FM receiver. By comparison of its resulting detected grid current at the limiter stage with that caused by an input carrier wave of known strength at the receiver's input terminals, the equivalent r.m.s. noise voltage at these input terminals could be determined. Now the l.f. noise ratios at the receiver's output at different frequency swings (15, 30, 60, and 75 kc/s) of the FM input signals were measured and the curves of Figure 225 obtained. Its vertical scale corresponds to the inverse output noise ratio and its horizontal scale to the ratio of r.m.s. input signal voltage to equivalent input noise voltage. From this Figure 225 we may conclude that the reduction of noise ratio predicted by the arguments of the preceding section VII.2.1 is entirely confirmed by experiment, the output noise ratio being inversely proportional to the square of the frequency swing $\Delta\omega$. At 75 kc/s frequency swing the r.m.s. input signal at AM must be 40 times the value at FM by Figure 225. With the set of Figure 223, a l.f. output of 50 m watts may be obtained at about 10 microv. r.m.s.

input signal voltage. At this input signal level the output noise ratio is still of such low value as not to impair reception, which is in most cases not true with AM sets of similar sensitivity.

Besides spontaneous fluctuation noise, disturbances by impulsive noise (e.g., atmospheric or man-made noise) and by interfering stations must also be accounted for. Corresponding tests have shown that a noise reduction similar to that of Figure 225 may be obtained if the input noise power issuing from any source is more than about 6 db below the input signal power. With spontaneous fluctuation noise the ratio of top square to m.s. values may be assumed at about 13 db. With singly periodic signals this ratio is about 3 db. Hence, if the m.s. noise power at the receiver input is about 10 db below the m.s. signal power, the noise tops will be of about equal power as the signal. The full noise reduction expressed by Eq. (VII.2.12*a*) may be obtained if the mean input noise power is about 16 db or more below the mean input signal power. The power contained in sharply peaked impulses is proportional to the square of the effective band width rather than to the band width itself. Hence smaller values of impulse noise power per c/s are needed to reach the above limit than with uniform fluctuation noise. In the case of extremely strong spaced impulses, reception is practically interrupted during short time intervals due to the action of the limiter stage. Signal reception is also interrupted during such intervals, but the resulting effect at the loudspeaker is often less disturbing with FM than with AM reception.

By the noise-reducing qualities of FM reception the surface area round a transmitting station in which tolerable conditions of reception prevail, taking account of interfering stations and noise, is larger at a given value of transmitting power in the case of FM than with AM broadcasting. Hence, if a network of transmitters covering a given area is contemplated, FM is preferable from this point of view.

REFERENCES: *74, 75, 115, 179, 230, 259.*

VII.2.22. Distortion and receiver design. We shall first examine the distortion of FM signals due to the mixer and i.f. stages preceding the limiter and converter-detector stages. The distortion effects caused by these stages with AM have been dealt with in sections VI.1.42 and VI.2.13. All of these effects are related directly to the curvature of anode current versus grid bias curves of the tubes in question. By these curvatures the anode current contains components proportional

to the second, third, $\cdots$, etc., powers of the input grid signal, the latter being $V_o \cos \{\omega t + m \sin (\Omega t + \varphi)\}$. Examining powers of this expression, it is obvious that anode current components are created which are proportional to the expression itself, to $\cos \{2\omega t + 2m \times \sin (\Omega t + \varphi)\}$, to $\cos \{3\omega t + 3m \sin (\Omega t + \varphi)\}$, etc. But of these expressions only the first one is passed by the h.f. and i.f. circuits preceding and interconnecting the stages in question, while the other ones are suppressed and do not play any further part in the reception process. The amplitude of the first expression above is altered by the curvatures under consideration, but this amplitude does not play any essential part due to the effect of the limiter stage (or to the frequency feedback if no limiter is applied). Hence we may conclude that curvatures of mixer and i.f. tube anode current curves do not cause distortions with FM reception. In a similar way the conclusion may be reached that cross-modulation in the case of two adjacent input FM signals due to tube curvature effects is also absent. Interference effects may arise from two FM input signals of angular carrier frequencies ω_1 and ω_2 if for instance $q_1\omega_1 \pm q_2\omega_2 \approx \omega_1$, q_1 and q_2 being integral numbers. These interference effects are somewhat similar to those discussed in the case of mixer stages in section VI.2.13.

Besides the tubes, we have to discuss effects caused by the h.f. and i.f. resonant circuits. It is known that these circuits do not in general pass all frequency components of a FM signal uniformly. We have discussed the effect of such mutilations of FM signals in section I.2.21 in connection with Figures 30 and 31. It was shown that serious distortion of the signals may result from too narrow band widths of the h.f. and i.f. circuits. The following table gives a condensed picture

SIGNAL:	AM	FM
Resonant circuits cause:	no distortion	distortion
Tube curvatures cause:	distortion	no distortion

of the distortion effects involved in mixer and i.f. stages with AM and FM signals. The band width of interstage circuits of FM receivers should be such that practically all relevant components of the FM frequency spectrum (see Fig. 31) are passed uniformly. The corresponding band widths are larger than twice the frequency swing $\Delta\omega/2\pi$.

In the design of FM receivers we may start from the input signal voltage required at the limiter stage, assuming this stage to be present

instead of the more expensive frequency feedback circuit. This input voltage must be well above the minimum value at which limiter action starts (see Fig. 222). In a number of practical cases this required level may be assumed at about 5 volts. If this voltage corresponds to an input signal voltage at the receiver entrance of 10 microvolts, we must achieve a voltage gain of 5×10^5. The interstage i.f. coupling circuits may be assumed to have resonant impedances of about 15 k ohms at 150 kc/s band width. If pentodes of, say, 9 m mhos transconductance are applied, voltage gain per i.f. stage works out at 135, while the voltage gain of the mixer stage may be estimated at 10. Thus one mixer and two successive i.f. stages would be required preceding the limiter stage in order to fit the assumed figures, if a further voltage gain of about 3 is obtained by the h.f. circuit preceding the mixer stage. The selectivity of the i.f. circuits may be somewhat less than in comparable AM receivers due to the effective suppression of spurious signals and noise by the FM reception process. Frequency drift of the local oscillator should be limited by suitable design (see section VI.2.33) to such figures that no serious distortion results from the ensuing non-uniform amplification due to the i.f. interstage circuits.

REFERENCES: *58, 76, 115, 176, 385, 387.*

VII.3. Impulse and single side-band reception. We shall now deal with the reception of IM (see section I.2.3) and of single side-band signals.

VII.3.1. Impulse reception. Impulse reception is applied in telegraph and other communication systems and in radar. The principles involved as well as the operation of corresponding receivers will be dealt with briefly.

VII.3.11. Impulse receivers. The impulses used in telegraph communication (with the original Morse system as well as with more modern systems) are of different lengths at different interspaces or of equal lengths at different interspaces. In all these cases the relation between the minimum impulse duration t_i and the band width is fixed by the argument of section I.2.31. This holds in the cases of input as well as of intermediate carrier frequencies. Subsequent to rectification (second detection) the individual pulse pattern must be passed and amplified by the l.f. stages. The corresponding relation between the upper angular frequency ω_u of these stages and the minimum impulse duration t_i has been discussed in section VII.1.21 in connection with

Figure 210. For telegraphic purposes the shape of the impulses passed by the l.f. stages need not satisfy such rigid requirements as for other purposes. Hence a value of, say, $\omega_u t_i \geqq 5$ may be adequate in the present case (see Fig. 210). This reasoning at once fixes also the values of resistance R_1 and bypass capacitance C_1 of the rectification stage, the required conditions being (ω_i is the angular i.f.): $\omega_i R_1 C_1 \gg 1$ and $\Omega R_1 C_1 \ll 1$ (see Fig. 197).

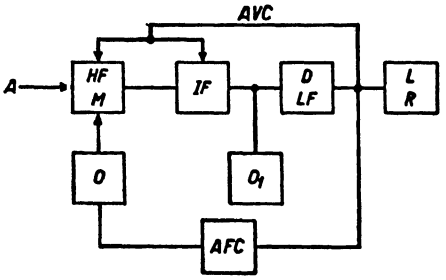

FIG. 226 Schematic diagram of a telegraph receiver. Legend: *A*, antenna; *HFM*, high frequency and mixer stages; *IF*, intermediate frequency stages; *DLF*, detector and low frequency stages; *LR*, loudspeaker and relay equipment; *AVC*, automatic volume control; *AFC*, automatic frequency control; *O*, oscillator of mixer *M*; O_1, beat frequency oscillator.

An over-all diagram for telegraph reception is shown in Figure 226. The signal issuing from the antenna terminals is amplified and mixed in the stages indicated by *HF* and *M*, subsequently passing through the i.f. stages indicated by *IF*. A second local oscillator O_1 of frequency differing only slightly from the i.f.—e.g., by about 1000 c/s—is shown in Figure 226 and is used in the case of aural reception. By this second local oscillator O_1 and the i.f. impulses at the input of the rectification stage, the resulting output sound issuing from the loudspeaker consists of a tone frequency, interrupted corresponding to the impulse shapes. If no sound reception is desired, the oscillator O_1 may be omitted and the l.f. impulses may then be used to activate suitable relays (indicated by *R* in Fig. 226). Subsequent to rectification an a.v.c. as well as an a.f.c. circuit are shown in Figure 226, the design of which will be discussed in section VII.4 (see also Figures 184-185).

As a second example of impulse reception an input signal of pulse-frequency modulation according to section I.2 will be considered. The individual impulses are of equal duration, but their number per unit of time is varied according to the requirements of modulation. Indicating the instantaneous number of pulses per second by q, a singly periodic modulation of angular frequency Ω would correspond to a variation of q according to $q = q_0\{1 + m_p \cos(\Omega t + \varphi)\}$, m_p being the coefficient of pulse modulation. Upon h.f. amplification, mixing, and i.f. amplification, the h.f. and i.f. angular carrier frequencies being

ω and ω_i respectively, the signal is passed on to the input of a rectification stage in which demodulation is to be obtained. The band width of the h.f. and i.f. stages is approximately $B = \alpha/t_i$, t_i being the duration of individual impulses and α a figure between, say, 1.5 and 5, the larger figures corresponding to a more accurate reproduction of the pulse shape at the detector input terminals. The average number q_o of pulses per second is assumed to be much lower than $\omega_i/2\pi$ and much higher than $\Omega/2\pi$, if Ω is the highest angular modulation frequency under consideration (e.g., $2\pi \times 10{,}000$ c/s). Thus, if ω_i is 20π mc/s, q_o

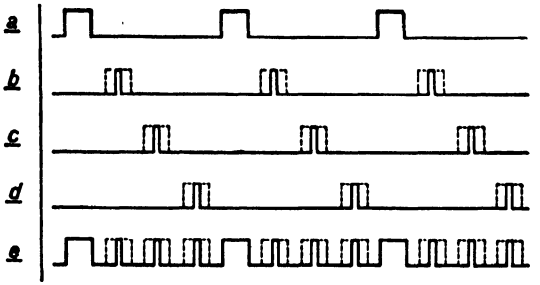

FIG. 227 Three-channel pulse position modulation. Diagram *a*: Marker pulses; diagrams *b*, *c*, and *d*: modulation channels with indications (dotted) of pulse position swings; diagram *e*: sum of previous diagrams.

might be 0.1 mc/s. The leakage resistance R_1 and bypass capacitance C_1 (see Fig. 197) of the rectification stage are required to satisfy the conditions: $\omega_i R_1 C_1 \gg 1$, $2\pi q_o R_1 C_1 \gg 1$, $\Omega R_1 C_1 \ll 1$. Under these conditions the instantaneous number of pulses per second arriving at the detector input is proportional to the corresponding l.f. detector output voltage, which thus offers a correct replica of the l.f. modulation imparted to the signal waves. This simple system may under certain conditions be applied to obtain a reduction of output noise ratio similar to that corresponding to FM. We shall go into this application in the succeeding section VII.3.12.

Only a single modulation channel of angular frequency-width Ω may be applied in the case discussed above. In order to modulate the impulse carrier with more than one signal, a slightly more complicated sequence of impulses must be applied, incorporating so-called marker or synchronizing pulses. An example of three modulation channels is shown in Figure 227. The upper diagram *a* contains the marker pulses, which are of somewhat larger width or duration than the signal

pulses. The diagrams *b*, *c*, and *d* each contain a set of signal pulses (full contours), the location of which with respect to the marker pulses may be varied within the limits indicated by the broken contours. A displacement of a sequence of signal pulses to the left of the mean or average positions shown in full contours corresponds to a variation or modulation of opposite sign compared with a displacement to the right. The three sequences of signal pulses are superimposed on the sequence of marker pulses in the diagram *e* of Figure 227, the full contours of which thus correspond to the input signal if all three channels

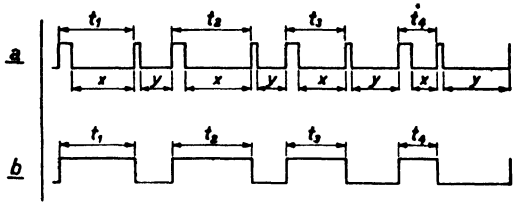

FIG. 228 Detection of one signal channel in pulse-position modulation. Differences in pulse-position are transferred to corresponding differences in width of output pulses, as indicated by t_1, t_2, t_3, etc., by suitable trigger devices.

are of zero instantaneous modulation. The detection and demodulation of impulse signals of this type (sometimes indicated as "pulse-time" modulated signals) is slightly more involved than was explained above in the case of a single modulation channel without marker pulses. We shall first discuss a method suitable for the demodulation of one single channel of the marker type. A particular modulation pattern is shown in Figure 228. The time intervals t_1, t_2, t_3, and t_4 correspond to the instantaneous values of modulation. Now if we consider the modulation corresponding to the distances x of Figure 228*a*, it is seen that the modulation corresponding to the complementary distances y is exactly equal but of opposite phase. Thus the application of a simple low-pass filter circuit (e.g., R_1, C_1 circuit of a detector stage) cannot bring about the desired demodulation, as the two modulations of opposite phase cancel and the resulting detector output would be zero. If a suitable trigger tube device is applied, a sudden change of bias voltage of an amplifier tube may be brought about by each successive pulse. Thus at a marker pulse the bias may be made less negative, changing to a more negative value at the subsequent signal pulse, etc. The resulting anode current of the l.f. amplifier tube is shown in Figure

228*b*, the i.f. having been filtered out by a suitable low-pass resistance-capacitance filter preceding the input of the trigger circuit. The width of the anode d. current pulses obviously varies in accordance with the signal modulation, and these pulses may be properly detected using a suitable detector circuit, the values R_1 and C_1 of which satisfy the conditions: $\omega_i R_1 C_1 \gg 1$, $2\pi q_o R_1 C_1 \gg 1$, $\Omega R_1 C_1 \ll 1$, q_o being the average pulse frequency and Ω the upper angular frequency limit of modulation.

With multiple-channel modulation, slightly more intricate devices are required, including a separation device for the individual modulation channels. Such separation may, for instance, be brought about by the use of three l.f. channels, one corresponding to each modulation channel, each sensitized by a trigger circuit which is synchronized by the marker pulses. Thus at each marker a suitable capacitance may be charged and subsequently discharged through a suitable resistance. At three different successive voltage levels across this resistance one of the three l.f. channels is sensitized by means of a suitable trigger device. As soon as the proper pulse of the channel at issue has passed, the channel in question is desensitized similarly to the procedure described above in connection with a single channel with markers. Upon separation each channel may further be treated in a similar manner as was explained above in connection with a single channel. At a carrier frequency of 1200 mc/s a twelve-channel system of this kind has been operated successfully.

All the above cases correspond to pulse-time or pulse-frequency modulation. Besides this, impulse-amplitude and impulse-duration have also been successfully applied as means for obtaining signal modulation. The discussion of these systems is, however, thought to be outside the scope of this book.

REFERENCES: *84, 133, 229, 267, 296, 378.*

VII.3.12. Noise reduction with impulse-frequency modulation. Several systems have been devised for the application of IM for the purposes of noise reduction. A simple system of this kind will be discussed in connection with a single-channel IM signal as considered at the start of the preceding section VII.3.11. Instead of the method of demodulation and detection discussed in that section, we shall now assume that a threshold is created in a stage subsequent to the normal i.f. stages, e.g., by application of a suitable bias voltage. A suitable filter circuit is interposed between the last i.f. stage and the threshold

stage, passing the individual impulses undistortedly but not the i.f. carrier frequency $\omega_i/2\pi$. As soon as an impulse voltage of the received signal exceeds a definite threshold value corresponding to the said bias voltage, it is passed and activates a trigger tube, e.g., of the well-known thyratron type. The current passed by this trigger tube is used for charging a suitable capacitance C_1, subsequently discharging through a resistance R_1 such that $\omega_i C_1 R_1 \gg 1$ and $2\pi q C_1 R_1 \gg 1$. The output voltage of this trigger or demodulator stage is then proportional to the instantaneous number q of impulses per second contained in the input signal. Demodulation is thus effectively carried out by a counting process indicating the number q. The output noise results mainly from the rises of level of the individual pulses taking place with random variations, causing random variations of the number q as counted and hence also random fluctuations of the output l.f. voltage. The output noise power is thus proportional to $\overline{(q - \bar{q})^2}$, being the m.s. value of the instantaneous fluctuation of pulse frequency q. The output signal power is, under the above conditions, proportional to $(\bar{q})^2$, being the square of the average frequency $\bar{q}$, the proportionality factor being the same as for the noise output power. Hence the output noise ratio is:

$$\frac{\overline{(q - \bar{q})^2}}{(\bar{q})^2} = \frac{1}{t_o \bar{q}},$$

t_o being the period of modulation: $t_o = 2\pi/\Omega$, while $\overline{(q - \bar{q})^2 t_o^2}$ has been equated to $\bar{q} t_o$, assuming the spontaneous fluctuations at issue to be uncorrelated. In a comparable case of AM, in which the peak values of the individual pulses (of duration t_i each) are modulated and not their spacing, the output noise power may be assumed to have a similar value as in the above case, the fluctuations of amplitude in the present case being proportional to the fluctuations in rise and fall of the pulses in the previous one. The output signal is, on the other hand, not proportional to $\bar{q} t_o$ but to $\bar{q} t_i$ in the present case. Thus we obtain a noise ratio:

$$\frac{1}{c_p} \frac{\bar{q} t_o}{(\bar{q} t_i)^2},$$

the proportionality multiplier c_p being of the order of magnitude of unity while its exact value does not matter in our present reasoning. From the above two expressions we directly obtain the ratio of noise

figure N_{IM} at IM of the type considered to the comparable noise figure at AM as stated:

$$\frac{N_{IM}}{N_{AM}} = c_p \left(\frac{t_i}{t_o}\right)^2 \approx c_p \left(\frac{\Omega}{2\pi B}\right)^2, \qquad \text{(VII.3.12}a\text{)}$$

Ω being the highest angular frequency of modulation and B the band width equivalent to the IM in question. This expression a is very similar to Eq. (VII.2.12a) in the case of FM. It is seen that a considerable reduction of noise figure may be obtained by the application of IM as described, a reduction entirely comparable to that obtained by the proper application of FM. This comparison may even be applied in detail, the present value $2\pi B$ being equivalent to the angular frequency sweep $2\Delta\omega$ in the case of FM. In both cases the reduction of noise figure is proportional to the square of the ratio of the modulation frequency to the applied band width.

VII.3.13. Radar. In brief, radar may be described as a system according to which a beamed impulse is transmitted, reflected by an object to be explored, the reflected impulse then being received. The time lapse necessary for the impulse to travel toward the object and back to the radar apparatus is measured and thus the location of the object is determined from the direction of the primary beam and the time interval. A simple argument may reveal the relation between transmitting power, receiver noise figure, distance to the object, and its radar coefficient (see section I.1.24). Assuming the transmitter power fed into the antenna to be P_t, the gain compared with a dipole of the transmitting antenna to be g, the distance of the object from the transmitter to be r, the specific power p_o at the object will be:

$$p_o = \frac{3}{2} \frac{P_t g}{4\pi r^2}. \qquad \text{(VII.3.13}a\text{)}$$

If the object has a radar coefficient O (see section I.1.24), the specific power p_r caused by reflection at the receiver (assumed to be coincident with the transmitter) is:

$$p_r = \frac{1}{4} p_o O = \frac{3}{2} \frac{O P_t g}{16\pi r^2} = \frac{3}{2} \frac{F^2 S_o}{(4\pi r^2)^2} P_t g,$$

S_o being the interception area of the obstacle and F its effective coefficient of reflection. Assuming the effective reception area of the

combined transmission-reception antenna to be S_e, the available reception power is: $P_r = S_e p_r$, or:

$$P_r = \frac{3}{2} \frac{F^2 S_o}{(4\pi r^2)^2} S_e g P_t. \qquad \text{(VII.3.13}b\text{)}$$

Equating this available reception power P_r to the minimum value P_{min} necessary to insure proper reception, we may obtain the maximum distance r_{max} between radar apparatus and object, at which an object can be spotted:

$$r_{max} = \sqrt[4]{\frac{3}{2} \frac{P_t}{P_{min}} \frac{g S_e F^2 S_o}{(4\pi)^2}} \cdot \qquad \text{(VII.3.13}c\text{)}$$

The gain g of the combined radar antenna bears a simple relationship to its effective area S_e, according to Eq. (III.1.13d). Inserting this into Eq. (c) we obtain a slightly modified equation for the maximum distance r_{max}:

$$r_{max}^4 = \frac{P_t}{P_{min}} \frac{S_e^2 F^2 S_o}{4\pi\lambda^2}, \qquad \text{(VII.3.13}d\text{)}$$

λ being the wavelength under application. Thus, with fixed values of transmission and reception power as well as of antenna and object, the maximum distance increases at decreasing wavelength. This relationship is, however, modified, if a fixed beam width is applied. With a circular reflector antenna the beam angle ψ between the adjacent half-power points is approximately (see sections III.3.22 and III.2.21):

$$\psi^2 \approx \frac{\lambda^2 \pi}{4 S_e}.$$

Hence, if ψ is fixed, the maximum distance r_{max} becomes:

$$r_{max} = \sqrt[4]{\frac{P_t}{P_{min}} \frac{F^2 S_o \pi \lambda^2}{64 \psi^4}}. \qquad \text{(VII.3.13}e\text{)}$$

Under these conditions the maximum distance increases if the wavelength is increased. But, if λ^2 is increased in the present case, the effective surface area of the radar antenna is increased proportionally and hence the apparatus at issue becomes more expensive.

We shall now consider the application of radar impulses of duration t_i at which the necessary band width B is approximately $1/t_i \approx B$.

The minimum available reception power P_{min} may be written as $P_{min} = NKTB$, N being the receiver's noise figure. Thus we obtain from Eq. (*d*):

$$r_{max} = \sqrt[4]{\frac{P_t t_i}{NKT} \frac{S_e^2 F^2 S_o}{4\pi\lambda^2}}. \qquad \text{(VII.3.13}f\text{)}$$

This equation is suitable for the discussion of various special cases. As an example we shall consider the reflection of radar waves by the moon's surface, as practically accomplished in the first months of 1946. Assuming the ratio S_e/λ^2 to be 25 and $S_e = 25\ \text{m}^2$, an estimate of the average coefficient of reflection F of the moon's surface is necessary. The surface in question is about $S_o = \pi(1.7)^2 \times 10^{12}$ and we shall assume: $F^2 S_o \approx \pi \times 10^{12}\ \text{m}^2$, while the distance r is approximately 3.8×10^8 m. With impulses of two microsecs duration and 1000 kw power $P_t t_i = 2$ joule, and hence the required noise figure becomes:

$$N \approx 4.$$

The experiment at issue thus requires receivers of a low noise figure.

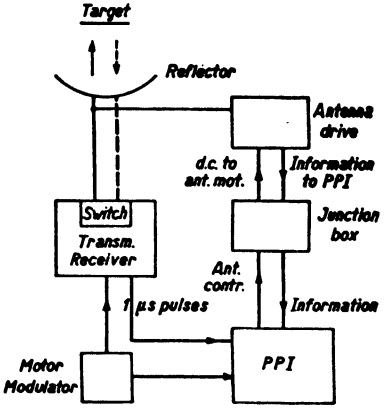

FIG. 229 Simplified block diagram of radar equipment. *PPI* is the plane position indicator.

In the actual experiments the carrier frequency was 111.6 mc/s, somewhat lower than was assumed in the above estimate (reference *245*). We may also use the above equations for the determination of the required transmission power for the detection of specified objects at a given distance if the receiver's noise figure is known.

Two types of visual radar applications have become widely known. With the first type the radar antenna system is given a definite direction and the transmitted and reflected impulse are recorded, using a cathode ray with a suitable time base. From the recorded distance between the two impulse images on the fluorescent screen of the c.r. tube the distance between radar antenna and object may then be read directly, the screen being provided with a suitably calibrated scale.

With the second type, sometimes indicated as surface-search radar, the antenna system is rotated in synchronism with the time base sweep of the c.r. tube. Thus a more or less detailed map of the objects swept by the beam is observed on the fluorescent screen. An over-all diagram of a surface-search radar is shown in Figure 229. In this particular case, 250 kw peak power is used at a pulse duration t_i of 1 microsec.

REFERENCES: *54, 69, 98, 109, 110, 139, 169, 245, 267, 323, 333.*

VII.3.2. Single side-band reception. Single side-band communication offers a number of advantages, especially for long distances, when the waves may be much affected by ionospheric conditions.

VII.3.21. General considerations. The suppression of one side-band of an AM signal together with partial or complete suppression of the carrier wave offers the advantage of an over-all band-width reduction to about one-half of its value with a pure AM signal. Thus more broadcast or communication channels can be accommodated within a given frequency interval than with pure AM. Furthermore, the required transmitter power is considerably reduced in comparison with AM, the continuous power used for the carrier of an AM signal being partly or entirely eliminated. Due to the reduced over-all band width required for single side-band transmission, the effects of fading and interference, especially at long-distance transmission, in most cases show a considerable reduction if compared with AM (see section I.1.4). By the reduced over-all band width the noise ratio may be less than with AM. Secrecy of single side-band transmission is in general greater than with AM, as no adequate direct reception using common AM sets is possible. Finally, distortion and interference effects due to non-linear tube curves may be less with single side-band signals.

In discussing the latter point we shall assume a single side-band signal, the carrier of which is completely suppressed. If one single frequency of modulation is considered, the signal thus consists of a single frequency. By curved tube characteristics overtones of this frequency are created, the frequencies of which are outside the reception band. Thus little harm is done by this sort of distortion. Effects like increase of modulation coefficient and distortion of modulation (see section VI.1.42 and VI.2.13) are not encountered in the present case. Interference by spurious modulation of the signal by l.f. dis-

turbances may, however, occur in the present case as well as with AM. Suppose that the spurious l.f. disturbance has a frequency f_b. By curvature effects the signal may be modulated by f_b and by its multiples, as shown schematically in Figure 230. If the carrier frequency is f_c, the l.f. output frequency is $|f_c - f|$ while the disturbances are at l. frequencies $|f_c - f \pm q \times f_b|$, q being an integral number. In most cases f_b is rather small compared with f; and then the disturbances corresponding to low values of q do not differ much in output frequency from the desired signal. Thus, if $|f_c - f| = 1000$ c/s and $f_b = 50$ c/s the disturbing frequencies are at 1050, 950, 1100, 900, etc., c/s. These disturbances are observed as a certain roughness of the output sound. If the same disturbing frequency f_b were modulated upon a pure AM signal, the resulting output sound disturbance would mainly correspond to f_b and to multiples of it. Hence an entirely different character of output disturbance is produced by the same disturbing frequency in the cases of pure AM and of a single side-wave signal.

FIG. 230 Representation of disturbing output frequencies resulting from tube curvature effects in single side-band reception. Carrier frequency f_c is broken line at the left. The spurious l.f. disturbing frequency is f_b, while the desired output l.f. is $|f_c - f|$. The resulting interfering spurious output frequencies are $|f_c - f \pm f_b\, q|$, q being an integral number, and are shown in the diagram with decreasing amplitudes for higher values of q.

Where two single side-wave signals are simultaneously present at the input of a tube, the resulting interference consists of sums and differences of the frequencies of both signals being created at the output. Most of these are outside the band under consideration and hence cause little or no trouble. This situation is again entirely different from that caused by the presence of two input signals of which one or both are A-modulated, the resulting disturbance being then cross-modulation (see sections VI.1.42 and VI.2.13). If a pure AM signal is present at the input of a tube simultaneously with a single side-wave signal, the resulting disturbing l.f. output frequencies caused by tube curvature effects are similar to those discussed above, i.e., $|f - f_c \pm f_d|$ if f_d is the modulation frequency of the AM signal, f the single side-wave frequency, and f_c its corresponding carrier frequency. This type of interference may be serious, and at its occurrence measures suitable to its removal

should be considered; they consist mainly of improving selectivity, thus excluding the disturbing signal at the input of the tube in question. In the above reasoning the carrier was assumed to be absent at the input of the tube in which the disturbing modulation effects occur. If a very weakened carrier is present, as in some actual cases, the argument is not much altered and the results remain substantially as stated.

VII.3.22. Reception. As already mentioned in section I.2.22 and VII.1.1, the reception of a single side-band signal is mainly based on its detection subsequent to an increase or addition of a suitable carrier. The stages preceding rectification or detection—i.e., h.f. (if any), mixer, and i.f. stages—are of a conventional character and designed to accommodate the entire side band in question, including the remainder of the signal carrier if present. The additional carrier or the reinforced carrier present at the input of the detector stage must be of an amplitude large compared with the average side-wave amplitudes. In this case distortion at demodulation may be negligible, as was discussed in section VII.1.11. If no carrier is contained in the input signal and an extra carrier is added preceding detection, its frequency must be exactly equal to that of the suppressed carrier at the transmitter. Its phase is, of course, random with respect to the side waves, but we may conclude from section I.2.22 that this phase angle is not a matter of importance and hardly affects demodulation in the detection stage as long as its amplitude is sufficiently large compared with the side-wave amplitudes and as long as its frequency does not show too large deviations from the exact carrier position. These deviations are by experiments required to be less than about 20 c/s with speech and less than about 5 c/s with music programs. In order to insure the adherence to these close requirements with signals having an entirely suppressed carrier, a subsidiary single-frequency pilot signal is in some cases provided for. Thus, with telephonic transmission, using a band of about 3000 c/s, a pilot signal at a distance of 5 kc/s from the suppressed carrier position may be used. This pilot frequency signal is then applied to keep the added fresh carrier at the right position by l.f. beat note control.

As an example, a single side-band receiver is shown schematically in Figure 231. The signal captured by the antenna A is amplified in a h.f. stage, mixed in a first mixer stage M_1 (the i.f. of which may be approximately 0.5 mc/s), then amplified in i.f. stages (marked ZF),

and brought to a second mixer stage M_2 in which the suppressed carrier frequency is converted to approximately 10 kc/s. The incoming signal is supposed to contain a pilot frequency of the type mentioned and a filter stage marked S is used to remove this pilot signal and to conduct it to an automatic frequency control stage marked AFR. In the filter stage the required frequency band to be passed on is strictly limited, then conducted to the subsequent demodulation stage marked Gl and thereupon to the l.f. stages NF and to the loudspeaker L. The pilot

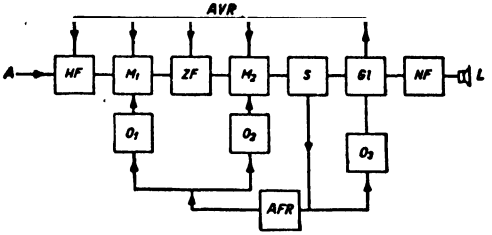

FIG. 231 Schematic block diagram of a single side-band receiver. Legend: A, antenna; HF, high frequency pre-mixer stage; M_1, first mixer stage with oscillator O_1; ZF, intermediate frequency stages; M_2, second mixer stage with oscillator O_2; S, filter circuits; Gl, detector stage with beat oscillator O_3; NF, low frequency stages; L, loudspeaker; AVR, automatic volume control; AFR, automatic frequency control.

frequency obtained from the filter stage S is applied to control the frequencies of the three oscillator stages O_1, O_2, and O_3, the first two of which are connected with the two mixer stages M_1 and M_2, while O_3 supplies the carrier to be added preceding the demodulation or detection stage Gl. From this detection stage the voltages necessary for the automatic gain control of the stages marked HF, M_1, ZF, and M_2 are also derived. The input signal carrier frequency may be 20 mc/s, entailing a frequency of O_1 of approximately similar amount. The frequency of O_2 is approximately equal to the i.f. created by the mixer M_1—e.g. 0.5 mc/s—while O_3 may be about 10 kc/s if the second mixer produces this carrier frequency at its output. The application of double mixing offers the advantage that the output i.f. of the first mixer M_1 may be chosen such that image response at its input is effectively suppressed, requiring a relatively high i.f. With the set under discussion, a frequency deviation from the pilot frequency of about 5 c/s creates a control voltage of the stage AFR resulting in a 3 kc/s frequency shift of the oscillator O_2.

Instead of one single side-band channel, several channels may be applied, calling for a proper separation in reception. For this and similar separation stages, adequate filter networks are required. In many cases quartz crystals are applied in such networks, insuring sharp cut-off characteristics at the ends of the bands to be passed on.

VII.4. Overall Design

Some questions connected with over-all design of reception sets and antennas suitable for the wave ranges at issue will be considered in this section. Most of these items apply to almost all of the different types of reception discussed previously.

VII.4.1. Fading compensation. One of the major disturbances of reception is fading. We shall deal with some aspects of its compensation here.

VII.4.11. Automatic bias control. Automatic fading compensation is mainly desirable in reception of long-distance signals, though some such compensation is also applied with television and other short-distance reception. One of the first questions to be settled is connected with the desirable shape of the l.f. output versus signal input voltage curve which should be obtained as a result of the automatic volume or gain control under discussion. Referring to AM first, a completely invariable output voltage could well be achieved at variable input carrier voltages and at a specified modulation coefficient. But in this case optimum output would be obtained only at a definite modulation level, the output power being too small at lower, and too high, involving distortion, at higher levels. In order to avoid this, a slowly increasing output at increasing input voltages is desirable. If a.v.c. starts directly at very low input signals, the output signal increases so slowly that optimum output power will hardly ever be obtained. This argument establishes the desirability of a threshold input signal, below which no a.v.c. is applied. A corresponding curve for a conventional sound reception set is shown in Figure 232.

The volume control itself is usually applied by biasing the control grids of the respective tubes, using bias voltage obtained from a special rectification stage, which is distinct from the normal demodulation or detection stage. A conventional circuit showing two directions of control—backward and forward from the rectification stage—is represented in Figure 233. The output resistance R (Fig. 233) of the rectifi-

cation stage and the capacitance C are chosen such that $\omega RC \gg 1$ in which ω may be the carrier or the modulation frequency. This condition is essential in order to obtain a purely direct bias voltage without l.f. ripple, which might cause disturbing interference by additional modulation in the h.f., mixer, and i.f. tubes. The threshold mentioned above may be obtained simply by biasing the diode, as shown in Figure 234. From curves like those of Figure 234 and from the transconduct-

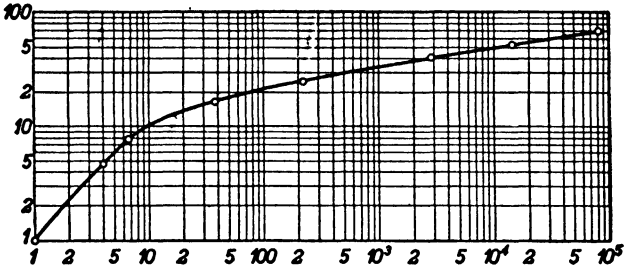

FIG. 232 Horizontal scale: Ratio of effective receiver input voltage to lowest input voltage. Vertical: Ratio of effective receiver output voltage to lowest output voltage. Curve corresponds to delayed automatic backward volume control at 30% AM.

ance versus bias curves of the mixer and amplifier tubes, the complete a.v.c. curve of a set may be obtained by graphical means. An example is given in the table below.

ANTENNA SIGNAL	MIXER VOLTAGE GAIN	I.F. VOLTAGE GAIN	BIAS CONTROL VOLTAGE	I.F. INPUT VOLTAGE OF DETECTOR	L.F. OUTPUT VOLTAGE OF DETECTOR	INCREASE OF OVER-ALL OUTPUT VOLTAGE
10 microv.	100	100	0	0.3	0.07	1×
40 microv.	100	100	0	1.2	0.33	4.7
67 microv.	100	100	0	2	0.55	7.8
380 microv.	46	77	2.3	4	1.15	16.4
2.2 mv.	18.5	50	5.0	6	1.75	25
28 mv...	5.1	23	10.5	10	2.9	41
140 mv...	2.8	11	14.5	13	3.8	54
800 mv...	1.2	5.9	20	17	5.0	71

In this example the rectifier threshold voltage is 3 volts and the AM coefficient $m_a = 0.3$. The manual volume control by potentiometer

should be applied behind the rectifier diode stage, as it would be less effective preceding this stage due to the a.v.c.

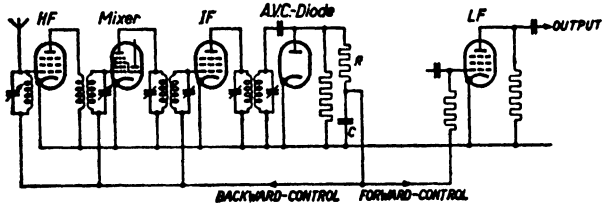

FIG. 233 Schematic receiver diagram illustrating automatic forward as well as backward volume control.

It is essential that the product of R and C of Figure 233 be not too large, as it determines the delay in time after which the bias voltage will have reached its full intended value. This delay is usually made

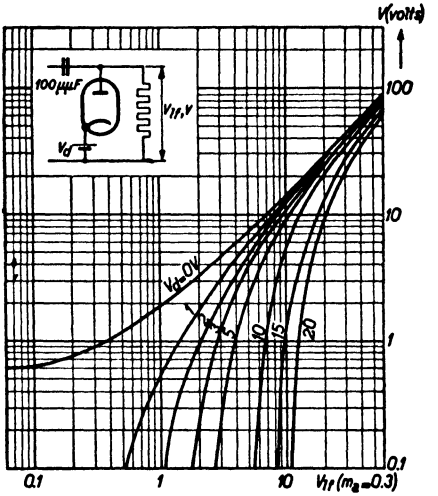

FIG. 234 Rectifier for the application of delayed or non-delayed automatic volume control. Vertical scale: Output direct voltage as dependent on the input intermediate frequency voltage, indicated by V_{lf}. Curves at different bias voltages V_d.

longer than 0.1 and shorter than 1 sec. and hence the value of the product RC is in this case required to be within these bounds.

By the application of suitable a.v.c. a number of disturbance effects that might occur at varying input signal levels may be avoided. Such

effects are, for instance: distortion by control grid current, distortion of modulation by tube curvature, and distortion by too large anode voltage swing. The automatic bias voltage of any one controlled tube must be such that effects like these are either eliminated or minimized. In some cases this may necessitate the application of different simultaneous control bias voltages to different tubes of a set, thus causing a complication if compared with Figure 233. A suitable rectification circuit supplying two different bias voltages is shown in Figure 235, the ratio R_1/R_2 being chosen accordingly. It is obviously also possible to provide for different time delays in the application of a.v.c. bias voltages using this circuit by choosing the RC products differently.

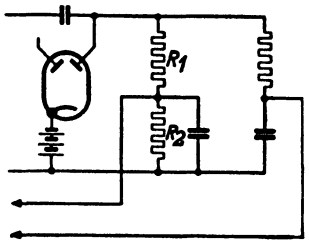

FIG. 235 Circuit for obtaining two different control voltages suitable for a.v.c. from a single diode. The delay is obtained by the application of a suitable bias voltage (indicated by a battery inserted in the cathode lead) of the diode.

A further aspect of the threshold voltage connected with the application of a.v.c. is related to noise. Transferring the available output noise power of a stage to its input by division by its gain figure, this equivalent input noise power is usually increased by the application of a.v.c. This holds for amplifier as well as for mixer stages using conventional tubes. Viewing the entrance stage of a set in this respect, its rise of equivalent input noise power must be chosen such that it lags behind the rise of input signal power which puts the a.v.c. into action. This may be achieved by simply applying a suitable threshold in the a.v.c. system. If under such conditions the equivalent input noise power starts rising, the input signal power has already risen to such a level that the noise ratio is less than previous to the application of a.v.c. and this is exactly what is desirable. Schematic curves for

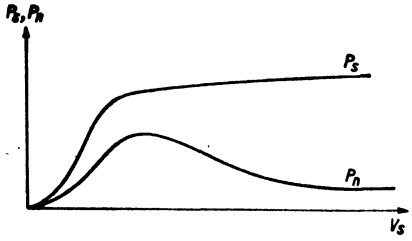

FIG. 236 Vertical scale: Output signal power P_s and output noise power P_n. Horizontal scale: Input signal voltage V_s. Both scales are linear. Curves are obtained with a.v.c.

the resulting output signal power and output noise power of a set applying a.v.c. with a suitable threshold are shown in Figure 236. It is seen clearly from these curves that the noise ratio is uniformly decreased if the input signal voltage is increased.

VII.4.12. Further methods of fading compensation. The bias-control method of fading compensation entails several disadvantages, some of which may be listed as follows: (1) By the variation of bias voltage, variations of tube input and output impedances are caused, which may result in distortion of frequency response of the attached circuits. (2) By the bias variations the supply voltages of the tubes in question may vary as a result of tube current variations. Such variations of supply voltages may affect other tubes and cause distortions of response by variations of impedances of the attached circuits. As already discussed in sections VI.1.42 and VI.2.13, the tubes in question have to be provided with remote cut-off anode current versus grid bias curves in order to limit distortion effects with volume control by bias voltage. Such remote cut-off curves, however, inevitably involve a higher ratio of anode current to anode transconductance than would be necessary with tubes having sharp cut-off characteristics, which are in turn unsuitable to bias control due to large distortion. (3) Finally, the application of bias voltage in many cases prevents the application of suitable feedback for reduction of noise figure, such as was discussed, for instance, in sections VI.2.42 and VI.1.32. For all these reasons it would be useful if a different means of effective volume control could be applied, avoiding all or most of the points mentioned.

Such means may be found in the application of electro-mechanical control. The actual device may be given various shapes and only one instance will be discussed briefly here. It consists of a tiny permanent magnet mounted on a common axis with one or more insulated condenser electrodes. The magnet moves between two poles of a suitable ferromagnetic circuit provided with one or more coils. These coils are energized by currents derived from a suitable rectification stage similar to that described in connection with bias control. By the d.c. through the coils the tiny magnet and its associated condenser plates are rotated and thus a variation of capacitance between these rotating plates and suitable adjacent fixed electrodes results. This capacitance may be used as a coupling capacitance between the antenna and the entrance resonant circuit or between any two consecutive stages of a set preceding the demodulation stage. The variation in capacitance

must be relatively considerable if satisfactory volume control is desired, e.g., 1 : 100 or 1 : 1000 between extreme positions. Such large variations may readily be achieved in various ways. One method has been dealt with already in section V.1.23 in connection with the attenuator stage of a standard signal generator. We may use a suitable modification of Figure 112 in the present case. Another way consists in the application of a push-pull circuit, the fixed condenser electrodes being of symmetrical position with respect to the set's chassis electrically. If the rotating plates are in a symmetrical position with respect to the fixed plates, the output voltage of the control device is zero at any input voltage. Hence a wide range of control may be obtained also in this case.

The construction of electro-mechanical devices of the type under discussion calls for a number of subsidiary considerations, the most important of which are connected with resonant frequencies and reaction time. The former are required to be much higher than the reciprocal time of reaction. The latter being about between 0.1 and 1 sec, the frequencies in question must be higher than, say, 10 c/s. At the same time, however, the reaction time must remain of the order of magnitude as stated and these two requirements together call for a very light structure. The supporting frame of the rotating parts may be molded of suitable plastic material. Another requirement is shielding. A suitable screen must be interposed between the control parts connected to h.f. or i.f. circuits and the parts connected with the rectification stage. Devices of this kind may also be used for automatic frequency control purposes.

Finally, we shall discuss briefly some aspects related to carrier amplification. If, by selective fading, the carrier of an AM signal is weakened considerably in relation to the side bands, very disagreeable l.f. distortion may result. Such effects occur especially in long-distance reception (see section I.1.4). They may be overcome by application of additional amplification to the carrier of an AM signal. This may be achieved in various ways; e.g., by using crystal filter circuits in the i.f. stages having sharp peak responses at the carrier frequency and less response at the side bands. If such carrier amplification is applied, automatic frequency control of the local oscillator becomes almost inevitable.

VII.4.2. Design and construction. Some problems connected with the over-all design and construction of reception sets at the frequencies under discussion will now be dealt with.

VII.4.21. Stabilized direct power supply. We have already mentioned in preceding sections (VII.4.12, VII.1.22, V.1.21) that the power supply stage of a receiver set should satisfy a number of requirements pertaining to stability of supply voltages under varying power drain

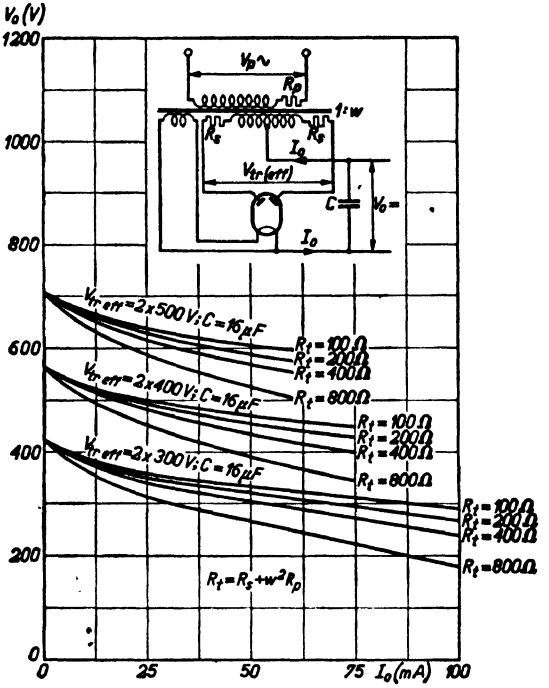

FIG. 237 Operational data of supply rectifier stage, the circuit being as shown in the diagram (R_s inherent secondary series resistance of the circuit and R_p inherent primary series resistance, w being the transformation ratio). Curves show output voltage V_o as dependent on output current I_o at different values of $R_t = R_s + w^2 \times R_p$. The sign Ω indicates ohms.

and to screening as regards h.f. currents. A rectifier circuit often used for supply purposes is shown in Figure 237, representing a so-called full-wave rectifier. The curves of Figure 237 show the decline of direct output voltage at increasing power drain (increasing d.c.). The resistance R_t at each curve is made up of components shown in the circuit: the primary transformer series resistance R_p and the secondary transformer series resistance R_s of each half: $R_t = R_s + w^2 R_p$, w being the transformation ratio. From these curves it is obvious that a reduced

internal resistance R_t of the power-supply circuit is conducive to a more constant output voltage at increasing d.c. values.

In order to reduce the ripple of the output voltage and to prevent l.f. voltages from entering the supply circuit and thence being conducted to other parts of the receiver, a choke of inductance L henry may be used in series with the positive output terminal, connecting its far end to ground across a capacitance C_1. If a ripple of angular frequency ω_r and voltage V_r is present at the output of the circuit of Figure 237, the reduced ripple voltage V_{ro} resulting from the choke-condenser circuit mentioned is:

$$\frac{V_{ro}}{V_r} = \frac{1}{1 - \omega_r^2 LC_1}.$$

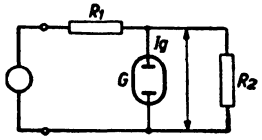

FIG. 238 Simple voltage stabilization circuit using a gas discharge tube G, the input source voltage indicated by the circle at the left being V and the output voltage across R_2 being V_2.

The stabilization of the output voltage V_o of a rectifier circuit under varying conditions of current drain has been the object of many special circuits, of which two will be mentioned here. The first one is based on a property of gaseous discharges, extremely useful for the present purpose. The electrode voltage of such a discharge is only little dependent on the d.c. passing through it. We shall indicate the increment of electrode voltage divided by a given increment of d.c. by R, whereas the ratio of electrode voltage to average d.c. of the discharge will be denoted by R_g. Considering a circuit as shown in Figure 238, G being the gaseous discharge tube, V the voltage generator of internal resistance R_1, and R_2 the load resistance, we may deduce:

$$\frac{V_2}{V} = \frac{1}{1 + \frac{R_1}{R_2} + \frac{R_1}{R_g}}. \qquad \text{(VII.4.21}a\text{)}$$

If a relatively small increment ΔV of V occurs, the corresponding increment ΔV_2 of V_2 is:

$$\Delta V_2 = \frac{\Delta V}{1 + \frac{R_1}{R_2} + \frac{R_1}{R}}, \qquad \text{(VII.4.21}b\text{)}$$

the difference from Eq. (*a*) being that R_g is replaced by R. By Eqs. (*a*) and (*b*) we have:

$$\frac{\Delta V_2}{\Delta V} = \frac{V_2}{V} \frac{1 + \frac{R_1}{R_2} + \frac{R_1}{R_g}}{1 + \frac{R_1}{R_2} + \frac{R_1}{R}} \qquad \text{(VII.4.21c)}$$

and the second right-hand multiplier is smaller than unity by virtue of R_g being much larger than R. From this expression it is obvious that a relatively considerable improvement of voltage stability calls for a

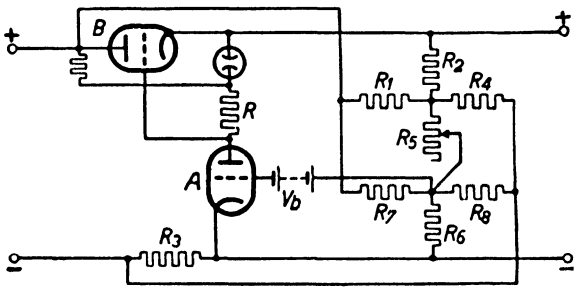

FIG. 239 Circuit for reducing output supply voltage variations of rectification stage, using two triodes. For description see text (reference *409*).

small ratio of R_1 to R_2. Under practical conditions this multiplier may be as small as 0.2. On this principle many applications have been based, using special gaseous discharge tubes with several electrodes, thus stabilizing several supply voltages at once.

If the internal resistance of a supply source such as represented in Figure 237 is zero, the variations of output d.c. would entail no corresponding variations of supply voltage. This internal resistance corresponds to the slope of the curves in Figure 237.

A circuit achieving a considerable reduction of output voltage variations by reducing the effective internal resistance of the supply source is shown in Figure 239, using two triodes and a bridge network.

In this circuit some relations between the various elements must be satisfied: $R_1/R_2 = R_7/R_6$, $R_1 + R_2 = n\mu R_2$, n being the amplification of tube A and μ the amplification factor of tube B. Furthermore: $R_2 + R_4 = R_3 R_2 n Y$, Y being the transconductance of tube B. Under these conditions the output voltage V_u may be varied with the aid of

the resistor R_5. Stability of output voltage is independent of its actual value. The effective internal resistance of the circuit if viewed from its output terminals may be made exactly equal to zero only at one single value of output d.c. The battery V_b shown in the circuit must be of constant voltage, this source serving as a pilot voltage to the circuit. We have: $R_4/R_2 = R_8/R_6 = n\ YR_3 - 1$.

VII.4.22. Antenna construction. In individual as well as commercial reception the problem of anti-noise antennas is often predominant.

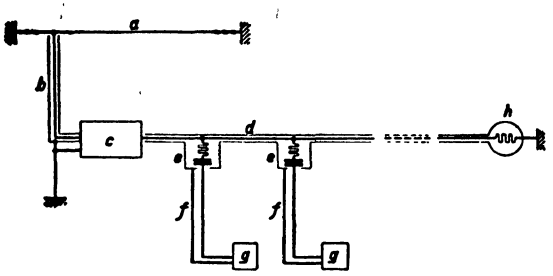

FIG. 240 Antenna system suitable for a plurality of receivers. Legend: *a*, antenna; *b*, coaxial shielded cable; *c*, antenna preamplifier; *d*, shielded coaxial cable; *e*, shunt connections of receivers; *f*, receiver coaxial cable; *g*, receiver set; *h*, wave impedance termination of *d*.

One of the most useful constructions aiming at a reduction of man-made noise consists of an antenna as far distant from the noise source as is practically feasible, connected to the receiver by a well-shielded coaxial cable of low attenuation. In some cases such anti-noise antennas may be used cooperatively, e.g., by the inhabitants of an apartment building (see Fig. 240). The signal level may be increased near or at the output of the antenna proper by application of a suitable antenna amplifier. This may incorporate a mixer, thus reducing the frequencies of the signals to be transmitted by cable. Its band width should be either sufficient to accommodate all the signal frequencies required or else be of adjustable center frequency. In the latter case remote tuning would often be required as the pre-amplifier set may be located in a poorly accessible place. The system might be recommended for high-quality television or short-wave (e.g., FM) reception in city areas.

The familiar antennas used in automobile, aircraft, naval, and similar reception need hardly any elaborate mention. Only two examples are

shown in Figures 241 and 242 of a direction-finder for naval and aircraft use (loop antenna) and a cycle-set with a small wire antenna.

In some cases commercial antennas have to be designed for reception from two opposite directions. This may be achieved by the use of a suitable phase-shifter. The effect of a device of this type is illustrated by Figure 243. Two antennas 1 and 2 oriented perpendicularly to the

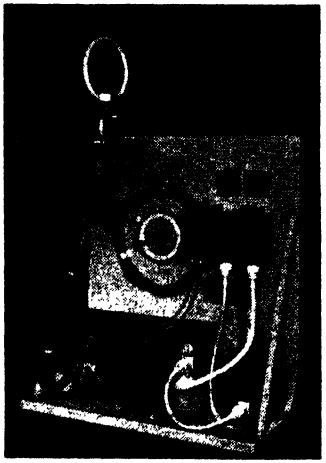

FIG. 241 Short-wave receiver including direction finder for ships and airplanes.

FIG. 242 Short-wave cycle set with short antenna.

directions of propagation are connected to a common point P, one directly and the other across the phase-shifter *Del*. The mutual distance between the individual antennas is $\lambda/4$, while *Del* causes a delay also corresponding to $\lambda/4$. Thus for waves arriving from the direction A the reception voltages are added at P, while for waves arriving from the direction B they cancel, assuming zero attenuation of *Del*. By transferring the device *Del* from the lead of the antenna 1 to the lead of 2, the direction of reception may be changed from A to B. The phase-shifter *Del* often takes the form of a suitable h.f. tube amplifier. By the insertion of similar phase-shifting devices other and more general variations of directive reception patterns may be obtained.

An extension of phase-shift practice to musa-systems incorporating six rhombic reception antennas (marked A) is illustrated by Figure 244. Each antenna is connected to an individual set containing a h.f. amplifier

stage *HF*, a first mixer stage M_1, an i.f. amplifier *IF*, and a second mixer stage M_2, the oscillators of the mixer stages being O_1 and O_2. At the outputs of five of the sets three phase-shifters *Ph* each are shown, indicated by 1, 2, and 3. These phase-shifters control the optimum response elevation angle of the antenna system. The shifters 1 vary their phase-shifts continuously and allow a continuous determination of the available antenna output power at various phase-shifts (or elevation angles). The shifters 2 and 3 are controlled manually or automatically and choose two optimum angles of elevation for long-distance reception on two particular paths. The shorter-path reception coaxial cable is interrupted by a suitable delay device *Del* providing for a delay such that virtually equal parts are created at the entrance of the two detector stages D_1 and D_2. The outputs of these stages are connected to a common l.f. amplifier *LF*. By the present reception system fading effects are reduced considerably.

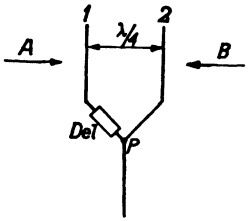

FIG. 243 The outputs of two identical antennas 1 and 2, of orientation perpendicular to the direction of reception, are brought together at a point *P*, an adjustable delay circuit *Del* being inserted in one branch. The directions of reception are either *A* or *B* according to the delay.

The construction of antennas involves a number of mechanical points such as strength under various conditions of wind (e.g., up to 100 m.p.h.), hail, snow, sleet, and durability under seasonal influences. The calculation of poles, towers, struts, and supporting structures under these conditions cannot be entered into here; for these the reader must be referred to texts on constructional design. Severe icing and humidity conditions must under some climatic circumstances be accounted for. In some cases special insulator design may be necessary, and sometimes de-icing circuits must be provided.

Antennas, especially of highly directive u.h.f. type, in planes, have to be built sometimes into wings or other structural parts in order not to impair aircraft operation. In such cases low-loss covers of the antennas and reflectors, flush with fuselage or body-surfaces, are appropriate.

With individual antennas, cost is a dominant factor and the choice between possible structures will often be decided upon according to best performance at a given expense. The data related to reception

properties may in most cases be obtained from chapter III while the data regarding expense are often obtainable from suitable texts and pamphlets.

REFERENCES: *5, 24, 31, 126, 136, 249, 282.*

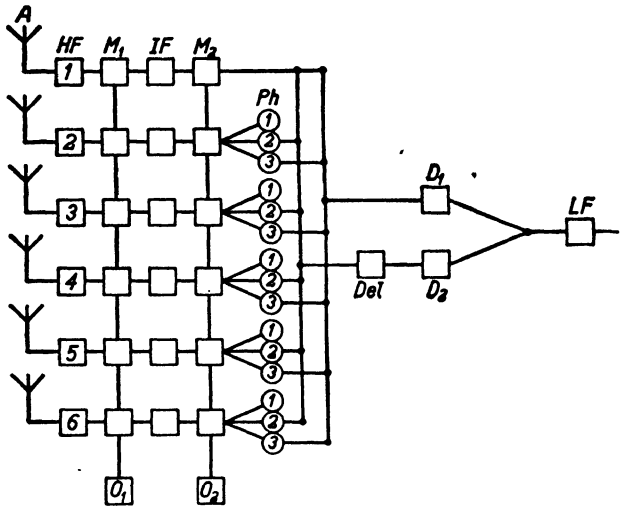

FIG. 244 Schematic diagram of diversity reception using six separate antennas *A* with six separate *HF*, mixer (M_1), intermediate frequency (*IF*), and second mixer (M_2) stages, the local oscillators being O_1 and O_2. Three phase-delay circuits *Ph* are provided in each of five reception paths. The circuits *Ph* 1 serve as a check for a most favorable choice of angles of incidence and are constantly rotating. The circuits *Ph* 2 and 3 are used for a manual or automatic adjustment leading to optimal output voltages. The delay circuit *Del* serves as a compensation of the difference in lengths of transmission paths. D_1 and D_2 are detector stages and *LF* are low frequency output stages.

VII.4.23. Set design and construction. Sets may be subdivided into portable, mobile, semi-portable, and fixed types. The construction of each of these types calls for special attention to the varying conditions of use, and widely different shapes have been adopted. An adequate treatment of the corresponding requirements and of the related constructions would unduly inflate the present section and hence we shall deal with only a few practical examples and with some simple rules.

The general trend of set construction has been directed toward increasing standardization and uniformization as regards parts and stages.

Thus standard i.f. stages have been built satisfying specific requirements for television and FM reception as well as for facsimile and u.h.f. or s.h.f. communication. Values of i.f. have in many cases been chosen with a special view to adequate image rejection, calling for relatively high i. frequencies. Uniformization has found a further expression in the so-called unit principle, manufacturers producing units of power supply, l.f. output stages, etc., and using them in various types of sets. The use of standardized parts has in many cases been halted by the advent of new and better parts. The same argument applies to tubes. Outstanding examples are the present 1946 miniature and subminiature types of which dimensions are shown in Figure 245. These extremely small tubes in conjunction with new and smaller parts such as resistances, condensers, coils, and sockets make for very small sets, which may be extremely useful in many cases (e.g., "personal" sets or "walkie-talkie" sets, the dimensions being comparable with medium or small-sized cigar

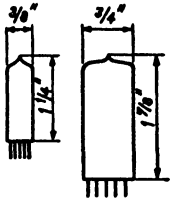

FIG. 245 External dimensions of miniature and subminiature receiving tubes.

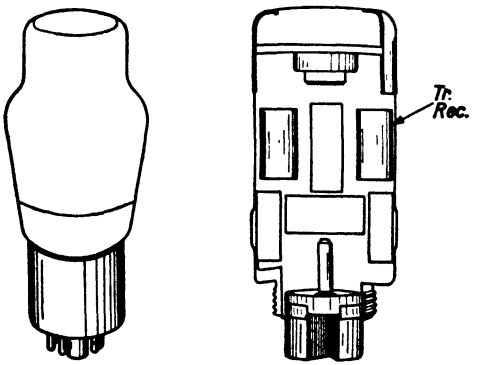

FIG. 246 Over-all sketch of fuse as used in artillery shell, incorporating complete receiver-transmitter using subminiature tubes (Fig. 245). For comparison of dimensions a 6 L 6 G tube is shown alongside.

boxes). A particular point with these small sets, if intended for the general public, relates to their loudspeakers; small-sized speakers often lack adequate l.f. response, thus impairing the quality of sound reproduction. One of the smallest sets yet produced is connected with the

so-called proximity fuses used in projectiles for antiaircraft and similar guns. An over-all picture of such a set, incorporating a transmitter and a receiver, using subminiature tubes, is shown in Figure 246. The entire set construction must withstand the tremendous acceleration imparted to it in the projectile (reference *167*, *172*). Test values were 20,000 times the acceleration of gravity at the earth's surface. All parts were enclosed by suitable rubber sleeves. The tubes had to be of special

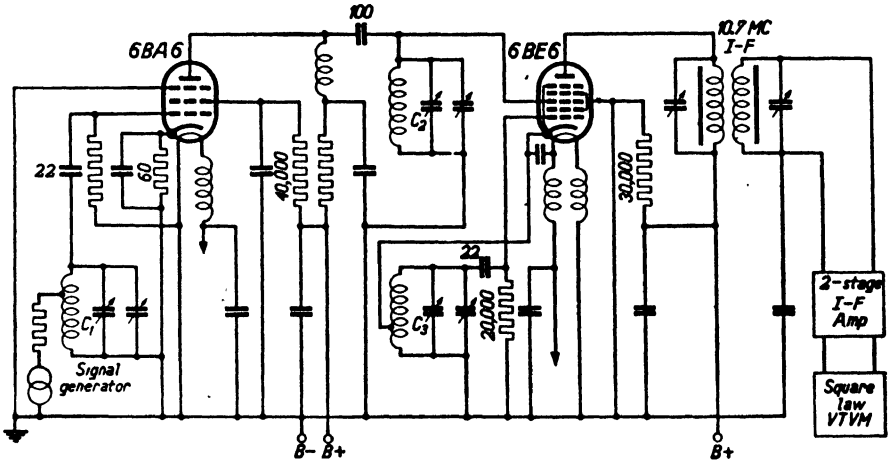

FIG. 247 Preamplifier (h.f.) and mixer stage of an FM receiver using two miniature types.

construction in order to avoid failures under such extreme conditions. These same tubes, by their rigid construction, are probably among the best antimicrophonic types ever marketed.

For FM reception special miniature tubes suitable for the h.f. and mixer stage have been developed, a pertinent wiring diagram being shown in Figure 247. The chokes inserted into the heater leads serve to prevent varying heater capacitance and resulting FM of the oscillator. This circuit is suitable at about 100 mc/s. As the i.f. is 10.7 mc/s, a considerable image rejection may be obtained, for instance 50 db. Voltage gain from the antenna input to the input of the first i.f. stage may be about 70.

Of special interest at present are u.h.f. and s.h.f. receivers. Sets tunable over frequency ranges of 2 to 1 with single dial control have been built giving continuous coverage up to 10,000 mc/s. At these

frequencies high image-rejection values have been obtained, e.g., 10 db at 1000 mc/s. The local oscillators between 1000 and 10,000 mc/s have often been lighthouse or reflex tubes using suitable circuits. The mixer stages are mostly of crystal type at these frequencies and a pertinent circuit is shown in Figure 248. The entire push-pull mixer circuit is based on the use of a suitable wave-guide combination as

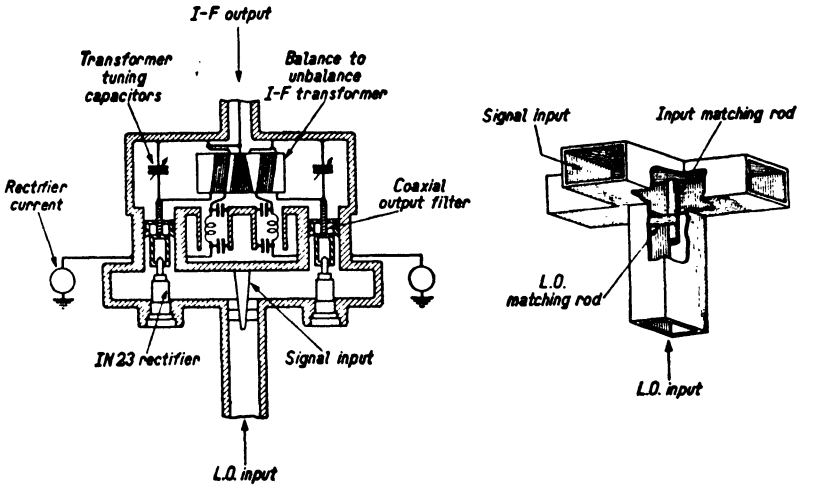

FIG. 248 Balanced s.h.f. mixer circuit using crystals and wave guide sections. The Tee-guide section is shown separately including its matching rods.

shown. Cavities and guides having no sliding contacts and often no dielectric in the h.f. circuit are used in constructions related to the present frequencies.

In some cases spurious v.h.f. or u.h.f. oscillations have been found in l.f. circuits of sets. Such oscillations may often be stopped by insertion of resistances of a few to 50 ohms into the tube electrode leads.

A considerable decrease of over-all weight of radar sets for aircraft use is necessary and has been partly obtained already. Original weight was about 300 lbs., present weight is about 100 lbs., and desired future weight is less than 50 lbs. (reference *323*). Similar decreases in weight of other mobile sets are required for many applications and present development is in this direction, using subminiature tubes and similarly small-sized parts.

REFERENCES: *2, 6, 94, 100, 167, 172, 177, 189, 323.*

LIST OF PRINCIPAL SYMBOLS

a. Latin Symbols

A	Amplitude of oscillation. Reciprocal of power attenuation.
a	Radius of circular conductor or disk (cm). Indication of anode.
B	Band width of frequency interval (cycles/sec or megacycles/sec).
b	Dimension of wave guide or reflector (cm).
C	Capacitance ($pF = \mu\mu F$).
c	Cycle in the expression c/sec. Indication of cathode.
D	Diameter or distance (cm).
d	Diameter of conductor (cm).
db	Decibel = 0.1 bel.
E	Electrical field strength (volts/cm).
e	Electronic charge: 1.6×10^{-19} coulombs.
e_o	Electronic charge/mass ratio: 17.6×10^{14} cm^2/sec^2 volt.
F	Coefficient of reflection and noise figure.
f	Frequency (c/s, kc/s, mc/s).
G	Function expressing v.h.f. decrease of noise currents (see Fig. 37).
g	Gain per stage. Indication of grid.
H	Magnetic field strength (ampere/cm).
h	Height (cm).
I	Current (ampere).
i	Fluctuation current (ampere).
j	Imaginary unit.
K	Boltzmann's constant: 1.38×10^{-23} joule/degree Kelvin.
k	Indication of $2\pi/\lambda$
L	Self-inductance (henry).
l	Length of antennas (cm).
M	Mutual inductance (henry).
m	Coefficient or index of modulation.
N	Noise figure.
n	Index of refraction.
n_o	Ratio of two indices of refraction.
O	Radar coefficient of reflection (section I.1.24).

P Power (watts, kilowatts).
p Specific power (watts/cm^2).
Q Quality figure of resonant devices.
q Integral number.
R Resistance (ohms, kiloohms, megohms).
r Radial distance (cm).
S Surface area (cm^2).
T Temperature (degrees Kelvin).
t Time (seconds).
U Indication of 2 ln ($2l$/a) (section III.2.11).
V Voltage (volts).
v Fluctuation voltage (volts).
w Transformation ratio of transformer.
X Reactance (ohms).
x Linear coordinate (cm).
Y Complex admittance (mhos) or transadmittance.
y Linear coordinate (cm).
Z Complex impedance (ohms).
Z_o Wave or surge impedance (ohms).
z Linear coordinate (cm).

b. Greek Symbols

α Coefficient of absorption (section I.1.23).
Γ Solid angle (see section III.1.21).
Δ Relatively small difference or interval between two separate values, e.g., Δf = frequency interval.
δ Loss angle of dielectric material (radians).
ϵ Dielectric constant or specific capacity.
ϕ Phase angle (radians).
φ Phase angle or azimuthal angle (radians).
κ Coupling index or coefficient.
Λ Ratio $4\pi h/\lambda$ (see Fig. 73).
λ Wavelength (cm or meters).
μ Symbol for micro, e.g., μ volt = microvolt.
μ_a Amplification factor of triode.
μ_0 $= 10^9/4\pi$ Dimensional constant.
Θ, ϑ Indications of angles, such as angle of elevation.

ω Angular frequency = $2\pi \times$ cycles/sec.
π $= 3.1417 \cdots$.
ρ_0 Specific resistance to eddy currents (section IV.1.11).
σ Specific conductivity (mhos/cm).
τ Electronic transit time (sec) (see section II.1.21).
χ Function of angular variables (section III.1.12).
ψ Phase angle.
η Coefficient (see section IV.2.12).
ζ Ratio of angular frequencies (section IV.2.11).

c. Abbreviations

a.f.c. Automatic frequency control.
a.v.c. Automatic volume control.
a.c. Alternating current.
a.v. Alternating voltage.
d.c. Direct current.
d.v. Direct voltage.
exp. Exponential function.
h.f. High frequency.
i.f. Intermediate frequency.
l.f. Low frequency.
lg Logarithm.
ln Napierian logarithm.
pF Picofarad = micromicrofarad.
r.f. Radio frequency.
r.m.s. Root mean square.
s.h.f. Super high frequencies (3000–30,000 mc/s).
u.h.f. Ultra high frequencies (300–3000 mc/s).
v.h.f. Very high frequencies (30–300 mc/s).

Bibliography

The following abbreviations have been used in the references:

American and British Periodicals

1. *A.J.* *Astrophysical Journal.*
2. *B.T.J.* *Bell System Technical Journal.*
3. *B.R.* *Bell Laboratories Record.*
4. *E.* *Electronics.*
5. *E.C.* *Electrical Communication.*
6. *E.E.* *Electrical Engineering.*
7. *E.E.T.* *Electrical Engineering Transactions.*
8. *E.I.* *Electronic Industries.*
9. *Ec.E.* *Electronic Engineering.*
10. *G.R.* *General Radio Experimenter.*
11. *J.A.P.* *Journal of Applied Physics.*
12. *J.F.I.* *Journal of the Franklin Institute.*
13. *J.I.E.* *Journal of the Institution of Electrical Engineers.*
14. *J.M.P.* *Journal of Mathematics and Physics.*
15. *N.* *Nature.*
16. *P.I.R.E.* *Proceedings of the Institute of Radio Engineers.*
17. *P.M.* *Philosophical Magazine.*
18. *P.P.S.* *Proceedings of the Physical Society.*
19. *P.R.* *Physical Review.*
20. *P.R.S.* *Proc. Royal Soc. London A.*
21. *P.T.R.* *Philips' Technical Review.*
22. *P.T.R.S.* *Phil. Trans. Royal Soc. London A.*
23. *R.C.A.* *R.C.A. Review.*
24. *R.S.I.* *Review of Scientific Instruments.*
25. *W.E.* *Wireless Engineer.*
26. *W.W.* *Wireless World.*

Dutch Periodicals

1. *P.* *Physica* (The Hague).

French Periodicals

1. *B.S.F.* *Bulletin de la société française des électriciens.*
2. *C.R.* *Comptes rendus de l'académie des sciences* (Paris).
3. *O.E.* *l'Onde électrique.*
4. *R.G.* *Revue générale de l'électricité.*

German Periodicals

1. *A.E.* *Archiv für Elektrotechnik.*
2. *A.P.* *Annalen der Physik.*
3. *E.E.N.* *Ergebnisse der exakten Naturwissenschaften.*
4. *E.N.T.* *Elektrische Nachrichten Technik.*
5. *E.Z.* *Elektrotechnische Zeitschrift.*
6. *F.* *Funk.*
7. *F.T.M.* *Funktechnische Monatshefte.*
8. *P.Z.* *Physikalische Zeitschrift.*
9. *T.R.* *Telefunken Roehre.*
10. *W.S.* *Wissenschaftliche Veroeffentlichungen des Siemens Konzerns.*
11. *Z.H.* *Zeitschrift für Hochfrequenztechnik und Elektroakustik.*

Italian Periodicals

1. *A.F.* *Alta frequenza.*

Swiss Periodicals

1. *H.P.A.* *Helvetica Physica Acta.*

U.S.S.R. Periodicals

1. *J.E.T.P.* *Journal of Experimental and Theoretical Physics.*
2. *M.P.U.* *Memoirs of Physics of the Ukraine.*
3. *T.P.U.* *Journal of Technical Physics of the U.S.S.R.*

If any article is not in English, its language is indicated. All titles are given in English.

References

1. Aceves, J. C., "Antennas for FM reception," *E.*, Sept. (1941), pp. 42–45.
2. Acheson, M. A. "Proximity fuze tubes." *E.*, vol. 19 no. 1 (1946), pp. 228–236.
3. Aiken, C. B., "Theory of the diode voltmeter," *P.I.R.E.*, vol. 26 (1938), pp. 859–876.
4. Alekseev, N. F. and Malairow, D. D., "Generation of high-power oscillations with a magnetron in the centimeter band," *P.I.R.E.*, vol. 32 (1944), pp. 136–139.
5. Alford, A. and Kandoian, A. G., "Ultra high frequency loop antennas," *E.E.T.*, vol. 59 (1940), pp. 843–848.
6. Allanson, J. T., Cooper, R. and Cowling, T. G., "The theory and experimental behaviour of right-angled junctions in rectangular-section wave guides," *J.I.E.*, Part III, vol. 93 (1946), pp. 177–187.
7. Armstrong, E. H., "Evolution of frequency modulation," *E.E.*, vol. 59 (1940), pp. 485–493.
8. Ataka, H., "On super-regeneration of an ultra-short-wave receiver," *P.I.R.E.*, vol. 23 (1935), pp. 841–884.
9. Babin, F., "Efficiency and radiation of antenna systems" (in French), *O.E.*, vol. 18 (1939), pp. 335–360, 375–390.
10. Bach, W., "Researches into the field near parabolic mirrors of rotation" (in German), *Z.H.*, vol. 53 (1939), p. 115.
11. Ballantine, S., "Schrot-effect in high-frequency circuits," *J.F.I.*, vol. 206 (1928), pp. 159–167.
12. Ballantine, S., "Grid induction noise in vacuum tubes at ultra-high frequencies," *P.I.R.E.*, vol. 28 (1940), p. 143.
13. Barrow, W. L., "On the impedance of a vertical half-wave antenna above an earth of finite conductivity," *P.I.R.E.*, vol. 22 (1935), pp 150–167.
14. Barrow, W. L., "Transmission of electromagnetic waves in hollow tubes of metal," *P.I.R.E.*, vol. 24 (1936), pp. 1298–1328.
15. Barrow, W. L., and Lewis, F. D., "The sectorial electromagnetic horn," *P.I.R.E.*, vol. 27 (1939), pp. 41–50.
16. Barrow, W. L., and Chu, L. J., "Theory of the electromagnetic horn," *P.I.R.E.*, vol. 27 (1939), pp. 51–64.
17. Barrow, W. L., and Shulman, C., "Multiunit electromagnetic horns," *P.I.R.E.*, vol. 28 (1940), pp. 130–136.
18. Barrow, W. L., and Mieher, W. W., "Natural oscillations of electrical cavity resonators," *P.I.R.E.*, vol. 28 (1940), pp. 184–191.
19. Barrow, W. L., and Mieher, W. W., "Hollow pipes of relatively small dimensions," *E.E.*, vol. 60 (1941), p. 119.
20. Bauer, G., "A semi-conducting highly resistive bolometer" (in German), *P.Z.*, vol. 44 (1943), pp. 53–62.

21. Bechmann, B., "Border-waves and stray radiation" (in German), *F.T.M.*, no. 6 (1941), pp. 81–88.
22. Benham, W. E., "A contribution to tube and amplifier theory," *P.I.R.E.*, vol. 26 (1938), pp. 1093–1170.
23. Bennett, W. R., "Response of a linear rectifier to signal and noise," *B.S.T.J.*, vol. 23 (1944), pp. 97–113.
24. Bennett, F. D., Coleman, P. D. and Meier, A. S., "The design of broad-band aircraft-antenna systems," *P.I.R.E.* vol. 33 (1945), pp. 671–701.
25. Bennington, T. W., "Short-wave (ionospheric) forecasting," *W.W.*, vol. 52 (1946), pp. 246–250, vol. 53 (1947) pp. 108–111.
26. Bennington, T. W., "The new sunspot cycle," *W.W.*, vol. 52 (1946), pp. 83–85.
27. Bereskin, A. B., "Improved high-frequency compensation for wide-band amplifiers," *P.I.R.E.*, vol. 32 (1944), pp. 608–611.
28. Bergmann, L., "Measurements of the radiation of straight wire antennas excited at fundamental and harmonic waves" (in German), *A.P.*, vol. 82 (1927), pp. 504–540.
29. Boella, M., "On the behavior of some types of high resistances in use in radio circuits at high frequencies" (in Italian), *A.F.*, vol. 3 (1934), p. 132.
30. Borgnis, F., "The electrical fundamental oscillations of cylindrical cavities" (in German), *Z.H.*, vol. 54 (1939), pp. 121–128.
31. Bowles, E. L., "40 cm. waves for aviation," *E.*, Nov. (1939), pp. 12–15.
32. Breazeale, W. M., "A note on noise and conversion-gain measurements," *P.I.R.E.*, vol. 35 (1947), pp. 31–34.
33. Brennecke, C. G., "Equivalent T and Pi sections for the quarter-wave-length line," *P.I.R.E.*, vol. 32 (1944), pp. 15–18.
34. Bressi, A., "Systematic measurements of high resistances at high frequencies" (in Italian), *A.F.*, vol. 7 (1938), pp. 551–571.
35. Brillouin, L., "Propagation of electromagnetic waves in a guide" (in French), *R.G.*, vol. 40 (1936), p. 227.
36. Brillouin, L., "Theoretical study of dielectric cables," *E.C.*, vol. 16 (1937–38), pp. 350–372.
37. Brillouin, L., "Hyperfrequency waves and their practical use," *J.F.I.*, vol. 229 (1940), pp. 709–736.
38. Brillouin, L., "Practical results from theoretical studies of magnetrons," *P.I.R.E.*, vol. 32 (1944), pp. 216–231.
39. Brown, G. H., "A turnstile antenna for use at ultra-high frequencies," *E.*, April (1936).
40. Bruce, E., "Developments in short-wave directive antennas," *P.I.R.E.*, vol. 19 (1931), pp. 1406–1433.
41. Bruce, E., Beck, A. C., and Lowry, L. R., "Horizontal rhombic antennas," *P.I.R.E.*, vol. 23 (1935), p. 24.
42. Bruene, K., "On the propagation of electromagnetic waves in water" (in German), *Z.H.*, vol. 50 (1937), pp. 73–81.
43. Buchholz, H., "Ultrashort waves in coaxial cables and cavity-resonators shaped as sections of such cables" (in German), *Z.H.*, vol. 54 (1939), pp. 161–174.
44. Burgess, R. E., "Noise in receiving aerial systems," *P.P.S.*, vol. 53 (1941), pp. 293–304.

45. Burgess, R. E., "Aerial characteristics," *W.E.*, vol. 21 (1944), pp. 154–160.
46. Burgess, R. E., "Screened loop aerials," *W.E.*, vol. 21 (1944), pp. 210 and 358.
47. Burgess, R. E., "Signal noise characteristics of triode input circuits," *W.E.*, vol. 22 (1945), p. 56.
48. Burgess, R. E., "Fluctuation noise in a receiving aerial," *P.P.S.*, vol. 58 (1946), p. 313–321.
49. Burrows, C. R., "Radiopropagation over plane earth. Field strength curves," *B.T.J.*, vol. 16 (1937), pp. 45–75.
50. Burrows, C. R., "The exponential transmission line," *B.T.J.*, vol. 17 (1938), pp. 555–573.
51. Burrows, C. R., and Gray, M. C., "The effect of the earth's curvature on ground-wave propagation," *P.I.R.E.*, vol. 29 (1941), pp. 16–25.
52. Busch, H., "Theory of Beverage antennas" (in German), *Z.H.*, vol. 21 (1923), pp. 290–312, 374–390.
53. Bushby, T. R. W. and Sherman, H., "Thermal frequency-drift compensation," *P.I.R.E.*, vol. 31 (1944), pp. 385–386, 232.
54. Byrnes, I. F., "Merchant marine radar," *R.C.A.*, vol. 7 (1946), pp. 54–66.
55. Campbell, N. R. and Francis, V. J., "A theory of valve and circuit noise," *J.I.E.*, Part III, vol. 93 (1946), pp. 45–52.
56. Carson, J. R., "Reciprocal theorems in radio communication," *P.I.R.E.*, vol. 17 (1929), p. 952.
57. Carson, J. R., Mead, S. P., and Schelkunoff, S. A., "Hyper frequency wave guides," *B.T.J.*, vol. 15 (1936), pp. 310–333.
58. Carson, J. R., and Fry, T. C., "Variable frequency electric circuit theory with application to the theory of frequency modulation," *B.T.J.*, vol. 16 (1937), pp. 513–540.
59. Carson, J. R., "Frequency-modulation. Theory of the feedback receiving circuit," *B.T.J.*, vol. 18 (1939), pp. 395–403.
60. Carter, P. S., "Circuit relations in radiating systems and applications to antenna problems," *P.I.R.E.*, vol. 20 (1932), pp. 1004–1041.
61. Carter, P. S., "Simple television antennas," *R.C.A.*, vol. 4 (1939), pp. 168–185.
62. Chaffee, J. G., "The application of negative feedback to frequency-modulation systems," *P.I.R.E.*, vol. 27 (1939), pp. 317–331.
63. Chipman, R. A., "Resonance curve methods for the absolute measurement of impedance at frequencies of the order of 300 mc/s," *J.A.P.*, vol. 10 (1939), p. 27.
64. Chu, En-Lung, "Notes on the stability of linear networks," *P.I.R.E.*, vol. 32 (1944), pp. 630–637.
65. Clayton, R. J., Houldin, J. E., Lamont, H. R. L. and Willshaw, W. E., "Radio measurements in the decimeter and centimeter wavebands," *J.I.E.*, Part III, vol. 93 (1946), pp. 117–125.
66. Colebrook, F. M., and Gordon-Smith, A. C., "The design and construction of a short-wave field strength measuring set," *J.I.E.*, vol. 84 (1939), pp. 388–398.
67. Colebrook, F. M., "The electric and magnetic fields of a linear radiator carrying a progressive wave," *J.I.E.*, vol. 86 (1940), pp. 169–178.
68. Colebrook, F. M., "Transmission line theory," *W.E.*, vol. 21 (1944), pp. 167–174.

69. Colton, R. B., "Radar in the United States Army," *P.I.R.E.*, vol. 33 (1945), pp. 740–752.
70. Condon, E. U., "Forced oscillations in cavity resonators," *J.A.P.*, vol. 12 (1941), p. 129.
71. Cornelius, E. C., "Silicon crystals for u.h.f. detection circuits," *E.I.*, vol. 4 (1945), no. 11, pp. 74–76, 136–140.
72. Cornelius, E. C., "Germanium crystal diodes," *E.*, vol. 19, no. 2 (1946), pp. 118–123.
73. Corrington, M. S., "F M distortion caused by multipath transmission," *P.I.R.E.*, vol. 33 (1945), pp. 878–891.
74. Crosby, M. G., "Frequency modulation propagation characteristics," *P.I.R.E.*, vol. 24 (1936), pp. 898–913.
75. Crosby, M. G., "The service range of frequency modulation," *R.C.A.*, vol. 4 (1940), pp. 349–371.
76. Crosby, M. G., "Band width and readability in frequency modulation," *R.C.A.*, vol. 5 (1941), pp. 363–370.
77. Crosby, M. G., "Exalted-carrier amplitude and phase modulation reception," *P.I.R.E.*, vol. 33 (1945), pp. 581–591.
78. Crosby, D. R. and Pennypacker, C. H., "Radio-frequency resistors as uniform transmission lines," *P.I.R.E.*, vol. 34 (1946), pp. 62–66.
79. Cruft Lab. war training staff, "Transmission lines, antennas and wave guides." Book, McGraw Hill, New York, 1945.
80. Daellenbach, W. and Kleinsteuber, W., "Reflection and absorption of decimeter waves at plane dielectric layers" (in German), *Z.H.*, vol. 51 (1938), pp. 152–156; vol. 52 (1938), p. 147.
81. Daellenbach, W., "Transformation line-section of smallest oscillating field energy" (in German), *Z.H.*, vol. 61 (1943), pp. 53–56.
82. Daellenbach, W., "On the first construction no. HB 14 of a resotank tube" (in German), *Z.H.*, vol. 61 (1943), pp. 161–164.
83. Daellenbach, W., "Is the term 'wave impedance of a wave guide' justified?" (in German), *Z.H.*, vol. 61 (1943), pp. 167–172.
84. Dahl, E. A., "2,660-Mc train communication system," *E.*, vol. 19, no. 1 (1946), pp. 118–122.
85. Darbord, R., "Reflectors and transmission lines at ultra-short waves" (in French), *O.E.*, vol. 11 (1932), pp. 53–82.
86. Darlington, S., "Synthesis of reactance 4-poles which produce prescribed insertion loss characteristics," *J.M.P.*, vol. 18 (1939), pp. 257–353.
87. Darrow, K. K., "Analysis of the ionosphere," *B.T.J.*, vol. 19 (1940), pp. 455–494.
88. Deviatkov, N. D., Gurevich, M. D., and Khokhlov, N. K., "A metal triode for ultra-high-frequency operation," *P.I.R.E.*, vol. 32 (1944), pp. 253–256.
89. Didlaukis, M. and Kaden, H., "The internal roughness of coaxial wide-band cables" (in German), *E.N.T.*, vol. 14 (1937), p. 13.
90. Dishal, M., "Theoretical gain and signal-to-noise ratio obtained with the grounded grid amplifier at ultra-high frequencies," *P.I.R.E.*, vol. 32 (1944), pp. 276–284.
91. Ditl, A., "Absolute measurement of voltage at decimeter waves" (in German), *Z.H.*, vol. 58 (1941), pp. 32–35.

92. Doering, H., "The slope of the detection curve at u.h.f." (in German), *Z.H.*, vol. 50 (1937), pp. 91–95.
93. Dumont, A. B. and Goldsmith, T. T., "Television broadcast coverage," *P.I.R.E.*, vol. 32 (1944), pp. 192–205.
94. Dunmore, F. W., "A unicontrol radio receiver for ultra-high frequencies using concentric lines as interstage couplers," *P.I.R.E.*, vol. 24 (1936), pp. 837–849.
95. Eaglesfield, C. C., "Characteristic impedance of transmission lines. A note on certain particular cases," *W.E.*, vol. 21 (1944), pp. 222–226.
96. Eastman, A. V., and Horle, L. C. F., "The generation of spurious signals by nonlinearity of the transmission path," *P.I.R.E.*, vol. 28 (1940), pp. 438–443.
97. Eckart, G. and Plendl, H., "The propagation of ultra-short waves" (in German), *E.E.N.*, vol. 17 (1938), pp. 325–366.
98. Elie, M., Gutton, H., Hugon, M., and Ponte, M., "Obstacle detection at navigation without visibility" (in French), *B.S.F.*, vol. 9 (1939), pp. 345–353.
99. Englund, C. R., "Dielectric constants and power factors at centimeter wavelengths," *B.T.J.*, vol. 23 (1944), pp. 114–134.
100. Engstrom, E. W. and Holmes, R. S., "Television receivers," *E.*, Part I April (1938), p. 28, *E.*, Part II June (1938), p. 20.
101. Esau, A. and Roth, O. H., "Disturbances of reception by short-wave diathermy appliances" (in German), *Z.H.*, vol. 48 (1936), p. 113.
102. Essen, L., "The measurement of balanced and unbalanced impedances at frequencies near 500 mc/s and its application to the determination of the propagation constants of cables," *J.I.E.*, vol. 91 Part III (1944), pp. 84–95.
103. Essen, L. and Oliver, M. H., "Aerial impedance measurements," *W.E.*, vol. 22 (1945), pp. 587–593.
104. Essen, L., "Cavity-resonator wavemeters," *W.E.*, vol. 23 (1946), pp. 126–132.
105. Everitt, W. L., "Frequency modulation," *E.E.T.*, vol. 59 (1940), pp. 613–625.
106. Fausten, H. J., "On optimal dimensions of double radiation-coupled directional antennas" (in German), *A.E.*, vol. 34 (1940), pp. 653–668.
107. Fendler, E., "The variations of propagation conditions of a border wave (10 m) in the years 1935–37" (in German), *Z.H.*, vol. 52 (1938), pp. 18–23, 147.
108. Fendler, E., "On the reception of antipodes at 10-m wavelength" (in German), *F.*, no. 5 (1941), pp. 77–79.
109. Fink, D. G., "The S C R—268 radar," *E.*, vol. 18, no. 9 (1945), pp. 100–109.
110. Fink, D. G., "The S C R—584 radar," *E.*, vol. 18 (1945), no. 11, pp. 104–109 no. 12, pp. 104–109.
111. Fink, D. G., "Cavity magnetrons," *E.*, vol. 19, no. 1 (1946), pp. 126–131.
112. Fisk, J. B., Hagstrum, H. D. and Hartman, P. L., "The magnetron as a generator of centimeter waves," *B.T.J.*, vol. 25 (1946), pp. 167–348.
113. Flint, H. T. and Williams, G., "A method for the measurements of impedance by means of Lecher wires," *P.M.*, vol. 32 (1941), pp. 489–495.
114. Ford, L. H. and Oliver, R., "An experimental investigation of the reflection and absorption of radiation of 9 cm wavelength," *P.P.S.*, vol. 58 (1946), pp. 265–280.
115. Foster, D. E. and Rankin, J. A., "Intermediate-frequency values for frequency-modulated-wave receivers," *P.I.R.E.*, vol. 29 (1941), pp. 546–551.
116. Fraenz, K., "Gain and absorption area of large directional antennas" (in German), *Z.H.*, vol. 54 (1939), pp. 198–224.

117. Fraenz, K., "The absorption of extremely short waves by clouds and fog" (in German), *Z.H.*, vol. 55 (1940), pp. 141–143.
118. Fraenz, K., "The amplitudes of noise-voltages" (in German), *E.N.T.*, vol. 19 (1942), pp. 166–173.
119. Fraenz, K., "Measurements of receiver sensitivity at short waves" (in German), *Z.H.*, vol. 59 (1942), pp. 105–112.
120. Fraenz, K., "Observations on the absorption area of directional antennas" (in German), *Z.H.*, vol. 61 (1943), pp. 51–53.
121. Francis, V. J. and James E. G., "The rectification of signal and noise," *W.E.*, vol. 23 (1946), pp. 16–25.
122. Frankel, S., "Characteristic impedance of parallel wires in rectangular troughs," *P.I.R.E.*, vol. 30 (1942), pp. 182–190.
123. Freeman, R. L., "Use of feedback to compensate for vacuum tube input capacitance variations with grid bias," *P.I.R.E.*, vol. 26 (1938), pp. 1360–1366.
124. Friend, A. W., "A summary and interpretation of ultra-short wave propagation collected by the late Ross A. Hull," *P.I.R.E.*, vol. 33 (1945), pp. 358–373.
125. Friis, H. T., Feldman, C. B., and Sharples, W. M., "The determination of the direction of arrival of short radio waves," *P.I.R.E.*, vol. 22 (1934), p. 47.
126. Friis, H. T. and Feldman, C. B., "A multiple-unit steerable antenna for short-wave reception," *B.T.J.*, vol. 16 (1937), pp. 337–419.
127. Friis, H. T., "Noise figures of radio receivers," *P.I.R.E.*, vol. 32 (1944), pp. 419–423, 729.
128. Friis, H. T., "A note on a simple transmission formula," *P.I.R.E.*, vol. 34 (1946), pp. 254–256.
129. Gaffney, F. J., "Microwave measurements and test equipments," *P.I.R.E.*, vol. 34 (1946), pp. 775–794.
130. Gainsborough, G. F., "The diode as a frequency-changer for measurements at ultra-high frequencies," *N.*, vol. 144 (1939), p. 548.
131. George, R. W., "A study of ultra-high-frequency wide-band propagation," *P.I.R.E.*, vol. 27 (1939), pp. 28–35.
132. George, R. W., "Field strength of motorcar ignition between 40 and 450 megacycles," *P.I.R.E.*, vol. 28 (1940), p. 145.
133. Gerlach, G. G., "A microwave relay communication system," *R.C.A.*, vol. 7 (1946), pp. 576–600.
134. Ginzton, E. L. and Harrison, A. E., "Reflex-klystron oscillators," *P.I.R.E.*, vol. 34 (1946), pp. 97–113.
135. Gordon, H. and George, L., "V.h.f. receiver (sensitivity) measurements," *E.*, vol. 19, no. 6 (1946), pp. 214–218.
136. Grammer, G. and Goodman, B., "The A.R.R.L. Antenna book," American Radio Relay League, Inc., West Hartford, Conn.
137. Gray, M. C., "Modification of Hallèn's solution of the antenna problem," *J.A.P.*, vol. 15 (1944), pp. 61–65.
138. Green, E. I., Leibe, F. A., and Curtis, H. E., "The proportioning of shielded circuits for minimum high frequency attenuation," *B.T.J.*, vol. 15 (1936), pp. 248–283.
139. Green, E. I., Fisher, H. J. and Ferguson, J. G., "Techniques and facilities for microwave radar testing," *B.T.J.*, vol. 25 (1946), pp. 435–482.

140. Grover, F. W., "The calculation of the mutual inductance of circular filaments in any desired position," *P.I.R.E.*, vol. 32 (1944), pp. 620–629.
141. Gruenberg, G., "On the theory of the action of a plane diode at high frequencies," *T.P.U.*, vol. 5 (1938), pp. 696–714.
142. Gundlach, F. W., "An electrodynamic current indicator at u.h.f." (in German), *Z.H.*, vol. 55 (1940), pp. 169–173.
143. Gundlach, F. W., "Decimeter wave measuring technique" (in German), *E.Z.*, vol. 61 (1940), pp. 853–858.
144. Gutton, H. and Ortusi, J., "Measurement of the field inside a wave guide" (in French), *C.R.*, vol. 27 (1943), pp. 18–20.
145. Haeff, A. V. and Nergaard, L. S., "A wide-band inductive output amplifier," *P.I.R.E.*, vol. 28 (1940), pp. 126–130.
146. Hansell, C. W. and Carter, P. S., "Frequency control by low-power-factor line circuits," *P.I.R.E.*, vol. 24 (1936), pp. 597–619.
147. Hara, G., "Radiation and current distribution of a linear antenna" (in German), *Z.H.*, vol. 44 (1934), pp. 185–193.
148. Harper, A. E., *Rhombic Antenna Design* (book), D. Van Nostrand, New York (1941).
149. Harris, W. A., "Fluctuations in space-charge limited currents at moderately high frequencies. V. Fluctuations in vacuum tube amplifiers and input systems," *R.C.A.*, vol. 6 (1941), pp. 114–124, 505–524.
150. Harris, W. A. and Dunn, R. F., "Recent developments in converter tubes," *E.* vol. 19, no. 1 (1946), pp. 240–242.
151. Harrison, C. W., "A note on the mutual impedance of antennas," *J.A.P.*, vol. 14 (1943), pp. 306–309.
152. Harrison, C. W., "A note on the characteristics of the two-antenna array," *P.I.R.E.*, vol. 31 (1943), pp. 75–79.
153. Harrison, C. W. and King, R., "The receiving antenna in a plane-polarized field of arbitrary orientation," *P.I.R.E.*, vol. 32 (1944), pp. 35–49.
154. Harrison, C. W., "Symmetrical antenna arrays," *P.I.R.E.*, vol. 33 (1945), pp. 892–896.
155. Harvey, A. F., *High Frequency Thermionic Tubes* (book), Chapman & Hall, London. (1944).
156. Heising, R. A., "Stability in high-frequency oscillators," *P.I.R.E.*, vol. 31 (1943), pp. 595–600.
157. Henyey, L. G. and Keenan, P. C., "Interstellar radiation from free electrons and hydrogen atoms," *A.J.*, vol. 91 (1940), pp. 625–630.
158. Herold, E. W., "An analysis of admittance neutralization by means of negative transconductance tubes," *P.I.R.E.*, vol. 25 (1937), pp. 1399–1413.
159. Herold, E. W., Harris, W. A. and Henry, T. J., "A new converter tube for all wave receivers," *R.C.A.*, July (1938), pp. 67–77.
160. Herold, E. W., "Superheterodyne converter system considerations in television receivers," *R.C.A.*, vol. 4 (1940), pp. 324–337.
161. Herold, E. W., "The operation of frequency converters and mixers for superheterodyne reception," *P.I.R.E.*, vol. 30 (1942), pp. 84–103.
162. Herold, E. W., "An analysis of the signal-to-noise ratio of ultra-high frequency receivers," *R.C.A.*, vol. 6 (1942) pp. 302–331.

163. Herold, E. W. and Malter, L., "Some aspects of radio reception at ultra-high frequency," Part I, "The antenna and the receiver input circuits," E. W. Herold, pp. 423–439; Part II, "Admittances and fluctuation noise of tubes and circuits," L. Malter, pp. 491–501; Part III, "The signal-to-noise ratio of radio receivers," E. W. Herold, pp. 501–510; Part IV, "General superheterodyne considerations at ultra-high frequencies," L. Malter, pp. 567–575; Part V, "Frequency mixing in diodes," E. W. Herold, pp. 575–581; *P.I.R.E.*, vol. 31 (1943).
164. Herold, E. W., Bush, R. R. and Ferris, W. R., "Conversion loss of diode mixers having image frequency impedance," *P.I.R.E.*, vol. 33, (1945), pp. 603–609.
165. Hershberger, W. D., "The absorption of microwaves by gases," *P.R.*, vol. 68 (1945), p. 284.
166. Hey, J. S., "Solar radiations in the 4–6 meter radio wavelength band," *N.*, vol. 157 (1946), pp. 47–48.
167. Hinman, W. S. and Brunetti, C., "Radio proximity fuze development," *P.I.R.E.*, vol. 34 (1946), pp. 976–986.
168. Hodgson, A. D., "Civil air transport communication," *J.I.E.*, vol. 87 (1940), pp. 317–350.
169. Holdam, J. V., McGrath, S. and Cole, A. D., "Radar for blind bombing," *E.*, vol. 19 no. 5 (1946), pp. 138–143.
170. Holmes, R. S. and Turner, A. H., "An urban field strength survey at thirty and one hundred megacycles," *P.I.R.E.*, vol. 24 (1936), pp. 755–770.
171. Hund, A., "Frequency and phase modulation," *P.I.R.E.*, vol. 32 (1944), pp. 572–573.
172. Huntoon, R. D. and Miller, B. J., "Generator-powered proximity fuze," *E.*, vol. 18 no. 12 (1945), pp. 98–103.
173. Jachnow, N., "Theoretical researches into the radiation diagram and radiation resistance with progressive waves of different phase velocities" (in German), *E.N.T.*, vol. 19 (1942), pp. 147–156.
174. Jaffe, D. L. and Hund, A., "Frequency and phase modulation," *P.I.R.E.*, vol. 33 (1945), pp. 487–488.
175. Jansky, K. G., "Minimum noise levels obtained on short-wave radio receiving systems," *P.I.R.E.*, vol. 25 (1937), pp. 1531–1541.
176. Jansky, K. G., "An experimental investigation of the characteristics of certain types of noise," *P.I.R.E.*, vol. 27 (1939), pp. 763–768.
177. Jenks, F. A., "Microwave techniques," *E.*, vol. 18 no. 10 (1945), pp. 120–127.
178. Johnson, J. B. and Llewellyn, F. B., "Limits to amplification," *B.T.J.*, vol. 14 (1935), pp. 85–96.
179. Johnson, R. N., "Interference in F M receivers," *E.*, vol. 18 no. 9 (1945), pp. 129–131.
180. Jones, F. and Sear, R., "Testing high-frequency cables," *W.E.*, vol. 21 (1944), pp. 512, 571.
181. Jouguet, M., "Natural electromagnetic oscillations of spherical cavities" (in French), *R.G.*, vol. 51 (1942), pp. 318–323.
182. Jouguet, M., "Natural electromagnetic oscillations of ellipsoidal cavities" (in French), *R.G.*, vol. 51 (1942), pp. 484–487.
183. Kallmann, H. E., "Standing wave meter," *E.*, vol. 20 no. 1 (1947), pp. 96–99.

184. Kalmus, H. P., "Some notes on super-regeneration with particular emphasis on its possibilities for frequency modulation," *P.I.R.E.*, vol. 32 (1944), pp. 591–600.
185. Kandoian, A. G., "Three new antenna types and their applications," *P.I.R.E.*, (Waves and Electrons) vol. 34 (1946), pp. 70–75.
186. Karplus, E., "Wide-range tuned circuits and oscillators for high frequencies," *P.I.R.E.*, vol. 33 (1945), pp. 426–441.
187. Kauzmann, A. P., "New television amplifier receiving tubes," *R.C.A.*, vol. 3 (1939), pp. 271–289.
188. Keen, R., Wireless Direction Finding London (Jliffe).
189. Kell, R. D. and Sziklai, G. C., "Miniature airborne television equipment," *R.C.A.*, vol. 7 (1946), pp. 358–366.
190. Kettel, E., "Measurements on the influence of space charge on input-capacity of amplifier valves" (in German), *T.R.*, vol. 9 (1937), pp. 15–32.
191. King, R. and Blake, F. G., "The self-impedance of a symmetrical antenna," *P.I.R.E.*, vol. 30 (1942), pp. 335–348.
192. King, R. and Harrison, C. W., "Impedance of short, long, and capacitively loaded antennas with a critical discussion of the antenna problem," *J.A.P.*, vol. 15 (1944), pp. 170–186.
193. King, R. and Harrison, C. W., "Mutual- and self-impedance for coupled antennas," *J.A.P.*, vol. 15 (1944), pp. 481–495.
194. King, R. and Harrison, C. W., "The receiving antenna," *P.I.R.E.*, vol. 32 (1944), pp. 18–35.
195. Kleen, W., "Position of ultra-short-wave valve technique" (in German), *Z.T.P.*, vol. 21 (1940), p. 357.
196. Kleen, W., "The behavior and especially the noise of triodes and pentodes in mixer circuits" (in German), *T.R.*, vol. 19–20 (1941), pp. 160–170.
197. Kleen, W., "Gain and sensitivity of ultra-short and decimeter wave reception valves" (in German), *T.R.*, vol. 23 (1941), pp. 273–296.
198. Kleen, W., "Grid-steering, cathode-steering and cathode-amplifiers" (in German), *E.N.T.*, vol. 20 (1943), pp. 140–144.
199. Klumb, H., "Bolometer for short electric waves" (in German), *Z.T.P.*, vol. 21 (1940), pp. 71–75.
200. Knol, K. S. and Strutt, M. J. O., "On a method for measuring complex admittances in the decimeter wave range" (in German), *P.*, vol. 9 (1942), pp. 577–590.
201. Kock, W. E., "Radio lenses," *B.R.*, vol. 24 (1946), pp. 193–196.
202. Koenig, H., "Self-excitation of triode circuits at ultra-short waves" (in German), *W.S.*, vol. 20 (1941), pp. 10–27.
203. Koenig, H., "The similarity laws of the electromagnetic field and their application to cavity-resonators" (in German), *Z.H.*, vol. 58 (1941), p. 174.
204. Kollak, R. and Wehde, H., *Short-wave Antennas* (in German) (book) Weidmann, Berlin.
205. Kompfner, R., "The travelling wave valve," *W.W.*, vol. 52 (1946), pp. 369–372.
206. Korshenewsky, N. von, "On the oscillations of an antenna in a radiation field" (in German), *Z.T.P.*, vol. 10 (1929), p. 604.

207. Kotowski, P., "Required band-width and efficiency of different radio telegraph systems," (in German), *E.N.T.*, vol. 20 (1943) pp. 270–276.
208. Kraus, J. D., "Multi-wire dipole antennas," *E.*, Jan. (1940), pp. 26–27.
209. Kraus, J. D., "The corner reflector antenna," *P.I.R.E.*, vol. 28 (1940), pp. 513–519.
210. Labus, J., "Calculation of self-impedance of antennas" (in German), *Z.H.*, vol. 41 (1933), pp. 17–23.
211. Laby, T. H., MacNeill, J. J., Nicholls, F. G. and Nickson, A. F. B., "Wave form, energy and reflection by the ionosphere of atmospherics," *P.R.S.*, vol. 174 (1940), pp. 145–163.
212. Lamont, H. R. L., *Wave Guides* (book), Methuen, London, (1942).
213. Landon, V. D. and Reid, J. D., "A new antenna system for noise reduction," *P.I.R.E.*, vol. 27 (1939), pp. 188–191.
214. Lindenblad, N. E., "Television transmitting antenna for Empire State Building," *R.C.A.*, April (1939).
215. Llewellyn, F. B., "Phase angle of vacuum-tube transconductance at very high frequencies," *P.I.R.E.*, vol. 22 (1934), pp. 947–956.
216. Llewellyn, F. B., "Equivalent networks of negative grid vacuum tubes at ultra-high frequency," *B.T.J.*, vol. 15 (1936), p. 575.
217. Llewellyn, F. B. and Bowen, A. E., "Production of ultra-high frequency oscillations by means of diodes," *B.T.J.*, vol. 18 (1939), p. 280.
218. Llewellyn, F. B., *Electron Inertia Effects* (book), Cambridge Univ. Press, New York. (1943).
219. Llewellyn, F. B. and Peterson, L. C., "Vacuum-tube networks," *P.I.R.E.*, vol. 32 (1944), pp. 144–167.
220. Loeb, E., "The dielectric coefficient and loss angle of dry and moist sand at decimeter waves," *Z.H.*, vol. 61 (1943), pp. 35–38.
221. Luedi, F., "Characteristic frequencies of E-type in a capacity loaded cylindrical cavity resonator" (in German), *H.P.A.*, vol. 14 (1941), p. 328.
222. Luedi, F., "Theory of slit-anode magnetrons" (in German), *H.P.A.*, vol. 16 (1943), pp. 60–82.
223. MacArthur, E. D., "Disk-seal tubes," *E.*, Feb. (1945).
224. MacDonald, D. K. C., "A note on two definitions of noise figure in radio receivers," *P.M.*, vol. 35 (1944), pp. 386–395.
225. Mackeown, S. S. and Miles, J. W., "The plane-wave resolution of guided waves," *P.I.R.E.*, vol. 33 (1945), pp. 805–808.
226. Maclean, W. R., "Ultimate band widths in high-gain multi-stage video amplifiers," *P.I.R.E.*, vol. 32 (1944), pp. 12–15.
227. Makinson, K. R., "Two methods of measuring u.h.f. electric fields," *P.M.*, vol. 35 (1944), pp. 355–371.
228. Malsch, J. and Frings, W., "A current and voltage measuring device of high sensitivity at u.h.f." (in German), *Z.T.P.*, vol. 23 (1942), pp. 50–53.
229. Marks, W. S., Perkins, O. D. and Clark, W. R., "Radio-relay communication systems in the U. S. Army," *P.I.R.E.*, vol. 33 (1945), pp. 502–522.
230. Maron, W., "Crystal tuned F M receivers," *E.*, vol. 18, no. 10 (1945), pp. 138–141.
231. Martyn, D. F., "Temperature radiation from the quiet sun in the radio spectrum," *N.*, vol. 158 (1946), pp. 632–633.

232. Mason, W. P. and Sykes, R. A., "The use of coaxial and balanced transmission lines in filters and wide-band transformers for high radio frequencies," *B.T.J.*, vol. 16 (1937), pp. 275–302.
233. Mataré, H., "The noise of diodes and crystal-detectors in static and dynamic operation" (in German), *E.N.T.*, vol. 19 (1942), pp. 111–126.
234. Mataré, H., "Input- and output-impedance of mixer-diodes" (in German), *E.N.T.*, vol. 20 (1943), pp. 48–59.
235. McPetrie, J. S., Perry, W. E. and Ford, L. H., "Sensitivity calibration of receivers," *W.E.*, vol. 22 (1945), p. 6.
236. McPetrie, J. S., Ford, L. H. and Saxton, J. A., "Polar diagrams of half-wave receiving aerials," *W.E.*, vol. 22 (1945), p. 263.
237. McPetrie, J. S. and Saxton, J. A., "The electrical properties of soil at wavelengths of 5 metres and 2 metres," *F.I.E.*, Part III vol. 92 (1945), pp. 247–255.
238. Megaw, E. C. S., "Voltage measurement at very high frequencies," *W.E.*, vol. 13 (1936), pp. 135, 201.
239. Meinke, H., "Characteristic detector curves of a diode at low and high frequencies" (in German), *T.R.*, vol. 21/22 (1941), pp. 250–264.
240. Meinke, H., "Power figures of a diode [redacted] and high frequencies" (in German), *T.R.*, vol. 23 (1941), pp. 297–315.
241. Melloh, A. W., "Damped electromagnetic waves in hollow metal pipes," *P.I.R.E.*, vol. 28 (1940), pp. 179–183.
242. Mertz, P. and Pfleger, K. W., "Irregularities in broad-band wire transmission circuits," *B.T.J.*, vol. 16 (1937), pp. 541–559.
243. Miller, J. M. and Salzberg, B., "Measurements of admittances at ultra-high frequencies," *R.C.A.*, vol. 3 (1939), pp. 486–504.
244. Moehring, G., "Investigation of diodes for the relative measurement of voltages at decimeter waves" (in German), *Z.H.*, vol. 58 (1941), pp. 57–61.
245. Mofenson, J., "Radar echos from the moon," *E.*, vol. 19, no. 4 (1946), pp. 92–98.
246. Moreno, T., "Engineering approach to wave guides," *E.*, vol. 19 no. 5 (1946), pp. 99–103.
247. Moullin, E. B., *Spontaneous Fluctuations of Voltage* (book), Oxford University Press, Oxford (1938).
248. Mouromtseff, I. E., "Development of electronic tubes," *P.I.R.E.*, vol. 33 (1945), pp. 223–233.
249. Mouroux, L., "Summary of some anti-noise schemes and systems" (in French), *O.E.*, vol. 17 (1938), pp. 575–581.
250. Moxon, L. A., "Noise factor, "Methods of measurement," "Sources of test signals," *W.W.*, vol. 53 no. 1 (1947), p. 11–14.
251. Mueller, J., "Investigation of electromagnetic cavities" (in German), *Z.H.*, vol. 54 (1939), pp. 157–161.
252. Mueller, J., "Sensitivity of valve-circuits with velocity-modulation" (in German), *Z.H.*, vol. 60 (1942), pp. 19–21.
253. Mueller, G. E., "Propagation of 6-millimeter waves," *P.I.R.E.*, vol. 34, (1946), pp. 181–183.
254. Mumford, A. H., "Radio communication developments," *N.*, vol. 157 (1946), p. 83.

255. Nagy, A. W., "An experimental study of parasitic wire reflectors on 2, 5 meters," *P.I.R.E.*, vol. 24 (1936), pp. 233–254.
256. Nergaard, S., "Electrical measurements at wavelengths less than two meters," *P.I.R.E.*, vol. 24 (1936), pp. 1207–1229.
257. Nergaard, S., "A survey of ultra-high-frequency measurements," *R.C.A.*, vol. 3 (1938), pp. 156–196.
258. Nergaard, S., and Salzberg, B., "Resonant impedance of transmission lines," *P.I.R.E.*, vol. 27 (1939), pp. 579–584.
259. Noble, D. E., "A state-wide FM police network," *E.*, vol. 13 Nov. (1940), pp. 18–22, 28–31, 66.
260. North, D. O., "Analysis of the effects of space charge on grid impedance," *P.I.R.E.*, vol. 24 (1936), pp. 218–234.
261. North, D. O., "Fluctuations in space-charge-limited currents at moderately high frequencies, Part II, Diodes and negative grid tubes," *R.C.A.*, vol. 4 (1940), pp. 441–472, Part III, vol. 5 (1940), pp. 214–260.
262. North, D. O., "Fluctuations induced in vacuum-tube grids at high frequencies," *P.I.R.E.*, vol. 29 (1941), pp. 49–50.
263. North, D. O., "The absolute sensitivity of radio receivers," *R.C.A.*, vol. 6 (1942), pp. 332–343.
264. North, D. O. and Friis, H. T., "Discussion on Noise figures of radio receivers," *P.I.R.E.*, vol. 33 (1945), pp. 125–126.
265. Norton, K. A., "The calculation of ground-wave field intensity over a finitely conducting spherical earth," *P.I.R.E.*, vol. 29 (1941), pp. 623–639; vol. 30 (1942), pp. 205–206.
266. Norton, K. A. and Landon, V. D., "Discussion on: The distribution of amplitude with time in fluctuation noise," *P.I.R.E.*, vol. 30 (1942), pp. 425–429, 526.
267. Norton, K. A. and Omberg, A. C., "The maximum range of a radar set," *P.I.R.E.*, vol. 35 (1947), pp. 4–24.
268. Ollendorff, F., "The absorption of short waves in buildings" (in German), *E.N.T.*, vol. 9 (1932), pp. 181–194.
269. Otto, R., "Electrical and mechanical problems connected with the construction of a signal source for frequencies up to 300 mc/s" (in German), *S.Z.*, vol. 22 (1942), pp. 126–130.
270. Pawsey, J. L., Payne-Scott, R. and McCready, L. L., "Radio frequency energy from the sun," *N.*, vol. 157 (1946), pp. 158–159.
271. Pawsey, J. L., "Observation of million degree thermal radiation from the sun at a wavelength of 1.5 meters," *N.*, vol. 158 (1946), pp. 633–634.
272. Pekar, S., "Rectifying effect of the semi-conductors with a blocking layer," *M.P.U.*, vol. 8 (1939), pp. 27–34.
273. Pekar, S., "A theory of a contact between metal and dielectric or a semiconductor" (in Russian), *J.E.T.P.*, vol. 10 (1940), pp. 1210–1224.
274. Percival, W. S., "An electrically cold resistance," *W.E.*, vol. 16 (1939), pp. 237–240.
275. Peterson, H. O. and Goddard, D. R., "Field strength observations of transatlantic signals, 40 to 45 megacycles," *P.I.R.E.*, vol. 25 (1937), pp. 1291–1299.

276. Peterson, H. O., "Ultra-high-frequency propagation formulas," *R.C.A.*, vol. 4 (1939), pp. 162–167.
277. Peterson, L. C. and Llewellyn, F. B., "The performance and measurement of mixers in terms of linear-network theory," *P.I.R.E.*, vol. 33 (1945), pp. 449–457.
278. Peterson, A., "Output systems of signal generators," *G.R.*, vol. 21 no. 1 (1946), pp. 1–8.
279. Pine, C. C., "A new type of automatic radio direction finder," *P.I.R.E.*, vol. 33 (1945), pp. 522–527.
280. Pockman, L. T., "The dependence of interelectrode capacitance on shielding," *P.I.R.E.*, vol. 32 (1944), pp. 91–98.
281. Poledrelli, C., "Considerations of optimal dimensions of two-conductor lines at u.h.f." (in Italian), *A.F.*, vol. 7 (1938), pp. 435–448.
282. Polkinghorn, F. A., "A single side-band musa receiving system for commercial operation on transatlantic radio telephone circuits," *B.T.J.*, vol. 19 (1940), pp. 306–340.
283. Pontecorvo. P., "On the behavior of resistors at high frequencies," *W.E.*, vol. 15 (1938), p. 500.
284. Prakke, F., Jonker, J. L. H. and [redacted] M. J. O., "A new 'all-glass' valve construction," *W.E.*, vol. 16 (1939), [redacted] 224–230.
285. Preisach, F. and Zakarias, I., "Input conductance. Measurements in high-slope h.f. amplifier valves," *W.E.*, vol. 17 (1940), pp. 147–157.
286. Prokott, E., "*Principles of modulation*," (Book, in German) Leipzig (1943), Hirzel.
287. Proudman, J., Doodson, A. T. and Kennedy, G., "Numerical results of the theory of the diffraction of a plane electromagnetic wave by a perfectly conducting sphere," *P.T.R.S.*, vol. 217 (1917), pp. 279–314.
288. Rack, A. J., "Effect of space charge and transit time on the shot noise in diodes," *B.T.J.*, vol. 17 (1938), pp. 592–619.
289. Ragazzini, J. R., "The effect of fluctuation voltages on the linear detector," *P.I.R.E.*, vol. 30 (1942), pp. 277–288.
290. Rao, V. V. L., "The Q meter and its theory," *P.I.R.E.*, vol. 30 (1942), pp. 502–511.
291. Reber, G., "Cosmic static," *P.I.R.E.*, vol. 30 (1942), pp. 378–383.
292. Reber, G., "Cosmic static," *A.J.*, vol. 100 (1944), pp. 279–287.
293. Reukema, L. E., "Transmission lines at very high radio frequencies," *E.E.*, vol. 56 (1937), pp. 1002–1011.
294. Rice, S. O., "Mathematical analysis of random noise," *B.T.J.*, vol. 23 (1944), pp. 282–336.
295. Riedinger, A., "Measurements of attenuation and propagation velocity of electromagnetic waves in metal tubes" (in German), *Z.H.*, vol. 58 (1941), pp. 21–25.
296. Roberts, F. F., and Simmonds, J. C., "Multichannel communication systems," *W.E.*, vol. 22 (1945), pp. 538–549, 576–580.
297. Robertson, S. D. and King, A. P., "The effect of rain upon the propagation of waves in the 1-and 3-centimeter regions," *P.I.R.E.*, vol. 34 (1946), pp. 178–186.
298. Rodwin, G. and Klenk, L. M., "High-gain amplifier for 150 megacycles," *P.I.R.E.*, vol. 23 (1940), pp. 260–275.

299. Rohde, L. and Opitz, G., "Conductivity measurements by rectification" (in German), *Z.H.*, vol. 54 (1939), pp. 116–121.
300. Roth, O. H., "On the mode of action of single and of multiple wire reflectors" (in German), *Z.H.*, vol. 48 (1936), p. 45.
301. Rothe, H. and Kleen, W., *Electronic Valves as Oscillators and Detectors* (in German) (book), Akademischer Verlag, Leipzig (1941).
302. Rothe, H. and Kleen, W., *Electronic Valves as First-stage Amplifiers* (in German) (book), Akademischer Verlag, Leipzig (1944) 2nd edition.
303. Russell, R. L., "Geometry of push-pull amplification," *W.E.*, vol. 21 (1944), p. 463.
304. Salzberg, B., "Notes on the theory of the single-stage amplifier," *P.I.R.E.*, vol. 24 (1936), pp. 879–897.
305. Samuel, A. L. and Sowers, N. E., "A power amplifier for ultra-high frequencies," *P.I.R.E.*, vol. 24 (1936), pp. 1464–1483.
306. Samuel, A. L., "A negative grid oscillator and amplifier for ultra-high frequencies," *P.I.R.E.*, vol. 25 (1937), pp. 1243–1252.
307. Santo Rini, P., "On double-diode field strength measurements at the low end of the decimeter-wave range" (in German), *Z.H.*, vol. 53 (1939), p. 157.
308. Saphores, J., "General properties [illegible]electric guides," *E.E.*, vol. 16 (1937–38), pp. 346–349.
309. Sarbacher, R. I. and Edson, W. A., "Tubes employing velocity modulation," *P.I.R.E.*, vol. 31 (1943), pp. 439–453.
310. Schelkunoff, S. A., *Electromagnetic Waves* (book), D. Van Nostrand, New York (1944).
311. Schottky, W., "The space charge reduction of shot effect," Part I (in German), *W.S.*, vol. 16/2 (1937), pp. 1–18.
312. Schottky, W., "On the theory of electronic noise in multi-grid valves" (in German), *A.P.*, vol. 32 (1938), pp. 195–204.
313. Scroggie, M. G., "Valve input resistance," *W.W.*, Nov. 10 (1938), pp. 400–402.
314. Seeley, S. W., "Frequency modulation," *R.C.A.*, vol. 5 April (1941), pp. 468–480.
315. Shardlow, L. R., "A new series of insulators for ultra high frequency tubes," *R.C.A.*, vol. 5 April (1941), pp. 498–504.
316. Sherbin, L. E., "Waveguide data," *E.*, vol. 20 no. 1 (1947), pp. 122–124.
317. Sherman, J. B., "Circular loop antennas at ultra-high frequencies," *P.I.R.E.*, vol. 32 (1944), pp. 534–538.
318. Shih, Tsonge, "Noise of electron valves in self-excitation" (in German), *Dissertation*, pp. 1–45, Technical University, Dresden (1937).
319. Shockley, W. and Pierce, J. R., "A theory of noise for electron multipliers," *P.I.R.E.*, vol. 26 (1938), pp. 321–332.
320. Sinclair, D. B., "New type vacuum thermocouple for use at high frequencies," *G.R.*, no. 13 (March 1939), pp. 5–8.
321. Smith, P. H., "Transmission-line-calculator," *E.*, Jan. (1939).
322. Smith-Rose, R. L., "The solar eclipse of 1945 and radio wave propagation," *N.*, vol. 157 (1946), pp. 40–42.
323. Smith, R. A., "Radar for civil aviation," *N.*, vol. 157 (1946), pp. 151–153.

324. Sommerfeld, A., "Reciprocity theorem in radio" (in German), *Z.H.*, vol. 37 (1931), pp. 167–169.
325. Southworth, G. C., "Hyper-frequency wave guides," *B.T.J.*, vol. 15 (1936), pp. 284–309.
326. Southworth, G. C., "Some fundamental experiments with wave guides," *P.I.R.E.*, vol. 25 (1937), pp. 807–822.
327. Southworth, G. C. and King, A. F., "Metal horns as directive receivers of ultra-short-waves," *P.I.R.E.*, vol. 27 (1939), p. 95.
328. Southworth, G. C., "A demonstration of guided waves," *B.R.*, vol. 18 (1940), pp. 194–198.
329. Southworth, G.C., "Microwave radiation from the sun," *F.F.I.*, vol. 239 (1945), pp. 285–297; vol. 241, March (1946).
330. Sproull, R. L. and Linder, E. G., "Resonant-cavity measurements," *P.I.R.E.*, vol. 34 (1946), pp. 305–312.
331. Stephens, W. E., "Crystal rectifiers," *E.*, vol. 19 no. 7 (1946), pp. 112–119.
332. Sterba, E. J. and Feldman, C. B., "Transmission lines for short-wave radio systems," *P.I.R.E.*, vol. 20 (1932), pp. 1163–1202.
333. Straus, H. A., "Fire-control radar M P G-1," *E.*, vol. 18 no. 12 (1945), p. 92–97.
334. Strieby, M. E. and Wentz, J. F., "Television transmission over wire lines," *B.T.J.*, vol. 20 (1941), pp. 62–81.
335. Strong, C. E., "The inverted amplifier," *E.*, July (1940), pp. 13–16.
336. Strutt, M. J. O., "The distribution of temperature in alternating-current conductors," *P.M.*, vol. 5 (1928), pp. 904–914.
337. Strutt, M. J. O., "Radiation of antennas in dependence of the properties of the soil" (in German), *A.P.*, vol. 1 (1929), pp. 721–772; vol. 4 (1929), pp. 1–16; vol. 9 (1931), pp. 67–91.
338. Strutt, M. J. O., "Reflection measurements using very short electromagnetic as well as acoustic waves" (in German), *E.N.T.*, vol. 7 (1930), pp. 387–395.
339. Strutt, M. J. O., "Measurements of electrical properties of soil between 20 c/s and 20 mc/s" (in German), *E.N.T.*, vol. 7 (1930) no. 10.
340. Strutt, M. J. O., "Detection of objects using u.h.f.," British Pat. Spec. no. 337904 (1930).
341. Strutt, M. J. O., "Skin effect" (in German), *A.P.*, vol. 8 (1931), pp. 777–793.
342. Strutt, M. J. O., "Mixing valves," *W.E.*, vol. 12 (1935), pp. 59–64.
343. Strutt, M. J. O., "Whistling notes in superheterodyne receivers," *W.E.*, vol. 12 (1935), pp. 194–197.
344. Strutt, M. J. O., "On conversion detectors," *P.I.R.E.*, vol. 23 (1935), pp. 981–1008.
345. Strutt, M. J. O., "Compensation of grid-anode capacity at short waves (in Dutch), Netherlands Pat. no. 46307 (1935–39).
346. Strutt, M. J. O. and Ziel, A. van der, "Simple circuit arrangements for improving the performance of h.f. amplifier valves" (in German), *E.N.T.*, vol. 13 (1936), p. 260.
347. Strutt, M. J. O., "Diode frequency changers," *W.E.*, vol. 13 (1936), pp. 73–80.
348. Strutt, M. J. O. and Ziel, A. van der, "Compensation of retroaction," British Pat. no. 492064 (1936).

349. Strutt, M. J. O. and Markus, N. S., "Compensation of induction effect in octodes at short waves" (in Dutch), Netherlands Pat. no. 51350 (1937–41).
350. Strutt, M. J. O. and Ziel, A. van der, "Rectification at ultra-high frequencies" (in German), German Pat. no. 715817 (1937–42).
351. Strutt, M. J. O., "Frequency changers in all-wave receivers," *W.E.*, vol. 14 (1937), pp. 184–192.
352. Strutt, M. J. O., "Characteristic constants of h.f. pentodes. Measurements at frequencies between 1, 5, and 300 mc/s," *W.E.*, vol. 14 (1937), pp. 478–488, *E.N.T.* vol. 12, (1935), pp. 347–354.
353. Strutt, M. J. O. and Ziel, A. van der, "The behavior of amplifier valves at very high frequencies," *P.T.R.*, vol. 3 (1938), pp. 103–111.
354. Strutt, M. J. O. and Ziel, A. van der, "The causes for the increase of the admittances of modern high-frequency amplifier tubes on short waves," *P.I.R.E.*, vol. 26 (1938), pp. 1011–1032.
355. Strutt, M. J. O., "The characteristic admittances of mixer tubes up to 70 mc/s" (in German), *E.N.T.*, vol. 15 (1938), pp. 11–18.
356. Strutt, M. J. O. and Ziel, A. van der, "Measurements of complex transadmittance of modern multi-grid tubes at u.h.f." (in German), *E.N.T.*, vol. 15 (1938), pp. 103–111.
357. Strutt, M. J. O. and Knol, K. S., "On the absolute measurement of alternating currents and the calibration of thermocouples in the decimeter-wave range up to 500 megacycles per second," *P.*, vol. 5 (1938), pp. 205–214.
358. Strutt, M. J. O., "Electron transit time effects in multi-grid valves," *W.E.*, vol. 15 (1938), pp. 315–321.
359. Strutt, M. J. O., "High-frequency, mixing, and detection stages of television receivers," *W.E.*, vol. 16 (1939), pp. 174–187.
360. Strutt, M. J. O. and Ziel, A. van der, "Some dynamic measurements of electronic motion in multi-grid valves," *P.I.R.E.*, vol. 27 (1939), pp. 218–225.
361. Strutt, M. J. O. and Knol, K. S., "Measurements of currents and voltages down to a wavelength of 20 centimeters," *P.I.R.E.*, vol. 27 (1939), pp. 783–789.
362. Strutt, M. J. O., *Modern Multi-grid Electron Valves* (in German), (book), Springer, Berlin, (1940) 2nd edition.
363. Strutt, M. J. O. and Ziel, A. van der, "A new push-pull amplifier valve for decimeter waves," *P.T.R.*, vol. 5 (1940), pp. 172–181.
364. Strutt, M. J. O. and Ziel, A. van der, "A variable bias amplifier valve with double cathode connection suitable for meter waves," *P.T.R.*, vol. 5 (1940), pp. 357–362.
365. Strutt, M. J. O. and Ziel, A. van der, "The noise in receiving sets at very high frequencies," *P.T.R.*, vol. 6 (1941), p. 178.
366. Strutt, M. J. O. and Ziel, A. van der, "The diode as a frequency-changing valve, especially at decimeter waves," *P.T.R.*, vol. 6 (1941), p. 285.
367. Strutt, M. J. O. and Ziel, A. van der, "Which quantities determine the operation of an electronic valve for the amplification of extremely small signals?" (in German), *P.*, vol. 8 (1941), pp. 424–425; vol. 9 (1942), p. 248.
368. Strutt, M. J. O. and Knol, K. S., "A diode for voltage-measurements at decimeter-waves," *P.T.R.*, vol. 7 (1942), pp. 124–128
369. Strutt, M. J. O. and Ziel, A. van der, "Suppression of spontaneous fluctuations

in amplifiers and receivers for electrical communication and for measuring devices," *P.*, vol. 9 (1942), pp. 513–527.

370. Strutt, M. J. O. and Ziel, A. van der, "Reduction of the effect of spontaneous fluctuations in amplifiers for meter- and decimeter-waves" (in German), *P.*, vol. 9 (1942), pp. 1003–1012.
371. Strutt, M. J. O. and Ziel, A. van der, "On the reduction of the effect of spontaneous fluctuations in amplifier valves for meter- and decimeter-waves" (in German), *P.*, vol. 10 (1943), pp. 823–826.
372. Strutt, M. J. O. and Ziel, van der, A., "Signal-noise ratio at v.h.f.," *W.E.*, vol. 23 (1946), pp. 241–249.
373. Strutt, M. J. O., "Noise-figure reduction in mixer stages," *P.I.R.E.*, vol. 34 (1946), pp. 942–950.
374. Sziklai, G. C. and Schroeder, A. C., "Cathode-coupled wide-band amplifiers," *P.I.R.E.*, vol. 33 (1945), pp. 701–709.
375. Thomas, H. A., *Theory and Design of Valve Oscillators* (book), Chapman & Hall, London (1939).
376. Thompson, B. J., North, D. O. and Harris, W. A., "Fluctuations in space-charge-limited currents at moderately high frequencies," Part I, "General survey," *R.C.A.* vol. 4 (1940), pp. 269–285; Part II *see* North; Part III *see* North; Part IV *see* Thompson and North; Part V *see* Harris.
377. Thompson, B. J. and North, D. O., "Fluctuations in space-charge-limited currents at moderately high frequencies," Part IV; "Fluctuations caused by collision-ionization," *R.C.A.*, vol. 5 (1941), pp. 371–388.
378. Trevor, B., Dow, O. E. and Houghton, W. D., "Pulse time division radio relay," *R.C.A.*, vol. 7 (1946), pp. 361–375.
379. Usselman, G. L., "A V-T voltmeter for coaxial line measurements," *E.*, July (1940), pp. 32, 79.
380. Waynick, A. H., "Experiments on the propagation of ultra-short radio waves," *P.I.R.E.*, vol. 28 (1940), pp. 468–474.
381. Weighton, D., "Coupled and staggered circuits in wide-band amplifiers," *W.E.*, vol. 21 (1944), p. 468.
382. Weissfloch, A., "A transformation rule on reactive four-poles and its application to the experimental investigation of decimeter and centimeter wave circuits" (in German), *Z.H.*, vol. 60 (1942), pp. 67–73.
383. Weissfloch, A., "A simple method for the determination of power losses in reception diodes at very high frequencies" (in German), *E.N.T.*, vol. 20 (1943), pp. 89–92.
384. Wells, H. W., "Effects of solar activity on the ionosphere and radio communications," *P.I.R.E.*, vol. 31 (1943), pp. 147–158.
385. Weston, J. D., "Response of reactive networks to frequency-modulated signals," *W.E.*, vol. 19 (1942), pp. 251–253.
386. Wheeler, H. A., "Transmission lines with exponential taper," *P.I.R.E.*, vol. 27 (1939), pp. 65–71.
387. Wheeler, H. A., "Two-signal cross modulation in a frequency modulation receiver," *P.I.R.E.*, vol. 28 (1940), pp. 537–540.
388. Wheeler, H. A., "Formulas for the skin effect," *P.I.R.E.*, vol. 30 (1942), pp. 412–425.

389. Wilder, M. P. and Brustman, J. A., "A picture signal generator," *E.*, vol. 13 Apr. (1940), pp. 25–29; Aug., pp. 30–33.
390. Williams, F. C., "Thermal fluctuations in complex networks," *J.I.E.*, vol. 81 (1937), pp. 751–760.
391. Williams, F. C., "The response of rectifiers to fluctuation voltages," *J.I.E.*, vol. 80 (1937), pp. 218–226.
392. Wilson, I. G., Schramm, C. W. and Kinzner, J. P., "High Q resonant cavities for microwave testing," *B.T.J.*, vol. 25 (1946), pp. 408–434.
393. Wolff, I., Linder, E. G. and Braden, R. A., "Transmission and reception of centimeter waves," *P.I.R.E.*, vol. 23 (1935), pp. 11–23.
394. Works, C. N., Dakin, T. W. and Boggs, F. W., "A resonant-cavity method for measuring dielectric properties at ultra-high frequencies," *P.I.R.E.*, vol. 33 (1945), pp. 245–254.
395. Yagi, H., "Beam transmission of ultra-short waves," *P.I.R.E.*, vol. 16 (1928), pp. 715–741.
396. Ziel, A. van der and Strutt, M. J. O., "Suppression of spontaneous fluctuations in 2 N-terminal amplifiers and networks," *P.*, vol. 9 (1942), pp. 528–538.
397. Zisler, S., "A wide-band antenna" (in German), *E.N.T.*, vol. 16 (1939), pp. 121–127.
398. Zuhrt, H., "Power amplification at u.h.f. and the limit of regeneration" (in German), *Z.H.*, vol. 49 (1937), p. 73; vol. 51 (1938), pp. 135–138.
399. Zuhrt, H., "Reduction of noise with FM in dependence on amplitude limitation" (in German), *Z.H.*, vol. 54 (1939), pp. 37–44.

Additional References

400. Moxon, L. A., "Variation of cosmic radiation with frequency," *N.*, vol. 158 (1946), pp. 758–759.
401. Strutt, M. J. O., "Properties of gain and noise figures at u.h.f.," *W. E.*, vol. 24 (1947).
402. Jordan, E. C. and Miller, W. E., "Slotted cylinder antenna," *E.*, Feb. (1947), pp. 90–93.
403. Kinzler, J. P. and Wilson, I. G., "End plate and side wall currents in circular cylinder cavity resonators," *B. T. J.*, vol. 26 (1947), pp. 31–79.
404. Scaff, J. H. and Ohl, R. S., "Development of silicon crystal rectifiers for microwave radar receivers," *B. T. J.*, vol. 26 (1947), pp. 1–30.
405. Hofweegen, J. M., van, "Impedance measurements," *P. T.R.*, vol. 8 (1946), no. 1.
406. Friis, H. T. and Lewis, D., "Radar antennas, "*B.T.J.*, vol. 26 (1947), pp. 219–317.
407. Lozier J. C., "Spectrum analysis of pulse modulated waves," *B.T.J.*, vol. 26 (1947), pp. 360–387.
408. Strutt, M. J. O. and Ziel, A. Van der, "Methods for the compensation of different kinds of shot-effect in electron tubes and attached circuits," (in German), *P.*, vol. 8 (1941), pp. 1–22.
409. Lindenhovius, H. J. and Rinia, H., "Stabilized d.c. power supply," *P.TR.*, vol. 6, Feb. (1941).

INDEX